

GEOSYNTHETICS '87

CONFERENCE PROCEEDINGS

Geosynthetics Conference '87

**Clarion Hotel, New Orleans, LA
February 24 & 25, 1987**

VOLUME 1

SPONSORED BY



SOLMAX

GEOSYNTHETICS '87

CONFERENCE PROCEEDINGS

Geosynthetics Conference '87

**Clarion Hotel, New Orleans, LA
February 24 & 25, 1987**

VOLUME 1

Sponsored by the Industrial Fabrics Association International under the auspices of the American Society on Geosynthetics and the International Geotextile Society.

GEOSYNTHETICS '87 CONFERENCE

SPONSORED BY:

THE INDUSTRIAL FABRICS ASSOCIATION INTERNATIONAL

UNDER THE AUSPICES OF:

AMERICAN SOCIETY ON GEOSYNTHETICS

AND

INTERNATIONAL GEOTEXTILE SOCIETY

GEOSYNTHETICS '87 CONFERENCE

ORGANIZING COMMITTEE

CHAIRMAN

JOSEPH E. FLUET, JR. President, American Society on Geosynthetics; Former Secretary/Treasurer, International Geotextile Society; Former Chairman, Geotextile Division, IFAI; Organizing Committee Member, 2nd International Conference on Geotextiles and 1st International Conference on Geomembranes; Former Committee Member Geotechnical Fabrics Conference '85.

COMMITTEE MEMBERS

RUDOLF BONAPARTE Charter Member of American Society on Geosynthetics.

RICHARD CAIN Chairman, Geomembrane Division, IFAI; Organizing Committee Member, Geotechnical Fabrics Conference '85.

KRISTI LEE JOHNSON Editor of Geotechnical Fabrics Report.

ROBERT M. KOERNER President Elect, American Society on Geosynthetics; Former Chairman, Geotechnical Fabrics Conference '85.

WILLARD PUFFER Chairman, Geotextile Division, IFAI; Organizing Committee Member, Geotechnical Fabrics Conference '85.

JUDY SHIMON Staff Director of Geomembrane and Geotextile Divisions, IFAI.

ROBERT WALLACE Chairman, Canadian General Standard Board, Subcommittee on Geotextile Test Methods; Former Chairman, Second Canadian Symposium on Geotextiles and Geomembranes; Former Chairman, Alberta Symposium on Geotextiles; Former Council Member, International Geotextile Society.

STEPHEN WARNER Executive Vice President, IFAI; Secretary General, American Society on Geosynthetics; Former Secretary General, 2nd International Conference on Geotextiles.

These papers are published by:
Industrial Fabrics Association International
345 Cedar Building, Suite 450
St. Paul, MN 55101
(612)222-2508
TWX: 910-563-3622

©Industrial Fabrics Association International

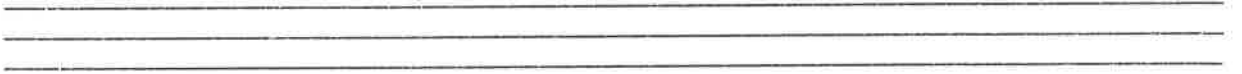


TABLE OF CONTENTS

TABLE OF CONTENTS

VOLUME 1

OPENING AND KEYNOTE ADDRESSES

Opening Address	1
FLUET, J.E., Jr., Chairman, Organizing Committee, Geosynthetic '87 Conference GeoServices Inc. Consulting Engineers, U.S.A.	
Keynote Address	4
GIROUD, J.P., President, International Geotextile Society GeoServices Inc. Consulting Engineers, U.S.A.	

SESSION 1A: UNPAVED AND PAVED ROADS

Co-Leaders: J.S. Freese, Mirafi, Inc., U.S.A.
J.D. Scott, University of Alberta, Canada

Field Tests on the Use of Geosynthetics to Support. Paved Roads Over Voids-Preliminary Conclusions T.C. KINNEY University of Alaska, U.S.A.	6
A Geosynthetics Post-Construction Assessment. R.B. WALLACE and J.F. BEECH GeoServices Inc. Consulting Engineers, U.S.A. R.J. GRAHAM EBA Engineering, Canada	14
The Behavior of Geotextiles as Separating Membranes on Glacial Till Subgrades D.T. GLYNN, and S.R. COCHRANE The Queen's University of Belfast, United Kingdom	26
Railroad Ballast Reinforcement Using Geogrids J.C. WALLS The Tensar Corporation, U.S.A. L.L. GALBREATH CSX Transportation, U.S.A.	38
Granular Base Reinforcement of Flexible Pavements Using Geogrids. R.G. CARROLL, and J.C. WALLS The Tensar Corporation, U.S.A. R. HAAS University of Waterloo, Canada	46

Polymer Grid Cell Reinforcement in Construction of
Pavement Structures 58
B. KAZERANI and G.H. JAMNEJAD
Sunderland Polytechnic, England

AC Overlay Strategies for PCCP Pavement Using Asphalt
Saturated Textiles. 69
J. HANNON
California Department of Transportation, U.S.A.
J. MINER and M. DONAHUE
Phillips Fibers Corporation, U.S.A.

New Mexico Study of Interlayers Used in Reflective Crack Control. 82
V.M. LORENZ
New Mexico State Highway Department, U.S.A.

SESSION 1B: SLOPES AND WALLS

Co-Leaders: W.C.B. Villet, Dames & Moore, U.S.A.
W.L. Deutsch, Roy F. Weston

A Design Procedure for Geotextile-Reinforced Walls. 95
D. LESHCHINSKY
University of Delaware, U.S.A.
E.B. PERRY
U.S. Army Engineer, U.S.A.

Design Charts for Geogrid-Reinforced Soil Slopes. 108
G.R. SCHMERTMANN, V.E. CHOUREY-CURTIS and R.D. JOHNSON
The Tensar Corporation, U.S.A.
R. BONAPARTE
GeoServices Inc. Consulting Engineers, U.S.A.

Slope Reinforcement Using Geogrids. 121
R.B. WALLACE and J.E. FLUET JR.
GeoServices Inc. Consulting Engineers, U.S.A.

The Importance of Stress-Strain Relationships in
Reinforced Soil System Design 133
J.F. BEECH
GeoServices Inc. Consulting Engineers, U.S.A.

Geogrid Reinforced Soil Retaining Wall to Widen an Earth
Dam and Support High Live Loads 145
B.R. CHRISTOPHER
STS Consultants, Ltd., U.S.A.

Design of the Devon Geogrid Test Fill	157
J.D. SCOTT, D.C. SEGO and B.A. HOFMANN Dept. of Civil Engineering, University of Alberta, Canada	
E.A. RICHARDS Dept. of Clothing and Textiles, University of Alberta, Canada	
E.R. BURCH Alberta Transportation, Canada	
Strain Development in Anchorage Zones	169
P.M. JARRETT and R.J. BATHURST Royal Military College of Canada, Canada	
Long-Term Allowable Tension for Geosynthetic Reinforcement.	181
R. BONAPARTE GeoServices Inc. Consulting Engineers, U.S.A	
R. BERG The Tensar Corporation, U.S.A	
<u>SESSION 2A: LABORATORY AND MODEL EVALUATION</u>	
Co-Leaders: W.G. Puffer, Puffer & Associates, U.S.A. B.L. Jeffery, Foss Manufacturing Company, U.S.A.	
Stitchbonded Composites	193
J.N. PAULSON and M.C. LANGSTON Exxon Chemical Company, U.S.A.	
Frictional Characteristics of Geotextiles With Compacted Lateritic Gravels and Clays	205
J. LAFLEUR, M.S. SALL and A. DUCHARME Ecole Polytechnique de Montreal, Canada	
Plate Loading Tests on Geogrid-Reinforced Earth Slabs.	216
V.A. GUIDO and J.D. KNUEPPEL The Cooper Union School of Engineering, U.S.A.	
M.A. SWEENEY Mueser Rutledge Consulting Engineers, U.S.A.	
Strength and Pullout Testing of Geogrids	226
S.R. BRAND Black and Veatch, U.S.A	
D.M. DUFFY Arizona State University, U.S.A.	
In-Soil Load Elongation, Tensile Strength and Interface Friction of Nonwoven Geotextiles.	238
D. LESHCHINSKY University of Delaware, U.S.A.	
D.A. FIELD CTC/GEOTEK, U.S.A.	

Soil-Geotextile Interaction Mechanism in Pullout Test 250
W.H. TZONG and S. CHENG-KUANG
University of Colorado at Denver, U.S.A.

In-Soil Stress-Strain Behavior of Geotextile. 260
B.D. SIEL
ATEC Associates, U.S.A.
W.H. TZONG
University of Colorado at Denver, U.S.A.
N.N.S. CHOU
Colorado Department of Highways, U.S.A.

SESSION 2B: EMBANKMENTS OVER WEAK SOILS

Co-Leaders: G.N. Richardson, Soil and Material Engineers, U.S.A
P. Lucia, Woodward-Clyde Consultants

Reinforcement of Embankments on Soils Whose
Strength Increases With Depth266
R.K. ROWE and K.L. SODERMAN
The University of Western Ontario, Canada

Use of Reinforcement for Embankment Widening278
D.N. HUMPHREY
University of Maine, U.S.A.
R.D. HOLTZ
Purdue University, U.S.A.

Stabilization of Very Soft Soils Using Geosynthetics289
J. FOWLER
U.S. Army Corps of Engineers, U.S.A
R.M. KOERNER
Drexel University, U.S.A.

Stability Consideration of Embankments on Soft Soils
Based on Improved Hydraulic Boundary Conditions301
G. WERNER and S. RESL
Chemie Linz AG, Austria
R.K. FROBEL
Chemie Linz US Inc., U.S.A.

Difficult Soil Problems on Cochrane Bridge Finessed
With Geosynthetics.309
L. LOCKETT
State of Alabama Highway Department, U.S.A
R.M. MATTOX
The Tensar Corporation, U.S.A

Design and Construction of a Geogrid Reinforced Embankment Over Waste Material.320
A. PAGOTTO Comune di Modena, Italy	
P. RIMOLDI RDB Plastotecnica, SPA, Italy	
The Effectiveness of Tensile Reinforcement in Strengthening an Embankment Over Soft Foundation.332
N.N.S. CHOU Colorado Department of Highways, U.S.A.	
W.H. TZONG University of Colorado at Denver, U.S.A	
B.D. SIEL ATEC Associates Inc., U.S.A.	
An Economical Solution to Increasing the Capacity of an Industrial Waste Facility with a Geogrid Reinforced Dike.341
H. SEAWELL Thompson Engineering, Testing, U.S.A.	
R.M. MATTOX The Tensar Corporation, U.S.A.	

V O L U M E 2

SESSION 3A: DESIGN/CONSTRUCTION

Co-Leaders: N. Schomaker, U.S. EPA, U.S.A.
C. Ryan, GEO-CON, U.S.A.

Design and Construction of a Hazardous Waste Landfill.353
L.O. YAMAMOTO International Technology Corporation, U.S.A.	
Current Practice in the Use of Geosynthetics in the Heap Leach Industry365
J.A. LEACH, T.G. HARPER, and R.T. TAPE Klohn Leonoff Consultants, Canada	
Geomembrane-Soil Composite Lining Systems Design, Construction Problems, and Solutions.375
D. BURANEK and J. PACEY Emcon Associates, U.S.A.	
Preventing Geomembrane Failures.385
A.A. MCCREADY Harding Lawson Associates, U.S.A.	

SESSION 3B: TRANSMISSION

Co-Leaders: M.J. Cowell, The Tensar Corporation, U.S.A.
I. Peggs, GeoSyntec Inc., U.S.A.

Geocomposite Drainage Systems: Mechanical Properties
and Discharge Capacity Evaluation. 393
A. CANCELLI
University of Milano, Italy
D. CAZZUFFI
ENEL's Research Centre for Hydraulics and Structures, Italy
P. RIMOLDI
Politecnico di Milano, Italy

Transient In-Plane Flow of Liquids in Fibrous Networks. 405
K.L. ADAMS and L. REBENFELD
Princeton University, U.S.A.

The Use of Geosynthetics in Conjunction With
Three-Dimensional Drainage Cores 417
J.O. SNYDER
GeoTech Systems Corporation, U.S.A.

Creep of Geocomposite Drains. 422
A.D. SMITH and S.R. KRAEMER
Haley & Aldrich, Inc., U.S.A

SESSION 4A: DURABILITY

Co-Leaders: N. Schomaker, U.S. EPA, U.S.A.
C. Ryan, GEO-CON, U.S.A.

An Analysis of the Durability Problems of Geotextiles. 434
H. SCHNEIDER
Chemie Linz, Austria
M. GROH
Polyfelt Inc., U.S.A.

Long-Term Durability of Geosynthetics Soil Reinforcement. 442
W.S. WHELTON
The Tensar Corporation, U.S.A.
N.E. WRIGLEY
Netlon Limited, United Kingdom

SESSION 4B: FILTRATION

Co-Leaders: M.J. Cowell, The Tensar Corporation, U.S.A.
I. Peggs, GeoSyntec, U.S.A.

Geosynthetic Filtration in Landfill Design. 456
A.L. ROLLIN
Ecole Polytechnique de Montreal, Canada
R. DENIS
Solmers Internationale, Canada

Permittivity of Geotextiles in Presence of Water
and Pollutant Fluids 471
A. CANCELLI
University of Milano, Italy
D. CAZZUFFI
ENEL's Research Centre for Hydraulics and Structures, Italy

Filtration Behavior Analysis of Thin Heat-Bonded Geotextiles. 482
G. LOMBARD and A. ROLLIN
Ecole Polytechnique, Canada

SESSION 5A: QUALITY ASSURANCE/QUALITY CONTROL

Co-Leaders: N.D. Williams, Georgia Institute of Technology, U.S.A.
J. Luna, Hoechst Fibers Industries

Geomembrane Seam Inspection Using the Ultrasonic Shadow Method. 493
R.M. KOERNER, A.E. LORD JR., and R.B. CRAWFORD
Drexel University, U.S.A.
M. CADWALLADER
Gundle Lining Systems, Inc., U.S.A.

Evaluating Polyethylene Geomembrane Seams 505
I.D. PEGGS
GeoSyntec, Inc., U.S.A

Construction Quality Assurance/Quality Control
for Land Disposal Facilities 519
T. HEBERT
Hebert Engineering Corp., U.S.A.

Geosynthetic Lining Systems and Quality Assurance-State of
Practice and State of the Art 530
J.E. FLUET JR.
GeoServices Inc. Consulting Engineers, U.S.A.

SESSION 5B: MATERIAL SELECTION

Co-Leaders: G. Kolbasuk, Precision Laboratories, U.S.A.
R. Carriker, Amoco Fabrics Company, U.S.A.

Selection of Geosynthetic Materials for Canal Liner 542
L.O. TIMBLIN JR.
Bureau of Reclamation, U.S.A.

High Density Polyethylene Liners: A Users Experience 554
I.L. PFALSER
Phillips Petroleum Co., U.S.A.

The Composite Advantage in the Mechanical Protection of
Polyethylene Geomembranes: A Laboratory Study 565
R. FROBEL
Polyfelt Inc., U.S.A.
W. YOUNGBLOOD and J. VANDERVOORT
PolyAmerica, Inc., U.S.A.

SESSION 6A: TESTING

Co-Leaders: N.D. Williams, Georgia Institute of Technology, U.S.A.
J. Luna, Hoechst Fibers Industries, U.S.A.

Laboratory Testing of Geosynthetics and Plastic
Pipe for Double-Liner Systems. 577
H.E. HAXO JR. and M.J. WALLER
Matrecon, Inc., U.S.A.

Performance of a Comprehensive Liner System
Compatability Testing Program. 595
M.F. COIA
Roy F. Weston, Inc., U.S.A.
L. SHERMAN
Fondessy Enterprises, Inc., U.S.A.
H.E. HAXO JR.
Matrecon, Inc., U.S.A.

The EPA Testing Program for Components of Treatment,
Storage, and Disposal Facilities 609
R.E. LANDRETH
United States Environmental Protection Agency, U.S.A.

SESSION 6B: OTHER GEOSYNTHETIC APPLICATION

Co-Leaders: G. Kolbasuk, Precision Laboratories, U.S.A.
R. Carriker, Amoco Fabrics Company, U.S.A.

Evaluation of Interface Friction Properties
Between Geosynthetics and Soils. 616

N.D. WILLIAMS
Georgia Institute of Technology, U.S.A.
M.F. HOULIHAN
Law Environmental Services, U.S.A.

Geoboard Reduces Lateral Earth Pressures. 628
A.M. PARTOS and P.M. KAZANIWSKY
SITE Engineers, U.S.A.



OPENING ADDRESS

KEYNOTE ADDRESS

FLUET, J.E., Jr.

Chairman, Organizing Committee, Geosynthetic '87 Conference
GeoServices Inc. Consulting Engineers, U.S.A.

Opening Address

On behalf of the organizing committee, the Industrial Fabrics Association International (IFAI), and the American Society on Geosynthetics (ASG), I wish to welcome you to Geosynthetics '87 and beautiful New Orleans.

I would like to begin by introducing the members of the organizing committee, who have worked very hard these past two years to bring you this national conference on geosynthetics.

- Dr. Rudolph Bonaparte is a charter member of the ASG, and has been a major contributor to the development of geosynthetic technology, particularly in the field of soil reinforcement.
- Mr. Richard Cain is Chairman of the Geomembrane Division of IFAI and served on the organizing committee of the predecessor to this Conference - Geotechnical Fabrics Conference '85.
- Dr. Robert Koerner is President-Elect of the ASG, the former Chairman of Geotechnical Fabrics '85, author of two textbooks and countless publications on geosynthetics, organizer and instructor of several short courses on geosynthetics, and a member of the ISSMFE committee on geosynthetics. Dr. Koerner is an acknowledged leader in this field, and he will demonstrate his leadership by moderating the panel discussion on durability/aging which immediately follows this session.
- Mr. Will Puffer is Chairman of the Geotextile Division of IFAI, served on the organizing committee for Geotechnical Fabrics '85, and is the author of a number of publications on geosynthetics.
- Mr. Bob Wallace is Chairman of the Canadian General Standards Board Subcommittee on Geotextile Test Methods, was chairman of the Second Canadian Symposium on Geotextiles and Geomembranes as well as the Alberta Symposium on Geotextiles, and is a former council member of the International Geotextile Society (IGS). Mr. Wallace is also the author of many publications on geosynthetics.
- Ms. Judy Shimon has, since December 1986, been the IFAI staff representative to the conference, and she has done a commendable job filling the capable shoes of Ms. Joan Haglund, who formerly held the position.

- Mr. Steve Warner is Executive Vice President of the IFAI, General Secretary of the ASG, a council member of the IGS, and he has served as the IFAI representative to the organizing committees of several conferences on geosynthetics - in fact, it was Steve who prompted IFAI to sponsor its first geosynthetics conference, the Second International Conference on Geotextiles, held in 1982 in Las Vegas.

I would like to take this moment, on behalf of the geosynthetics industry, to extend our thanks to the Industrial Fabrics Association International. The IFAI has certainly been a moving force in the growth of our industry. They founded and sponsored the two major trade associations of our industry: the IFAI Geotextile and Geomembrane Divisions. The IFAI has also contracted to act as professional manager in support of the ASG. Perhaps most importantly, the IFAI has sponsored every major conference on geosynthetics ever held in North America: the 1982 Second International Conference on Geotextiles, the 1984 International Conference on Geomembranes, the 1985 Geotechnical Fabrics Conference '85, and now they bring us Geosynthetics '87. Every one of these conferences has been very professionally managed and has reflected honorably on our discipline. Each one has been a technical conference in the best sense of the word, witness the fact that the proceedings from each of them have served as major technical references which have significantly advanced the state of the art.

I think you will agree with me that this conference and its proceedings have continued in this fine tradition. The technical sessions cover every major topic related to geosynthetics, and, selecting the more than sixty technical papers from the many submittals was indeed a challenge for the technical program committee. Many of the papers address state of the art developments: high modulus and high strength soil reinforcement applications, new and innovative materials and composites, and, of course, the proliferation of geosynthetic applications in the waste disposal industry. These topics are at the leading edge of our discipline, and the excellent quality of the papers presented this week have certainly advanced the state of our art.

Similarly, the panel discussion to be held later this afternoon will address one of the most topical aspects of geosynthetics: durability/aging. For the first time, leading experts from all facets of our industry have been assembled to focus and discuss this critical issue. Most of us will agree that the lack of long term research on durability/aging is a glaring deficiency in our discipline, and this assembly may well prove to be the long awaited impetus to the initiation of this research.

Following the panel discussion and the reception this evening, the American Society on Geosynthetics will hold a General Assembly meeting. The ASG was founded as the American Chapter of the International Geotextile Society. One of the primary goals of both the IGS and the ASG is to provide a forum for communications between designers, manufacturers and users of geosynthetics. This conference is one such forum, hence it is being held under the auspices of the IGS and the ASG. Other excellent forums are the societies themselves - the IGS and the ASG have active committees who address the most critical issues in our field. The real driving force behind any emerging discipline is concerted and cohesive action by those who are involved in its emergence. Those of you who are already members of the ASG know the power of such concerted efforts. To those of you who are not yet involved, I offer this challenge - you can make a difference,

you can have an effect. Join right now and help us guide the growth of this industry. We need your competence, your professionalism, your ideas, your participation. With a little help from each of us, both the industry and the discipline of geosynthetics will grow rapidly and be characterized by the professionalism we all so dearly cherish. I, for one, recognize the many benefits I have reaped from my association with geosynthetics: it has provided me with a challenging career, interesting work, a growing list of friends and colleagues, a chance to visit far-away places (perhaps a little more often than I might choose), a decent livelihood, and, it even gives me something to do with my spare time. In appreciation of all these benefits, I view my participation in the ASG as an opportunity to repay some of the debt I owe to geosynthetics. For all of us here, it's time to repay a little debt and/or to jump on the bandwagon and start reaping some benefits. In either case, it's time to participate in the ASG, so join us this evening. This is one time when your voice will not only be heard - I assure you the echo will resound for many years to come.

Now, I am proud to have the opportunity to introduce Dr. J.P. Giroud, President of the International Geotextile Society. Dr. Giroud is perhaps the best known individual in our field. He has authored a book and over sixty technical papers on geosynthetics, he developed many of the fundamental engineering formulations upon which the discipline is founded (including coining the terms "geotextile" and "geomembrane"), and he has been and continues to be involved in virtually every state of the art technical development in geosynthetics. Furthermore, Dr. Giroud has provided us with much more than technical leadership - he has been involved in geosynthetics committee work around the world, including ASTM, RILEM, and the French and Swiss National Committees, and in his spare time, he chaired the Second International Conference on Geotextiles, and the International Conference on Geomembranes, as well as the ISSMFE Technical Committee on Geotextiles and Geosynthetics including the geosynthetics session of the last ISSMFE conference in San Francisco. Dr. Giroud's keynote address at the Third International Conference on Geotextiles in Vienna this past spring was widely regarded as a highlight of the conference, and, today, those of you who missed Vienna will see why. Ladies and gentlemen, Dr. J.P. Giroud.

GIROUD, J.P.

President, International Geotextile Society
GeoServices Inc. Consulting Engineers, U.S.A.

Keynote Address

The International Geotextile Society - the IGS - is very happy to participate in Geosynthetics '87, the first national conference organized under its auspices. The IGS is also very pleased that this has happened in the USA, the country with the largest IGS chapter (the first to have more than 100 members) and the country with the largest market for geotextiles and related products.

The IGS is grateful to the leader of this success, J.E. Fluet, Jr., president of the American Society on Geosynthetics, which is the US chapter of the IGS, and chairman of the organizing committee of this conference. Also, Mr. Fluet is one of the founders of the IGS and was its first treasurer.

The IGS would also like to thank S.M. Warner, IGS Council member and secretary general of the American Society on Geosynthetics. Mr. Warner is executive vice president for the Industrial Fabrics Association International (IFAI), the sponsor of Geosynthetics '87. The IGS has enjoyed working with IFAI on this conference, and hopes to have opportunities for more cooperation in the future.

There have been conferences on geotextiles and on geomembranes in the past, but this is the first to have the word "geosynthetics" in its name. The term, first proposed by Fluet to ASTM in June of 1983, has great merit because of its broad scope. Regardless of the terms you use - geotextile, geomembrane, geogrid, geomat, geoweb, geonet, geoproduct, geoetcetera - your presence here shows you are involved with these products. If you are not already a member of the IGS, we believe that you would further the profession by adding your efforts and joining in the Society's work. With your support, the IGS will continue to work towards a better organized profession. Another reason for joining the IGS is to enjoy the benefits reserved to members. One of them is to have your name mentioned in the IGS Directory published every year. No one who is involved with geosynthetics can afford not to be in this "Who's Who" of the geosynthetics community.

The IGS Directory shows that we already have members in 37 countries. However, in most of these countries, membership must grow and chapters must be formed to ensure a strong basis for the IGS. The American chapter should set an example for the countries where chapters are being formed. To set this example, the American chapter has several tasks on its agenda.

First, the US chapter - the American Society on Geosynthetics - needs to grow larger. In countries like Japan and France, there are approximately four IGS members for every square meter of geotextile annually used. Using the same ratio, the American Society on Geosynthetics should have more than 400 members. This goal can be reached before the next International Conference on Geotextiles to be held in The Hague, Netherlands, in 1990. Such a large membership would not only be beneficial to the US chapter, but would also set an example for all other countries.

Increased involvement of the geomembrane community in the organization of our profession is another goal of the IGS. Federal legislation and the US Environmental Protection Agency, in their admirable effort to protect the environment, have paved the way for the rapid growth of the geomembrane industry in the United States. As a result, the US chapter of the IGS is in a unique position to promote cooperation between geotextile and geomembrane specialists and set an example for other countries.

With Geosynthetics '87, the US chapter is setting an example of quality and, I am sure, will set an example in the near future for membership growth and geomembrane involvement. In addition, everyone expects the US chapter to be a leader in many areas of technical development. However, the capability of the US chapter to set technical examples will be increasingly hampered by a communication problem if the engineers in this country continue to use a system of units that is not understood in any other country in the world. I am amazed at seeing that many American engineers do not realize the extent of the damage they do to themselves and their country by not using the International System of Units. In a discipline like ours, where materials are easily transported from one continent to another, a growing discipline where exchange of ideas is essential, ease of communication becomes a critical issue. For that reason, the IGS is committed to use only one official language and has adopted English, although more than two thirds of its members do not have English as their mother tongue. By the same token, the IGS encourages all its members to use the International System of Units, and I urge the American Society on Geosynthetics to take a firm stance on that matter. And, believe me, it is much easier to master the SI system than the English language!

As we can see, there is much to be accomplished by the geosynthetic community, but it is fair to say that much has already been accomplished. A survey of the emergence of the geotextile discipline was the theme of the lecture I presented at the opening session of the Third International Conference on Geotextiles in Vienna (April 1986). I am grateful to the organizers of Geosynthetics '87 who have invited me to repeat this lecture. To be consistent with the goals of the IGS, I have expanded the subject, which is reflected by its title: "Geosynthetics - From the Products to the Engineering Discipline".

REFERENCE. There is no written text for "Geosynthetics - From the Products to the Engineering Discipline". However, the text of the original lecture, delivered at the Vienna conference, can be found in the proceedings of that conference, as follows:

Giroud, J.P., "From Geotextiles to Geosynthetics: A Revolution in Geotechnical Engineering", Proceedings of the Third International Conference on Geotextiles, Vol. 1, Vienna, Austria, April 1986, pp. 1-18.



SESSION 1A
UNPAVED AND PAVED ROADS

KINNEY, T.C.

University of Alaska, U.S.A.

Field Tests on the Use of Geosynthetics to Support Paved Roads Over Voids-Preliminary Conclusions

ABSTRACT

A series of studies are being conducted to determine the viability and practicality of using geosynthetics to support roads across voids created by thawing ice masses in ice rich permafrost. A design procedure was established, and three field tests have been run to verify the design procedure. The tests verify the design procedure and suggest that commercially available geosynthetics can be used to support unpaved roads across voids in excess of 3 m wide. It also appears that it would be viable to pave the road under certain conditions. This report only discusses the last field test. The design procedure and two previous field tests have been published elsewhere.

INTRODUCTION

The test discussed herein is part of a continuing series of studies to develop design criteria for the use of geosynthetics in roads crossing polygonal ground (permafrost terrain containing ice wedge polygons). The geosynthetics are used to totally support roads over the voids created when ice melts out from under the embankment materials.

A preliminary design scheme was developed in 1981, and a field test was performed in 1984 to establish the viability of the scheme and the validity of the design procedure. The study up to the fall of 1984 suggested that the design approach was reasonable, but the field test sections failed to carry the design load.

The design procedure was upgraded, and a new field test was performed in the fall of 1985. This test was successful, demonstrating that at least a 2 m wide void could be spanned with commercially available materials and that the design procedure was indeed reasonable. The deflections under traffic loading were lower than anticipated, leading to the conclusion that paving may be a viable option.

The field tests reported herein were performed in the fall of 1986 to extend the void widths to 2.4 m to explore the ramifications of the void being at a 45° angle to the road (and the machine direction of the geosynthetics), and to study the possibility of paving the road. The test have been constructed and preliminary trafficking and analysis has been completed. The test facility has been left in place with the intent of continuing trafficking, making additional measurements, and completing the analysis in the spring.

The original concept was presented to the Alaska Department of Transportation and Public Facilities (DOT&PF) Research Section(1). The design procedure was outlined at the 3rd International Conference on Cold Regions Engineering in Edmonton, Alberta, Canada(2). The design parameters were further defined and the summer 1984 tests results were discussed in a report to the DOT&PF Research Section(3). The design procedure was further refined, the results of the 1985 tests were discussed, a computer program was presented, and a design chart was presented to DOT&PF in an interim report(4). This work was summarized at the 4th International Conference on Cold Regions in Anchorage, Alaska(5). A condensed version of the work until June 1986 has been submitted to the ASCE Cold Regions Journal(6). This report presents only the newest set of test results. All background information is readily available.

TEST FACILITY

The test facility consisted of constructing a road 3.6 m wide, and 0.76 m high of pit run sand and gravel across four trenches. Two trenches, 1.8 m and 2.4 m wide, were constructed perpendicularly to the center line of the road. Two other trenches, 1.2 m and 1.8 m wide, were constructed at 45° angles to the road center line. The trenches were shored with timbers. The top timber had a beveled edge for the geosynthetic to ride over. The layout is shown in Figure 1, and a typical cross section is shown in Figure 2.

Sections of geosynthetic, 15.2 m long and 3.6 m wide, were stretched loosely across the trenches. Pit run sand and gravel were placed 0.76 m deep over the ends of the geosynthetic to hold it in place. Pit run sand and gravel were pushed gently over the trenches with a small bulldozer. An attempt was made to

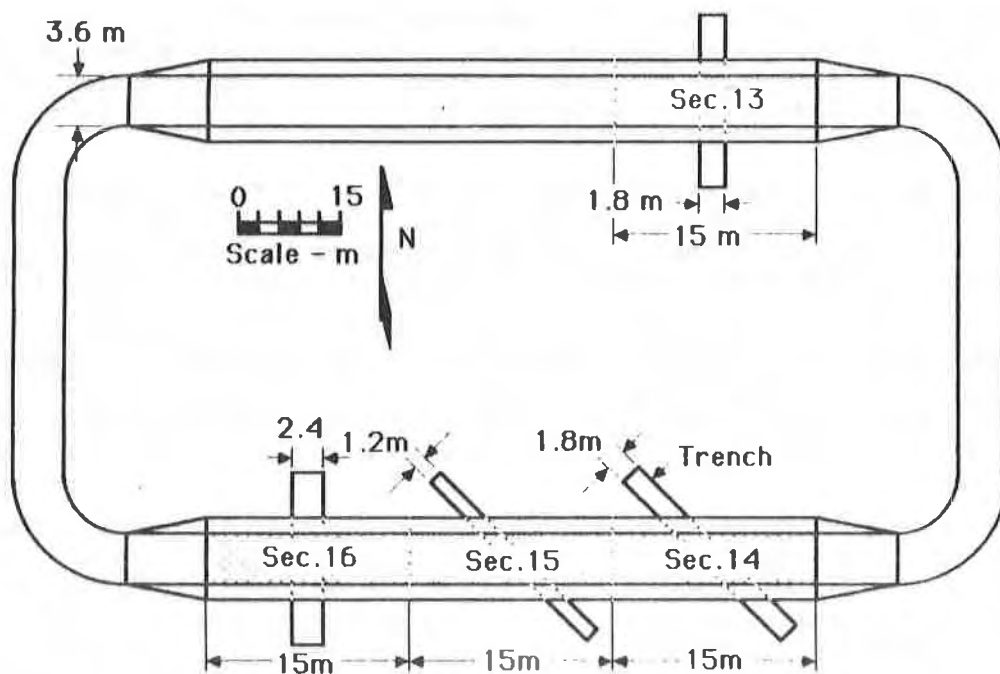


Figure 1. Test section layout.

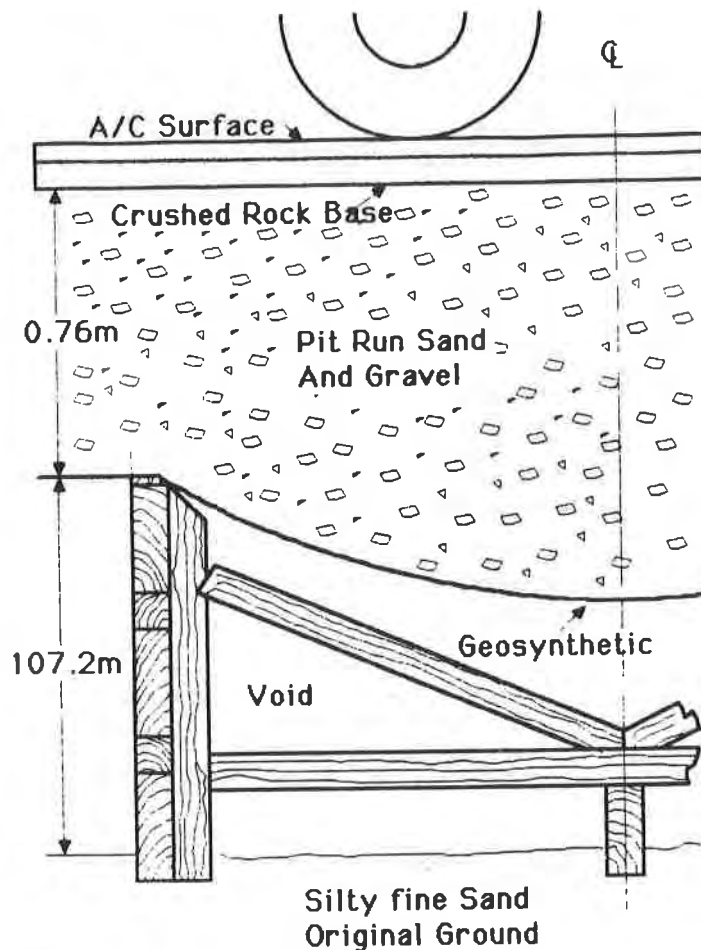


Figure 2. Typical cross section.

load the area over the trenches evenly from both sides. The surface was then bladed with a road grader, and a steel wheeled vibratory compactor was run over the surface with a total of 10 coverages.

A 100 mm layer of crushed rock base course material (State of Alaska Specification D-1) was placed on the surface of the two test sections that had trenches perpendicular to the road. The test road was then compacted with five coverages. Fifty mm of hot mix asphaltic concrete were placed on one wheel track, and 50 mm of D-1 were placed on the other wheel track. Both materials were compacted with five coverages of the compactor.

Two different geosynthetics were used. GTF 800, made by EXXON, is four layers of a woven split film polypropylene fabric sewn together with Malamo stitching. The Signode materials are both geogrids constructed of 11.9 mm wide by 1.02 mm thick orientated polyester strands, each with a tensile strength of 5.34 kN at a strain of about 10 to 12 percent.

A summary of the test section configurations is shown in Table 1. The properties of the geosynthetics are shown in Table 2.

TABLE 1. Summary of test configurations and falling weight deflectometer data.

Sec. No.	Trench width (m)	Trench dir. deg.	Geo-synthetic	Sand & gravel (m)	Crushed rock (mm)	A/C pavement (mm)	Maximum (1) disp. (mm)
13a	1.8	90	GTF 800	0.76	0	0	2.01
b	1.8	90	GTF 800	0.76	150	0	1.83
c	1.8	90	GTF 800	0.76	100	50	0.89
14	1.8	45	TNX 800	0.76	0	0	2.44
15	1.2	45	GTF 800	0.76	0	0	2.06
16a	2.4	90	TNX 8002	0.76	0	0	4.57
b	2.4	90	TNX 8002	0.76	150	0	---
c	2.4	90	TNX 8002	0.76	100	0	1.07
Ca	No trench		Either	0.76	---	---	1.93
b	No trench		Either	0.76	150	---	1.83
c	No trench		Either	0.76	100	50	0.81
d	On subgrade		None	0	0	0	4.06

- (1) All maximum deflection data have been adjusted to a 35.6 kN force on the 0.3 m diameter falling weight deflectometer plate.
- (2) The limit of accurate readings of the falling weight deflectometer is on the order of 2.5 mm.

TABLE 2. Geosynthetic properties.

Geosynthetic	Direction deg.	Maximum tension (kN/m)	Failure strain (%)	Secant modulus (kN/m)
Signode TNX 8002	0	140	10-12	2,630*
	90	70	10-12	1,460
	45			
TNX 800	0	140	10-12	2,630*
	45	140	10-12	2,630*
EXXON GTF 800	0	110	25-30	496
	90	90	25-30	496
	45			

* Measured from 0 to 2% strain.

Falling weight deflectometer (FWD) measurements were made on the surface of the pit run sand and gravel, after compaction, on the surface of the 15.2 mm of D-1 on one wheel path, and on the asphaltic concrete on the other wheel path. Measurements were made over the center of each of the trenches and in between the test sections for control. The deformed shapes of the geosynthetics were

measured with a measuring tape from a base line to an accuracy of about 2 mm. The strain in the geogrids was determined by measuring between the strands with a micrometer caliper to a precision of 0.02 mm. The results of these measurements are summarized in Table 3.

TABLE 3. Summary of measured and calculated data.

Sec. No.	Center line displacement		Radius of curvature		Average strain	
	Meas. (mm)	Calc. (mm)	Meas. (m)	Calc. (m)	Meas. (%)	Calc. (%)
13	370	429	1.31	1.25	---	5.4
14.x (1)	429	394	1.19	1.29	4.9	4.3
.y (2)	429	460	1.90	1.90	2.0	1.6
15.x (1)	310	300	0.75	0.83	---	5.8
.y (2)	310	371	1.33	1.19	---	4.9
16	391	427	2.09	1.80	2.2	1.77

(1) Assuming the direction of support is perpendicular to the trench.

(2) Assuming the direction of support is parallel to the road.

Following these measurements, a fully loaded dump truck was run over the test sections for a total of 200 times. The truck had dual wheels on tandem axles with a total load on the eight wheels of 142 kN. The test sections were observed during trafficking and the surface of the paved sections was examined at the end of the 200 passes of the truck.

TEST RESULTS

The visual observations indicated that there was up to 10 mm of downward movement of the center of the geosynthetics during trafficking. The FWD measurements shown in Table 1 indicate a total of about 2 mm and 1 mm of vertical movement of the surface under the unpaved and paved sections, respectively, under a 36 kN load. The truck moved at about five miles per hour, while the FWD was adjusted to represent a load moving at about 50 miles per hour. The data collected to date suggest the FWD measurements yield deflections that are too low and, therefore, do not represent the conditions that should be used for design of a paved surface. The author suggests a combination of FWD data and Benkleman Beam data for design.

In addition, even the deflection measurements on the control sections were much higher than would ordinarily be considered acceptable under a paved surface. This is probably due to the generally loose condition of the fill materials. Density tests were taken at many locations and depths in the fill materials after trafficking was complete. There was considerable scatter in the data at all depths, and it was not possible to detect a difference in the density between the soil over the trenches and the soil between the trenches. There was, however, a

clear trend toward decreasing density with depth. The density of the sand and gravel was on the order of 19.8 kN/m^3 near the surface, 18.0 kN/m^3 at a depth of 0.3 m, and 16.6 kN/m^3 at a depth of 0.6 m. The minimum and maximum densities for this material are about 15.7 kN/m^3 and 21.0 kN/m^3 , respectively. This leads to the conclusion that significantly more compaction would be necessary after the void has formed than was used on these test sections if the road is to be paved. It is the intent at this time to recompact the test sections and repeat the trafficking and testing in the spring. In spite of the large deflections, the pavement did not show signs of cracking under the traffic loading.

The design procedure developed for this purpose was used to analyze the test sections. The necessary design parameters are summarized in Table 4. The

TABLE 4. Summary of parameters used in calculations.

Sec. No.	Void width (m)	Embedment length (m)	Shear stress (Kpa)	Geosynthetic modulus (kN/m)	Average pressure (Kpa)
13	1.8	6.7	6.0	500	21.6
14.x (1)	1.8	1.5	8.4	730	24.4
14.y (2)	2.6	4.5	8.4	2,920	24.2
15.x (1)	0.9	1.5	6.0	292	20.6
15.y (2)	1.7	4.9	6.0	500	20.6
16	1.8	6.4	8.4	2,920	28.8

(1) Assuming the direction of support is perpendicular to the trench.

(2) Assuming the direction of support is parallel to the road.

average pressure on the geosynthetic was considered to be the weight of all of the material above the void, plus the total load over the trench due to the loaded truck calculated using elastic theory divided by the horizontal area of the trench (Figure 3). Note that no consideration was given to soil arching over the trench. In addition, it should be noted that the truck applied nearly half of the total load considered on the geosynthetic. But during trafficking, the deflection as the truck passes over the trench (Table 1) is negligible compared to the total deflection (Table 3). One explanation for this may be that the truck load is locked in during construction by reverse arching and this stress is merely relieved during traffic loading. Another explanation, although somewhat less palatable to the author, is that the design technique is seriously in error, the deflection is caused by the weight of the soil, and the truck load is transferred to the edges of the trench through arching. Either explanation could be considered for narrow trenches, but both mechanisms should diminish as the trench width increases. The design procedure seems to accurately predict the performance in terms of maximum deflection and radius of curvature.

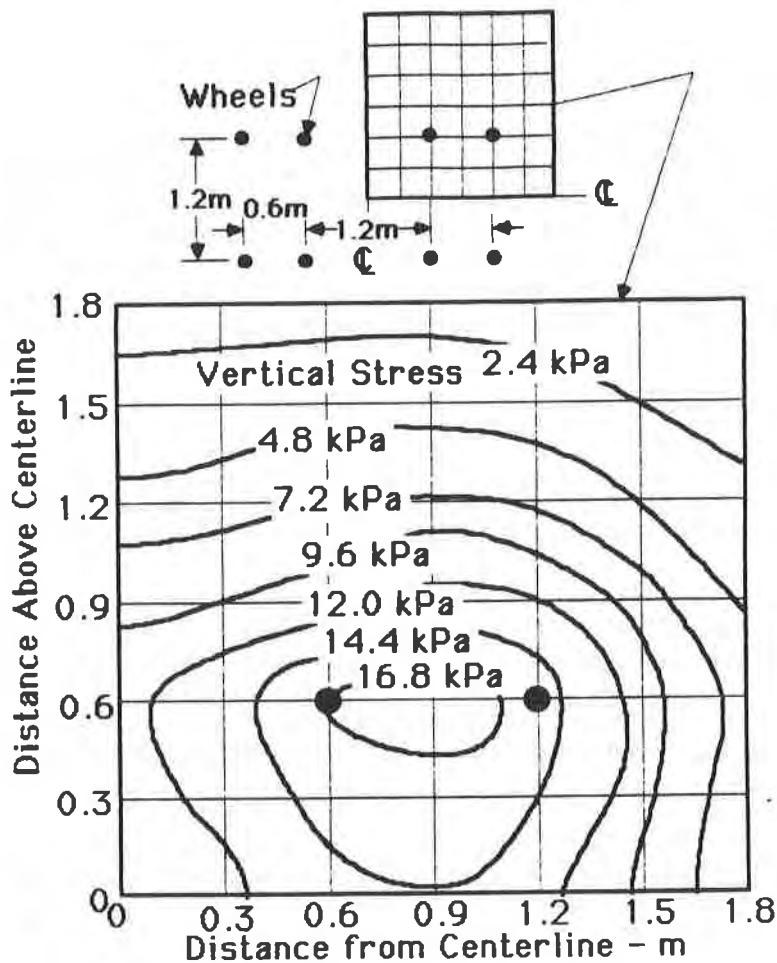


Figure 3. Pressure at a depth of 0.9 meters under dual wheels on tandem axles with a total load of 142 kN.

The results of the trenches at a 45° angle to the road are of special interest. The calculations indicated that the effective modulus of the woven geotextile must have been more than half of the modulus measured in the machine direction. This is considerably more than would be expected if the geotextile were not confined on the one side by the soil. The strain in the geogrid could be measured fairly accurately. It appears that there was very little strain in the direction of the strips all of the deflection was developed through distortion of the grid. The distortion of the grid was minimal compared to what might be expected if the same material were placed under the same tension without the soil confinement.

CONCLUSIONS

The test results presented herein provide additional verification that the design procedure developed elsewhere for this application is usable in its present form. It appears that it is possible and economically viable to consider spanning a 3 m void with currently available materials. While these data are inconclusive, it appears that a road spanning a void could be paved if it were properly designed and the embankment materials were compacted well enough.

ACKNOWLEDGMENTS

The study was funded primarily by the Alaska Department of Transportation and Public Facilities (DOT&PF) Research Section using Federal Highway Administration funds. Signode Corporation and EXXON Chemical Company also contributed funding. The falling weight deflectometer was provided by DOT&PF. The test site and the embankment materials were donated by H&H Contractors of Fairbanks, Alaska. Special thanks go to Mr. Don Graffin and Mr. Art Slater of Signode, Mr. Tom Miller of EXXON and Mr. Billy Connor of the DOT&PF Research Section for their assistance during the test.

REFERENCES

- (1) Kinney, T.C., "Use of Geotextiles to Bridge Thermokarsts," State of Alaska, Department of Transportation and Public Facilities, Division of Planning and Programming, Research Section, Aug. 1981, Report No. AK-RD-82-21, 30 pp.
- (2) Kinney, T.C., and Abbott, R.A., "Geotextiles Used to Reinforce Roads Over Voids," Proceedings of the 3rd International Conference on Cold Regions Engineering, Edmonton, Alberta, Canada, April 4-6, 1984, Vol. 1, pp. 493-505.
- (3) Kinney, T.C., "Field and Laboratory Study on the Use of Geotextiles and Related Products to Bridge Thermokarsts," May 1985 Report No. FHWA-AK-RD-85-31, 124 pp.
- (4) Kinney, T.C., "Tensile Reinforcement of Road Embankments on Polygonal Ground by Geotextiles and Related Materials - Interim Report," State of Alaska, Department of Transportation and Public Facilities, Division of Planning and Programming, Research Section, June 1986, FHWA-AK-RD-86-29, 40 pp.
- (5) Kinney, T.C., "Reinforced Roads Bridging Voids," Proceedings ASCE 4th International Conference on Cold Regions Engineering, Anchorage, AK, Feb. 24-26, 1986, pp. 329-329.
- (6) Kinney, T.C., "Geosynthetics Used to Support Unpaved Roads Over Thermokarsts," submitted to the ASCE Cold Regions Technical Journal.

WALLACE, R.B., and BEECH, J.F.
GeoServices Inc. Consulting Engineers, U.S.A.
GRAHAM, R.J.
EBA Engineering, Canada

A Geosynthetics Post-Construction Assessment

Geosynthetics used for area stabilization must satisfy an inherent reinforcement requirement, but the design is primarily one of separation to prevent intermixing of the subgrade and fill materials. A project is outlined for which a large area of storage yard was developed with a geotextile and granular fill. Construction operations are outlined, along with particular difficulties and the operations over the first winter. Problems which were encountered in the first spring thaw afforded an opportunity to review the design, as well as to examine problem areas and to appreciate the nature of the fabric performance.

1. INTRODUCTION

The use of geosynthetics for area stabilization of sites subjected to concentrated and extensive loads has become a part of standard geotechnical practice. All too frequently, however, there is very little design input to the selection of the reinforcement materials. This is in spite of the fact that many design procedures exist, of both product-specific and generic natures. It is extremely difficult, however, to verify the suitability of a particular design, as the design is seldom supported by performance data. Inadequate design will always be evident in the failure of a structure. Overdesign, however, will usually only be determined by analysis of the performance of the project, in conjunction with some form of research program. We do want to know how conservative we are in our design procedures, in order to optimize the benefits of geosynthetics usage.

It is possible for the practicing engineer to carry out a post-construction assessment, based on the performance observations of the area, and perhaps some excavation to examine the condition of the geotextile or geogrid and subgrade. Opportunities for this seldom arise for the practicing engineer, who must usually rely on reimbursement to justify this work. This paper presents the results of a post-construction evaluation of the design of a storage yard, which was possible due to the carry-over of work to a second season. After construction, and in the light of the performance of the structure over the first two years, the design has been re-evaluated, in part on the basis of the observed behaviour and in part on the basis of the problems which occurred.

2. BACKGROUND

The subject site is that of a small steel mill on a 50 hectare (125 acre) property in Red Deer, Alberta. The present owners of the mill were not the original developers. The mill was producing pipe and tubular products, and operations were round-the-clock at the time of this program of work. The project consultant was first contacted in 1984 after the spring thaw. The 180 and 270 kN (20 and 30 ton) forklift equipment used to transport the finished product from the mill to the storage area, and from the storage area to the transport areas had caused severe rutting, and in fact significant portions of the storage area became inaccessible. Subsequent to the spring thaw, the same conditions would exist after even modest periods of rainfall. On the other hand, the subgrade would dry out after one or two days of dry weather, and would be extremely hard, giving good accessibility to all areas.

At the time of the initial investigation, the conditions at the site were at their best, during a period of continued dry weather. In fact, aside from the geotechnical investigation information, it took a visit to the site after only one day of rain, to really appreciate the short term deterioration of the site.

3. SITE CONDITIONS

The investigation of the site revealed a combination of problems, each of which alone could be sufficient to necessitate major expenditures, but which, in combination, will eventually result in off-site activities which were not anticipated by the owner. These problems related to the initial development of the site, the soil conditions at the site, the ground water conditions at the site, and the regional drainage patterns which affected the site.

3.1 Site Development

Prior to the initial site development, the land was in agricultural use. When the site was developed, it was stripped of topsoil, with no real site grading. The building elevations were set at existing grades, which in turn set the benchmark for all future site development. No granular materials were placed for storage areas, and only a skiff of gravel was placed on the main roadways.

Since no granular cross section was developed for the yard area, any subsequent preparation would first involve excavation to a new subgrade level, to preserve and establish the grades fixed by the buildings.

3.2 Soil Conditions

The subgrade material at the site is a cohesionless silt, with only modest amounts of clay and sand (less than 10 to 15 %). In a dry state, the soil mass would be very hard, and afforded good traffickability. Upon wetting, however, the silt evidenced very little strength, resulting in very deep ruts, which would eventually lead to loss of access. The silt is very susceptible to ice aggradation upon freezing. Below-freezing temperatures can be expected to prevail in this area from November to early April (latitude 52 degrees North). When fine-grained, cohesionless soils thaw, the loss in perceived strength when changing from a frozen to a non-frozen condition is severe, and the presence of the usually excess amounts of pore water result in a very low strength subgrade. The same condition is approximated after rainfall. In a dry state, however, the silt exhibited good

support for even the heavy wheel loads and high repetitions experienced at this site.

3.3 Ground Water and Drainage

The ground water table at the site is very close to the surface, and is perched on the relatively shallow shale bedrock. This perched level is subject to fluctuation, responding to prolonged periods of rainfall with a rise of over 0.3 meters (1.0 foot). The site is sloping, with a drop of about 3 meters (10 feet) from north to south. The land immediately to the south of the site is the low point, and becomes a small lake after a period of rain. Drainage from the area is hampered by the presence of a railway embankment and a highway embankment along the east side of the site. Due to the lack of drainage provisions on the site, localized ponding was always a problem after rainfall, which compounded the other site problems.

4. REMEDIAL WORKS AT THE SITE

4.1 Design

The design for this site involved a detailed drainage system, to remove water from precipitation, as well as to preferentially deflect the runoff away from roadways and other areas requiring critical access. The siting of the existing structures set the required grades, so that the placement of the gravel base and surface course first entailed excavation of as much as 1.5 meters (5 feet) of the silt in some areas, and filling in other areas. The cutting (excavating) was the single largest problem with the implementation of the design.

A detailed design of the yard area was carried out using a geotextile to serve as both reinforcement and separator. Although the design was ostensibly for the reinforcement of the subgrade, the separation of the subgrade silt from the granular fill materials was essential to keep the granular materials from being contaminated, and thereby preserve the integrity of the fill.

The design was carried out in accordance with the method proposed by Giroud and Noiray (1982). The design was complicated by virtue of the extremely heavy axle loads being imposed, and the very high design repetitions (at that time, the mill was operating 24 hours per day). After revising the design several times by the iteration of different parameters, a design incorporating 0.6 meters (2 feet) of gravel, overlying a nonwoven, needlepunched geotextile (Bidim U34) was selected. At the loading area, where continuous input of the feedstock resulted in higher repetitions of loads, this gravel thickness was increased to 0.9 meters (3 feet) somewhat arbitrarily.

The second design task was to provide good surficial drainage through a network of ditches. This involved considerable regrading in some areas in which drainage patterns had to be reversed in order to prevent ponding. The ditch section selected was to be lined with geotextile, and covered with a nominal thickness of the gravel. The design of this system is incidental to the topic at hand, and is not discussed further herein.

There were concerns with regard to the end-of-year construction schedule, which called for an October startup. The possibility of having to carry out the work in below-freezing temperatures was subordinate to the absolute need to have an operational yard in the spring. It was therefore agreed that the work would

proceed, and that provisions could be made for cold weather operations, should the need arise.

4.2 Construction

The construction in the first year involved the areas around the mill, all roadways throughout the site, areas adjacent to the rail spur feeding the site, and about two-thirds of the storage areas. In addition, all of the drainage ditches were to be completed throughout the site. The total area to be covered was approximately 120,000 square meters (1,300,000 square feet).

On the first day of field work the first snowfall of the season arrived and, although the weather cleared shortly thereafter, subsequent melting of this precipitation resulted in softening of the subgrade (see Figure 1). At that time, however, it was believed that sufficient time was available to carry out the work prior to the onset of very cold weather.



Figure 1: Example of softened subgrade during subcutting operations after precipitation

Due to the combination of factors influencing the site, the most difficult aspect of the remedial works for the yard area was the excavation of the existing silty materials down to the design subgrade level, which was 0.6 meters (2 feet) below the final design grade, as dictated by the existing building location, and the requirements for proper drainage across the site. The high water table, which was typically 1.5 to 2.4 meters (5 to 8 feet) below the then-existing grade, was very close to the excavated surfaces in some locations, due to the necessity of cutting up to 1 to 1.5 meters (3 to 5 feet) of soil to attain the required grade. Extensive piping occurred in a few locations (Figure 2), causing considerable difficulty in preparing an acceptable surface for placement of the geotextile.

It had been the original intention to carry out the construction in such a manner that drainage of the site would be enhanced and accelerated by the progression of

the excavation and regrading, and the construction of the drainage ditches. It was not possible to optimize this approach, however, because of the fact that the mill was operating on a 24 hour per day basis. A considerable proportion of the area to be developed was in current and active use for storage and shipping of steel products. As a result, shipping requirements and deadlines dictated by the owner's contracts governed the areas which could be worked on at any given time. It was possible to outline this at the beginning of the project, however this still necessitated a piecemeal progression from one portion of the site to another, and subdivided areas were completed incrementally.



Figure 2: Piping due to excavation and construction

As noted previously, virtually the day of commencement of the project, the temperature dropped and it started to snow. At first, this represented more of an inconvenience than anything else, in that the snow soon melted, resulting in the poor traffickability that we had noted after periods of rainfall. After about 10 days, however, the temperature rapidly dropped to about -22 degrees F. (-30 degrees C.). This reduced the problem with the snow, which continued to fall almost daily in light quantities, in that it was not melting and could be removed with the excavated materials. Unfortunately, however, the temperature continued to drop to the point where daily highs were in the range of -22 to -40 degrees F. (-30 to -40 degrees C.). Even though discussed, it was apparent that suspending construction really was not an option, and our attentions were directed toward identification of the new constraints placed on the project by the weather, and the manner in which the design would be compromised, if at all, by these conditions.

Both the in situ densities and the testing of the subgrade surface and granular fill materials were curtailed, primarily due to the fact that although compactive efforts were initially applied, densification of the gravel beyond placed and graded densities was not possible. On the other hand, the gravel surface would be exposed to considerable traffic from the large forklift equipment, and so there was a reasonable expectation that the surface would at least be nominally

compacted in high traffic areas over the course of the winter.

The windfall benefit of the cold weather was that difficulties in excavation experienced due to the soft soils virtually disappeared. Frost penetration was sufficiently rapid that excavation of at least partially frozen soils was much easier, and the working surfaces afforded reasonable access. With time, however, it became necessary to rip the soils in order to excavate to the subgrade level (Figure 3). The benefit of this was also realized during the backfilling stage, in that the exposed subgrade was allowed to freeze prior to any geotextile or fill being placed, so that soft subgrades were not a problem. The preparation of uniform subgrade surfaces was impossible due to this, but such was not considered to be a shortcoming.



Figure 3: Ripping of frozen subgrade necessitated by the very low freezing temperatures

The net result of the change in weather was that the productivity increased, although the quality of the product represented an unknown. It was clear, however, that there would likely be some problem areas upon spring thaw due to the lack of proper dressing of the subgrade and the compaction of the fill materials. Due to the fact that the soils were all frozen prior to fill placement, any settlement or other accommodation of the new system would not occur until thaw. During the thawing process, they would be subjected to repetitive loading, so severe rutting in localized soft spots could be expected.

The work took several weeks to complete, but there were few problems aside from the inconvenience of the weather conditions. In the end, a small portion of the work was actually suspended until the spring, but this was in a remote area and was not critical to the operations at the site. In general, however, the finished product was excellent, under the circumstances. Those areas which had been prepared prior to the poor weather were particularly good. (See Figures 4,5).

4.3 Winter Operations - The First Year

Subsequent to the completion of construction in mid December, no problems were encountered by the owner through the winter with regard to the work that had been



Figure 4: Finished surface prepared prior to the cold weather work



Figure 5: Gravel placement during -40 degree C. weather

completed. In fact, the only point raised by the owner was the fact that there had been a noticeable decrease in previously high maintenance costs for the forklifts, in the form of wheel bearing wear due to silt infiltration.

4.4 Spring Thaw - The Remedial Works

In the spring of 1985, following a long cold winter, areas exhibiting excessive rutting, combined with evidence of a ruptured geotextile, were noticed at several locations throughout the total developed area. In these locations, the silty subgrade had worked its way to the surface of the gravel layer, indicating that the geotextile had indeed been damaged (Figure 6). In all, there were fourteen areas which exhibited this type of damage, although the total combined area of the damage was only about one per cent of the total area treated. Other areas evidenced rutting to varying degrees of severity, but with no apparent damage to the geotextile. (Figure 7).



Figure 6: Severe rutting with the geotextile exposed subsequent to spring thaw.



Figure 7: Minor rutting was noted primarily at corners

Even in spite of the conditions which had been experienced during the construction of the yard areas, some of the damaged areas seemed excessive for the traffic that had been imposed (areas of only minor traffic levels). At least some of the problem became apparent after observation of the damage, and discussion with the owner's representatives. When the first rutting occurred, the owner undertook to carry out some regrading to fill in the ruts and reestablish the working surface, which was consistent with good practice. Unfortunately, however, the grader operator, in his enthusiasm, had been subcutting the grade in some locations in order to redistribute the gravel. Consequently, a few of the failed areas occurred subsequent to the initial thaw of the soil, in areas which had experienced the removal of as much as 0.15 meters (6 inches) of gravel, which was 25 per cent of the thickness placed.

Additional gravel was imported and the areas exhibiting minor rutting were repaired by infilling and compacting. The pervasively rutted areas in which the geotextile had apparently failed, or at least had been ruptured in some manner were excavated, the geotextile removed, the subgrade undercut to remove the worst material, and then reconstructed with new geotextile and clean fill. There were about twelve locations that had to be repaired in this manner, although the largest area was only about 4.5 meters (15 feet) square.

Prior to the remedial works to repair the areas which had failed, some investigation of the soil strength was undertaken using a cone penetrometer and a shear vane. The results of this testing indicated that for the most part, the soil strengths were very similar to those indicated in the initial investigation. Correlation to unfailed areas indicated fairly consistent results from one area to another.

Our initial assumption that localized soft spots would be the obvious reason for the failures was not borne out. It was noted, however, that the top 0.15 to 0.2 meters (6 to 8 inches) of the silt directly below the geotextile was pervasively disturbed in the worst locations, due to the failure of the geotextile. In general, however, the worst locations were in high traffic areas, almost always at corners where the equipment would be turning, which would create 'shoving' forces. These locations were also noted to be very wet at the geotextile/subgrade interface, upon excavation, which may have been an indication of excessive ice lensing or even snow within the gravel when it was placed.

4.5 Observations from the Excavated Areas

All of these areas which had to be excavated showed similar conditions, namely very soft soils directly beneath the fabric, a wet zone at the base of the gravel, and silt contamination of the gravel through a hole or holes in the fabric. The first two conditions are not considered to be unusual in that it was anticipated that at least some of the runoff drainage to the ditch system would be through the gravel rather than over it, since no effort had been taken to seal the surface.

Although a gradient had been provided in the design of the subgrade to provide at least a positive slope to inhibit ponding on the subgrade surface, the excavation conditions in the cold weather made the realization of this objective difficult at best. It is likely therefore that localized ponding of meltwater at the interface of the geotextile and subgrade contributed at least in part to the greater degree of softening in these locations subsequent to the spring thaw. Two locations which

did not exhibit any distress were probed at random, and it was confirmed that the excess water noted in the excavated locations was absent in these locations.

The damage to the geotextile was another factor, however, which was not so easily explained. Care was taken when excavating the gravel to avoid dragging the fabric, or the gravel across it, with the bucket of the backhoe. Hand excavation was undertaken near the fabric in order to recover samples without further damage. Several samples were collected and visually examined in the laboratory.

Two types of damage were noted, apparently from different causes. The first consisted of tears, and we were fairly confident that they had not been caused by the exhumation. These tears appeared to have resulted at least partly from the deformation of the fabric in the "classic" rut mode. It is quite possible, however, that elongation of the fabric was restricted by the adjacent confinement in a frozen state, in that the wet areas would tend to thaw before the areas without excess water. Overstressing of the fabric beyond levels that would normally be expected in this situation was therefore possible, resulting in some tearing of the fabric. This would certainly be the worst case of fabric damage, as it would destroy both the membrane-effect, as well as the positive separation between the gravel and the subgrade silt. In the areas where this was noted, the gravel was completely contaminated with the silt.

The second type of damage which was noted in the geotextiles was a severe degree of puncturing, in which many about 200 per square meter (20 per square foot)) small punctures, each about 5 millimeters (0.2 inches) in diameter, were noted throughout the failed area. (Figure 8).

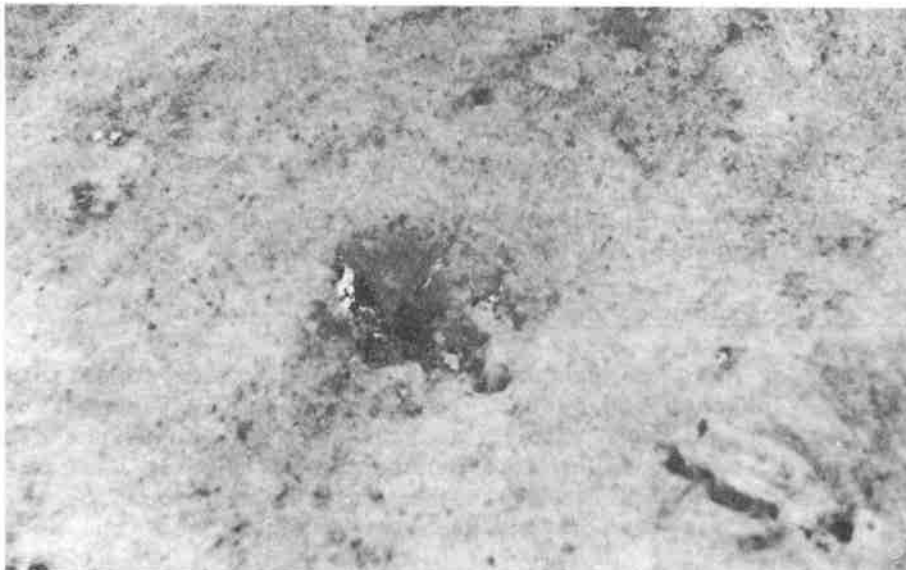


Figure 8: Multiple puncture damage to geotextile

The gravel that was used for the development of the yard was not angular in shape, and in fact was very rounded. It is believed that the puncturing could have occurred immediately upon placement onto the frozen subgrade. Even though normal

care was taken with the placement of granular materials directly onto the fabric, the subgrade in the frozen state would approximate the hardness of concrete. It is easy to visualize severe puncturing of the geotextile placed directly onto concrete, and then dropping gravel up to 75 millimeters (3 inches) in diameter from even a short distance. This evaluation is substantiated in part by the fact that this puncturing was noted primarily in those areas which experienced the immediate subgrade freezing. In fact, there were only two locations which required repair in the area prepared before the onset of the very cold weather (this represented about 14 per cent of the locations needing repair, in about 40 per cent of the total area).

4.6 Two Years Later

In areas which experience very cold winters, and consequent deep seasonal frost penetration, the absolute indicator of the quality of performance of any trafficked area, whether a pavement or a gravel surface, is the period during, and immediately subsequent to the spring thaw. It is generally accepted that even roads constructed under more ideal conditions than we endured will require some work after their first spring thaw. In fact, wherever possible, new roads constructed in one year will not be given their final surfacing until after the first winter.

This site has now been through two complete winters and summers. Since the repairs performed in May 1985, no additional problems have arisen with the site related to the development of the granular geotextile-reinforced surface. The continued traffic under heavy vehicular loads has served to compact the surface to a very tight state, and only nominal maintenance has been required. In general, the structure is believed to be performing in a satisfactory manner, and the savings that were realized, both in the capital cost due to savings in gravel thickness (and excavation) required, as well as in the ongoing maintenance costs for both the yard and the equipment, are significant.

5. CONCLUSIONS - PERFECT HINDSIGHT

It is difficult for anyone actively involved in designing with geosynthetics to look back on the work performed two years previously and be perfectly content, as the state of the art is changing at such a rapid rate. Even so, applying the then existing state of design using geotextiles, the conclusion that the work was satisfactory is easy to make. Relative to the owner's alternatives, a solution was attained that saved them a great deal of money, so one of a consultant's prime criteria has been satisfied. The performance of the structure has been very good, so the design adequacy criterion has been satisfied. The owner is happy with his product, so the value criterion has been satisfied.

An honest evaluation has to consider what would be done different today, were the project to arise independently on another site. The conclusion is - not much. The design is certainly not conservative, and we would have to obtain a much better idea of what levels of stress are really imposed on fabrics in this type of situation in the field than we do now, before we could justify revision of the design. If there had not been spring thaw damage, then the design would have been considered to be conservative.

Although holes were encountered in the fabric at the locations which were repaired in the spring, this problem appeared to be peculiar to those locations. With minimum disturbance, a couple of locations were examined in which no failure had occurred, and no particular damage was evident. It should be noted that although, by the nature of its construction, the nonwoven, continuous filament fabric would still be flexible in the very low temperatures (as long as it was dry). With the hard, frozen subgrade, it is likely that some damage to individual fibers could result from the shock of the impact of the gravel dropped onto it. This certainly does not appear to have significantly affected the performance of the system, and it is very likely that damage was generally confined to the areas which had to be repaired.

The proper design and construction of these works is a geotechnical problem, not a geosynthetics problem. The unusual constraints that arose at this site were essentially independent of the geotextile, and really did not impact the geotextile component of the design at all. If a proper understanding of soils and soil behaviour is not part of the design process, the application of geo-anything will not be optimized.

6.0 ACKNOWLEDGEMENTS

The authors are indebted to EBA Engineering Consultants Ltd. for their assistance in the preparation of this paper, and for whom Messrs. Wallace and Graham were working when the project was carried out. Particular thanks are due to Messrs. D. Lines, D.G. Anderson, and H. Braun, all of IPSCO Inc. for their confidence and support during this program, and permission to prepare this paper. We also thank and acknowledge Mr. D. Danyluk, of Reid, Crowther and Partners, who prepared the grading plan and drainage design.

7.0 REFERENCE

Giroud, J.P. and Noiray, L., "Geotextile Reinforced Unpaved Road Design", ASCE Journal of the Geotechnical Engineering Division, Vol. 107, No. 9, September, 1981, pp.1233-1254.

GLYNN, D.T., and COCHRANE, S.R.

The Queen's University of Belfast, United Kingdom

The Behavior of Geotextiles as Separating Membranes on Glacial Till Subgrades

This paper describes experimental investigations into the influence of subgrade type on clay contamination of stone sub-bases and its prevention or reduction by the use of permeable fabric membrane filters/separators. The performance of various types of geotextiles is assessed in both statically-loaded and dynamically-loaded laboratory models for a range of subgrade soils. These tests, which are designed specifically to examine stone penetration and clay pumping behaviour of soil/fabric/stone aggregate systems, show that unreinforced subgrades with a large clay or silt fraction and at moisture contents above optimum produce conditions where serious contamination of the stone sub-base layer is likely. However, the results suggest that geocomposites with suitable equivalent opening size and stiffness, particularly sand-filled nonwovens, greatly reduce both contamination by sub-grade fines and stone penetration and best preserve the integrity of the road sub-base.

INTRODUCTION

Civil Engineers involved in road construction are now becoming more aware that a pulsating dynamic load on a road surface (such as might occur with heavy traffic flows) can lead to clay particles being 'pumped' upwards from the fine cohesive subgrade into the voids of the unbound granular sub-base material, so causing permanent contamination. Furthermore, the granular sub-base may intrude down into the subgrade by direct penetration. With repeated traffic loading plastic flow of softened clay can occur (ie squeezing upwards of failed subgrade into the stone layer interstices above). This can lead to a dispersion of the sub-base particles within the subgrade and a consequential loss of useful depth of sub-base. Such contamination not only lowers the permeability of the stone layers and restricts drainage (1) but also acts as a lubricant which significantly reduces the shear strength of the stone sub-base aggregates (2). Failure of the road pavement results.

Although it is difficult to quantify it will be clear that such failures are extremely expensive to deal with when they occur. Preventive road maintenance to avoid major problems is just as expensive, and delays which result for the travelling public add their own not inconsiderable cost.

Within the last decade the use of synthetic permeable fabrics in road construction has become more common for separating soil subgrades and stone sub-base materials, for spreading surface loadings, reinforcing soils, relieving porewater pressures and allowing cheap on-site fill material to be used in embankments. In order to extend their geotechnical applications the idea of using fabrics to prevent sub-

grade fines migration was conceived, and in 1977 a course of research was initiated at The Queen's University of Belfast by Drs. Snaith and Bell (3) to study the problem. They showed, under laboratory-simulated conditions, that for filter membranes beneath road sub-bases normal filter principles (for unidirectional flow conditions) did not seem to apply. Indeed the problem of prevention of clay fines rising up from a cohesive subgrade to foul the sub-base materials differs from many other filtration problems; the subgrade, sub-base and intervening geotextile filter layers are all subjected to dynamically varying normal and shear stresses; flow through the filter may be of the reversing type; the filter is essentially required to allow free passage of water and yet restrict the movement of a fine-grained slurry.

To extend the work of Bell, McCullough and Snaith (4) and later Saunders (5), a comprehensive series of laboratory model tests was devised and carried out within the last year at this research centre. The present paper describes these laboratory investigations.

OBJECTIVES AND SCOPE OF STUDY

The main objectives of the research programme were to assess the dynamic filtration performance and separation function effectiveness of a range of geotextiles when used as separating membranes between clay subgrades and stone sub-bases and to investigate the various parameters which influence their behaviour in this role. A related objective was to study subgrade-sub-base interaction in order to gain a better understanding of the physical processes involved in clay pumping under dynamic cyclic loading.

The major part of the experimental study comprised of an extensive series of performance tests which were carried out with the geotextile under compression and in contact with soil/stone. The tests simulated operational in-soil conditions (ie for specific working environmental and loading conditions) for a variety of model soil/fabric/aggregate systems which in this instance represented discrete sections of the sub-base/subgrade boundary region in 'typical' road pavements.

Two kinds of performance test were used in this study (depending on the type of applied loading employed):

1) Static Load Penetration Test

This test simulates the severe loading of construction traffic before full road pavement depth has been attained and is designed to investigate the susceptibility of a subgrade soil to surface deformation by the sub-base layer. More specifically, it evaluates the effect of static loading on a sample of clay subgrade in terms of the average sub-base stone penetration into the subgrade. With a reinforced sub-grade, the test was also used to monitor the performance of the reinforcing fabric in reducing stone penetration.

2) Dynamic Load Filtration Test

Developed primarily to study the behaviour of clay pumping in roads and to identify the mechanisms causing the clay particle migration. In this form of the test the cell (road model) was subjected to a sinusoidally varying dynamic load of fixed amplitude and frequency. When the subgrade was reinforced with a separating membrane the performance of the fabric could be measured in terms of its effectiveness in preventing clay contamination of the sub-base layer, thereby enabling a relative assessment to be made of the geotextile's filtration properties.

Cochrane (6) drew up a framework or hierarchy of factors which could possibly

influence clay contamination of road sub-bases. The list in Table 1 shows that there are several controlling variables involved - in fact, far too many to be investigated on an individual basis. Therefore, in order for the project to be completed within the time and resources available, a selection of key variables was made to streamline the testing programme. Consequently, the experimental work was concentrated specifically on three sets of definitive tests. Each set included a series of both static load and dynamic load tests in which the main variables were: (i) subgrade soil, (ii) type of geotextile filter/separating membrane (including the unreinforced case where no geotextile was used) and (iii) initial moisture content of subgrade. Also in a separate set of filtration experiments the effect of variation of dynamic stress level (or load range) with soil moisture content was investigated for a 'typical' Northern Irish subgrade. Two extreme cases were examined - (i) with no filter layer present, and (ii) using a special thick nonwoven fabric/fine sand composite filter.

To compliment this work a range of 'index' tests were carried out to determine important geotextile index properties, ie values indicative of physical mechanical and hydraulic characteristics under standard environmental and loading conditions.

MATERIALS, EQUIPMENT AND TEST PROCEDURES

The subgrade soils used in the tests can be described as 'boulder clays' or more correctly 'glacial lodgement tills'. Such till soils cover much of Northern Ireland and are extremely varied in nature. Their particle size distribution ranges from heavy clayey tills (zone 1) with clay contents in excess of 25%, through the medium clay tills of zone 2 with 10% to 25% clay fraction, to zone 3 silts and sands with clay percentages less than 10% - the three grading zones were established to permit classification of the till grading curves and are shown in Fig. 1. Zone 1 included the relatively impermeable, high plasticity soils while zone 2 might be considered 'average' clay tills for this region having medium clay contents and generally poor drainage properties. Zone 3 represented the low plasticity, sandy silty tills with better than average drainage characteristics.

To reflect the wide spectrum of subgrade types found beneath roads in the Province, three different clay soils were selected for testing. The soils, which can be described as zone 1, zone 2 and zone 3 type glacial tills, were obtained from road construction sites in County Fermanagh (Southern Lakeland District), Whiteabbey (North Belfast) and at Newtownbreda (Co. Down) respectively. Particles larger than sand size were removed before using the soils for laboratory tests. Grain size distribution curves for each are shown in Fig. 1 and classification data is listed in Table 2.

In order to keep the test rig specimens to a manageable size it was decided to use scaled-down 'model' sub-base materials in all the performance tests. Instead of the 2" and 4" single-sized aggregates often employed in full scale roads in Northern Ireland a 20mm single-sized crushed basalt stone was selected to model the sub-base layer.

Both existing civil engineering fabrics and a specially developed sand mat composite were adopted as filters/separators in the performance tests.

As fabric pore size or equivalent opening size is considered to be the single most significant parameter controlling clay contamination, four different types of commercially available geotextile membranes with low O_{90} values were used ie generally less than 100 microns. Details of the fabrics are given in Table 3.

In addition to the geotextiles a geofabric/granular composite was used as a filter in a separate series of dynamic tests in which the filter's performance over a wide range of soil moisture and applied loading combinations was assessed. The filter itself was made up of a compacted layer of fine sand in an 8mm thick fibrous nonwoven matting. The matting, which could be described as similar to an air filter, was 'open' structured to facilitate the inclusion of the sand filling. Collectively, it was known as the Bondina sand mat.

Static Load Penetration Test

Samples for the test were prepared by placing and compacting the subgrade soil into a shallow cylindrical mould, followed by placing of the geotextile separating membrane and the model sub-base material. A typical arrangement of the test sample is shown in Fig. 2.

Preparation of each sample was carried out by mixing a quantity of distilled water - the exact amount depending on the prescribed target moisture content - with a representative sample of dried and sieved boulder clay. This was then left in an airtight container to ensure equilibration of moisture throughout the soil mass. After 24 hours the subgrade material was placed in two layers each approximately 40mm deep in the bottom of a 250mm diameter steel mould. Each layer was initially compacted under standard compactive effort using a 2.5kg drop hammer conforming to BS1377 (7). This method assisted in kneading the soil uniformly into the mould without entrapping pockets of air. Final compaction was achieved using a compression test machine - a vertical static pressure of 500kN/m^2 was applied to the formation surface. At this stage the test specimen was trimmed and the weight of the subgrade and mould together was determined. During the trimming operation small samples of soil were taken for moisture content determination. Also a set of depth measurements was recorded to establish the position and profile of the subgrade surface relative to the top of the mould - this served as a fixed reference plane - and from this the volume of the soil mass was estimated.

Once the subgrade was prepared a separating membrane which had previously been weighed was positioned on top of the soil surface. The fabric sample was cut so that its plan dimension was greater than that of the mould, approximately 400mm in diameter. The extraneous or overlap material was then folded up the sides of the mould to ensure continuity of separation layer and interface boundary at the edges and also provide good anchorage during testing. Several 'control' tests were also carried out with no fabric present. These tests simulated the unreinforced condition.

Finally a fixed mass of air dried 20mm single-sized aggregate was placed on the fabric layer to model the road sub-base. To prevent possible rocking of the loading platen the sub-base surface was carefully levelled before commencing the test.

When the preparation procedure was completed the test sample was transferred to the loading platform of a compression test machine and a vertical load of 2.5 tonnes (equivalent to a normal stress of 500kN/m^2) was applied. The load was sustained for a short period of 4-5 sec and then released. This loading pattern was repeated a total of 12 times at 5 minute intervals for the duration of the test to model the effect of heavy construction traffic on the road sub-base material.

On completion of the static load test the sub-base layer together with the geotextile were removed from the mould to reveal a depressed and uneven soil surface due to the penetration of the stone into the subgrade. Having previously established the mean initial surface level of the preloaded subgrade, a series of

depth readings (total of 30 in all) was made of the post-test surface. This involved taking fifteen measurements from the fixed reference plane to the bottom of each randomly selected indentation (trough) formed by individual sub-base particles and a corresponding set of measurements to the peaks (areas of local heave) adjacent to these indentations. Consequently average trough and peak levels were calculated and comparative measurements of the depth of stone penetration and the degree of surface 'unevenness' (ie average amplitude) occurring in each test were obtained from the following equations:

Average Amplitude of Penetration = Average Trough Level - Average Peak Level

Average Stone Penetration Value = Average Trough Level - Mean Depth to Surface Before Test

Dynamic Load Filtration Tests

The procedure adopted for the preparation of the sample in this test was similar to that used in the stone penetration test. The subgrade soil, geotextile filter and sub-base material were all prepared and arranged according to the technique described above. In the case of the Bondina sand mat composite, a known quantity of sand was spread on to the surface of the fabric and gently tamped into its matrix until completely filled. Before the test sample was transferred to the loading apparatus, however, 500ml of distilled water was poured into the mould to simulate ponded water (Fig. 2). This modelled the uneven condition of a road pavement in which water collected on the subgrade surface, either in a wheel rut or local depression, and because of the altered lateral gradients was unable to drain quickly away. In the laboratory experiment therefore, as in the real situation, this free water promotes the formation of a fine-grained slurry at the sub-base-subgrade interface and thus serves as a carrier for the waterborne clay particles to migrate into the stone layer.

When fully prepared the test sample was placed under the loading ram of an electronically controlled servo-hydraulic dynamic MAND testing machine (Fig. 3). This was used to apply a mean vertical stress of 50kN/m^2 to the surface of the sample via a rigid bearing platen. The load was then varied sinusoidally at a rate of 5Hz between the set limits of 25kN/m^2 and 75kN/m^2 over a period of six hours, during which time the sample was subjected to 108000 load cycles. In a limited number of tests applied loading levels of $30\pm 15\text{kN/m}^2$ and $70\pm 35\text{kN/m}^2$ were also used to examine the effect of increased or reduced mean stress levels.

A comparative measurement of the amount of clay material penetrating the fabric filter and contaminating the stone layer at the completion of the test was devised. This was known as the 'Soil Contamination Value' (SCV) and was strictly defined as the dry weight of subgrade-derived contamination (gms) passing the filter per unit area of subgrade/sub-base interface (units of gm/m^2). SCV's were determined in the following manner. After each dynamic loading test both the contaminated sub-base and geotextile layers were removed from the mould and oven dried at a moderate temperature (55°C) for 24 hours. Once dry the materials were weighed and the increase in dry weight over their original pre-test weight was recorded. Given the area of the mould (ie 0.05m^2) the SCV was calculated.

Throughout a typical experiment such variables as fluctuations in dynamic load, deflection of hydraulic ram from the mean position and total number of load cycles over the test period were monitored. These variables were periodically output from the MAND system as analogue voltages and processed into readable units via an analogue to digital convertor (PCI). The data was then stored on a microcomputer.

The software for this computer-based data acquisition facility was designed and written in-house⁽⁸⁾.

RESULTS AND OBSERVATIONS

A summary of the results for the static load test programme is shown in Figs.4-6. These graphs clearly show the weakening effects of excessive soil moisture but also demonstrate the relative performances of the fabric membranes in preventing or minimising sub-base penetration for the different subgrades. All the fabrics successfully reduced stone point penetration, however, the thicker compressible membranes (Lotrak composite and needled nonwoven) performed markedly better at higher soil moisture contents than the two thinner relatively incompressible membranes (woven and spunbonded nonwoven). It is also apparent from the low values recorded for average amplitude of penetration that plastic flow of softened clay into the stone interstices above was virtually eliminated by the presence of a geotextile. This was partially attributed to a local restraining effect being imposed on the subgrade due to the development of tensile forces in the geotextile between individual aggregate particles.

Fig. 7 shows the results of a series of 12 dynamic load tests conducted using no filter (unprotected subgrade). They clearly indicate the major importance of both loading levels and soil moisture content on clay contamination. For instance, at moisture contents of about 18% (optimum for the soil used), average stress levels of 50 kN/m² produce SVC's of just over 500 gm/m² - this value has often been considered the acceptable limit of clay contamination. However, at 25% moisture content the contamination has worsened considerably with the same stress level producing SCV's over three times the acceptable limit. At moisture contents above 25% the soil contamination becomes progressively worse.

Results for a series of dynamic load tests to compare the performance of a range of fabrics are presented graphically in the form of SCV-moisture content relationships (Figs. 8, 9 and 10). They show that all the fabrics were effective in reducing contamination of the sub-base due to pumping, and that the capacity of the fabrics to act as dynamic filters was related to the size and shape of their pores. It was noticeable therefore that the performances of the thick nonwoven and composite were distinctly better for each of the three soil types than that of the woven and thin nonwoven fabrics. This would also indicate that thickness has an important cushion effect as well as providing good in-plane permeability for drainage and porewater pressure relief. The relatively poor protection afforded the sub-base by the Scottlay woven would appear to indicate that relatively little advantage is to be gained by its use over the unreinforced condition in preventing clay contamination.

The final set of tests incorporated the Bondina sand mat filter in the pumping test rig. The results show that for extreme and adverse conditions this filter was very successful in limiting clay contamination to values generally less than 450 gm/m² (Fig. 11). The sand mat also produced the most rigid filter yet tested. It exhibited a high resistance to local deformation by the sub-base particles. Correspondingly, only minor disruption of the subgrade was observed. It was noted however that larger stress levels caused sand particles to penetrate through the fabric and become embedded in the subgrade surface. This behaviour demonstrated the importance of matching the density of the fibre mat to the particle size grading of the granular material.

Table 1 Factors influencing clay contamination of road stone layers

Response Variables of Interest	Possible Contributory or Explanatory Variables or Factors		
	Primary Factors	Secondary Factors	Tertiary Factors
1. Soil Contamination Value (SCV) 2. Stone penetration 3. Rutting 4. Pore-water pressure behaviour	1. Load	1. During construction 2. During lifetime	1. Mean loading 2. Range of cyclic loading 3. Frequency 4. Duration (no. of cycles)
	2. Stone layer	3. Crusher run 4. Single size	5. Grading 6. Shape
	3. Separating layer or membrane	5. Unreinforced 6. Granular 7. Woven 8. Nonwoven 9. Composites	7. Grading 8. Porosity 9. Through-plane permeability 10. In-plane permeability
	4. Subgrade	10. Glacial lodgement tills	11. Strength 12. Weight 13. Thickness 14. S.S.C. 15. M/C 16. Density 17. PL 18. LL 19. Cu 20. CBR

Table 2 Physical properties of subgrade soils

Soil Type	Liquid Limit (%)	Plastic Limit (%)	Plasticity Index (%)	Natural W/C (%)	Optimum W/C (%)	Clay Content (%)
Fermanagh Boulder Clay	71	32	39	37	28.5	48
Whiteabbey Boulder Clay	39	20	19	18	19	21
Newtownbreds Boulder Clay	32	15	17	11.5	11	12

Table 3 Details of geotextiles

Fabric	Construction	Material	Weight (g/m ²)	Thickness (mm)	0 ₁₀₀ (µm)
Moven (Scottlay)	Plain woven monofilament tapes	P'propylene	194	0.68	233
Thin Non-woven (Terram)	Melt-bonded continuous filament fibres	P'propylene P'ethylene	340	1.68	40
Thick Non-woven (Bidim)	Needle-punched continuous filaments	Polyester	550	4.38	74
Composite (Lotrak)	Plain woven top with fleece needed to under-surface	P'propylene	840	4.02	60

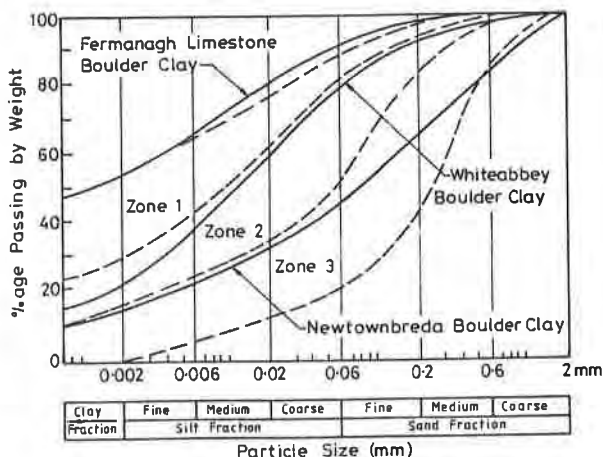


Fig. 1 Grading curves of subgrade soils.

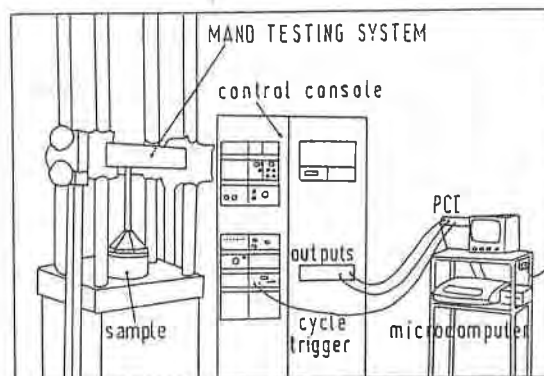


Fig. 3 Dynamic cyclic load test

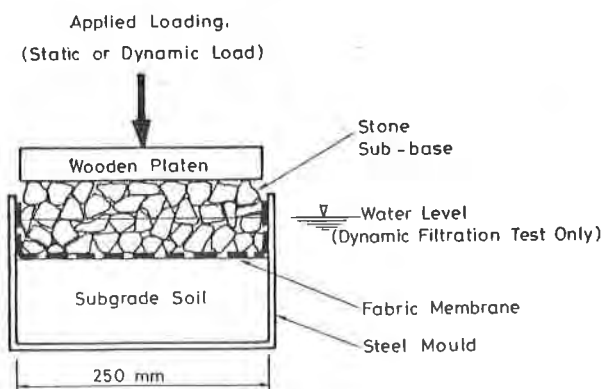


Fig. 2 Stone penetration / dynamic filtration test

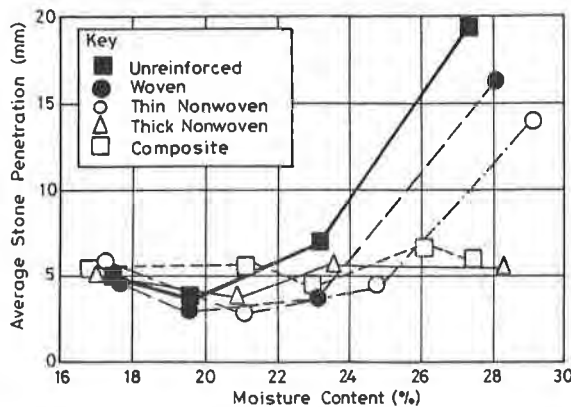


Fig. 4 Influence of soil moisture on stone penetration into subgrade for Whiteabbey Boulder Clay

DISCUSSION

Visual inspection of the post-test samples revealed that in no instance did any geotextile fail to act as a separating membrane between sub-base stone and subgrade soil. The results of the static load tests confirm that geotextiles reduce stone penetration levels dramatically and virtually eliminate local heave (plastic flow) of the subgrade. It is apparent however that the benefits of a particular fabric are more pronounced for the medium and high plasticity soils (Whiteabbey and Fermanagh Boulder Clays respectively), with the Scottlay woven generally performing less well in this role and possibly the Bidim nonwoven or Lotrak composite providing the greatest benefits over the full range of moisture contents.

In Fig. 12 the influence of fabric thickness on the maximum depth of stone penetration for the three soil types is investigated and suggests that a strong relationship exists between this index property and response variable. In each case a significant decrease in maximum stone penetration occurs when thicker fabrics are used. It is not known what proportion of this decrease may be attributed to the fabric thickness property as other index properties such as compressibility and tensile strength may also play a part. Also the influence of fabric thickness may vary for different moisture content levels. This trend is particularly evident with the silty and stoney boulder clay from Newtownbreda, where somewhat surprisingly maximum stone penetration value for each fabric does not coincide with highest soil moisture level.

The performance of the various geotextiles in terms of minimum contamination levels vary significantly in the pumping tests. Contamination levels as low as 250gm/m² may be achieved when a composite fabric is used on the Newtownbreda clay. This is compared to a minimum SCV level of 750gm/m² for Whiteabbey Boulder Clay and 2500gm/m² for Fermanagh Limestone Boulder Clay. A similar trend is

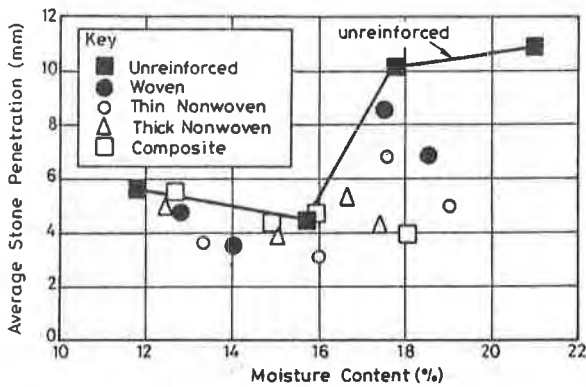


Fig. 5. Influence of m/c on stone penetration for Newtownbreda boulder clay.

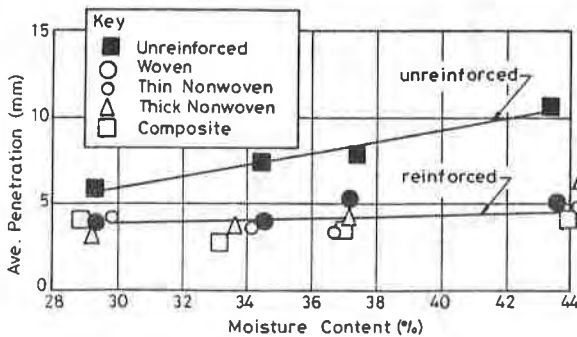


Fig. 6. Influence of m/c on stone penetration for Fermanagh Boulder Clay.

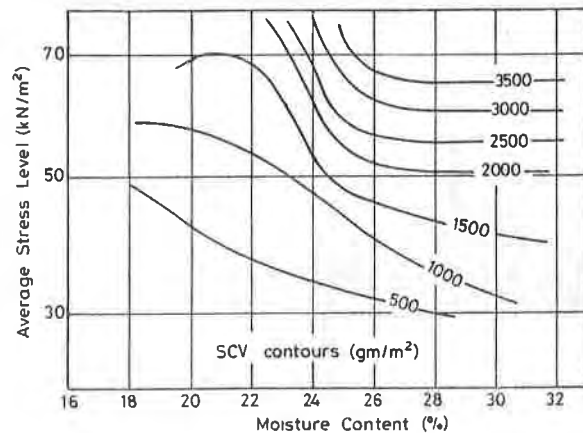


Fig. 7. Effect of soil m/c and applied stress level on SCV for unreinforced subgrade (zone 2 till)

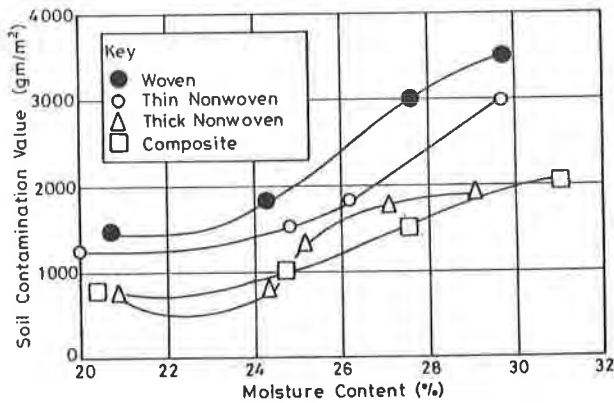


Fig 8. Relationship between subgrade moisture content and contamination (SCV) for Whiteabby Boulder Clay.

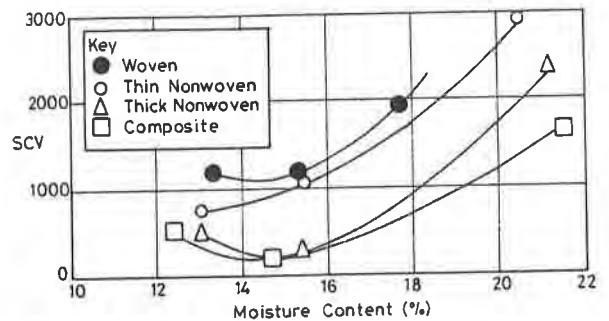


Fig 9. Relationship between subgrade m/c and SCV for Newtownbreda Boulder Clay.

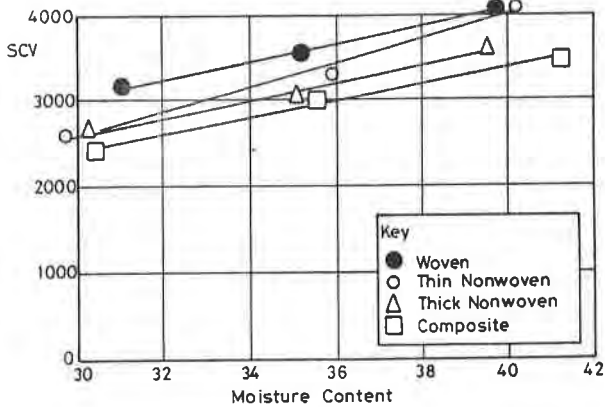


Fig 10. Relationship between subgrade m/c and SCV for Fermanagh Limestone Boulder Clay.

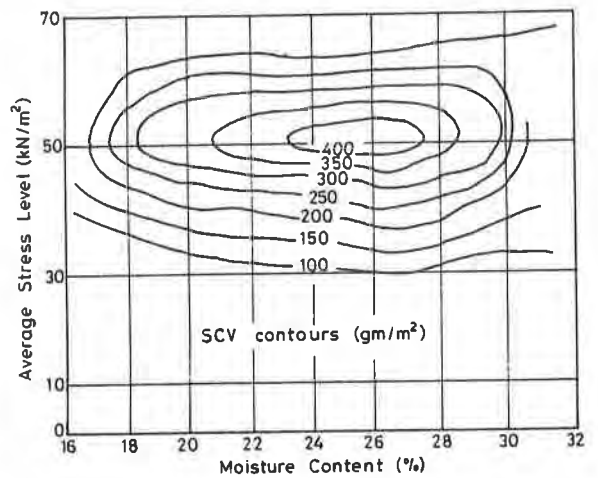


Fig 11. Effect of soil m/c and applied stress level on SCV for zone 2 till subgrade using Bondina sand mat filter.

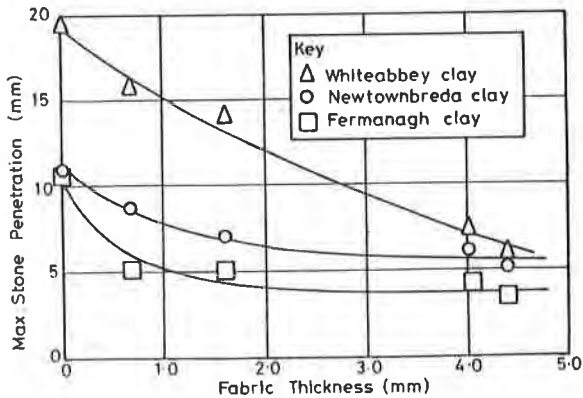


Fig 12. Influence of fabric thickness on stone penetration

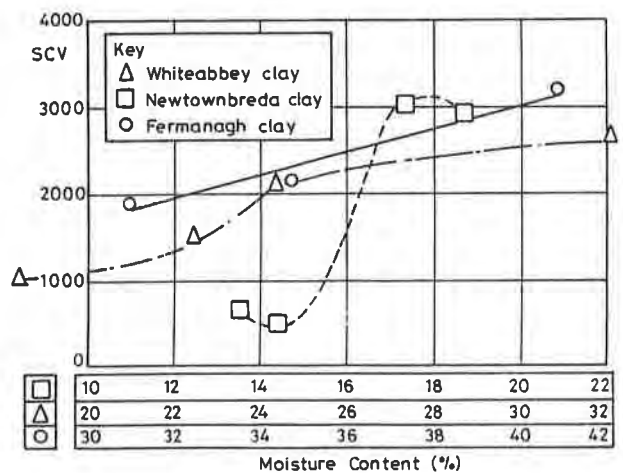


Fig 13. Relationships between m/c and SCV for unreinforced subgrades.

observed for the unreinforced subgrades. Fig. 13 shows that greater contamination due to pumping occurred with the heavy clay soil and generally lessened with the clay percentage of the subgrade. This would seem to indicate that, given their susceptibility to pumping over particular 'working' ranges of soil moisture content, medium and heavy clay subgrades are considerably more likely to be the source of sub-base contamination problems and that the degree of the contamination will primarily depend on the clay content of the subgrade.

For each clay the fabric performance over the range of moisture contents tested also varies. For example, in the case of the Fermanagh clay the SCV-m/c relationship approximates to a linear increasing one, whereas in the case of the Whiteabbey clay the distribution of SCV's over the m/c range is in the form of a pseudo S-curve possibly due to the particular behaviour of the soil at or below optimum moisture levels as in the case of the driest tests. A U-curve is characteristic of the relationship for the Newtownbreda clay. This reflects the diverse nature of the three soils and supports the argument that there is clearly a relationship between clay contamination of the sub-base material and clay content of subgrade. However, there appears to be other factors or soil properties determining the shape or form of the SCV-moisture content graphs.

A consistent finding of the dynamic load test series (with only one exception) is that although the amount of contamination varies for the different clays the relative performances of the various fabrics remains the same. For example, the Lotrak composite fabric is the best overall performer, the rate of increase of contamination (SCV) with increase in moisture content being much less than for any of the other geotextile fabrics. The next most successful filters are the non-wovens, the Bidim being the more effective of the two. Finally, the Scottlay woven, although still providing some protection to the sub-base at higher moisture contents, is the least effective fabric in reducing clay contamination. This behaviour holds true for silty, medium clay, or heavy clay subgrades.

Post-test examination of the dynamically-loaded geotextile specimens reveals that distinctive soil contamination patterns form on and through the fabric matrix. In the case of the thin nonwovens (Terram) mud staining occurs at locations corresponding to the contact areas between sub-base particles, filter and subgrade. Between the contact areas little or no staining is visible. This would suggest that fines migration takes place beneath the high stress contact points. Since also the fabric may be stretched in this area of particle contact the nominal effective opening size (O_{90} value) of the fabric will increase locally further decreasing its resistance to soil migration. As a result the contaminant is jetted vertically through the fabric into the base of the stone layer. Similar behaviour is observed for the woven geotextiles although the contamination patterns are not so distinguishable.

In contrast to this a somewhat different behaviour is observed for the thicker fabrics, namely for the Bidim polyester nonwoven and the Lotrak composite. The mud staining in this instance occurs between the particle contact areas with little or no contaminant visible directly below the stone points. It would appear that due to the compressible nature of these filters the pore size becomes locally reduced beneath individual sub-base particles. Consequently, the clay slurry is forced sideways along the plane of the geotextile bringing into play a three-dimensional filtration effect. The slurry is eventually directed up into the sub-base between the contact areas where the fabric's porosity remains relatively unaltered.

Dawson (9) suggested that a thick geotextile performs better as a dynamic filter

because the passages through it tends to be longer and more convoluted. He debated that hydraulic gradient along the flow path will thus be less (than for a thinner less compressible fabric) and the 'dropping' of suspended solids within the fabric will be corresponding more likely. A similar argument is applicable to this three-dimensional filtration effect described above. Since the flow path of the migrating slurry is longer the effective filtration length must also increase with the result that the fabric has more opportunities to entrap soil particles within its matrix.

By far the most successful dynamic filter/separating membrane tested was the Bondina sand mat composite. It combines a fabric filter with a layer of compacted granular material. Its big advantage over conventional fabric filters is that its mechanical and hydraulic properties do not change significantly under test conditions. For instance, sand is a highly incompressible material and will remain permeable under load. By incorporating sand into the voids of a fabric, the fabric is prevented from collapse when stressed and serves to maintain the filtration characteristics of the composite. The fabric can complement this by providing the sand layer with a tensile resistance to movement. Under cyclic loading the sub-base particles may tend to punch into and through the sand, however, any displacement of the granular material is impeded by the fabric.

CONCLUSIONS

1. All the geotextiles tested perform a useful separating function in reducing the stone penetration down into soft clay subgrades and in preventing plastic flow of the clay up into the stone interstices. The thicker compressible fabrics were found to be particularly effective in this role over a wide range of moisture contents and soils.
2. Clay pumping, or fines migration upwards into the stone layers above, under dynamic cyclic loading on a model stone sub-base, was found to be dependent mainly on stress level, soil moisture content, and clay content of the sub-grade soil. Geotextiles with effective opening sizes of less than 100 μ m reduce clay pumping significantly when used as separating membranes between the clay subgrade and stone sub-base.
3. The mechanism of clay pumping was found to arise mainly from slurry filled depressions formed by stone penetration into the clay subgrade surface. The stone point depressions, filled with water, acted as clay slurry pump sumps under repeated cyclic loading, squirting the clay slurry upwards into the stone interstices.
4. The thick geotextiles were most successful in reducing clay pumping. The cushion effect of their thickness reduced stone point penetration into the sub-grade, and slurry penetration through the fabric only occurred between the stone point depressions where the fabric was relatively uncompressed. The thin geotextiles performed less well in reducing clay pumping. Slurry penetration was found to take place at the highly stressed areas around the stone points probably due to enlargement under stress of the fabric openings.
5. A thick sand-filled fabric was found to be the most effective in controlling clay pumping under a wide range of loads and soil moisture contents. This was principally due to its stiffness in resisting stone penetration and hence minimising the formation of depressions in the clay subgrade surface which might then fill with water and become sources of clay slurry.

ACKNOWLEDGEMENTS

The authors wish to extend their appreciation to the United Kingdom Science and Engineering Research Council who made this study possible through its financial support. Thanks are also due to Mr. E. Uprichard, Lambeg Industrial Research Association for providing technical assistance throughout the project.

REFERENCES

- (1) Cedregren, H.R., Drainage of Highway and Airfield Pavements, John Wiley and Sons, Inc., New York, 1974, 285 pp.
- (2) Bell, A.L., McCullough, L.M. and Gregory, B.J., "Clay Contamination in Crushed Rock Highway Sub-bases", Proceedings of Conference on Engineering Materials, New South Wales, Australia, 1981, Session II, pp 355-365.
- (3) Snaith, M.S. and Bell, A.L., "The Filtration Behaviour of Construction Fabrics Under Conditions of Dynamic Loading", Geotechnique, London, 1978, Vol. 28, No. 4, pp 466-469.
- (4) Bell, A.L., McCullough, L.M. and Snaith, M.S., "An Experimental Investigation of Sub-base Protection Using Geotextiles", Proceedings of Second International Conference on Geotextiles, Las Vegas, USA, 1982, Vol. 2, pp 435-440.
- (5) Saunders, A.T., Bell, A.L. and Green, H.M., "The Role of Geotextiles in the Dynamic Filtration of Road Pavements", Third International Conference on Polypropylene Fibres and Textiles, York, England, 1983, pp 36.1-36.10.
- (6) Cochrane, S.R., "The Clay Contamination of Road Stone Layers on Glacial Till Subgrades", Proceedings of International Conference on Glacial Tills, Edinburgh, Scotland, 1985, pp 87-91.
- (7) British Standard BS1377, Methods of Test for Soils for Civil Engineering Purposes, British Standards Institution, London, England, 143 pp.
- (8) Davis, C. and Cochrane, S.R., "Microcomputer Controlled Dynamic Testing of Geotextile Separating Membranes in Road Construction", Proceedings of Second International Conference on Civil and Structural Engineering Computing, Edinburgh, Scotland, 1985, Vol. 2, pp 377-380.
- (9) Dawson, A.R. and Brown, S.F., "Geotextiles in Road Foundations", Report to ICI Fibres Group, University of Nottingham, England, 1984, 77 pp.

WALLS, J.C.

The Tensar Corporation, U.S.A.

GALBREATH, L.L.

CSX Transportation, U.S.A.

Railroad Ballast Reinforcement Using Geogrids

ABSTRACT

The following is a case study on the use of geosynthetics to stabilize and reinforce ballasted track over an unstable subgrade. The project involves the repair of a section of track in Alabama where a combination of weak soils and a high ground-water table had caused repeated track failures. After several attempts to stabilize the track had failed, the track section was successfully repaired using a unique combination of geotextile and polymer grid reinforcement. Although geotextiles have been widely used in railroad track structures for separation and drainage, this project represents the first use of polymer grids in North America to reinforce railway ballast.

INTRODUCTION

This paper describes the use of polymer grids to reinforce the ballast under a 2000 m section of track, near Milstead, Alabama. The track section, which is owned and operated by CSX Transportation, formerly Seaboard System Railroad, was a continual source of maintenance problems, requiring frequent realignment to overcome repeated settlements that were caused by a high ground-water table and poor soil conditions.

Railroad track maintenance accounts for a large percentage of railroad companies' total operating costs. A common cause of track failure is excessive settlement due to the large dynamic loads under 120 tonne freight cars. Research (1) at Queens University and the Royal Military College of Canada (RMC) in Kingston, Ontario has indicated that polymer geogrid reinforcement of railway ballast can significantly reduce total settlements under railway tie loadings and thereby offer potential for reducing total maintenance costs. The function of the grid is to preserve the integrity of the ballast by rigidly confining the aggregate material. Furthermore, the grid carries tensile stresses to restrict both vertical and lateral movement of the ballast. The research at RMC demonstrated that geogrid reinforced ballast sections over flexible subgrades could carry up to 10 times the number of model tie loadings before a permanent deformation of 50 mm occurred, as shown in Figure 1.

RESULTS OF RAILWAY BALLAST TESTS at Queens University

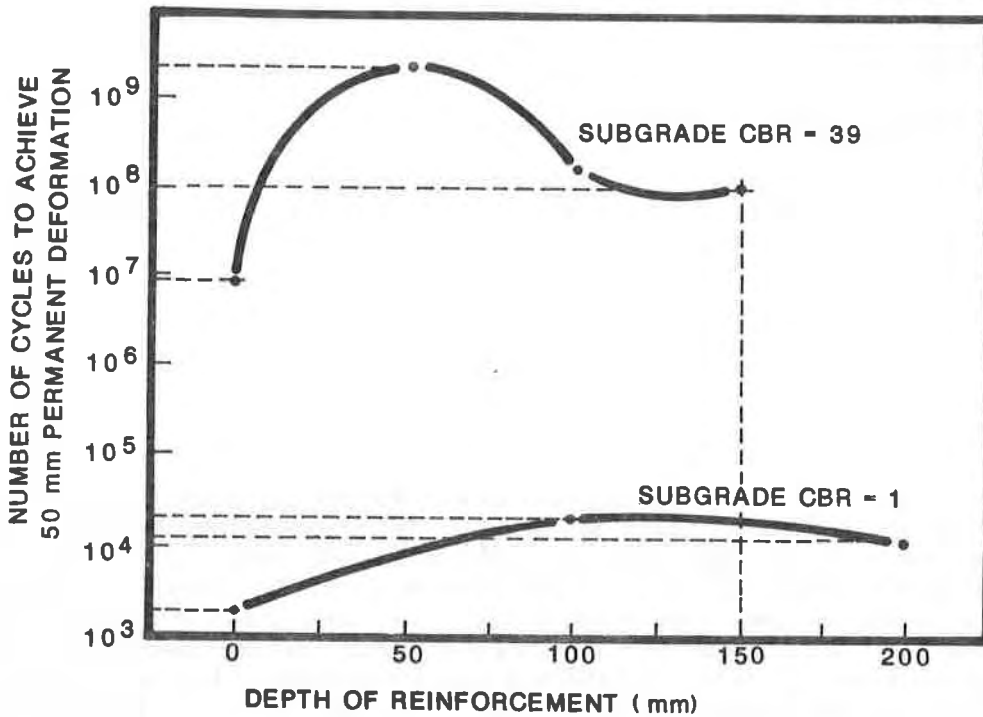


Figure 1 Results of Railway Ballast Tests.

SITE CONDITIONS

The original track structure was located along the bank of the Tallapoosa River high above the water line. Since continual erosion of the embankment toe caused repeated slope failures, the alignment of the track was moved to a new location about 365 m east of the original site. The 2000 m long section of track was re-constructed in 1976. Much of the re-aligned track was placed in a deep, wide cut through interbedded sand and weak clay layers about 7.5 m below the original phreatic surface. The cut sections had 2:1 side slopes with benches at vertical intervals of approximately 7.5 m. Deep side ditches were constructed beside the track to provide drainage for the inevitably large accumulations of run-off water. Within months after relocating the track, erosion of the cut slopes and benches filled the ditches with sediment and blocked drainage. This resulted in trapped water saturating the subgrade soils beneath the track structure, further reducing the effective shear strength of the clay. Heavy rail traffic therefore caused progressive shear failure of the railway embankment and heaving of the shoulders. Quick conditions also occurred due to the dynamic loads, causing excessive settlements and pumping of fines through the ballast and into the side ditches as shown in Figure 2.



Figure 2 Condition of track structure in May, 1983, showing fouled ballast and clogged ditches.

As a result of the very poor conditions, it was necessary to maintain, realign and surface the track every 2 to 4 weeks. Furthermore, the situation was so severe that a speed restriction of 8 km/hr. was usually necessary for that section of track.

Previous efforts to stabilize the track had failed. For example, rail sections had been driven vertically into the ground beside the track to try and prevent lateral displacement of the ballast and track, as shown in Figure 3.

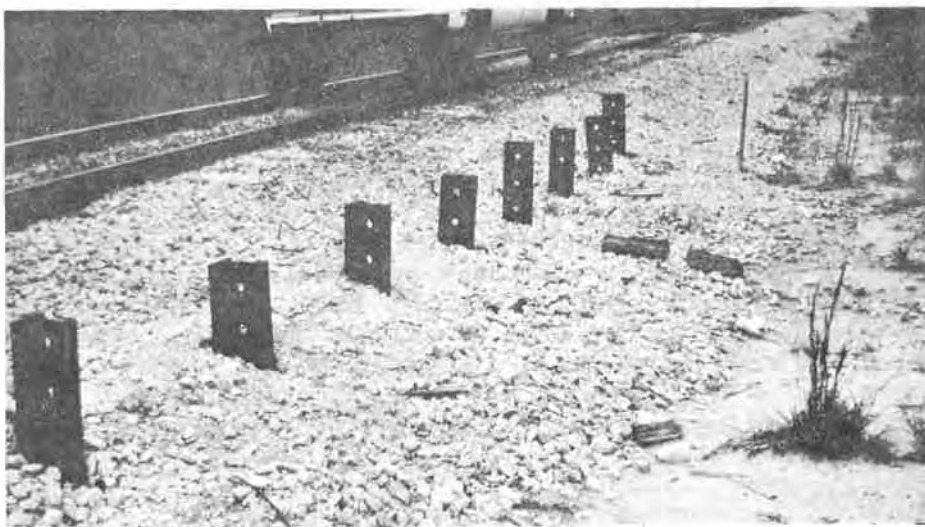


Figure 3 Rail sections driven into ground in effort to stabilize railway embankment.

DESIGN ALTERNATIVES

In May, 1983, the railroad's geotechnical consultant was called in to assess the track condition and recommend a solution. In order to stabilize the track and eliminate the need for continual maintenance, three alternatives were proposed (2).

Alternative 1

The first, and the most costly, alternative was to relocate the track structure. To ensure stability of the new track the subgrade would have to be excavated to a minimum depth of 0.30 m below the base of the ballast and the top 0.15 m of the new subgrade compacted to 90% of optimum density. A 540 g/m² geotextile was specified on top of the prepared subgrade followed by 0.30 m of subballast and 0.20 m of ballast.

Alternative 2

The second alternative was to stabilize the existing subgrade under the existing track structure. The recommended procedure was to remove the existing ballast beneath the track, install a specified geotextile (810 g/m²) on top of the old subballast and place standard ballast to a minimum depth of 0.30 m below the base of the tie.

Alternative 3

The third alternative was to remove the fouled ballast under the existing track and replace with new clean ballast reinforced with polymer grids. The recommended procedure was to undercut and remove the existing ballast, install a specified geotextile (380 g/m²) on top of the existing subballast and place TENSAR Geogrids directly on top of the geotextile prior to placing standard ballast to a minimum depth of 0.30 m.

The function of the geotextile in this design was to provide separation and prevent fines from pumping into the clean ballast. The function of the polymer grid was to provide tensile reinforcement to the ballast and thus minimize lateral and vertical movement of the ballast under the dynamic loads. Use of the polymer grid eliminated the need for using a much heavier geotextile which would have been required to provide some of the required reinforcement.

Although large scale test results had previously demonstrated the potential for polymer grid reinforcement of railway ballast, there were no case histories of this application in North America at that time. Since this alternative offered the most cost effective solution to the problem, the decision was made to incorporate the polymer grids into the track repair. It was estimated that the grid solution would cost about \$90,000 compared to \$570,000 for the relocation alternative.

CONSTRUCTION

Construction of the polymer grid reinforced ballast was carried out in December, 1983. With the exception of placing the geotextile and geogrid in the same operation, construction was very similar to routine track maintenance.

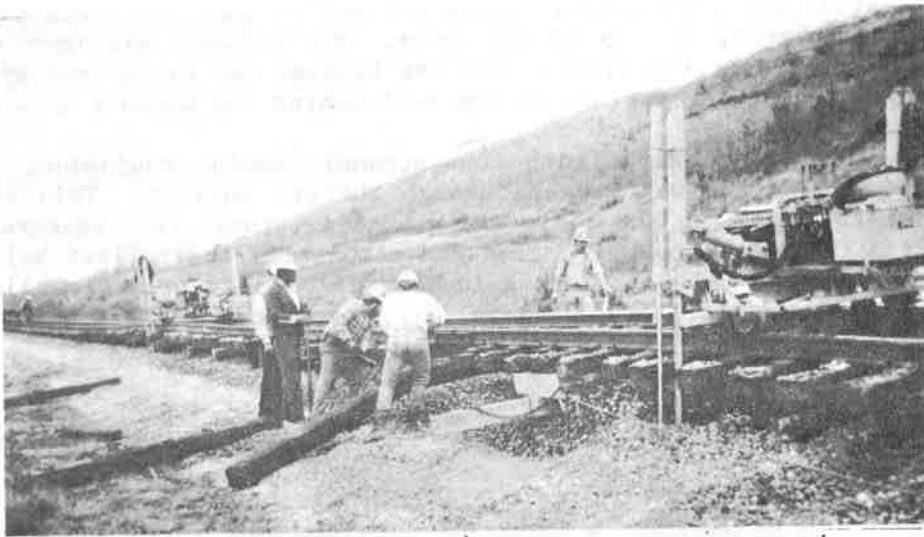


Figure 4 Removing fouled ballast from beneath raised track.



Figure 5 Installing geogrid and geotextile on top of existing subballast.

Firstly, the track, including rails and ties, was raised and the fouled ballast was removed by a "sled" being pulled by two cables connected to a backhoe. When completed, the track was again raised by the power jacks and the geotextile and geogrid were unrolled simultaneously over the existing subballast. Figures 4 and 5 illustrate the sledding and geotextile/grid placement operations.

When the geotextile and grid were in place and pulled taut the track was then lowered to rest temporarily on top of the grid. New ballast was then dumped from gondola cars passing over the track. The new ballast was bladed out by a railroad tie being dragged along the surface of the rail behind the gondola car.

Finally, the ballast was tamped with conventional tamping equipment, as shown in Figure 6, while the track was raised through the new ballast. This machine uses grips to raise the track by the rails and vibrating prongs that penetrate into the ballast shaking it down through the ties and compacting the ballast below the ties in the vicinity of the rails. Laser guidance was used to properly align the rail during this operation. Figure 7 shows the completed track immediately after construction.

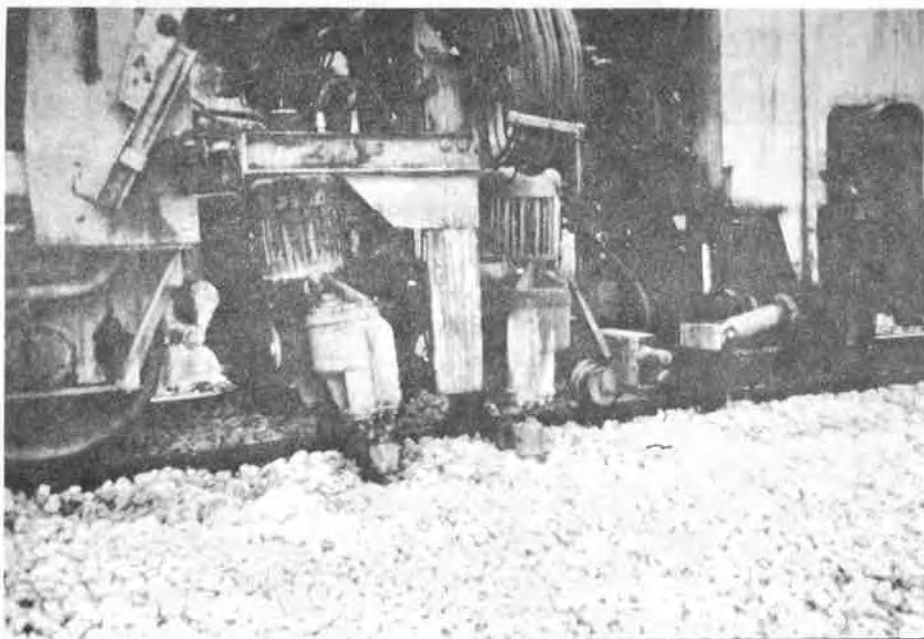


Figure 6 Raising track through ballast and compaction of ballast beneath ties.

CONCLUSIONS

High strength, rigidly structured polymer geogrids have proven to be effective and economical in reinforcement of railway ballast to minimize or prevent track stability problems. Properly sized grids will interlock with and confine ballast rock thereby resisting lateral and vertical deformation under typical railroad track loads. Reinforcement of the ballast reduces the magnitude of the shearing stresses transmitted to the subballast and subgrade. This is particularly important when track structures are built over low shear strength or highly elastic soils. When partially saturated or saturated conditions are present, polymer grids will be most effective when used in conjunction with appropriate geotextile fabrics that provide adequate separation between subgrade and ballast or subballast.

Inclusion of polymer grid reinforcement into the ballast during track rehabilitation is possible during routine maintenance in which fouled ballast is to be replaced and/or new ballast is to be added. No difficult or additional steps are required to incorporate the grid at or near the bottom of the new ballast.

Conventional tamping equipment can be used to prepare the ballast without damage to the grid provided that a minimum of 8 inches of ballast is placed between the grid and the base of the tie before tamping begins.

Since completion of the first project utilizing polymer grid to reinforce railway ballast, other railroad companies have used geogrids to successfully stabilize problem sections of track. Several of these are currently being monitored for permanent settlements and overall performance. To date, all reports have been very favorable.



Figure 7 Track structure after construction.

PERFORMANCE

Within three months after completion of the reinforced track structure, the 8 km/hour speed restriction was raised to 56 km/hour and no track stability problems had been encountered. At the time of writing, nearly 3 years have passed since construction and no additional maintenance has been required over the reinforced section of track. Furthermore, the slow order has been completely lifted.

ACKNOWLEDGEMENTS

The authors wish to commend Mr. Jack Newby, Newby Soils, Inc, for having the foresight to recognize the potential of polymer grid reinforcement in railway ballast and including it in his original recommendations to Mr. R. E. Frame of CSX Transportation, formerly Seaboard System Railroad.

REFERENCES

1. Bathurst, R.J., Raymond, G.P. and Jarret, P.M., "Performance of Geogrid-Reinforced Ballast Railroad Track Support", Proceedings of the 3rd International Conference on Geotextiles, Vienna, Austria, 1986.
2. Newby, Jack E., "Seaboard System Railroad, Subgrade Stabilization, Mile Post 146+ Near Milstead, Alabama", Geotechnical Report for Seaboard System Railroad, May 18, 1983.
3. Raymond, G.P., Bathurst, R.J., Jarrett, P.M., Hawrysh, T.A., "Large Scale Testing of TENSAR Geogrid Reinforced Railway Ballast", Draft Report for The Tensar Corporation, June 1985.

CARROLL, R.G., Jr. and WALLS, J.C.
The Tensar Corporation, U.S.A.
HAAS, R.
University of Waterloo, Canada

Granular Base Reinforcement of Flexible Pavements Using Geogrids

ABSTRACT

A comprehensive program investigating geogrid reinforcement of granular base layers of flexible pavements was carried out at the University of Waterloo, Ontario. The program consisted of repeated load tests on varying thicknesses of reinforced and unreinforced granular bases. Other controlled variables included reinforcement location and subgrade strength. The results of this program were used to develop an empirically based design guide for grid reinforced base layers of flexible pavements.

This paper will review the program results and review the design guidelines that have been developed for geogrid reinforced base layers of flexible pavements.

INTRODUCTION

For more than a decade geotextile fabrics have been used for subgrade stabilization of soft foundation soils. In subgrade stabilization, the separation function of the fabric is the key to performance. As a separator, fabric prevents granular base material from punching into soft foundation soils under the wheel or track loads of construction vehicles. By preventing this base punching or localized shear failure, the subgrade can develop its full bearing capacity.

This separation function provides an increase in subgrade load capacity when the soil shear strength is very low ($<50 \text{ kN/m}^2$) and the subgrade is prone to deep rutting. As subgrade shear strength increases ($>50 \text{ kN/m}^2$) however, these benefits diminish.

Fabric applications have been limited for the most part to high deformation systems where surface deflections of 75 mm or greater are allowable, for example haul and access roads over soft ground. Fabric use below the granular base of pavements has also been promoted in more recent years. But there is no evidence to support improvements via fabric separation or reinforcement in such low deformation systems.

Recent developments in grid technology, however, suggest that the interlock and tensile modulus characteristics of certain grid products might prove beneficial as a reinforcement within the granular base of low deformation systems such as flexible pavements.

Grid reinforcement is used to contribute a confinement effect within a granular layer that reduces strain. The principle of confinement is best illustrated by a pyramid of billiard balls held together at their base by a plastic ball rack. Without a rack at the base, the pyramid of balls would collapse under its own weight. The bottom layer of balls would roll away under the load. But the rack provides confinement against lateral movement at the pyramid's base, and the effect is passed from one layer of balls to the next so the structure is stable. Not only is the pyramid stable due to confinement, it can also support load.

HAAS/WATERLOO TESTS

A research program was performed by Haas, et al. (1) at the University of Waterloo to evaluate the benefit of grid in base layers of flexible pavements.

The purpose of the program was to quantify the benefit of geogrid reinforcement within the granular base of a flexible pavement system (i.e., asphalt concrete surface, granular base and subgrade).

Specifically the experiments had the following objectives:

1. To analyze and explain geogrid reinforcement mechanisms in paved road applications through the use of stress, strain, and deflection measurements.
2. To develop layer coefficients or equivalency factors for geogrid-reinforced, granular base materials.
3. To establish structural design procedures for geogrid reinforced paved roads utilizing the developed layer equivalency factors.

The experimental program consisted of cyclic load tests on both reinforced and unreinforced pavement sections, varying reinforcement locations and varying subgrade strengths. Asphalt surfaces, 75 to 100 mm (3 to 4 inches) thick, were used for all tests. Variables in the test included subgrade bearing capacity, base layer thickness, asphalt concrete layer thickness and grid location within the base layer.

Test Facility

The test facility at the University of Waterloo consisted of a large rectangular box, 4.5 m x 1.8 m x 0.9 m deep (15 ft. x 6 ft. x 3 ft.), constructed with plywood reinforced by a steel frame and lined with galvanized steel sheeting.

Loads were applied by a 300 mm (12 inch) diameter steel load plate driven by a servo hydraulic unit rated at 58 kN (13 kips). Each test section was subjected to an identical loading sequence consisting of a series of dynamic loads followed by a single static load at predetermined cycle counts. The load applied to the pavement surface for both types of loading was 40 kN (9,000 lb.) applying a pressure of 550 kPa (80 psi) through the load plate. The configuration and magnitude of applied load were selected to simulate a set of dual wheels of an equivalent 80 kN (18-kip) single axle load. Dynamic loads were applied at a frequency of 8 cycles per second.

Each test set up was instrumented as illustrated in Figure 1. Five dial gages were placed on the asphalt surface and load plate along with the actuator LVDT to measure surface deflections and permanent deformations of the asphalt surface. In addition, foil type strain gages were placed on the mesh at several locations of increasing radial distance from the load center.

In selected tests pressure cells were placed 35 mm (1.5 inch) below the top of the subgrade to compare differences in stress distribution between reinforced and unreinforced sections.

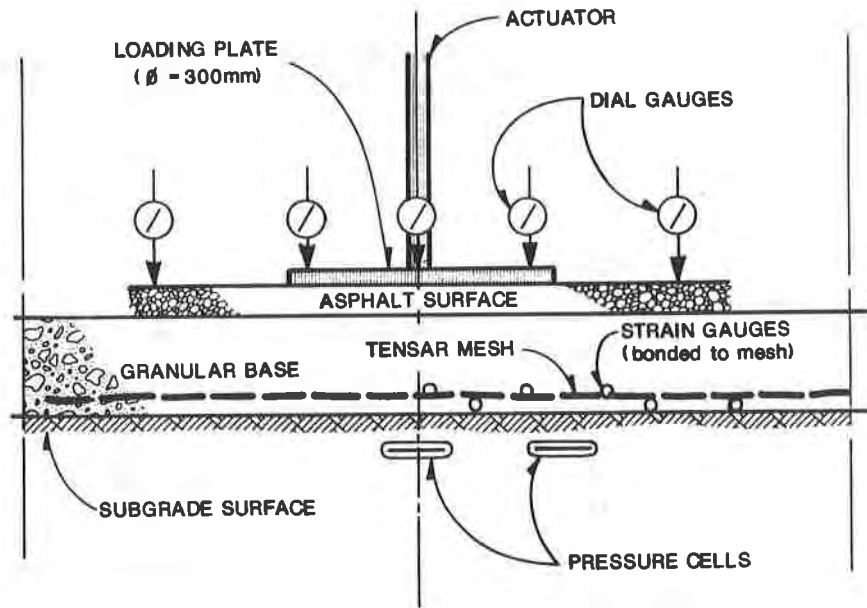


Figure 1 General arrangement of the instrumentation.

Subgrade

The prepared subgrade consisted of a very fine grained beach sand, SP, (99% passing the No. 40 sieve, 32% passing the No. 100 sieve, 4% passing the No. 200 sieve). Because it had an almost uniform grain size, it was ideal for varying support strength by changing the moisture content.

Aggregate Base

The base material for all tests was a well graded crushed stone aggregate, GW, (100% passing the 1 inch sieve, 49% passing the No. 4 sieve, 4% passing the No. 100 sieve, 2.3% passing the No. 200 sieve). The optimum moisture content and maximum dry density were determined to be 6 percent and 23 kN/m^3 (146 lb/ft^2), respectively.

Asphalt Concrete

The asphalt surface layer for all tests was a dense-graded material with 15 mm (0.6 inch) maximum aggregate particle size and a 85/100 penetration grade asphalt cement.

Geogrid Reinforcement

The geogrid used for all tests was TENSAR SS1 Geogrid. The key performance properties of this grid are shown in Table 1.

TABLE 1
TENSAR SS1 GEOGRID

PROPERTIES		TEST METHOD	UNITS	TYPICAL VALUES
Tensile Strength at 2% Strain	M	TTM 1.1 ¹	kN/m (1b/ft)	4.1 (280)
	XM			5.8 (400)
5% Strain	M			8.3 (570)
	XM			12.1 (830)
Junction Strength		TTM 1.2 ³	%	90
Stiffness	M	ASTMD 1388-64	mg-cm x 1000	400
	XM			250
Aperture Size	M		mm (in)	25 (1.0)
	XM			33 (1.3)
Thickness	rib		mm (in)	0.5 (0.02)
	junction			2.8 (0.11)
Polymer				pp ⁴

1 Tensar Test Method (TTM) for single rib tensile strength tested at 50 mm per minute (2 inches) per minute strain rate . . . strength per unit length calculated based on rib count per unit length.

2 M = machine or longitudinal direction of grid.
XM = cross machine or transverse direction of grid.

3 Tensar Test Method (TTM) for strength of junction between machine and cross-machine ribs expressed as % of single rib ultimate strength.

4 pp = polypropylene.

TEST RESULTS

The experimental program was divided into six test series or "loops" with each loop containing four (4) separate tests. Each loop was carefully designed to control certain key variables in order to isolate and examine the effects of the geogrid reinforcement.

Loop 1

The purpose of Loop 1 was to compare performance of reinforced and unreinforced pavement sections with the same base thickness over relatively firm subgrades (CBR=8), and to examine the effects of reinforcement location within the granular base layer. The test results clearly indicated that reinforcement of the base layer improves the deformation resistance of the asphalt surface layer and extends the load life of the pavement with respect to permanent deformation. Figure 2 shows that the reinforced section (Test 2) carried 3 times the number of load cycles than the unreinforced (Test 1) before developing a rut depth of 20 mm (0.8 inches).

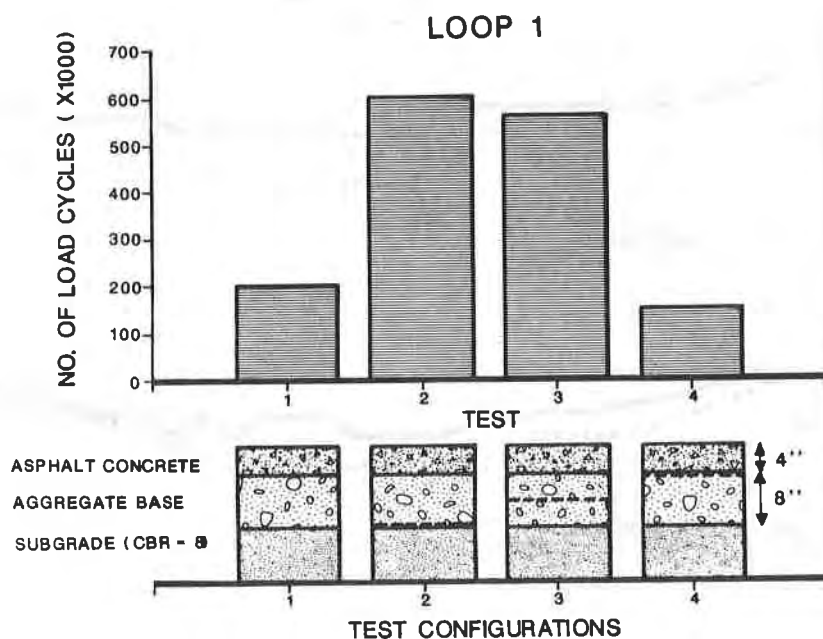


Figure 2 Number of load cycles to yield permanent deformation of 20 mm (0.8 inches). Loop 1.

Figure 2 also notes the significance of grid location on performance. The optimum location was within the lower half of the granular layer and in a zone of high horizontal stress. Reinforcing the top of the granular layer had no positive effect in improving performance. These results are not surprising since the grid is providing tensile reinforcement to the granular base much like rebar in a concrete beam.

Another observation of Loop 1 suggests that grid reinforcement of the base layer is effective in distributing the load and reducing the stress levels acting on the subgrade. A comparison of profiles taken on the subgrade sand before and after testing indicated a punching type of shear failure in the subgrade in the case of the unreinforced section and very little permanent deformation in the reinforced cases of Tests 2 and 3. Furthermore, it can be seen from Figure 3 that the relatively uniform deformation below the reinforced sections of Tests 2 and 3 more closely resembles the deformation that might be expected under a fairly rigid slab.

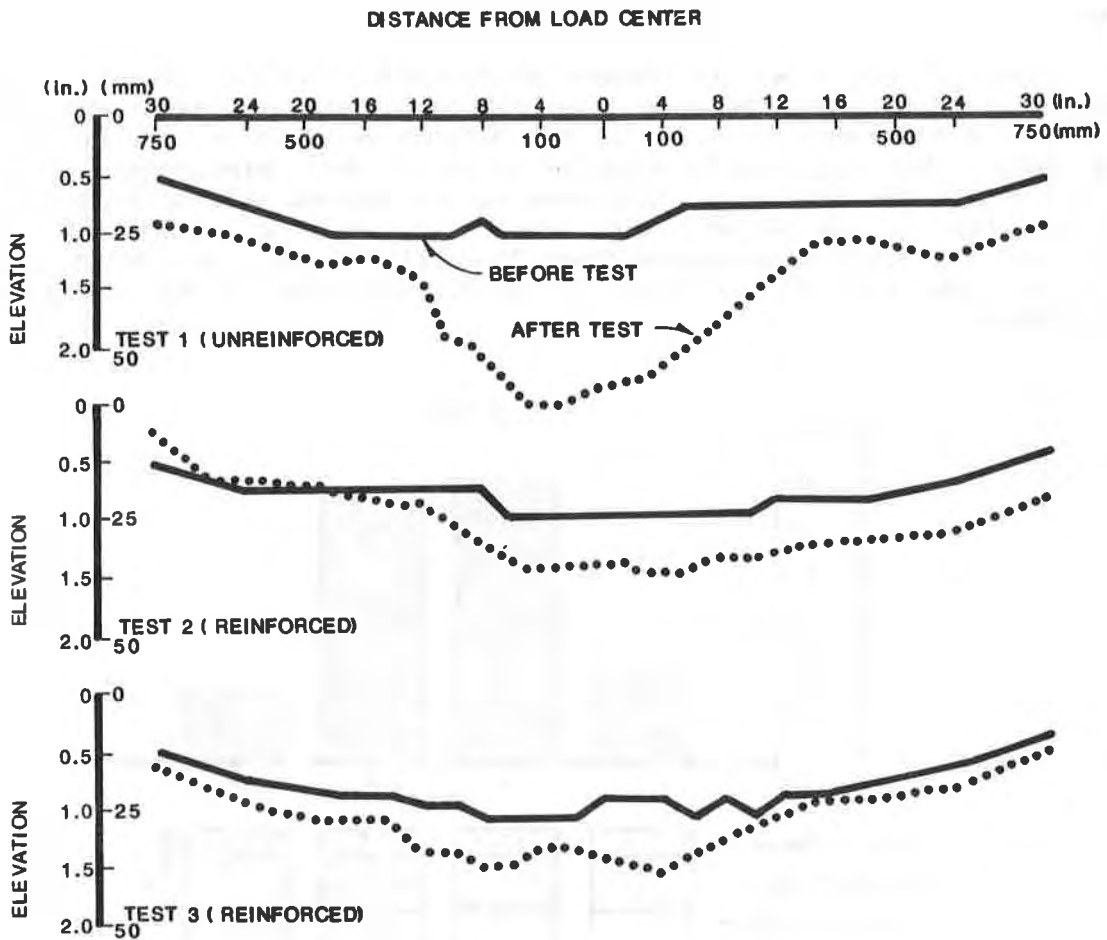


Figure 3 Profiles of the subgrade sand before and after testing. Loop 1.

Loop 2

The second loop was designed to determine the possible reduction in base thickness due to grid reinforcement over marginal strength subgrades (CBR=4). Again, an unreinforced test section was compared to a reinforced test section having the same thickness. In all tests, the geogrid reinforcement was placed at the bottom of the granular layer.

Figure 4 reveals that both 150 mm (6 inch) and 200 mm (8 inch) reinforced sections withstood approximately 3 times more load cycles than the unreinforced 200 mm (8 inch) control section for the same 20 mm (0.8 inch) deformation. In addition, the very thin 100 mm (4 inch) reinforced section performed slightly better than the control section. Thus, the result of the second loop indicated that reductions in base thickness up to 50 percent are possible with the inclusion of geogrid reinforcement.

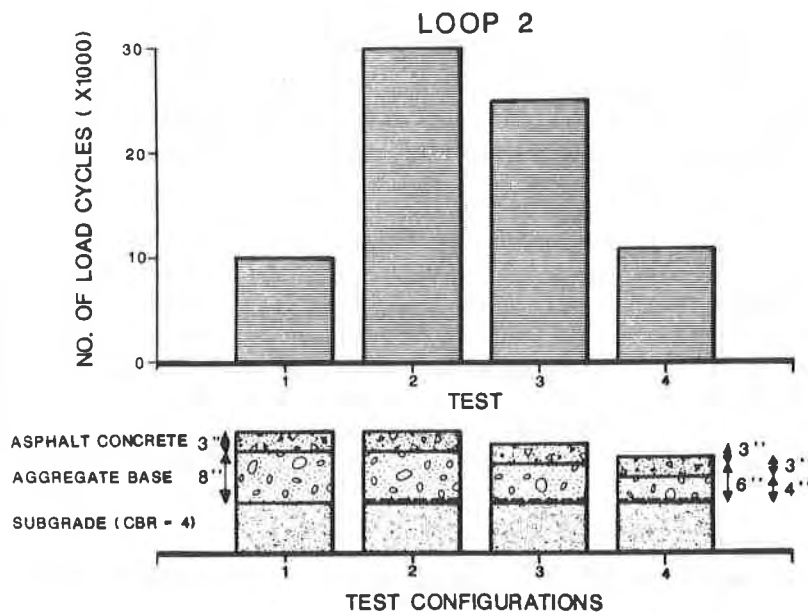


Figure 4 Number of load cycles to yield permanent deformation of 20 mm (0.8 inches). Loop 2.

Loop 3

The purpose of the third loop was to extend the range of granular thicknesses tested and to re-examine the effects of geogrid location. Two 250 mm (10 inch) reinforced sections were tested alongside 250 mm (10 inch) and 300 mm (12 inch) unreinforced sections. The subgrade sand was left in its semi-saturated condition but evaporation and leakage from the corners of the box lowered the moisture content and significantly increased the subgrade strength by the end of the loop.

Therefore, an additional variable was added to this test loop making direct comparison of reinforced and control sections impossible. However, by measuring the CBR value of the subgrade before and after testing, the data was still able to be used in the final program analysis.

Loop 4, 5 & 6

The final three loops (4, 5 and 6) all had weakened subgrades created by mixing peat moss into the top 200 mm (8 inch) of sand. The CBR's of Loops 4 to 6 ranged from 0.5 to approximately 1. Since physical constraints prevented the construction of much thicker pavement sections, the test sections in Loops 4 to 6 were theoretically underdesigned. Therefore, 20 mm (0.8 inch) deformations occurred very early in the load history. Since the pavement sections were underdesigned for the weak subgrade, the failure criteria for comparison analysis was taken to be 38 mm (1.5 inch).

The results of Loop 4 (subgrade CBR = 1.0) indicated that geogrid reinforcement provided a threefold improvement to the service life of a pavement structure over soft ground.

The main objective of Loop 5 was to determine whether there are any advantages gained by pretensioning the reinforcement grid. The results showed that pretensioning of the geogrid had no beneficial effect on the strength of the structure when compared with normal grid placement. This finding suggests that the stiff, prestressed geogrid tested does not require deformation within the pavement system to mobilize reinforcement.

Loop 6 was conducted in order to investigate the grid's effect when it is placed in the subgrade, at the subgrade-granular layer interface, and when it is located at the mid-point and base of the granular layer simultaneously. All tests that included the geogrid performed significantly better at a permanent deformation of 38 mm (1.5 inch). The test which had grid at both the mid level and base of the granular layer was the strongest and did not reach 38 mm (1.5 inch) deformation until 15,000 cycles. This was more than a threefold improvement over the unreinforced section which reached 38 mm (1.5 inch) deformation after 4,000 cycles.

Test Conclusions

The major conclusions drawn from the test program can be summarized as follows:

1. Grid reinforcement reduces permanent deformation in flexible pavement systems.
2. Pavement sections incorporating polymer grid reinforcement in the granular base layer carried three times the number of load applications as conventional unreinforced pavements.
3. Grid reinforcement allowed up to a 50% reduction in the thickness requirements of granular base based on load-deformation performance.
4. Two layers of geogrids, one at the middle and one at the bottom of the aggregate base layer, allowed more than 3 times the number of loads to be carried over very weak subgrades.
5. The optimum location of grid reinforcement is at the bottom of thin bases and at the midpoint of bases 10 inches thick or greater. Over very weak subgrades, optimum benefit may be derived by placing one layer of grid at the bottom of the base and a second layer of grid at the midpoint.

DESIGN GUIDELINE

One of the purposes of this experimental program was to develop design guidelines for grid reinforced flexible pavements. The AASHTO Guide for Design of Pavement Structures (2) is the most widely recognized empirically-based design guide for flexible pavements. Therefore, it was chosen as a basis for analyzing test results and developing design guidelines for reinforced pavements.

Data from the experimental program were used to calculate the structural number, SN (AASHTO Guide) of control (unreinforced) sections in each Loop according to the formula:

$$SN = a_1d_1 + a_2d_2$$

where a_1, a_2 , etc. = layer coefficients for asphalt and base layers, respectively;
 d_1, d_2 , etc. = thickness (in.) of asphalt and base layers, respectively.

For each test Loop, the SN for the control section was calculated using a layer coefficient of 0.40 for the asphalt concrete and 0.14 for the granular base, which are typical values from the AASHTO Guide. These variables remained constant throughout the test program.

Using the AASHTO design nomograph, the design total equivalent 80-kN (18-kip) single axle loads were calculated for the control pavement knowing the SN (as calculated above) and the subgrade soil support value (S). The soil support value (S) was estimated from average in situ CBR determinations.

A load correction factor was then calculated as the ratio of design total equivalent 80-kN (18-kip) single axles (as calculated above) to the actual number of 40 kN load repetitions to failure of the section from the experimental results. The load correction factor was applied to account for differences between laboratory and field loading patterns and arbitrary failure criteria.

The load correction factor was then used to calculate the design equivalent 80-kN (18-kip) axles for reinforced pavement sections within each test Loop. This was done by multiplying the actual number of 40 kN load repetitions to failure by the load correction factor. An estimate of the structural number (SN) of the reinforced pavement was then derived from the AASHTO design nomograph using the known soil support value (S) and the design equivalent 80-kN (18-kip) single axles.

The structural number of the granular base layer (SN_{gr}) was calculated from the formula:

$$SN_{gr} = SN - a_1 d_1$$

where a_1 = layer coefficient for the asphalt concrete (assumed = 0.4)
 d_1 = thickness of the asphalt concrete layer in the test section (inches).

The ratio of granular layer coefficients reinforced/unreinforced (A_r/A_u) was then determined using the AASHTO formula:

$$\frac{A_r}{A_u} = \frac{(SN_{gr})_r \times d_u}{(SN_{gr})_u \times d_r}$$

where

$(SN_{gr})_r$ & $(SN_{gr})_u$ = structural number of reinforced and unreinforced granular layers, respectively
 d_r and d_u = granular base thickness of reinforced and unreinforced sections.

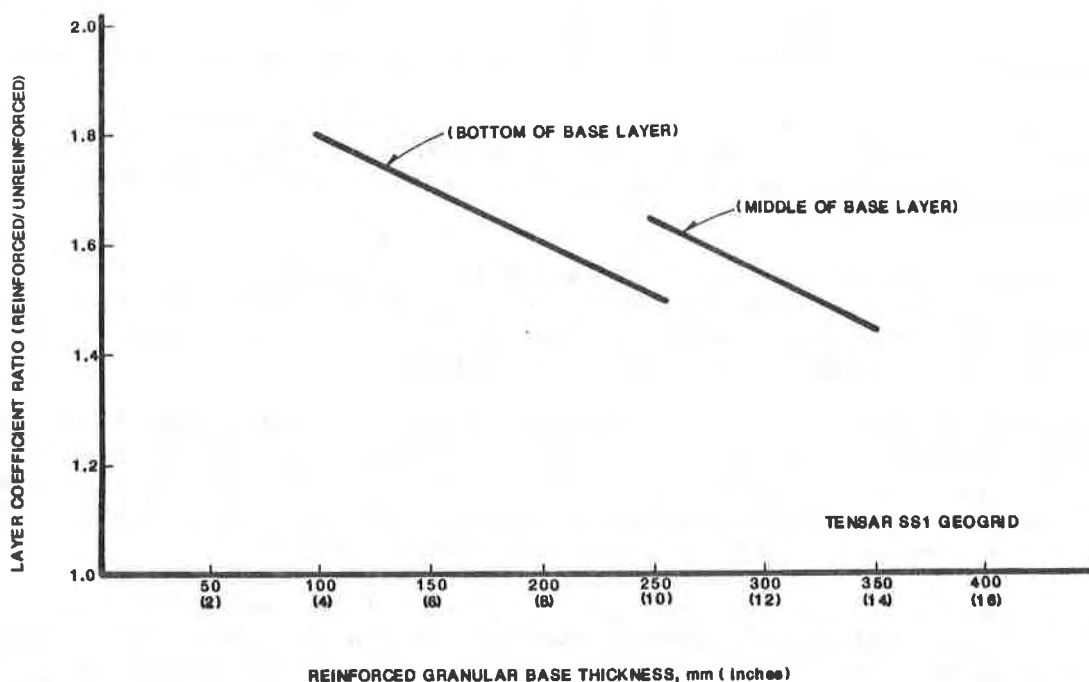


Figure 5 Relationship for layer coefficient ratio, (A_R/A_U) (reinforced/unreinforced) as a function of reinforced granular base thickness.

The ratio A_R/A_U expresses the effect of the geogrid on the structural capacity of the granular base layer. The higher this ratio the higher the structural layer coefficient of a reinforced base layer in comparison with a conventional unreinforced layer.

A close relationship was discovered between the layer coefficient ratio and reinforced base thicknesses as shown in Figure 5. The layer coefficient ratio was found to be greatest for a 100 mm (4 inch) reinforced base layer approximating a value of 2. As reinforced base thicknesses increased, the layer coefficient ratio decreased to a factor of approximately 1.5 for a 250 mm (10 inch) thick base layer, reinforced at the bottom.

For a reinforced base thicknesses of 250 mm (10 inch) a further increase in the layer coefficient ratio was found by placing geogrids at the midpoint of the layer. The layer coefficient would again decrease as reinforced base thickness increased beyond 250 mm (10 inches). The layer coefficient ratio determined from Figure 5 can be used as a "multiplier" to calculate the structural layer coefficient of a grid-reinforced granular base.

In order to make the design relationships adaptable to other methods of design, a simple chart was developed to show structural equivalencies between unreinforced and grid reinforced pavements. Using this chart, conventional unreinforced design can be quickly converted to reinforced design alternatives.

The graph of Figure 6 was developed by calculating the thickness requirements for unreinforced bases through a range of reinforced base thicknesses and corresponding layer coefficient ratios determined from Figure 5. In order to keep the relationship as simple as possible, a conservative linear relationship was then plotted to include the transition from reinforcement at the bottom of the base to that of reinforcing at the midpoint. This, of course, occurs when the required thickness of reinforced base exceeds 250 mm (10 inch).

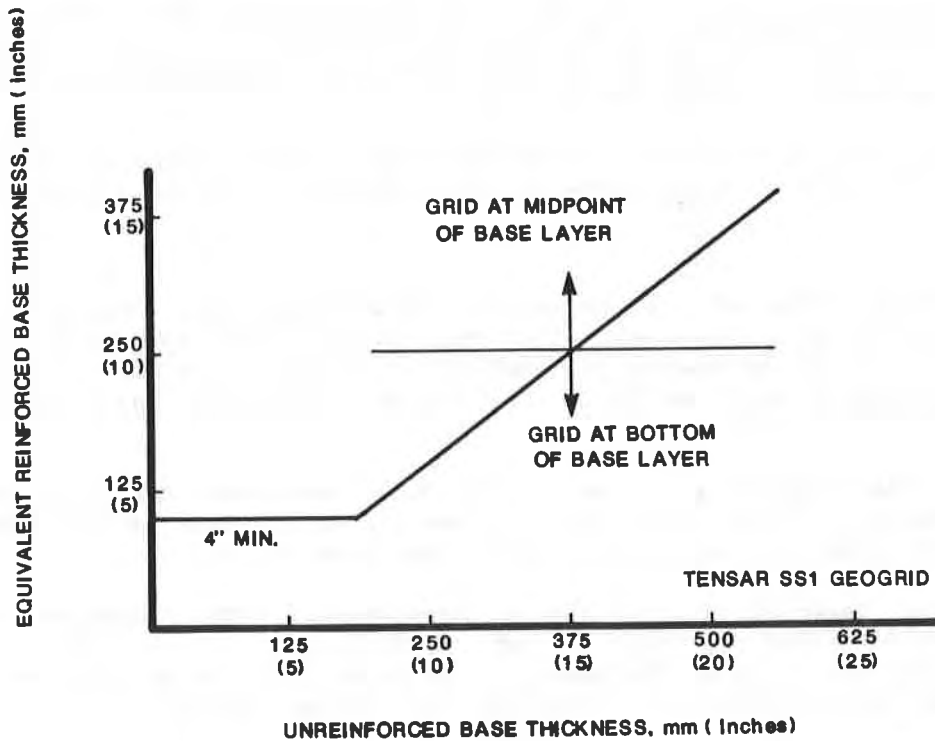


Figure 6 TENSAR Geogrids reinforced base thicknesses for flexible pavements.

MECHANISTIC ANALYSIS

In addition to the empirical approach for developing the above design guidelines, a mechanistic analysis of the test data was also carried out to determine whether elastic layer theory is applicable to reinforced pavements.

Elastic layer theory has been introduced into the new AASHTO Design Guide as an alternative approach to design and is increasingly being used to predict stresses and strains within a pavement under an applied load. Calculated strains are then used to limit the occurrence of specified distress modes. For example, tensile strain at the bottom of the asphalt layer can be limited to preclude fatigue type cracking and the compressive strain on the subgrade can be used to control rutting.

Because of the relatively thin sections in this experimental program rutting was the overriding criterion. The analysis was therefore limited to relating the permanent deformations to strain levels in the subgrade.

An iterative technique was used to solve for the elastic moduli of the asphalt, base and geogrid layers. For the conditions of this study the layer representing the grid was determined to have an elastic modulus of 6.9 MPa (100,000 psi) when represented by a thickness of 10 mm (0.4 inch).

Predicted vertical strains at the top of the subgrade were then compared with the number of load applications to failure determined by the test results. The relationship developed (3) was found to be similar to design criteria developed by other investigators to predict rutting.

Although more work is required to develop a mechanistic approach to design, it does appear that elastic layer theory can be applied to reinforced pavements.

SUMMARY

The strengthening effect of grid in pavement base layers comes from interlock with and confinement of base particles. Test results show that grid reinforcement can decrease the rate of permanent deformation in pavement structures. Therefore, reinforced pavements will support more loads or can be built with reduced thickness.

Empirically based design guidelines have been developed for grid reinforced flexible pavements. These guidelines incorporate equivalency factors between unreinforced and reinforced base layers that range from 1.5 to 1.8.

The improvement benefits of grid can be incorporated into a pavement design by applying these equivalency factors to layer coefficients such as used in the AASHTO Design Guide for Flexible Pavements. The simplified design chart presented in this paper has been developed to abbreviate that design process.

A mechanistic analysis of test data suggests that grid reinforcement benefits can be analyzed by elastic layer theory.

The concept of base stabilization is far from new. In fact lime, cement and other pozzalons have long been used to increase the structural capacity of both base and subgrades. Grid reinforcement provides an alternative to these base treatments that is less sensitive to moisture conditions and field installation, yet one that strengthens the base through confinement.

REFERENCES

1. Walls, J., Penner, R., and Haas, R., "Final Project Report on TENSAR Reinforced Granular Bases," Report to The Tensar Corporation, University of Waterloo, January 31, 1985.
2. American Association of State Highway and Transportation Officials, "AASHTO Guide for Design of Pavement Structures", 1986.
3. Penner, R., Haas, R., Walls, J., and Kennepohl, G., "Geogrid Reinforcement of Granular Bases," Paper presented to Roads and Transportation Association of Canada, October, 1985.

KAZERANI, B. and JAMNEJAD, G.H.
Sunderland Polytechnic, England

Polymer Grid Cell Reinforcement in Construction of Pavement Structures

1. ABSTRACT

The stabilisation technique discussed in this paper involves confinement of soil in a honeycomb type polymer grid cell reinforcement developed at the WES. The system is comprised of vertical walls joined together intermittently to provide discrete and stable cells open at the top and bottom. In a grid cell reinforced pavement structure the lateral movement and shear failure are resisted by both the tensile hoop strength of the cell walls and the passive resistance of the full adjacent cells, thereby enhancing its structural performance and in-service life, as well as reducing associated costs. A geotechnical testing facility incorporating a servo-controlled hydraulic actuator was used to carry out large scale sustained repeated and monotonic plate loading tests on a number of reinforced and unreinforced pavement arrangements. The effectiveness of the grid cells when filled with poorly and well graded granular fill was studied. The surface deformation and transmitted stresses at base/subgrade interface were monitored. A computer program based on the finite element method of analysis was used to predict the theoretical stresses and deformations. The results of this study demonstrate clearly that grid cell reinforcement significantly improves the load/deformation and stress distributing characteristics of pavements.

2. INTRODUCTION

The construction of unbound pavements and temporary access or haul roads often requires stabilisation of the constituting fill materials. The conventional methods include compaction, chemical treatment and cement stabilisation. These techniques improve the shear strength of granular materials in an attempt to achieve an enhanced pavement performance. The increase in stiffness and compressive strength derived from the addition of cement, for example, is frequently achieved at the expense of increased brittleness in respect of tensile strains.

However, mechanically stabilised bases with geotextiles and geogrids give stiffness advantages without the disadvantages associated with brittle failure. Extensive research work has been conducted to evaluate the most influential parameters affecting the structural behaviour of the synthetic reinforced pavements (1,2,3,4).

This paper describes the effectiveness of using a three-dimensional grid cell confinement system for the construction of unbound pavements. An illustration of the grid cell network and its dimensions are shown in Plate 1 and Table 1 respectively.

Plate 1. Partially filled grid cell confinement system

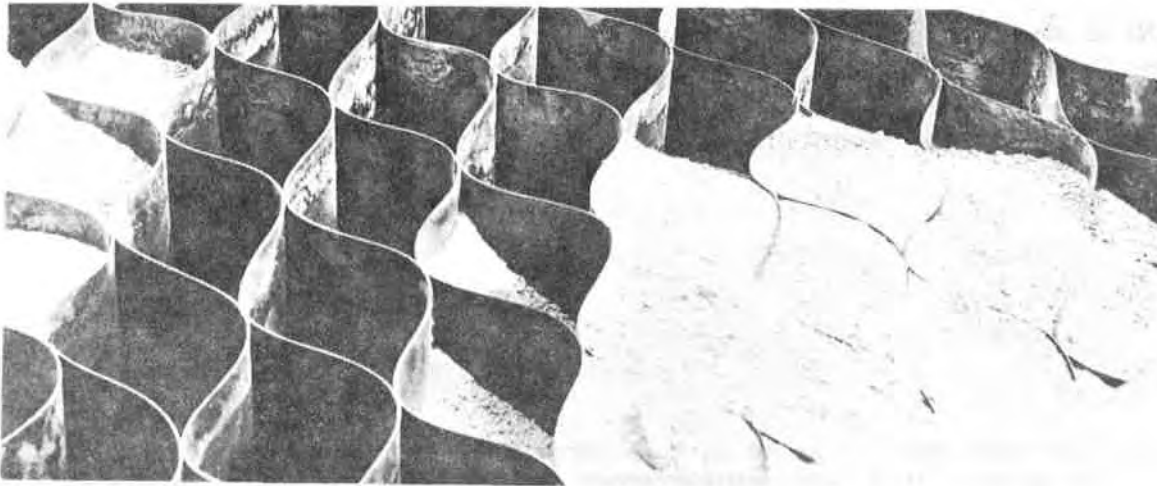


Table 1. Grid cell dimensions (by courtesy of Presto Products)

Expanded dimension	2.5m x 6m x 20cm
Collapsed dimension	3.4m x 13cm x 20cm
Panel thickness normal	0.119cm
Weight	3.1 kg/m ³
Cell area	265cm ²

When the grid cell confinement system is filled with a granular fill and is subjected to monotonic or repeated loading, each cell shares its load with the adjacent cells to form a well stabilised composite material in which lateral movement and shear failures are resisted by both the tensile hoop strength of the cell walls and the passive resistance of the adjacent cells. As a result, a grid cell reinforced pavement structure offers a substantial increase in stiffness and the ability to support large traffic loads with minimal vertical deformation.

Research on this form of synthetic material was initiated at the WES, (5,6). The grid cell system is commercially known as the "Geoweb" and is manufactured in the U.S.A. (7). The grid cell confinement concept can be used in construction with low grade materials which may not otherwise exhibit suitable behaviour when subjected to long term repeated loading, (8). The inclusion of grid cell reinforcement in pavement structures could lead to substantial reduction in construction thickness, see Fig.1.

The grid cell confinement media can be used effectively in conjunction with other materials which may be brittle in nature or may deteriorate when subjected to repeated loading. The confinement of these materials improves the overall structural behaviour of the composite layer.

The improvement in the bearing capacity of a grid cell reinforced pavement is partially due to the confinement mechanism which prevents failure wedges forming in the base, see Fig.2. The frictional interlock between the fill material and the

cell walls assists in the distribution of concentrated loads to adjacent cells, thereby reducing transmitted stresses at base/subgrade interface.

3. GEOTECHNICAL TESTING FACILITIES

Large scale experiments were conducted in a concrete pit with plan dimensions of 2m x 2m and 2m deep. A firm subgrade was provided using a 600mm thick layer of well graded and well compacted granular medium, prepared using a plate vibrator, and a softer subgrade by means of 150mm thick polystyrene blocks. The physical properties of the subgrades used are shown in Table 2.

A servo-controlled hydraulic actuator (Dartec, capacity ±300 kN and stroke ±150mm) was used for the application of monotonic and sustained repeated plate loading tests, see Fig.3. Sustained-repeated loading was chosen to simulate the worst cumulative permanent deformation of the pavement under repeated loading. The actuator was mounted on a reaction frame over the test pit. Monotonic loadings had a displacement rate of 3mm/min. A frequency of 0.2 Hz was selected for the sinusoidal sustained-repeated loading patterns. When possible, a maximum number of 180,000 cycles were applied. The magnitude of sustained load was 0.5 kN. A plate bearing of 300mm diameter was used throughout the testing programme.

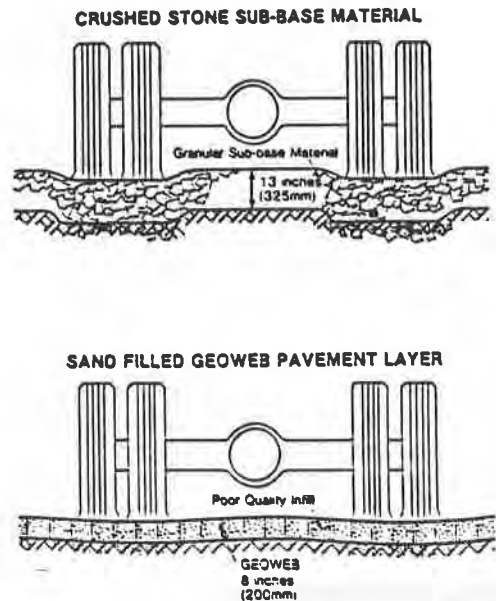


Fig.1 Thickness of reinforced and unreinforced sub-base of equal flexural stiffness and bearing capacity (by courtesy of Presto Products)

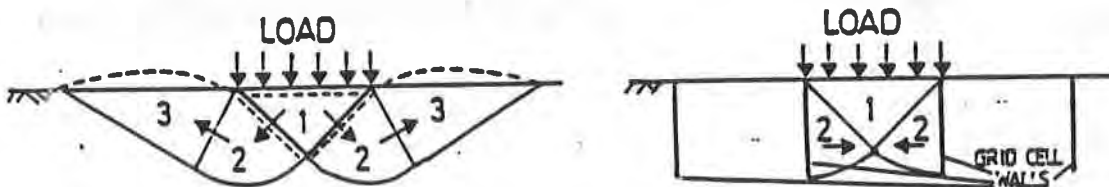


Fig.2 Unreinforced and reinforced soil behaviour

The reinforced base courses were prepared by placing expanded grid cells on the subgrade, and filling each cell with poorly or well graded fill. In the absence of grid cells an equivalent thickness of fill, i.e. 200mm, formed the unreinforced bases. The reinforced base layers were provided with a 30mm cover course in order to prevent direct application of the load onto the cell walls.

Table 2. Properties of firm and soft subgrades

<p><u>Firm Subgrade : CRUSHED DOLOMITE</u></p> <p>Well graded soil with particles slightly angular in shape Angle of friction = 43° ; specific wt. = 24.5 kN/m^3 Modulus of Subgrade Reaction = $0.164 \text{ N/mm}^2/\text{mm}$</p> <p><u>Soft Subgrade : POLYSTYRENE</u></p> <p>Type - normal density Elastic modulus 5 N/mm^2 Poisson's ratio 0.42</p>
--

For the paved systems, rectangular block paving units provided a rigid and stable surface course. The blocks were laid in herringbone pattern and restrained at the edges to mobilise full interlocking mechanism between the individual blocks, and spread the applied load over a wider area of the test bed. A typical cross-section of pavements is shown in Fig.4.

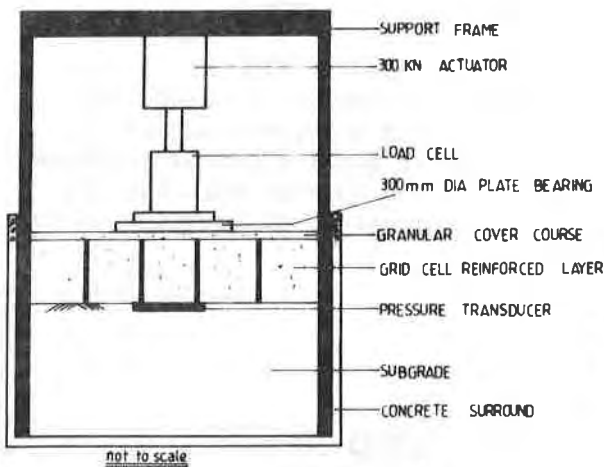


Fig.3 Schematic diagram of the testing facilities

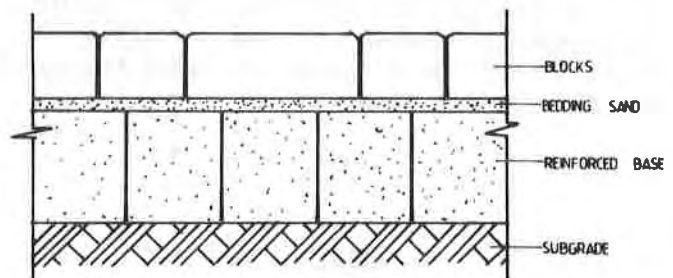


Fig.4 A cross-section of reinforced pavement structure

4. THE EXPERIMENTAL INVESTIGATIONS

The experimental results for two different pavement arrangements are shown in Fig.5. It is clear that the cumulative surface deformation of the grid cell reinforced pavement has significantly reduced. This can be attributed to the confinement mechanism and to the additional stiffness of the base layer provided by the inclusion of the grid cells. The unreinforced pavement sustained approximately 60% greater deformation after the application of 80,000 cycles of load compared with that of the reinforced pavement subjected to the same number of load repetitions.

Evidently the inclusion of the grid cells considerably improves the mechanical properties of the poorly graded granular fills by preventing the degradation of the fill particles.

From Fig.5 it can also be observed that the stresses at the base/subgrade interface are reduced due to the inclusion of the grid cells.

It is interesting to note that the stresses at base/subgrade interface under repeated loading reduce as the number of cycles increases. In the case of the reinforced unpaved structure, a drastic reduction in transmitted stresses was detected after approximately 16000 cycles. This can be attributed to the compaction action of cyclic loading which improves the interlock between grid cell and fill material, resulting in a semi-rigid layer capable of transmitting the applied concentrated load to a larger area.

The reduction in stresses is due to the ability of the system to transmit the applied stresses to a large interface area, and to the transformation of applied load to frictional force between soil and grid cell walls.

The effects of providing a rigid and stable surface course, i.e. concrete blocks, were also investigated. This easily constructed surface course reduces the cumulative deformation by approximately 80%. Overall, the addition of paving blocks considerably enhanced the structural performance of the reinforced pavement.

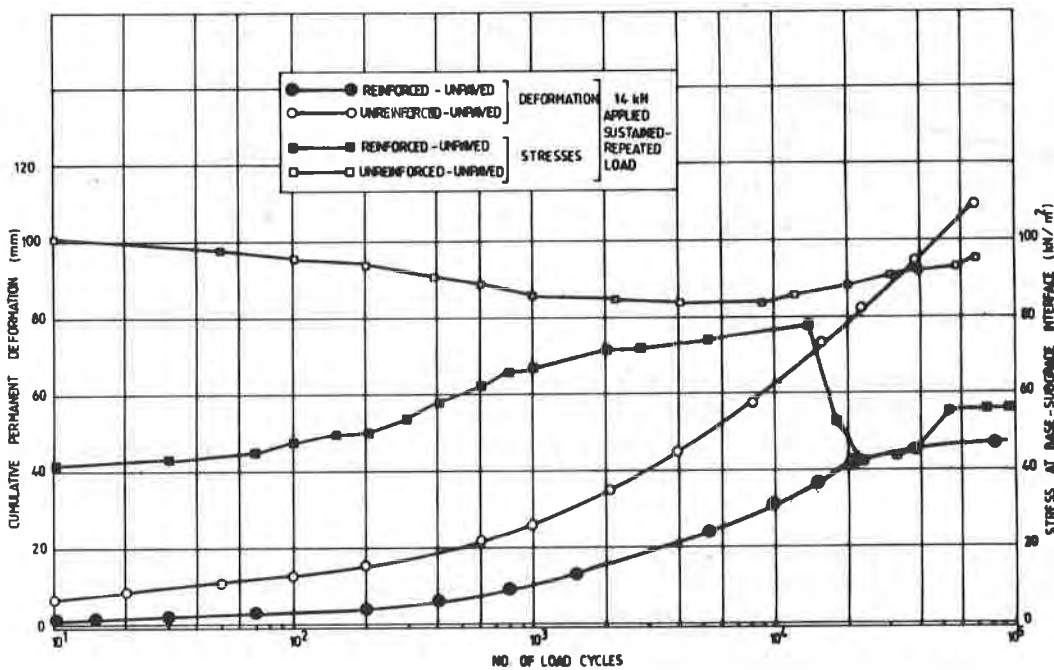


Fig.5 Load/deformation and stress distribution characteristics of pavements with poorly graded fill overlying the firm subgrade

Figs.6 and 7 present results from plate loading tests on different pavement arrangements with a soft subgrade. The soft subgrade was simulated using blocks of medium density polystyrene. Two types of base soil were tested, i.e. poorly graded and well graded. The effect of reinforcement on the cumulative deformation of pavement with poorly graded base soil is illustrated in Fig.6. The cumulative deformation of the reinforced structure after 20000 loading cycles is approximately 60% of that of unreinforced pavement.

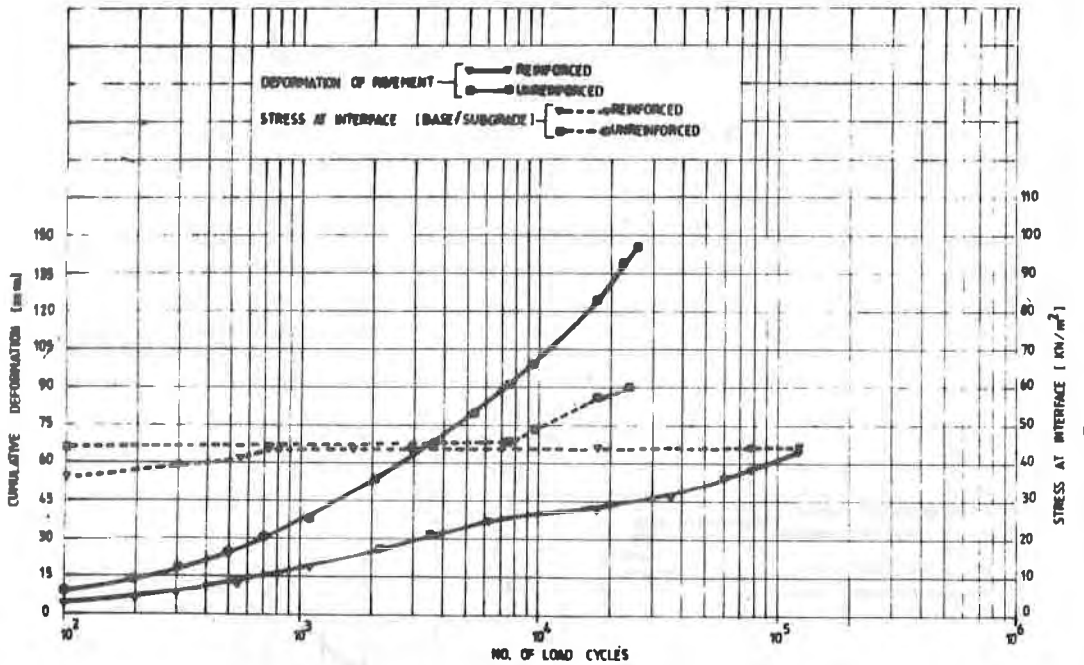


Fig.6 Deformation and interface stresses of pavements with poorly graded base soil on the soft subgrade

Reduction in the transmitted stresses at the base/subgrade interface for a poorly graded base soil is not substantial, whereas for a well graded soil (Fig.7) it is more pronounced. Fig.7 demonstrates that the deformation characteristics of the pavements with well graded material are also improved by the use of grid cell reinforcement.

Further experimental investigations are currently being conducted to establish an allowable load level based on permissible vertical strain at the interface of the reinforced layer and supporting foundation media.

5. THEORETICAL ANALYSIS OF THE PAVEMENTS

The traditional methods of analysis for the prediction of deformations and stresses are based on the elastic theory. Unfortunately, such procedures do not provide reliable estimates of the structural behaviour of grid cell reinforced pavements. This is due to uncertainties over boundary constraints and difficulties in modeling the stress-strain relationship for the soil-grid composite system.

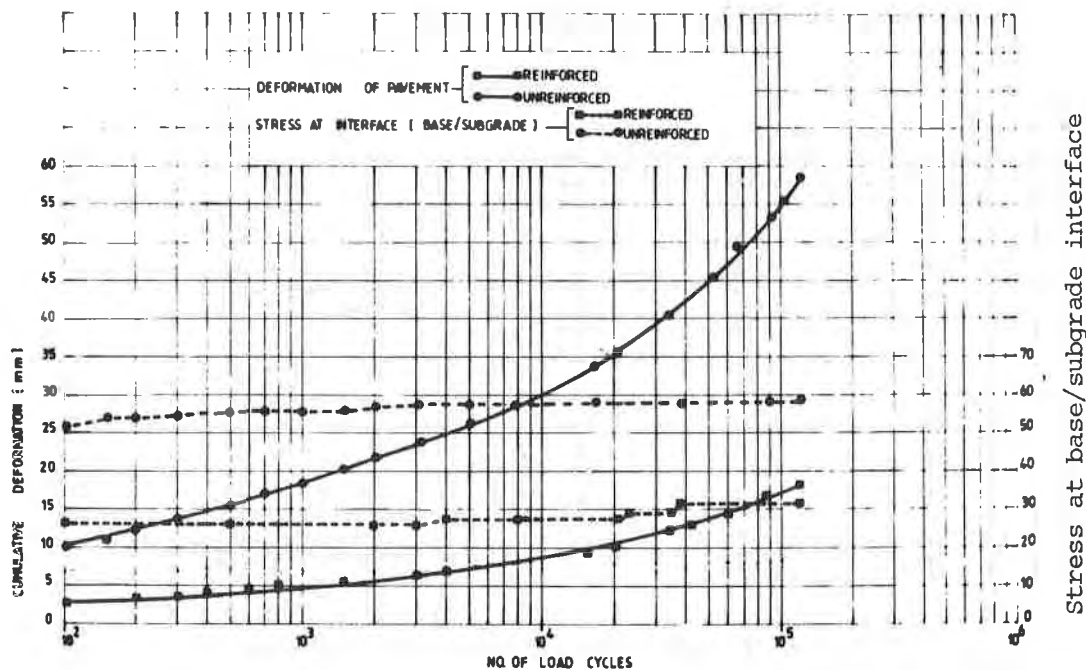


Fig.7 Deformation and interface stresses of pavements with well graded base soil on the soft subgrade

A finite element method of analysis was adopted to predict the stresses and deformations of pavement structures. A suite of finite element programmes (PAFEC) was used to perform linear axisymmetric analysis of the pavements using four noded quadrilateral isoparametric elements. A typical finite element mesh is shown in Fig.8. This approach has also been used by other investigators (9,10).

A Clegg hammer (11) was used to measure the in-situ elastic moduli of the reinforced and unreinforced base layers. The values obtained are shown in Table 3. Evidently, the stress-strain relationship shows a marked improvement due to the confinement of fill material within polymer grid cells.

Table 3. Elastic constants for different layers

Type of layer	E (N/mm ²)	Poisson's ratio
Reinforced base with poorly graded fill	13.72	0.23
Unreinforced base with poorly graded fill	6.86	0.40
Subgrade (firm)	48	0.30
Reinforced base layer with well graded fill	21.72	0.17
Unreinforced base layer with well graded fill	10.86	0.32
Subgrade (soft)	5	0.42

Using the finite element programmes of PAFEC, and the properties shown in Table 3, the theoretical deformations and stresses for different pavements were determined. Table 4 present typical experimental and predicted values of surface deformation and interface stresses. The results indicate an acceptable comparability between

the experimental and the predicted behaviour of the pavements.

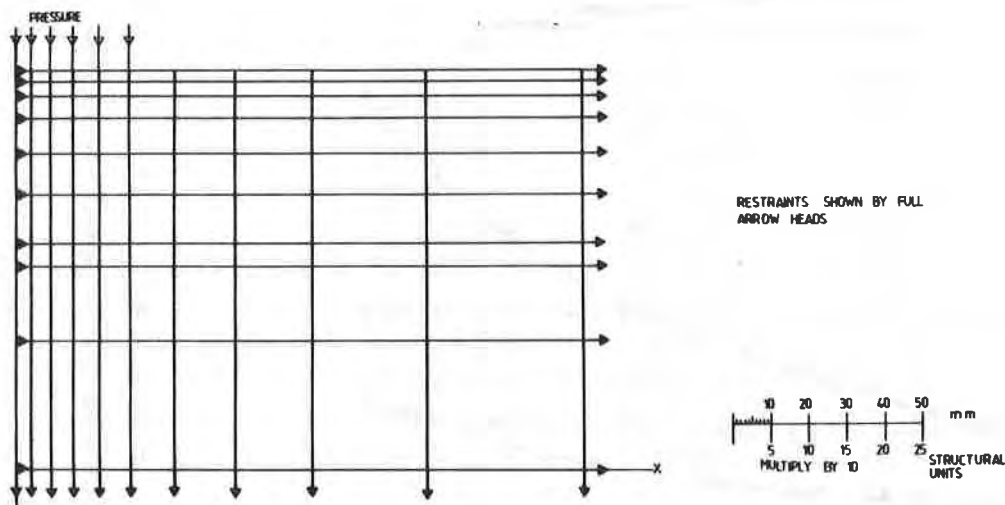


Fig.8 Typical finite element mesh for axisymmetric analysis of pavement structures

Table 4. Experimental and predicted stresses and deformations for two pavement structures with a firm subgrade

Type of fill	Applied Stress kN/m ²	Elastic surface deformations (mm)		Interface Stresses (kN/m ²)	
		Exp.	Predicted	Exp.	Predicted
Well graded	212	2.44	2.11	38	68
Poorly graded	198	2.10	2.71	48	60

The experimental and the predicted values of elastic surface deformation and stresses at the base/subgrade interface with the applied surface stresses for reinforced pavements with poorly graded fill are graphically represented in Figs.9 and 10 respectively.

The analysis presented in this paper considers constant values of 'E' for the computational procedures. However, the stress-strain relationship for reinforced and unreinforced pavements exhibit non-linear behaviour. This type of relationship can be modelled by adopting a piece-wise linearisation of the stress-strain curve. The changes in loading conditions can be implemented in a series of increments. Analytical work is currently being undertaken to adopt a non-linear methods of analysis to predict the deformation and stresses in grid cell reinforced pavements.

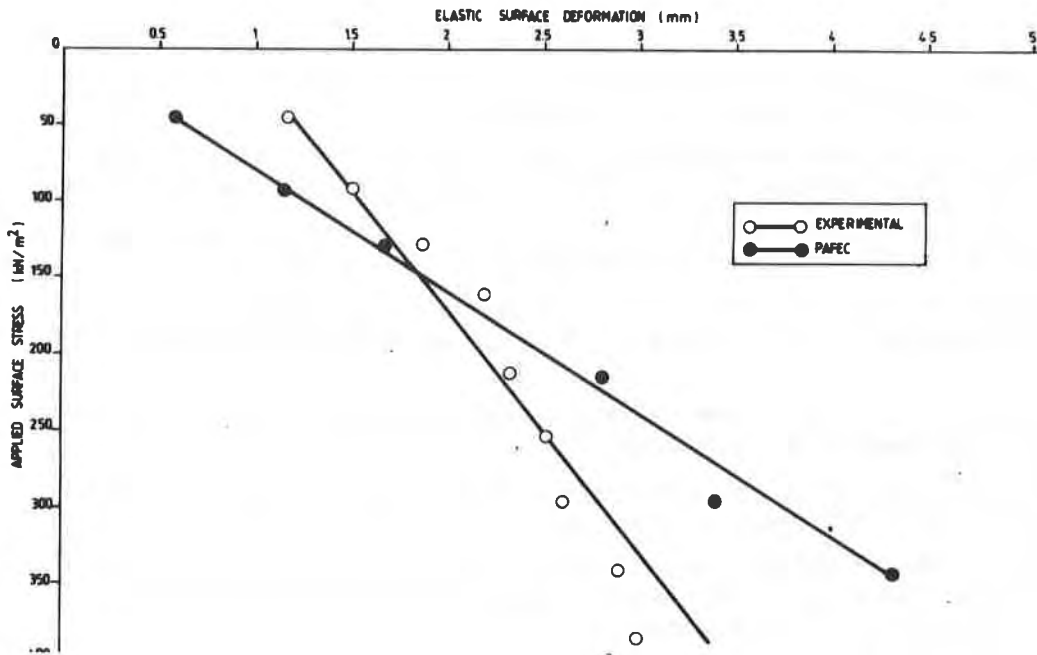


Fig.9 Experimental and predicted surface deformation for a reinforced pavement (unpaved) with poorly graded fill and overlying a firm subgrade

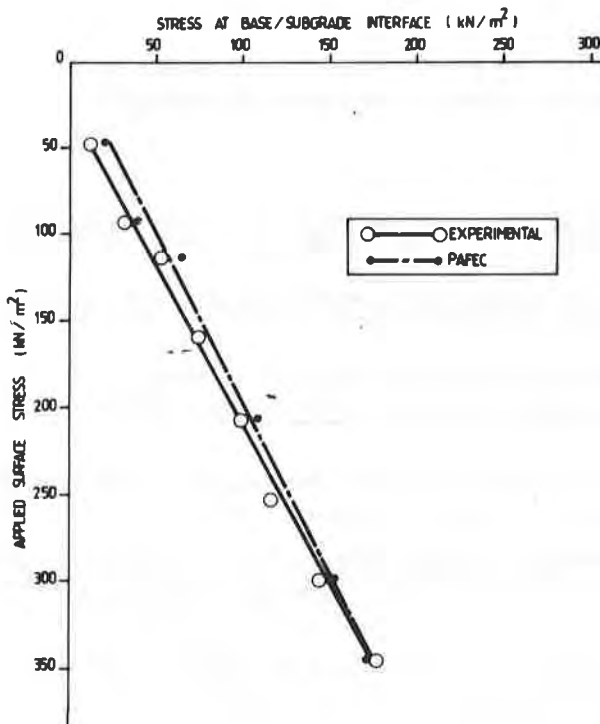


Fig.10 Experimental and predicted interface stresses for a reinforced pavement (unpaved) with poorly graded fill and overlying a firm subgrade

6. CONCLUSIONS

The conclusions drawn from the present studies on the effectiveness of polymer grid cell reinforcement of base layers are as follows:-

- 1) Load-deformation and stress distributing characteristics of poorly graded materials can be significantly improved by the grid cell reinforcement system.
- 2) The behavioural characteristics of a base layer with well graded soil are also improved when it is reinforced with the polymer grid cell media.
- 3) The cyclic response of a grid cell reinforced base is considerably improved, and cyclic degradation is retarded, when the base is overlaid by block paving units.
- 4) The elastic properties of the base layer are significantly improved when reinforced with the polymer grid cell media.
- 5) Finite element analysis is a satisfactory technique in predicting the performance of a soil/grid cell composite structure.
- 6) The grid cell reinforcement of a granular base layer reduces the thickness requirements of an equivalent unreinforced layer by approximately 20-30% depending on the soil elastic properties.
- 7) A design procedure for grid cell reinforced pavement structures could be developed, based on limited allowable vertical compressive strain at the base/sub-grade interface.

ACKNOWLEDGEMENT

The authors wish to acknowledge the support of the Science and Engineering Research Council through the research and development grant, reference GR/D/O8159.

REFERENCES

- 1) Jewell, R.A. "Some Effects of Reinforcement on the Mechanical Behaviour of Soils", Ph.D. Thesis, University of Cambridge, March 1980.
- 2) Mashour. "Behaviour of Model Granular Embankments With and Without Fabrics", Ph.D. Thesis, University of Strathclyde, 1979.
- 3) Brown, S.F. "The Potential of Fabrics in Permanent Road Construction", Proceedings of the Conference on Textiles in Civil Engineering, UMIST, Manchester, 1978.
- 4) Ruddock, E.C. "Fabrics and Meshes in Road and Other Pavements: A-State-of-the-Art Review", Technical Note, CIRIA, London, October, 1977.
- 5) Webster, S. and Watkins, J.E. "Investigation of Construction Techniques for Tactical Bridge Approach Roads Across Soft Ground", Technical Report S-77-1, U.S. Army WES, Vicksburg, 1977.
- 6) Mitchell, J.K. and Kavazanjian, E. "Analysis of Grid Cell Reinforced Pavement Bases", Technical Report GL-79-8, U.S. Army WES, Vicksburg, 1979.
- 7) Presto Products Incorporation. "Introducing Presto Road Base", Internal Report, Wisconsin, February 1982.

- 8) Jamnejad, G., Kazerani, B, Harvey, R.C. and Clarke, J.D. "Grid Cell Reinforcement in Foundation Engineering", Proceeding of 14th Conference on Building Foundation, Brno, Czechoslovakia, November 1986.
- 9) Andrawes, K.Z., and McGown, A. et al. "The Finite Element Method of Analysis Applied to Soil-Geotextiles System", Proceeding of International Conference on Geotextiles, Las Vegas, 1982.
- 10) Al-Hussani, M.N. and Radhakrishnan, N. "Analysis of Plane Strain Tests using the Finite Element Method", Proceeding of Conference on Application of Finite Element Method, Vicksburg, 1972.
- 11) Clegg, B. "Design Compatible Control of Basecourse Construction", Proceeding of Australian Road REsearch, No.18, Vol.2, June 1983.

HANNON, J.

California Department of Transportation, U.S.A.

MINER, J. and DONAHUE, M.

Phillips Fibers Corporation, U.S.A.

AC Overlay Strategies for PCCP Pavement Using Asphalt Saturated Textiles

ABSTRACT

Three basic asphalt concrete (AC) overlay strategies are presented which provide a variable level of service for rehabilitating distressed portland cement concrete pavements (PCCP). These strategies vary from a thin 2.5 cm (1") fabric-reinforced AC overlay to a thick (10.7 cm or 4.2"), fabric-reinforced AC overlay with cracking and seating of the PCCP (for a rehabilitation of mainline pavements for a high level of service subject to heavy truck traffic).

The mechanisms of reflection cracking and PCCP joint displacement are addressed in development of the three overlay strategies. An asphalt saturated textile membrane (paving fabric) is used as a combined stress relieving interlayer and moisture barrier to improve overlay performance. Several case histories are described and a generic fabric specification is provided.

INTRODUCTION

Many state and local highways constructed of portland cement concrete pavement (PCCP) have achieved their design life, and are in poor condition. This paper addresses rehabilitation design strategies for these pavements using paving fabric with asphalt concrete (AC) overlays. The optimum rehabilitation strategy delays and limits cracking of the overlay, thereby lengthening pavement life for a given level of service.

Three design strategies for AC overlays on PCCP that provide different levels of service will be discussed in this paper: 1) design strategy 1, a 2.5 to 7.6 cm (1 to 3") AC surface course, placed over the asphalt-textile, which is installed directly on the PCCP, 2) design strategy 2, which, in addition to the features of design strategy 1, includes a 2.5 to 5 cm (1 to 2") AC leveling course beneath the asphalt-textile and, 3) a 7.6 cm (3") AC surface course over the asphalt-textile, which is installed onto a 3 cm (1.2") AC leveling course, with the PCCP having been cracked and seated. Considerations for the overlay design include: condition of the PCCP prior to the rehabilitation, maximum daily and seasonal temperature differential, anticipated time to cracking and failure, and initial cost. The focus of this report is to summarize theory and laboratory testing, and to support this through case histories, to show that the use of the asphalt-textile system can optimize cost and increase longevity for AC overlays on PCCP.

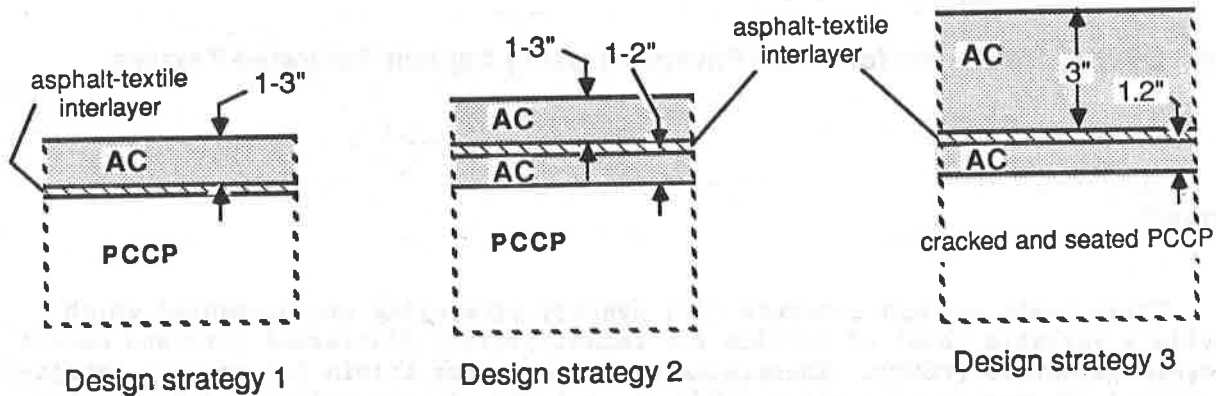


Figure 1

MECHANISMS OF REFLECTIVE CRACKING

The objective of an AC rehabilitation overlay on PCCP is to lengthen the life of the pavement by restoring both rideability and structural adequacy to the existing pavement. Reflective cracking in the AC overlay can impede this objective and accelerate pavement failure. The mechanisms of reflective cracking must be understood to properly develop a rehabilitation strategy.

Reflective cracking generally results from displacements in the underlying PCCP (1). The displacements can be a combination of deflection under a moving wheel load and thermal strain from temperature variation. The severity of reflection cracking in the AC overlay is dependent on: 1) the magnitude and number of wheel load applications which, with the modulus of rigidity, determine the magnitude of joint deflections and 2) the magnitude and frequency of the thermal strain. Deflection in response to moving wheel loads may occur at unsupported joints between PCCP slabs or in areas of local structural weakness.

Stormwater can infiltrate into the area beneath the PCCP joints; in the absence of positive drainage (i.e., a road that does not allow water to drain freely out of the base), this water can remove unstabilized, fine-grained material through pumping caused by the deflection of the slab ends (Fig 2a); erosion of the base under the joints, and eventual slab faulting with poor ride results from this action. Additionally, a difference in deflection between adjacent slabs may develop. If sufficiently large, this differential deflection, unless corrected, will cause reflective cracking in any thin AC overlay placed over these pavements, as shown schematically in Figure 2b. An ideal rehabilitation overlay should therefore provide permanent waterproofing, i.e., by a fabric interlayer,

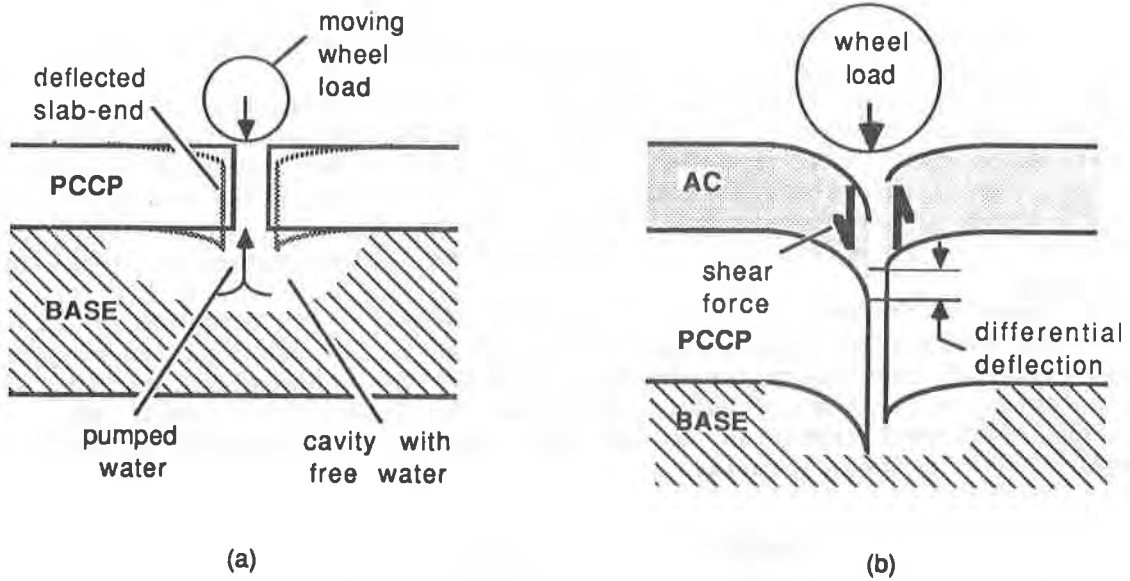


Figure 2
Slab end deflection and pumping (a); differential deflection (b).

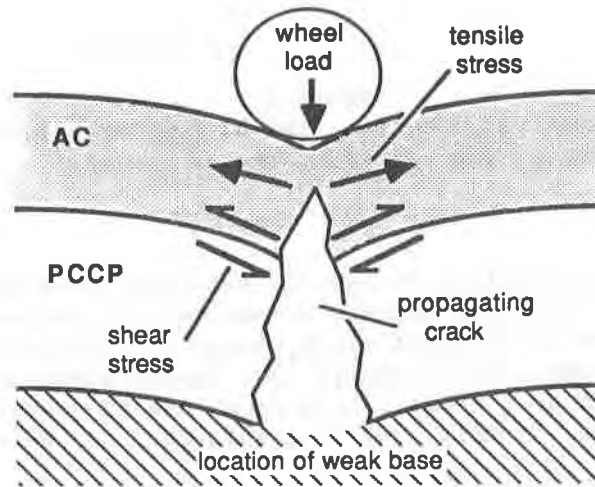


Fig 3
Deflection over an area of local structural weakness leads to tensile stress in the AC overlay.

to prevent a continued increase in differential deflection caused by infiltration of water through the surfacing (2).

In a zone of local structural weakness, vertical deflection may cause cracking in the PCCP through tensional stress (Fig 3). The displacement in the PCCP leads to shear stress at the PCCP/AC interface, which in turn causes tensional stress in the AC overlay; unless this process is deterred by a component of the design strategy, a reflection crack in the AC will soon develop. Additionally, a waterproofing component of the overlay will protect the base from further weakening from water infiltration.

Two types of thermal strain occur in PCCP: 1) daily and seasonal temperature variation can cause axial displacements (Fig 4a) and, 2) a vertical temperature gradient resulting from daily temperature variation can cause slab curl (Fig 4b). Both displacements (with magnitude dependent on the temperature change, the coefficient of thermal expansion for the PCCP, and the slab dimensions) lead to tensional stress in the AC overlay.

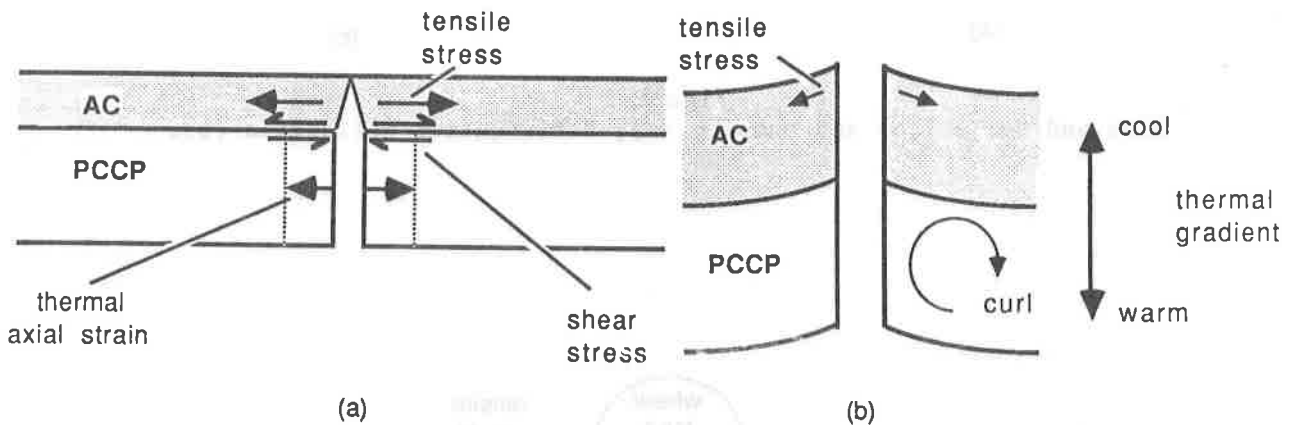


Figure 4

a) Temperature change causes axial strain and b) bending strain, or curl; both lead to tensile stress in the AC overlay.

The seasonal temperature variation, frequently referred to as the temperature differential, is defined to be the maximum temperature in the hottest month, minus the minimum temperature in the coldest month, based on a 30 year average (3). Although difficult to prevent, particularly in climates with severe temperature variation, cracking caused by thermal displacement can be somewhat retarded with the design strategies discussed in this paper; in this context, design strategy 3 is the most effective.

DESIGN STRATEGIES AND CASE HISTORIES

For a minimal level of service, PCC pavements subjected to light (low average daily traffic and low axle weights) traffic, a thin (3.8 cm or 1.5") AC

rehabilitation overlay is frequently specified. This minimal design provides a new riding surface and a temporary moisture barrier; however, it incorporates no feature for the retardation of reflective cracking and subsequent water infiltration into the base (3). In a typical installation, a majority of the cracks and joints in the PCCP will reflect through the overlay within 1-2 years; failure (i.e., extensive spalling and poor rideability of the AC) occurs typically at the reflected joint cracks within 4 years or less.

Design Strategy 1

In the first design strategy, for light traffic, an asphalt-textile is installed directly on the PCCP surface beneath a 3.8 to 7.6 cm (1.5" to 3") AC overlay. The asphalt-textile is comprised of a nonwoven synthetic fabric saturated with asphalt. The asphalt not only binds the fabric to the pavement below and the AC above, but also contributes to the overall physical properties of the asphalt-textile system.

The asphalt insures that the system is waterproof, and can retain this property after cracking has occurred, since nonwoven fabric sustains in excess of 50% strain before failure. Weakening of the subbase (the native material beneath the roadway) or base, and pumping, can thus be delayed or prevented (1, 4).

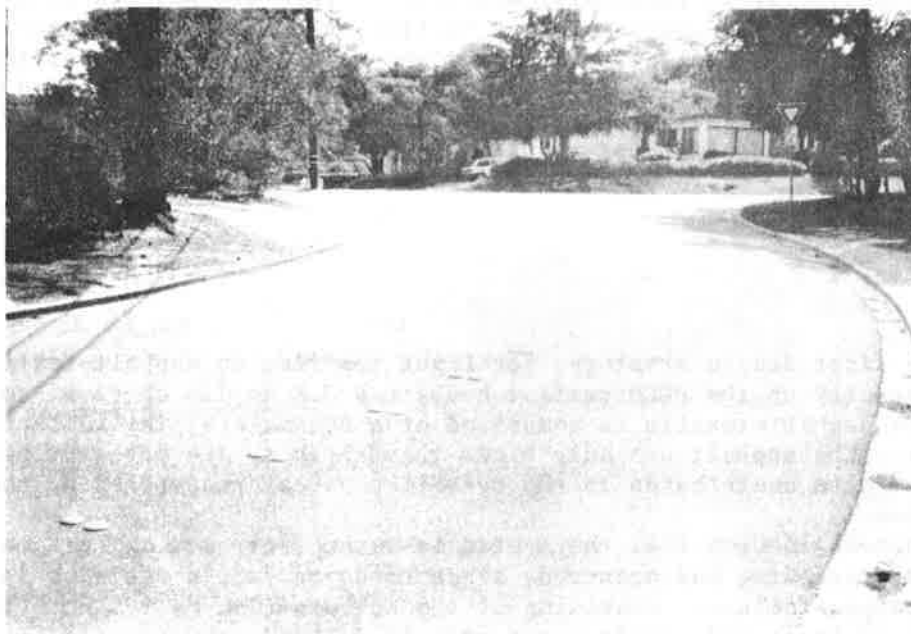
Cracks reflecting displacement in the underlying PCCP will first encounter the asphalt-textile. The stress is concentrated in the propagating crack tip; the lower viscosity (relative to the PCCP and AC) of the asphalt-textile can dissipate this concentrated stress so that the critical fracture strength of the overlying AC is not attained (5). Laboratory testing (6) has shown that the fatigue life of AC can be increased substantially through this mechanism.

The expected performance of this design is the retardation of reflective cracking for 3 to 4 years; good rideability can persist for 10 or more years until failure occurs due to severe spalling. A similar performance might be expected for a thicker overlay (>10 cm or 4") without an asphalt textile, but not without incurring significantly greater cost and creating problems with overhead clearance and gutter heights (termed vertical control). Three case histories involving an asphalt-textile placed directly on PCCP will be discussed.

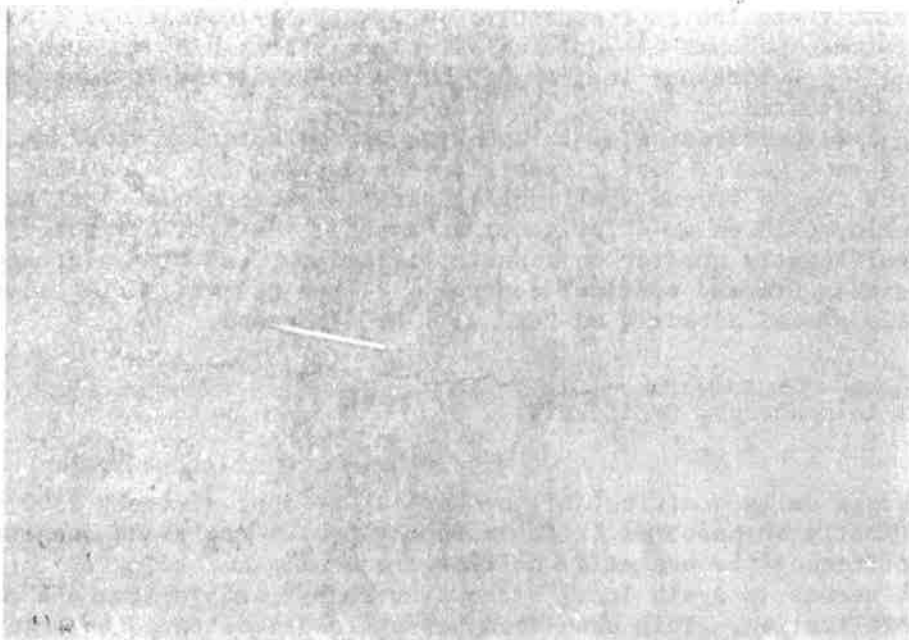
Martin Street in Monterey, California.

The average daily traffic (ADT) on Martin St, approximately 2300 vehicles per day, is low (mostly automobiles, with an hourly bus). Daily and seasonal temperature differentials are mild, neither frequently exceeding 17°C (30°F). The street itself serves to drain local stormwater runoff, subjecting the pavement to high water infiltration. This case then serves to demonstrate the waterproofing capabilities of this design.

The rehabilitation was performed in July 1982 on the existing distressed PCCP. Pavement preparation included: 1) portions of broken PCCP smaller than 1m x 1m (3' x 3') were removed and replaced with new PCCP to form 4m x 4m (12' x 12') slabs, 2) all cracks were filled with emulsified asphalt and 0.64 cm (0.25") aggregate chips, and 3) the pavement was cleaned with a sweeper.



(a)



(b)

Figure 5
a) Martin Road in September 1986, b) one of the few transverse cracks.

Following this, AR₂4000 (hot liquid asphalt) was distributed over the PCCP at a rate of 0.22 gallons/yd²; the paving fabric was rolled onto the asphalt with tractor mounted equipment. Finally, a medium-graded AC was placed over the fabric, 3.8 cm (1.5") thick at the centerline, tapered to 3.18 cm (1.25") at the curb line.

In September 1986, after four years, a condition survey showed that the rehabilitation was in excellent condition with excellent rideability and little cracking (Fig 5a). The few visible cracks (Fig 5b) are narrow and show no faulting (a difference in height across the crack that indicates movement of the underlying PCCP). Evidently water infiltration has been prevented and the PCCP slabs remain stable, leading to a long lasting and smooth-riding pavement.

Pacific Avenue in Long Beach, California.

This installation occurred in October 1975 over existing 20 cm (8") thick PCCP that showed a moderate amount of block cracking. Since the time of the construction of the PCCP in 1925 and the rehabilitation project, the Long Beach area has been subject to differential subsidence. The high ADT, 13,500 vehicles per day with frequent bus passages, required a durable rehabilitation. Curb heights, however, precluded the application of a thick structural AC overlay. An asphalt-textile under a 7.6 cm (3") AC overlay comprised the selected design. Eleven years after the rehabilitation, in October 1986, a condition inspection discovered only 10% reflective cracking over the longitudinal PCCP joints, and 15% reflection of the transverse PCCP joints. Since thermal differentials and annual precipitation totals are small in Long Beach, this case history exemplifies the ability of design strategy 1 to resist cracking due to elastic displacements in the underlying PCCP.

73rd Street in Windsor Heights, Iowa.

The PCCP, prior to overlay, showed some spalling at transverse joints and random cracking throughout the slabs. The rehabilitation, performed in October 1982, began with milling the PCCP (i.e., mechanically removing a thin layer). The asphalt-textile was placed directly on the milled surface, and was followed by a 5 cm (2") AC overlay. The very high ADT (the traffic has grown since 17,000 vehicles per day were measured in 1978) and temperature differential 40°C (73°F), serve as an extreme test of this economical design. The overlay survived the unusually severe winter of 1982-1983 without any signs of cracking. In October 1986, the transverse joints had reflected through, but no potholes or other signs of failure were evident. Recognizing its practicality, the City of Windsor Heights has since utilized this design strategy in three rehabilitation projects.

Design Strategy 2

Design strategy 2, indicated for larger ADT values with a somewhat higher level of service than design strategy 1, includes a 2.5 cm (1") leveling course below the asphalt-textile. Experimental study (1) and numerical modeling (7)

indicate that this is the ideal placement (the lower 1/3 of the overlay) of the asphalt-textile as a stress relieving interlayer.

Expected performance for this design is cracking after 5 to 10 years under moderate truck loading. Time to failure is unknown, since this design was not utilized before 1970, and few failures have since been observed. Three case histories are presented for this design strategy.

Wardlow Road in Long Beach, California

The pavement existing before rehabilitation consisted of two highly fractured, 18 cm (7") thick, 5.5 m (18') wide roadways, separated by 5.2 m (17'). A very high ADT (21,000 vehicles per day, including bus traffic) exists on this road; the case history demonstrates the capability of this design strategy to impede reflection cracking, despite many deflections of large magnitude. As with the Pacific Avenue rehabilitation, gutter height disallowed a thick structural overlay. Figure 7 diagrams the rehabilitation project, which began with placement of new 18 cm (7") thick PCCP between the two existing lanes of PCCP.

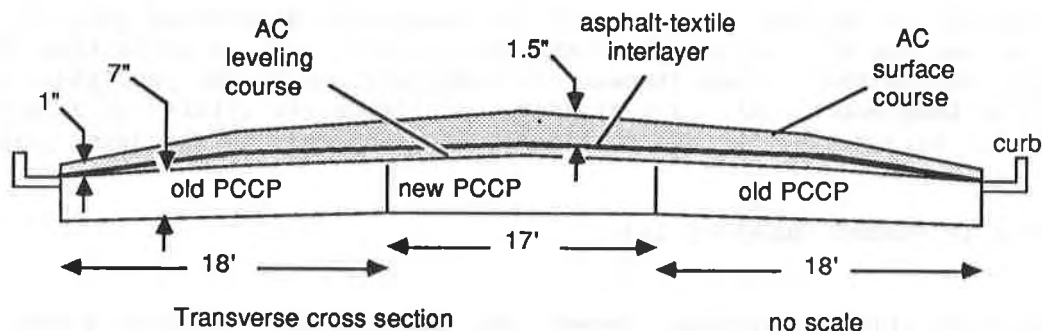


Figure 6
Rehabilitation design schematic of Pacific Ave in Long Beach, CA

The AC leveling course varied in thickness from a maximum of 2.5 cm (1") at the centerline, to zero at the gutters. The asphalt-textile was placed atop the leveling course. The AC surface course varied from 3.8 cm (1.5") at the centerline to 2.5 cm (1") at the gutters.

The performance of this 1975 rehabilitation was evaluated eleven years later in September 1986. Cracking observed included: less than 10% reflection of the longitudinal joint, 20% reflection of the transverse PCCP joints as 30 cm (1') long cracks at the taper (adjacent to the curb), and 10% reflection of the transverse joints as extending more than 3 m (10'). The pavement was still smooth and not showing evidence of failure.

South Airport Boulevard in South San Francisco, California

This rehabilitation project was completed in November 1977. The PCCP prior to the AC overlay showed moderate to severe block cracking. The rehabilitation consisted of a 5 cm (2") maximum-depth AC leveling course beneath the asphalt-textile and a 3.8 cm (1.5") surface course. The aggregate grading for the AC was 1.3 cm (0.5") maximum. A smooth riding surface with an extended life and minimal maintenance were the objectives of the rehabilitation. To meet these objectives, the large ADT (as measured in 1974, 3,000 vehicles per day in the north-bound lanes, 9,000 in the south-bound lanes) necessitated a heavy structural AC overlay, or the application of design strategy 2. Design 2 was chosen because a thick overlay, in addition to being more expensive than this design, would have created problems with vertical control.

An inspection in November 1981 (four years after the rehabilitation) found the pavement in excellent condition, with no apparent cracking. An ADT count performed in 1984 showed traffic had increased significantly (to 9,000 vehicles per day in the north-bound lanes and to 12,000 in the south-bound lanes). In October 1986, a second inspection found the rehabilitation still performing well (Fig 7).



Figure 7
South Airport Boulevard, South San Francisco, October 1986

Transverse cracking was rare (a detailed assessment of the pavement between Utah and Belle Air found one transverse crack 3 m (10') in length) and rideability was still very good. Intermittent cracking over the longitudinal joints was mostly

hairline with some cracks up to 1.3 cm (0.5") in width (Fig 7). After nine years of heavy traffic, the rehabilitation appears to offer many more years of serviceability.

Maryville Road in Granite City, Illinois

This case history is another illustration of the success of design strategy 2 in an application of primarily providing waterproofing. The 20 cm (8") thick, wire mesh reinforced PCCP with doweled joints was constructed in 1978, with an expected design life of 20 years. The ADT count in 1983 was 8,100 vehicles per day. By 1980 popouts were becoming a problem. Chemical analysis of the PCCP showed that excessive particles of magnesium oxide present in the Portland cement were reacting with water, expanding, and causing the popouts. An overlay to shield the PCCP from water was chosen as an alternative to costly chronic maintenance.

The 1982 rehabilitation consisted of patches for the existing popouts, a 1.9 cm (0.75") leveling course, an asphalt-textile, and a 3.8 cm (1.5") surface course. Although the ADT is low, the climate is severe, with an annual temperature differential of 38°C (68°F); in combination with the 30.5 m (100') slab lengths, (7.3 m, or 24', width), this results in a large thermal strain in the PCC. A heavy structural overlay with cracking and seating of the slabs and a stress relieving membrane would have been required to delay reflection cracking over the PCCP joints (3).

An inspection of the overlay four years later in October 1986 showed that the large temperature range had led to reflection cracking over the PCCP joints; the asphalt-textile interlayer, however, due to its capability for large strain without failure, remained intact. The objective of the overlay design had been achieved; the popouts had ceased since the PCCP had been isolated from water by the waterproofing rehabilitation.

Design Strategy 3

Design rehabilitation strategy 3 (Fig 1), which is generally utilized to provide a high level of service (10 years) under heavy truck loading or large thermal strains, has been used successfully by the California Department of Transportation (Caltrans) since 1982. This rehabilitation strategy utilizes cracking and seating of the PCC pavements that are distressed to the extent that rehabilitation to maintain the structural integrity and ride quality of the PCCP, i.e., by subsealing, slab replacement and grinding, is cost prohibitive.

In the cracking and seating procedure, it is only necessary to crack PCCP into rectangular sized blocks 1.8 m (6') transversely by 1.2 m (4') longitudinally. Experience supports the theoretical judgment (9) that these dimensions will produce thermal strains in the cracked PCCP that are small enough in most California environments to be tolerated by a nominal 10.8 cm (4.2") thick fabric-reinforced AC overlay. The seating process with a heavy pneumatic roller following the cracking procedure provides a stable base for the AC overlay.

Although fabric-reinforcement is included in the AC overlay system for reflection crack retardation and waterproofing, an edge drain system with outlets is

LORENZ, V.M.

New Mexico State Highway Department, U.S.A.

New Mexico Study of Interlayers Used in Reflective Crack Control

I. INTRODUCTION

The primary objective of any pavement design system is to provide a roadway that is not only safe and rides comfortably, but also extends these characteristics over a maximum useful life with a minimum amount of required maintenance. Since the pavement generally deteriorates in the forms of cracking, rutting, and other surface deformations, rehabilitation frequently involves applying a thin overlay over a properly prepared cracked pavement. This method of restoration may subsequently result in a new problem--that of reflective cracking patterns that migrate into and eventually through the overlay. Once the overlay is fractured, erosion can occur rapidly. The ride and safety performance of the roadway is eventually severely affected resulting in further and costly maintenance. It is the perception of many highway agencies that placing some form of interlayer between the old deteriorated pavement and the new overlay will prevent or, at the very least, retard reflective cracking thereby increasing the life of the overlay and resulting in a savings in maintenance costs.

The objective of this study was to finalize the evaluation of several New Mexico Experimental Projects which were established under Category 2 Experimental Construction and to provide an overall evaluation of several interlayer systems which New Mexico has implemented for the purpose of retarding reflective cracks. This abridged report discusses in minimal detail only the first four of the original six reported projects.

II. MECHANISMS OF REFLECTIVE CRACKING (1,2)*

Horizontal and vertical movements between the original pavement and the overlay are the basic mechanisms which result in the development of reflective cracking. Although several field observations and theoretical analyses of reflective cracking have been made, there have not been many controlled projects where sufficient data were taken to accurately determine the cause or factors associated with this type of cracking. Most of the projects which have been studied consisted of an asphalt overlay over a portland cement concrete pavement. Hence, a generally accepted well-developed description of the mechanisms and response variables is not available.

*Numbers in parentheses refer to references listed at the end of this report.

Reflective cracking is generally accepted to be partially due to horizontal movements resulting from the expansion and contraction of the existing pavement from temperature and moisture changes. Tensile stresses which are produced from movements at the joints or cracks become critical in that area because of the bond between the overlay and the existing pavement. The amount and rate of temperature change, slab length, gage length across the joint or crack, and the properties of the overlay materials are all contributing factors to the development of reflective cracking.

Repeated traffic loading produce differential vertical movements at joints and cracks which result in shear-stress concentrations at the joints and cracks in the overlay. The magnitude of load, the amount of load transfer across the joint or crack, and the differential subgrade support under the existing pavement are important factors involved in differential deflections.

III. THE INTERLAYER SYSTEMS

Several projects have been undertaken in New Mexico where interlayers were utilized in the hopes of reflective crack retardation. The following describes the types of interlayers which were incorporated into the four different experimental project locations.

The ARIZONA RUBBERIZED ASPHALT membrane is produced by the Arizona Refining Company of Phoenix, Arizona. An 85-100 pen asphalt was combined with 20% reclaimed Replasticized rubber and a 2% extendor oil and then heated to 210°C. (410°F.). (A 120-150 pen asphalt was used in lieu of the 85-100 pen asphalt on one of the projects.) As the material was uniformly applied at an average rate of 2.85 l/m² (0.63 gal/sq.yd.) across the roadway, the small cracks were filled. Chips were then spread across the membrane at an average rate of 20.6 kg/m² (38 lbs/sq.yd.).

The ARKANSAS MIX consisted of an open-graded bituminous pavement with a coarse gradation with aggregate less than 5.1 cm (2") in size and 3% of AC20 grade asphalt. The material was placed in one 8.9 cm (3½") lift and then rolled by 4536 kg (five-ton) roller.

The HEATER-SCARIFICATION consisted of two separate units which were used to preheat the pavement. The second unit scarified the existing mat to a depth of 1.9 cm (¾"). The rejuvenating agent Reclamite was applied to the scarified surface by a distributor at a rate of 0.36 l/m² (0.08 gal/sq.yd.). A steel roller then followed the distributor to compact the material.

MIRAFI 140, which is manufactured by Celanese Fibers Marketing Company, is a nonwoven fabric uniquely constructed from two types of continuous filament fibers. One fiber consists of a polypropylene homofilament, and the other type is a heterofilament composed of a polypropylene core covered with a nylon sheath. During the webmaking process, the heterofilaments are heat-bonded or fused together where they intersect. At the same time, during this process, the homofilament polypropylene, which is unaffected by the heat, becomes mechanically interlocked with the other fibers, thereby giving the fabric its high tear strength and elongation capability.

PETROMAT, a nonwoven fabric, is manufactured by Philips Fibers Corporation whereby a needlepunching process utilizes polypropylene filaments to form the fabric.

The SAHUARO RUBBERIZED ASPHALT membrane is produced by the Sahuaro Petroleum and Asphalt Company of Phoenix, Arizona. The rubberized asphalt which is blended at 177°C. (350°F.) consists of 25% vulcanized granulated rubber and 120-150 pen asphalt. The mixture is diluted between 5.5% to 7.5% by volume with kerosene. The asphalt rubber mixture was applied at 163°C. (325°F.) on the roadway at an average rate of 2.7 l/m² (0.6 gal/sq.yd.). Chips were then spread across the membrane at an average rate of 20.6 kg/m² (38 lbs./sq.yd.).

The STANDARD BASE COURSE which was placed directly on top of the existing mat, consisted of a finer gradation with aggregate 1.9 cm (3/4") in size and smaller. The moisture content was maintained at 5% and a vibratory roller was used for compacting the 10.1 cm (4") layer.

IV. THE EXPERIMENTAL PROJECTS

The four experimental projects where these interlayers were used are listed below. Their locations are shown in Figure 1 below.

1. I-25 11.2 km (7.0 mi.) South of Raton -- North, Colfax County
2. I-40 7.2 km (4.5 mi.) East of Clines Corners -- East, Torrance County
3. I-25 13.1 km (8.2 mi.) North of T. or C. -- North, and Mitchell Point Interchange -- North, Sierra County
4. I-40 West of Grants, M.P. 70.15-79.0, (Bluewater Interchange to Milan Interchange), Cibola County

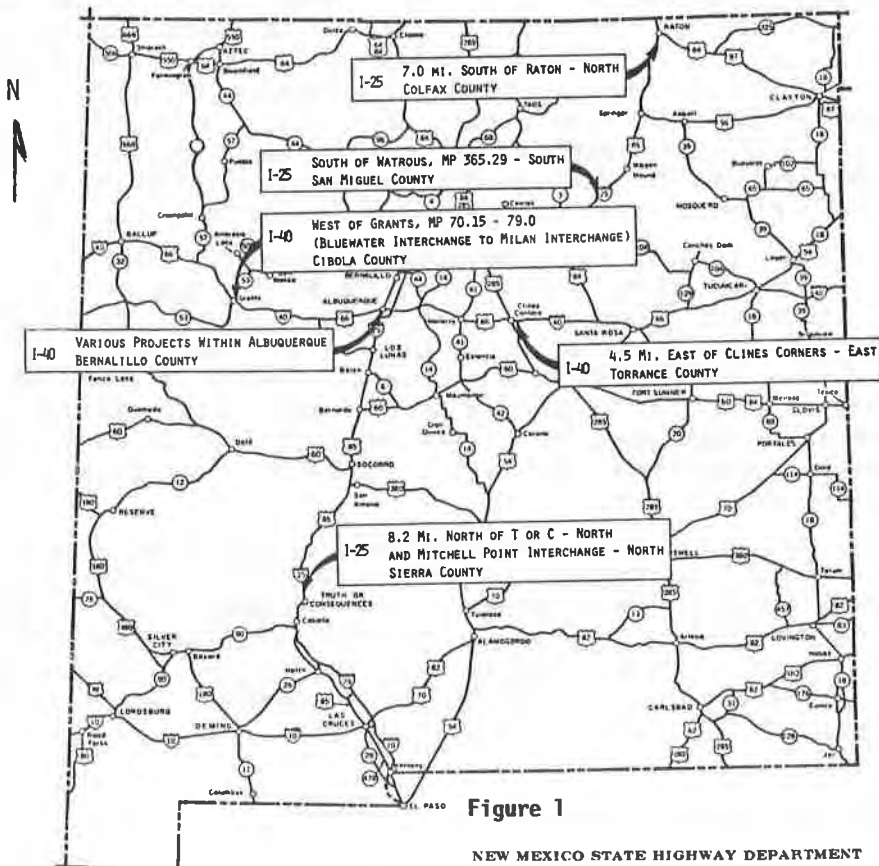


Figure 1
NEW MEXICO STATE HIGHWAY DEPARTMENT
NM Experimental Project Locations

Environmental conditions which affect the pavement structure were collected for a three-year period (1980-1982) at a national weather station which is located in close proximity to each project site. Provided by the National Climatic Data Center in Asheville, North Carolina, the data was compared and was found to be similar for the following projects: 1. I-25 at Raton; 2. I-40 at Clines Corners; and 4. I-40 at Grants.

1. I-25, South of Raton

The original roadway was completed in 1968 with thicknesses and the types of layers as follows: 1.6 cm (5/8") Plant Mix Seal Coat, 11.4 cm (4½") Plant Mix Bituminous Pavement, 15.2 cm (6") Untreated Base, 15.2 cm (6") Cement Treated Base Course, 10.2 cm (4") Untreated Subbase. The project was designed using the R-value, traffic index, and gravel equivalent design concept rather than the AASHTO Interim Design Guide Procedures for Pavement Design.

The experimental project consisted of overlaying the existing roadway and utilizing two types of crack relief systems. Prior to construction, several pavement distresses were observed. Some rutting had occurred in the wheelpaths of the driving lanes. Extensive longitudinal and transverse cracking could be seen as well as some localized alligator-type cracking. There was no indication that the pavement failed structurally which would require the removal and replacement of the underlying structure. Six 183 m (600 ft.) monitor sections were demarcated so that each of the types of crack relief systems was represented in the construction of two sections, while the remaining four sections were constructed as control sections with different thicknesses of plant mix bituminous layers and without the use of an interlayer. All cracks in each monitor section were photographed and logged in a field book for future reference. The overlay thicknesses consisted of 6.4 cm (2½") and 10.2 cm (4") for the no interlayer sections and 5.1 cm (2") for the Mirafi 140 and Petromat sections. A 1.6 cm (5/8") plant mix seal coat was constructed on the entire project.

This experimental project was completed in November, 1978 at an initial cost of \$45,132/ln-km (\$72,212/ln-mi). All cracks in the existing pavement had been blown clean and filled with 120-150 pen asphalt. An 85-100 pen asphalt was spread as a tack coat, prior to placing the Mirafi 140 fabric at a rate of 0.68 to 0.91 l/m² (0.15 to 0.20 gal/sq.yd.) and at an approximate temperature of 191°C. (375°F.). Prior to placing the Petromat fabric, the 85-100 pen asphalt was applied as a tack coat at a rate of 1.13 l/m² (0.25 gal/sq.yd.) and at an approximate temperature of 163°C. (325°F.). No specific problems were reported during construction.

This project has since been inspected several different times with the last inspection occurring on October 18, 1983. Only the monitor sections were inspected and all cracks were noted in the log book. The primary distresses which occurred in one or all of the monitor sections were rutting, raveling, and fatigue cracking. Table 1 summarizes the number of cracks observed before the overlay construction and during each inspection after the construction, and the percent of the reflective cracks of the original cracks for each monitor section.

Summary and Conclusions

Cracks were first observed during the final inspection which took place almost

five years after the overlay construction. The two monitor sections with 10.1 cm (4") of PMBP and no interlayer have both the greatest percentage (39%) and the smallest percentage (20%) of reflective cracks. The section utilizing Mirafi 140 fabric had 28% of the cracks return. The section constructed with Petromat fabric had 27% of the original cracks return. There a 6.4 cm (2½") layer of PMBP was built without an interlayer, 23% of the original cracks reflected through in one section and 28% occurred in the other section. Figure 2 below is a graph of the percent of cracks returned versus the number of years since the overlay was constructed. As shown, after almost five years of service, less than 30% of the cracks reflected through the overlay in five out of the six sections. The pavement distresses which had developed indicate that the reflective cracks could be caused by repeated traffic loads. The Petromat section and two control sections had the best performance of all the experimental sections in reducing reflective cracking.

Table 1. Reflective Cracks. I-25, South of Raton

TEST SECTION NUMBER Type of Interlayer	Total No. of Original Cracks	Number of Cracks Observed Percent of Total Number of Original Cracks			
		Date of Inspection (Age of Overlay in Years)	4/26/79 (0.4)	1/22/80 (1.2)	10/15/81 (2.9)
SECTION I Control Section No interlayer	23	0 0%	0 0%	0 0%	9 39%
SECTION II Mirafi 140 Fabric	32	0 0%	0 0%	0 0%	9 28%
SECTION III Petromat Fabric	37	0 0%	0 0%	0 0%	10 27%
SECTION IV Control Section No interlayer	46	0 0%	0 0%	0 0%	9 20%
SECTION V Control Section No interlayer	35	0 0%	0 0%	0 0%	8 23%
SECTION VI Control Section No interlayer	32	0 0%	0 0%	0 0%	9 28%

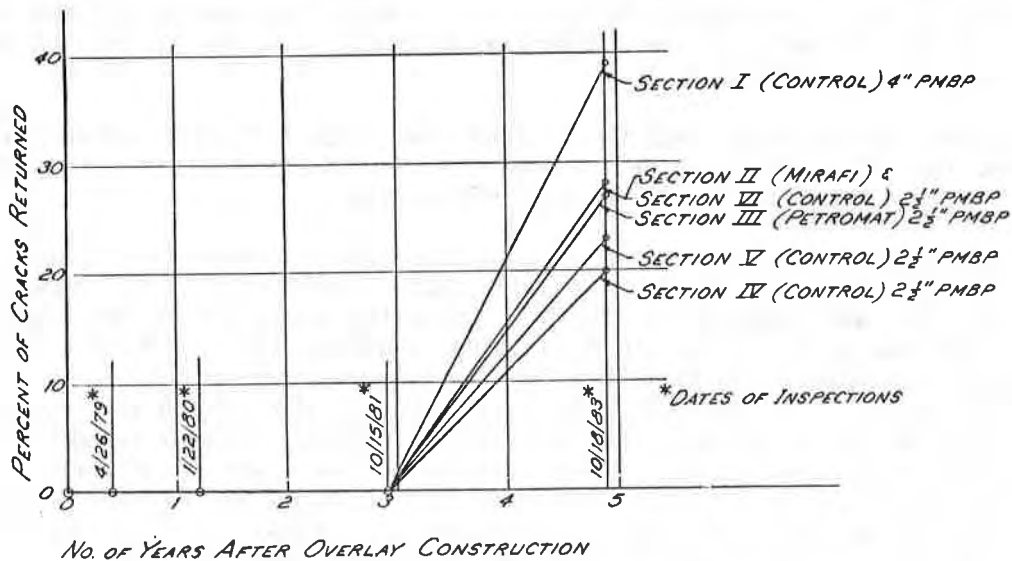


Figure 2. Reflective Cracks vs Overlay Life
I-IR-025-6(49)439, 7 Mi. S. of Raton-N., Colfax County

2. I-40, East of Clines Corners

Completed under three contracts, the original roadway was built in 1956, 1957, and 1958 with layer thicknesses and the types of materials used in the construction as follows: 1.6 cm (5/8") Plant Mix Seal Coat, 7.6 cm (3") Plant Mix Bituminous pavement, 10.2 cm (4") Base Course, 10.2 cm (4") Subbase. Stage construction surfacing was designed using a R-value, traffic index and gravel equivalent. Records indicated that a 5.1 cm (2") overlay was anticipated to be structurally sufficient to complete the stage construction for the anticipated life expectancy.

The entire experimental project which was completed at a cost of \$63.936/ln-km (\$102,297/ln-mi), consisted of overlaying the existing roadway with 14 cm (5½") PMBP and implementing four different types of crack relief systems -- Sahuaro Rubberized Asphalt, Arizona Rubberized Asphalt, Mirafi 140, and Petromat. Extensive transverse, longitudinal, and alligator cracks which were observed prior to construction were photographed and logged in a field book for future reference. Some pavement areas were removed and replaced since they were so badly deteriorated.

Six 183 m (600 ft.) sections completed by July, 1978 were selected to be monitored. Five were constructed with one type of crack relief system and one section was built without an interlayer. The sixth section was added to the project during construction when problems occurred during the construction of the section with Sahuaro Rubberized Asphalt. Section VI was constructed with the same interlayer but only a 10.2 cm (4") PMBP layer was built. The tack coat for the fabrics was a 120-150 pen asphalt. For Mirafi, the application rate varied from 0.68 to 0.91 l/m² (0.15 to 0.20 gal/sq. yd.).

Several problems arose during the construction of the overlay project. An investigation attributed the raveling of the rubberized asphalt mixture to incorrect mixing times. An incomplete reaction between the rubber and the asphalt resulted in the stripping of the rubberized material. At this point, it was decided to construction Section VI.

Problems occurred in other sections. When the chips that were spread over the rubberized asphalt were too fine, a poor bond to the next layer resulted. The problem disappeared after the chips were rescreened.

Other problems experienced were related to the fabric blowing and "parachuting" because it was not adhering to the tack coat. Additional labor was used to straighten, cut, and replace the fabric. Since the spray bar on the distributor was not long enough to apply the full width required for the Mirafi fabric, a second pass was made which then resulted in an excess of asphalt where the two passes overlapped. In addition, the tack coat was not spread uniformly. The laydown machine had a tendency to pull on the fabric, thereby wrinkling it or pulling it apart at the joints. Since shoving of the plant mix bituminous pavement occurred in some areas, those sections were removed and replaced. Throughout the entire project, the contractor made an attempt to fill the existing cracks with 120-150 pen asphalt. It was estimated that only half the cracks were partially filled and the other half were left unfilled.

Flushing occurring in the initial lifts on top of one fabric was attributed to the segregation of the aggregate which had occurred during several handling operations. The percent of asphalt and fines had both been increased in an attempt to reduce segregation, but the voids in the mix were reduced thus producing a dense mix. Segregation became a cumulative situation due to improper storage of the aggregate and loading, unloading and placing of the plant mix bituminous pavement. The flushing was eventually eliminated by reducing the percent of asphalt and the percent of fines was reduced to provide voids in the mix.

Since construction was completed, this project has been inspected several times with the most recent inspection occurring on September 8, 1983. All new cracks were logged in the book for only the monitor sections. Pavement distresses which were observed in one or more sections were severe bleeding, rutting, and transverse and longitudinal cracking.

Core samples were taken in each monitor section in this project and analyzed to verify the causes of the pavement distresses which were observed. In general, the following was ascertained:

1. Bleeding occurring in the pavement surface resulted from too high an asphalt content in the plant mix seal coat or the plant mix bituminous pavement, or the asphalt stripped from the aggregate.
2. The original cracks had not been properly cleaned and sealed.
3. Stripping of the asphalt from the aggregate caused portions of the cores to disintegrate.
4. In most cases the interlayer remained intact, even though the original crack propagated through the pavement layers to the top.

Table 2 indicates the number of cracks observed before the overlay construction and during each inspection.

Table 2. Reflective Cracks. I-40, East of Clines Corners

TEST SECTION NUMBER Type of Interlayer	Total No. of Original Cracks	Number of Cracks Observed Percent of Total Number of Original Cracks				
		1/15/80 (1.4)	7/31/80 (2)	2/19/81 (2.4)	10/6/81 (3.2)	9/8/83 (5.1)
SECTION I Sahuaro Rubberized Asphalt	25	0 0%	1 4%	2 8%	3 12%	11 44%
SECTION II Arizona Ref. Co. Rubberized Asphalt	28	1 4%	0 0%	1 4%	1 4%	7 25%
SECTION III Mirafli 140 Fabric	40	0 0%	0 0%	0 0%	0 0%	12 30%
SECTION IV Petromat Fabric	37	0 0%	0 0%	0 0%	0 0%	8 22%
SECTION V Control Section No Interlayer	41	0 0%	0 0%	5 12%	6 15%	21 51%
SECTION VI Sahuaro Rubberized Asphalt	53	0 0%	0 0%	3 6%	3 6%	15 28%

Summary and Conclusions

Cracks began appearing as early as nineteen months after the overlay construction in the Arizona Rubberized Asphalt section. After two years, cracks were observed in the first Sahuaro Rubberized Asphalt section. Cracks then appeared in the control section and the second Sahuaro Rubberized Asphalt section after almost two and a half years. After more than five years, cracks were observed in all sections. The greatest percentage (51%) of reflective cracks, which was observed during the final inspection occurred in the control section where no interlayer was used. The smallest percentage (22%) of cracks returned was observed in the Petromat section. The percent of cracks in the remaining sections ranged from 25 to 44 percent. Figure 3 is a graph of the percent of cracks returned versus the number of years since the overlay was constructed for each monitor section. After more than five years of service, less than 30% of the cracks returned in three out of the six sections. The pavement distresses which were observed indicate that repeated traffic loads and temperature and moisture changes possibly aided in the development of the reflective cracking. The Petromat, Sahuaro, and Arizona sections performed the best in reducing the number of reflective cracks.

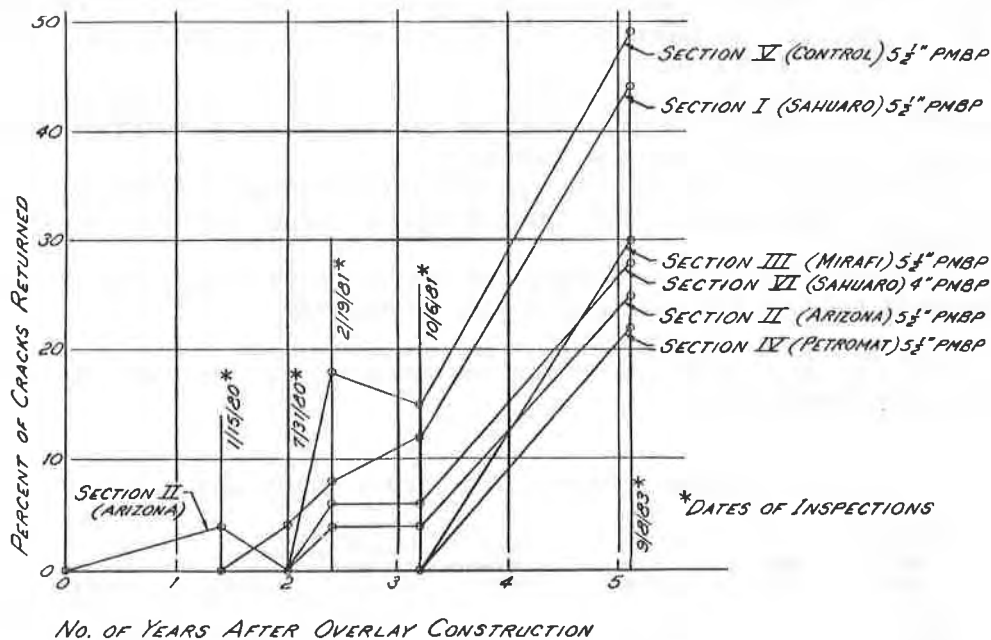


Figure 3. Reflective Cracks vs Overlay Life
I-IR-040-4(31)223, 4.5 Mi. E. of Clines Corners-E., Torrance County

3. I-25, North of T. or C.

The original roadway was built in July, 1966 with the configuration of materials and layer thicknesses as follows: 3.8 cm (1 1/2") Surface Course, 5.1 cm (2") Binder Course, 10.2 cm (4") Asphalt Treated Base, 10.2 (4") Subbase. Design data were not available in the project files.

The experimental project consisted of incorporating four crack relief systems (Sahuaro Rubberized Asphalt, Arizona Rubberized Asphalt, Petromat, and Mirafi 140) and the heater-scarification process with a 5.1 cm (2") PMBP overlay.

Prior to construction, numerous transverse cracks were observed with widths ranging from 0.6 cm to 2.5 cm ($\frac{1}{4}$ " to 1") and with depths of approximately 20.3 cm (8"). No alligator cracking was apparent. An 152 m (500 ft.) monitor section was laid out in each experimental test section and one in the control section. All cracks in each monitor section were photographed and logged in a field book for future reference.

This experimental project was completed in July, 1979 at an initial cost of \$70,271/ln-km (\$112,434/ln-mi). The contractor attempted to fill all cracks in the existing pavement with 120-150 pen asphalt; however, because of the depth and width of each crack, not all cracks were filled. Other problems occurred during construction. In the heater-scarification section, while the second heater unit was scarifying the old pavement, the asphalt in the previously filled cracks began to bleed through the scarified material. Excessive asphalt from crack sealing also caused a problem in the Sahuaro section. Bleeding occurred through the chips when the hot rubberized asphalt blend was applied to the area where cracks had been filled. Minor wrinkles occurred in both fabric sections, but did not present any problems.

Since the date when construction was completed, several inspections have taken place. During an interim inspection, several cores were sampled. An analysis resulted in the following comments:

1. The rubberized asphalt membranes and the fabrics appeared to be intact.
2. Small cracks had remained filled with crack sealant while large cracks had voids as large as 5.1 cm (2") deep between the interlayer and PMBP. Where no crack sealant was used, the cores fell apart into pieces.
3. Old cracks in the control section reflected through the new surfacing.
4. There was no evidence of reflective cracking in the heater-scarification section.

The final inspection was performed on September 27, 1983 when the monitor sections were observed in detail and all new cracks were noted in the logbook. The pavement distresses which were observed in one or more sections are raveling, rutting, transverse and longitudinal cracks.

Table 3. Reflective Cracks. I-25, North of T. or C.

TEST SECTION NUMBER Type of Interlayer	Total No. of Original Cracks	Number of Cracks Observed Percent of Total Number of Original Cracks Date of Inspection (Age of Overlay in Years)				
		9/12/79 (0.1)	1/7/80 (0.4)	12/11/80 (1.4)	10/13/81 (2.2)	10/12/83 (4.2)
SECTION I Heater-Scarify & Rejuvenate	30	0 0%	0 0%	3 10%	6 20%	23 77%
SECTION II Sahuaro Rubberized Asphalt	22	0 0%	0 0%	7 32%	9 41%	23 100%
SECTION III Arizona Ref. Co. Rubberized Asphalt	25	0 0%	5 20%	14 56%	15 60%	28 100%
SECTION IV Petromat Fabric	19	0 0%	1 5%	9 47%	11 58%	20 100%
SECTION V Mirafi 140 Fabric	25	0 0%	3 12%	8 32%	9 36%	20 80%
SECTION VI Control Section No Interlayer	31	0 0%	13 42%	19 61%	19 61%	31 100%

Table 3 shows the number of cracks and the percent of original cracks which were observed during all reported inspections. Figure 4 represents the increase of percent of cracks returned versus the age of the overlay construction.

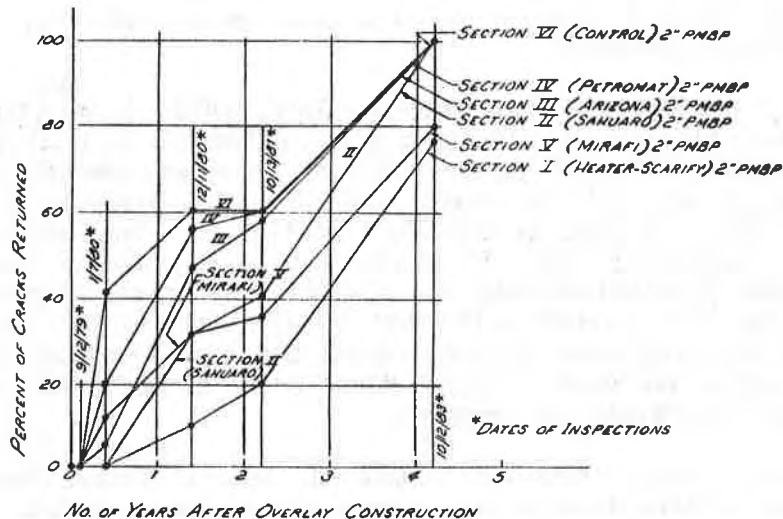


Figure 4. Reflective Cracks vs Overlay Life
I-025-2(35)89, 8.2 Mi. N. of T. or C. - N.
& Mitchell Point Interchange - North, Sierra County

Summary and Conclusions

Cracks began to appear within the first year after the overlay construction in four of the six monitor sections. Cracks appeared in the remaining two sections within the next six months following that first year. The pavement distresses indicate that both vertical and horizontal movements possibly contributed to the development of reflective cracking. The heater-scarification section and the Mirafi section had the best performance for reducing reflective cracking after four years with cracks returning at 77% and 80%, respectively.

4. I-40, West of Grants

The project for constructing the original pavement was completed in 1970 with the following configuration of the thicknesses and materials: 7.6 cm (3") Asphalt Concrete, 15.2 cm (6") Cement Treated Base, 10.2 cm (4") Subbase. Design data were not available for this project.

Two types of systems were incorporated as stress relieving interlayers in this experimental project. The Arkansas Mix was overlaid with 6.4 cm (2½") PMBP and the Standard Base Course was overlaid with 8.9 cm (3½") PMBP. A 152 m (500 ft.) monitor section was laid out in each experimental test section where all major cracks were photographed and logged in a field book.

This project was completed in November, 1979 at a cost of \$47,528/ln-km (\$76,044/ln-mi). No major problems developed during the construction of the Standard Base Course or the Arkansas Mix. Only construction traffic was allowed

on these sections prior to placement of the hot mix and all traffic was discouraged on the Arkansas Mix until it had completely cooled.

Since project completion, three inspections have been documented. The last inspection occurred on October 5, 1983 where the monitor sections were observed in detail. New cracks which had appeared since the overlay construction were logged in the field book. The primary pavement distress which occurred in each section was rutting which had an average depth of 0.9 cm (3/8"). Some flushing or bleeding also occurred in both sections of the driving lane. In addition, transverse and longitudinal cracks were observed.

Table 4. Reflective Cracks. I-40, West of Grants

TEST SECTION NUMBER Type of Interlayer	Total No. of Original Cracks	Number of Cracks Observed Percent of Total Number of Original Cracks Date of Inspection (Age of Overlay in Years)			
		2/6/80 (0.3)	4/80 (0.4)	10/8/81 (1.9)	10/5/83 (3.0)
SECTION I Open-Graded Bituminous Pavement	24	0 0%	0 0%	0 0%	9 37%
SECTION II Standard Base Course	41	0 0%	0 0%	0 0%	2 5%

Table 4 indicates the number of cracks returned for each inspection and the percent of the original cracks. Figure 5 is a graph depicting the percent of reflective cracks versus the years after the overlay construction.

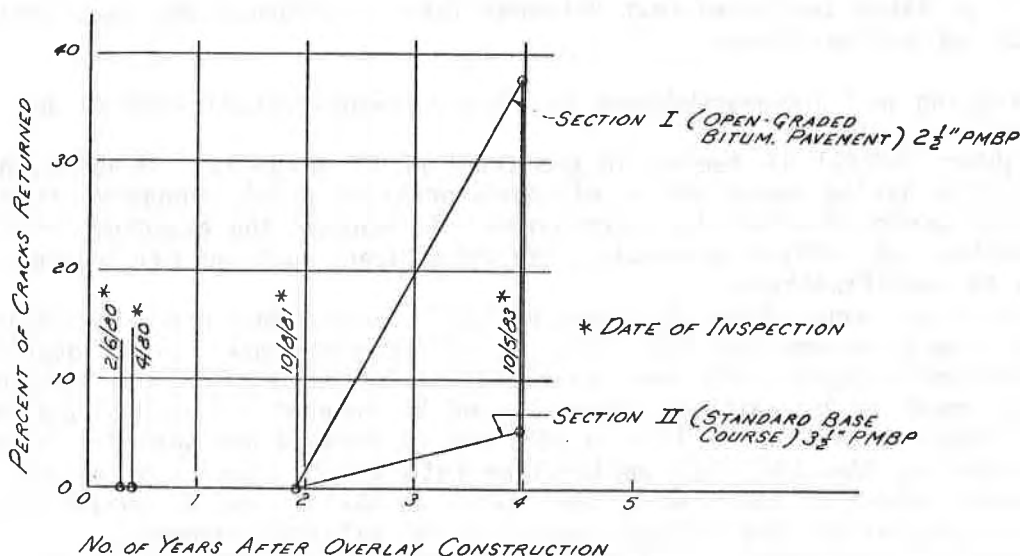


Figure 5. Reflective Cracks vs Overlay Life
I-040-2(34)71, W. of Grants, MP 70.15 - 79.00
(Bluewater Interchange to Milan Interchange), Cibola County

Summary and Conclusions

Cracks first began appearing in each section after slightly less than four years. Pavement distresses indicate that the reflective cracks were possibly developed by repeated traffic loads. Thirty-seven percent of the cracks had returned in the Arkansas Mix section. The Standard Base Course performed better with only 5% reflective cracks.

V. CONCLUSIONS AND RECOMMENDATIONS

The following conclusions were derived from this study:

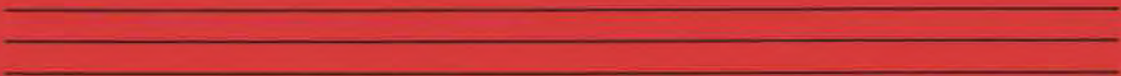
1. Interlayers do retard the rate of reflective cracks, and can therefore produce a savings in maintenance costs.
2. Interlayers do not necessarily prevent crack reflection.
3. Petromat fabric performed the best when all of the New Mexico experimental projects were compared.
4. Arizona's and Sahuaro's Rubberized Asphalt membranes were close competitors to Petromat in reducing reflective cracking.
5. Two control sections on I-25 at Raton performed just as well as the Petromat fabric and the Arizona and Sahuaro Rubberized Asphalt Membranes on the project on I-40 at Clines Corners. One section had a 10.2 cm (4") overlay and the other section had only a 6.4 cm (2½") overlay. It therefore appears that a thicker overlay can reduce crack propagation, but it would not be as cost-effective as the fabric or rubberized asphalt membrane.
6. Two of the three projects with similar weather data had similar results. The results from both the I-40 project at Clines Corners and the I-25 project at Raton indicated that Petromat fabric performed the best with 30% or less reflective cracks.

The following are recommendations for future experimental/research and routine construction projects:

1. Tighter control is needed in construction of projects. Numerous problems occurred during construction of these projects which probably affected the actual performance of the interlayers. To achieve the expected results of a reduction of reflective cracks, the interlayers must be constructed according to specifications.
2. Interlayers consisting of a paving fabric or a rubberized asphalt membrane are highly recommended for reducing reflective cracks in an overlay construction project. For the interlayer to be successful, the existing surface needs to be patched, cleaned, and be free of irregularities and dry. All cracks wider than 1.3 cm (0.50") are to be cleaned and sealed. In the case of fabrics, the tack coat application rate should consist of a total of the asphalt retention required by the fabric as tested, and an amount of asphalt needed to satisfy the surface hunger of the existing pavement.
3. Heater-scarification is a plausible alternative if cracking in the existing pavement is excessive. The initial cost of this process could be less than cleaning and sealing the cracks followed by the placement of an interlayer.

REFERENCES

1. GEORGE SHERMAN, "Minimizing Reflection Cracking of Pavement Overlays," NCHRP Synthesis of Highway Practice No. 92, TRB September, 1982.
2. HARVEY J. TREYBIG, B. FRANK McCOLLOUGH, PHIL SMITH, and HAROLD VON QUINTUS, Overlay Design and Reflection Cracking Analysis for Rigid Pavements, FHWA-RD-77-66, August, 1977.



SESSION 1B
SLOPES AND WALLS

LESHCHINSKY, D.

University of Delaware, U.S.A.

PERRY, E.B.

U.S. Army Engineer, U.S.A.

A Design Procedure for Geotextile-Reinforced Walls

INTRODUCTION

Geotextiles have been utilized in the construction of retained soil walls in the U.S. since the early 70's. In these walls the geotextile sheets are used to wrap layers of compacted soil producing a stable composite structure. Advantage of reinforced walls over conventional concrete walls include:

1. In many cases the reinforced wall cost-effectiveness compares favorably with conventional walls. Geotextile walls are very competitive.
2. The construction of reinforced walls is simple and rapid. This is especially true with geotextile reinforced walls.
3. The reinforced wall is flexible, thus it can undergo significant deformation or sustain significant dynamic impacts.

Some disadvantages are:

1. The construction of reinforced walls in cut regions requires a wider excavation than conventional concrete walls.
2. Excavation behind the reinforced wall is restricted.

It should be stated that due to limited experience with embedded geotextiles there is still a question regarding its endurance, i.e., its ability to resist chemical and biological degradation or to resist creep over the long-run (1). However, up-to-date performance of geotextiles in walls is encouraging (e.g., (2), (3), (4), (5), (6), (7)).

Applications of geotextile reinforced walls range from construction of temporary road embankments to permanent structures remedying slide problems and effectively widening highways. Such walls can be constructed as noise barriers or even as abutments for secondary bridges. Because of their flexibility, they can be constructed in areas where poor foundation material exists or areas susceptible to earthquake activity.

ANALYSIS AND MECHANISMS

The internal stability of reinforced walls, where a material possessing high compressive strength (soil) interacts with a material possessing high tensile strength (reinforcement), is a key problem in design. The analytical approach to this problem is based on a limiting equilibrium analysis following the procedure suggested by Baker and Garber (8),(9). The results of this analysis procedure satisfy all global equilibria requirements producing the minimal factor of safety

for the failure mechanism used. Details of the modified mathematical formulation are given elsewhere (10).

The problem is presented schematically in Fig. 1. The backfill is characterized by unit weight γ and friction angle ϕ . Each geotextile sheet possesses a tensile resistance of t_j where j is the sheet number. In developing a design methodology it will be shown that (1) the allowable value of t may exceed only a fraction of the actual geotextile's tensile strength, (2) because of practical considerations, all geotextiles extend to the same vertical plane $x=(H\cot i+l+l_e)$, (3) the geotextile restraining is along l_e , i.e., the pullout resistance portion developing between the slip surface and $x=(H\cot i+l)$ is neglected, and (4) the determination of the required t_j value is coupled with the geotextile pullout resistance. Based on the above one can assume that t_j is a function of the overburden pressure, obtaining the following linear relationship

$$t_j = t_1(H-y_j)/H \tag{1}$$

where y_j is the elevation of geotextile j , and t_1 is the pullout resistance of the geotextile at $y_1=0$.

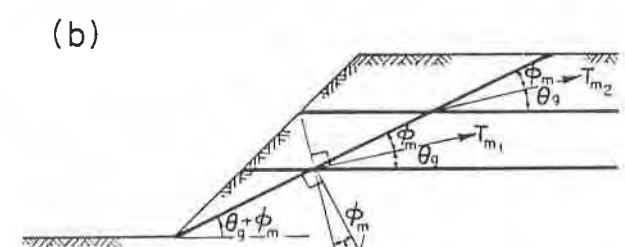
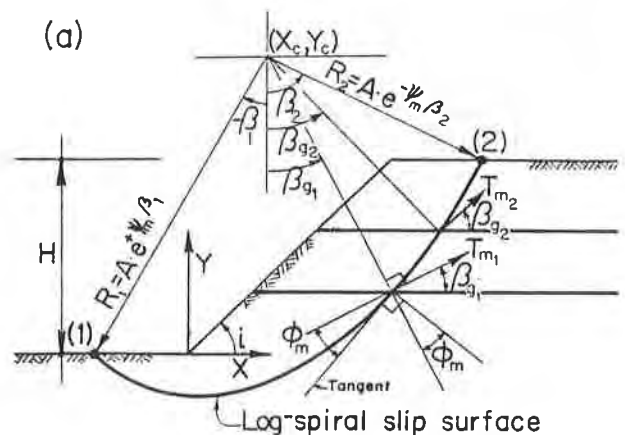
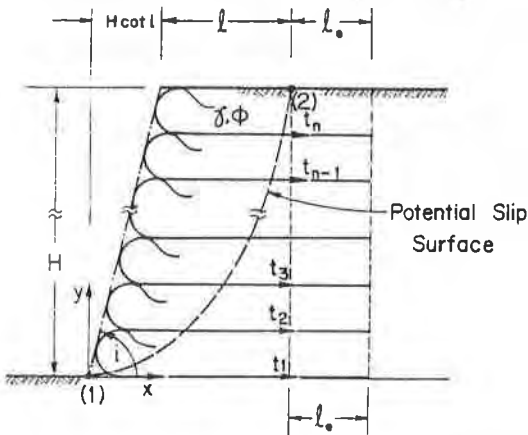


Figure 1. Basic Definitions.

Figure 2. Failure Mechanisms:

(a) Rotational, and (b) Translational.

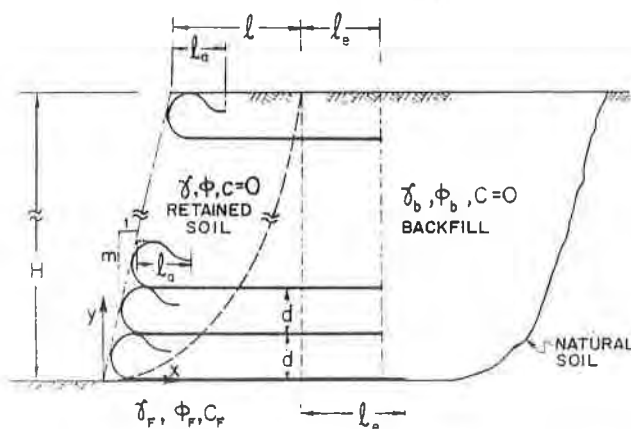


Figure 3. General Wall Configuration.

Two possible failure modes are considered: rotational and translational. The slip surface geometry corresponding to the first mode is log-spiral and to the second mode is plane. The failure mechanism that is likely to develop, however, is the one rendering the lowest factor of safety, F_s , with respect to the shear strength of soil and reinforcement. To completely define the failure mechanisms for the

actual problem, one can assume that when the soil mass is at the verge of collapse (i.e., state of limit equilibrium), all geotextile sheets remain horizontal at their intersection with the slip surface. Such an assumption is commonly employed in the simplified tieback analysis. However, since geotextiles have no significant lateral stiffness and t_j is activated by soil differential movement, it is assumed that, when failure of the composite structure occurs, the membrane at the slip surface will be inclined so as to contribute the most resistance, i.e., be most effective. It can be verified (10) that for rotational failure the geotextile is orthogonal to the radius of the log-spiral at their intersection. In the case of translational failure, the geotextile is inclined at ϕ_m to the failure plane where $\phi_m = \tan^{-1}[(\tan(\phi))/F_s]$. These two failure mechanisms are presented in Fig. 2. It is interesting to note that these collapse geometries are identical to the admissible mechanisms used in the upper bound analysis in plasticity where a rigid body is considered and the geotextile's tensile force is opposing the velocity.

To develop design charts, a closed-form solution for each failure mode was assembled (11).

GENERAL CONSIDERATIONS

The conceptual configuration of a geotextile-retained soil wall is illustrated in Fig. 3. Notice that all geotextile sheets, except for the lowest one extend to the same vertical plane. Although this configuration requires, apparently, an excessive embedment length of geotextiles at the lower elevations, it is recommended because of the following:

1. The structure resembles conventional reinforced earth walls for which extensive experience has been gained. Thus, applying the well established design approach, concerned with various potential external failure mechanisms, is straightforward.
2. Due to complex interaction there are some uncertainties in estimating geotextiles' pullout resistance contributed by their embedded portion next to the idealized potential slip surface (i.e., restraining within the "passive block"). This resistance, in turn, produces an internally stable structure. Extending the geotextile sheets beyond l , neglecting any resistance effect generated along portions underneath the sliding mass, adds confidence in design.
3. Construction is facilitated due to simpler specifications.

As shown in Fig. 3 the wall face is not necessarily vertical. This can be due to structural reasons (e.g., internal stability), ease of construction or architectural purposes (e.g., see Fig. 4). Also notice that all geotextiles are equally spaced so that construction is simplified.

Geotextiles exposed to ultra-violet (UV) light may degrade rapidly. At the end of construction, therefore, protective coating should be applied to the exposed face of the wall (e.g., (4), (12)). To protect the wall from possible vandalism, a layer of about 3 inches of gunnite can be applied (e.g., (4), (6)). When aesthetics is important, a low cost solution may utilize a facing system comprised of used railroad ties (7). Fig. 4 illustrates a rather expensive solution; however, its facing can be used as part of a simpler construction procedure, i.e., each facing module is placed before each layer lift thus acting also as a form.

Note that no weepholes are specified although the UV and vandal protection measures may render an impermeable wall. To ensure the fast removal of seeping water in a permanent structure, however, it is recommended to replace one to two feet of the natural foundation soil (in case it is not free-draining) with a crushed-stone layer (6). This layer should provide adequate drainage from within and behind the wall. The crushed-stone should be separated from the natural soil by a heavy weight filter fabric.

PROPERTIES OF MATERIALS

Retained Soil

The soil wrapped by the geotextile sheets is termed "retained soil". This soil must be free-draining and non-plastic. The ranking (most desirable to less desirable) of various retained soil for permanent walls, using the Unified Classification System, is as follows: 1. SW, 2. SP, 3. GW, 4. GP and 5. Any of the above as a borderline classification, dual designated with GM or SM. Notice that the amount of fines in the above soil is limited to 12% passing sieve #200. This restriction limits possible migration of fines, being washed by seeping water. The fines may be trapped by the geotextile sheets (or accumulated at the lower wall elevation), thus eventually creating low permeability liners. Generally, the permeability of the retained soil must be more than 10^{-3} cm/sec.

Although crushed rock possesses high permeability and, possibly, high strength, its utilization requires special attention. Crushed rock contains angular grains which can puncture the geotextile sheets during construction. Consequently, consideration must be given to geotextile selection so as to resist puncture. It should be noted, however, that if a geotextile possessing high puncture resistance is available, then GP and GW should replace SP and SW, respectively, in their ranking order.

The geotextile-retained soil wall is a flexible structure, possibly deriving its composite strength from shear deformations of the retained soil, occurring mainly during construction. Since these deformations might be of large magnitude, it is recommended to determine the retained soil internal angle of friction, ϕ , based on its ultimate strength (i.e., shearing at constant volume). It should be emphasized that proper selection of ϕ is particularly important since it is a key factor affecting the stability of the wall.

The retained soil unit weight should be specified based on conventional laboratory compaction tests. Since the retained soil will probably be (1) further densified as additional layers are placed and compacted, and (2) subjected to transitional external sources of water, such as rainfall, it is recommended to use for design the value of γ equal to the maximum density as calculated for zero air voids.

Backfill Soil

The soil supported by the reinforced wall (i.e., the soil to the right of (l_e+l) --see Fig. 3) is termed "backfill soil." This soil has a direct effect on the external stability of the wall and, therefore, should be carefully selected.

Generally, the backfill specifications used for conventional retaining walls should be employed here as well. Such specifications are given in most geotechnical handbooks (e.g., (13)). Because of limited experience with geotextile reinforced walls, however, clay, silt or any other material with low permeability should be avoided next to a permanent wall (i.e., adjacent to $(l+l_e)$). Fig. 5 presents a possible arrangement for using such low grade backfill. Notice that a filter fabric separates the fine and the free-draining backfills, thus preventing fouling of the higher quality material. Since both backfills may have an effect on the reinforced wall external stability, the properties of both materials are needed. The unit weight should be estimated similar to the retained soil; for analysis take γ equals the maximum density at zero air voids. The strength parameters should be determined under drained conditions for the permeable backfill. For the low permeability backfill, drained and undrained strength parameters should be determined so that the short- and long-term external stability of the wall could be assessed.

The backfill and the retained soil (line AB in Fig. 5) must have similar

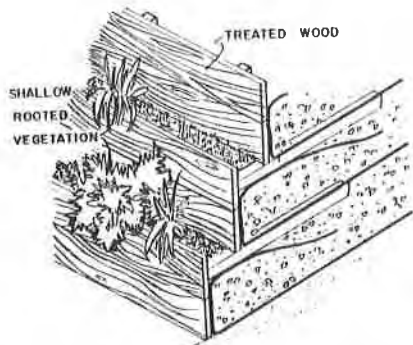


Figure 4. Aesthetic Arrangement of a Wall Face.

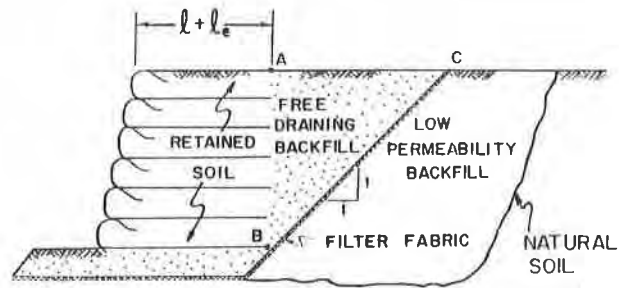


Figure 5. Arrangement for Low Permeability Backfill.

gradation at their interface so as to minimize the potential for lateral migration of soil particles. If such requirement is not practical, then a filter should be designed based on the grain-size distribution of the two materials. Alternatively, a filter fabric can be used along AB.

Geotextiles

Either woven or nonwoven geotextiles may be used, provided they meet the required specifications.

The potential for developing an allowable geotextile tensile resistance, t_j , must be ensured. As long as t_j , determined in the next section, is not fully mobilized, the reinforced wall must be internally stable. Most polymers, however, exhibit significant creep elongation when subjected to tensile force. This creep tendency increases rapidly with the level of tensile force. Specifying a geotextile possessing tensile strength equal to t_j , therefore, may result in intolerable wall deformations due to excessive creep. It is recommended that t_j be selected as a fraction of the geotextile tensile strength t_{ult} (14):

Geotextile Type	$\frac{\text{allowable tensile resistance}}{\text{ultimate tensile strength}} = \frac{t_j}{t_{ult}}$
Polyester	0.50
Polyamide	0.40
Polyethylene	0.25
Polypropylene	0.25

It should be noted that t_{ult} has to be determined using a wide width tensile test. Depending primarily on polymer type and density and on environmental conditions, the ultimate strength of some geotextiles may decrease with time. Since the full extent of this phenomenon is not well known yet, a single reduction factor of t_{ult} is suggested for all geotextiles. It is recommended to reduce by 30% the value of t_{ult} determined from the wide width tensile test. Furthermore, although proper selection of geotextiles as related to the associated construction equipment and technique is given due consideration later on, it is assumed that some imminent damage will occur during construction. Since information regarding the extent of this damage is scarce, it is recommended to further reduce t_{ult} by 20% to account for potential construction damage. Subsequently, in estimating the allowable tensile resistance, t_j , as a fraction of t_{ult} , the experimentally determined value of t_{ult} should be reduced by 50% to account for potential aging and construction damage. As more information becomes available, this reduction factor should be modified accordingly.

Mobilization of tensile force may require large elongation in the geotextile sheets. Consequently, large shear strains may be induced into the adjacent soil that restrain the geotextile from slippage thus enabling the development of t_j . These induced strains must be acceptable (i.e., compatible). It is recommended, therefore, to ensure that for the required tensile resistance, t_j , the corresponding geotextile sheet elongation shall not exceed 10%. Both the creep and elongation criteria must be satisfied in selecting a geotextile based on t_j .

Research indicates that non-woven geotextiles tend to increase their strength as well as their stiffness as their confining pressure increases (e.g., (15), (16), (17)). Because of insufficient experience, however, it is recommended to ignore this phenomenon in design.

An important component of the soil-geotextile interaction is the friction and adhesion developed at their interface. In the next section it is assumed that the friction angle between the retained soil and geotextiles is $2\phi/3$. Experience has shown that the assumed friction value is conservatively valid for most geotextiles. In specifying a geotextile, however, one must ensure that the assumed design values for the interface are met. These values can be determined from a direct shear test using the soils involved.

If the retained soil is comprised of coarse and sharp-edged aggregate, the question whether the geotextile will survive installation arises; i.e., will it resist puncture during construction. This survivability is heavily dependent on the construction technique and equipment. Based on experience related to highways (18), the following modified recommendations are given for walls with geotextile sheets spacing of up to one foot. If the aggregate average diameter is less than one-half lift thickness, use minimum puncture strength of 110 lbs. The minimum puncture strength required for all other types of retained soil must be 40 lbs. The above strength values are for construction equipment exerting ground pressures up to 8 psi. If the exerted pressures are higher than 8 psi, the first lift should be, at least, 10 inches. Note that in this case, there will practically be only one lift equal to the geotextiles specified spacing (which is limited to a maximum of 12 inches). If coarse angular aggregate is used and the structure is anticipated to carry external loads, the thickness of the soil layer above the top geotextile sheet must be at least 18 inches and preferably of finer grade material. This should protect the top sheet from possible puncture and abrasion damage during its service life. It should be noted that the above specified strength is measured by puncturing the geotextile with a 5/16 inch diameter solid steel cylinder with hemispherical tip.

Most commercially available geotextiles possess equivalent permeability which will not alter the free-draining characteristic of the wall. It is recommended, however, to specify geotextiles with equivalent permeability of, at least, 10^{-2} cm/sec.

Finally, when selecting a geotextile it is worthwhile to bear in mind its cost. Barrett (7) has indicated that the geotextile cost amounts to only 5 to 10% of the total construction cost. Therefore, factors such as availability of geotextiles and construction schedule should also be considered in selecting a geotextile.

INTERNAL STABILITY

Internal stability is a result of sufficient resistance to collapse developed by the retained soil and the geotextiles' tensile force. This stability can be viewed from two different perspectives. In the first one it is assumed that all shear resistance components are equally mobilized; i.e., both soil and geotextile approach their prescribed strength simultaneously. It is regarded as the internal stability of the composite structure and conceptually, it is similar to the conven-

tional slope stability approach where the cohesion and the friction are assumed to be equally mobilized. The second prospective assumes that the soil attains failure first (i.e., fully mobilized), thus activating geotextiles' tensile force. It implies that the structure's margin of safety against collapse depends now on the degree of the geotextiles' tensile resistance mobilization. This type of stability is analogous to the common approach used in design of geotextile-retained soil walls.

When the composite structure is actually at the verge of failure, both of the above prospectives coincide. Adequate design, however, requires a specified margin of safety against collapse which may be different for each prospective of failure. It is recommended, therefore, to carry out a design trail based on each approach, using the more stringent result as the final design. This ensures that the safety, based on both criteria, is satisfied.

Composite Structure

In assessing the internal stability of the composite structure, it is assumed that the soil's friction, $\tan\phi$, and the geotextiles' tensile resistance, t_j ($j=1,2,\dots,n$), are equally mobilized. Only failures potentially developing within the reinforced wall block are considered.

Typically, the following parameters are given: H and m (i.e., the height and face inclination of the wall, respectively); and γ and ϕ (i.e., the unit weight and internal angle of friction of the retained soil, respectively). For a prescribed factor of safety, F_s , one has to determine the required tensile resistance of the geotextile sheets, t_j , as well as their embedment length, $l+l_e$.

It is assumed that the effective restraining zone over which the geotextiles' tensile forces dissipate is l_e -- see Fig. 3. The geotextiles' restraining force capacity must be, at least, equal to their required tensile resistance. Assuming these forces to be proportional to the overburden pressure one gets

$$t_j = \gamma(H-y_j) l_e (\mu_t + \mu_b) \quad (2)$$

where y_j is the elevation of geotextile j , measured from the toe; and μ_t , μ_b are the friction coefficients between geotextile j and the soil above and below it, respectively. Generally, μ is a function of ϕ . It is recommended to use the following relationship

$$\mu_t = \tan(0.67\phi_{\text{top}}) \quad (3a)$$

$$\mu_b = \tan(0.67\phi_{\text{bottom}}) \quad (3b)$$

Since a uniform soil is retained, μ_t equals μ_b for all geotextiles $j=2,3,\dots,n$. This, however, may not be the case for the geotextile interfacing the foundation soil (i.e., $j=1$). Utilizing eqns. (1) through (3), the following expressions are obtained

$$l_e = t_1 / [2\gamma H \tan(0.67\phi)] \quad (4a)$$

$$l_{e1} = t_1 / \{\gamma H [\tan(0.67\phi) + \tan(0.67\phi_F)]\} \quad (4b)$$

$$\text{If } l_{e1} < l_e \text{ then take } l_{e1} = l_e \quad (4c)$$

where ϕ_F is the friction angle of the foundation material, and l_{e1} is the effective

embedment length of the geotextile at the bottom -- see Fig. 3. The condition in eq. (4c) (i.e., $l_{e1} < l_e$) can exist only when $\phi_F > \phi$.

The restraining force t_j counterbalances a force generated within the sliding mass. To ensure that t_j can indeed develop within the active mass as well as to retain the soil at the wall face, each geotextile sheet is folded back at the wall face and re-embedded over a length $(l_a)_j$ --see Fig. 3. To determine $(l_a)_j$, the following assumptions are combined with the rationale used in stating eq. (2):

1. The average elevation of l_a is at the center in between two adjacent geotextile sheets.
2. The full intensity of t_j is carried along $(l_a)_j$.
3. For non-vertical walls the average overburden pressure acting along l_a is proportional to $(ml_a+d)/2$ so long as $m(l_a/2)+d$ is less than H . One can see the geometrical interpretation of this assumption by looking at Fig. 3.

Based on the above, the following approximate expressions are assembled

$$l_a = \begin{cases} (d/2m) \left\{ \sqrt{1 + 8mHl_e/d^2} - 1 \right\} & \text{only for } m < \infty \text{ and } (ml_a/2) \leq (H-d) \\ 2l_e & \text{for all cases} \\ \geq 3 \text{ ft.} & \text{for all cases} \end{cases} \quad (6)$$

For each problem, the longest l_a should be selected. Notice that a minimal value of $l_a=3$ ft., adopted from Steward et al. (12), should ease construction and, physically, will ensure adequate embedment. It is interesting to note that, in most practical cases, eq. (6) will indicate that l_a is specified by its required minimal value.

Figures 6a and 6b are design charts. They represent the results only for the critical mode of collapse, i.e., either planar or log-spiral failure surface.

It is recommended to use a factor of safety of $F_s=1.5$ for the composite structure. This F_s value is typical in design of slopes where long-term stability is concerned. The following are the steps necessary to utilize the charts in the design process:

1. Determine the wall's geometry; i.e., height H and face average inclination -- 1 (horizontal): m (vertical).
2. Determine the retained soil properties; i.e., unit weight γ and friction angle ϕ .
3. Select a value for the composite structure factor of safety F_s .
4. Select the geotextile sheets spacing, d . To ease construction, this spacing should be limited to a maximum of $d=12$ inches.
5. Compute $\phi_m = \tan^{-1}[(\tan\phi)/F_s]$.
6. For the given m and computed ϕ_m , determine T_{m1} utilizing Fig. 6a.
7. The number of the required equally spaced geotextile sheets is $n=H/d$.
8. Compute the required tensile resistance of the geotextile sheet at the toe elevation $t_1 = T_{m1} F_s \gamma H^2 / n$.
9. Calculate the required tensile resistance of all other geotextile sheets using eq. (1); i.e., $t_j = t_1 (H - y_j) / H$.
10. Based on the recommendations in the last section and the required t_j , select the proper geotextiles. In case the specified geotextile tensile strength is exces-

- sively high as compared to available geotextiles, decrease the spacing d and return to step 7. If only one type of geotextile is used, skip step 9; t_1 will be used to determine this geotextile type.
11. Use eq. (4) to compute the required length of the restraining zone so that the geotextiles' tensile resistance can actually develop; i.e., calculate l_e and l_{e1} .
 12. Compute $\lambda_{T\phi} = (nt_1) / (\gamma H^2 \tan\phi)$.
 13. Based on m and $\lambda_{T\phi}$, determine L from Fig. 6b.
 14. Compute $l = L \cdot H$ where l defines the location at which the potential slip surface intersects the crest.
 15. Based on eq. (6) select the geotextile re-embedment length l_a at the wall face--see Fig. 3.
 16. Determine the required length of each geotextile sheet j : $l_{e1} + l + d + l_a + (H - y_j) / m$. For geotextile $j=1$ use l_{e1} rather than l_e . Add one foot as tolerance permitting curvature along l_a and over the wall face.

Equal application of F_s to two different materials (i.e., to $\tan\phi$ and t_j) appears rather arbitrary although such an approach is common in similar problems (e.g., conventional stability analysis of layered slopes). In retrospect, however, one can come up with a justification for this F_s application as far as the geotextile reinforced problem is concerned. Combining eqns. (1) and (4) (or steps 9 and 11 above) yields $t_j = 2\gamma(H - y_j)l_e \tan(0.67\phi)$; i.e., t_j is controlled and, in fact, is equal to the pullout resistance. Thus applying F_s to t_j or to $\tan(0.67\phi)$ is equivalent. Consequently, F_s is actually related only to the retained soil friction making the concept of equal mobilization reasonable.

Geotextile Tensile Resistance

As was stated before, the internal stability can be viewed from another prospective. One can assume that the soil is fully mobilized (i.e., $\phi_m = \phi$) and that the margin of safety then is solely contributed by the geotextile tensile resistance. This margin of safety is defined as

$$F_g = t_j / t_{mj} \quad (7)$$

where F_g is the factor of safety with respect to geotextile tensile resistance; $t_{mj} = T_{mj} \gamma H^2 / n$ = the tensile resistance of geotextile j yielding a composite structure which is at the verge of failure (i.e., $F_s = 1.0$); and t_j is the required tensile resistance of geotextile j so that F_g is attained. It is recommended to use $F_g = 2.0$. It can be verified that this F_g value combined with the suggested design procedure will render structures possessing safety factors greater than one when their stability is analyzed using the design methods introduced by Steward et al. (12) and Murray (19).

To design a wall possessing a specified F_g value, the design charts (Figs. 6a, 6b) are utilized. The composite factor of safety, however, must be taken as $F_s = 1.0$ when using these charts. The following are the steps necessary to utilize the charts, assuming that a preliminary design, based on F_s , has been carried out:

1. Select a value for F_g .
2. Take $F_s = 1.0$; hence, $\phi_m = \phi$.
3. Use Fig. 6a to determine T_{m1} for m and ϕ_m .
4. Compute the required tensile resistance of the geotextile sheet at the toe elevation $t_1 = F_g T_{m1} \gamma H^2 / n$.
5. Calculate the required tensile resistance of all other geotextile sheets using eq. (1); i.e., $t_j = t_1 (H - y_j) / H$.
6. Compare t_j for all n sheets with those obtained based on a prescribed F_s in the previous section. If t_j here is smaller, take the previous t_j for

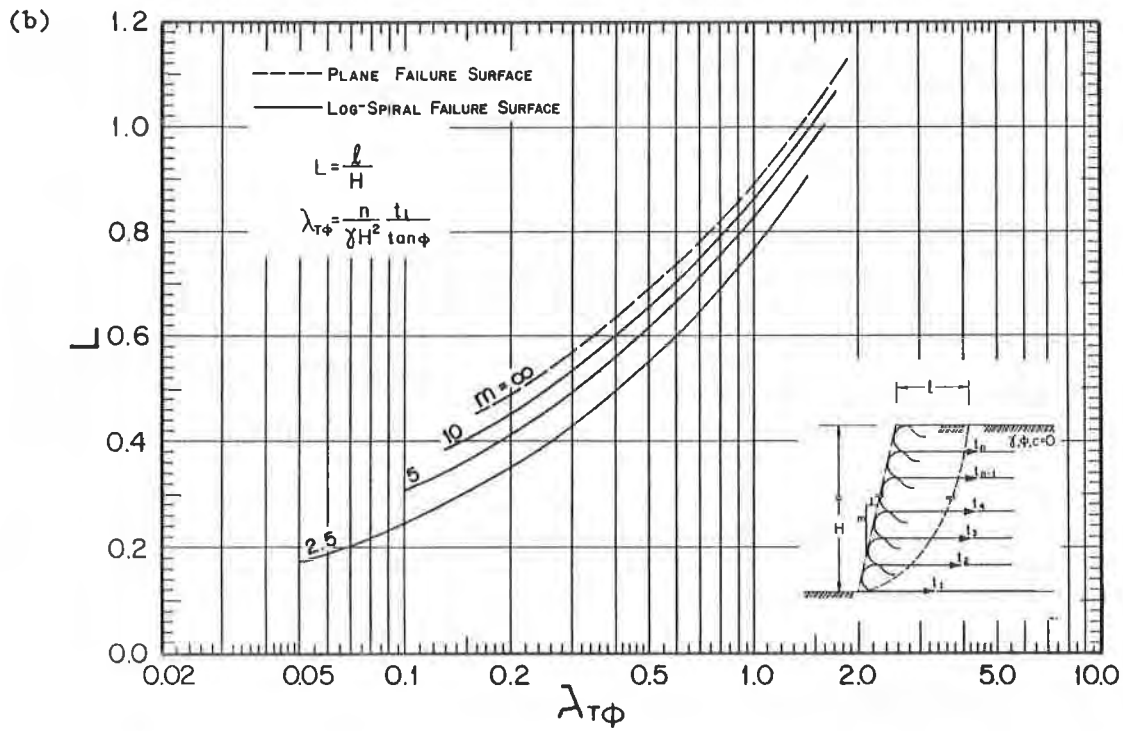
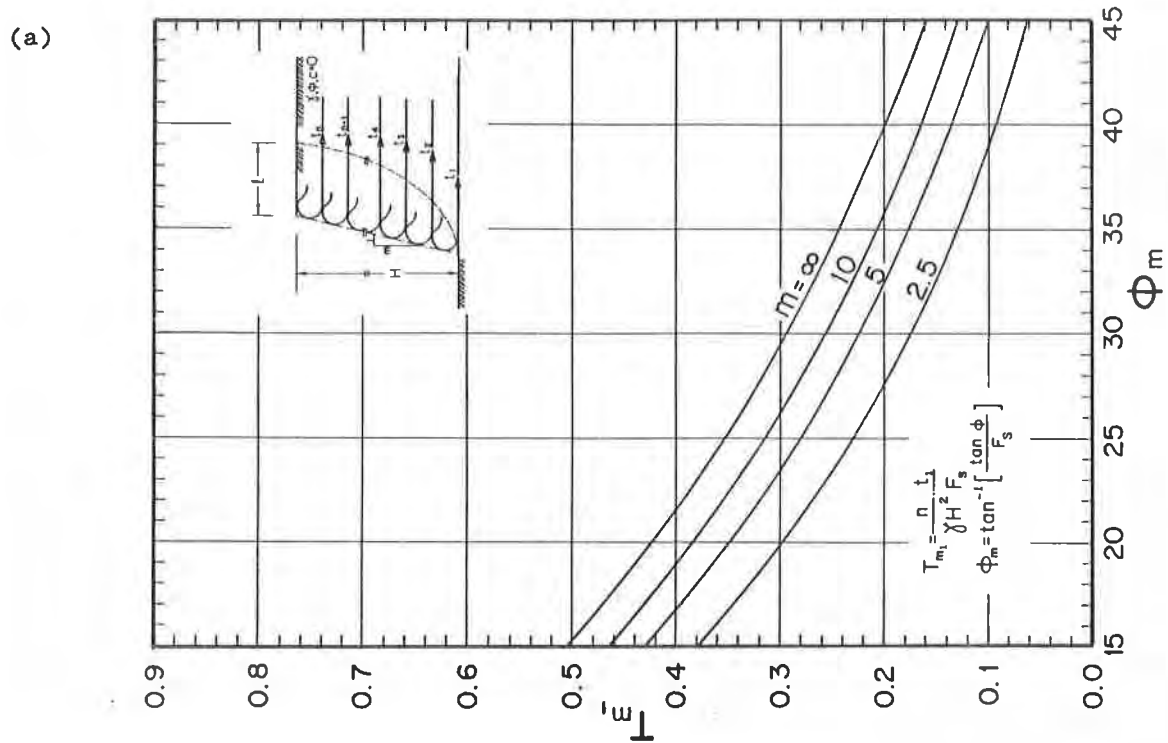


Figure 6. Design Chart.

- design and skip to the next step. If it is larger than the previously required, select the proper geotextiles based on the recommendations in the last section. In case the specified geotextile tensile strength is excessively high, increase the number of geotextile sheets n and return to step 4.
7. Regardless of the conclusion in step 6, in steps 7 and 8 use t_1 as computed in step 4. Use eq. (4) to compute the required length of the restraining zone l_e and l_{e1} .
 8. Compute $\lambda_{T\phi} = (nt_1) / (F_g \gamma H^2 \tan \phi)$. Notice that t_1 / F_g is used here, whereas before only t_1 was used.
 9. Use Fig. 6b to determine L and m and $\lambda_{T\phi}$.
 10. Compute $l = L \cdot H$.
 11. Is $(l + l_e)$ smaller than the value obtained based on a prescribed F_s ? If yes, then the embedment length is dictated by the procedure based on the safety factor for the composite structure F_s . If no, proceed.
 12. Select l_a based on eq. (6).
 13. Determine the required length of each geotextile sheet j : $l_e + l + d + l_a + (H - y_j) / m$. Add one foot as tolerance. Use l_{e1} instead of l_e for geotextile #1.

Surcharge Load

Design charts, similar in nature to Fig. 6, which deal with uniform and strip surcharge loads are given elsewhere (11).

Example

Given a wall data: height $H=10$ ft. and face inclination $1:\infty$ ($m=\infty$, i.e., vertical wall). The retained soil data: total unit weight $\gamma=120$ lb/ft³ and friction angle $\phi=35^\circ$. The foundation possesses $\phi_F=20^\circ$.

Design based on $F_s = 1.5$: Following the presented procedure one can choose a spacing of $d=1$ ft. Computing ϕ_m gives $\phi_m = \tan^{-1}[(\tan 35^\circ) / 1.5] = 25^\circ$. For $m=\infty$ and $\phi_m=25^\circ$, it follows from Fig. 6a that $T_{m1}=0.35$. For a spacing of $d=1$ ft., the number of required geotextile sheets is $n=H/d=10/1=10$ sheets. Hence, the required tensile resistance of the geotextile sheet at the toe elevation is $t_1 = T_{m1} F_s \gamma H^2 / n = 0.35 \cdot 1.5 \cdot 120 \cdot (10)^2 / 10 = 630$ lb. per foot width. Using the equation $t_j = t_1 (H - y_j) / H$, where y_j is zero at the toe and H at the crest, one can calculate the required tensile resistance of each geotextile sheet:

Geotextile # (j)	1	2	3	4	5	6	7	8	9	10
Elevation y_j [ft]	0	1	2	3	4	5	6	7	8	9
t_j [lb/ft]	630	567	504	441	378	315	252	189	126	63

Now, a geotextile can be selected based on the recommendations. If only one type of geotextile is to be used, t_1 should be the key value for selecting this type. If, however, geotextiles with decreasing strength properties are preferred, take the maximum t_j for each cluster of homogeneous geotextiles as the key value.

The required length of the restraining zone, so that t_j can realize without pullout, should be calculated based on eq. (4); i.e.,

$$l_e = 630 / [2 \cdot 120 \cdot 10 \cdot \tan(0.67 \cdot 35^\circ)] = 0.61 \text{ ft} \approx 8''$$

$$l_{e1} = 630 / \{120 \cdot 10 \cdot [\tan(0.67 \cdot 35^\circ) + \tan(0.67 \cdot 20^\circ)]\} = 0.78 \text{ ft} \approx 10''$$

For all practical purposes a uniform value of l_e equals one foot can be selected.

Now, calculate $\lambda_{T\phi} = (10 \cdot 630) / (120 \cdot 10^2 \cdot \tan 35^\circ) = 0.75$. For $m = \infty$ and $\lambda_{T\phi} = 0.75$ read $L = 0.8$ from Fig. 6b. Hence, the potential slip surface is located at a distance of $l = 0.8 \cdot 10 = 8$ ft. Using eq. (6) one obtains $l_a = 3$ ft. Allowing one additional foot as tolerance, the length of each geotextile sheet should be equal to $[l_e + l + d + l_a + (H - y_j) / m] + 1 = (1 + 8 + 1 + 3) + 1 = 14$ ft.

Design based on $F_g = 2.0$: Taking $F_s = 1.0$, ϕ_m then equals ϕ . Using Fig. 6a for $\phi_m = 35^\circ$ and $m = \infty$, the corresponding T_{m1} is 0.241. Hence, $t_1 = F_g t_{m1} \gamma H^2 / n = 2.0 \cdot 0.241 \cdot 120 \cdot (10)^2 / 10 = 580$ lb per foot width. Using eq. (1), the required tensile resistance of each geotextile is:

Geotextile # (j)	1	2	3	4	5	6	7	8	9	10
Elevation y_j [ft]	0	1	2	3	4	5	6	7	8	9
t_j [lb/ft]	580	522	464	406	348	290	232	174	115	58

Comparing t_j 's based on $F_g = 2.0$ and $F_s = 1.5$ implies that the key value for t_j is dictated by the composite structure stability (i.e., by $F_s = 1.5$). Hence, the previous results are taken for design.

Based on eq. (4) the following is obtained: $l_e = 0.57$ ft and $l_{e1} = 0.72$ ft. Once again, take $l_{e1} = l_e = 1$ ft. Compute $\lambda_{T\phi} = (10 \cdot 580) / (2.0 \cdot 120 \cdot 10^2 \cdot \tan 35^\circ) = 0.35$. For $m = \infty$ and $\lambda_{T\phi} = 0.35$ read $L = 0.6$ from Fig. 6b. Consequently, $l = 0.6 \cdot 10 = 6$ ft and $(l + l_e) = 7$ ft. This embedment length is less than the one resulted from the prescribed $F_s = 1.5$ (i.e., less than 9 ft.). In this particular problem the predominant factor is the design based on the safety for the composite structure. It determines both the required tensile resistance ($t_1 = 630$ lb/ft) and the embedment length ($l + l_e = 9$ ft). The resulted structure will have F_s equals 1.5 but F_g somewhat greater than 2.0.

EXTERNAL STABILITY

The composite wall interacts with its foundation soil and is subjected to lateral earth pressures induced by the soil retained behind the reinforced portion. The effects of these factors were not considered in the internal stability design. Consequently, an internally stable reinforced wall may have unacceptable external stability. Typically, the reinforced wall is taken as a monolithic block having to be stable under the following conditions:

1. Overturning about the toe of the wall.
2. Sliding of the wall along its base or above it.
3. Overall slope stability.
4. Bearing capacity failure of the base of the wall.

Satisfaction of the above stability criteria does not guarantee tolerable settlements. Therefore, this subject, which may affect serviceability but will not cause catastrophic failure, may need special attention as well.

External stability can be assessed using available procedures for reinforced or conventional walls (e.g., (11)). Due to restricted publishing space, however, these procedures are not represented here.

REFERENCES

- (1) Mitchell, J.K., "Earth Walls," TR News, Transportation Research Board, National Research Council, No. 114, September-October, 1984, pp. 24-31.

- (2) Bell, J.R., Stilley, A.N. and Vandre, B., "Fabric Retained Earth Walls", Proceedings of the 13th Annual Engineering Geology and Soils Engineering Symposium, University of Idaho, Moscow, April 2-4, 1975, pp. 271-287.
- (3) Bell, J.R. and Steward, J.E., "Construction and Observation of Fabric Retained Soil Walls," Proceedings of the International Conference on the Use of Fabrics in Geotechnics, April 20-22, 1977, Paris, Vol. 1, pp. 123-128.
- (4) Bell, J.R., Barrett, R.K. and Ruckman, A.C., "Geotextile Earth-Reinforced Retaining Wall Tests: Glenwood Canyon, Colorado," Transportation Research Record, 916, 1983, pp. 59-69.
- (5) Mohny, J., "Fabric Retaining Wall-Olympic N. F.," Highway Focus, May 1977, Vol. 9, No. 1, pp. 88-103.
- (6) Douglas, G.E., "Design and Construction of Fabric-Reinforced Retaining Walls by New York State," Transportation Research Record, 872, 1982, pp. 32-37.
- (7) Barrett, R.K., "Geotextiles in Earth Reinforcement," Geotechnical Fabrics Report, March/April 1985, Vol. 3, No. 2, pp. 15-19.
- (8) Baker, R. and Garber, M., "Variational Approach to Slope Stability," Proceedings of the 9th International Conference on Soil Mechanics and Foundation Engineering, Tokyo, Vol. 2, 1977, pp. 9-12.
- (9) Baker, R. and Garber M., "Theoretical Analysis of the Stability of Slopes," Geotechnique, Vol. 28, No. 4, 1978, pp. 395-411.
- (10) Leshchinsky, D., "Geotextile Reinforced Earth, Part I & II," Research Report Nos. CE 84-44/45, July 1984, Department of Civil Engineering, University of Delaware, Newark, DE.
- (11) Leshchinsky, D., "Design Manual for Geotextile-Retained Earth Walls," Research Report No. CE 85-51, Sept. 1985, Department of Civil Engineering, University of Delaware, Newark, DE.
- (12) Steward, J., Williamson, R. and Mohny, J., Guidelines for Use of Fabrics in Construction and Maintenance of Low-Volume Roads, Chapter 5, USDA, Forest Service, Portland, Oregon, June 1977 (Also Revised Version, June 1983).
- (13) Terzaghi, F. and Peck, R.B., Soil Mechanics in Engineering Practice, 1967, 2nd Edition, John Wiley & Sons, Inc., p. 364.
- (14) R. Veldhuijzen Van Zanten (editor), Geotextiles and Geomembranes in Civil Engineering, John Wiley & Sons, 1986, p. 159.
- (15) McGown, A., Andrawes, K.Z. and Kabir, M.H., "Load-Extension Testing of Geotextiles Confined In-Soil," Proceedings of the 2nd International Conference on Geotextiles, August 1-6, 1982, Las Vegas, USA, Vol. 3, pp. 793-798.
- (16) El-Fermaoui, A. and Nowatzki, E., "Effect of Confining Pressure on Performance of Geotextiles in Soils," Proceedings of the 2nd International Conference on Geotextiles, August 1-6, 1982, Las Vegas, USA, Vol. 3, pp. 799-804.
- (17) Leshchinsky, D. and Field, D.A., "In-Soil Load Elongation, Tensile Strength and Interface Friction of Nonwoven Geotextiles," Proceedings of Geosynthetics '87, Feb. 1987, New Orleans, LA.
- (18) Christopher, B.R. and Holtz, R.D., Geotextile Engineering Manual, 1985, Course Text, Prepared for FHWA, National Highway Institute, Washington, D.C., Contract No. DTFH61-80-C-00094.
- (19) Murray, R.T., "Fabric Reinforced Earth Walls: Development of Design Equations," Ground Engineering, Vol. 13, No. 7, pp. 29-36.

SCHMERTMANN, G.R., CHOUERY-CURTIS, V.E., and JOHNSON, R.D.
The Tensar Corporation, U.S.A.
BONAPARTE, R.
GeoServices Inc. Consulting Engineers, U.S.A.

Design Charts for Geogrid-Reinforced Soil Slopes

ABSTRACT

This paper describes the development of design charts for reinforced soil slopes. A review and comparison of existing design charts shows that treatment of reinforcement lengths has not been completely satisfactory. In this study, simple limit equilibrium slope stability analyses are used to predict the number and lengths of reinforcement layers required to stabilize steep slopes of drained frictional fill. A general truncation rule is used in determination of reinforcement lengths. The simple analysis results are compared to more detailed analysis methods and to previously published charts. Design charts are synthesized from the analyses and comparisons. An example problem is presented.

INTRODUCTION

Geogrids and other geosynthetic reinforcement materials have expanded the practical options for design of soil slopes. These materials permit construction of slopes at angles steeper than the angle of repose of the soil fill (Figure 1), thereby reducing land requirements for slope construction and often eliminating the need for retaining walls. Steep reinforced soil slopes frequently provide economic advantages over traditional design alternatives.

This paper describes the development of design charts which allow for the rapid evaluation of geogrid reinforcement requirements for steep slopes of simple geometry constructed of drained frictional fill. The charts provide the number and lengths of geogrid reinforcement layers needed to achieve a desired soil factor of safety for slopes of varying slope angle and soil strength. A soil-reinforcement interface shear strength equal to 90% of the internal soil shear strength was used. The charts have been developed with the goal of providing geotechnical engineers with practical, yet conservative, design guidelines for geogrid slope reinforcement.

BACKGROUND

Previous Work

Design charts for reinforced soil slopes have been presented by Ingold (6), Murray (10), Jewell et al. (7), Leshchinsky and Reinschmidt (9), Schneider and Holtz (12), and Ruegger (11). All used limit equilibrium models to investigate the amount of reinforcement required to maintain slope stability. A summary of

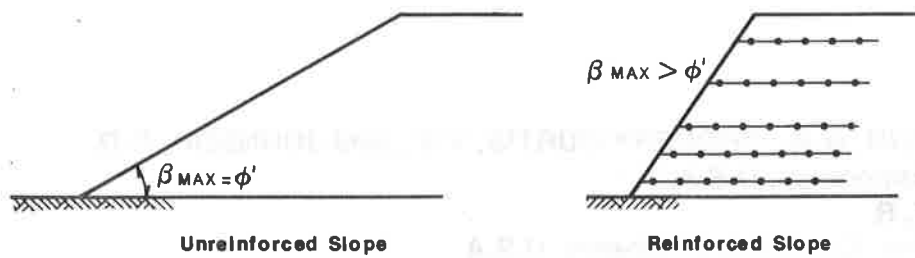


Figure 1. Reinforced Slope Concept

each investigation is given in Table 1. Only Jewell et al. (7) and Ruegger (11) present charts for the required reinforcement length. As determination of the reinforcement length is a necessary step in design, these are the only two sets of charts providing complete design solutions. Both sets of charts are restricted, however, by the assumption that the reinforcement layers are truncated along a plane parallel to the slope face.

The authors' experiences on numerous projects have shown that the assumption of parallel truncation often restricts the applicability of design charts in sidehill or embankment cuts (Figure 2), and often reduces the cost effectiveness of reinforcement compared to conventional design alternatives. The authors have also found that reinforcement lengths in existing charts are frequently longer than lengths determined with more detailed analysis methods. The charts presented herein incorporate a general reinforcement truncation scheme and are in agreement with more detailed slope stability analysis methods.

Table 1. Summary of Slope Reinforcement Design Charts

Investigator	Limit Equilibrium Model	Soil Type	Pore Pressures	Slope Angle	Length of Reinforcement	Comments
Ingold (6)	Infinite Slope	ϕ' (30° only)	N.A.	30°-80°	N.A.	Surficial stability only.
Murray(10)	Two-Part Wedge	ϕ'	r_u (0,0.25,0.5)	10°-40°	N.A.	Reinforcement load-elongation relationship included in model.
Jewell, et al. (7)	Two-Part Wedge	ϕ'	r_u (0,0.25,0.5)	30°-80°	Parallel Truncation	Basis for Schmertmann, et al. study.
Leshchinsky and Reinschmidt (9)	Log Spiral	c', ϕ'	N.A.	15°-90°	N.A.	Rigorous equilibrium model.
Schneider and Holtz (12)	Two-Part Wedge	c', ϕ'	r_u	0°-40°	N.A.	Extended work of Murray. Charts do not give critical failure surfaces.
Ruegger (11)	Circular	ϕ'	N.A.	30°-90°	Parallel Truncation	For FS = 1.3 only.
Schmertmann, et al.	Two-Part Wedge	ϕ'	N.A.	30°-80°	General Truncation	This study. Extended work of Jewell, et al.

N.A. - Not Addressed

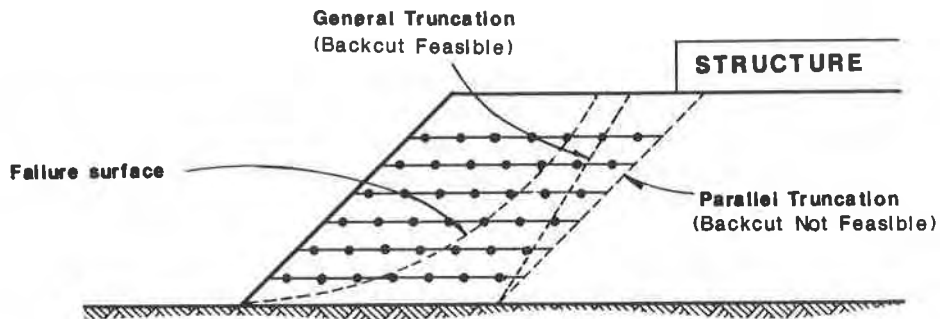
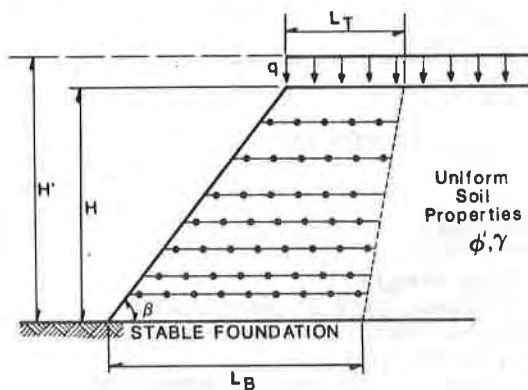


Figure 2. Feasibility of Slope Failure Repair with Parallel and General Reinforcement Truncation

Class of Problems

This investigation was limited to the conditions and assumptions listed in Figure 3. An implicit assumption in the development of the charts is that surficial stability of the slope face is adequate. Conditions not considered herein include slopes founded on soils with insufficient shear strength to support the slope, slopes with internal pore pressures, non-homogenous slope fills, slopes with rock close to the surface, seismic stability of slopes (1), and short-term undrained stability of clay slopes. If a particular problem does not match the assumptions of Figure 3, the design charts may not be applicable.



ASSUMPTIONS

1. ϕ' only ($c' = 0$) analysis is appropriate.
2. Uniform soil properties throughout slope.
3. Stable slope foundation.
4. Flat slope face and horizontal slope crest.
5. No pore pressures within the slope.
6. No seismic loading.
7. Uniform surcharge load on top of slope.
8. Horizontal reinforcement layers with coefficient of interaction equal to 0.9.

- H - Slope Height ,m
- H' - Modified Slope Height ,m (Not to exceed 1.2 H)
- q - Uniform Surcharge on Top of Slope , kPa
- β - Slope Angle from Horizontal,deg.
- ϕ' - Effective Soil Friction Angle, deg.
- γ - Moist Unit Weight of Soil , kn/m^3
- L_B - Reinforcement Length at Base of Slope ,m
- L_T - Reinforcement Length at Top of Slope ,m

Figure 3. Slope Geometry Parameters and Assumptions

SIMPLE WEDGE MODELS

General Description

Two-part wedge, or bilinear, limit equilibrium models have been used for reinforced slope stability analyses due to their simplicity and to the fact that for unreinforced slopes they yield results similar to those obtained from analyses based on more complex failure mechanisms (10). Three simple wedge models were used in this study and are illustrated in Figure 4. Horizontal and vertical force equilibrium equations for each model were set up in non-dimensional form and were programmed for computer solution. The soil was modelled as a purely frictional material complying with the Mohr-Coulomb failure criterion. All failure surfaces were assumed to enter behind the slope crest and exit through the toe. The models use a soil-reinforcement interface shear strength equal to 90% of the internal soil shear strength (coefficient of interaction, μ , equal to 0.9). Interwedge friction angles, δ , were assumed to be equal to factored soil friction angles, ϕ'_f , defined below. This assumption is consistent with the recommendation of Seed and Sultan (13) and significantly influences the predicted reinforcement lengths as will be illustrated subsequently. Jewell et al. (7) used similar two-part wedges but assumed zero interwedge friction.

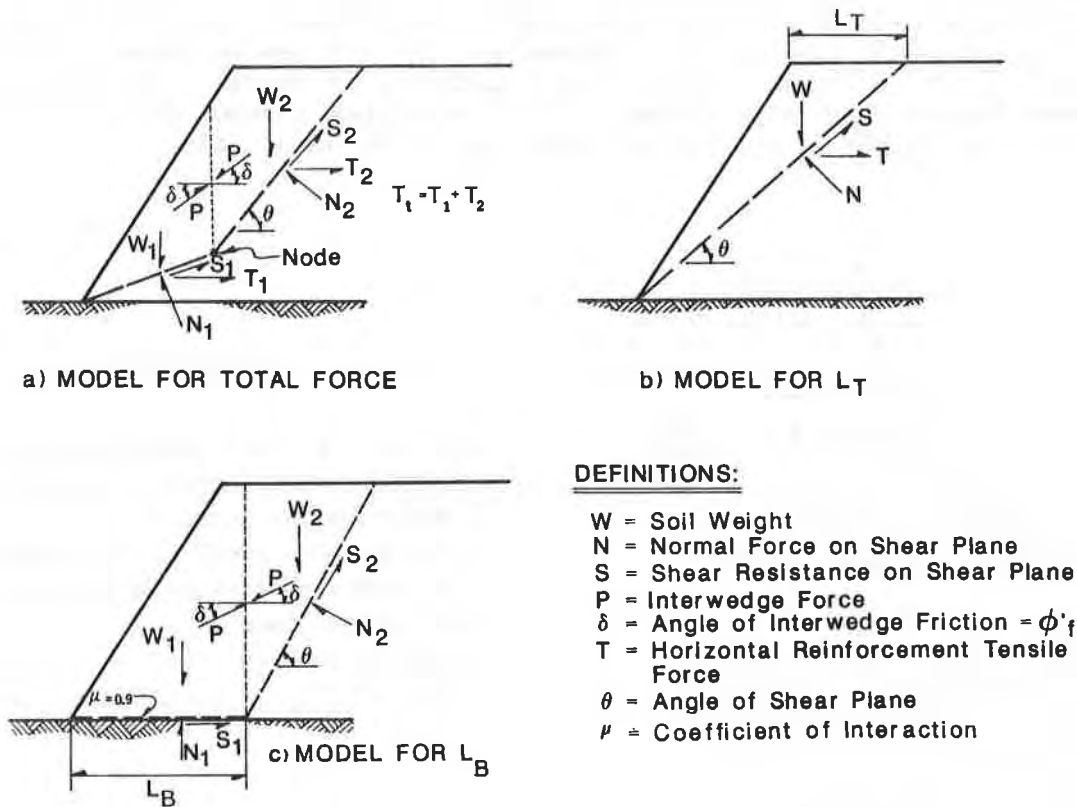


Figure 4. Simple Wedge Models

Factor of Safety

The equilibrium nature of the models means that solutions are for a factor of safety, FS, equal to one. The desired overall soil factor of safety is accounted for by using factored soil shear strengths. The factored soil friction angle, ϕ'_f , is calculated as follows:

$$\phi'_f = \tan^{-1} (\tan \phi' / FS) \quad (\text{Eq. 1})$$

where ϕ' is the soil friction angle. With extensible soil reinforcement materials such as geogrids and geotextiles, it is important to select soil and reinforcement strengths corresponding to compatible limiting strains. Therefore, the value of soil friction angle used in Eq. 1 depends on the selected limit strain of the soil-reinforcement system. Peak soil friction angles, ϕ'_p , may be used if the limit strain is sufficiently small. Otherwise, the large-strain, constant volume friction angle, ϕ'_{cv} , should probably be used as suggested by Jewell et al. (7). The amount of strain required to mobilize the long-term reinforcement design strength should be not more than the selected system limit strain.

The above definition of factor of safety is consistent with that used in classical limit equilibrium slope stability methods where the factor of safety equals the soil shear strength divided by the shear stress required to maintain slope equilibrium (5). With this approach, the authors believe that no overall factor of safety need be applied to the reinforcement design strength. The selected long-term reinforcement design strength should, however, account for reinforcement creep, long-term degradation and construction-induced material damage (3). The investigators listed in Table 1 used slightly differing definitions of factor of safety. Discussions of factors of safety for reinforced soil structures are given by Jewell (8) and Bonaparte et al. (3).

Total Reinforcement Force

The two-part wedge model shown in Figure 4a was used to predict the required total reinforcement force, T_t (kN/m). The ratio between the magnitudes of the two free-body reinforcement forces T_1 and T_2 shown in Figure 4a was determined based on an assumed triangular reinforcement tension distribution which increased proportionally with depth below the slope crest. A search was performed for the critical combination of node location and wedge angle, θ , producing the largest total required reinforcement force, T_t . For cases where the lower sliding surface was horizontal, the soil shear strength along the horizontal surface was multiplied by a value of 0.9. The nodal search was based on a procedure described by Jewell et al. (7). In the design charts, T_t is presented non-dimensionally as horizontal reinforcement force coefficient, K , which is calculated using the equation:

$$K = 2(T_t) / \gamma(H')^2 \quad (\text{Eq. 2})$$

where γ is the moist unit weight of the soil fill and H' is the modified slope height. The modified slope height is calculated as follows:

$$H' = H + (q/\gamma) \quad (\text{Eq. 3})$$

where H , q and γ are defined in Figure 3.

Reinforcement Lengths

It was assumed that the reinforcement length at the bottom of the slope, L_B , would be controlled by external stability requirements and that the reinforcement length at the top of the slope, L_T , would be controlled by internal stability requirements. These assumptions are analogous to those used in the design of reinforced soil retaining walls.

The straight-line wedge model shown in Figure 4b was used to predict L_T . This model was found to predict greater values of L_T than the two-part wedge of Figure 4a. A search was performed to find the wedge angle, θ , producing the maximum horizontal reinforcement force, T . The intersection of this critical wedge with the slope crest was assumed to define a minimum value for L_T . In the design charts, the required length is presented non-dimensionally as the ratio of L_T to modified slope height, H' .

The two-part wedge model shown in Figure 4c was used to predict L_B . A search was performed to find the wedge angle, θ , producing the largest L_B . The soil shear strength along the horizontal surface was multiplied by 0.9. This model represents a sliding failure mode in which no reinforcement tension is mobilized across the potential failure surface. In the design charts, the required length is presented non-dimensionally as the ratio of L_B to modified slope height, H' .

Typical Results

The simple wedge models were used to generate results for a range of slope angles and soil strengths. Results for $\phi'_f = 25^\circ$ are shown in Figure 5. The horizontal axis of each plot is slope angle, β . It can be seen that all curves reach an ordinate value of zero at the point where $\beta = \phi'_f$. No reinforcement is required at this point because the slope is stable due to the soil shear strength. The trend of increasing K and L_T/H' with increasing slope angle is not surprising. The shape of the L_B/H' curve, however, is not intuitively obvious. The largest value

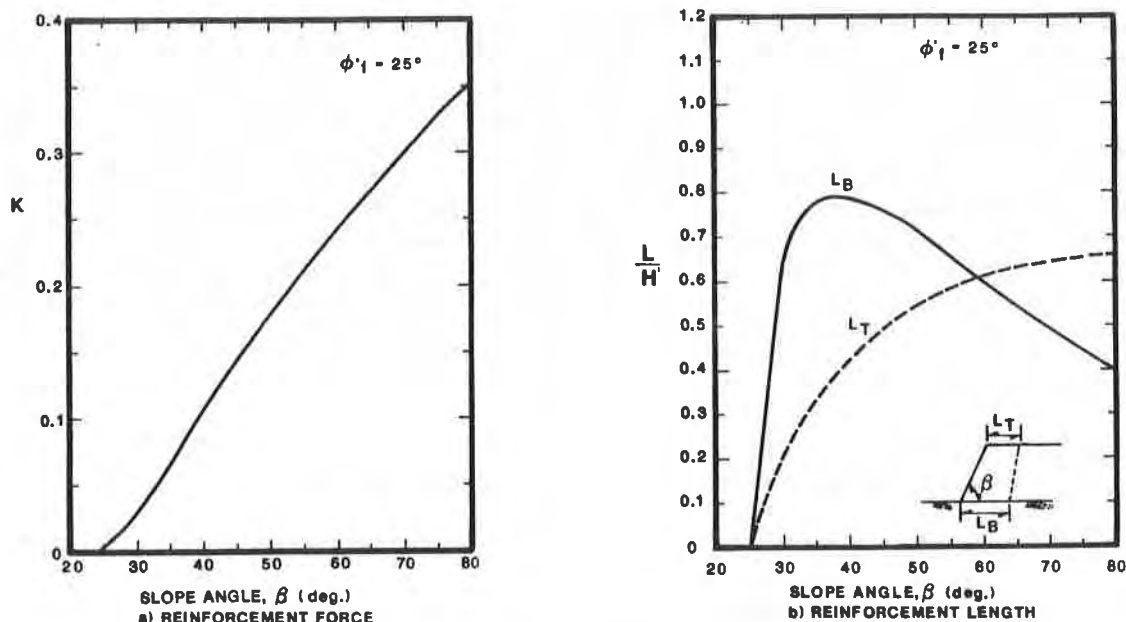


Figure 5. Typical Results from Simple Wedge Models

of L_B occurs at a flat slope angle primarily because the vertical stress (and hence the shearing resistance) at the base of the slope near the toe is much lower in a flat slope. A numerical summary of the results from the simple wedge analyses is given in Table 3.

Effect of Assumptions

The influence of assumptions regarding interwedge friction, reinforcement force distribution, and coefficient of interaction was investigated and representative findings are shown in Figure 6 for $\phi'_f = 25^\circ$. Figure 6a shows the effect of assumptions on the horizontal reinforcement force coefficient, K. The effect of using a uniform reinforcement tension distribution over the height of the slope, rather than a triangular distribution, is insignificant. The use of zero interwedge friction, rather than interwedge friction corresponding to ϕ'_f , results in an increased K value. This increase ranges from about 0.02 to 0.04 which is significant for flat slopes but relatively insignificant for steep slopes.

The effect of interwedge friction and coefficient of interaction assumptions on the reinforcement length at the bottom of the slope, L_B , is presented in Figure 6b. There is no effect on reinforcement top length, L_T , because the predictive model (Figure 4b) assumed a straight-line wedge failure mechanism. Reducing the value of coefficient of interaction from 0.9 to 0.8 increases predicted L_B values by 0% to 10%. Eliminating interwedge friction increases predicted L_B values by as much as 35% to 45%.

DETAILED ANALYSIS METHODS

Results from the simple wedge analyses were compared to results obtained from the more detailed limit equilibrium analysis methods described in this section. These slope stability methods are familiar to geotechnical engineers and provide a valuable practical check on the wedge results.

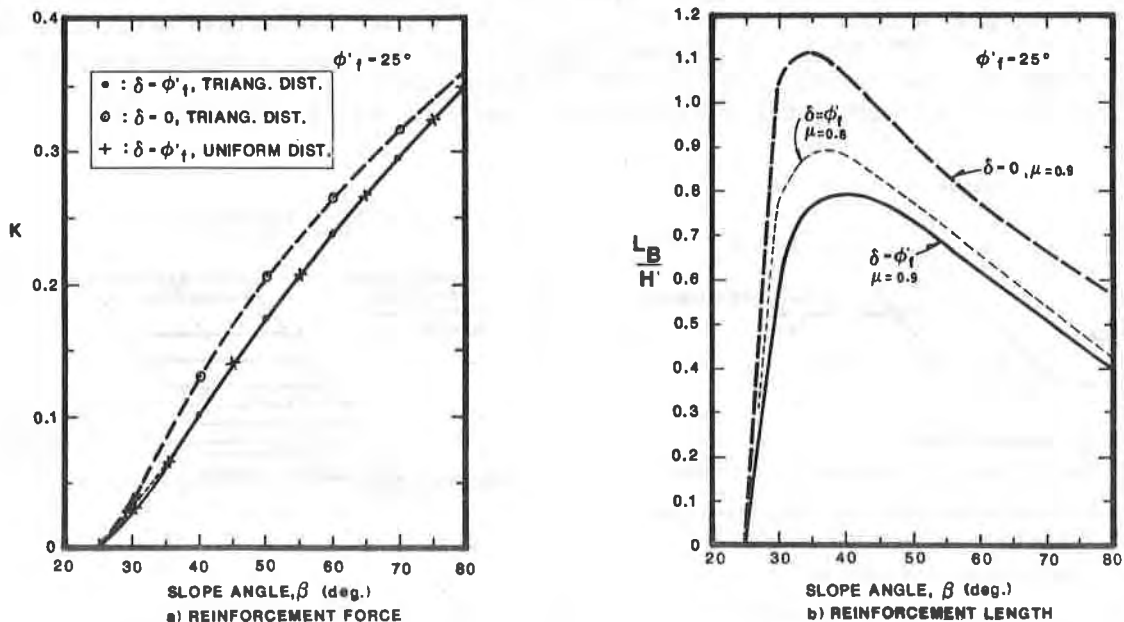


Figure 6. Effect of Assumptions on Simple Wedge Models

Bishop Modified Method

Bishop's modified method (BMM) of analysis can be extended to include the effect of tensile reinforcement (6). When a failure surface intersects a reinforcement layer, an additional resisting moment is added to the overall moment equilibrium. The precise manner by which the additional resisting moment is calculated and included in the safety factor computation is subject to debate (2).

An extended version of the BMM has been developed and implemented in a computer program ('TENSLO1') by the authors. The resisting moment from the reinforcement is calculated as shown in Figure 7. The BMM neglects interslice friction forces and while the effect on FS has been shown to be negligible for circular failure surfaces in unreinforced slopes (5), the effect in steep reinforced slope analysis is as yet unknown. 'TENSLO1' was used to evaluate K and L_T by considering circular surfaces passing through the reinforced soil zone (Figure 8). The program evaluates both reinforcement pullout and rupture failure mechanisms.

Spencer's Method

The sliding failure mode shown in Figure 4c was checked with conventional slope stability analyses for unreinforced slopes since no reinforcement intersects the failure surface. The 'PCSTABL5' program developed at Purdue University analyzes non-circular failure surfaces using Spencer's method (4). This method uses interslice friction and satisfies all equations of equilibrium. 'PCSTABL5' was used to evaluate L_B by considering sliding failure modes (Figure 8).

Results

Results from the detailed and simple wedge analyses are presented in Table 2. A comparison shows several general trends. The values of K determined with the BMM are within 10% of the wedge results. The slight disagreement is in part due to differences in the way the reinforcement force was included in the BMM and wedge analyses. The values of L_B/H' determined with Spencer's method are also within 10% of the simple wedge results. The values of L_T/H' determined with the BMM, however, are up to 40% larger than the simple wedge results. The disagreement can be attributed to the dissimilar assumed failure surface shapes and to the different methods of including the reinforcement force(s) in the analyses.

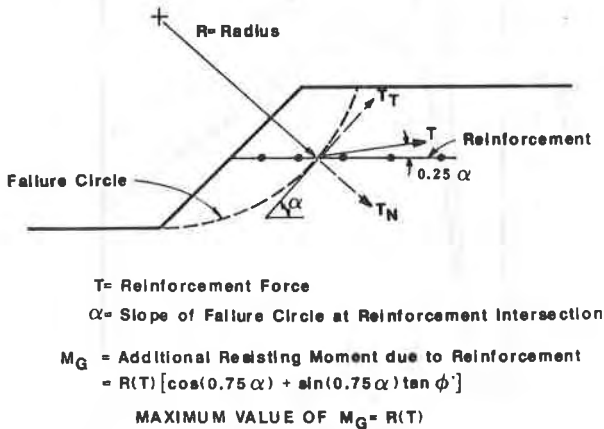


Figure 7. Calculation of Reinforcement Moment in 'TENSLO1' Program

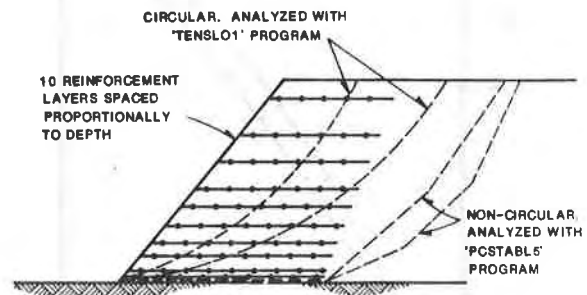


Figure 8. Typical Failure Surfaces Checked with Detailed Analyses

Table 2. Results of Simple Wedge and Detailed Analyses

Slope Angle	Factored Friction Angle	Simple Wedge Results			Detailed Analysis Results		
		K	L_T	L_B	K	L_T	L_B
30°	15°	0.25	0.83	1.84	0.27	0.86	1.83
35°	20°	0.16	0.57	1.22	0.17	0.57	1.22
45°	15°	0.38	0.99	1.47	0.40	1.23	1.40
45°	25°	0.14	0.49	0.76	0.15	0.67	0.76
60°	20°	0.34	0.77	0.83	0.31	0.91	0.78
75°	25°	0.32	0.65	0.44	0.32	0.94	0.42

DESIGN CHARTS

Design charts have been prepared based on the results from the simple wedge and detailed analyses and on comparison with other published results presented subsequently. The K , L_B and L_T values predicted by the simple wedge models were used as a baseline for the charts. These baseline values were then increased in some cases in order to be more consistent with the BMM and Spencer analyses and with the other published results. The authors also assumed that in no case should L_B be smaller than L_T .

It is important to note that the K and L values in the design charts are linked. Though the individual values for K , L_B , and particularly L_T , presented in the charts are not always conservative with respect to the individual K , L_B , and L_T results from the detailed analyses, the minimum factors of safety from the charts and from the detailed analyses are very consistent. It is believed that the design charts are practical, yet conservative, because they are the product of a careful synthesis of differing analysis methods. The charts are presented in Figure 9, and have been patterned after those of Jewell et al. (7).

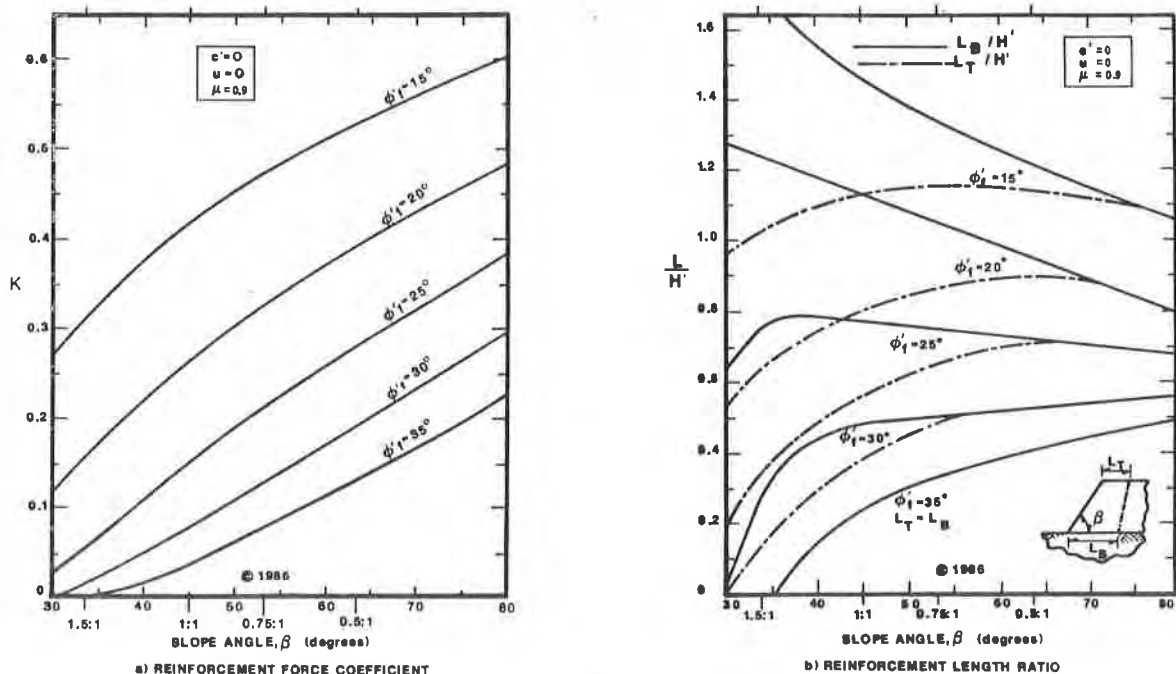


Figure 9. Design Charts

COMPARISON TO OTHER PUBLISHED RESULTS

A comparison between other published results and results from the simple wedge analyses and design charts is shown in Table 3. The variation in K is given in Table 3a. Results from Ingold (6) are not compared because his analysis was for infinite slopes. Results from Schneider and Holtz (12) are not compared because their charts require a manual search for the critical failure surface. The wedge results for K are generally slightly higher than the more rigorous results of Leshchinsky and Reinschmidt (9), and slightly lower than Jewell et al.'s (7). The wedge results were conservatively increased by 10% to obtain the K values for the design charts. There is good agreement in K values among most investigators, with the design charts from this study being slightly conservative.

The variation in L/H' is given in Table 3b. The simple wedge results for L_B are smaller than other published results. The values of L_B from the design charts are on the average 20% smaller than those from Jewell, et al. (7). Results for L_T are not comparable because the other charts assume constant reinforcement length throughout the slope height. Significant differences between the design chart

Table 3. Comparison of Other Published Results to Results from This Study

Slope Angle	Factored Friction Angle	a) K						b) L/H'					
		Murray (10)	Leshchinsky and Reinschmidt (9)	Ruegger (11)	Jewell, et al. (7)	Simple Wedge Models. This Study	Design Charts (Fig.9a)	Ruegger (11)	Jewell et al. (7)	Simple Wedge Models. This Study		Design Charts (Figure 9b)	
										L _T	L _B	L _T	L _B
30°	20°	0.05	0.10	-	0.12	0.10	0.11	-	1.40	0.46	1.28	0.53	1.28
	15°	-	-	-	0.27	0.25	0.27	-	-	-	-	-	-
40°	30°	0.04	-	-	0.06	0.04	0.05	-	-	-	-	-	-
	25°	-	-	0.12	0.13	0.10	0.11	-	-	-	-	-	-
	20°	0.10	-	0.20	0.22	0.20	0.22	-	-	-	-	-	-
	15°	-	-	-	0.38	0.34	0.38	-	-	-	-	-	-
45°	35°	-	0.04	-	0.06	0.03	0.04	-	0.47	0.20	0.24	0.25	0.25
	30°	-	0.08	-	0.10	0.07	0.08	-	0.73	0.33	0.48	0.38	0.48
	25°	-	0.13	0.14	0.16	0.14	0.15	0.86	0.98	0.49	0.76	0.56	0.77
	20°	-	0.21	0.22	0.26	0.24	0.27	1.18	1.28	0.70	1.03	0.80	1.12
	15°	-	-	-	0.43	0.38	0.42	-	-	-	-	-	-
60°	40°	-	0.07	-	0.08	0.06	0.07	-	0.42	0.28	0.16	0.28	0.28
	35°	-	0.10	-	0.13	0.10	0.11	-	0.54	0.37	0.29	0.38	0.38
	30°	-	0.15	-	0.18	0.16	0.17	-	0.70	0.48	0.44	0.52	0.52
	25°	-	0.20	0.21	0.26	0.24	0.26	0.84	0.88	0.61	0.60	0.70	0.73
	20°	-	0.28	0.29	0.36	0.34	0.37	1.09	1.14	0.77	0.83	0.89	0.98
	15°	-	0.36	-	0.52	0.47	0.51	-	-	-	-	-	-
80°	40°	-	-	-	0.17	0.16	0.18	-	0.44	0.42	0.12	0.42	0.42
	35°	-	-	-	0.22	0.21	0.23	-	0.52	0.49	0.18	0.49	0.49
	30°	-	-	-	0.29	0.27	0.30	-	0.62	0.56	0.26	0.56	0.56
	25°	-	-	0.33	0.36	0.35	0.38	0.81	0.72	0.65	0.40	0.68	0.68
	20°	-	-	0.41	0.46	0.44	0.48	0.99	0.93	0.76	0.63	0.80	0.80
	15°	-	-	-	0.57	0.55	0.61	-	-	-	-	-	-

values for L/H' and the other published results are partially due to the inclusion of interwedge friction and to the use of a high value of coefficient of interaction ($\mu = 0.9$). This discrepancy in L/H' values is consistent with the authors' experience that the previous design charts give longer reinforcement lengths than those determined from detailed analyses.

EXAMPLE PROBLEM

An example slope design using the design charts is given in Figure 10. A detailed explanation of the design process can be found in (14). The example design was evaluated using the BMM and the minimum factor of safety was found to be 1.52. This illustrates the consistency between the charts and detailed analyses, even for a case in which a considerable discrepancy exists between the L_T values from the wedge and detailed analyses (see Table 2).

CONCLUSION

Design charts for geogrid-reinforced soil slopes have been synthesized from the results of simple wedge equilibrium analyses, detailed equilibrium analyses, and from other published results. The design charts presented herein are believed to be practical, yet conservative.

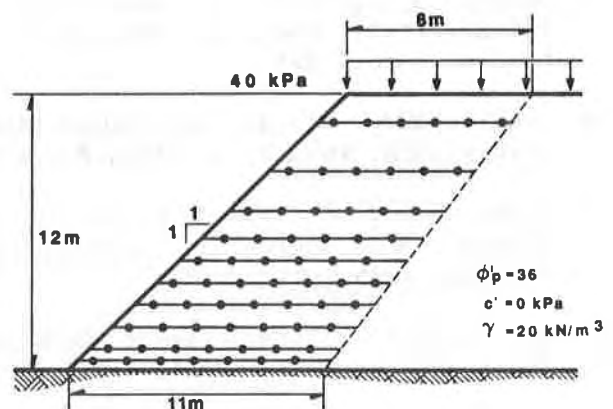
Substantial agreement exists among required reinforcement force predictions from the available design charts. Only a few investigators have developed design charts for reinforcement length, and discrepancies exist between their results. The design charts presented herein, which are based on a high soil-reinforcement interaction coefficient ($\mu = 0.9$) and a general truncation rule, give reinforcement lengths which are significantly smaller than other published results. The reinforcement length results presented herein have been found to provide slope factors of safety that are in agreement with detailed slope stability analyses. Additional work is needed in the area of reinforcement length, as evidenced by the disparities noted and the limited published information.

EXAMPLE PROBLEM

GIVEN: ALL ASSUMPTIONS VALID. REQUIRED FS = 1.5
SOIL PROPERTIES - $\phi_p = 36^\circ$, $c = 0$, $\gamma = 20 \text{ kN/m}^3$
SLOPE PARAMETERS - $H = 12 \text{ m}$, $\beta = 45^\circ$, $q = 40 \text{ kPa}$

DESIGN STEPS:

1. CALCULATED MODIFIED SLOPE HEIGHT.
 $H' = 12 \text{ m} + 40 \text{ kPa} / (20 \text{ kN/m}^3) = 14 \text{ m}$
2. CALCULATED FACTORED SOIL FRICTION ANGLE.
 $\phi_f = \tan^{-1}(\tan 36^\circ / 1.5) = 25.8^\circ$
3. OBTAIN K AND CALCULATE TOTAL GEOGRID FORCE.
 $K = 0.15$ (from Figure 9a)
 $T = 1/2 (0.15)(20 \text{ kN/m}^3)(14 \text{ m})^2 = 294 \text{ kN/m}$
4. SELECT GEOGRID DESIGN STRENGTH AND CALCULATE NUMBER OF GEOGRID LAYERS.
 $\alpha_d = 30 \text{ kN/m}$ (from review of product data (3))
 $N = (294 \text{ kN/m}) / (30 \text{ kN/m}) = 9.8$ Use 10 layers



5. OBTAIN LENGTH RATIOS AND CALCULATE GEOGRID LENGTHS.
 $L_T/H' = 0.55$ $L_B/H' = 0.76$ (from Figure 9b)
 $L_T = 0.55 (14 \text{ m}) = 7.7 \text{ m}$ Use 8 m
 $L_B = 0.76 (14 \text{ m}) = 10.6 \text{ m}$ Use 11 m
6. SPACE GEOGRID LAYERS INVERSELY PROPORTIONAL TO DEPTH (SEE REF. (14)).

Figure 10. Example Problem

ACKNOWLEDGEMENTS

The authors thank Ryan Berg for his significant input to this study and review of the paper, and Jean Pierre Giroud for his review. We also thank Doris Campbell and Barbara Hutcheson who expertly typed the manuscript, as well as Rick Komada and Sherry Chauncey who drafted the figures.

REFERENCES

1. Bonaparte, R., Schmertmann, G.R., and Williams, N.D., "Seismic Design of Slopes Reinforced with Geogrids and Geotextiles", Proc. of Third International Conference on Geotextiles, Vol. 1, p. 273, Vienna, April 1986.
2. Bonaparte, R. and Christopher, B.R., "Design and Construction of Reinforced Embankments over Weak Foundations", Proc. Symposium on Reinforced Layered Systems, Transportation Research Board, January 1987 (in press).
3. Bonaparte, R., Holtz, R.D., and Giroud, J.P., "Soil Reinforcement Design Using Geotextiles and Geogrids", ASTM Special Technical Publication #952, Geotextile Testing and the Design Engineer, 1987 (in press).
4. Carpenter, J.R., "STABL5/PCSTABL5 User Manual", School of Civil Engineering, Purdue University, May 1986.
5. Duncan, J.M. and Wright, S.G., "The Accuracy of Equilibrium Methods of Slope Stability Analysis", In: S.L. Koh (editor), Mechanisms of Landslides and Slope Stability, Engineering Geology, No. 16, p. 5, 1980.
6. Ingold, T.S., "An Analytical Study of Geotextile Reinforced Embankments", Proc. of Second International Conference on Geotextiles, p. 683, Las Vegas, August 1982.
7. Jewell, R.A., Paine, N., and Woods, R.I., "Design Methods for Steep Reinforced Embankments", Proc. of Conference on Polymer Grid Reinforcement, p. 70, London, March 1984.
8. Jewell, R.A., "Limit Equilibrium Analysis of Reinforced Soil Walls", Proc. of 11th ICSMFE, Vol. 3, p. 1705, San Francisco, August 1985.
9. Leshchinsky, D. and Reinschmidt, A.J., "Stability of Membrane Reinforced Slopes", ASCE Journal of Geotechnical Engineering, Vol. 111, No. 11, p. 1285, November 1985.
10. Murray, R.T., "Reinforcement Techniques in Repairing Slope Failures", Proc. of Conference on Polymer Grid Reinforcement, p. 47, London, March 1984.
11. Ruegger, R., "Geotextile Reinforced Soil Structures on Which Vegetation can be Established", Proc. of Third International Conference on Geotextiles, p. 453, Vienna, April 1986.
12. Schneider, H.R. and Holtz, R.D., "Design of Slopes Reinforced with Geotextiles and Geogrids", Geotextiles and Geomembranes, No. 3, p. 29, 1986.

13. Seed, H.B. and Sultan, H.A., "Stability Analyses for a Sloping Core Embankment", ASCE Journal of the Soil Mechanics and Foundations Div., Vol. 93, No. SM4, p. 75, July 1967.
14. "Slope Reinforcement with TENSAR Geogrids: Design and Construction Guideline", Tensar Technical Note SRI, The Tensar Corporation, May 1986.

WALLACE, R.B. and FLUET, J.E., Jr.
GeoServices Inc. Consulting Engineers, U.S.A.

Slope Reinforcement Using Geogrids

Slope reinforcement using geogrids is now accepted as a construction aid which can greatly reduce quantities of fill materials, as well as construction-related costs. This paper reviews several procedures which have been developed by others to rationalize the addition of geogrid reinforcement to classical geotechnical engineering slope design concepts and methods. A discussion of the philosophy underlying the design of reinforced slopes is presented, and the concept of strain compatibility between the soil and the geogrid is stressed. Design procedures are reviewed, and a sample problem is presented.

1. INTRODUCTION

There exists firm archeologic evidence (reinforced soil structures which were constructed thousands of years ago and still stand [5]) which confirms the effectiveness of the soil reinforcement concept. Yet, soil reinforcement is still considered by many civil engineers to be an innovative, if not experimental, concept. In North America, the reinforcement of soil structures was essentially restricted to a proprietary procedure (Reinforced Earth) prior to the relatively recent proliferation of geosynthetics applications. Thanks to an adventurous few - those researchers and practicing engineers who have, over the past decade, sought to develop innovative design methods to increase the scope and contribution of geotechnique to civil engineering - geosynthetics are now used to reinforce soil as a standard practice in many areas and jurisdictions. Yesterday's innovation has become today's routine.

The principal applications of geogrid soil reinforcement include: embankments, walls, foundations, landfills, and steep slopes. Steep slopes are a particularly important application since they may be constructed alone or in combination with each of the other major applications. In the case of embankments, for example, in addition to incorporating geosynthetics for reinforcement at the contact of the embankment and foundation to provide support over soft soils, geogrids are often used for multi-layer reinforcement of the embankment slopes. This paper specifically addresses the topic of slope reinforcement.

Some common examples of routine applications of slope reinforcement are natural slopes requiring repair, cut slopes requiring support, and embankment slopes requiring steepening. Design procedures have been developed which, when properly applied, result in economical, well-engineered soil reinforcement solutions to slope stability problems.

2. DESIGN METHODS

Several papers exist which have addressed the topic of slope reinforcement. Murray [11, 12] outlined a procedure which emphasized the optimization of the layer spacing of reinforcement in the slope. This method uses a bilinear (two component) slip surface which models the problem in a simplified manner. An example is presented in his more recent paper [12] presenting values of permissible (allowable) geosynthetic tension (T_{perm}) for given values of soil parameters [unit weight (γ), friction angle (ϕ'), and pore pressure ratio (r_u)] and geometry [slope angle (β) and slope height (H)]. Charts are then presented which plot β vs factor of safety for given values of γ , ϕ' , and r_u , from which a value of $T_{perm}/s_v H$ is obtained, where s_v is the vertical spacing between layers of reinforcement. This method is particularly useful for the application for which it was derived, which was to allow the re-use of debris soil from landslides in conjunction with geosynthetic reinforcement and thereby realize savings by eliminating the need to import granular materials.

Similarly, Jewell et al [8] use limit equilibrium analysis to define a "gross reinforcement quantity" based also on a two component linear slip surface. In the Jewell method, a value for the coefficient of lateral earth pressure (K) is presented as a function of ϕ' and β . Charts can then be developed for fixed values of r_u . Unlike the Murray procedure, however, Jewell then developed charts to determine the required length of reinforcement into the slope (L_z), by relating L_z/H , ϕ' , and β . Figure 1 illustrates some of these parameters.

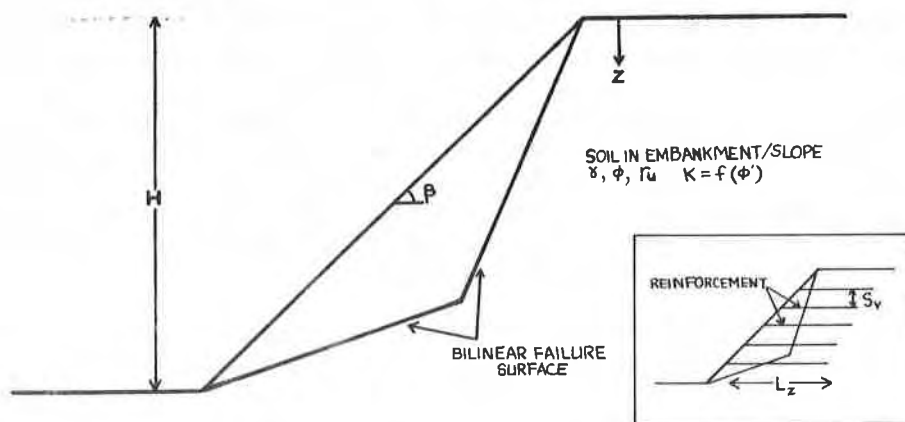


Figure 1: Slope geometry and notation

The attractiveness of these design procedures is that they are generic and independent of product-specific bias. Products are therefore selected strictly on the basis of their stress-strain characteristics, other material properties, and cost. Other research efforts, both reported and ongoing, build on these basic methods, and further enhance product selection. The method outlined by Bonaparte et al [3] is particularly useful and is discussed herein.

3. DESIGN PHILOSOPHY

3.1 Strain Compatibility

Although the movements associated with a catastrophic slope failure are massive in scale, potentially resulting in the displacement of many hundreds or thousands of tonnes of material, the incremental displacements leading up to the failure, (the point at which the limit equilibrium is exceeded) are very small. These micro-scale soil strains are the governing consideration in the evaluation of the stability of a slope, and are typically less than 5 per cent. It is desirable, therefore, when considering reinforcement of the slope, to seek reinforcement which will exhibit strain behavior of a compatible nature and magnitude. In order for the reinforcement to be effective, it must provide the required tensile properties at levels of strain that are compatible with the particular soils. Figure 2 illustrates this requirement. The band which is shaded represents the range of strains which are compatible with soil behavior (0-5 per cent), and the range of reinforcement tension which is required to provide slope stability, for desired factors of safety with a given reinforcement configuration.

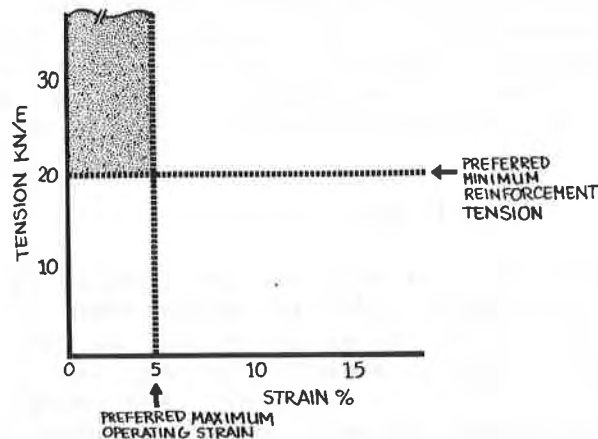
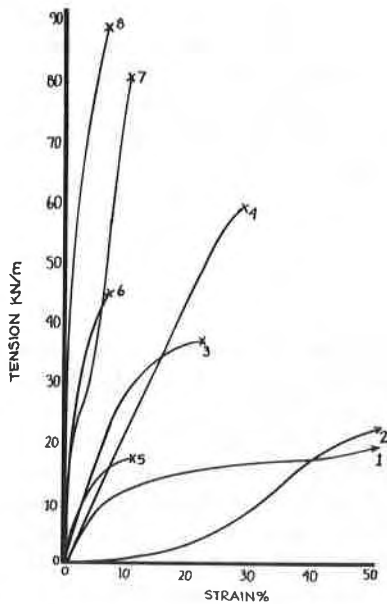


Figure 2: Ranges of desirable strain and tension for reinforcement materials

Figure 3 shows the characteristic unit tension-strain curves for a variety of geosynthetic products. Relatively few of these materials fall within the shaded area from Figure 2.



1. Nonwoven, heatbonded geotextile
2. Nonwoven, needle punched geotextile
3. Woven monofilament geotextile
4. Woven multifilament geotextile
5. Geogrid Tensar SS-2
6. Geogrid Signode TNX 250
7. Geogrid Tensar SR-2
8. Geogrid Signode TNX 5001

(Geogrid strengths shown for machine direction. Geotextiles from Figure 2.2 [9]. Test conditions not reported.)

Figure 3: Unit tension-strain curves for various geosynthetics (from Koerner [9] and product literature)

For the purposes of reinforcement of soil structures, therefore, it is often possible to short-list the candidate materials on the basis of strain compatibility even before the design issue is addressed. High geogrid strength is required to provide adequate tensile strength to the soil, and high geogrid modulus is required because it is necessary to preserve strain compatibility between the soil and reinforcement. The reinforcement must undergo strain in order to develop any strength. Similarly, the soil must yield to reach the active state. This can be related to the case of a vertical wall, for which the deformation at the top of the wall required to mobilize the active conditions is usually represented as:

$$\Delta x = 0.001 H \quad (1)$$

Although the stresses imposed on a wall are considerably different than within a slope, the initiating movements, although larger than for a wall, will be of similar small magnitude. It should be noted that we must distinguish between designing to structural working strain, whereby the geogrid reinforcement minimizes deformation of the structure itself, and designing to limit strain, whereby we design to the largest allowable geogrid reinforcement tension which is compatible with the soil. In the case of slopes, we are able to design to limit strain conditions, which usually means that greater deformations can be tolerated when designing to structural working strains. Nonetheless, the allowable soil strain remains the governing parameter.

The design philosophy for this type of structure is therefore to properly understand the soil behaviour and the deformation characteristics, and apply those criteria to the reinforcement. Strain compatibility allows the selection of working stress levels in the reinforcement which can in turn allow the use of actual stress levels in design.

3.2 Geogrid Strength Requirements

Once the strain compatibility of the system has been conceptually achieved, it is necessary to examine the strength component of the reinforcement. The required unit tension in the reinforcement, presented in kN/m (lb/in or ppi), must be provided at the very low working strains, which are compatible with those of the soil, hence the requisite high geogrid modulus. Using any of the geogrid design methods, values of unit tension in the order of 10 to 75 kN/m (57 to 429 ppi) are necessary in order to obtain layer spacings at reasonable levels. Table 1 illustrates the reported values for initial modulus, as well as tension at 2 and 5 per cent for some commercially available geogrids.

TABLE 1: REPRESENTATIVE STRENGTH PARAMETERS FOR GEOGRIDS

PRODUCT	INITIAL MODULUS (kN/m)	UNIT TENSION @ 2% STRAIN (kN/m)	UNIT TENSION @ 5% STRAIN (kN/m)	UNIT TENSION @ FAILURE (kN/m)	FAILURE STRAIN (%)
TENSAR					
SS 1	438	4	8	12	11
SS 2	657	5	10	17	11
SR 1	1021	9	20	34	11
SR 2	2189	22	45	79	11
SR 3	2918	29	60	109	11
SIGNODE					
TNX 250	1330	23	40	44	8
TNX 5001	2650	45	79	88	8

NOTE: Machine direction only (direction of applied force on slope reinforcement). Tensar - Tensar Test Method 2.1;
Signode - ASTM Wide Strip Test D 4595-86 (modified).

3.3 Factors of Safety

The design philosophy for reinforced slopes must also include some justification for the selection of the factor of safety, a very critical parameter from the viewpoint of both the integrity and the economics of the system. Bonaparte et al [3] present a particularly good discussion of soil reinforcement factors of safety. Two approaches are available: the more conventional definition, i.e., the ratio of the resistance of the structure to the driving forces acting on it; and second, the application of a factor of safety to the soil parameters. For reinforced structures, these two approaches provide different, and potentially misleading results.

The first approach needs no elaboration herein, since it represents the standard or conventional practice in geotechnical engineering.

Although not widely utilized in North America, one version of the second approach [3] advocates a procedure incorporating partial factors of safety, in which different factors of safety are applied to the different parameters. This approach does not apply a factor of safety to the strength properties of the reinforcement, but rather undertakes a careful analysis of all relevant factors affecting the stress-strain characteristics of the material: breaking load, anticipated strain levels, and creep characteristics (which are particularly relevant for any permanent structure). Isochronous creep curves as developed by McGown [10] are recommended as a basis for the evaluation of creep characteristics.

The factors of safety of the external stability of the reinforced slope can be evaluated using the ratio of the resisting forces to the driving forces in exactly the same way as unreinforced slopes are designed. Internal stability, (i.e., failure surface entirely within the slope) can be evaluated conventionally by the application of a factor of safety to the factored strength parameters for the soil:

$$\tan \phi_f = \tan \phi / FS \quad (2)$$

and
$$c_f = c / FS \quad (3)$$

- where:
- ϕ_f and ϕ are the factored and unfactored angles of internal friction of the soil;
 - c_f and c are the factored and unfactored soil cohesion; and
 - FS is the factor of safety.

4. GEOGRID SLOPE REINFORCEMENT DESIGN

In the past, the actual design of geogrid reinforced slopes has been based on various methods as previously discussed (e.g., Murray, Jewell). For purposes of this paper, we shall use the more current procedure discussed by Bonaparte et al [3]. We will discuss only the internal stability of the slope, since external stability is examined using the same analytical procedures as unreinforced slopes. Internal stability is of special concern in reinforcement design, since the specific purpose of the reinforcement is to steepen the slope to an angle in excess of that which would be stable in the unreinforced case.

Schmertmann et al [13] present an excellent simplified design approach for slopes reinforced with geogrids. This procedure is an extension of the method developed by Jewell [8]. The evaluation of the internal stability of a reinforced soil slope is essentially dependent on the determination of four parameters: the allowable reinforcement tension, defined as α_a ; the total tensile load required to be picked up by the reinforcement (T); and the number of layers and distribution of reinforcement (N and s_v). The equations that are utilized in this procedure are as follows:

$$T = 0.5 \gamma H^2 K \quad (4)$$

$$N = T / \alpha_a \quad (5)$$

$$s_v = T / K \gamma z = H^2 / 2 N z \quad (6)$$

- where:
- γ is the unit weight of the soil;
 - H is the slope height;
 - K is the lateral force coefficient; and
 - z is the depth from the top of the slope.

The real challenge with respect to the design of reinforced slopes is in the proper selection of the relevant criteria for design, notably FS, α_a , and K .

4.1 Selection of the Factor of Safety

The selection of the factor of safety is a geotechnical decision based on the critical nature of the slope. In natural slopes, a factor of safety of 1.2 is often considered acceptable. In general, however, the design of man-made slopes should target a higher safety factor, usually around 1.35 to 1.5 in non-critical applications, and possibly higher in certain critical applications. The incorporation of geogrid reinforcement in low to medium height slopes (up to 4.5 m) can often result in higher factors of safety at a modest premium cost. The consequences of failure of a higher slope, on the other hand, are usually more severe. As a result, the selection of the factor of safety is often more conservative, even at a much higher cost of materials.

The factor of safety selected for any reinforced slope will depend on the confidence level on the design parameters. In geotechnical structures, there are always unknowns with regard to the homogeneity of the soils. Even in embankment fills, in which we have a degree of control over the consistency of the material as it is placed, it is impossible to attain a completely homogeneous structure. Due to layering and compaction difficulties, the fill properties will not be isotropic. Similarly, the soil parameters used for design are not actual, but rather representative values. Even though it is possible that many designs are therefore overly conservative, we do not yet have sufficient data to allow us to lower the factors of safety. Only projects which are well instrumented and take particular care in the preparation of the site, and then taken to failure, will provide the missing input data for refinement of these designs.

4.2 Selection of the Allowable Reinforcement Tension

The second design parameter which requires determination is the allowable tension in the reinforcement (α_a). For a slope, the stress conditions close to the slope face are close to being constant, whereas the stress conditions within the slope vary considerably. The near-surface overburden stress conditions at different levels of reinforcement do not change in the same proportion as the overburden stress conditions well into the slope. For example, in the case of a 45° slope, the overburden stress (σ_z) is as follows:

- close to the slope: $\sigma_z = \omega \gamma z$ (7)

- well into the slope: $\sigma_z = \gamma z$ (8)

where: ω is a dimensionless factor which is a function of the soil properties and slope geometry, and

$$\omega \leq 1 \quad \text{and} \quad \lim_{x \rightarrow 0} \omega = 0$$

and: x is the horizontal distance into the slope from the face.

Consequently, the overburden stress into the slope from the slope face is governed by equation 8 (the normal overburden case, for which $\omega = 1$), whereas the overburden stress at and near to the slope face is governed by equation 7. From this we can deduce that the stress distribution along the reinforcement is not a constant, even at a constant elevation within the slope. We do know that the friction and pull-out interaction between the soil and reinforcement is a function, in part, of the normal stress on the reinforcement layer (McGown et al [10]). We also know that in the absence of the reinforcement, the failure of the slope will start at the face of the slope and work its way into the slope. This is the typical retrogressive failure seen in most slope failures. The presence of the reinforcement will not tend to change this mechanism, and so the failure will still start at the face. Consequently, the first component of the reinforcement that will be stressed will be that located close to the slope face. As it is tensioned, therefore, at the first loading, the only stressed portion of the reinforcement layer would be that at the face.

Beech [1] has shown the load distribution along the reinforcement. He shows that regardless of the distribution of stresses within the reinforcement, it is still necessary to extend the reinforcement beyond the failure surface. In addition, the load distribution relates solely to the internal stability considerations for the slope, and therefore extrapolation to external stability is not appropriate.

The selection of the allowable reinforcement tension must consider the limit strain in the geogrid and must also relate the loading to the strains under which the loading takes place. Some movement must take place, however small, to develop tension in the geogrid. The short term strains that are appropriate for these purposes are in the order of 2 per cent (Bonaparte et al [3]). However, long-term loading conditions must also consider the creep phenomenon, and, consequently, working level strains closer to 5 per cent to 10 per cent may be more appropriate. The research by McGown et al [10] provides a rational approach to the creep component of design. In any event, selection of the allowable geogrid tension (α_a) should be consistent with these strains, even though this may lead to the selection of a value considerably below the ultimate value (i.e., the tension at failure).

The second factor that affects the allowable tension of the reinforcement, after examining the material strength, is the pullout resistance. This corresponds to the frictional resistance and the passive resistance between the reinforcement and the soil. This is a site-specific consideration, and representative values have been published for different soils (Koerner [9]). Within the constraints set by these parameters, therefore, the reinforcement must be able to strain a prescribed amount without pullout. Hence, at a given level of force on the reinforcement, its strain must be compatible with that of the soil. Consequently, the limiting consideration on the soil strength is not necessarily the properties

of the soil (c and ϕ), but the pull-out interaction between the soil and the reinforcement.

4.3 Selection of the Lateral Force Coefficient

The third parameter which requires some interpretation in order to input to design is the value of the dimensionless coefficient K , which relates indirectly to the coefficient of lateral earth pressure. Bonaparte et al [3] and Schmertmann et al [13] present values for this force coefficient as a function of the factored frictional strength characteristic, ϕ_f , and the slope angle, β . For most cases, involving relatively shallow slopes and moderate values of ϕ_f , this factor falls in the range 0.1 to 0.4, generally corresponding to the coefficient of active earth pressure for walls (K_a). For steep slopes and low factored friction angle values, the force coefficient K has a limiting value of about 0.7, which is conceptually consistent, since we would not expect to attain the generally accepted at-rest value of 1.0 (for $\phi = 0$).

5. DESIGN EXAMPLE

To illustrate the application of the design procedures referred to herein, we present the following brief design example. We take a case of a sand slope which is to be reinforced using geogrids. The properties and geometry are as follows:

$$\begin{array}{lll} c = 0 & \phi = 35^\circ & \gamma = 19 \text{ kN/m}^3 \text{ (121 pcf)} \\ \beta = 60^\circ & H = 6 \text{ m (20 ft)} & \end{array}$$

(a) Determine the factored value of friction angle to be used:

$$\phi = 35^\circ \rightarrow \text{select a factor of safety (in this case, FS = 1.4)}$$

$$\phi_f = 35/1.4 = 25^\circ$$

(b) Determine the total load to be picked up by the reinforcement:

$$\begin{array}{ll} T = 0.5 \gamma H^2 K & \text{(equation 4)} \\ = 0.5 \cdot 19 \cdot 6^2 \cdot 0.26 & \text{(K from Figure 9 of} \\ = 88.92 \text{ kN/m} & \text{Schmertmann et al [13])} \end{array}$$

(c) Select an allowable working level strain which is compatible with the soil:

$$\rightarrow \text{select for this case, 5 \%}$$

(d) Select a trial allowable tension for the reinforcement:

$$\alpha_a = 15 \text{ kN/m}$$

(e) Determine the requisite minimum number of layers:

$$\begin{array}{ll} N = T / \alpha_a & \text{(equation 5)} \\ = 88.92/15 & \\ = 5.93 \rightarrow 6 \text{ layers} & \end{array}$$

(f) determine the requisite layer spacing:

$$\begin{aligned}
 s_v &= H^2 / 2 N z && \text{(equation 6)} \\
 &= 36 / 2 \cdot 6 \cdot z \\
 &= 3/z
 \end{aligned}$$

- at the bottom, $z = 6$ m, $s_v = 0.5$ m
- at the midpoint, $z = 3$ m, $s_v = 1.0$ m
- near the top, $z = 1$ m, $s_v = 3$ m

(g) Select an appropriate value for s_{vmax} :

→ in this case, select 1 m

(h) Iterate for different allowable tensions to satisfy s_{vmax} .

There is a practical and functional limit to layer spacing. Taking a conservative value for s_{vmax} of 1.0 m (1.5 m is frequently used in practice), layers of reinforcement would be required at $z = 1, 2, 3, 3.75, 4.5, 5, 5.5,$ and 6 meters (i.e., $N = 8$) in order to satisfy equation 6 at all elevations within the slope. We have not violated any of the requirements of the design, but rather have shown that to accommodate the distribution of stresses within the slope which are to be resisted by the reinforcement, more layers than the minimum are needed. In some instances, this can be an economic benefit, since the value of α_a for 8 layers can be reduced. Therefore, reworking equation 5:

$$\begin{aligned}
 \alpha_a &= T/N \\
 &= 88.92/8 \\
 &= 11.12 \text{ kN/m} \rightarrow \text{say } 11.5 \text{ kN/m}
 \end{aligned}$$

This could represent a significant saving, depending on the stepdown that results from one type of reinforcement to another. Eight layers of the revised design reinforcement may cost less than 6 layers of the original reinforcement. In addition, we must not forget the practical considerations relating to soil placement and compaction. In this particular example, constant layer thicknesses of 0.25 m (10 in) could be used, which for this type of soil is a reasonable choice.

6. DESIGN VERIFICATION

Any design procedure of this nature requires full-scale testing in order to determine whether or not the design is being optimized. With slopes, full scale testing is not usually possible outside the venue of a research organization. When such an opportunity does arise, however, it is desirable to maximize the informational value of the work. Scott et al [14] have commenced an instrumented full-scale slope test section, incorporating several different types of geogrid. It is intended that this project be several years in duration, so that data at several stages of load development and redistribution can be obtained. This test fill will ultimately be built up to a height of about 20 m (66 ft).

7. CONCLUSIONS

High modulus polymeric geosynthetic materials are ideally suited for the reinforcement of soil structures. The use of geosynthetics for reinforcement has been widely practiced for several years now, and is well documented in the literature. The development of very high modulus geosynthetics, in particular geogrids, has allowed the design of these structures to be optimized, drawing upon the high allowable tensile stress at low strain levels compatible with typical soil strains.

Slope reinforcement is one area in which the use of high modulus geosynthetics for reinforcement can maximize economic benefits of geosynthetic usage. Soils do not naturally (unreinforced) remain in a stable configuration at other than relatively shallow angles (approximately 30°). Reinforced with geogrids, steep slopes up to and including the limiting case of a reinforced wall (although the analysis differs for parametric selection) are possible. Test data are available for geogrids tested in isolation (McGown [10]), which are known to be conservative relative to the in-soil case. Sufficient testing in-soil has not been carried out to develop reliable correlations between the two cases. In any event, extrapolation of the results from one soil to another should only be done with caution, and in fact, site-specific soil-geogrid interaction should be carried out in cases where the project size or critical nature require it. More research on long term in-soil creep of these materials is required. In addition, full scale, instrumented test sections will greatly contribute to the development of design methods and optimization of the benefits of geogrid usage.

ACKNOWLEDGEMENTS

The authors wish to thank the Signode Corporation for its support in the research leading to the preparation of this paper. In addition, we appreciate the comments of Dr. J.F. Beech, of GeoServices, Inc.

REFERENCES

1. Beech, J.F., "Reinforcement design using high modulus geosynthetics", To be presented at Geosynthetics '87, New Orleans, 1987.
2. Bonaparte, R. and Margason, E., "Repair of landslides in the San Francisco Bay area", Polymer Grid Reinforcement, London, 1984, pp. 64-68.
3. Bonaparte, R., Holtz, R.D. and Giroud, J.P., "Soil reinforcement design using geotextiles and geogrids", ASTM Symposium, Geotextile Testing and the Design Engineer, 1985.
4. Devata, M.S., "Geogrid reinforced earth embankments with steep side slopes", Polymer Grid Reinforcement, London, 1984, pp. 82-87.
5. Giroud, J.P., "From Geotextiles to Geosynthetics: A Revolution in Geotechnical Engineering", Proceedings of the Third International Conference on Geotextiles, Vienna, 1986, Volume 1, pp. 1-18.

6. Ingold, T.S., "An analytical study of geotextile reinforced embankments", Proceedings of the Second International Conference on Geotextiles, Las Vegas, 1982, Volume 3, pp. 683-688.
7. Jewell, R.A., Milligan, G.W.E., Sarsby, R.W. and DuBois, D., "Interaction between soil and geogrids", Polymer Grid Reinforcement, London, 1984, pp. 18-30.
8. Jewell, R.A., Paine, N. and Woods, R.I., "Design methods for steep reinforced embankments", Polymer Grid Reinforcement, London, 1984, pp. 70-81.
9. Koerner, R.M., Designing With Geosynthetics, Prentice-Hall, Englewood Cliffs, NJ, 1986.
10. McGown, A., Andrawes, K.Z., Yeo, K.C. and DuBois, D., "The load-strain-time behaviour of Tensar geogrids", Polymer Grid Reinforcement, London, 1984, pp. 11-17.
11. Murray, R.T., "Fabric reinforcement of embankments and cuttings", Proceedings of the Second International Conference on Geotextiles, Las Vegas, 1982, Volume 3, pp. 707-713.
12. Murray, R.T., "Reinforcement techniques in repairing slope failures", Polymer Grid Reinforcement, London, 1984, pp. 47-53.
13. Schmertmann, G.R., Bonaparte, R., Chouery, V.E. and Johnson, R.D., "Design Charts for Geogrid Reinforced Soil Slopes", To be presented at Geosynthetics '87, New Orleans, 1987.
14. Scott, J.D., Richards, E.A., Sego, D., Hofmann, B.A. and Burch, E., "Design of the Devon Geogrid Test Fill". To be presented at Geosynthetics '87, New Orleans, 1987.
15. Terzaghi, K., Theoretical Soil Mechanics, John Wiley and Sons, Inc., New York, 1943.

BEECH, J.F.

GeoServices Inc. Consulting Engineers, U.S.A.

Importance of Stress-Strain Relationships in Reinforced Soil System Designs

INTRODUCTION

In the last decade the development of different geosynthetics and new soil reinforcement techniques have provided the geotechnical engineering profession with new methods to solve old problems. However, in using these new methods the designer often reapplies traditional design methods founded in limit equilibrium theory. Using a limit equilibrium approach does not necessarily guarantee compatibility between the strains in the soil and the geosynthetic reinforcement. Also, these traditional design methods often do not fully account for the differences in geosynthetic properties.

This paper first outlines the philosophy of stress-strain relationships in civil engineering design and discusses why a limit equilibrium approach is often acceptable for traditional geotechnical design. Secondly, slope reinforcement is used as an example to demonstrate why compatibility between soil and geosynthetic reinforcement strains must be accounted for in design. Thirdly, the load transfer method is proposed as a procedure for predicting the pullout tension as a function of the displacement relationship of reinforcement material. Finally, the effects of strength and modulus on pullout tension are briefly addressed.

STRESS-STRAIN RELATIONSHIPS IN CIVIL ENGINEERING DESIGN

All engineering materials have stress-strain characteristics, and the ease with which they are incorporated into design methods depends upon the complexity of these characteristics. For example, materials whose stress-strain characteristics can be accurately modeled as linear elastic functions are routinely incorporated into structural engineering design.

As shown in Figure 1, soils have nonlinear stress-strain characteristics which vary as functions of such variables as stress level and void ratio. Consequently the incorporation of soil stress-strain characteristics into design is quite complex. (The results shown in Figure 1, are for a concrete sand, tested in direct shear, under an initial normal confining stress of 18.3 kN/m^2 , and will be used again later in this paper). As a result, many of the early geotechnical engineering design procedures were based on limit equilibrium theory [Terzaghi, (1943)] and this philosophy has continued today. By using a limit equilibrium approach, the strain in the soil can be ignored leaving only the equilibrium of

stresses as a requirement for design. For example, this concept is routinely used in unreinforced slope stability analysis.

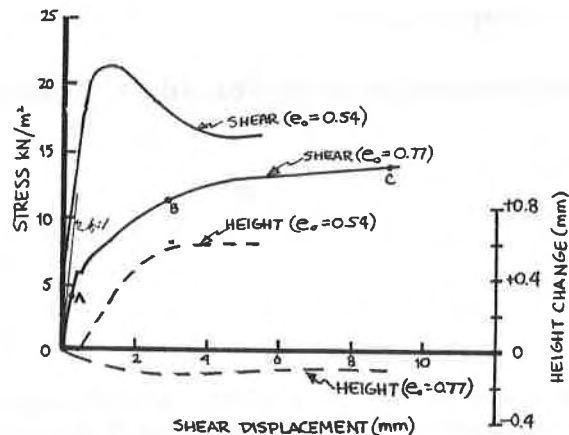


Figure 1. Typical Soil Stress-Strain Properties
Source: After Boyce and Kulhawy [1983]

Unfortunately, in many cases strains cannot be completely ignored in geotechnical design, and the importance of strains was recognized by Roscoe [1970]. However, it is difficult to account for the stress-strain behavior of soils in routine design, and as a result, the design is often performed in two parts. For example, in shallow foundation design, the verification of adequate bearing capacity of the foundation (limit equilibrium) and the settlement analysis (verification of strain level) are performed separately. This uncoupling of stress and strain is not always permissible. In particular, if there is more than one stress-strain relationship involved, then uncoupling of stress and strain can lead to erroneous results. The load carrying capacity of deep foundations is composed of a combination of shearing resistance along the foundation side surfaces and end bearing resistance at the foundation tip. A limit equilibrium approach requires that these two resistances be superimposed. However, because these two resistances are mobilized at different rates of displacements, superposition is not applicable. As this example illustrates, when more than one stress-strain relationship exists, the design procedure must account for strain compatibility.

STRESS-STRAIN RELATIONSHIPS IN REINFORCED SOIL STRUCTURES

Reinforced soil structures are composed of materials with different but complementary stress-strain (or tension-strain) characteristics. Soils, which transmit load through shear and compression, perform well when loaded in compression but have little or no tensile strength. Reinforcement materials, on the other hand, carry loads best in tension. Typical soil stress-strain properties were presented in the previous section, and prior to discussing reinforced soil structures, typical geosynthetic tension-strain properties will now be presented. Next, a discussion of limit equilibrium in reinforced slope

design will be presented, followed by a discussion of strain compatibility of reinforced structures.

Typical Geosynthetic Tension-Strain Curves

The tension-strain relationships of reinforcement can vary significantly depending upon the nature of the material. A typical range of tension-strain relationships for several different geosynthetics measured from wide strip tension tests is shown in Figure 2. Details of material properties and testing procedures are shown in Table 1. It can be observed from Figure 2 that material C has the highest strength while material A has the highest initial tensile modulus. The relative importance of these two properties relative to reinforcement performance will be discussed later in this paper.

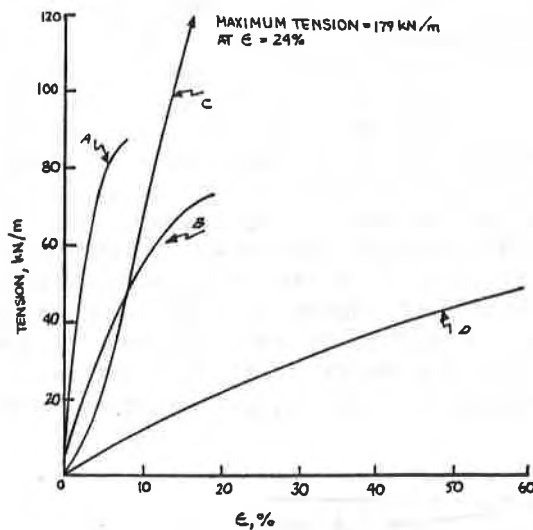


Figure 2. Typical Geosynthetic Tension-Strain Curves

TABLE 1. CHARACTERISTICS OF GEOSYNTHETICS SHOWN IN FIGURE 2

Curve	Geosynthetic	Description	Mass Per Unit Area (g/m ²)	Test Procedure	Strain Rate (%/min)	Test Temp. °C
A ^a	Signode TNX-5001	Geogrid	550 ^d	ASTM D4595-86	10%	e
B ^a	Tensar SR-2	Geogrid	920 ^d	ASTM D4595-86	10%	e
C ^b	Geolon 1250	Woven Geotextile	722 ^d	CGSB draft Standard	2%	22±1
D ^c	Bidim U64	Needlepunched nonwoven Geotextile	550 ^d	N.R.	50%	e

a - measured by STS Consultants Ltd., Northbrook, Illinois
 b - Rowe and Ho [1986]
 c - Baudonnel et. al [1982]
 d - obtained from manufacturer's literature
 e - not reported

Limit Equilibrium Design

Design procedures for reinforced soil walls and slopes have been extrapolated from traditional design procedures for similar unreinforced structures. As discussed earlier, these traditional design procedures are founded in limit equilibrium theory, a concept which is valid only if strains can be ignored. This is not the case for reinforced soil because it is composed of two materials with distinctly different stress-strain properties, i.e., the design requires compatibility between the strains in the soil and the reinforcement materials. Simply stated, a limit equilibrium approach should not be applied to reinforced soil structures because the materials involved are characterized by different stress-strain properties.

Strain Compatibility in Design

In the last few years, the importance of strains in the design of reinforced structures has been recognized [McGown et. al. (1984), Bonaparte et. al (1987)]. Both McGown et. al. [1984] and Bonaparte et. al. [1987] recommend an empirical approach for guaranteeing strain compatibility. One of the primary reasons for this is that various types of strain are involved, as can be observed for the case of a reinforced slope shown in Figure 3. At point A, the failure surface will intersect the reinforcement material at some angle and the soil strains will have to be compatible with the reinforcement strains at this point. Also, strain compatibility will have to be guaranteed along segment AC of the reinforcement material. Along AC, the reinforcement material is undergoing axial tensile strain, while the soil in contact with it is being subjected to shear strains. Accounting for the compatibility of these strains can be complex. A more rigorous technique for taking compatibility into account is presented by Delmas et. al. [1986] who work with displacements instead of strains. Their procedure is used as a basis for a reinforced soil slope design procedure and which is outlined in the next section.

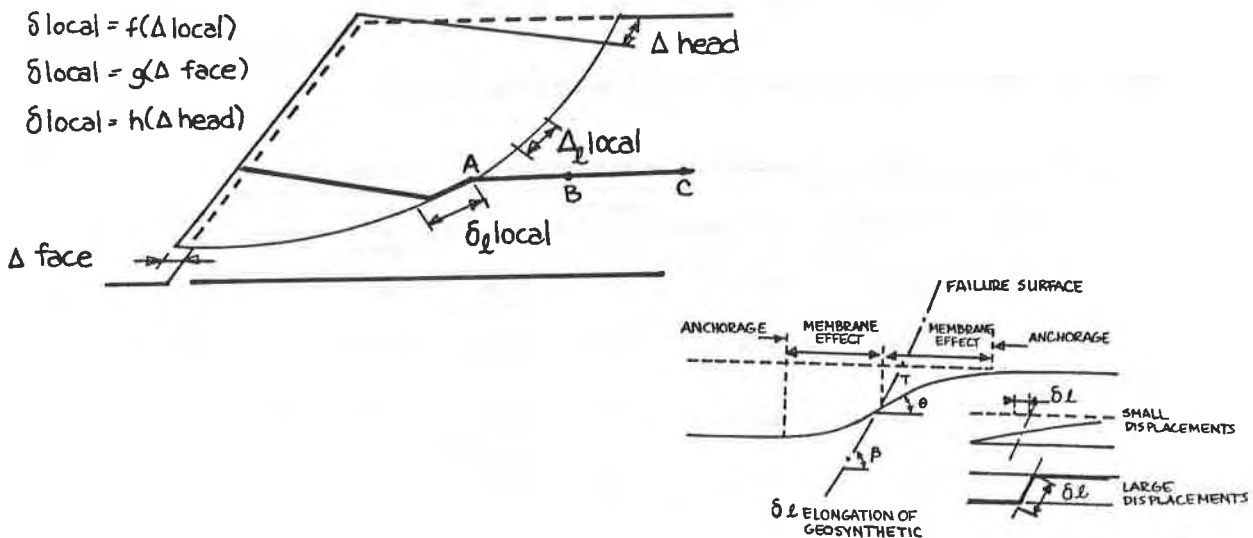


Figure 3. Displacements Mobilized in Reinforced Slope
Source: After Delmas et. al. [1986]

REINFORCED SLOPE DESIGN

The procedure for the design of reinforced slopes which is presented herein is based on the work of Delmas et. al. [1986] and incorporates the work of others [Beech and Kulhawy (1987), Bonaparte et. al. (1987), Coyle and Reese (1966), McGown et. al. (1986)]. This procedure guarantees compatibility between the displacements in the soil and reinforcement material. As was indicated in the previous section, displacement compatibility must be accounted for in two zones: at the intersection of the soil failure surface and geosynthetic reinforcement; and along the length of the reinforcement material embedded beyond the failure surface. The proposed design procedures for each of these two zones are presented separately.

Displacement Compatibility Along Soil Failure Surface

In this design procedure, the equilibrium of stresses and compatibility of displacements are accounted for prior to the soil reaching a failure state. Therefore, the first step is to determine the allowable displacement which can occur within the reinforced soil mass. Delmas et. al. [1986] do not recommend an approach for establishing the allowable soil displacement, however, an approach is presented here. A plot of mobilized soil friction angle as a function of displacement can be established from the results plotted in Figure 1, and an example for the test at an initial void ratio of 0.77 is shown in Figure 4. As discussed by Bonaparte et. al. [1987], the working strength of the soil can be established by dividing $\tan \phi$ by the required factor of safety. Entering Figure 4 with this value, the corresponding allowable soil displacement can be established, as shown by the dashed line in Figure 4.

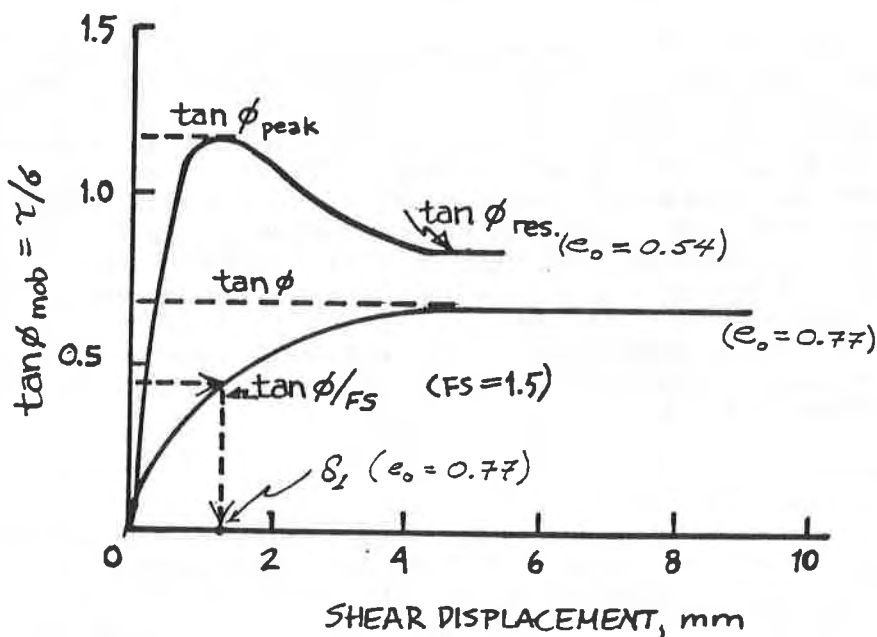


Figure 4. Mobilized Friction Angle as a Function of Shear Displacement

At this small displacement it is likely that the displacements will vary throughout the reinforced soil mass (i.e., the displacement at the face, Δ_{face} , will be different from that at the head, Δ_{head} , or along the potential failure surface, Δ_{local}) and the displacement along the potential failure surface is better defined as a band instead of a well defined discontinuity. However, at large displacements, a well defined failure surface will exist and the unstable soil will move as a rigid body (i.e., $\Delta_{\text{face}} = \Delta_{\text{head}} = \Delta_{\text{local}}$).

The second step is to calculate displacement δ_1 in the reinforcement material at point A to guarantee compatibility along the potential failure surface. At large displacements, when a discontinuity exists, the displacement in the reinforcement material is equal the displacement along the failure surface. At small soil displacements, the verification of compatibility is more complex because of what Delmas et. al. [1986] call the membrane effect. Gourc et. al [1986] present a procedure for calculating δ_1 , however, the accuracy of this procedure needs to be verified.

The third step is to determine the tension in the reinforcement material necessary to maintain equilibrium. The reinforcement tension is calculated to be the tension which provides enough additional resisting moment (in addition to that provided by the soil shear stresses) to stabilize the soil.

From the above steps, the minimum tension and maximum displacement which can occur in each geosynthetic reinforcement can be determined. The properties of the geosynthetic reinforcement need to be selected such that the embedded length of the reinforcement material, AC, provides the required minimum tension and maximum displacement at point A.

Pullout Resistance of Reinforcement Material

The length and properties of the reinforcement material, AC (Figure 3), must be selected such that the minimum tension and maximum displacement described above are provided. This information can be obtained from a plot of tension versus geosynthetic displacement, which is commonly referred to as a pullout curve. Pullout tests can be performed on geosynthetics embedded in soil. While pullout tests can provide the information required for a given set of conditions (e.g., geosynthetic type, soil type, confining stress, embedment length, etc.) they are of limited design use because they apply only to a specific set of conditions. Another limitation of the pullout test is that the results may be affected by the boundary conditions of the test apparatus, and, as a result, they are not representative of field conditions. An alternate approach is to use an analytical or analogical approach which predicts the pullout curve from the intrinsic properties of the soil and geosynthetic.

Load Transfer Method

The approach presented here is based on the load transfer method [Coyle and Reeve (1966)] which was developed for deep foundations. The application of the load transfer method to soil reinforcement, results in the prediction of a pullout curve that accounts for both displacement of the soil and the elongation of the geosynthetic. It is important that the elongation of the geosynthetic be taken into account because the same shearing resistance will not be mobilized at all points along the reinforcement, as shown in Figure 5.

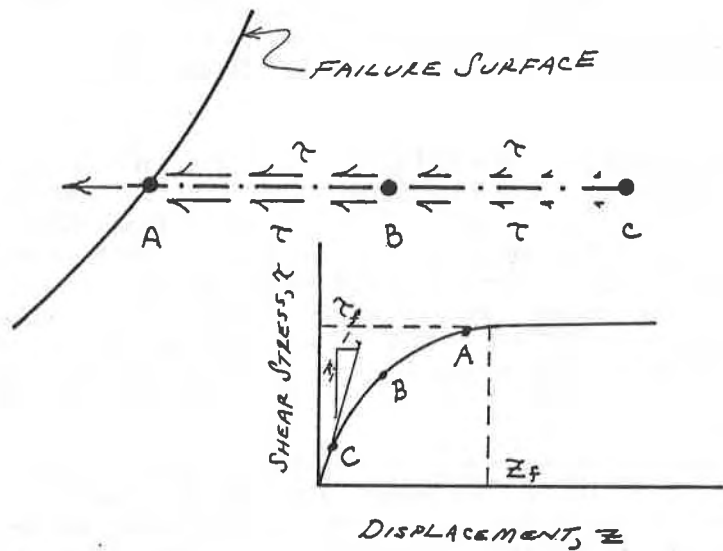


Figure 5. Variation of Shear Stress Along Reinforcement

Using the load transfer approach, the reinforcement material is divided into a series of elements, as shown in Figure 6. The shear stress is assumed to be constant across each element, however, the tension within each element decreases from one end to the other (e.g., point A to point B). The strain within each element will also decrease across the element because of the variation of tension within the element. This decrease in strain will generate a smaller displacement in the next element (e.g., point B, element 2) than in the previous element (e.g., point A, element 1). The smaller displacement at point B results in a smaller shear stress being generated along element 2 than was generated along element 1. The overall effect is a decrease in mobilized shear resistance with length, along the surface of the geosynthetic reinforcement.

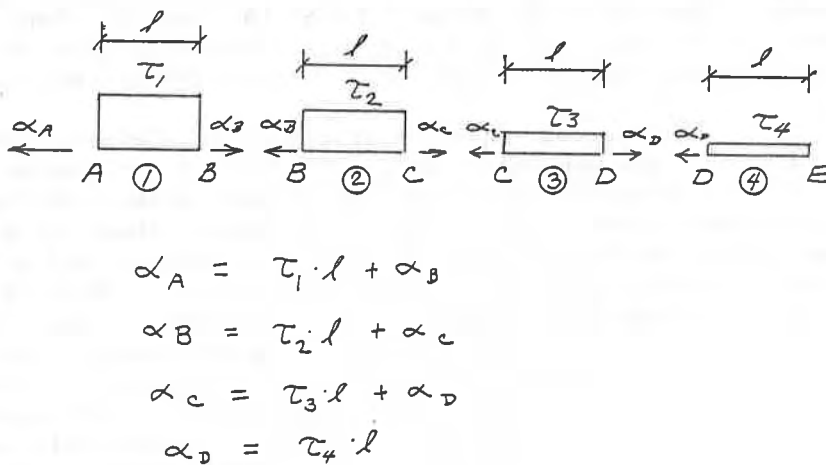


Figure 6. Conceptual Presentation of Load Transfer in Reinforcement

Application of the load transfer method requires knowledge of the geosynthetic tension-strain properties and the soil-geosynthetic interface shear resistance as a function of displacement. The procedures for evaluating both are discussed below.

Geosynthetic tension-strain properties. The geosynthetic tension-strain properties can be measured by performing a wide strip tensile test. The properties of geosynthetics are time and temperature dependent, which must be accounted for in design. Andrawes et. al. [1986] present a test method, for measuring geosynthetic tension-strain properties, which incorporates time and temperature effects. The author recommends using this or a similar test method at expected field temperatures and times representative of the proposed design life in order to determine the geosynthetic tension-strain properties of the geosynthetic.

Soil-geosynthetic interface properties. The soil-geosynthetic interface properties are more difficult to determine than the geosynthetic tension-strain properties. Coyle and Reese [1966] prescribed an empirical method employing the undrained shear strength of the soil. A more accurate procedure was recommended by Beech and Kulhawy [1987] in which the interface shear resistance is:

$$\tau = \frac{\tau_f}{(k_i \tau_f + 1)} \frac{z}{(1/k_i + z/\tau_f)} \quad z \leq z_f \quad (1)$$

$$\tau = \tau_f \quad z > z_f$$

in which k_i = initial tangent stiffness (units: F/L³), τ_f = shear stress at failure, and z_f = displacement at failure. The above equation can be used to estimate a soil-geosynthetic interface shear resistance; but, it is necessary to use the following alternate procedures to evaluate the parameters k_i , z_f , and τ_f .

In foundation analysis, k_i is a function of the foundation radius. A limited comparison with geosynthetic pullout data revealed that k_i is relatively independent of the geosynthetic thickness and could be determined directly from direct shear tests. Therefore, k_i appears to be the initial slope of the shear stress-displacement curve measured in the direct shear test, as shown in Figure 1. However, this approach should be confirmed through additional testing.

The calculation of τ_f is dependent upon a variety of parameters. The first step is to determine the soil-geosynthetic interface failure mechanism. Jewell et. al. [1984] performed a detailed review of the failure mechanisms that can occur when the soil-geosynthetic interface is loaded in direct shear or pullout. When loaded in pullout, the interface failure for both geotextiles and geogrids can be a continuous failure surface parallel to the geosynthetic. This failure surface can occur at the soil-geosynthetic interface or in the soil a small distance from the geosynthetic. A bearing capacity failure mechanism also exists for geogrids, in which each member perpendicular to the direction of loading acts as an anchor, exhibiting passive resistance immediately. The type of failure mechanism that occurs will be controlled primarily by the soil particle size distribution and soil density. Jewell et. al. [1984] present a procedures for calculating τ_f for the different possible failure modes. (These procedures are not repeated here because of space restrictions, and the reader is referred to

the original publication.) The use of the procedure presented by Jewell et. al. [1984] should also be confirmed (or calibrated) through additional testing.

Alternatively, τ_f can be back-calculated from pullout tests. However, care should be taken to account for the elongation of the geosynthetic. The best procedure for back-calculation is to use the load transfer method to predict a series of pullout curves by varying τ_f . The value of τ_f is that value which gives the best correlation between the predicted and measured pullout curve.

The displacement at failure, z_f , is based on empirical observations rather than a theoretical approach. The side resistance of deep foundations is typically mobilized at displacements of 2 to 4 mm, and the same range of values should apply to geosynthetic reinforcement. As an alternate approach, the value of z_f can be obtained from direct shear tests. It should be noted that z_f is the displacement of the soil, which is in contact with the geosynthetic along the length AC, and should not be confused with the pullout displacement, δ_1 , at point A.

Typical pullout curves predicted using the load transfer method are presented in the next section as part of a parametric study. Although not presented here, when compared with existing pullout test results, the load transfer method results appear to be promising.

PARAMETRIC ANALYSIS OF GEOSYNTHETIC MODULUS

In the previous section it was shown that the geosynthetic will undergo some strain under the working stresses to which the reinforced system is subjected. The amount of geosynthetic strain will be controlled by the factor of safety selected and the spacing the geosynthetic layers, among other variables, one of which is the modulus of the geosynthetic. Geosynthetic modulus is the rate at which the tension in the geosynthetic reinforcement is developed as a function of strain. In this section, the effect of the geosynthetic modulus on the pullout resistance is studied.

The soil properties presented in Figures 1 and 4 along with the geosynthetic properties presented in Figure 2 are used in the load transfer method to develop conceptual pullout curves shown in Figures 7 and 8. For this example, the shear stress-displacement curve is modeled using equation 1 in which the three input parameters are: initial tangent stiffness, $k_1 = 20,000 \text{ kN/m}^2$; shear stress at failure, $\tau_f = 20 \text{ kN/m}^2$ and; the displacement at failure, $z_f = 5 \text{ mm}$.

It should be noted that this comparison is not necessarily a true representation of how these geosynthetic products will behave, but is just an example of the influence of modulus. For example, the nonwoven geotextile, Product D, will actually have a higher in situ modulus than that shown in Figure 2, because of soil confinement. Also, the geosynthetic tension-strain curves presented in Figure 2 have been measured by several different sources. Ideally, the curves should be generated by one laboratory. However, these curves are felt to be satisfactory for the comparison being made here.

Predicted pullout curves were generated for a geosynthetic reinforcement 0.5 m long in the direction of load application and 1 m wide in the direction perpendicular to loading. For the analysis, the reinforcement was divided into

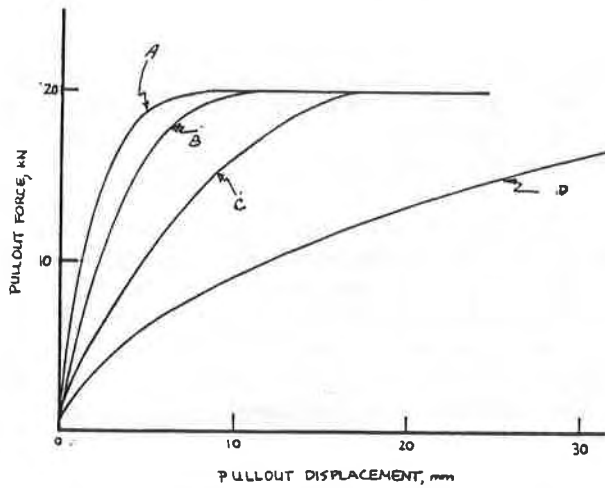


Figure 7. Predicted Pullout Curves for Typical Geosynthetics

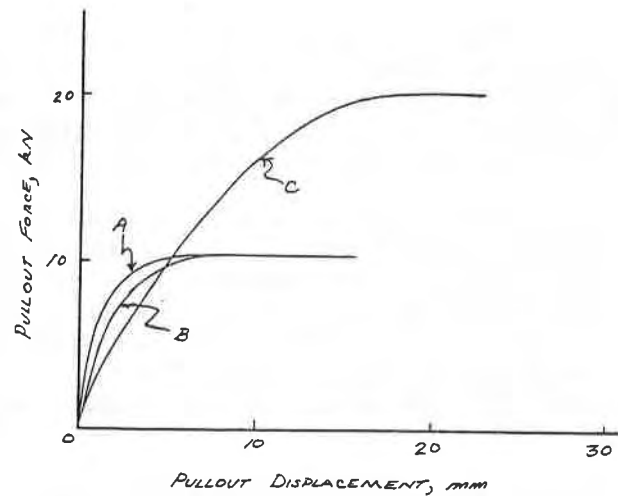


Figure 8. Predicted Pullout Curves, Assuming Reduced Interface Shear Strength for Geogrids

20 elements, which satisfied convergence criteria. The predicted pullout curves for four different geosynthetic tension-strain curves are shown in Figure 8. For the given dimensions and properties, all four geosynthetics are predicted to fail in pullout rather than by rupture of the geosynthetic. The pullout resistance develops at a faster rate (as a function of displacement) for the higher modulus geosynthetics. The rate at which the pullout resistance develops is important because, in the design procedure presented above, the controlling factor is the pullout resistance at a specified displacement, not the pullout resistance at failure of the geosynthetic. It can be observed from Figure 4, that, for this soil and a factor of safety of 1.5, the controlling displacement is approximately 1.5 mm. At this displacement, material A has the highest pullout force, even though it has a lower strength than material C.

In reality, all geosynthetics will not have the same interface strength, τ_f . For example, in a fine-grained soil, a geogrid may have a lower value of τ_f than a geotextile. This may be demonstrated by considering the value of τ_f for materials A and B to be 10.4 kN/m^2 , in which case a smaller pullout capacity will be developed than in the case previously considered in Figure 7. However, as shown in Figure 8, both material A and material B will develop a greater pullout resistance than material C at a displacement of 1.5 mm. At large displacements, material C will have a larger capacity. Again, this difference is because of the modulus of the geogrid, not the strength.

An example of the predicted distribution of axial force along the length of the geosynthetic, for materials A, B, and C, is shown in Figure 9, at a pullout displacement of 1.5 mm. (These load distributions correspond to the pullout curves shown in Figure 7.)

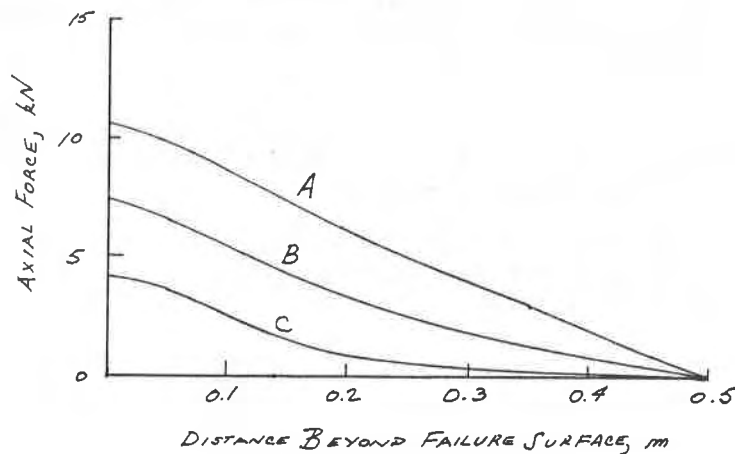


Figure 9. Variation of Tension Along the Length of the Geosynthetic, at a Displacement of 1.5 mm

SUMMARY

Often in traditional geotechnical engineering design, strains can be ignored in order to permit the use of a limit equilibrium approach. However, in the design of reinforced soil systems, compatibility between reinforcement and soil strains must be considered. For the case of a reinforced slope, compatibility can be accomplished more easily through displacements than through strains. The displacement of a geosynthetic will depend upon its pullout characteristics. The load transfer method can be used to predict the pullout characteristics of geosynthetic reinforcement. The modulus of the geosynthetic will influence its pullout characteristics, with high modulus geosynthetics being more efficient at developing pullout resistance at working strains.

ACKNOWLEDGEMENTS

This work is part of an ongoing study for Signode High Performance Plastics Division. The author would like to thank Mr. Art Slaters, Jr. for his permission to publish this work and for his continued support. The author would also like to thank Mr. Joe Fluet for reviewing the manuscript and Ms. Henny Benson for her assistance in typing the manuscript.

REFERENCES

- Andrawes, K.Z., McGown, A., and Murray, R.T., "The Load-Strain-Time-Temperature Behavior of Geotextiles and Geogrids", Proceedings, Third International Conference on Geotextiles, Vienna, Austria, Vol. III, April 1986, pp. 707-712.
- Baudonnel, J., Giroud, J.P., and Gourc, J.P., "Experimental and Theoretical Study of Tensile Behavior of Nonwoven Geotextiles", Proceedings, Second International Conference on Geotextiles, Las Vegas, Nevada, U.S.A., August 1982, pp. 823-828.

Beech, J.F., and Kulhawy, F.H., "Experimental Study of the Undrained Uplift Behavior of Model Drilled Shafts", Report in press, Electric Power Research Institute, Palo Alto, 1987.

Bonaparte, R., Holtz, R.D., and Giroud, J.P., "Soil Reinforcement Design Using Geotextiles and Geogrids", Report in press, Symposium on Geotextile Testing and the Design Engineer, ASTM Committee D-35, 1987.

Boyce, S.C., and Kulhawy, F.H., "Laboratory Determination of Horizontal Stress in Cohesionless Soil", Geotechnical Engineering Report 83-1, Cornell University, Ithaca, New York, January 1983, 324 p.

Coyle, H.M. and Reese, L.C., "Load Transfer for Axially Loaded Piles in Clay", Journal of the Soil Mechanics and Foundations Division, ASCE, Vol. 92, No. SM2, Mar. 1966, pp. 1-26.

Delmas, P., Berche, J.C., Gourc, J.P., "Le Dimensionnement des Ouvrages Rénforcés par Géotextile Programme CARTAGE", Bulletin Liaison Laboratoire des Ponts et Chaussées, Vol. 142, Mars-Avril 1986, pp. 33-44.

Gourc, J.P., Ratel, A., and Delmas, P., "Design of Fabric Retaining Walls: The 'Displacement Method'", Proceedings, Third International Conference on Geotextiles, Vienna, Austria, Vol IV, April 1986, pp. 1067-1072.

Jewell, R.A., Milligan, G.W.E., Sarsby, R.W., and DuBois, D., "Interaction Between Soil and Geogrids", Proceedings, Polymer Grid Reinforcement, London, Mar 1984, pp. 18-30.

McGown, A., Paine, N., Dubois, D., "Use of Geogrid Properties in Limit Equilibrium Analysis", Proceedings, Polymer Grid Reinforcement, London, Mar 1984, pp. 31-36.

Roscoe, K.H., "The Influence of Strains in Soil Mechanics", Geotechnique, Vol. 20, No. 2, June 1970, pp. 129-170.

Rowe, R.K., and Ho, S.K., "Determination of Geotextile Stress-Strain Characteristics Using a Wide Strip Test", Proceedings, Third International Conference on Geotextiles, Vienna, Austria, April 1986, pp. 885-890.

Terzaghi, K., "Theoretical Soil Mechanics", John Wiley and Sons, New York, 1943, 510 p.

CHRISTOPHER, B.R.
STS Consultants, Ltd., U.S.A.

Geogrid Reinforced Soil Retaining Wall to Widen an Earth Dam and Support High Live Loads

INTRODUCTION

To allow access of construction equipment for reconstruction of the Cascade Dam hydroelectric facility in Cascade, Michigan, the owner, STS Consultants, Ltd., designed and constructed a geogrid reinforced soil wall to increase the width of the crest of the dam from 4.5 m (15 ft) to 9 m (30 ft). Complicating the design was a requirement for the support of an 840 kN (95 ton) crane with a 100 kN (20 ton) lifting capacity and the construction of the wall within a limited working area on a 2 horizontal to 1 vertical slope. The 3.1 m (10 ft) high wall was constructed using high modulus geogrid reinforcing elements supplied by the Signode Corporation. The wall was fully instrumented to monitor internal and external lateral movement as well as strain levels in the geogrid elements.

The wall was constructed in the summer of 1986 and was monitored throughout reconstruction of the hydroelectric facility. This paper reviews the design and construction of the wall and presents the results of the monitoring program.

BACKGROUND

The Cascade Dam hydroelectric facility is located at the center portion of a concrete core wall earthen-fill dam. Access to the facility was by a 4.5 m (15 ft) wide service road along the crest of the dam. The earth-fill embankment downstream of the service road was constructed at a 2 horizontal to 1 vertical slope. Reconstruction of the facility would require access by construction equipment including a 6 axle, 840 kN (95 ton) crane for placing the turbine and 180 kN (20 ton) generator. The crane with its outriggers extended would require a maneuvering and operating space of approximately 9 m (30 ft) wide. Therefore, a wall was required to be constructed on the side slope of the embankment to expand the crest of the dam. It was decided to use a reinforced soil wall due to the ease of construction in the limited work area and lower cost as compared to a reinforced concrete wall. In addition, the wall would be built with a geosynthetic reinforcement to provide a flexible face and allow for anticipated lateral displacement under temporary, very high surcharge loading. After reconstruction of the hydroelectric facility, a permanent precast panel or wood facing would be attached to the wall and the surface above the wall would be used for parking.

WALL DESIGN

Figure 1 shows a profile view of the proposed wall section along with anticipated surcharge loads. The reinforced soil retaining wall was designed by analyzing the external and internal stability of the system. The external stability was evaluated by treating the reinforced soil section as a gravity retaining wall and analyzing its potential for failure by sliding, bearing capacity, overturning, and overall deep seated slope failure. Conventional soil mechanic stability methods were used to evaluate each stability criterion (1). Once it was determined that the wall could be supported by the existing embankment, the internal stability and reinforcement requirements were evaluated.

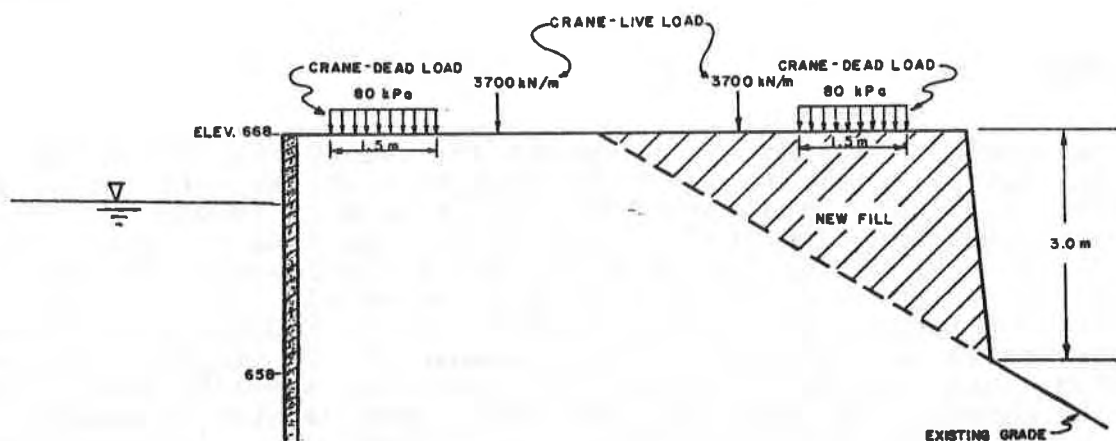


FIGURE 1: Design Requirements for Cascade Dam Retaining Wall

The internal stability analysis involved selecting a geosynthetic layer spacing to fit the construction sequence and facing requirements. The reinforcement tensile strength required to resist horizontal stresses and the length of the reinforcement to resist pullout at those stress levels was then determined. Three methods that are summarized in the FHWA "Geotextile Engineering Manual" (2) were utilized in the analysis of internal stability including; Steward, Williamson and Mohny (1977); Netlon (1982); and Netlon (1984). Each method essentially uses the same analytical approach with the tension in the reinforcement (α_d) determined by:

$$\alpha_d = K\sigma_v(s)$$

where:

- K = a lateral stress ratio
- σ_v = vertical stress resulting from the soil mass + the deadload surcharge
- s = spacing of the elements.

The value of the stress ratio depends upon the amount of lateral yield that can occur and is usually somewhere between the active lateral earth pressure and the at-rest condition. The stress ratio used varied

between the different procedures. The vertical stress, σ_v , results from the reinforced soil mass and any long-term surcharge loads. The vertical stress is distributed over the depth of the reinforcement using either the Meyerhof's or Trapezoidal stress distribution methods, which again varied between the referenced methods. An additional vertical stress also results from live surcharge loads.

In the case of the Cascade Dam, the major surcharge loads resulted from the wheel loads of the crane while moving it into position and the dead load of the crane as applied through the outrigger jacks. The load from the four outrigger jacks was transferred to the subgrade through 1.5 m (5 ft) wide by 3.0 m (10 ft) long timber mats. The actual surcharge stress during lift at the base of the timber mats was calculated at 80 kPa (1670 psf). The wheel loads of the crane were analyzed as a line load of 3700 kN/m (1700 lbs/ft) which, of course, did not occur simultaneously with the crane dead load. Load distribution evaluation of such high surcharge loads on reinforced soil walls, especially low height walls, is not well covered in the literature.

Early in the analysis, it was determined that the upstream reinforced concrete core wall would be only marginally stable under the lateral pressure resulting from the crane loads. Therefore, tiebacks were placed between the two walls, the reinforced concrete wall and the reinforced soil wall, at the support arm locations to reduce the risk of cracking the upstream face of the wall. This complicated the analysis of the reinforced soil wall as the tiebacks also reduced the stress in the upper levels of that wall. For the reinforced soil wall analysis, the tiebacks were assumed to take all of the surcharge stress down to the tieback level. The stress immediately below the tieback was then analyzed using a 2 vertical to 1 horizontal distribution and then distributing the stress at that level as a constant stress over the remainder of the wall as shown in Figure 2. The distribution of the wheel load, also shown in Figure 2, was distributed using elastic theory (1).

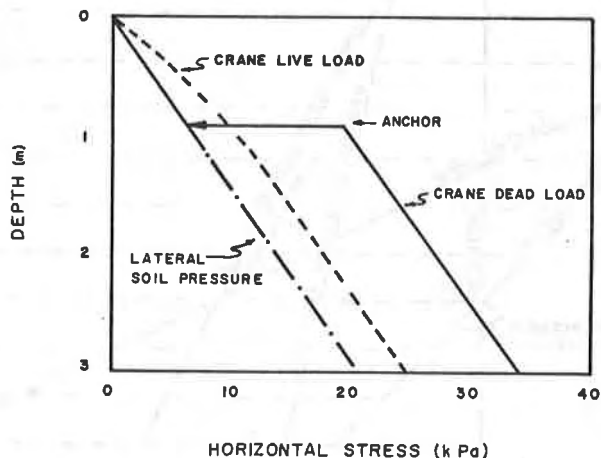


FIGURE 2: Horizontal Stress Distribution

Based on using a 0.30 m (1 ft) geosynthetic layer for ease of construction, the design strength (α_d) required to provide a factor

safety of 1.5 against rupture during crane loading was found to be approximately 14 kN/m (80 lbs/inch) at a maximum tolerable strain of 5%. Using a factor safety of 3 to take into account creep and longevity of the geosynthetic, the ultimate strength (α_u) required was therefore 42 kN/m (240 lbs/in). Based on these requirements and other factors such as pullout resistance, a geogrid reinforcement was selected.

In order to develop the required strength, the geogrid must be extended far enough behind the potential failure surface to develop sufficient pullout resistance. The potential failure surface is the location of the maximum tensile stresses in the reinforcement. For extensible reinforcement, such as geogrids or geotextiles, in cohesionless ($c = 0$) soils, it is usually assumed to occur along the Rankine failure surface or at an angle from the base equal to 45° plus one-half the soil friction angle, ϕ , (2). The pullout resistance of geogrids is a function of: the length of the grid behind the failure plane; the type, density and frictional characteristics of the soil; the size of the grid opening; the frictional resistance of the grid surface; and, to some extent the thickness of the transverse grid elements.

Preliminary pullout design was based on the assumed friction angle of the fill to be used and the methods recommended in the three procedures used for the analysis. On that basis and other assumptions used in each of the design methods, the reinforcement lengths determined from each method are shown in Figure 3. Variations between methods are mainly due to differences in surcharge load distribution procedures. The actual lengths used are also shown and were selected based on the design requirements as well as particular construction features. The final design is shown in Figure 4.

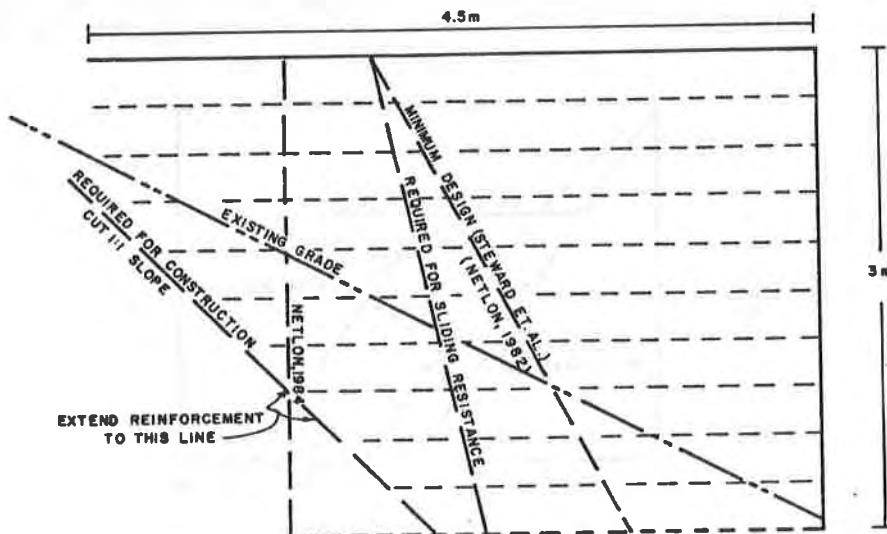


FIGURE 3: Length of Reinforcement Summary

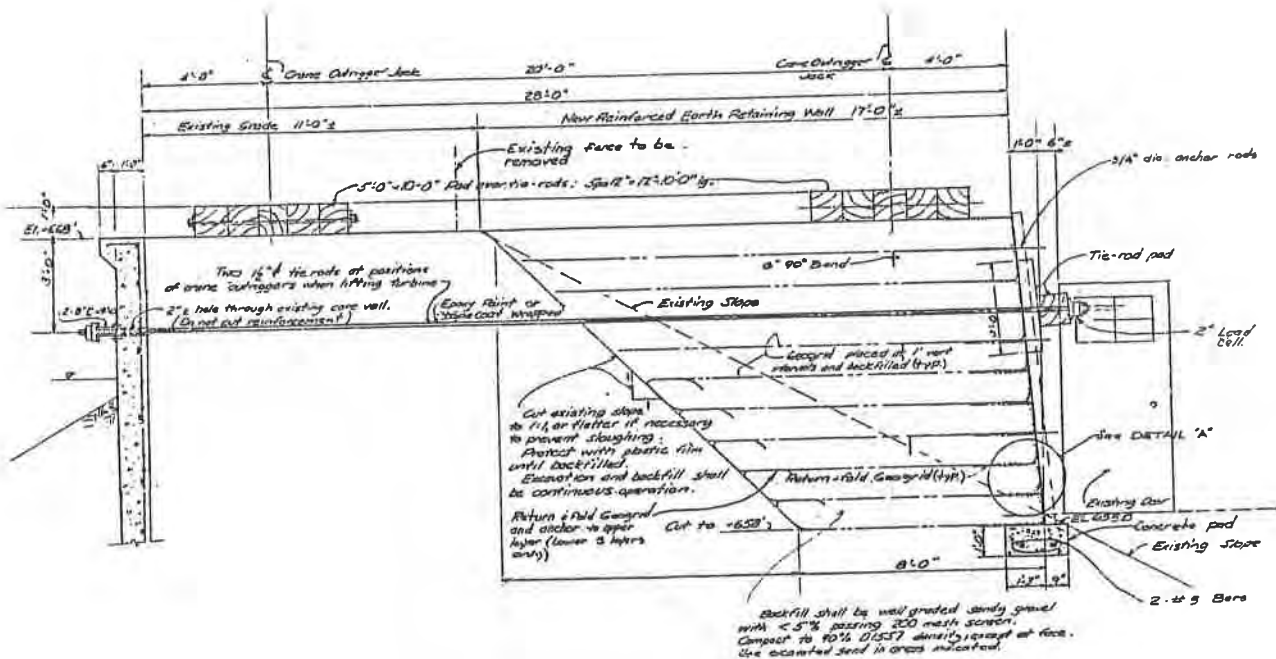


FIGURE 4: Final Design of Cascade Dam Reinforced Soil Wall

MATERIAL CHARACTERISTICS

Soil Profile

The embankment upon which the wall was to be placed generally consisted of medium dense fine sand with some clay ($\phi=30^\circ$, $c=0$) extending to the base of the dam at a depth of 12 m (approx. 30 ft). The embankment was supported on alternating layers of natural, very stiff fine sandy clay and extremely dense fine sand.

Backfill

Imported sandy gravel fill was used in the front portion of the wall and extended back from the face of the wall about 3 m. Thus, the imported sandy gravel encompassed both the active and reactive portions of the reinforced soil mass. Behind the imported soil, the fine sand excavated to allow the reinforced soil wall to be keyed into the embankment was used.

The imported sandy gravel consisted of a bank run fine to course sand and fine to course gravel with some cobbles and approximately 5% was finer than 75 μm . Large 150 mm (6 in) diameter triaxial tests indicated $\phi = 37^\circ$ and $c = 20$ kPa (420 psf) when compacted to the as placed density of 2000 kg/m^3 (125 lbs/ft^3).

Geogrid

The geogrid selected for this project was Signode TNX 250. This particular geogrid is comprised of orthogonal strands of highly oriented polyester that have been welded together at the crossover points. The strands are approximately 12 mm (0.5 in.) wide by 1 mm thick with nodes spaced at 76 mm (3 in) on center in both the longitudinal (machine) and transverse (cross machine) directions. The characteristic tensile strength properties of the grid based on ATSM D-4595 Wide Width Test are shown in Figure 5. The strain gauge plot shown on the figure was obtained from bonding gauges on individual strands. As such, the strain gauge plot does not include the influence of the welded connections and is more representative of the polymer stress-strain characteristics than the total grid characteristics.

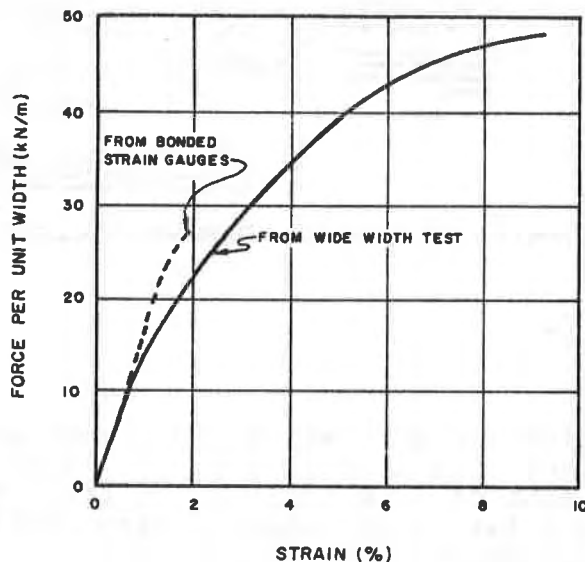


FIGURE 5: Tensile Strength Characteristics of Geogrid

Pullout tests were performed on the geogrid using a 0.8 m wide by 1.2 m long by 0.4 m deep pullout box. The pullout resistance for a 1.2 m (4 ft) embedment was found to increase linearly with overburden pressure up to the maximum pullout resistance required (equal to the ultimate strength required of the grid) at an overburden pressure of 30 kPa (equivalent to 1.5 m of soil).

INSTRUMENTATION PROGRAM

An instrumentation monitoring program was developed to evaluate the performance of the wall both during construction and loading. The program involved measuring; 1) the tension in the longitudinal grid strands through measurement of localized strain, 2) the total and incremental lateral displacement of the grid at various depths, 3) the lateral movement of the face of the wall, and 4) the magnitude of stress transferred to the tiebacks during surcharge loading.

The tension in the longitudinal grid strands (in the direction perpendicular to the wall face) at various locations was measured using both bonded electrical resistance strain gauges and electro-magnetic inductance type strain gauges. Micro-Measurements Group, Inc. bonded resistance foil strain gauges (type EP-08-250BG-120) were used as the primary strain measurement gauges. As a backup to the bonded resistance gauges, Bison electro-magnetic inductance strain gauges (Model 4101-A) were installed at five gauge locations in Section A. To measure the lateral displacement of the grid over sections of significant length, mechanical wire extensometers were attached to the grid at 0.6 m (2 ft) intervals from the wall face. Gage locations are shown on Figure 6.

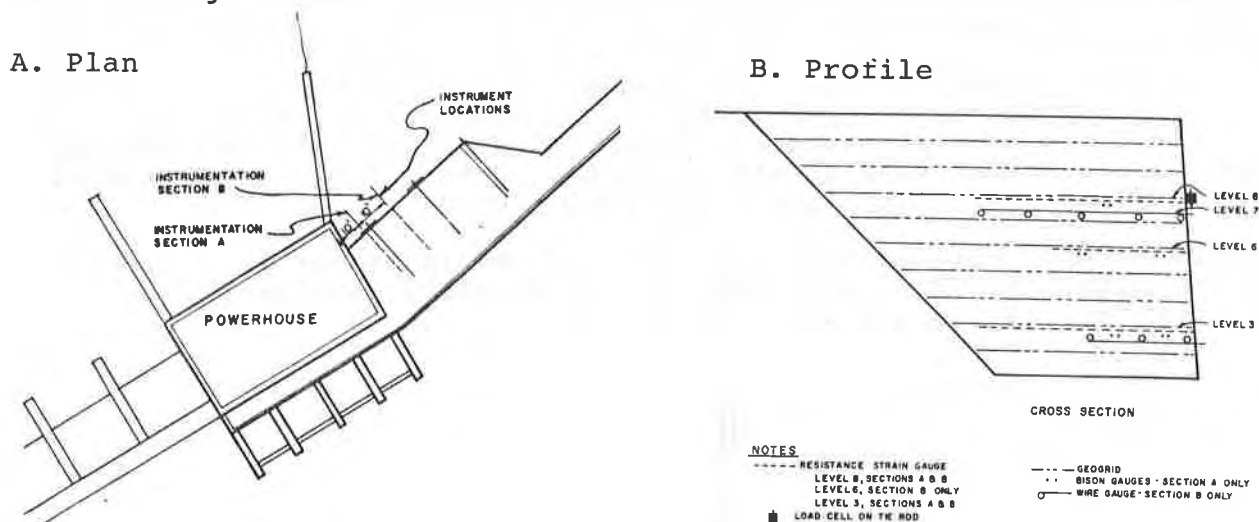


FIGURE 6: Instrumentation Layout

Direct measurements of the horizontal position of the wall face were also obtained at several stages and were referenced to the concrete footing. Inaccessibility to the footing terminated the readings prior to moving the large crane on site.

Load cells, Sinco Model 51351911-890 kN (100 ton) capacity, were installed on the two tieback rods prior to low load service crane loading. To seat the tiebacks, anchor bolts were torqued to an initial 44.5 kN (5 tons) load after which load readings were periodically taken.

CONSTRUCTION

The wall was constructed using conventional construction equipment. The original embankment was excavated back to a one to one side slope to key the reinforced soil wall into the embankment. A 0.6 m (2 ft) wide by 0.3 m (1 ft) deep concrete leveling pad was constructed at the toe of the wall. Fill was end dumped on top of the embankment and lowered to the base of the wall with a backhoe. The fill was then manually spread and leveled to an approximate 0.3 m (1 ft) lift thickness. The backfill was then compacted with a hand operated vibratory compactor to a minimum density of 90% of ASTM D-1557, Modified Proctor density method.

Geogrid was placed at each lift level with the longitudinal direction perpendicular to the face of the wall. Adjacent rolls of geogrid were overlapped a minimum of 2 grid spaces. At the base of the wall, the geogrid was folded at the back of the reinforced soil section as shown on the design drawings to maximize pullout resistance.

The face of the wall was constructed using removable braced plank form work similar to that used by the New York Department of Transportation(3). A unique facing support was used which consisted of overlapping and tying adjacent layers of geogrids (Figure 7) as opposed to using a conventional return type system. Metal clips (grit seals) and high strength 350 N (80 lb) polypropylene plastic ties were used to tie off the successive grid layers. A silt film woven geotextile was placed behind the geogrid at the wall face to prevent raveling of the soil through the grid. This type of construction proved to be easier than the conventional return system and resulted in a savings of 1.4 m (1.5 yards) of material per grid level. In addition, minimal sloughing of the face after removal of the forms was noted. Forms were removed after an additional three levels had been placed.

The instrumented grid layers were installed at locations previously shown on Figure 6. Hand placement of the backfill facilitated in protecting the gauges and wire leads.

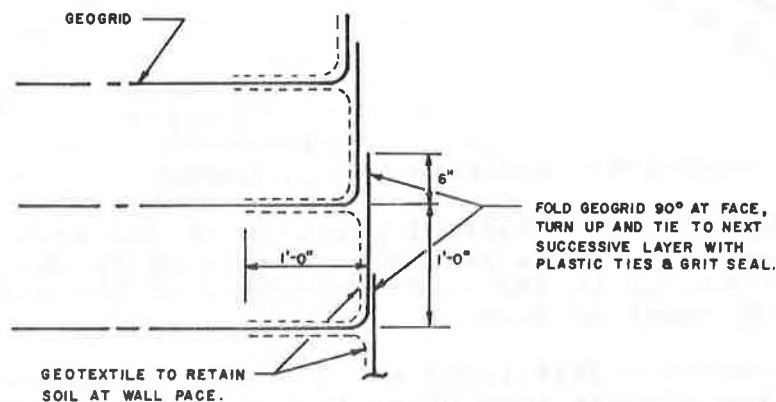


FIGURE 7: Wall Facing Connection Detail

The wall was constructed with an inexperienced crew in three days. At 21 days after construction, the tiebacks were seated by applying a 90 kN (10 ton) force and a 310 kN (35 ton) service crane was moved onto the site. Five months after construction, the high capacity crane was moved into position. The large crane was utilized for a period of approximately four hours, one hour of which was used to move into position and support the 180 kN (20 ton) generator.

MONITORING PROGRAM RESULTS

The wall was monitored during construction, the five month period following construction when a service crane and other construction equipment was operated on the wall, and during high capacity crane

loading. Monitoring will be continued to evaluate long-term performance.

The strain gage data provided the principal information obtained from the monitoring program. Figure 8 shows a typical set of data obtained at a particular section and level for each event that occurred during the monitoring program. The cumulative total strains that occurred at the end of each significant event are shown in Figure 9 as a function of distance from the face of the wall.

The most significant event was the high capacity crane loading. For that event, the lateral stress at the tierod locations could be measured directly from the increase in tierod reaction force and the area of the reaction pad. Significant increases in stress were measured as the generator was swung out over the reinforced soil wall and held in position at the back of the crane (Instrumentation Section A) during installation. Figure 10 presents the strain developed in Section A, the location of highest loading, as compared to the measured stress.

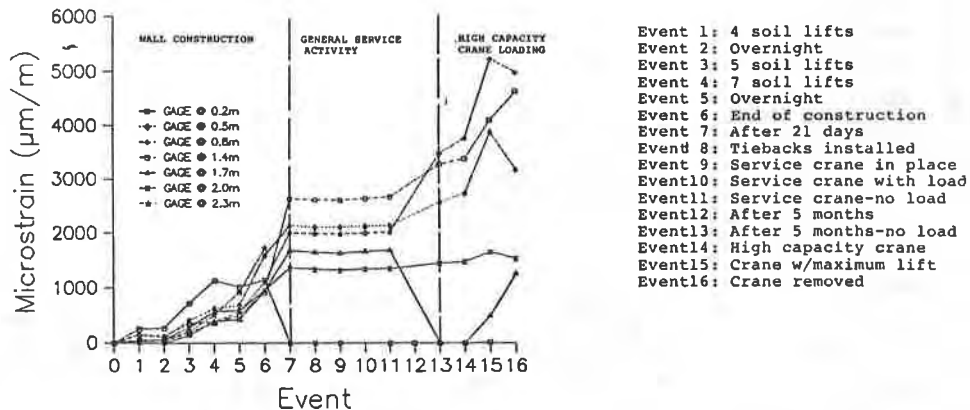


FIGURE 8: Strain Readings During Construction Sequence for Level 3, Section A

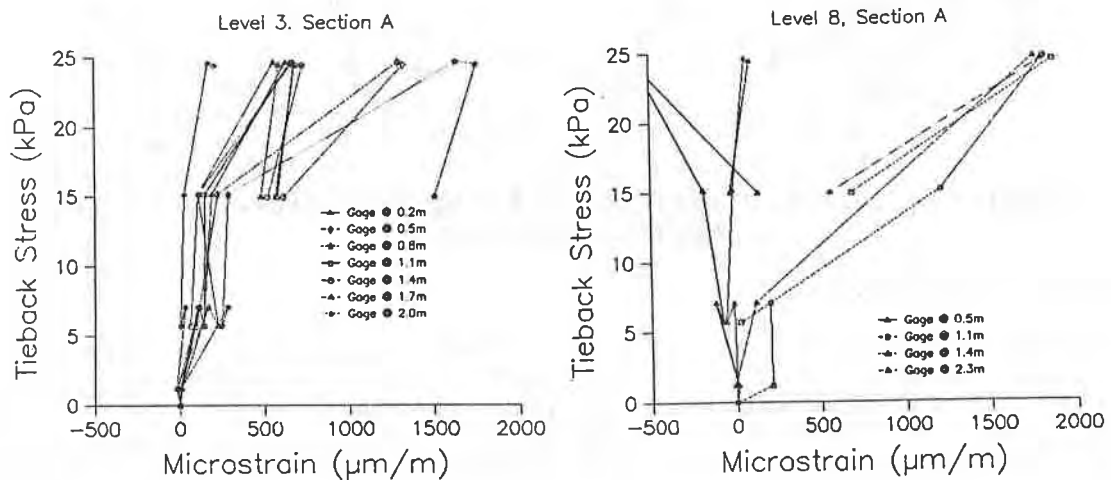


FIGURE 10: Strain Measurements Under Crane Loading

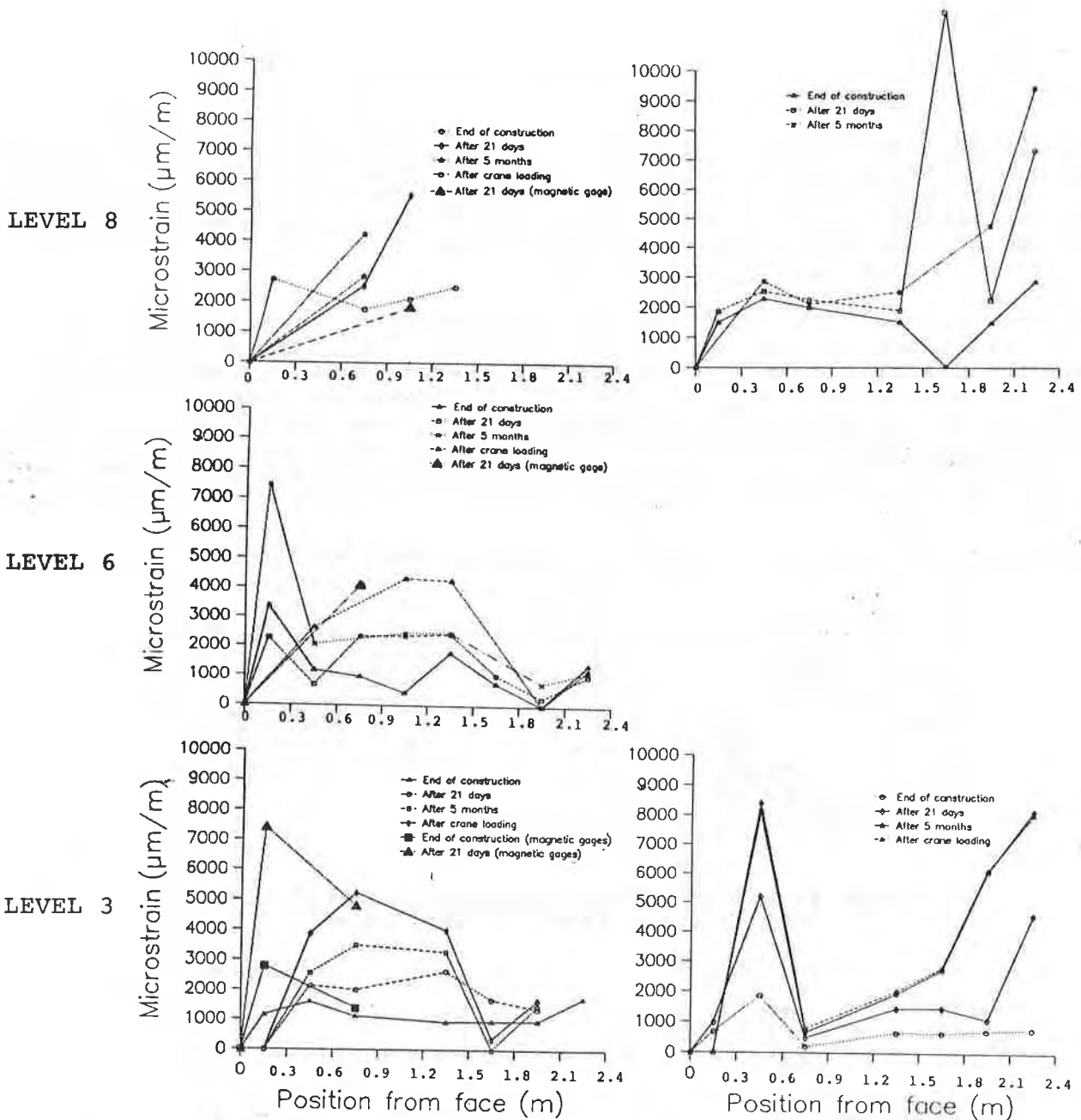
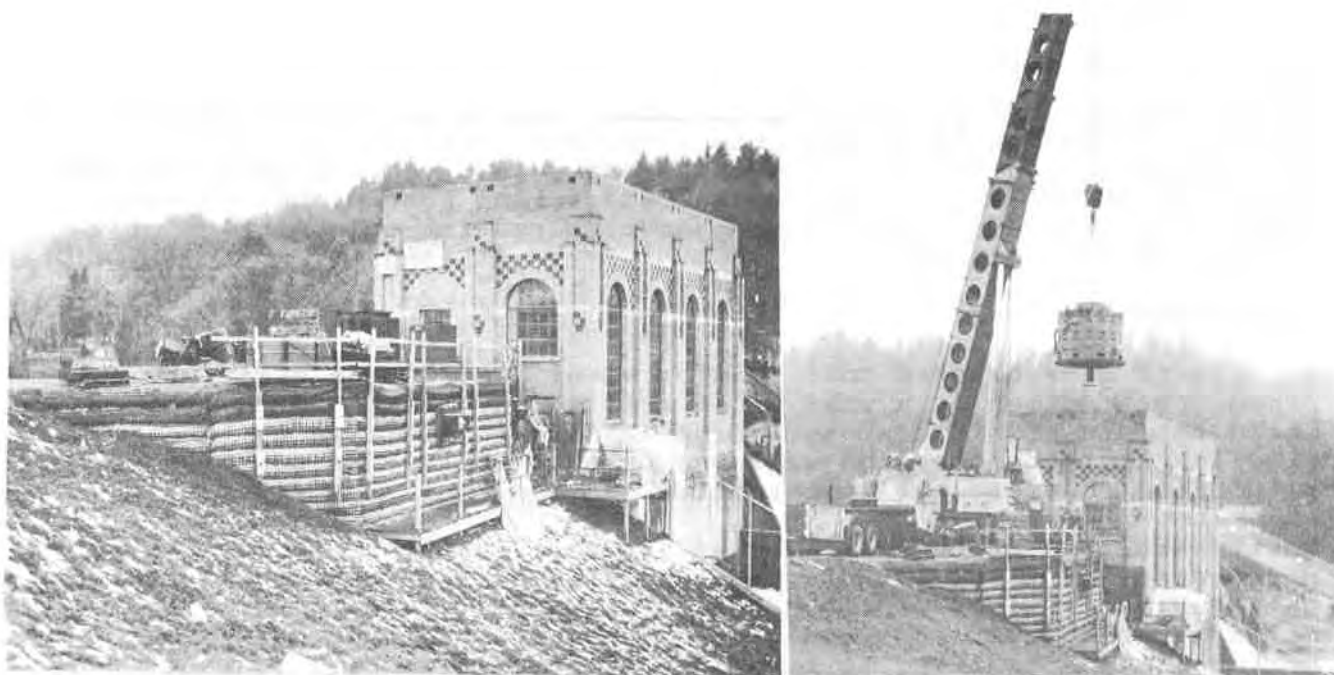


FIGURE 9: Strain Distribution Along Reinforcement During Monitoring Events

Performance Evaluation

The overall performance of the wall is best described by the photographs shown in Figure 11 which show the high capacity crane in position. It is apparent from the photographs that the wall performed its intended function with no apparent distress to the reinforcement. Negligible settlement of the crane platforms were observed during crane loading as indicated by the leveling bar on the crane which remained at a constant level position throughout operation.



A. Geogrid wall after construction

B. High capacity crane loading

FIGURE 11: Cascade Dam Reinforced Soil Retaining Wall

Measurements from the instrumentation program indicated a maximum strain in the upper level wall reinforcement on the order of 1% and, in the lower portion of the wall, 0.85%. Based on the stress-strain characteristics of the geogrid shown in Figure 5, these strain levels would equate to tension in the geogrid of 16.5 kN/m (94 lbs/in) and 14 kN/m (80 lbs/in), respectively. The maximum tension measured in the geogrid at the lower portions of the wall was very close to that estimated for the design. However, the upper level tension in Section B was higher than anticipated. As shown in Figure 8, even higher strains may have occurred at greater depths behind the face of the wall than the 2.4 m instrumentation locations.

With regard to the higher stress levels measured, the conventional rigid body theory used for the design would have predicted the maximum stress in the lower portion of the wall. Such analytical procedures do not take into account strains in the reinforcement, stress transfer, and concentrated stress from high loading forces near the front edge of the wall. In addition, analyzing the stress at the Section B location is complicated by the tieback. Research by Wichter, et.al.(4) indicated when loading is concentrated directly above the reinforced soil wall section, the failure plane is shifted to the rear edge of the load platform. Correspondingly, an increase in tensile forces in the upper level reinforcement occurs and, as a result of increase in normal stress, the structure is apparently less yielding in the area of the loading platform. The tiebacks are located directly beneath the loading pads, which apparently transferred stress to the Section B location between the tiebacks. As the face of the wall was not restrained at that location, higher lateral movement than anticipated occurred. Figure 10, shows that the strains in the upper level of Section A were restrained by the tiebacks.

Another measure of performance is cost. The total cost of the wall was \$19,000, including \$4,000 for the tiebacks. The cost of the geogrid reinforcement was \$3,000. The cost of a reinforced concrete wall was estimated at \$21,000, including the additional cost of the tiebacks. Additional time would have also been required for construction of the reinforced concrete wall.

CONCLUSIONS

The use of geosynthetic soil reinforcement allowed the efficient and rapid construction of a wall, in a restrictive working area, which would support significant surcharge loads. In addition to the excellent performance, the wall was cost effective, as compared to a reinforced concrete wall alternative.

Instrumentation of the wall proved extremely valuable in evaluating the performance of the wall. Further analysis of the strain-distribution data may assist in refining predicative capabilities. From the data, it is apparent that additional research needs to be performed and design methods modified to take into consideration high concentrated stresses within the zone of reinforcement near the front edge of reinforced soil walls.

ACKNOWLEDGMENTS

The author wishes to acknowledge Ms. Cynthia Bonczkiewicz for her valuable assistance in the instrumentation program, Ms. Diane Moe for her diligence in mounting the instruments, and Ms. Maria Flessas for help in preparing the paper. The author and STS Consultants, Ltd. wish to extend their gratitude to the Signode Corporation, High Performance Plastics Division, for their extensive support as sponsors of the instrumentation program.

REFERENCES

- (1) Terzaghi, K., and Peck, R.S., Soil Mechanics in Engineering Practice, John Wiley and Sons, New York, 1967.
- (2) Christopher, B.R., and Holtz, R.D., Geotextile Engineering Manual, Report No. FHWA-TS-86/203 for the Federal Highway Administration, 1985.
- (3) Douglas, G.E., "Design and Construction of Fabric Reinforced Retaining Walls by New York State" presented to the annual meeting, Transportation Research Board, 1982.
- (4) Wichter, L., Risseuw, P., and Gay, G., "Large Scale Tests on the Bearing Behavior of Woven Reinforced Earth Wall", Proceedings of the Third International Conference on Geotextile, Vienna, Austria, Volume IV, pp. 1073-1078.

SCOTT, J.D., SEGO, D.C., and HOFMANN, B.A.,
Dept. of Civil Engineering, University of Alberta, Canada
RICHARDS, E.A.
Dept. of Clothing and Textiles, University of Alberta, Canada
BURCH, E.R.
Alberta Transportation, Canada

Design of the Devon Geogrid Test Fill

ABSTRACT

The design requirements of a 12 m high geogrid reinforced embankment, to be constructed with 1:1 slopes using cohesive soil, are presented. The primary objective of the test fill is to determine the mechanism whereby geogrid layers reinforce cohesive soil slopes. The embankment geometry, geogrid layout, and properties of both the fill and foundation soils are outlined. The instrumentation installed on the geogrid, within the soil embankment and within the foundation soil to monitor the performance of each and establish the interaction of the soil and the geogrids are discussed in detail.

INTRODUCTION

Soil reinforcement has recently gained much interest in geotechnical engineering design and construction. Its advantages are reduction in costs and ease of construction, coupled with a basic simplicity (1). For these reasons, Alberta Transportation has experimented in the field with reinforcing of pavements and of weak foundations for embankments and has established a research program on reinforcing steep slopes in soil embankments.

The advantages in reinforcing soil slopes are cost savings with respect to the volume of soil material used in a fill or in a bridge approach embankment, cost savings with respect to narrower right-of-ways for embankments, elimination of retaining structures, and decreasing the length of culverts through fills due to steeper slopes.

The reinforced slope research, conducted by the University of Alberta and funded by Alberta Transportation, includes development of both testing apparatuses and testing procedures for geogrids and high strength geotextiles to determine interfacial friction and pullout resistance, development of a design methodology for reinforced soil slopes, and field testing of several geogrid materials. This paper is concerned with the design of the field test of three different geogrid materials. The field test is a reinforced cohesive soil embankment, containing four instrumented sections; one for each geogrid and an unreinforced slope for comparison.

Most reinforced soil structures use a well graded cohesionless fill because granular materials are usually stable, free draining and are not frost susceptible. The high cost of importing such materials, however, in many areas of Alberta is a distinct disadvantage. The field research program therefore used a silty clay soil representative of many soil deposits in Alberta.

The test fill is located near Devon, Alberta, approximately 30 km from Edmonton (Fig. 1). It is being constructed in conjunction with a new bridge crossing of the North Saskatchewan River which requires approach fills up to 22 m in height. Initially, the test sections were planned to be part of the bridge approach fills, but the potential for interference with construction of the approach fills and the desire to monitor the performance of the test sections for several years, dictated the construction of a 23,000 m³ embankment solely devoted to the research program.

OBJECTIVES OF TEST FILL

The primary objective of the test fill is to determine how individual geogrid layers reinforce a mass of cohesive soil. An understanding of the mechanisms should lead to an understanding of the most critical modes of failure and result in a more efficient and economic design method for slope reinforcement.

Additional objectives are to evaluate the current methods for designing fills using geogrids for reinforcement, to compare the performance of three different geogrid materials, to evaluate the field performance of the compacted fill and its foundation soils, and to evaluate the field construction procedures involved in constructing geogrid reinforced slopes.

DESIGN REQUIREMENTS

Rowe and Soderman (2) consider that failure of a geotextile reinforced embankment can be deemed to have occurred if the shear strength of the soil is fully mobilized along a potential rupture surface and (a) the geotextile fails; or (b) the geotextile-soil interface fails; or (c) the maximum strain in the geotextile reaches the allowable compatible strain. They show that prior to failure modes (a) or (b), the contribution of the geotextile to the embankment stability is governed by a condition of strain compatibility and the relative moduli of the soil and geotextile. Although they were examining the stability of embankments on soft foundations, their reasoning is also true for the stability of reinforced slopes.

With the high strength and high modulus geogrids used in the Devon geogrid test fill, the lateral strain in the soil could be significantly reduced by the geogrids and failure condition (a) or (b) would govern. As the purpose of the test fill is to measure the stress transfer from the soil to the geogrids during construction of the embankment, the test fill was designed to allow lateral strain of the soil to stress the geogrids, mobilizing their allowable working strength. The dimensions of the embankment are such that, if desired, the fill height can be subsequently increased and the geogrids loaded into their creep range or to failure.

Figure 2 shows a typical geogrid layout (3) where the geometry and soil properties of the fill shown correspond to a factor of safety of 1.5. The close vertical spacing of the geogrids (approximately 0.5 m) in the bottom third of the fill would not only prevent lateral straining with subsequent low stresses in the geogrids but would also result in interference between individual reinforcing members. To allow lateral straining to occur and to ensure that each reinforcing layer would act independently, three primary reinforcing layers at 2 m vertical spacing were chosen for the test fill design (Fig. 2). The minimum number of geogrid layers and the minimum length of each layer were chosen in order that both local and overall stability of the slope was achieved while the deformation was not inhibited.

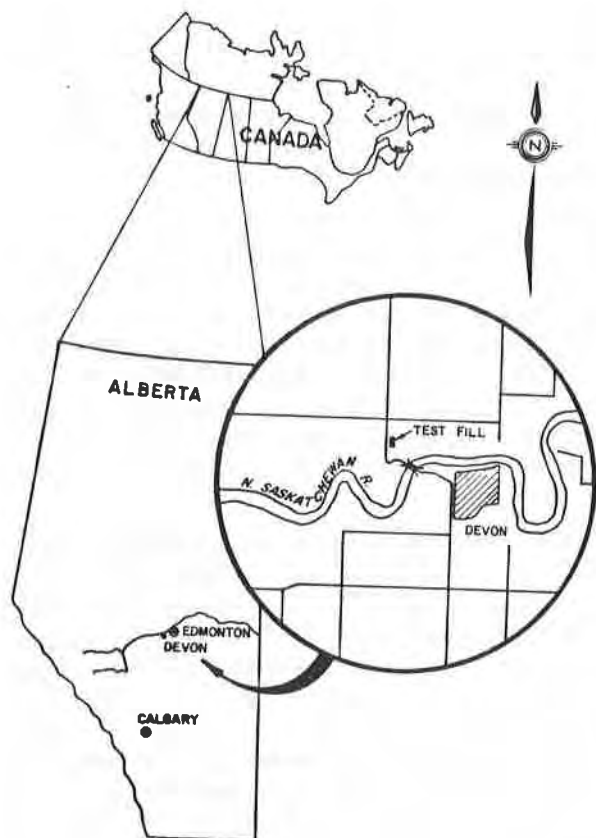


Figure 1 - Location of Geogrid Test Fill

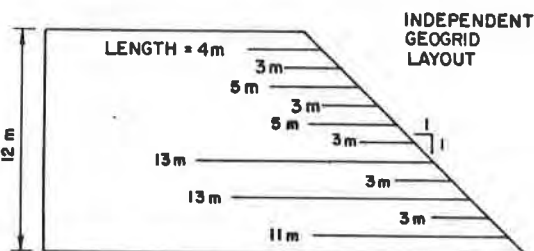
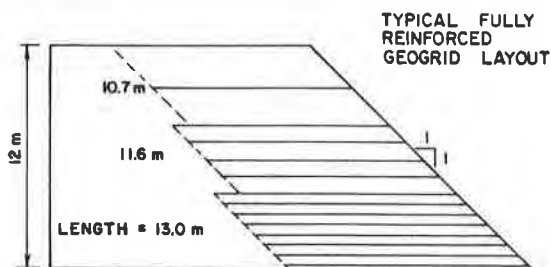


Figure 2 - Fully Reinforced Layout versus independent layers of geogrid.

An advantage of the test fill design is that the possibility of a design method utilizing fewer but stronger geogrids can be examined. Jones (1), when reviewing the work by Jewell (4), suggests that given a choice of reinforcement, that stronger reinforcement placed at wider spacing is more efficient than a greater number of smaller reinforcements placed close together. With the stronger geogrids now being developed by manufacturers, such a design method may be appropriate.

Other design requirements for the test fill were to use a locally available soil, preferably similar to the soil being used for the bridge approach fills, and that the soil have stress-strain properties which would ensure that sufficient lateral strains occurred under the embankment stresses. In addition, the site for the fill required good foundation conditions in order that strains from foundation deformations would not make the analyses of the field measurements onerous.

EMBANKMENT SOIL PROPERTIES

The grain size curve of the compacted fill material is given in Figure 3.

The soil is composed of 25% sand sizes, 50% silt sizes, and 25% clay sizes. Although this material would be described as a clayey silt on the basis of the grain size curve, the Atterberg limits are indicative of an inorganic clay of low to medium plasticity. The liquid limit of the fill soil is 42% and the plastic limit is 18%. The activity of the soil is therefore approximately equal to one, which suggests that the clay fraction is largely montmorillonite.

Standard compaction tests were conducted on the embankment soil. The resulting compaction curve is shown in Figure 4b, where the optimum water content is approximately 21.5% and the corresponding maximum dry density is 1,600 kg/m³. Unconfined compressive strength tests were conducted on the compacted samples and it was found that beyond the optimum water content, the undrained shear strength of the compacted soil dropped rapidly. The compaction specifications for construction of the fill were chosen such that the undrained shear strength of the soil would permit substantial deformations in the completed embankment. The range of allowable water contents and densities shown in Figure 4b correspond to a factor of safety of approximately 1.0.

Consolidated undrained triaxial tests with pore pressure measurements were also conducted on the compacted embankment soil (Figure 5). The soil was compacted in a standard compaction mould at water contents between 22 and 24%. Specimens were then removed from the mould using thin walled, 1.5" diameter Shelby tubes. The specimens were consolidated under confining pressures of 75, 150, 200, and 300 kPa prior to shearing. Typically, the soil exhibited strain hardening behaviour, where the deviatoric stress had not yet reached a maximum at 18% strain. It therefore became necessary to define failure in terms of the maximum principal effective stress ratio reached during shearing of the specimens. In most cases, the principal effective stress ratio reached a maximum of 3.0 at strains of about 12%. The pore pressures, however, rapidly increased, reaching a maximum at 4% strain. The pore pressure parameter A was equal to approximately 0.50 for high confining stresses and equal to about 0.16 for low confining stresses. The tests gave strength parameters of $\phi' = 22^\circ$ and $c' = 13$ kPa.

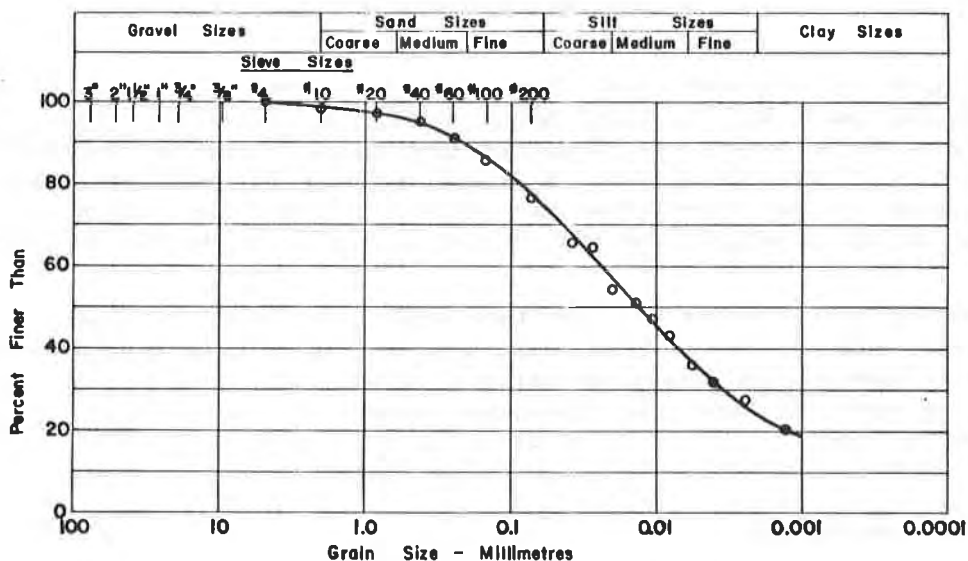


Figure 3 - Grain Size Curve of Compacted Fill Material.

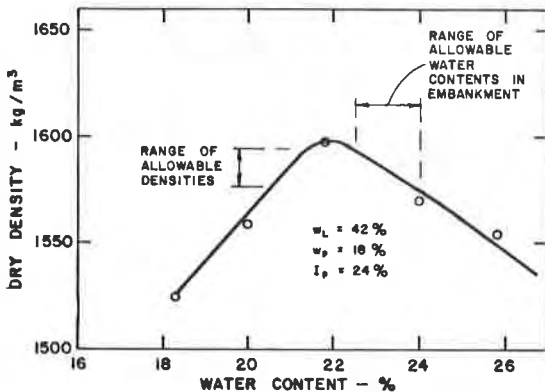


Figure 4a - Undrained Shear Strength of Compacted Soil

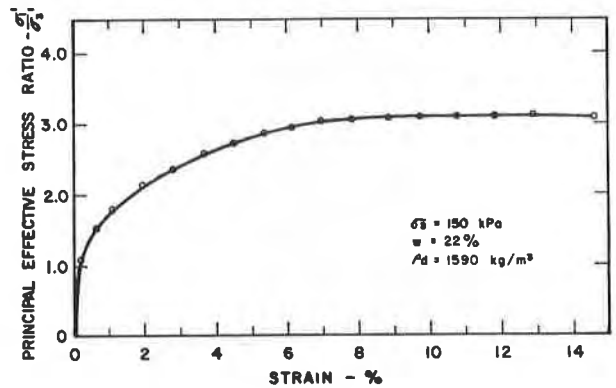


Figure 5a - Stress Strain Curve of Compacted Soil

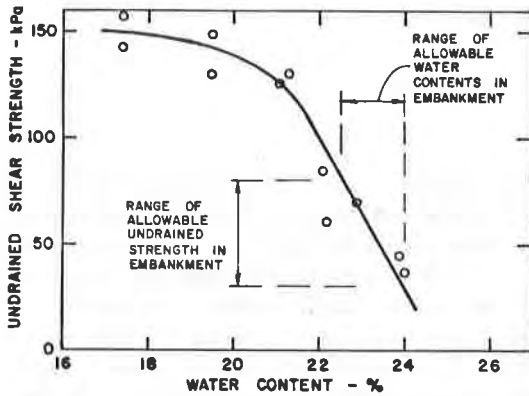


Figure 4b - Compaction Curve

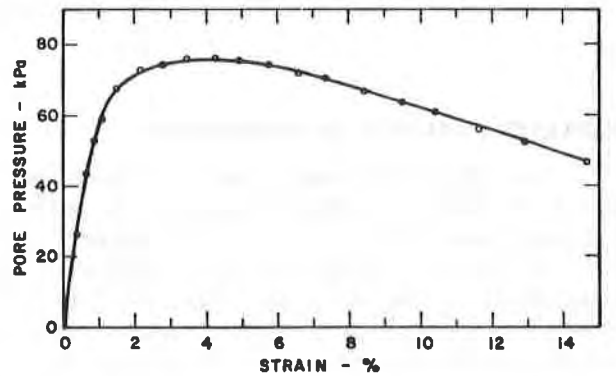


Figure 5b - Pore Pressure

FOUNDATION SOIL

A number of boreholes were drilled in the foundation soil to a depth of 10 m with a wet rotary drill rig. One borehole was drilled down to bedrock a distance of 27 m and a bench mark was then installed. Standard penetration tests and Shelby tube samples were taken alternately in a continuous manner, beginning 1 m below the ground surface and extending to a depth of 10 m. A typical profile is shown in Figure 6. The uppermost layer of soil consists of a soft silty clay at a relatively high water content of 35%. This is underlain by 2 m of a stiffer sandy, silty clay. Beyond 6 m, a fine, very dense layer of grey sand exists and this is underlain by a hard clay till. Preliminary consolidation tests have shown that the effective preconsolidation stress in the soft silty clay is approximately 350 kPa. Since the maximum vertical effective stress expected to be induced in the foundation is only 300 kPa, foundation settlements should not be significant.

Consolidated undrained triaxial tests with pore pressure measurements have been conducted on undisturbed samples of the foundation soil obtained from the soft silty clay. The tests indicate that $\phi' = 27^\circ$ and $c' = 20$ kPa. Hence, the foundation soil is strong compared to the embankment soil, and a slip surface which extends into the foundation soil is not expected.

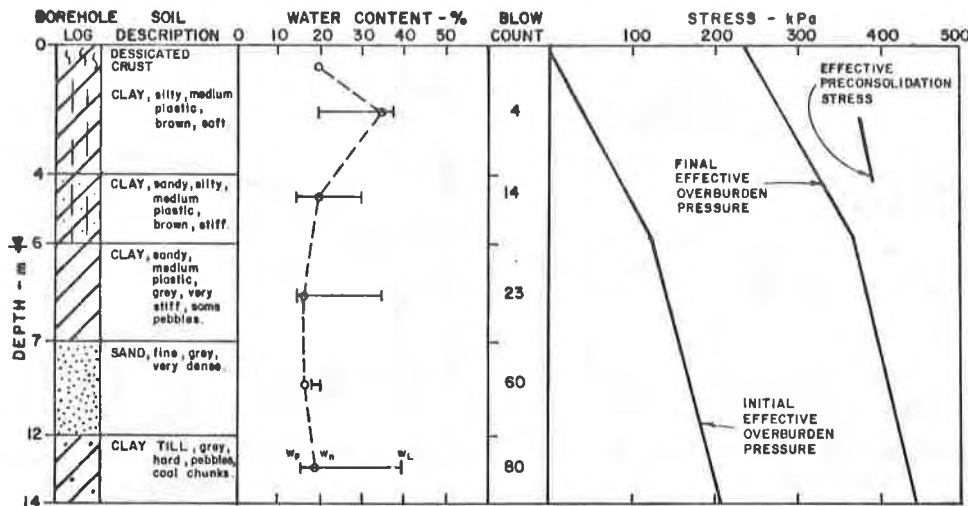


Figure 6 - Foundation Soil Profile.

STABILITY ANALYSIS OF EMBANKMENT

The test fill has been designed with 1:1 side slopes such that the factor of safety against a slope failure is close to 1.0, thus ensuring that significant deformations will occur. The height of the fill was established on the basis of both undrained and drained stability analyses. The factor of safety for an unreinforced, 12 m high fill, using $\phi = 0^\circ$ and an undrained shear strength of 45 kPa, was 1.1. The effective friction angles and cohesive strengths of the fill and foundation soils obtained from the consolidated undrained triaxial tests were used for the short term drained analysis. Here the factor of safety was 0.96, when the pore pressure parameter, ru , was assumed to be 0.15. Figure 7 shows the critical slip circle, C, which corresponds to these conditions. The long term soil strength parameters were estimated for the long term drained analysis. The corresponding critical slip circle, B, is also shown in Figure 7, where the factor of safety is 0.94. Note that there is very little difference in the positions of circles B and C, indicating that the required geogrid lengths may be determined based on either criterion. Inclusion of the proposed geogrid layout shown in Figure 7 increases the factor of safety by only 0.1.

Once the geometry of an individual slope had been chosen, the entire test fill was designed to incorporate three instrumented slope sections, each reinforced with different types of geogrid, and one unreinforced slope section. The following constraints had to be met: the behaviour of opposite slopes must not influence each other and plane strain conditions must exist. A plan view of the resulting fill is shown in Figure 8. The dimensions of the base of the fill are 42 m by 72 m, and the dimensions at the top of the fill are 18 m by 36 m. Each test section is therefore 18 m across at the crest of the slope. The north and south slopes of the fill are 1.5:1, with a more gently sloping approach ramp located on the north end.

GEOGRID LAYOUT

The geogrids used in each reinforced slope have three distinct roles. The

primary geogrids as shown in Figure 7, are installed to reinforce the slope against a toe failure within the embankment. The secondary geogrids reinforce the slope against shallow slope failures. The tertiary geogrids provide reinforcement of the slope such that compaction to the edge of the steep slope is possible and the potential frost heaving of the surface layer is reduced.

The primary geogrids are up to 13 m long and are vertically spaced at 2 m to ensure that each geogrid acts independently within the soil mass. To guard against any possibility of pull out each geogrid is embedded in the soil at least 4 m beyond the critical slip surface predicted from the short-term analysis (Figure 7). The geogrids reinforce the soil mass as the soil begins to strain under self weight. Each geogrid is instrumented to examine the load transfer from the soil to the geogrid as well as the load distribution along the geogrid. Details of the geogrid instrumentation are presented later. The length of secondary geogrids vary between 3 and 5 m and are spaced 1 m vertically. Each secondary geogrid is installed to resist the stresses imposed by potential shallow slope failures. No instrumentation is installed on the secondary geogrids. The tertiary geogrid, 1.5 m long, is installed every 1/3 m where no primary or secondary geogrids were installed. They are not instrumented.

Figure 8 shows a plan view of the test fill indicating the regions reinforced with the different products. The dimensions of the reinforced sections along with locations of the instrumented sections are also illustrated. Table 1 summarizes the different types of reinforcement and amounts used in the test fill.

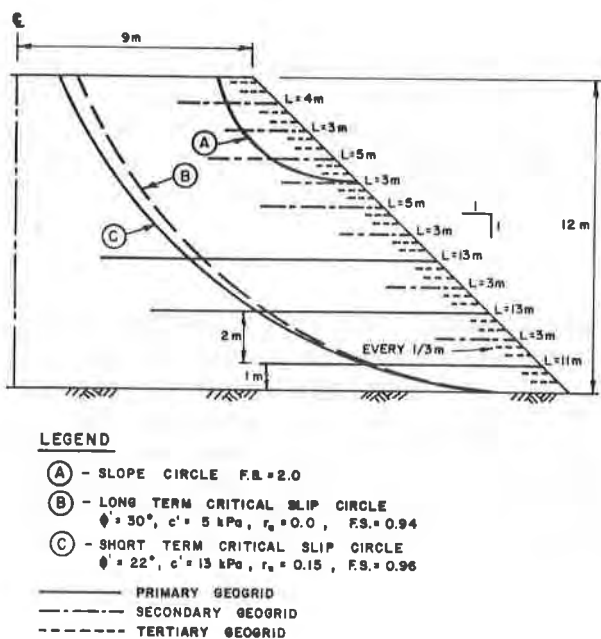


Figure 7 - Typical Geogrid Layout

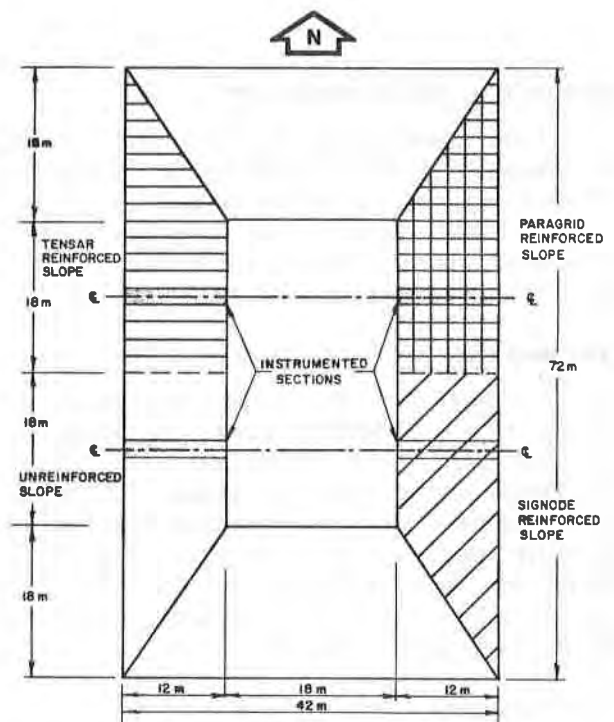


Figure 8 - Plan View of Reinforced Test Fill

INSTRUMENTATION

Extensive instrumentation has been installed to measure the performance of the foundation, the test fill and the geogrids. The types of instruments used as well as the purpose of each instrument are outlined in the following sections. The role of the instruments is to indicate the overall deformation of the test fill and how each geogrid interacts with the soil deformation. The number and location of individual instruments are dictated by the need to know the response of both the soil and the geogrids at specific locations within the test fill. This information then allows a detailed understanding of the soil geogrid interactions.

Table 1. Type and Quantity of Geogrids Used to Reinforce Test Fill.

Type of Reinforcement	Mirafi				Bay Mills			
	Paragrid	Area (m ²)	Signode	Area (m ²)	Tensar	Area (m ²)	Glasgrid	Area (m ²)
Primary	50S/50S	1240	TNX5001	1240	SR2	1020	-	-
Secondary	5T	820	TNX250	820	SR1 SS1	360 450	-	-
Tertiary	-	-	-	-	-	-	Glasgrid	4200

FOUNDATION INSTRUMENTATION

Instrumentation within the foundation is needed to measure foundation settlements during and after construction. The lateral deformations in the foundation must also be measured to determine their influence on the deformation of the test fill. As the test fill is being constructed the pore pressure response within the foundation must be known to understand the lateral and vertical deformations of the foundation soils.

Piezometers

A total of 20 Sinco pneumatic piezometers (Model #514178) were installed within the foundation soils to study the pore pressure response of the foundation to the test fill construction. The layout of the piezometers at a typical instrumented section is shown in Figure 9. Piezometers were installed at depths of 3 m and 6 m in the foundation below the toe, the top of slope and the center line of the final 12 m high test fill. These will provide information on the build up and dissipation of the foundation pore pressure during and after construction. These piezometers will be monitored to ensure stable conditions are maintained during construction.

Inclinometers

Vertical Sinco inclinometer casing (Model #51111) was installed at the toe and crest of the fill at each instrumented section. Each inclinometer was installed to a depth of 12 m below the ground surface to ensure that it was

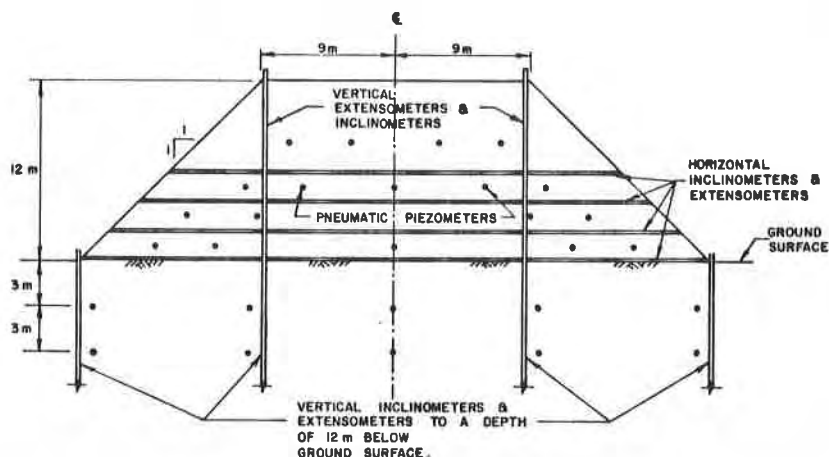


Figure 9 - Soil Instrumentation in Test Fill.

founded in the stiff till and its bottom would not be displaced by the test fill. They measure the lateral deformations within the foundation soils. These deformations are needed to evaluate any influence of the behaviour of the foundation soils on the test fill.

Vertical Extensometers

Multipoint magnetic extensometers are also installed beneath the toe and crest of the slope at each instrumented section. The extensometers will measure the vertical displacements of the foundation soils during and after construction. The deepest extensometer magnet was placed 12 m below the ground surface in the stiff till. Since some vertical deformation may occur at the 12 m depth level surveys referenced to the deep bench mark will be used to measure the elevation change of the deepest magnet.

Magnets were installed at 3, 6, 9 and 12 m beneath the ground surface. This allows for vertical strains within the foundation soils to be calculated.

TEST FILL INSTRUMENTATION

The test fill was designed to strain laterally and vertically so that the primary geogrids would be significantly loaded. The role of the instrumentation within the test fill is to record this deformation as well as information which influences the deformation such as pore pressure, temperature changes and frost heave of the soil near the slope surfaces. All instruments are being installed as the test fill is constructed.

Piezometers

An extensive grid of 36 pneumatic piezometer is being installed. Their locations at each instrumented section is shown in Figure 9. The spacing was dictated by a load-deformation analysis which indicated that the majority of the deformation and load changes would occur within the regions defined by the piezometer locations (Figure 9). This region also is illustrated in Figure 7 by

the critical slip circles B and C. Piezometers are being installed at the center line within the fill to record the maximum pore pressure response during construction.

Inclinometers

Vertical and horizontal Sinco inclinometers are being installed within the test fill. The vertical slope inclinometers extend from the foundation to the top of the slope. The horizontal telescoping slope indicators (Model #51103) were installed in the test fill beneath and above the layers of primary geogrid reinforcement to provide information on the vertical displacement of the test fill at each instrumented section.

Extensometers

Vertical and horizontal multipoint magnetic extensometers are being installed at the same locations as the inclinometers. The vertical extensometers measure vertical displacements and the horizontal extensometers measure lateral displacements of the test fill.

Auxillary Slope Instrumentation

Deformation points are being installed along the slope surface to measure the vertical and lateral deformations of plates close to the slope surface. Survey techniques will be used to establish the deformations of these points. To ensure accurate survey control, four deep survey monuments were installed at each instrumented section. A permanent bench mark to bedrock also was installed beyond the settlement influence of the test fill. The survey monuments are also used for survey control on all instruments installed both in the foundation and the test fill.

Frost heave gauges with thermocouples are being installed in each slope to a depth of 2 m. The thermocouples record the advance of the frost front and the frost heave gauges measure the heave normal to the slope during the frost advance. Similar instrumentation will be installed in the top of the fill. These gauges will allow for evaluation of the tertiary geogrid performance in limiting frost heave on steep reinforced slopes.

GEOGRID INSTRUMENTATION

The primary geogrids have been instrumented with electrical wire resistance strain gauges, Bison strain gauge sensors, and thermocouples to monitor the strains induced in the geogrids as they reinforce the test fill. Figure 8 shows a plan view of the test fill with the location of the instrumented geogrid sections. Each instrumented geogrid was up to 13 m in length and 1 m in width. The instrumented positions began at 0.5 m and then 1 m from the face of the slope. Beyond 1 m they were spaced at 1 m centers along the geogrid. The close spacing at the slope was chosen to monitor the influence of rapid temperature changes on the geogrid. The 1 m spacing was chosen to ensure that the region of larger deformations within the test fill was monitored. Figure 10 shows the location of the instruments along the primary geogrids as well as a detail of the instrumentation at a given location.

A pair of electrical resistance strain gauges were installed at each location on the top and bottom of a longitudinal member to measure small strains. Each gauge was bonded to the geogrid using epoxy and then waterproofed after the

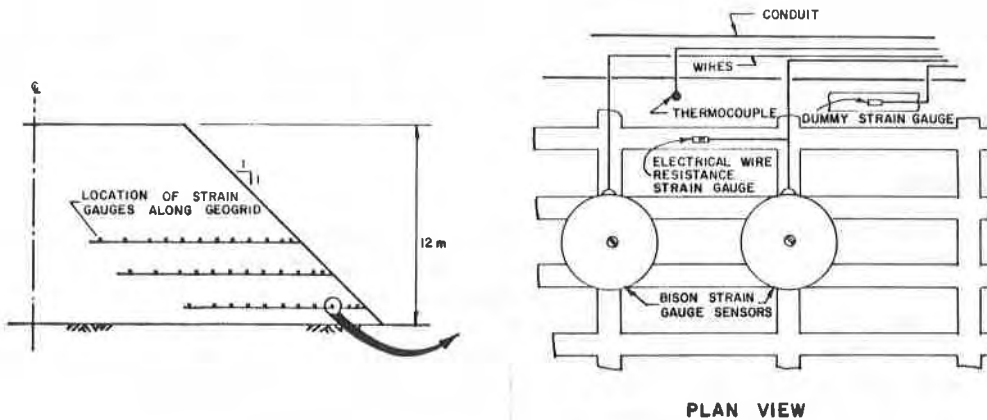


Figure 10 - Geogrid Instrumentation

electrical leads were installed. The electrical resistance strain gauges measure the strains induced in the geogrid by the test fill. Since the mechanical properties of the geogrids vary with temperature, a thermocouple has been installed at each set of strain gauges. A dummy electrical strain gauge was also placed in the test fill at 0.5, 1 and 5 m distances from the slope face to aid in accounting for temperature influences. A total of 240 electrical resistance strain gauges are being installed.

Pairs of Bison strain gauges were attached by a plastic bolt placed through the center of adjacent transverse members. These gauges will measure the global strains of the geogrid and will continue working beyond the range of the electrical resistance strain gauges. The Bison strain gauge has been previously used to measure strains in geogrids as reported by Chouery (5), Fluet (6), and Rowe, MacLean and Barsvary (7). The global strains recorded by the Bison gauges along with the local strains recorded by the electrical resistance strain gauges will be used to evaluate the stresses and loads induced in the geogrids as the test fill deforms. A total of 188 Bison strain gauges in 94 pairs are being installed.

The electrical leads at each location were laid in a conduit which was installed parallel to the instrumented geogrid. The conduit guards against excessive deformation in the leads as the test fill deforms.

LABORATORY TESTING OF GEOGRIDS

To determine the loads in the geogrids, the measured strains must be analyzed using the appropriate moduli for the geogrid material taking into account the field strain rate, temperature and loading history. Devata (8) avoided this complex problem by using aluminum strain gauge connectors, which acted as load cells, at intervals along the geogrid strip. Because of the large number of strain gauge locations, however, it was decided to mount strain gauges directly on the plastic material. A comprehensive series of tension tests on the three geogrid materials, therefore, is planned to develop isochronous load-temperature-strain curves similar to those shown by McGown et al. (9) and van Zanten (10).

CLOSURE

At the time of writing this paper (November 1986) approximately 8,000 m³ of fill has been placed to a height over 3 m. Construction will be shutdown for the winter at this stage. All installed instrumentation is working well. The only surprise to date is that the pore water pressures in the compacted fill are higher than anticipated.

ACKNOWLEDGEMENTS

The authors appreciate the help of many colleagues in Alberta Transportation and at the University of Alberta, especially that of Rick Chalaturnyk who was responsible for the early planning and design of the test fill. In addition, Bernard Myles of ICI Fibres; Ted Gailer of Signode Corporation; John Kerr and Michael Cowell of The Tensar Corporation; John Price, formerly of Mirafi Inc.; and Bob Wallace and Joe Fluet of GeoServices Inc. have provided invaluable advice and experience towards the planning and construction of the test fill.

REFERENCES

1. Jones, Colin J.F.P., Earth reinforcement and soil structures. Butterworths Advanced Series in Geotechnical Engineering, Butterworth and Co. (Publishers) Ltd., 1985, 183p.
2. Rowe, R.K. and Soderman, K.L. An approximate method for estimating the stability of geotextile-reinforced embankments. Canadian Geotechnical Journal, vol. 22, no. 3, August, 1985, pp. 392-398.
3. Tensar Technical Note: SR1. Slope reinforcement with Tensar Geogrids, Design and Construction Guideline. The Tensar Corporation, March, 1986, 45p.
4. Jewell, R.A. Some effects of reinforcement on the mechanical behaviour of soils. Ph.D. Thesis, University of Cambridge, March, 1980.
5. Chouery, V.E., Personnel Communication. The Tensar Corporation, Morrow, Georgia, 1986.
6. Fluet, J.E., Personnel Communication. GeoServices Inc., Boynton Beach, Florida, 1986.
7. Rowe, R.K., MacLean, M.D., and Barsvary, A.K., The observed behaviour of a geotextile-reinforced embankment constructed on peat. Canadian Geotechnical Journal, vol. 21, no. 2, May, 1984, pp. 289-304.
8. Devata, M.S., Geogrid reinforced earth embankments with steep side slopes. Proceedings of a Conference on Polymer Grid Reinforcement, Thomas Telford, London, March 22-23, 1984, pp. 82-87.
9. McGown, A., Andrawes, K.Z., Yeo, K.C. and DuBois, D., The load-strain-time behaviour of Tensar geogrids. Proceedings of a Conference on Polymer Grid Reinforcement, Thomas Telford, London, March 22-23, 1984, pp. 11-17.
10. van Zanten, R. Veldhuijzen, Geotextiles and geomembranes in civil engineering. John Wiley & Sons, 1986, 658p.

JARRETT, P.M. and BATHURST, R.J.
Royal Military College of Canada, Canada

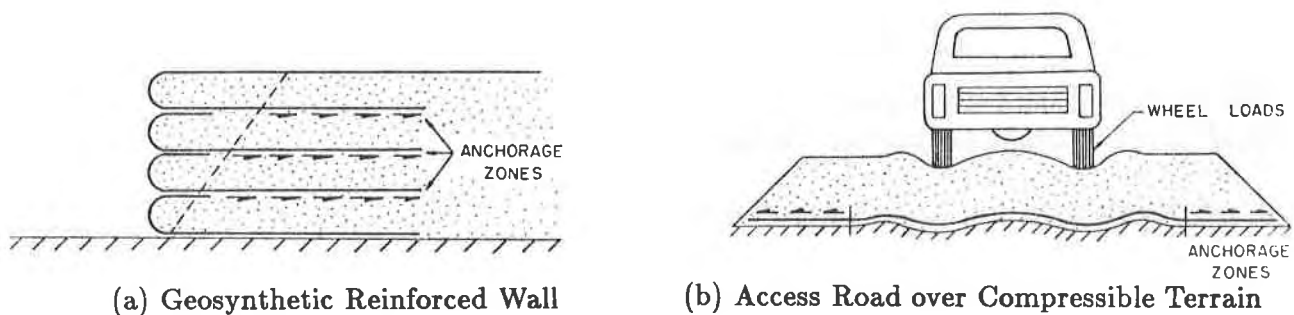
Strain Development in Anchorage Zones

Introduction

Tensile reinforcement can only be provided to the extent that anchorage is available to restrain the reinforcing material as it resists the tensile loads applied to it. When geosynthetics are used as tensile reinforcement in soils, the anchorage is usually developed by interlocking and/or frictional resistance between the geosynthetic and the soil on either side of the inclusion. Many common problems have readily identifiable anchorage zones which are usually modelled as a simple Coulomb-type frictional interface (Figure 1). In the two cases depicted on the figure, anchorage is provided to resist the pull of essentially horizontal tensile forces. In order to develop rational design methods which can incorporate the mobilized anchorage capacity of these geosynthetic-soil composites it is necessary to understand the mechanics of these systems.

Previous studies of geosynthetic-soil interface resistance have used shear box tests (1), (2), (3) and pullout tests (4), (5), (6). Comparisons between these two test methods have been presented in (7), (8), (9) and (10). Interesting developments in testing methodologies have been reported in (3) and (9). Over the period of time represented above considerable discussion has occurred concerning the applicability of the results obtained from these tests to field problems. The main area of concern is the compatibility of stresses and strains between the laboratory and field cases and particularly the fact that both forms of laboratory tests tend to generate unrealistic stress or strain concentrations. Schlosser and Elias (5) reported field tests in which the reinforcing elements had been pulled out of reinforced earth structures in an attempt to correlate laboratory and field results. A general discussion of many of the problems involved in predicting or measuring geosynthetic-soil interface friction was prepared by Mitchell (11).

The paper by Jarrett and Bathurst (10) also compared the results of shear box tests to pullout tests. The problem studied, however, was different from most of the previously annotated work as it dealt with the resistance at an interface in which markedly dissimilar soils (e.g. gravel and peat) were separated by the geosynthetic. Only Collios et al. (7) and Yamauchi and Kitamori (6) have considered problems of this nature.



(a) Geosynthetic Reinforced Wall

(b) Access Road over Compressible Terrain

Figure 1 Soil Reinforcement Examples Using Geosynthetics

A large portion of the test results presented by the authors in this earlier paper were based on data from two different pullout test configurations: One configuration involved pulling the geogrid while restraining the upper gravel layer in the horizontal direction (this arrangement represents a conventional pullout test); the second configuration left the front of the gravel face unrestrained and thereby allowed the gravel base to *travel with* the geogrid reinforcement. The latter configuration is considered to be a good model of the anchorage zone observed in plane-strain beam tests which have been used by the authors to simulate the access road over compressible terrain problem. From the results of these unrestrained pullout tests the authors have concluded that the ultimate pullout resistance developed by the geosynthetic-gravel composite over the anchorage zone is due to the fully mobilized shearing resistance of the underlying peat.

Comparison of ultimate pullout capacity from the restrained and unrestrained test configurations emphasized the importance of lateral gravel restraint in these tests. Specifically, these tests showed that when the front face was restrained the ultimate pullout capacity was *doubled*.

Objectives

The current paper reports the results of further unrestrained pullout tests in which several parameters have been varied and the configurations more comprehensively instrumented. The principal objectives of the test program were to:

- a) Determine the deformation-load response of pullout tests comprising different granular base depths, surcharge material types and geogrid reinforcements of different stiffnesses.
- b) Examine strain propagation in geogrid reinforcement during pullout.

In order to achieve the second objective it was first necessary to develop a method to instrument the geogrid so that strains in the reinforcing element could be recorded for the full duration of the pullout tests.

Test Apparatus

3

The general test arrangement for the large-scale pullout tests is shown on Figure 2. The peat subgrade comprised a finely fibrous Sphagnum peat with a low degree of decomposition. For each test the peat was reconstituted to a moisture content of $650 \pm 50\%$ and gave an average shear vane resistance of 4 kN/m^2 . Two different base materials were used in the current investigation: A crushed limestone Granular A gravel with a top size of 20 mm was placed and compacted in 150 mm lifts to give an average density of 1950 kg/m^3 . Additional tests were carried out using a uniform-size, angular coarse sand containing some fine gravel. This material was placed in the same manner as the gravel and gave an average density of 1750 kg/m^3 . Two Tensar Geogrids were used in the current study. The high-density polyethylene GM1 with grid apertures nominally 50 mm apart was used in one series of tests. In a second test series, the less extensible SS2 was used which is a biaxial polypropylene geogrid with mesh apertures nominally 40 mm apart in the transverse direction (i.e the strong direction) and 28 mm apart in the longitudinal direction.

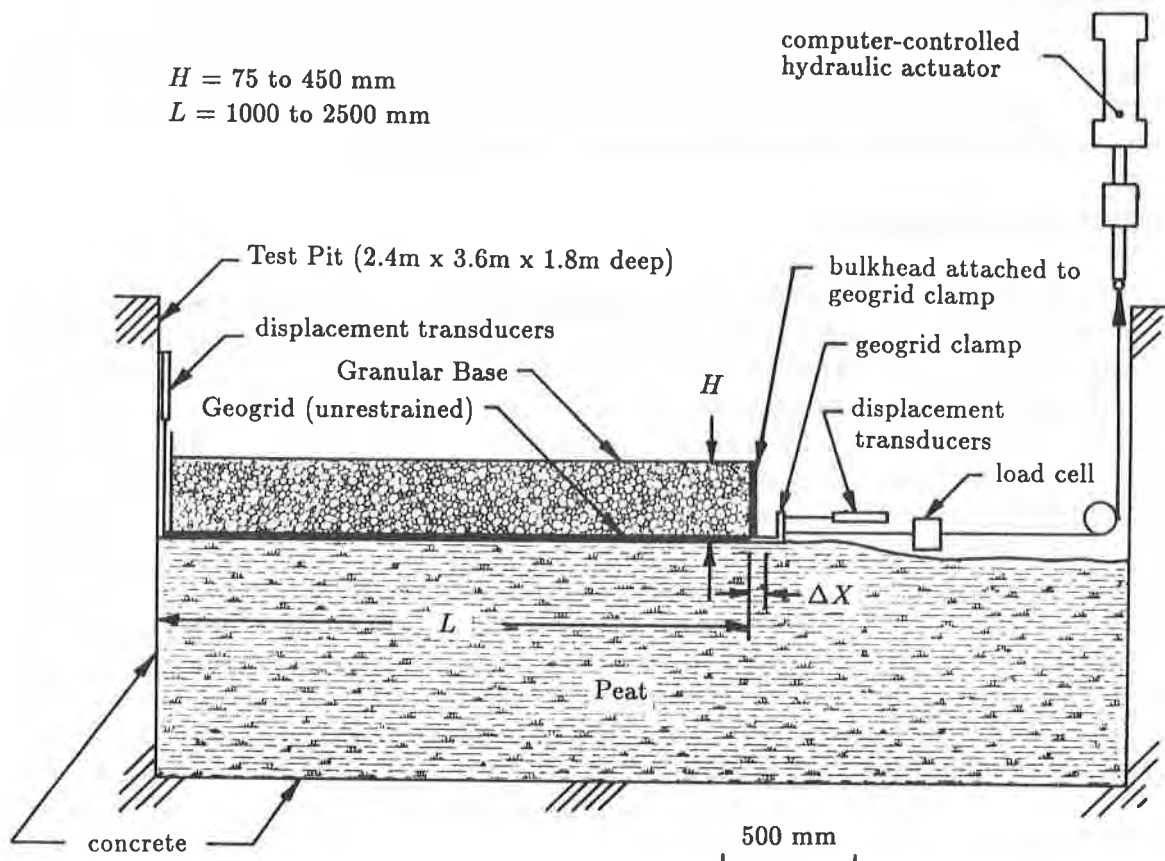


Figure 2 General Arrangement for Pullout Tests

In each test a strip of geogrid nominally 1.0 m wide by 2.1 to 2.5 m long was attached to a rigid clamp and this assembly pulled by the MTS hydraulic actuator as illustrated on the figure. In the first two tests a manual jack was used but otherwise all the tests were carried out in a similar manner. In plan view the entire width of the test pit behind the clamp was surcharged to the same depth as the cover placed over the geogrid. The surcharge above the test strip was isolated from the surrounding granular material by vertical strips of aluminium to minimize the effect of side friction as the granular soil/geogrid system was pulled. The front granular soil face at the location of the geogrid clamp was left unrestrained during the test by attaching the front vertical bulkhead to the geogrid clamp. This bulkhead served primarily to allow initial compaction of the granular base materials and also to prevent spalling of the front face during pullout. Each test was loaded by a series of monotonically increasing tensile loads applied for a duration of 15 minutes each.

The unrestrained form of pullout test described above was developed as a result of model studies of access roads over peat which showed well-defined anchorage zones. It is also believed that tests of this form may more closely model the anchorage zones of many other geosynthetic-reinforced earth systems than do the fully restrained pullout test configurations. In essence, all systems in which lateral support within the reinforced soil mass is decreasing as the anchorage is tensioned, approach the unrestrained condition. Such a condition includes most reinforced earth walls and slopes.

Geogrid Instrumentation

A large number of the pullout tests reported in the current study were carried out with strain gauges attached at selected mid-rib locations distributed along the length of the reinforcement. In addition, thin steel wires were attached through a pulley system to vertically mounted electronic displacement transducers as shown on Figure 2. The wires were protected from the granular surcharge by running them through stiff plastic tubes. These two forms of instrumentation were employed in order to monitor the full range of tensile strains and displacements which were generated in each pullout test. The type of strain gauge, adhesive and bonding technique employed was arrived at after much experimentation. A high-strain, foil-type gauge (Showa Measuring Instruments Co., Ltd.) was ultimately selected and a careful process of grid surface preparation adopted to ensure a good bond between the gauge and the polymer reinforcement. A two-part RTC epoxy adhesive was used. The final step in strain gauge preparation was to surround the gauge in a pliable water-proof silicone bubble. The strain gauge assemblies proved to be functional up to about 2% strain. At 2% strain, however, displacements recorded from the wire/transducer assemblies were large enough that grid strains could be calculated from these devices with some confidence.

It is well known that strain distribution in high-density open-mesh polymer reinforcements such as the Tensar Geogrids is not uniform. This non-uniformity is a consequence of grid geometry and variable material moduli. In order to make comparable strain measurements between strain gauge readings and strains deduced from displacements recorded over

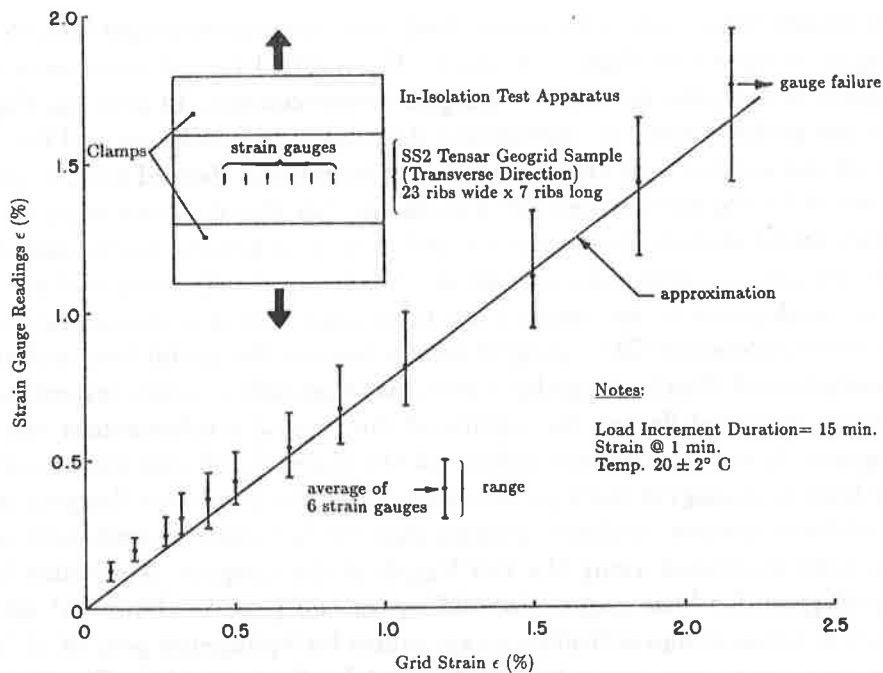


Figure 3 Results of In-Isolation Test on SS2 Geogrid for Calibration of Strain Gauges to Grid Strain

several grid apertures, the strain gauge readings were correlated to gross average strain in the grid. In this paper, strains measured over a gauge length consisting of one or more apertures are called *grid strains*. It can be appreciated that grid strain is a more meaningful parameter since it facilitates comparison of mechanical response between different sheet reinforcement types and is more easily implemented in analytical models. The correlation between strain gauge readings and grid strain was made by carrying out in-isolation tests on sections of geogrid material on which strain gauges had been mounted. The in-isolation test specimens were subjected to the same loading program as that applied to the pullout tests. The results of the in-isolation test using a SS2 specimen loaded in the transverse direction are shown on Figure 3. The figure shows that there is a roughly linear relationship between the strains recorded by the rib-mounted gauges and grid strain measured over the sample length. The gauges in this test were arranged over the same row of ribs. Nevertheless, the range of strains recorded by the six(6) gauges at a given grid strain was observed to increase with load level. This variability is thought to be due to the sensitivity of gauge response to small differences in gauge positioning, rib dimensions and possibly, non-uniform load between ribs. An interesting observation which can be made from this figure is that grid strains are greater than strains recorded directly at mid-rib locations. The relatively greater modulus of the highly-oriented polymer at the central rib locations is responsible for this phenomenon.

Test Results

6

Test results with respect to tensile load-displacement response recorded at the front of each geogrid are given on Figures 4 and 5. The applied tensile loads have been normalized with respect to the plan area of the geogrid reinforcement. In general, Figures 4a, 4b and 4c show that as the surcharge increases so does the initial stiffness and the ultimate pullout capacity of the geogrid/soil composite. Tests in general showed good repeatability except for the two 9.0 kPa tests shown on Figure 4a. No observations were made during these tests which could explain this variation and it may be simply attributed to test variability in fill placement and subgrade formation. Interestingly, the shape of the curves for tests using SS2 reinforcement are similar for both sand and gravel surcharges. For the tests with the more extensible GM1 geogrid reinforcement the initial load-deformation response is noticeably less stiff indicating that the initial load-deformation response of these systems is influenced by grid stiffness. No rupture of the geogrid reinforcement was observed in this test program. Instead, ultimate failure of the geogrid-soil composite occurred when the granular base and geogrid were pulled as a monolithic unit over the peat subgrade. Under these conditions it is reasonable to assume that the full shearing resistance of the underlying peat has been mobilized along the full length of the geogrid. A sensible friction angle for the geogrid-granular base composite sliding on the peat is about 35° which corresponds favourably with the range of friction angle values for Sphagnum peat of 27° to 34° measured using the ring shear apparatus by Landva and La Rochelle (12). On Figure 5 the *average shear stress* at pullout has been plotted as a function of surcharge pressure for all tests including similar tests with 1000 mm lengths of SS2 reported in an earlier paper by Jarrett and Bathurst (10). The data show that within the range of experimental accuracy there is no systematic effect of geogrid type and surcharge material type on ultimate pullout capacity nor does the geogrid length between 1.0 m and 2.5 m length influence this value in a consistent manner.

If attention is now focused on the behaviour of the composite system prior to ultimate failure then, the distributions of grid strain plotted on Figure 6 for the tests using SS2 reinforcement are of interest. Grid strains at the front of the reinforcement were not measured directly but were estimated from the grid strains at comparable tensile loads applied during the in-isolation calibration tests on SS2 geogrid materials. In-isolation and pullout tests were subjected to similar load-increment time paths.

It can be noted that the plots of grid strain against horizontal location show some abrupt changes in grid strain gradient. These irregularities may be a consequence of the inherent warp in these reinforcement materials (as manufactured) and local variations in geogrid-gravel interlock which can both lead to non-uniform load transfer along nominally parallel rib strands. Another source of irregularity may be due to changes in measurement device which is the case when grid strains are inferred from strain gauge results at one point and then from an electrical transducer at an adjacent location.

Nevertheless, as may be expected, the plots show that grid strain increases with increasing tensile load. In general, the strain distributions are linear over much of the geogrid length with perhaps an increase in strain gradient towards the front of the reinforcement. The overall degree of linearity is a noticeable feature of these curves especially during the

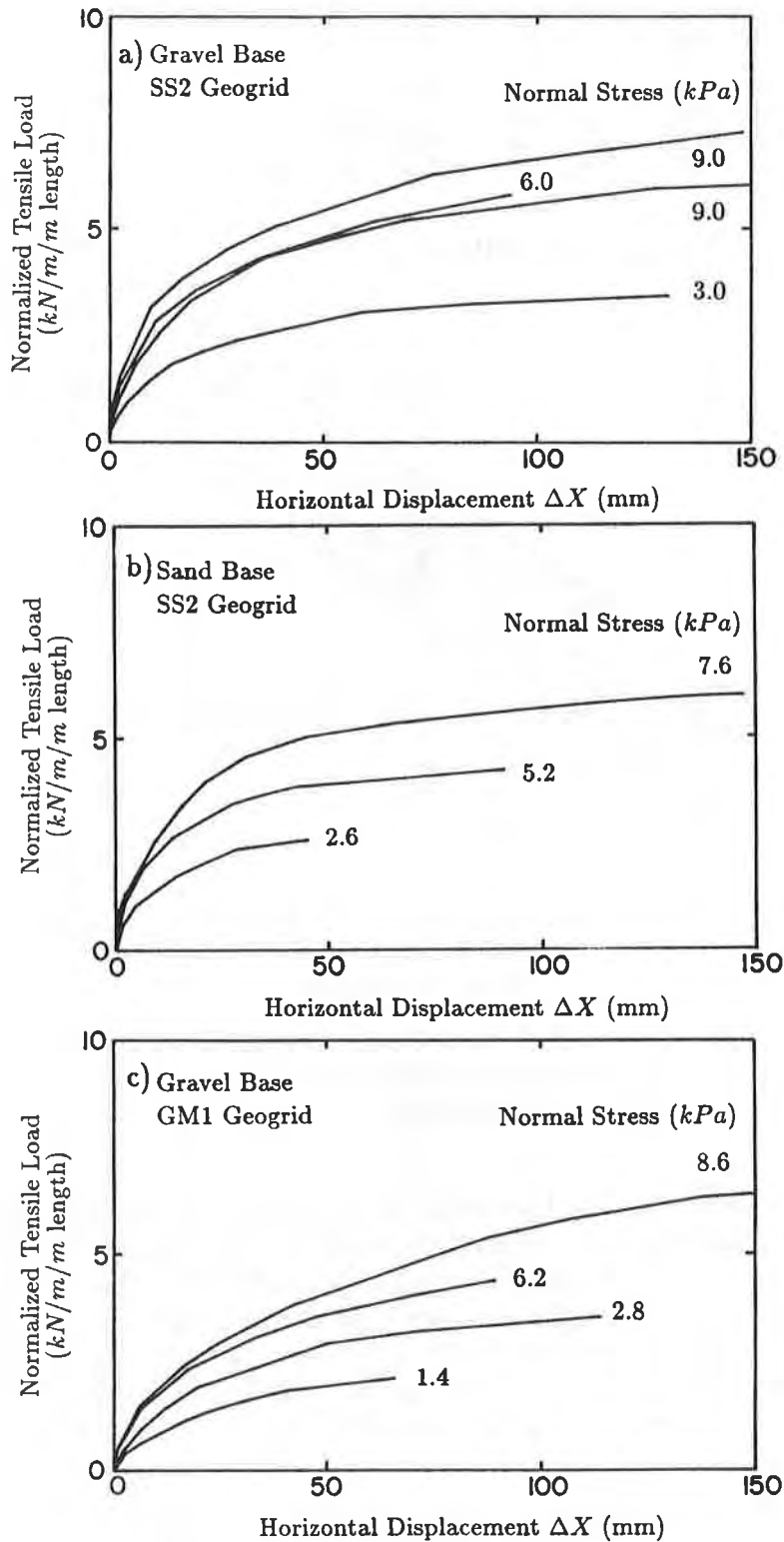


Figure 4 Load-Deformation Response of Pullout Tests

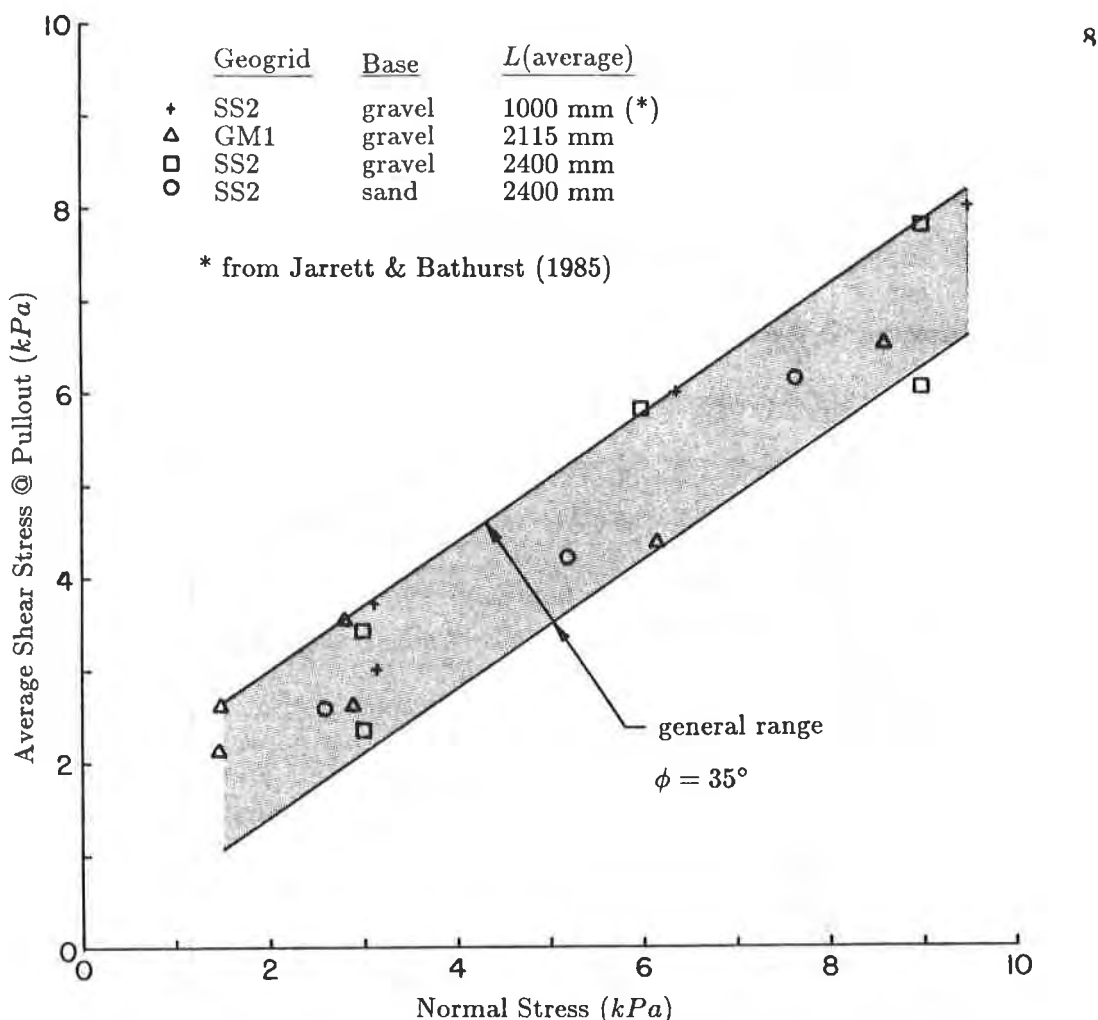


Figure 5 Average Shearing Resistance @ Pullout versus Normal Stress

earlier load stages when one may have expected more pronounced strain gradients at the front of the reinforcements. After studying data of this type and grid node displacement results, the tests show that anchorage at low tensile loads is provided by only a portion of the grid length since no movements were recorded at the unrestrained end of the geogrid strip during these early stages. When strains were observed to propagate to the back of the reinforcements, measurable slippage of the grid-gravel composite over the peat subgrade was simultaneously recorded and clearly a greater length of fully-mobilized peat shearing resistance generated.

Another approach by which the anchorage mechanism may be assessed is presented on Figure 7. In this figure the applied tensile load required to produce 1 and 2% grid strain contours at various distances from the front of the geogrid is plotted for the SS2 tests with gravel bases. Considering the 150 mm test first, it is observed that due to the

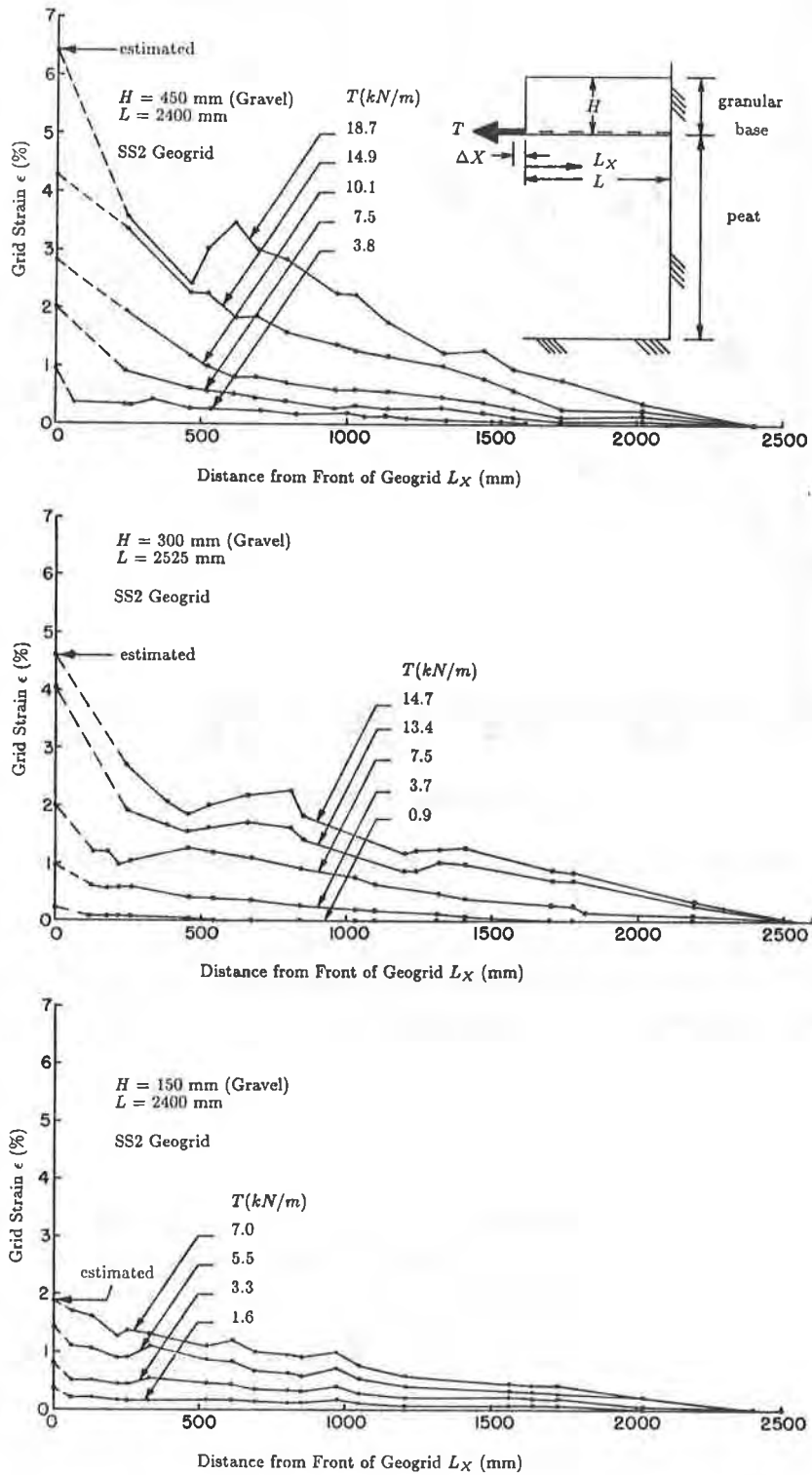


Figure 6 Distribution of Grid Strain during Pullout Tests

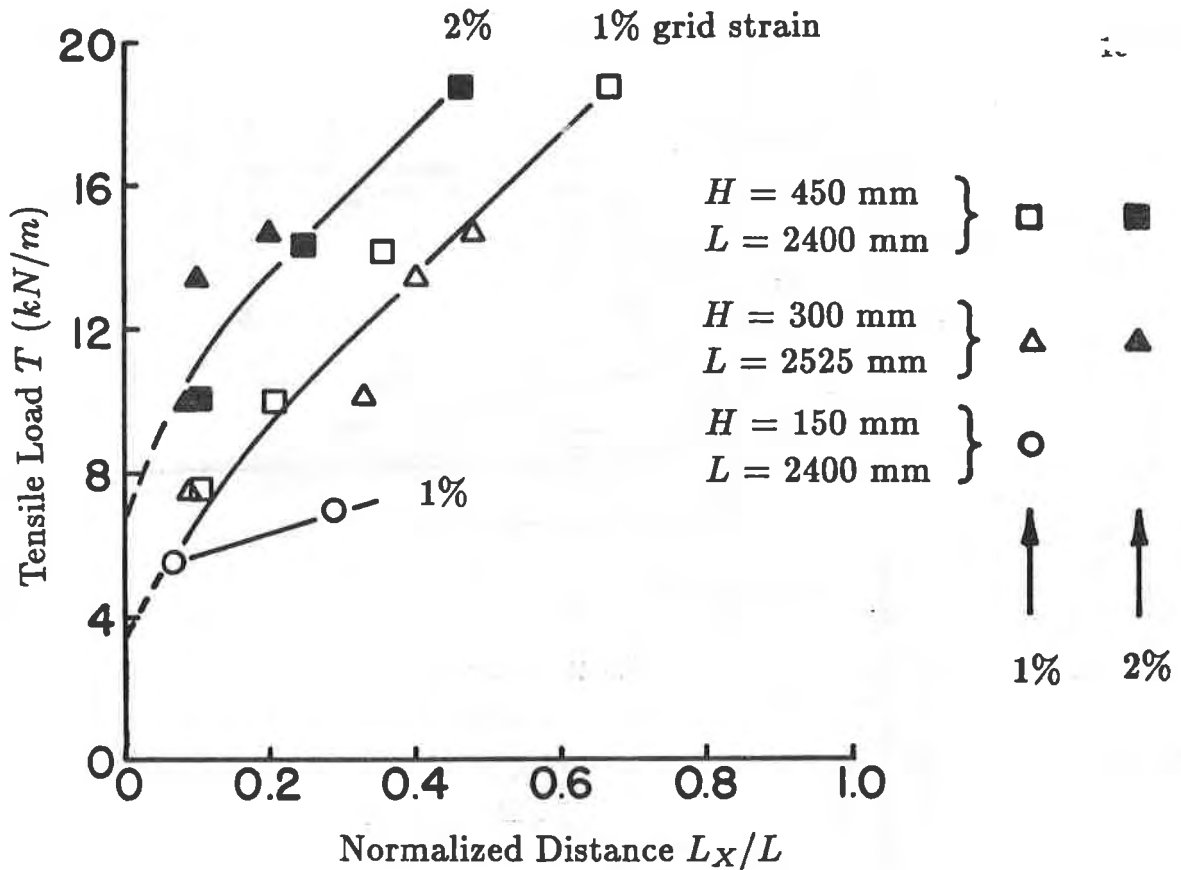


Figure 7 Grid Strain Propagation during Pullout Tests

limiting anchorage available, only a maximum 1% grid strain was observed to propagate into the front one third of the reinforcement. With greater normal stress, the same level of grid strain was observed to propagate further into the reinforcement in a near-linear fashion.

Discussion

There are many factors involved in the mobilization of anchorage resistance. It is understood that the forces in the grid are transferred to the granular base and the peat. In addition, the initial movements of the reinforcement in this study were observed to be much larger at the front of the grid than at the unrestrained end. Simple concepts of soil strength mobilization would lead us to expect that larger movements lead to larger mobilized bearing resistance at the front of soil-geogrid interface. This larger resistance would lead to a rapid non-linear decrease of force and hence strain in the remaining reinforcement. However, this simple model does not fit the linear grid strain distributions observed. Again, at a simple level, the linear variation in grid strain would tend to indicate that force is being shed from the reinforcement uniformly along its length. This mechanism is difficult to relate to shear mobilization in the underlying peat and explanations must

await further analysis of the data and perhaps a more comprehensive model for soil-geogrid interaction.

Another complicating factor is the time-dependent properties of the polymer reinforcement material and the peat subgrade. It is reasonable to expect that under sustained loading these pullout tests would generate lower ultimate tensile capacity, reduced system stiffness and possibly other grid strain distributions.

Conclusions

Based on the results of the reported pullout tests, the following conclusions can be made:

- (1) Grid strains in pullout tests using high-density polymer geogrids were monitored up to about 2% using high-strain foil-type gauges. At higher strain levels, electronic displacement transducers attached to grid nodes by thin steel wires proved to be successful in measuring both grid strains and grid displacements.
- (2) The shearing resistance developed at the bottom of granular base-geogrid composites up to 2.5 m long is considered to be equivalent to the shearing resistance of the underlying peat.
- (3) The ultimate pullout capacity of test configurations was not observed to be measurably dependent on grid length, geogrid type and granular base material. However, the initial load-deformation response was seen to be sensitive to geogrid type. Specifically, the more extensible GM1 geogrid was observed to give a less stiff system response than comparable configurations with SS2 geogrid.
- (4) Measureable grid strains were observed to propagate the entire length of the test specimens with the magnitude of grid strains increasing with applied tensile load level. The distribution of grid strains was essentially linear along the length of the grid particularly at low tensile load levels.

Acknowledgements

The authors would like to acknowledge the efforts of Research Assistants J.Bell, R.Hickman and J.Rehkopf for developing the test apparatus and carrying out the tests. This work was supported by the Department of National Defence (Canada).

References

- (1) MYLES, B. (1982), "Assessment of Soil Fabric Friction by Means of Shear", *Proceedings 2'nd International Conference on Geotextiles*, Las Vegas, Vol. 3, pp. 787-791
- (2) MARTIN, J.P., KOERNER, R.M. and WHITTY, J.E. (1984), "Experimental Friction Evaluation of Slippage between Geomembranes, Geotextiles and Soils", *Proceedings International Conference on Geomembranes*, Denver, Vol. 1, pp. 191-196
- (3) RICHARDS, E.A. and SCOTT, J.D. (1985), "Soil Geotextile Friction Properties", *Second Canadian Symposium on Geotextiles and Geomembranes*, Edmonton, Alberta, pp. 13-24
- (4) HOLTZ, R.D. (1977), "Laboratory Studies of Reinforced Earth using a Woven Polyester Fabric", *Proceedings International Conference on the Use of Fabrics in Geotechnics*, Vol. 3, pp. 149-154
- (5) SCHLOSSER, F. and ELIAS, V. (1978), "Friction in Reinforced Earth", *Symposium on Earth Reinforcement*, Pittsburgh, pp. 735-762
- (6) YAMAUCHI, H. and KITAMORI, I. (1985), "Improvement of Soft Ground Bearing Capacity using Synthetic Meshes", *Geotextiles and Geomembranes*, Vol. 2, pp. 3-22
- (7) COLLIOS, A., DELMAS, P., GOURC, J-P. and GIROUD, J-P. (1980), "Experiments on Soil Reinforcement with Geotextiles", ASCE National Convention, Portland, Oregon, Preprint 80-177, in *The Use of Geotextiles for Soil Improvement* pp. 53-74
- (8) INGOLD, T.S. (1984), "A Laboratory Investigation of Soil-Geotextile Friction", *Ground Engineering*, Vol. 17, Nov., pp. 21-28
- (9) ROWE, R.K., HO, S.K. and FISHER, D.G. (1985), "Determination of Soil-Geotextile Interface Strength Properties", *Second Canadian Symposium on Geotextiles and Geomembranes*, Edmonton, Alberta, pp. 25-34
- (10) JARRETT, P.M and BATHURST, R.J. (1985), "Frictional Development at a Gravel-Geosynthetic-Peat Interface", *Second Canadian Symposium on Geotextiles and Geomembranes*, Edmonton, Alberta, pp. 1-6
- (11) MITCHELL, J. (1979), "General Report Session 1", *Proceedings International Conference on Soil Reinforcement*, Paris, Vol. 3, pp. 25-62
- (12) LANDVA, A.O. and LA ROCHELLE, P. (1983), "Compressibility and Shear Characteristics of Radforth Peats", *ASTM Special Technical Publication 820, Testing of Peats and Organic Soils*, pp. 157-191

BONAPARTE, R.

GeoServices Inc. Consulting Engineers, U.S.A

BERG, R.

The Tensar Corporation, U.S.A.

Long-Term Allowable Tension for Geosynthetic Reinforcement

ABSTRACT

A methodology is described for selection of long-term allowable reinforcement tension to be used in the design of permanent, critical reinforced soil structures. The methodology accounts for reinforcement creep, in-ground material degradation, and construction-induced material damage. An example is given of the application of the methodology to one particular geosynthetic soil reinforcement product.

INTRODUCTION

Polymer based soil reinforcing materials are finding increasing use in permanent, critical applications such as reinforced soil retaining walls, steep fills, and earth dams. These uses are in contrast to early soil reinforcement applications such as unpaved roads, temporary retaining walls, and low-height embankments where the reinforcement function was often temporary or where the consequences of failure were not severe.

In this paper, an earth structure is considered permanent if it is built to current U.S. Federal Highway Administration (FHWA) guidelines for permanent highway construction which means the structure has a minimum design life of from 75-100 years. A reinforcement application is considered critical if there is mobilized tension in the reinforcement for the life of the structure, if the structure would fail should the reinforcement lose its ability to transmit tension, and if the consequences of failure include personal injury or significant property damage.

The use of polymer materials in permanent, critical soil reinforcement applications has recently been questioned. For instance, the FHWA's Geotechnical and Materials Branch issued a letter (April, 1986) to engineers, academicians, and manufacturer's representatives soliciting "comments and technical guidance regarding the durability and construction induced damage of geotextiles and geotextile related materials for long-term reinforcement applications." Due to uncertainty over long-term performance, Broms (3) recommended against the use of polymer materials in applications requiring permanent reinforcement tension. These views indicate the need for a better understanding of polymer behavior and for a rational methodology for selecting long-term properties for design.

The purpose of this paper is to present a methodology for selecting long-term polymer reinforcement properties for design of permanent, critical earth structures and to show how the methodology has been applied to one particular soil reinforcement product. The methodology considers the effects of reinforcement creep, long-term reinforcement degradation, and reinforcement damage during construction. It evolved into its current form through the senior author's participation in guideline development for the AASHTO-AGC-ARBTA Joint Committee on New Materials Task Force 27, and is therefore presented in the form of a guideline. It is pointed out, however, that the views and opinions expressed subsequently are solely those of the authors.

BACKGROUND

ASTM Committee D35 on Geotextiles and Related Products has developed a standard wide-strip test method (D4595-86) for determining the tensile properties of geosynthetics. The wide-strip test is performed at a strain rate of 10% per minute at a temperature of 21°C (70°F). Geosynthetic project specifications often call for a minimum wide-strip tensile strength. The current state-of-practice for selection of a long-term allowable reinforcement tension is often to: (i) obtain the tension-strain behavior of the reinforcement from ASTM D4595-86; (ii) reduce the results from the wide-strip test to account for reinforcement creep using generalized reduction factors such as those provided in Villet and Mitchell (11); (iii) ignore any potential for long-term material degradation; and, (iv) ignore construction induced material damage while minimizing its effects through selection of a suitably robust material.

The above-described approach is direct and simple and may be acceptable for selection of reinforcement properties in noncritical or temporary applications. The long-term properties derived from this approach, however, can only be considered indices of a specific product's true long-term behavior. For permanent, critical applications, these indices contain an unacceptably high degree of uncertainty, since it is known that relatively minor variations in polymer formulation, product geometry, manufacturing process and other factors can lead to significant changes in long-term behavior. Therefore, an approach is required which rationally accounts for these factors.

METHODOLOGY

The methodology for selection of product-specific long-term reinforcement properties described herein relies on the use of constant-load creep tests as described by McGown et al. (6) and on interpretation of the test results in terms of isochronous (constant-time) parameters (1,2,6,7). It further requires consideration of the long-term, in-ground durability of the reinforcement as well as the effect of construction-induced material damage. The end result is a product-specific long-term reinforcement tension that can be used in limit equilibrium calculations. Both reinforcement rupture (limit state) and reinforcement load-elongation response (serviceability state) are considered. A flow chart outlining the methodology is given in Fig. 1.

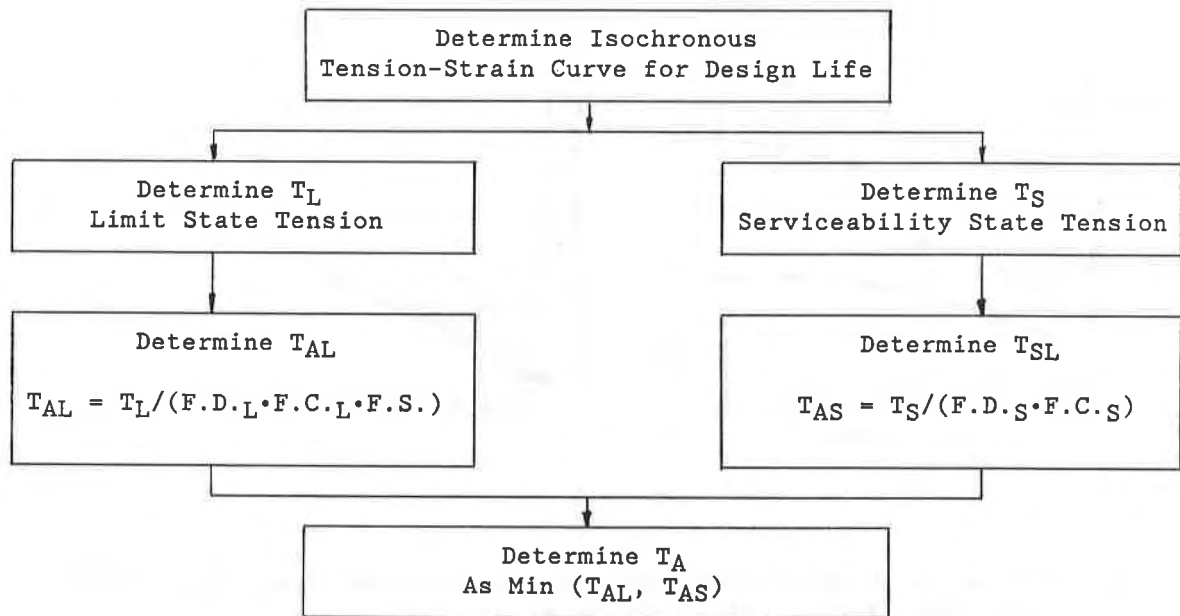


Figure 1. Flow chart

Reinforcement Creep

Discussion - A tension-strain curve must be established which corresponds to confined in-soil loading of the reinforcement for the design life (approximately 10^6 hours) of the earth structure. Ideally, this curve would be determined from the results of in-soil constant-load creep tests carried out for a duration long enough to allow extrapolation of the test results to the design life of the earth structure. This testing goal is not achievable since it requires in-soil testing, which is complex, for a time period on the order of ten years (since it is generally stated that polymer creep test results should not be extrapolated in time more than about one order of magnitude). Practically, creep tests are most often carried out in an unconfined state with durations limited to not more than one year (10^4 hours).

The results from creep tests can be presented in terms of isochronous (constant-time) tension-strain curves as shown in Fig. 2. Isochronous curves can be extrapolated, either mathematically (1,6,12), or based on judgment, to the design life of the earth structure. Extrapolation can be carried out with a reasonable degree of confidence only if the relationship between load, strain, and log-time is linear. Above the limit of linear viscoelasticity, extrapolation is difficult. Furthermore, extrapolation should be limited to stress levels less than those associated with transition from a ductile failure mode to a brittle one within the specified design life (14).

Method - The tension-strain-time behavior of the reinforcement should be determined using constant-load creep tests conducted for a duration of 10^4 hours for a range of load levels. Tests should be carried out on samples large enough and of such a shape so as to minimize scale and shape effects. Samples should be tested in the direction in which the load will be applied in use.

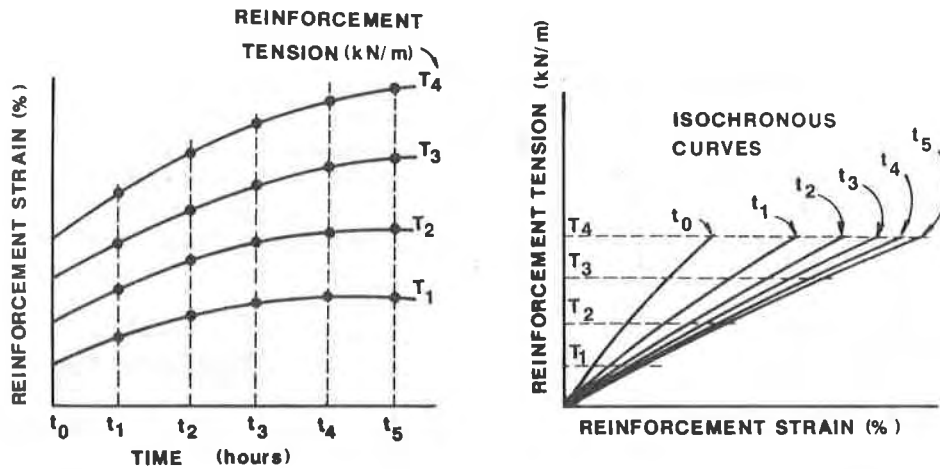


Figure 2. Derivation of isochronous tension-strain curves from constant-load creep test results (after McGown et al. (7)).

Based on the creep test results, an extrapolated isochronous tension-strain curve should be defined corresponding to the anticipated service temperature and design life. From this isochronous curve the following two parameters can be determined:

- 1) The reinforcement tension at the strain corresponding to the limit state of the soil-reinforcement system. This value of tension will be termed the limit state reinforcement tension and will be designated T_L . The strain corresponding to T_L should be within the range of linear viscoelastic behavior for the considered reinforcement material. The stress level corresponding to T_L should be low enough to preclude transition from a ductile to brittle failure mode.
- 2) The reinforcement tension at a strain value defined by a structural serviceability limit. This value of tension will be designated the serviceability state reinforcement tension, T_S .

Unless otherwise specified, the design life and in-ground service temperature can be assumed to be 75 years and 55°F, respectively, for most of the geographic U.S. The requirement for a 10,000 hour minimum creep test period may be waived for new products if it can be shown that they are sufficiently similar to proven creep-tested products for their performance to be predictable from a comparison of shorter term tests. In no case, however, should the creep test duration for a product be less than 1,000 hours. Creep tests may be carried out in-air (unconfined) or confined in soil.

Based on published creep test data for different products, T_L will vary from about 15% to about 70% of the reinforcement tensile strength measured in ASTM D4595-86.

Long-Term Material Degradation

Discussion - The isochronous tension-strain response determined previously does not account for long-term material degradation which might reduce the load carrying capacity of the reinforcement. Potential sources of degradation include internal "aging" of the polymer microstructure, attack by microorganisms, chemicals (including adsorption of water), or ultra-violet light (UV), thermal oxidation and environmental stress cracking. The importance of any one of these factors will depend on resin type and grade, the presence of additives such as anti-oxidants and carbon black, the manufacturing process and the final product physical structure. Time-dependent degradation has been discussed in (5,10,14) and a wide body of information on this subject can be found in the literature of the plastics industry. This information, along with test results from manufacturers, should be used to ascertain the potential for long-term reinforcement degradation.

Method - Product-specific studies (both literature reviews and laboratory tests) should be carried out to determine the potential for long-term reinforcement degradation. These studies should include an evaluation of, but not be limited to, the effects of aging of the microstructure, microbiological, chemical and UV attack, thermal oxidation, and environmental stress cracking as well as any possible synergism between individual factors. The results from these studies should be incorporated into two durability factors of safety:

- 1) $F.D.S$ equal to the durability factor of safety on the limit state reinforcement tension;
- 2) $F.D.L$ equal to the durability factor of safety on the serviceability state reinforcement tension.

The above factors should be determined for the range of soil environments to which the reinforcement may potentially be exposed.

Based on published information on different polymer types, grades and additive packages, the durability factor of safety will range from 1.0 to more than 2.0.

Construction Induced Damage

Discussion - The effects of construction operations should be considered in the selection of reinforcement properties for design. Ideally, these effects should be incorporated by performing creep tests on specimens that have been subjected to project-specific fill placement and compaction procedures. This is not practical. Instead, manufacturers should provide data on the tension-strain properties of their materials after they have been subjected to full-scale construction damage tests. These tests consist of subjecting large size product specimens to fill placement and compaction operations and then evaluating the change in product tensile properties due to the operations. Tests should be carried out using fills which span the range of those normally encountered in earthwork construction. The tests should utilize standard construction equipment and fill lift thicknesses. It is suggested that comparison of the before and after specimens be made using ASTM D4595-86. Sufficient testing should be done to minimize uncertainty in the results.

Method - The effect of construction damage on the reinforcement should be determined from the results of full-scale construction damage tests using fill materials and construction procedures representative of the site conditions. The test results should be converted into construction damage factors of safety:

- 1) F.C._L equal to the factor of safety on the limit state reinforcement tension;
- 2) F.C._S equal to the factor of safety on the serviceability state reinforcement tension.

Based on published information of different products, the construction damage factor of safety will range from 1.0 to more than 1.7.

Long-Term Reinforcement Tension

The long-term allowable reinforcement tension, accounting for creep, time-dependent degradation and construction induced damage, is taken as the lesser of:

- 1) Limit state determination:

The long-term reinforcement tension based on the load limited criterion, T_{AL}, is given by:

$$T_{AL} = \frac{T_L}{F.D.L \times F.C.L \times F.S.} \quad (1)$$

where F.S. is an overall factor of safety against internal failure of the earth structure. F.S. accounts for uncertainties in applied loads, soil strength, geometry, etc. Typical values for F.S. are 1.3 to 1.5 for reinforced slopes and 1.5 for reinforced soil retaining walls. It is noted that conventional practice in reinforced soil wall design is to apply F.S. to the reinforcement tension, as indicated in Equation 1. An alternative approach, recommended in (2) is to apply F.S. to the soil shear strength. While differences in the two approaches are small for reinforced soil walls constructed with free-draining granular backfills, they can be significant for other reinforced soil structures. The alternative approach is the one recommended by the authors.

- 2) Serviceability state determination:

The long-term reinforcement tension based on the serviceability criterion, T_{AS}, is given by:

$$T_{AS} = \frac{T_S}{F.D.S \times F.C.S} \quad (2)$$

As this is a working stress calculation, no overall factor of safety is required. F.D._S and F.C._S may be smaller than F.D._L and F.C._L since limited data (8) suggests that long-term degradation and construction damage have a larger effect on peak strength than on initial modulus.

APPLICATION OF METHODOLOGY

The methodology described above has been applied to a uniaxially drawn high density polyethylene (HDPE) geogrid having a mass per unit area of approximately 920 g/m² (27 oz/yd²) and a longitudinal (machine direction) ASTM D4595-86 wide strip tensile strength of 78 kN/m. (The product is TENSAR SR2 Geogrid, manufactured in the United States by The Tensar Corporation, Morrow, Georgia, and in the United Kingdom by Netlon Ltd., Blackburn, England.)

Reinforcement Creep

Constant-load creep test results on U.K. manufactured samples of the considered geogrid have been reported in (1,6,7,8). Results from tests by the authors on U.S. manufactured product are shown in Figs. 3 and 4. Fig. 3 shows total strain versus log-time. Fig. 4 presents a plot suggested by Wilding and Ward (13) of total strain versus log-strain rate. From Fig. 3 it can be seen that for values of T less than about 32 kN/m, the strain versus log-time response of the reinforcement is approximately linear (actually, the derivative $d\epsilon/d\log_{10}t$ is decreasing slightly). At T=36 kN/m, the response is nonlinear and $d\epsilon/d\log_{10}t$ is increasing. Based on these results, extrapolation of the isochronous curves to 10⁶ hours should be limited to reinforcement tensions less than about 32 kN/m. The isochronous load-strain curve for 10⁶ hours obtained by linear extrapolation of the creep test results is shown in Fig. 5.

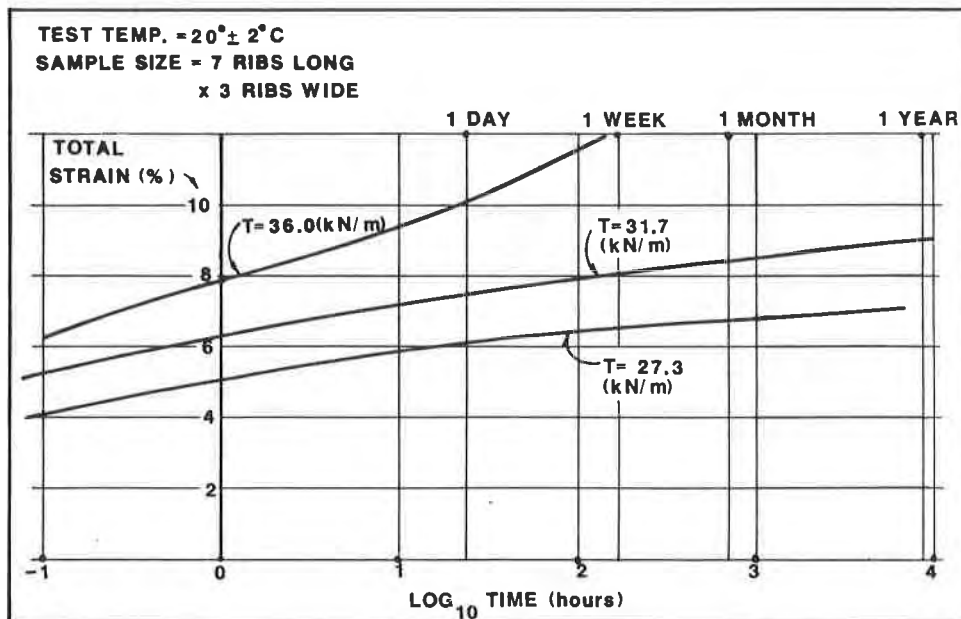


Figure 3. Creep strain versus log-time. Results from constant-load creep tests on TENSAR SR2 Geogrid.

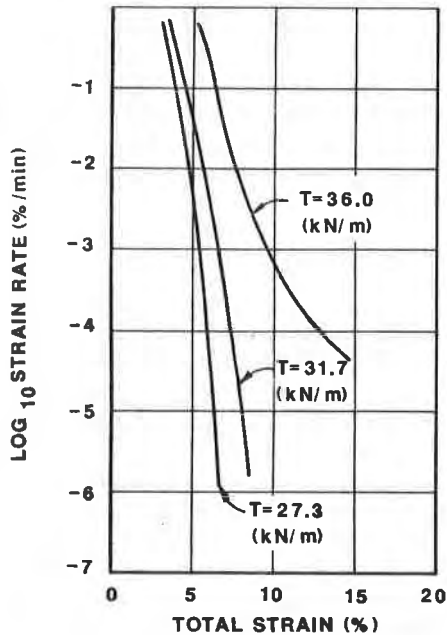


Figure 4. Log strain-rate versus total strain.

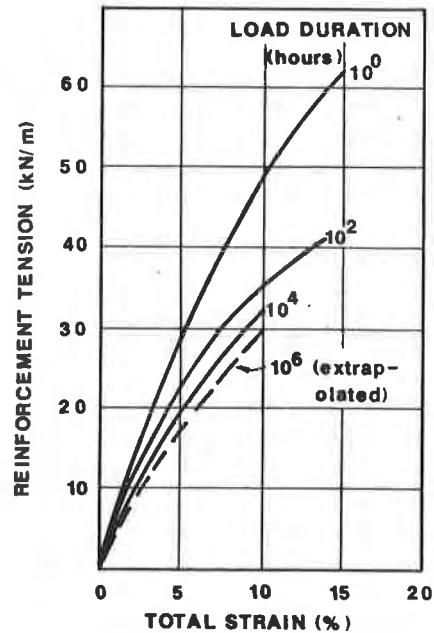


Figure 5. Isochronous load-strain curves.

The strain corresponding to the limit state of the soil-reinforcement system depends primarily on the type of fill, its compaction density, and on whether the soil shear strength is based on peak (ϕ'_p) or large-strain, constant-volume (ϕ'_{cv}) conditions. McGown et al. (7) suggested that for well compacted granular fills and strengths based on ϕ'_{cv} , a "performance limit strain" of 10% could be adopted for the soil-reinforcement system. This value was taken herein as the limit state strain used to evaluate T_L . The authors selected a serviceability state strain of 5% based on experience and judgment.

For limit state and serviceability state strains of 10% and 5%, respectively, T_L and T_S can be evaluated using Fig. 5. From Fig. 5, $T_L=30$ kN/m (2055 lbs/ft) and $T_S=18$ kN/m (1230 lbs/ft).

Long-Term Material Degradation

The mechanisms for potential long-term degradation of buried high density polyethylene reinforcement include attack by micro-organisms or chemicals, thermal oxidation and environmental stress cracking. As shown in (10,14), it appears that each of these factors can be largely mitigated through proper selection of resin type (molecular weight, density, amount of copolymerisation, amount of cross-branching), resin additive formula (carbon black and anti-oxidants) and manufacturing process. (The geogrid tested is manufactured with rib dimensions of 5.5mm (220 mil) wide by 1.2mm (48 mil) thick which results in a relatively low surface area to mass ratio of 2×10^{-3} m²/g. The geogrid tested

also has an average longitudinal orientation ratio of approximately five. Orientation decreases HDPE permeability and increases polymer environmental stress crack resistance (10).)

Of particular interest is the environmental stress crack resistance of HDPE reinforcing materials. This question has recently been raised in the literature (5). Creep test results on a HDPE geogrid manufactured with the same process and resins as the geogrid considered in this section, but with slightly different geometry, are shown in Fig. 6. These results compare unconfined creep performance of the geogrid in air and in a detergent solution (a surfactant causing severe environmental stress cracking conditions) for periods up to 2000 hours at a temperature of 23°C. The results show a negligible effect of the detergent solution on creep performance under the test conditions.

Based on the information provided in (10,14) both F.D.L and F.D.S are taken as 1.0 for the HDPE geogrid considered herein.

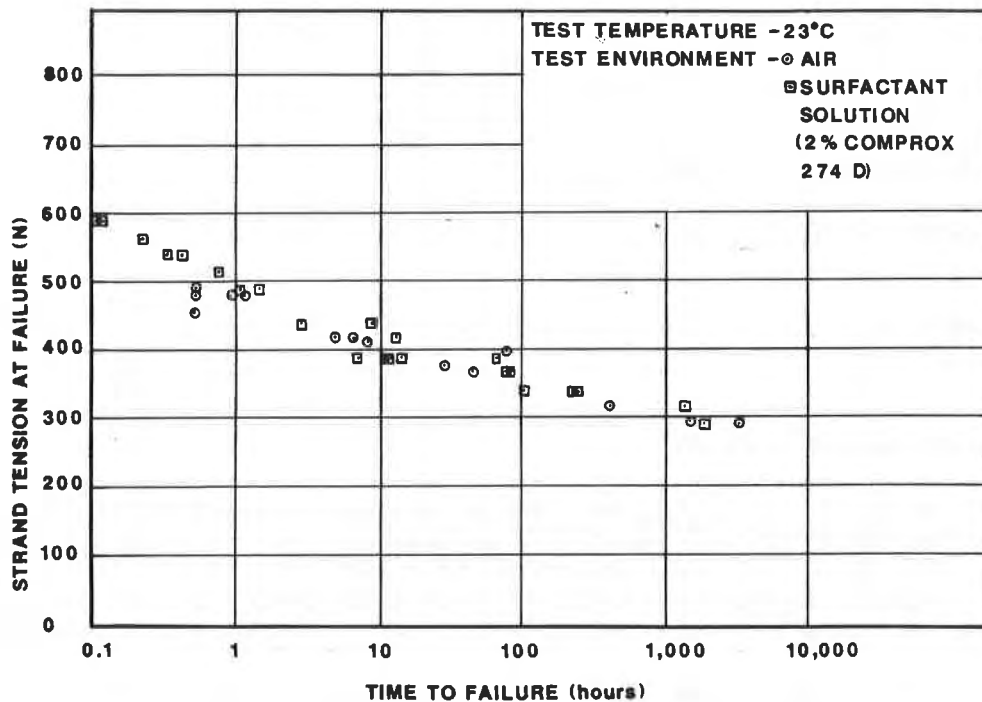


Figure 6. Comparative behavior of HDPE geogrid tested in air and in surfactant solution (from Wrigley (14)).

Construction Induced Damage

Full-scale construction damage tests (8) were carried out on three different uniaxially oriented HDPE geogrids with masses per unit area ranging from 500 - 1100 g/m² (Table 1). Three different well-graded crushed limestone fills were placed under and over the geogrids and compacted using conventional procedures. The effect of construction damage was evaluated by comparison of the wide strip tensile strength of "construction damaged" samples with "undamaged" control samples. The test results are reported in Table 1 as the ratio of "undamaged" to "damaged" geogrid strength. The values given define F.C.L. The construction operations were found to have a negligible effect on the initial tensile modulus of the reinforcement. Thus, F.C.S equals 1.0.

Based on the mass per unit area of the considered geogrid (920 g/m²), a value of F.C.L midway between the values for geogrids with masses per unit area of 750 and 1,126 g/m² would seem to be appropriate.

TABLE 1 (adapted from (9))

Fill Descriptions	Geogrid Mass per Unit Area (g/m ²)		
	522	750	1,126
Well-graded gravel with 60-mm max particle size	1.45	1.30	1.20
Well-graded gravel with 20-mm max particle size	1.25	1.20	1.10
Sands and Clays	1.15	1.10	1.05

Long-Term Reinforcement Tension

The long-term allowable reinforcement tension for the considered geogrid can be determined using the previously described methodology and discussion. If it is assumed that the reinforced soil structure is a concrete-panel-faced retaining wall with a backfill specification corresponding to a well-graded crushed rock with a maximum particle size of 60mm (2.5 in), the following calculations can be carried out:

$$T_{AL} = \frac{T_L}{F.D.L \times F.C.L \times F.S.} = \frac{30.0 \text{ kN/m}}{1.0 \times 1.25 \times 1.5} = 16.0 \text{ kN/m} \quad (3)$$

$$T_{AS} = \frac{T_S}{F.D.S \times F.C.S} = \frac{18.0 \text{ kN/m}}{1.0 \times 1.0} = 18.0 \text{ kN/m} \quad (4)$$

Taking the minimum of T_{AL} and T_{AS} :

$$T_A = T_{AL} = 16.0 \text{ kN/m} \quad (5)$$

Comparing T_A to the wide strip tensile strength of the reinforcement (78 kN/m) shows that the long-term allowable reinforcement tension to be used in limit equilibrium design equations is approximately 20% of the wide strip strength. The authors limited review of the literature suggests that T_A may be less than 10% of the corresponding wide strip tensile strength for some geosynthetic materials.

CONCLUSION

A methodology to determine the long-term allowable geosynthetic reinforcement tension for use in design of permanent, critical applications has been proposed. The methodology accounts for reinforcement creep, in-ground material degradation, and construction-induced material damage. The methodology has been applied to a HDPE geogrid product. Due to the fact that the design life of a reinforced soil structure is much longer than the duration of tests used to evaluate long-term performance, extrapolation of test results based on mathematical models, literature reviews and judgment is required.

ACKNOWLEDGEMENTS

The authors would like to acknowledge V. Elias, N.E. Wrigley, and W.S. Shelton for their stimulating discussions with the authors with respect to long-term allowable design loads. The authors would like to thank J.P. Giroud for reviewing a draft of the paper, Grace Saunders for typing the paper, and Sherry Chauncey for drafting the figures.

REFERENCES

1. Andrawes, K.Z., McGown, A. and Murray, R.T. (1986), "The Load-Strain-Time-Temperature Behavior of Geotextiles and Geogrids", Proceedings of the Third International Conference on Geotextiles, Vol. 3, Vienna, pp. 707-712.
2. Bonaparte, R., Holtz, R.D. and Giroud, J.P. (1985), "Soil Reinforcement Design Using Geotextiles and Geogrids", ASTM Symposium on Geotextile Testing and the Design Engineer, Special Technical Publication #952 (in press).
3. Broms, B. (1986), Oral Discussion, Session 3A, Third International Conference on Geotextiles, Vienna.
4. Cheok Y.K. (1985), "The Behavior of Polymeric Grids Used for Soil Reinforcement", Ph.D. Thesis, Strathclyde University, Glasgow.

5. Ingold T.S. and Miller, K.S. (1986), "Short, Intermediate and Long-Term Stability of Geotextile Reinforced Embankments Over Soft Clay", Proceedings of the Third International Conference on Geotextiles, Vol. 1, Vienna, pp. 337 -342.
6. McGown, A., Andrawes, K.Z., Yeo, K.C. and DuBois, D.D. (1984), "The Load-Strain-Time Behavior of Tensar Geogrids", Proceedings of the Symposium on Polymer Grid Reinforcement in Civil Engineering, The Institution of Civil Engineers, London, pp. 11-17.
7. McGown, A., Paine, N. and DuBois, D.D. (1984), "Use of Geogrid Properties in Limit Equilibrium Analysis", Proceedings of the Symposium on Polymer Grid Reinforcement in Civil Engineering, the Institution of Civil Engineers, London, pp. 31-35.
8. Netlon Ltd. (1986), "Procedures for Assessing the Site Damage of TENSAR SR 55, SR80, and SR110", Internal Report, Blackburn, England. (Available from The Tensar Corporation, Morrow, Georgia.)
9. Netlon Ltd. (1986), Tensar SR55-SR80-SR110 Geogrids, Product Brochure, Blackburn, England. (Available from The Tensar Corporation, Morrow, Georgia.)
10. Shelton, W., and Wrigley, N.E. (1987), "Long-Term Durability of Geosynthetic Soil Reinforcement", Proceedings of the Symposium Geosynthetics '87, New Orleans, February.
11. Villet, W.C.B., Mitchell, J.K., et al. (1985), "Reinforcement of Earth Slopes and Embankments", Report to National Cooperative Highway Research Program, Project 24-2, Washington, D.C.
12. Ward, I.M. (1984), "The Orientation of Polymers to Produce High Performance Materials", Proceedings of the Symposium on Polymer Grid Reinforcement in Civil Engineering, The Institution of Civil Engineers, London, pp. 4-10.
13. Wilding, M.A. and Ward, I.M. (1978), "Tensile Creep and Recovery in Ultra-High Modulus Polyethylenes", Polymer, Vol. 19, p. 969.
14. Wrigley, N.E. (1986), "The Durability of TENSAR Geogrids", Internal Report, Netlon Ltd., Blackburn, England. (Available from The Tensar Corporation, Morrow, Georgia.)

SESSION 2A

LABORATORY AND MODEL EVALUATION

PAULSON, J.N. and LANGSTON, M.C.
Exxon Chemical Company, U.S.A.

Stitchbonded Composites

I. INTRODUCTION

The use of geotextiles has grown and developed significantly from the mid 1960's, when the first geotextile was installed in the United States (1). The applications have increased in both size and complexity as designers have recognized the benefits in cost and time that can be derived from use of geotextiles in their projects.

As the use of geotextiles expanded, the need to understand the material characteristics and the functions these fabrics perform also increased. Design engineers were no longer satisfied with the explanation that "it worked for me" as the design basis. Thus began the period in the practicing Geotechnical engineering history, wherein the rational basis for why a geotechnical solution worked was investigated. The science of designing with geotextiles has grown and expanded as a result of this desire to fit design procedures to the art and experience of using geotextiles.

Along with this development came the need to understand the physical properties of fabrics, and the relationships that these materials' properties had to soils and soil-structure performance. This functional approach to design is seeing acceptance as a logical basis for designing structures, and for selecting geotextiles that provide the physical properties required by that design.

Finally, multi-function geotextiles are the logical extension to this development, where a single product exhibits more than one desirable physical property. Design benefits and construction cost and time savings can be realized when one construction material serves dual roles.

This paper investigates a technique of combining geotextiles into multi-layered composites which exhibit just such multi-function properties. This composition allows the possibility of producing materials which satisfy several design functions with one material. Two combinations are presented and tested: multiple layer woven composites and woven/non-woven composites. Resulting physical properties are presented and compared.

II MANUFACTURING PROCESS

Review of a number of conference proceedings revealed few references where fabric construction was discussed to any extent. Although presented extensively in textile publications, geotechnical and geotextile conferences have concentrated primarily on applications and physical properties, with little discussion of manufacturing techniques, and how they can significantly influence these physical properties. Understanding of these processes is critical to the correct and intelligent use of the end products, which are geotextiles. Information on geotextile construction can be obtained in a number of references (1,2). The following is a brief discussion of the two predominant geotextile manufacturing processes, woven and non-woven.

WOVEN GEOTEXTILE CONSTRUCTION

Traditional woven geotextiles are formed by weaving single yarns in both warp and fill directions to form a dimensionally stable end product. Increases in tensile strength are accomplished by weaving with larger sized yarns or multifilament yarns with higher total denier (fiber diameter).

Geotextile construction is of the plain weave type, with one over one (or two by two) the predominant configuration. More complicated weaving techniques are typically not used except in specialized fabric construction.

Physical properties attributed to woven geotextiles primarily relate to tensile strength and elastic modulus. Permeability normal to the plane of the woven geotextile is limited. Apparent opening size is normally relatively ununiform, and governed by the largest opening(s) in the sample. The use of monofilament yarns with light heat calendaring results in more uniform opening size, useful in filtration applications.

NON-WOVEN CONSTRUCTION

Non-Woven geotextiles are formed by combining many randomly oriented small denier fibers into a stable fabric. As the name implies, no pattern or ordered weaving process is used in construction. Rather, mechanical (needlepunching) or thermal (heatbonding) techniques are used to give the finished product shape, strength and uniformity.

Physical properties generally attributed to non-woven geotextiles are deformability (high elongation), high permeability normal to the plane of the fabric (permeability), in-plane flow capacity (hydraulic transmissivity) and good filtration. These characteristics are significantly affected by heatbonding. As such caution must be exercised when selecting a non-woven for these functional requirements.

GEOSYNTHETIC COMPOSITES

The combining of multiple layers of geotextile was first mentioned in 1983 (ref 3). Non-woven geotextile filtration characteristics of combinations of different types of non-woven geotextiles are discussed in ref (4). These are formed using needle punching techniques.

Other composites, such as prefabricated drainage structures, are formed using either bonding adhesives, or by partially melting one or the other of the materials to be fastened. These composites normally consist of a geotextile attached to a core structure of unique/different construction. The core provides void space to facilitate flow, with the geotextile providing filtration and drainage of the soil. Multi-function products providing filtration, drainage and high in-plane flow volumes are the end result (5).

III STITCHBONDING

Stitchbonding is a method of sewing multiple geotextile layers together using knitting manufacturing techniques. The sewn stitches consist of a series of chainstitches installed in closely spaced rows. This process serves to mechanically combine the individual layers into one composite. Variations in both the stitch line spacing and the number of stitches per inch of stitchline are possible.

A wide variety of combinations are possible with this process. For this paper two product groups were investigated; multiple layers of woven geotextile, and woven/nonwoven geotextile combinations. All composites were stitched with 500 denier polyester sewing thread with 2.5-3.0 stitches per cm, and one cm between stitchlines. This results in 2.5 to 3.0 stitches per sq cm of geotextile.

A. MULTIPLE LAYER WOVEN COMPOSITES

Combinations of a medium strength slit tape polypropylene geotextile, stitchbonded to form three and four layer composites were tested. The influence of stitchbonding on the individual layer physical properties were evaluated and included grab tensile strength, wide width strength, puncture, burst, and trapezoid tear. Table 1 lists pertinent physical properties of these three geotextiles.

Figure 1 shows wide width test results for the three materials. As the number of layers increases so does both the ultimate tensile strength and the slope of the stress-strain curve.

The wide width test results were replotted to investigate the efficiency of the stitchbonding process. The normalized results are shown in figure 2 and were obtained by taking the tensile strength and dividing by number of layers and then by the strength of an unstitched single layer. There is a reduction in efficiency resulting from the stitchbonding process of approximately 15%.

Table 1
Woven Geotextile Physical Properties

Physical Properties	Grab Tensile Strength ASTM 1682	Wide Width Strip Tensile ASTM D4595	Secant Modulus at 10% Strain ASTM D4595	Trapezoid Tear ASTM D1117	Puncture ASTM D751	Burst ASTM D751
Single Layer	890 N (200 lb)	30 KN/m (170 lb/in)	117 KN/m (670 lb/in)	400 N (90 lb)	445 N (100 lb)	3272 KPa (475 psi)
3 Layer Composite	3335 N (705 lb)	77 KN/m (440 lb/in)	613 KN/m (3500 lb/in)	890 N (200 lb)	1780 N (400 lb)	10,000 KPa (1500 psi)
4 Layer Composite	4000 N (900 lb)	104 KN/m (590 lb)	875 KN/m (5000 lb/in)	980 N (220 lb)	2000 N (450 lb)	10,000 KPa (1500 psi)

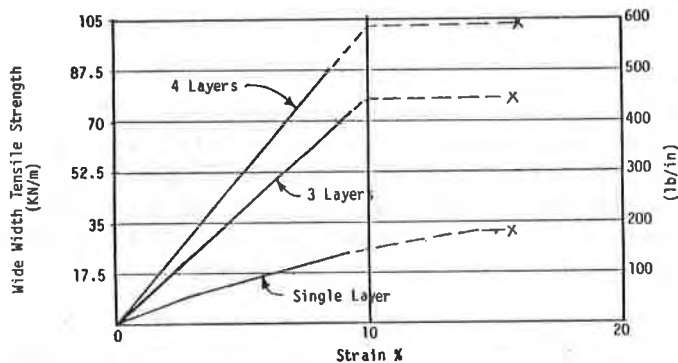


Figure 1 Wide width tensile strength comparisons

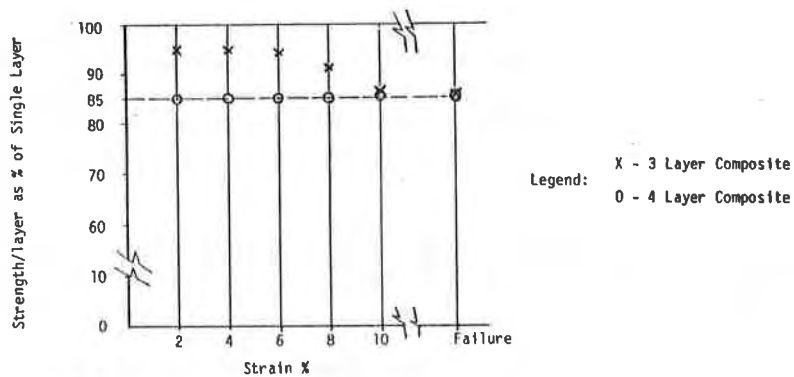


Figure 2 Stitchbonding efficiency as measured by individual layer strength retention using wide width testing

OFFSET STRAIN

As yarn size increases, the strain required to straighten the yarns in a woven fabric and thus provide tensile strength increases. When tested using wide width procedures, an off-set strain is the result. This is discussed in ref (2) and is defined as "the distance between the daylight point and the intercept of the extended modulus line with the strain axis".

Evaluation of offset strain is important in soil-geotextile interaction, as evidenced by the total resulting strain required to achieve a desired stress level in the material. Conversely, the maximum stress level that can be achieved in that same product may be limited by the allowable strain in the structure.

Depending on the manufacturing technique used the offset strain can amount to several percent. This is depicted graphically in figure 3. Defined as crimp in fabric construction terminology, this is the strain required to straighten out the yarn, allowing it to take load. All woven geotextiles exhibit some degree of offset strain.

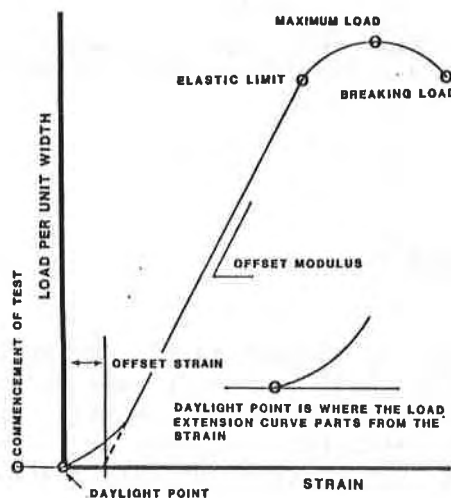


Figure 3 LOAD - STRAIN CURVES FOR GEOTEXTILES FROM MYLES (6)

Figure 4 shows wide width test results of a 4 layer stitchbonded composite geotextile plotted alongside an equivalent strength, single layer woven geotextile. Although the overall slope of both materials are similar, the offset strain exhibited by the heavy single layer Geotextile is absent for the composite.

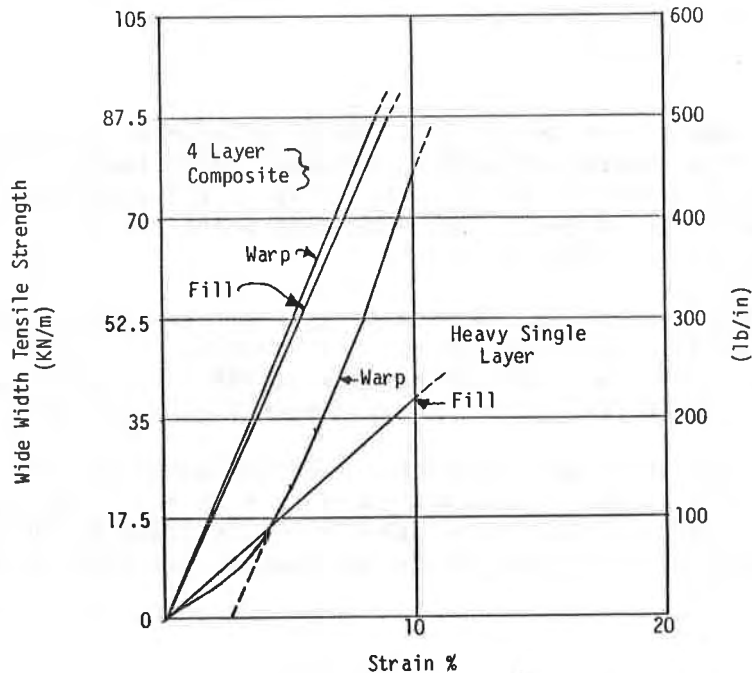


Figure 4 Comparison of single layer and multiple layer composite load/strain characteristics

FLEXURAL RIGIDITY (STIFFNESS)

Installation conditions can be significantly affected by the stiffness or flexibility of the geotextile used. For very soft sites geotextile stiffness may benefit installation by improving field workability and increasing construction progress. Additionally, dimensional stability is increased, resulting in few or no folds or wrinkling during installation and fill placement.

Although somewhat indirect in nature, attempts have been made to quantify flexibility using Textile industry methods, specifically ASTM D-1388 (75). In this method a 5 cm(2 in) wide specimen is slid out cantilever fashion over an edge of a table or test platform, and the length of sample that can be supported by itself is measured. one-half the length which can stand at a 41.5 degree angle from the horizontal is then cubed, with that quantity multiplied by the weight per unit area of the fabric to determine the geotextile flexural rigidity.

Table 2 lists flexural rigidity values for a number of tested materials. The stitchbonding process results in an order of magnitude higher flexural rigidity than a comparable strength/weight material.

TABLE 2 Geotextile Flexural Rigidity

	Weight W	Bending Length (c)	Flexural Rigidity $G = Wc^3$
Lightweight Single layer Slit tape woven	15.9mg/cm ² (4.7 oz/sy)	7.2 cm	6185 mg-cm
High Strength Multi-Filament woven	72.5mg/cm ² (21 oz/sy)	5.7 cm	13426 mg-cm
4 layer Stitch- bonded woven composite	67 mg/cm ² (19.8 oz/sy)	16.3 cm	292560 mg-cm

SOIL FABRIC FRICTION

Determination of embedment length required to design against geotextile pull-out as a potential failure mode is dependent on the soil-fabric friction. This is determined from either laboratory direct shear or pull-out tests, and is commonly expressed as either a value in degrees, or as a percentage of the angle of internal friction of the soil to be used on the project.

Typical results for slit tape woven geotextiles in granular material are in the range of $2/3 \phi$, or approximately 65-70% of the soil friction angle (1,8).

Testing was performed to verify these values, and to evaluate the effect (if any) that the stitchbonding process had on this interaction. Tests were run using Ottawa Silica Sand with particle size between the #20-30 U.S. Standard Sieve. Several geotextiles were tested, with all tests run using a 12" square direct shear apparatus as described in ref (7). Results are presented below.

SOIL-GEOTEXTILE FRICTION

Ottawa Silica sand	<u>Friction angle</u> = 36
<u>Three layer composite</u>	
Parallel to stitchlines	= 23
Perpendicular to stitchlines	= 26
<u>Four layer composite</u>	
Parallel to stitchlines	= 23
Perpendicular to stitchline	= 25

These results are consistent with previous work performed (8). It is interesting to note the slight increase in frictional resistance transverse to the stitchline direction, indicating a slightly rougher surface.

DESIGN SIGNIFICANCE

The importance of the reduction in offset strain, and the increase in geotextile flexural rigidity to the practicing engineer is described below. In many reinforcing applications geotextile strength at a given strain is more critical than the material ultimate strength. The ability of the geotextile to provide high strength at low strains can be vital.

An example of this would be an embankment to be built over soft ground. The embankment width requiring reinforcement is approximately 30m. Required geotextile tensile strength of 25 KN/m has been determined by analysis, and the design criteria dictates that lateral spreading be held to a minimum.

Using results presented in figure 4 it is seen that a difference in strain required to reach this stress level in the single layer geotextile versus the stitchbonded material is approximately 2-1/2 %. Assuming uniform, horizontal extension, this equates to approximately an additional 0.7 meters of lateral spreading. As important, if small strains were needed in the geotextile to limit soil shear strain, the strength available for these two materials at the desired strain would be dramatically different.

Geotextile flexural rigidity can be of significant benefit if the site conditions reveal that the subgrade to be traversed is extremely soft. This was the case earlier this year when a bentonite filled muck pond had to be covered and capped with soil. The muck shear strength was estimated to be less than 5 kPa (100 psf) and in many areas was nothing more than a bentonite slurry.

For this project the strength properties specified dictated that a four layer stitchbonded composite be used. The high flexural rigidity of the stitchbonded composite allowed workmen to walk on top of the geotextile immediately after it was spread. As well, installation went smoothly with little delay due to straightening folds or wrinkling of the fabric. The site contractor stated that the fabric stiffness greatly improved his installation time. Placement of the soil cap proceeded without incident.

B. WOVEN/NON-WOVEN COMPOSITES

The features and benefits of two types of geotextile construction processes have been discussed. The prime features of a woven geotextile are strength and modulus, whereas the nonwoven (non-heatbonded) manufacturing process results in a higher elongation, more permeable geotextile in both in-plane and normal to the plane directions. Stitchbonding allows two (or more) material types to be mechanically fastened. The desirable end result is a product that embodies the best features of both. This section discusses one such combination of materials.

A woven/non-woven stitchbonded composite geotextile was investigated. It consisted of a 160g/sq.m. (4.7 oz./sy) polypropylene tape woven layer sandwiched between two polypropylene needlepunched non-woven layers of approximate weight of 200g/sq.m. (6 oz./sy). This combination was considered representative of the possibilities of the stitchbonding process. Table 3 presents physical properties of each individual layer along with results obtained for the composite.

Table 3
Woven/Non-Woven Geotextile Physical Properties

Physical Properties	Grab Tensile Strength ASTM 1682	Wide Width Strip Tensile ASTM D4595	Secant Modulus at 10% Strain ASTM D4595	Trapezoid Tear ASTM D1117	Puncture ASTM D751	Burst ASTM D751
Woven Layer	890 N (200 lb)	30 KN/m (170 lb/in)	117 KN/m (670 lb/in)	400 N (90 lb)	445 N (100 lb)	3272 KPa (475 psi)
Non-Woven Layer	711 N (160 lb)	7.88 KN/m (45 lb/in)	1.75 KN/m (10 lb/in)	310 N (70 lb)	290 N (65 lb)	1550 KPa (225 psi)

TENSILE STRENGTH

Figure 5 shows the wide width tensile test results for the woven layer and the composite. Both the warp and fill direction composite show considerable strength increase over the individual woven geotextile layer. For the warp direction this increase is due to the strength contribution from the non-woven layers. Fill direction strengths increased also, a result of offsetting factors namely, non-woven strength contributions being balanced by strength loss in the woven geotextile from needling during stitchbonding.

A second factor in both the observed strength increases is the lateral constraint provided by the stitchbonding process. This is felt to be a result that is experienced in the geotextile in the ground when soil provides confinement. The stitchbonding process allows this effect to be seen in laboratory testing.

One additional feature this combination provides is a material that experiences a load strain curve which peaks early, but still retains strength at higher strains and, in fact, goes on to gain strength with increasing strain. This may prove to be of significant value for some selected design conditions.

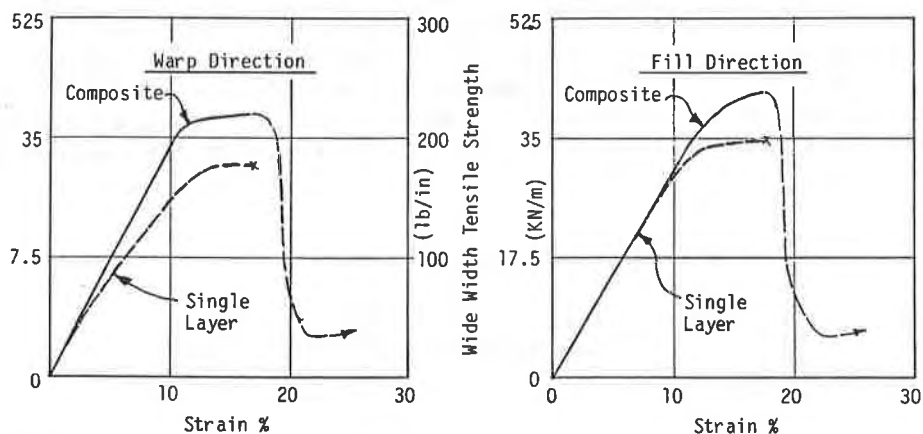


Figure 5 Comparative load/strain curves for woven/non-woven composite and woven geotextile

SOIL-FABRIC FRICTION

Soil-fabric friction has been discussed previously in this paper as related to woven stitchbonded composites. Experience has shown that the frictional resistance of a non-woven geotextile tends to be higher than that of a smooth surfaced geotextile (8). Consequently, by combining materials which exhibit a rougher surface on the outsides of the strength providing layer, a higher friction angle would be expected.

Soil-fabric friction of the woven/non-woven composite was investigated. Results are as follows:

SOIL-GEOTEXTILE FRICTION

Friction angle

Ottawa Silica sand = 36

Composite

Parallel to stitchlines = 26

Perpendicular to stitchlines = 26

These results are somewhat lower than expected. The lightweight and thinness of the non-woven geotextile used to construct this composite may be a factor.

Additionally, the interface friction angle can be significantly affected by the soil particle size, particle shape and the density of the fill used. For the above tests, the relatively large soil particle size (US sieve #20-30) compared to the fabric A.O.S. (#70-100 US standard sieve) is undoubtedly a contributing factor. Additional work is currently being performed in this area. In an application where this interaction is critical, individual testing of the soil and geotextile to be used should be performed.

HYDRAULIC TRANSMISSIVITY

Planar flow within a reinforcing geosynthetic can provide drainage and reduce or eliminate internal pore pressures which may build within an embankment fill. As slope stability is significantly affected by the pore pressure regime within the fill section, elimination of excess hydrostatic pressure thru internal drainage would be of significant benefit. A typical application is shown in figure 6.

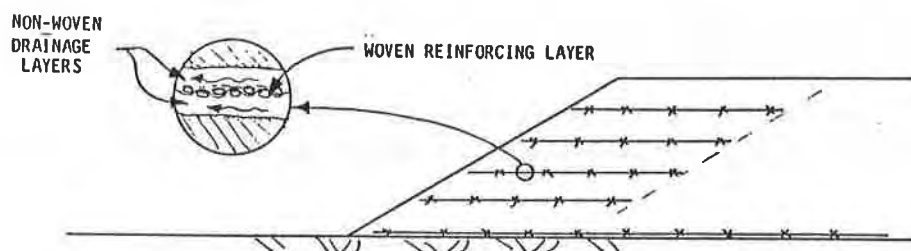


Figure 6 Embankment reinforcing and drainage combination geotextile

This is another distinct potential use of stitchbonded composites, and one which is being investigated. Results will be presented as these materials are developed and tested further.

Acknowledgements

The soil-geotextile friction testing was performed at Georgia Institute of Technology under the guidance of Prof. N.D. Williams. All other testing was performed in the technology laboratories of Exxon Chemical Company in South Carolina.

References

1. Christopher, B.R. and Holtz, R.D. Geotextile Engineering Manual, FHWA, 1984
2. Koerner, R.M. and Welsh, J.P., Construction and Geotechnical Engineering Using Synthetic Fabrics, John Wiley and Sons, Inc., New York, 1980
3. Giroud, J.P. and Carroll, R.G. Jr., "Geotextile Products", Geotechnical Fabrics Report, Vol. 1, No. 1, IFAI, St. Paul MN, 1983, PP. 12-15
4. Muhring, W. and Saathoff, F., "Testing of Filter Characteristics of Composite Materials", Proceedings of the Third International Conference on Geotextiles Vienna, Austria, 1986, pp. 809-814.

5. Koerner, R.M., Luciani, V.A., Freese, J.S., Carroll, R.G., Jr., "Prefabricated Drainage Composites: Evaluation and Design Guidelines", Proceedings of the Third International Conference on Geotextiles, Vienna, Austria, 1986, pp 551-556
6. Myles, B. and Carswell, I.G., "Tensile Testing of Geotextiles", Proceedings of the Third International Conference on Geotextiles, Vienna, Austria, 1986, pp.713-718
7. Williams, N.D. and Houlihan, M. "Evaluation of Friction Coefficients between Geomembranes, Geotextiles and Related Products", Proceedings of the Third International Conference on Geotextiles, Vienna, Austria, 1986, pp. 891-896
8. Myles, B. "Assessment of Soil Fabric Friction By Means of Shear", Proceedings of the Second International Conference on Geotextiles, Las Vegas, Nevada, 1982, pp.787-792

LAFLEUR, J., SALL, M.S., and DUCHARME, A.
Ecole Polytechnique de Montreal, Canada

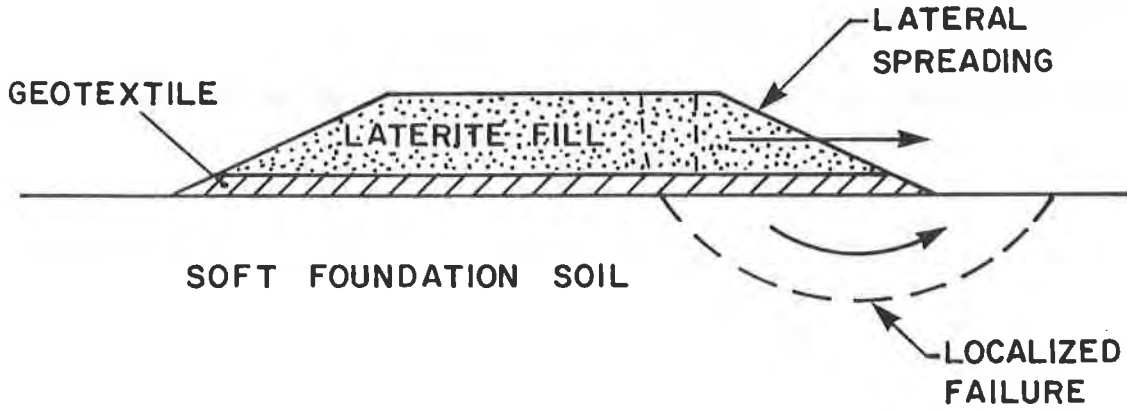
Frictional Characteristics of Geotextiles With Compacted Lateritic Gravels and Clays

ABSTRACT

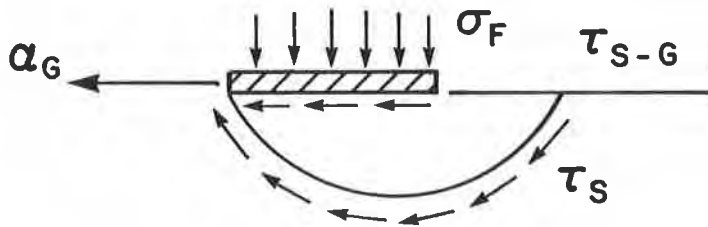
Direct shear tests have been made to evaluate the adherence between geotextiles and various soils with respect to the design of reinforced lateritic gravel embankments laid over a soft clay foundation. The two gravels samples were typical of those used as highway fill in Sénégal on the west african plateau; although of the same geological origin, they were different in grain size distribution. Three geotextiles were tested: one thick needle-punched, one thin needle-punched and one woven. The soil strength and the soil-geotextile adherence parameters were obtained from direct shear box tests. The tests results show on one hand, that the grain size distribution of a soil strongly influences the adherence of soils to woven geotextiles: for the coarser laterite, the adherence angle δ (44°) was substantially larger than for the silty gravels (32°) and the remoulded clay (22°). On the other hand, the dominant effect of the geotextile texture on the relative friction ($\tan \delta / \tan \phi$), is considerable with cohesive soils: it is exceeding 100% for the non wovens, whereas it decreases to 60% for the wovens. This difference has been attributed to the presence of the randomly oriented fibres at the non woven interface, that promotes interpenetration of the soil into the geotextile and reinforces it locally. This lead to recommend the use of non woven geotextiles in reinforcement with cohesive soils, when interface friction is relied upon.

INTRODUCTION

In tropical countries, the presence of lateritic soils is very frequent, so they are often used as highway fill material. When properly compacted, some lateritic gravels can have excellent strength properties. This paper refers to situations where lateritic fills are laid over low bearing capacity soils as for example, alluvial unconsolidated clays and silts. Amongst engineered solutions, the use of a geotextile reinforcement can prevent local failures, thereby insuring uniform settlements of the structure and a better serviceability. Fig. 1. gives a schematic view of such an application and the mobilized forces associated with two failure mechanisms that can be prevented by the use of a reinforcing geotextile: a) a localized failure plane developing mainly through the foundation soil and b) lateral spreading of the sloped part of the fill.



LOCALIZED FAILURE



LATERAL SPREADING

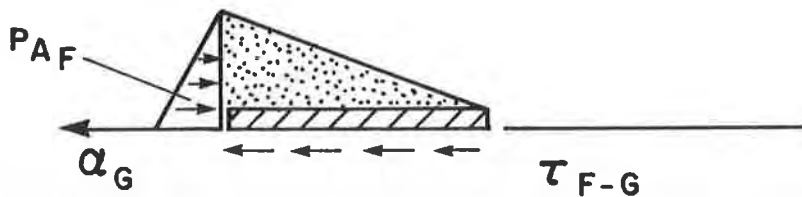


FIG. 1 — LIMIT EQUILIBRIUM IN REINFORCED EMBANKMENT

The acting and reacting forces are given in the lower part of the figure: for the localized failure, the disturbing stress is the weight of the fill (σ_F) resisted by the tensile strength of the geotextile (α_B), the shearing resistance of the foundation soil (τ_B) and the lower interface adherence (τ_{B-G}). For the case of lateral spreading, the disturbing stress is the lateral earth pressure of the fill wedge (p_{AF}) and the resisting stresses are the tensile strength of the geotextile (α_B) and the upper interface adherence (τ_{F-G}). The existing models for assessing the stability or for analysing the behaviour of such works, (4,7,8) rely on mechanical parameters obtained from laboratory tests:

- soil properties (foundation and fill): cohesion c , friction angle ϕ , elastic modulus E , and Poisson's ratio ν , either in drained or undrained conditions depending upon the rate of construction of the fill.
- geotextiles properties: tensile strength α_f , elongation at failure ϵ_f , tensile stiffness J .
- interface strength: adherence angle δ on both interfaces

Most of these parameters can be obtained from current laboratory procedures, but properties related to soil-geotextile interaction, like the interface strength, are site specific, and a testing programme bearing on this topic has been undertaken.

MATERIALS AND PROCEDURES

a) lateritic gravels:

The laterite deposits are essentially localized in the tropical regions; these are residual soils that are the product of the in-place weathering of the parent rock. Gidigas (3) gives an extensive review of the origin of these materials and their engineering properties. The fill samples that were used in the programme, are representative of highway materials used in Sénégal, on the west african plateau. They come from two sites 50 km apart, where they are quarried as base and subbase. The grain size curves of fig. 2 indicate that Leona Niang (LN) is coarser than Dougar (D); both soils are gap-graded since their gravel "skeleton" (40 to 50% in mass) is lacking sand size particles and it is confined in a more or less plastic matrix having a plasticity index in the order of 18% (see table 1). As indicated by the shifting of the grain size curves on fig. 2, these residual soils are highly sensitive to crushing, since compaction of a sample following the standard Proctor procedure can increase the fine content by 5%.

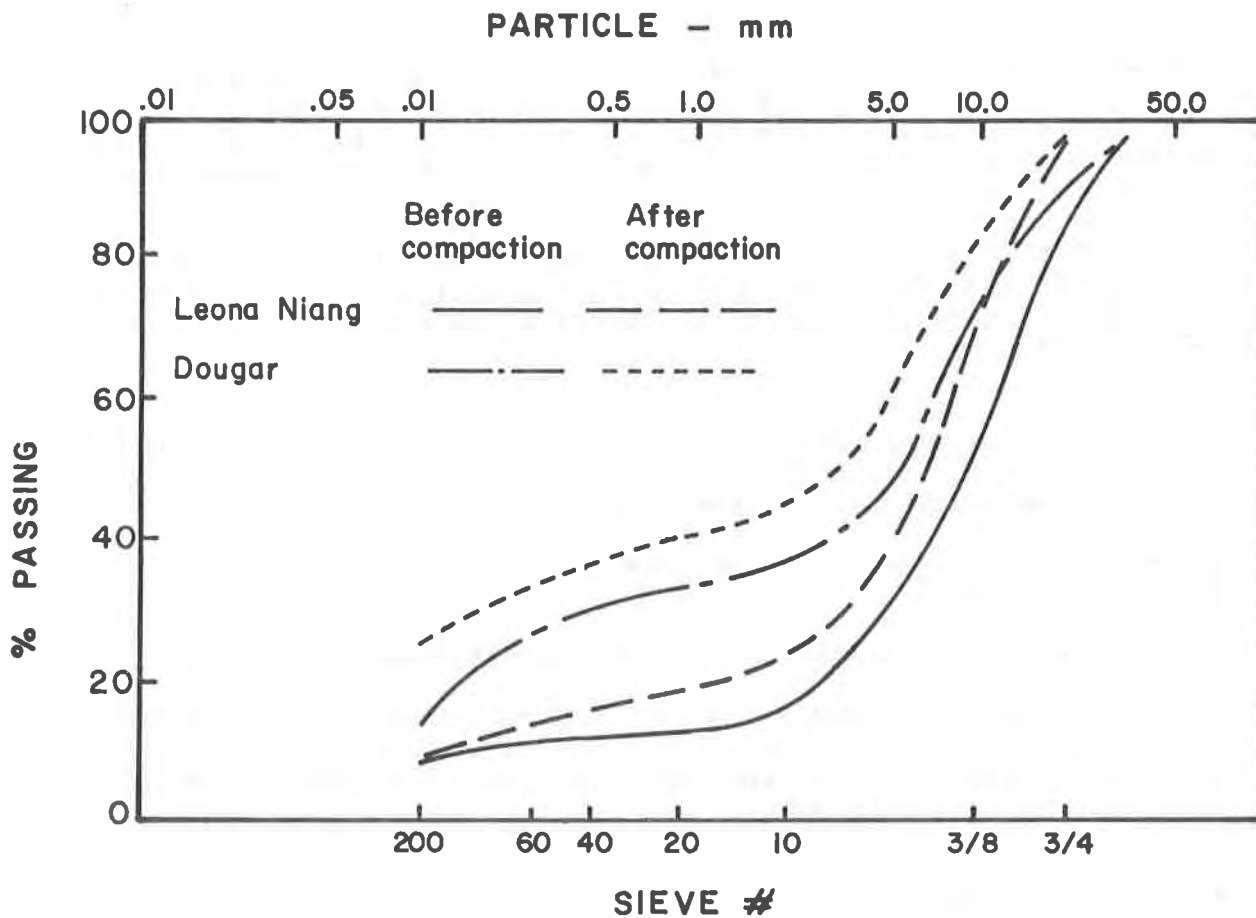


FIG. 2 — GRAIN SIZE CURVES — LATERITIC GRAVELS

The internal shear strength properties have been evaluated in a 150 x 150 mm shear box described in Akber et al. (1), using samples with 20 mm maximum particle size, compacted under static load (to avoid particle crushing) and molded at the optimum water content; the energy was adjusted in order to produce samples with densities corresponding to fill specifications, i.e. 90% of the standard Proctor reference given on table 1. After consolidation under normal stresses in the range compatible with current fill heights (50 to 150 kPa), the shearing stresses were applied at a constant rate of 1 kPa/min. The resulting strain rates were slow enough to assume that the tests were fully drained; in fact the time to failure ranged between 20 minutes and 3 hours. The shear tests have been made on two series of samples to have the full spectrum of responses: one group was soaked for 4 days before testing and the other group was sheared without water available, in order to modelize unsaturated fills standing above water level.

Table 1 Geotechnical Properties

	Lateritic gravels		Clay
	LN	D	
Liquid limit	35	32	56
Plastic limit	16	14	26
Plasticity index	19	18	30
Max dry density (std, Proctor) (kg/m ³)	2020	2090	--
Optimum water content (%)	8	9	--

From table 2, one can appreciate the influence of grain size distribution on the shearing behaviour: the friction angle (ϕ) of the coarser material (LN), being in the order of 44 to 48, is not substantially influenced by soaking period; it behaves as a relatively pervious granular material whereas the second one (D), has its friction angle significantly decreased from 49° to 27° by the presence of water; in the same way, the cohesion (c) passes from 50 kPa to nearly 0.

Table 2 Soils Shear Strength Parameters

Lateritic gravel				
	LN		D	
	soaked	unsoaked	soaked	unsoaked
c' (kPa)	19	35	5	53
ϕ' (°)	44	49	27	49°
Remolded plastic clay				
w (%)	25	40	60	
c' (kPa)	8	6	9	
ϕ' (°)	35	32	29	

b) plastic clay:

A plastic clay was used to modelize the soft foundation soil; table 1 gives a liquid limit of 56% and a plastic limit of 26%. The shear strength parameters were determined in a 50 mm square shear box on samples molded at different water contents: 25, 50 and 60%, and under consolidation stresses of 50, 100 and 150 kPa. A constant strain rate of 0.024 mm/min was adopted on the basis of a c_v value of 10^{-4} cm²/min, in order to assume fully drained conditions. The resulting failure envelopes were almost linear and the internal friction angles given on table 2, were seen to decrease from 35° to 29° when the water content varied from 25 to 60%. Cohesion intercepts were very small, in the range of 5 to 10 kPa.

c) geotextiles:

The table 3 gives the main physical properties of the three geotextiles used in the testing programme: two needle-punched non wovens, one thick and one thin, and one woven. The woven appears to be stiffer than the non woven, since its strain at failure is around 20% compared to 65% for the non wovens. The interface strength was measured using the same procedures and samples as those used for the determination of the internal strength parameters. Both parts of the box were filled with soil on a height of 50 mm, the geotextile were bound to the upper half and the shear strains were applied by moving the lower box. The following combinations were tested:

- plastic clay at different water contents (25, 50 and 60%) and the three geotextiles.
- lateritic gravels and the woven geotextile only. No tests were made with non wovens, because the results of tests on clays, indicated that lower bound values were obtained with wovens.

Table 3 Geotextile Properties

Designation Polymer	TX-7643 Polyester	PF-700 Polypropylene	MP-500 Polypropylene
Masse per unit area (g/m ²)	1470	297	170
Thickness (mm)	7.3	1.7	0.4
Tensile strength (kN/m)	64	16	12
Strain at failure	70-100	50-80	22

TEST RESULTS

The test results for the lateritic gravels are given on fig. 3 and table 4, in terms of Mohr-Coulomb parameters. The envelopes are linear and the intercept on the shear stress axis are almost negligible. This last point can

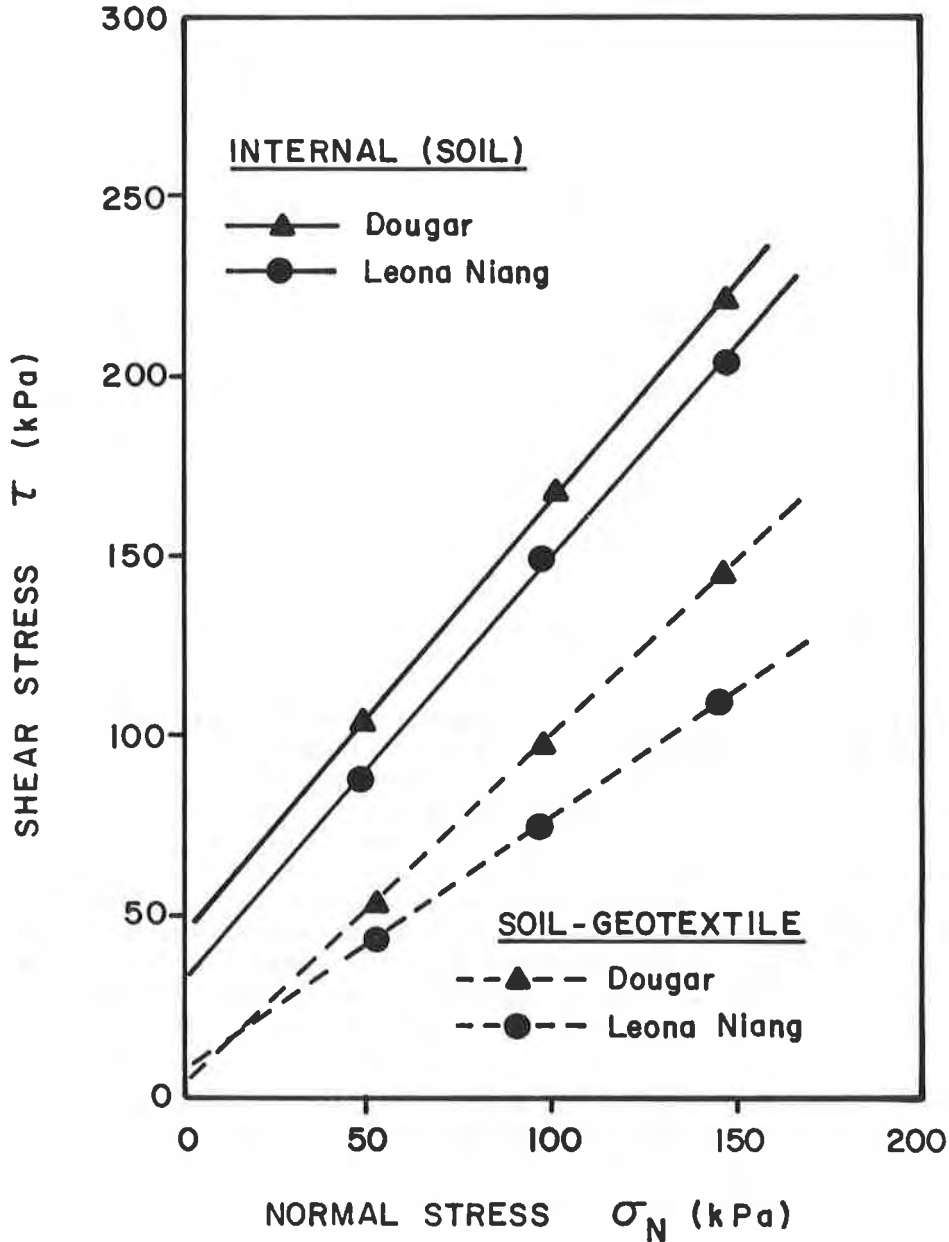


FIG. 3 – MOHR - COULOMB ENVELOPE - UNSOAKED LATERITIC GRAVELS VS WOVEN GEOTEXTILE

Table 4 Interface Adherence

Unsoaked laterite - vs - MP - 500		
	Adherence angle (δ) ($^{\circ}$)	Relative friction * (%)
LN	44	85
D	35	60
Plastic clay - vs - MP - 500 (woven)		
w = 25	22	59
40	21	61
60	15	47
Plastic clay - vs - PF - 700 (thin non woven)		
25	37	109
40	33	103
60	29	98
Plastic clay - vs - TX - 7643 (thick non woven)		
25	39	115
40	34	109
60	28	94
* $\tan \delta / \tan \phi$		

be explained by the fact that the high internal cohesion was related to the negative pore pressures associated with the partial saturation of the sample so the presence of a geotextile at the interface in the latter tests significantly contributed to release these pore pressures. One can see that for the gravel with the finer matrix (D), the relative friction is 60% compared with 85% for (LN). This difference illustrates that in the former case, the gravel particles are more or less surrounded by the fines matrix and they have a lesser influence on the frictional behaviour, whereas in the case of LN, the friction angle is not substantially decreased by the presence of the geotextile and the adherence between the gravel skeleton and the relatively smooth woven geotextile is still appreciable.

The fig. 4 gives the stress displacement curves for these tests: one can see that the maximum interface strength is fully mobilized after a displacement ranging between 1 and 3 mm depending upon the applied normal stress. This displacement corresponds to less than 2% of the total length of the box and it is comparable to those between the plastic clays and the woven, shown on fig. 5. With the non woven however, the displacements at failure are greater, being in the order of 4 to 10%. These larger strains can be associated to the particles adjustment and interpenetration into the geotextile that takes place at the interface. This phenomenon has also been observed upon dismantling of the samples at the end of the tests.

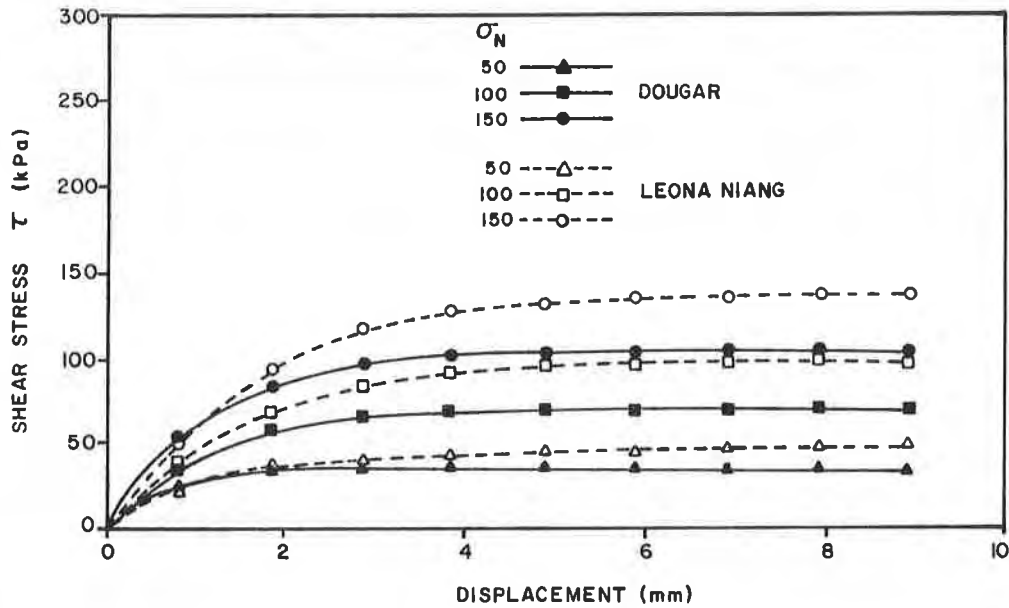


FIG. 4 - SHEAR TEST RESULTS - LATERITIC GRAVELS - VS - WOVEN GEOTEXTILE

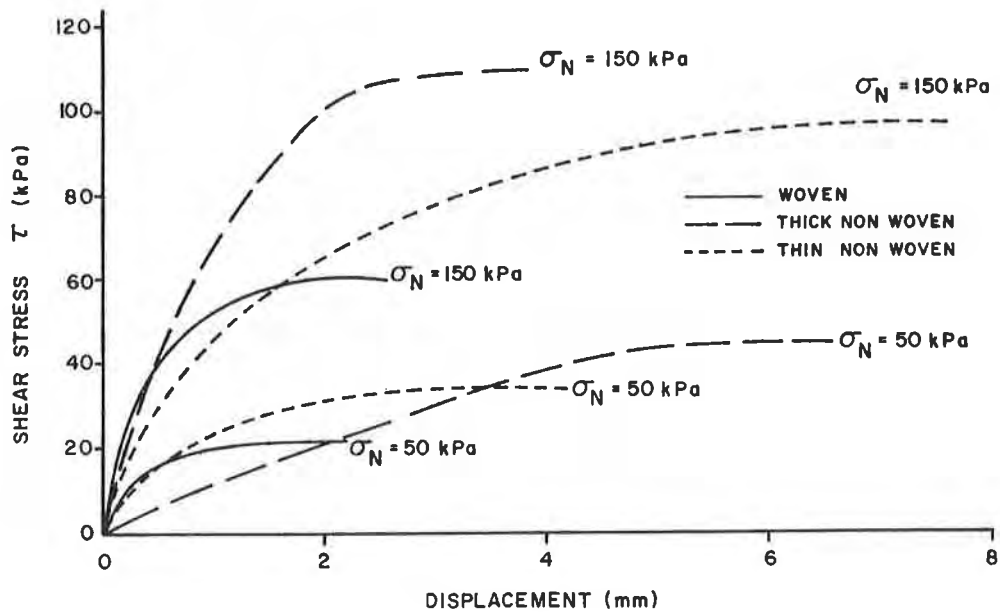


FIG. 5 - SHEAR TEST RESULTS - PLASTIC CLAY (W = 40%)

Finally, the table 4 gives the adherence values for the clays as a function of the water content. When comparing results between woven and non wovens, one can easily appreciate that in the second case, the mobilized interface strength is the same or even superior to the internal strength; this result could be related to the soil interpenetration that has just been described above. With wovens, the relative friction drops to less than 60% and this reflects the inability of the smooth interface to promote strong adherence between the soil particles and the geotextiles filaments.

CONCLUSIONS

A shear testing program has been undertaken to justify the choice of a geotextile in reinforced fill applications at the interface of lateritic gravels fills laid over soft clayey foundation soils. Two failure mechanisms of the soil have been identified: lateral spreading due to insufficient adherence of the fill material to the upper surface of the geotextile and the localized failure in the soft foundation, this last mechanism involving a relative tangential displacement between the foundation soil and the lower surface of the geotextile. The design and the choice of a geotextile, can be carried out by computing adherence strength on both sides of the geotextile, by using a Mohr-Coulomb criterion.

The shear test results of our programme indicate that the adherence of the fill material to woven geotextiles, is strongly dependent on the grain size distribution of the laterites: when the fines contents (smaller than sieve #40) is less than 10%, the adherence angle δ for a woven (therefore a lower bound value) can be as high as 44° , corresponding to an efficiency ($\tan \delta / \tan \phi$) of 85%. For a lateritic gravel with a fines content of 30%, the contribution of the coarse skeleton was substantially reduced and the efficiency dropped to 60%. This conclusion on the influence of the particle size on the adherence of soils to thin geosynthetics, also stems from the results of Eigenbrod and Locker (2) and of Martin et al. (5) who shear tested geotextiles with different soils. The use of thick geosynthetics however tends to eliminate this influence of coarser particles (1).

When considering the lower interface of the geotextile with the clay foundation, this study has shown that the use of non woven geotextiles allowed the mobilization of an adherence comparable to the internal friction of the cohesive foundation material; with woven geotextiles, the relative friction felt to 60%. Such results have already presented in the literature (5,6) This difference however, can be attributed to the texture of the contact along the induced failure plane: the smooth surface of the woven does not permit particules interpenetration and the creation of strong adhesion between the soil and the synthetic.

Finally when interface friction is a controlling factor in the choice of a reinforcing material and when cohesive materials are involved either as fill or as foundation soil, the non woven offers superior qualifications because the adherence values are higher and in the case that the loads are applied at a fast rate, it can convey water coming out of the soil from consolidation, a non-existent possibility with woven. However, if non-cohesive materials are involved and if tensile strength controls the design, the use of a woven can appear justified, because it is many times stiffer than the needle-punched and its tensile capacity (ratio of the tensile strength to the mass per unit weight) is the double of that of non wovens.

ACKNOWLEDGEMENTS

The authors gratefully acknowledge the financial support from the Gouvernement du Québec (grant FCAR-EQ-2151), from the Gouvernement du Sénégal and from the World Bank.

REFERENCES

- (1) AKBER, S.Z., HAMMAMJI, J. and LAFLEUR, J. "Frictional Characteristics of Geomembranes, Geotextiles and Geomembrane- Geotextiles Composites". Proceedings of the 2nd Canadian Symposium on Geotextiles and Geomembranes, Edmonton, Can. 1985, pp. 209-217.
- (2) EIGENBROD, K.D. and LOCKER, J.G. "Determination of Friction Values for the Design of Side Slopes Lined or Protected with Geofabrics." Proc. of the Annual Conference of the Canadian Society for Civil Engineering, Saskatoon, Can. 1985, pp. 281-300.
- (3) BIDIGASU, M.D. Laterite Soil Engineering - Pedogenesis and Engineering Principles. Elsevier, Amsterdam, 1976, 554 p.
- (4) JEWELL, R.A. "A Limit Equilibrium Design Method for Reinforced Embankments." Proc. of the 2nd Int. Conference on Geotextiles. Las Vegas, NV, 1982, Vol 2, pp. 671-676.
- (5) MARTIN, J.P., KOERNER, R.M. and WHITTY, S.E. "Experimental Friction Evaluation of Slippage between Geomembranes, Geotextiles and Soils". Proc. International Conf. on Geomembranes, Denver, Colo. 1984, Vol I, pp. 191-196.
- (6) MYLES, B. "Assessment of Soil Fabric Friction by means of Shear". Proc. Second International Conference on Geotextiles, Las Vegas NV, 1982, pp.787-791.
- (7) ROWE, R.K., MAC LEAN, M.D. and SODERMAN, K.L. "Analysis of a Geotextile-Reinforced Embankment Constructed on Peat". Canadian Geotechnical Journal, 1984, Vol 21. No. 3, pp. 563-576.
- (8) ROWE, R.K. and SODERMAN, K.L. "An Approximate Method for Estimating the Stability of Geotextile-Reinforced Embankments." Canadian Geotechnical Journal, 1985, Vol 22, No. 3, pp. 392-398

GUIDO, V.A. and KNUEPPEL, J.D.
The Cooper Union School of Engineering, U.S.A.
SWEENEY, M.A.
Mueser Rutledge Consulting Engineers, U.S.A.

Plate Loading Tests on Geogrid-Reinforced Earth Slabs

SYNOPSIS

Presented herein is a comparison of the results of laboratory model plate loading tests used to study the bearing capacity of geogrid reinforced earth slabs. A number of different parameters will affect the bearing capacity of a reinforced earth slab. The parameters studied were: The pull-out resistance between the geogrid and the soil, the number of layers of geogrids, the width size of a square sheet of geogrid, depth below the plate of the first layer of geogrid, the vertical spacing of the layers, the tensile strength of the geogrid, and the aperture size of the geogrid. For the tests performed, the bearing capacity of geogrid-reinforced earth slabs increased by a factor between two and three. After an optimum number of layers or width of reinforcement the bearing capacity was largest for those geogrid-reinforced earth slabs where the first layer was closest to the footing and the spacing between the layers was the smallest. Aperture size and reinforcement tensile strength must be looked at simultaneously.

INTRODUCTION

Since soil has very low tensile resistance an effective means of reinforcing it is the inclusion of tension-resistant members. This additional tensile strength, however, is only available to the soil if an effective bond between the soil and reinforcement is formed. Bond may be achieved either through friction or interlock at the soil-reinforcement interface. This paper will investigate the reinforcing capabilities of polymer grids (which achieve bond through interlock at the soil-grid interface), namely, their effect on the bearing capacity of earth slabs.

ment and soil. Series A and Series B tests used square stiffened plexiglass and wooden boxes, respectively. Each box was 1.22 m (48 in.) wide and 0.92 m (36 in.) deep. A total of 80 plate loading tests were performed, 55 from Series A and 25 from Series B. The polymer grids used were Tensar SS1, SS2, and SS3 geogrids. Series A tests were performed using either Tensar SS1 or SS2 geogrids as the reinforcement and Series B tests used only Tensar SS3 geogrids as the reinforcement.

LABORATORY MODEL

Two series of laboratory model plate loading tests were performed, each using a different box to contain the reinforcement.

The following information on Tensar geogrids was obtained from the manufacturer's literature. Tensar geogrids are high tensile strength polymer grids formed from polyolefine resins to produce consistent and chemically inert engineering materials, suitable for long-term reinforcement. The

grid geometry supplies an interlocking and supporting mechanism for both granular and cohesive soils, while the polymer construction of the reinforcement promotes in-soil durability. The junction strength and continuous structure characteristic of Tensar geogrids allows the soil bearing forces to be distributed throughout the grid structure. Tensar geogrids can be used over a wide temperature range, retain their properties despite exposure to ultraviolet light for extended periods of time (stabilized with carbon black), and are resistant to the corrosive environment found in some naturally occurring soils. Uniaxially oriented geogrids are stretched in one direction only, while biaxially oriented geogrids are stretched in mutually perpendicular directions. The former are typically used for retaining structures and steep slopes where strength in one direction is required, while the latter are typically used in roadway projects where strength in two directions is needed.

Beneath a footing strength would be required in two directions, necessitating the use of biaxially oriented geogrids. The Tensar SS1, SS2, and SS3 geogrids used were biaxially oriented geogrids. See Table I and Fig. 1 for typical dimensions and mechanical properties of the aforementioned geogrids.

The sand used in both the series A and Series B tests was a uniformly graded sand (SP). The properties of this sand can be found in Table II. Depending on the vertical spacing between the layers of reinforcement the sand was placed in 25 mm (1 in.) to 76 mm (3 in.) lifts. Subsequent model plate loading tests with a different type of reinforcement investigated the effect of relative density on the bearing capacity of a reinforced earth slab. It was found that the most dramatic increases in bearing capacity for reinforced earth slabs occurred at relative densities between 50 and 70 percent. Therefore, the use of a sand, throughout both the Series A and Series B tests, at a relative density of 55 percent dramatically demonstrated the benefits to be

derived from the use of Tensar geogrids to increase the bearing capacity of earth slabs.

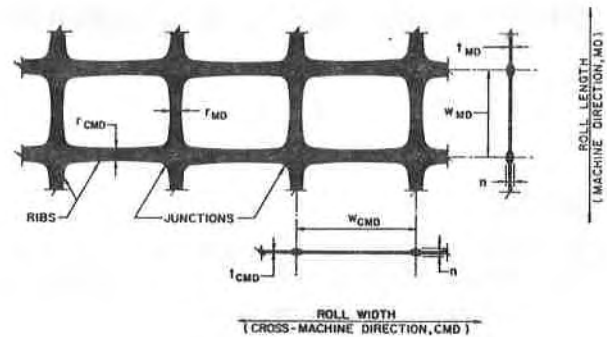


Fig. 1 Geometry of Tensar Geogrids used in this study.

The plate used for both the series A and Series B tests was square with a 305 mm (12 in.) width. It consisted of a 25 mm (1 in.) thick piece of exterior grade plywood stiffened by 3mm (0.125 in.) thick steel plates at the top and bottom. The vertical load was applied to the plate through the use of a 223 kN (25 ton) capacity hydraulic cylinder and hand pump. The load applied in small increments was recorded on an 89 kN (10 ton) capacity load ring, and the resulting plate displacements recorded by two dial gages placed at the corners along a diagonal through the center of the plate. These dial gages had a 51 mm (2 in.) capacity with a 25 μ m (0.001 in.) sensitivity. For both the Series A and Series B tests performed the differential settlement recorded by these gages was very small. The geogrids were used in square sheets placed concentrically under the square plate. To insure that damaged reinforcement was not being used no sheet of

TABLE I

Properties of the Tensar Geogrids Used in the Model Tests

Geogrid	Dimension of Geogrid				Characteristic Tensile Strength*	
	n ⁺ (mm)	t ⁺ (mm)	r ⁺ (mm)	w ⁺ (mm)	Actual ⁺ (kN/m)	Spec ⁺ (kN/m)
SS1	2.5	0.8/0.8	2.8/2.5	28/38	16.8/24.8	12.5/20.9
SS2	4.1	1.3/1.3	2.8/2.5	28/38	23.0/36.8	17.9/32.0
SS3	4.3	1.0/0.8	4.3/4.3	46/71	17.8/28.7	16.0/27.3

+ The numbers above the line are for the machine direction (along the roll length) and the numbers below the line are for the cross-machine direction along the roll width).

* Samples 3 junctions long and 1 rib wide, were extended at a constant rate of 5.1 cm/min, at a temperature of 20°C±1°C. For the column headed "Actual" this is the characteristic tensile strength for the actual geogrid as tested by the Tensar Corporation in Atlanta, Georgia. The column headed "Spec" is the characteristic tensile strength for a specified geogrid as given in the Tensar literature.

geogrid was used more than once. In all 80 plate loading tests no sheet of geogrid was ever found to have ruptured during testing. The geometry of the test model is shown in Fig. 2. The authors feel that since the plan area of the test box was sixteen times that of the loaded plate and the depth 75% of its width, boundary effects were not reflected in the results obtained. The sides of the box did not interfere with the development of the failure surfaces, especially with the sand at a relative density of 55%. The size of the box was arrived at by trial.

TEST RESULTS

As was indicated previously geogrids transfer stress from the soil to the reinforcement through bearing at the soil to mesh cross bar interface. An efficient anchoring effect is achieved through the interlocking of the soil through the apertures of the geogrid, mobilizing the high tensile strength of the grid as loads are applied. In order to determine the failure mechanisms of the Tensar geogrids a series of Pull-Out Tests were performed.

TABLE II

Properties of the Sand Used in the Model Tests

Uniformity Coefficient, Cu	1.90
Coefficient of Concavity, Cc	1.23
Effective Size, D ₁₀ , mm	0.086
Specific Gravity	2.66
Minimum Dry Unit Weight, γ _{dmin} , kN/m ³	13.10
Maximum Dry Unit Weight, γ _{dmax} , kN/m ³	15.65
Dry Unit Weight, γ _d , kN/m ³	14.39
Relative Density, D _r , %	55
Angle of Internal Friction, φ, °	37

PULL-OUT TESTS

Two series of pull-out tests were performed. Series C contained 35 pull-out tests using the Tensar SS1 and SS2 geogrids and the soil in Table II, while Series D contained 15 pull-out tests using the Tensar SS3 geogrids and the soil in Table II. Square split shear boxes were used with a slit located at the mid depth of the boxes. Because of the very large apertures in the SS3 geogrids as compared to those in the SS1 and SS2 geogrids the same shear box could not be utilized to perform the pull-out tests on all the geogrids tested. In addition, the clamp used on the SS1 and SS2 geogrids to pull them from the shear box was different from the one used on the SS3 geogrids. In Table III is found a comparison of the two shear boxes used.

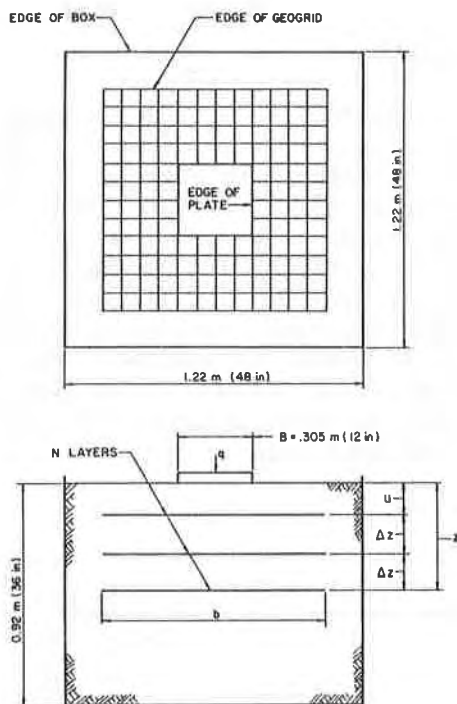


Fig. 2 Geometry of the Test Model.

The geogrids were pulled out of the shear boxes along the roll length (machine direction) which is the weaker direction. The range of normal stresses used were from 2 kPa (42 psf) to 48 kPa (1000 psf), while two relative densities were investigated, 55% and 75%. A rate of strain of 0.033%/s of the first section of embedded ribs was used.

In Fig. 3 is shown the relationship between the applied normal load, σ_n , and the average maximum shear stress mobilized, τ , which is equal to the maximum pull-out force divided by twice the embedded area of the reinforcement. The geometrically similar SS1 and SS2 geogrids show similar and superior values of maximum shear stress than those for the SS3 geogrid. For both the SS1 and SS2 geogrids, the higher soil density improved the interlocking effect of the soil grains around the geogrid and a higher maximum shear stress was obtained. For the two relative densities investigated, the maximum shear stress mobilized by the SS3 geogrid was independent of the relative density.

Two modes of failure were observed: slippage of the grid from the soil and tension failure of the grid, the latter being observed at high normal stress levels. The horizontal portions of the curves for both the SS1 and SS2 geogrids in Fig. 3 were created by premature grid breakage. It is the authors' belief that the clamp used to pull these grids created stress concentrations, resulting in breakage of the grid structure at pull-out forces well below the tensile capacities of the SS1 and SS2 geogrids. For example, the greatest value of maximum shear stress mobilized by the SS2 geogrid just prior to breakage was 21.6 kPa (450 psf) at an applied normal stress of approximately 36.4 kPa (760 psf) and a relative density of 75%. The corresponding pull-out force for this value of shear stress is 13.1 kN/m (900 lbs./ft.), a value significantly less than the 23.0 kN/m (1575 lbs./ft.) capacity of the geogrid in the direction of pull-out,

TABLE III

Comparison of Modified Shear Boxes Used on Series C and D Pull-Out Tests

	Series C	Series D
Inside Dimensions	305x305x205 mm	535x380x150 mm
Base Plate Material	Steel	Aluminum
Base Plate Dimensions	400x405x25 mm	660x510x13 mm
Normal Load Plate Material	Steel	Aluminum
Normal Load Plate Dimensions	305x305x19 mm	325x380x13 mm
Thickness of Wooden Side Walls	50 mm	38 mm
Width of Slot	280 mm	520 mm
Approximate Number of Grid	63	49
Apertures within Box	(7 wide & 9 back)	(7 wide & 7 back)

see Table I. Had premature breakage not occurred, the SS1 and SS2 geogrids would have shown even larger values of maximum shear stress. The results clearly show the SS3 to possess a weak bonding capability with the sand tested relative to the bonding capabilities of the SS1 and SS2 geogrids. The larger aperture size and consequently lesser lateral bearing area of the SS3 geogrid was the cause of this poor bonding capability.

PLATE LOADING TESTS

In addition to the pull-out resistance between the geogrid and the soil, the effect of six other parameters on the bearing capacity of geogrid-reinforced earth slabs were investigated. They were:

- 1.) Number of layers of geogrid, N.
- 2.) Width size, b, of the square sheet of geogrid, expressed in dimensionless form as b/B, where B is the width of the footing.
- 3.) Depth below the footing of the first layer of geogrid u, expressed in dimensionless form as u/B.
- 4.) Vertical spacing of the layers of geogrid Δz, expressed in dimensionless form as Δz/B.
- 5.) and 6.) Tensile strength and aperture size of the geogrid. These two parameters must be considered simultaneously. By testing Tensar SS1, SS2, and SS3 geogrids the investigation of these two parameters is satisfied.

The Series A and Series B plate loading tests had an ultimate bearing pressure,

q_o for the unreinforced sand of 93.8 kPa (1,960 psf) and 98.7 kPa (2,960 psf), respectively at a settlement, of 21.3 mm (0.84 in.), or s/B of 0.07. This difference in ultimate bearing pressure, albeit only 5%, was due to the difference in the relative stiffnesses of the two boxes used. For convenience in expressing and comparing test data the term bearing capacity ratio (BCR) will be used:

$$BCR = q_r / q_o \quad (1)$$

where q_o is defined as above and q_r is the bearing pressure of the geogrid-reinforced sand at a settlement corresponding to the settlement at the ultimate bearing pressure for the unreinforced sand. By using the BCR to compare test results it is possible to compare the Series A and Series B plate loading tests, even though their ultimate bearing pressures in the unreinforced state are different, since all bearing pressures will be relative. Typical load-settlement curves are shown in Fig. 4 for different values of Δz/B.

Vesic (7) proposed three possible failure modes can develop in soil upon application of load to a plate at the surface of a soil medium: general shear failure, local shear failure and punching shear failure. General shear failure will develop in very dense soil with the failure surface extending completely to the soil surface and exhibiting large surface heaving. Local shear failure will develop in soils of medium compaction

with the failure surface extending to the soil surface and exhibiting small surface heaving; upon failure the plate will continue to displace with very little increase in load. Punching shear failure will develop in loose soils without extension of the failure surface to the soil surface, and beyond the ultimate failure sand from the test model the geogrid reinforcement directly below the plate was visibly deflected downward, indicating a punching type failure mode. The above observations were true for all plate loading tests performed.

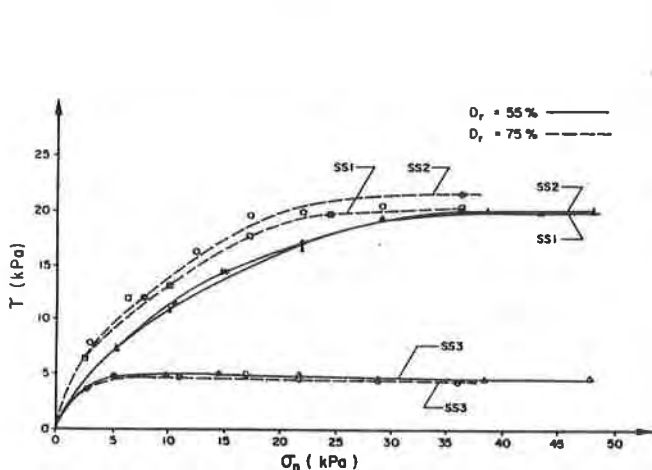


Fig. 3 Variation of Average Maximum Shear Stress with Applied Normal Stress.

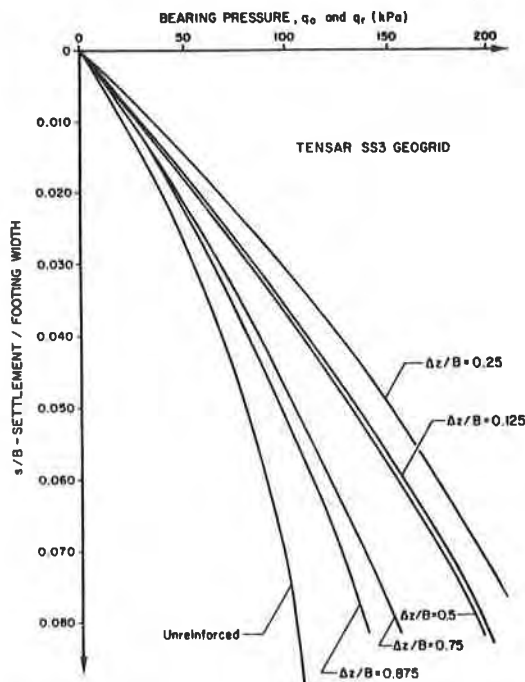


Fig. 4 Load-Settlement Curves for $u/B = 0.25, N=3$ and $b/B = 3.0$.

load an almost linear relationship exists between load and settlement. The load-settlement curve in Fig. 4 for the unreinforced sand at a $D_r=55\%$ (medium compact density) demonstrates a local shear failure mode; very little surface heaving was observed for this test. The remaining load-settlement curves in Fig. 4 for the geogrid-reinforced sand condition should exhibit a failure mode approaching general shear since the earth slab is more rigid, however, the presence of the geogrid-reinforcement interfere with the development of the failure surfaces not allowing them to reach the sand surface; no surface heaving was observed in these tests. These load-settlement curves have a shape typical of punching shear. Upon removal of

1. Number of Layers of Geogrid-Reinforcement

The variation of BCR with the number of layers of geogrid reinforcement is shown in Fig. 5 for the Tensar SS1 and SS2 geogrids. For both geogrids there is a steady increase in BCR with an increasing number of layers of geogrid-reinforcement up to an optimum value of $N=3$, after which no additional benefit was gained by increasing the number of layers. Similar results for different

reinforcing materials were observed by Binquet and Lee (2), Akinmusuru and Akinbolade (1), University of California, Davis (6), Guido et al (5). For $N=4$, the depth of the bottom layer of geogrid-reinforcement is at $1.25B$ indicating that all layers of geogrid-reinforcement should be placed within an effective depth ($z/B=1$).

geogrid yielded a BCR value 20% larger than the SS2 geogrid, this will be discussed subsequently.

Beneath the plate there exists a zone of soil extension. Only that portion of the geogrid-reinforcement within this zone will have its tensile strength effectively mobilized. Geogrid-reinforcement area beyond this zone will be in compression and serve only as anchorage. For b/B values greater than 2.5 a significant portion of the geogrid-reinforcement area functioned ineffectively, being neither in the zones of soil extension or anchorage; the grid did nothing.

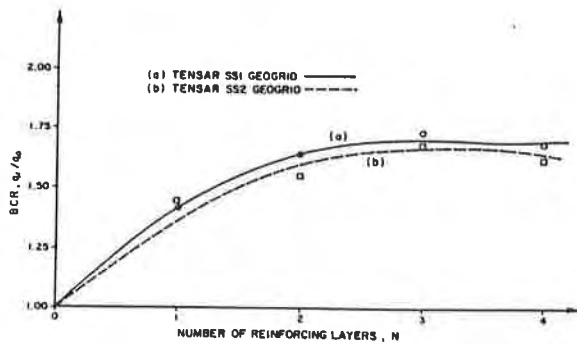


Fig. 5 BCR Variation with Number of Reinforcing Layers, $u/B = 0.5$, $\Delta z/B = 0.25$ and $b/B = 3.0$.

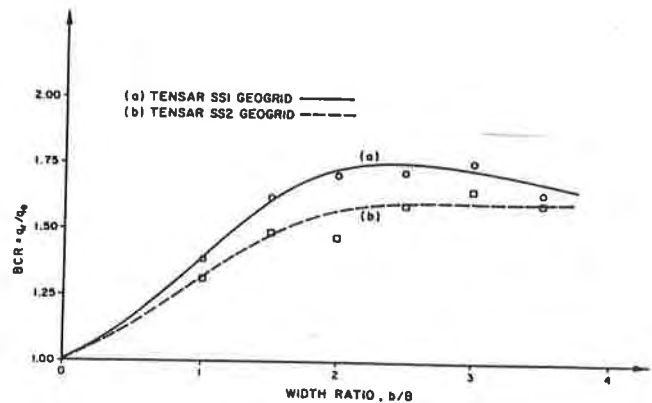


Fig. 6 BCR Variation with Width Ratio, $u/B=0.5$, $\Delta z/B=0.25$ and $N=3$.

2. Width Size of a Square Sheet of Geogrid-Reinforcement

In Fig. 6 is shown the variation of BCR with the width ratio b/B for the Tensar SS1 and SS2 geogrids. For both geogrids, there was a steady increase in the BCR with an increase in b/B up to a value of approximately 2.5 after which additional embedded area of reinforcement was ineffective. Similar results have been observed by Fragasy and Lawton (4) and Guido et al (5) for different reinforcing materials. At a value of $b/B=2.5$ the SS1

3. Depth of Top Layer of Geogrid-Reinforcement

In Fig. 7 is shown the variation of BCR with u/B for the Tensar SS1, SS2, and SS3 geogrids. For all three geogrids, the BCR increases with decreasing u/B , however, the trend observed for the SS1 and SS2 geogrids was not the same as that

for the SS3 geogrid. Akinmusuru and Akinbolade (1) and Guido et al (5) have observed similar results with different reinforcing materials. For the SS1 and SS2 geogrids there was a steady increase in BCR with decreasing u/B from a value of u/B of approximately 1.0, before which there was essentially no increase in BCR with decreasing u/B . This would substantiate the idea that placement of geogrid reinforcement beyond an effective depth $u/B=z/B=1$ is not beneficial. The SS3 geogrid exhibited three regions: The BCR steadily increases as u/B decreases from 1.25 to 0.75, increases rapidly as u/B decreases to 0.5, and increases only slightly as u/B decreases to 0.25.

and b/B large). For series A and B plate loading tests with u/B values greater than 0.67 ($u/B=0.75, 1.00, \text{ and } 1.25$), it can be concluded that the geogrid-reinforcement improved the ultimate bearing capacity and settlement response by creating a rigid boundary into which the shear zone would not penetrate. For Series A and B plate loading tests with u/B values less than 0.67 ($u/B=0.5 \text{ and } 0.25$), the geogrid-reinforcement performed more efficiently by directly interfering with the shear surfaces. Since breakage of the reinforcement was never encountered, it can be concluded that the failure mode for reinforcement schemes with u/B values of less than 0.67 involved pull-out.

4. Vertical Spacing of the Layers of Geogrid-Reinforcement

The variation of BCR with $\Delta z/B$ is shown in Fig. 8 for the Tensar SS1, SS2, and SS3 geogrids. The SS1 and SS2 geogrids exhibited similar trends with a steady increase in BCR with decreasing $\Delta z/B$, indicating that as the density of the reinforcement increases ($\Delta z/B$ decreases) the BCR increases. For the SS3 geogrid two regions are exhibited: The BCR increases steadily as $\Delta z/B$ decreases from 0.875 to 0.25, after which the BCR decreases slightly as $\Delta z/B$ is further reduced to value of 0.125; indicating that below a certain spacing interference occurred, with the consequence that the increase in shear strength provided by each layer of geogrid-reinforcement decreased. The SS1 geogrid had a BCR value approximately 73% greater than the SS3 geogrid at $\Delta z/B=0.125$, the reason for this will be discussed subsequently. Similar trends were observed by Akinmusuru and Akinbolade (1) and Guido et al (5) for different reinforcing materials.

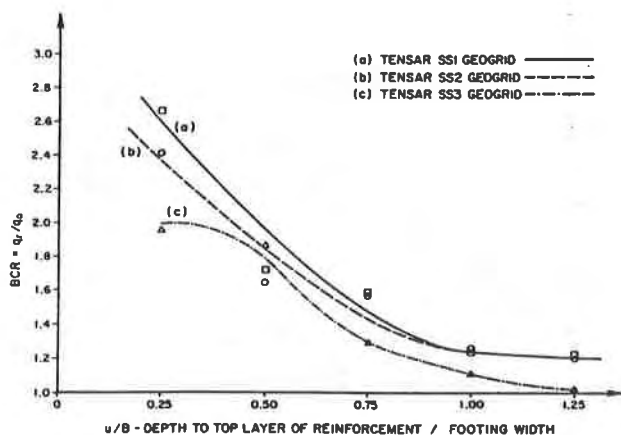


Fig. 7 BCR Variation with Depth to Top Layer, $\Delta z/B=0.25$, $N=3$ and $b/B=3.0$.

Binquet and Lee (3) have indicated that three possible modes of bearing capacity failure exist for reinforced earth slabs, depending on the arrangement and strength of the reinforcement these three modes involve soil shear above the reinforcement ($u/B > 0.67$), reinforcement pull-out ($u/B < 0.67$ and $N < 2$ or 3, or b/B small) and reinforcement breakage ($u/B < 0.67$, $N > 3$,

5. and 6. Tensile Strength and Aperture Size of the Geogrid-Reinforcement

To discuss the effects of tensile strength and aperture size of the geogrid-reinforcement on the bearing capacity of geogrid-reinforced earth slabs, the

curves for the SS1 and SS2 geogrids in Figs. 5 to 8 will be discussed concurrently and then the curves for the SS1 and SS3 geogrids in Figs. 7 and 8 will be discussed concurrently. It seems the SS1 geogrid was the most effective for the particular sand and relative density used.

In contrast, the sand particles were more apt to pass around the extremely rigid (stiff) structure of the SS2 geogrid. It would appear that the properties of the sand were more compatible with the properties of the SS1 geogrid. The high stiffness of the SS2 geogrid and the small particle sizes of the sand led to an earlier breakdown of the interlock based bond as the sand particles traveled around the rigid structure of the SS2 geogrid.

From Figs. 7 and 8 it can be seen that the SS1 geogrid yielded considerably higher BCR values than the SS3 geogrid. Although the SS3 geogrid has characteristic tensile strengths approximately 20% larger than the SS1 geogrid, see Table I, its aperture size is 3 times that of the SS1 geogrid. Grid geometry was a major factor in the superior performance of the SS1 geogrid over the SS3 geogrid. The considerably larger aperture size of the SS3 geogrid consequently provided less lateral bearing area for the sand. In fact, there were approximately four SS1 geogrid apertures for every one SS3 geogrid aperture. Thus, for the plate loading tests conducted the SS3 geogrid established less bonds with the sand than did the SS1 geogrid. Pull-out (bond breakdown) developed quickly for the SS3 geogrid in the direction containing the larger aperture dimension (cross-machine direction, CMD), see Fig. 3. The geogrid largely deflected in this direction of greater tensile strength but lesser lateral bearing area. Akinmusuru and Akinbolade (1) observed that the BCR increased as the linear density of reinforcement (LDR) increased, where

$$\text{LDR} = \frac{\text{width of reinforcement}}{\text{spacing of reinforcement}} \times 100\% \quad (2)$$

the LDR can vary from 0% (unreinforced) to 100%. This would indicate smaller aperture sizes would yield higher BCR values; as was demonstrated above. The aperture size is limited to how small it can get, since the soil must be able to penetrate it in order to achieve the desired interlocking between the soil and grid.

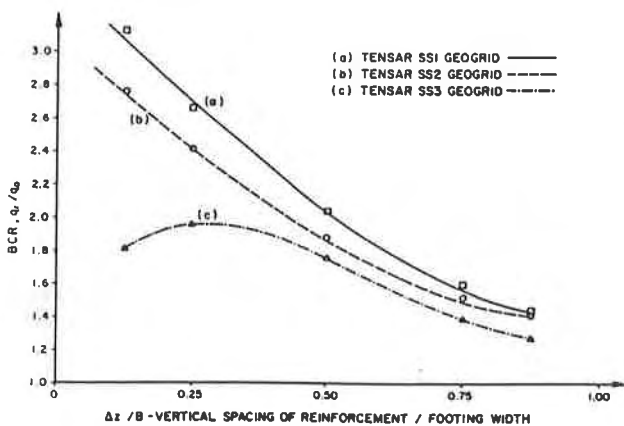


Fig. 8 BCR Variation with Vertical Spacing of Reinforcement, $u/B=0.25$, $N=3$ and $b/B=3.0$.

In all cases the Tensar SS1 geogrid yielded higher BCR values than the Tensar SS2 geogrid despite its considerably lower characteristic tensile strength and lesser thickness, see Table I. Geogrid geometry cannot be used to explain the superior performance of the SS1 geogrid over the SS2 geogrid since the two geogrids are geometrically similar except for thickness, see Table I. Thus, it can be concluded that for the test models used, soil strain caused geogrid-reinforcement strain more efficiently in an SS1 geogrid-reinforced earth slab. The sand particles originally in contact with a layer of SS1 geogrid-reinforcement remained so under load and high tensile strength was deve-

CONCLUSIONS

Based on the test results presented here, it would appear that the SS3 geogrid is an inefficient means of reinforcing a sand subgrade for a shallow foundation. Rather, the SS1 geogrid should be used for this application since its properties are more compatible with sand and its aperture size provides considerable lateral bearing area. When optimally placed in their respective test models, SS1 geogrid-reinforcement increased the ultimate bearing capacity of unreinforced sand by a factor of 3, compared to a factor of 2 for SS3 geogrid-reinforcement. When the results of the Series A and B plate loading tests and the Series C and D pull-out tests are considered together, it is apparent that sand-geogrid bond performance is greatly dependent upon the amount of geogrid lateral bearing area available to the sand.

General practice and design of reinforced concrete suggests the use of many smaller reinforcing bars well distributed over the tensile cross-sectional zone of a concrete member. It is believed that this will lead to a better distribution of the tensile stresses to the reinforcement rather than one or two larger rods supplying the needed area of steel. The authors believe this to be the case with reinforced earth slabs as long as the aperture size is much much larger than the soil particle, which was the case with the sand used and the SS3 geogrid. It is suggested that instead of using fewer stronger (stiffer) ribs (such as the SS3 geogrid provides), the use of many weaker ribs (such as the SS1 geogrid provides) will lead to a better distribution of the tensile stress as supplied to the geogrid reinforcement. As the particle size approaches the aperture size, a larger aperture should be used.

REFERENCES

- (1) Akinmusuru, J.O. and Akinbolade, J.A., "Stability of loaded footings on reinforced soil", ASCE Journal of Geotechnical Engineering, 1981, 107 (GT6), p.p. 819-827.

- (2) Binquet, J. and Lee, K.L., "Bearing capacity tests on reinforced earth slabs", ASCE Journal of Geotechnical Engineering, 1975, 101(GT12), p.p. 1241-1255.
- (3) Binquet, J. and Lee, K.L., "Bearing capacity analysis of reinforced earth slabs", ASCE Journal of Geotechnical Engineering, 1975, 101(GT12), p.p. 1257-1276.
- (4) Fragaszy, R.J. and Lawton, E., "Bearing capacity of reinforced sand subgrades", ASCE Journal of Geotechnical Engineering, 1984, 110(GT10), p.p. 1500-1507.
- (5) Guido, V. A., Biesiadecki, G.L. and Sullivan, M.J., "Bearing capacity of a geotextile-reinforced foundation", Proceedings of Eleventh International Conference on Soil Mechanics and Foundation Engineering, San Francisco 1985, Vol. 3, p.p. 1777-1780.
- (6) University of California, Davis, "Plate bearing tests on Tensar SS1 Geogrid-reinforced granular base on weak clay subgrade", A Progress Report prepared by the Department of Civil Engineering for the Tensar Corporation 1984. (unpublished)
- (7) Vesic, A. S., "Analysis of ultimate loads of shallow foundations", ASCE Journal of the Soil Mechanics and Foundation Division, 1973, 99(SM1), p.p. 45-73.

BRAND, S.R.

Black and Veatch, U.S.A.

DUFFY, D.M.

Arizona State University, U.S.A.

Strength and Pullout Testing of Geogrids

Practicing geotechnical engineers have been quick to appreciate the advantages that geotextiles and geogrids can bring when their properties are compatible with project requirements and soil conditions. The engineer examining the potential application of geogrids to problems that require long term stability or where deformation must cease soon after loading, must understand the creep potential of geogrids. Geogrid creep, or the potential of the material to elongate with time, when subjected to a constant load, is a serious consideration if a structure or soil mass is mobilizing sustained tensile stresses in the geogrid. Besides the concern for creep, the engineer is often concerned with staged construction which may require increased tensile stresses to be induced in the geogrid after the initial phase of construction has reached equilibrium. How tensile strength has changed after small creep deformations is a question that would have to be answered.

If the maximum application of geogrids is to occur, a better understanding of tensile strength and creep characteristics of geogrids must be developed. In addition to better understanding the physical properties of geogrids, a paucity of information exists on pullout resistance of geogrids in clay soils.

This research effort focused on geogrid: tensile strength; creep characteristics; tensile strength after creep has occurred; and pullout resistance in low moisture content expansive soils.

PREVIOUS WORK

Research to date has concentrated on the interaction between geogrids and granular soils. This is primarily due to the almost exclusive use of granular backfill in reinforced soil embankments. The rather stable granular soil properties with time, and changing moisture contents, have made them the backfill material of choice during the early life of reinforced earth and geogrid applications.

A number of investigators have studied the sand-geogrid interaction. A comparison study was initiated by Ingold (1) to investigate the variability in test results as a function of the test method. Ingold concluded that the pullout test is a more realistic model of geogrid performance where field pullout resistance is the criterion governing design.

Jewell, et al. (2) demonstrated that both short and long term shear strength of cohesive soil may be increased by geogrid reinforcement. It was also found that geogrid reinforcement produced higher failure strains than for non-reinforced clay in horizontal shear boxes. Several structures have been built in Great Britain

using reinforced clay backfill, Jones (3). To supplement the British experience there exists a need for additional information on how geogrid reinforcement interacts with and modifies cohesive soil behavior.

Manufacturer's recommended design stress levels for geogrid reinforced embankments is generally less than 40 percent of maximum strength. The primary reason to restrict the design stresses to a rather low level is to minimize creep or continued deformation of the geogrid. Additional research studying the effects of higher stress levels on the tensile strength and elastic properties of geogrids is necessary.

EXPERIMENTAL WORK

The experimental work was conducted in the laboratories of Arizona State University. Tensile strength, creep characteristics, strength after creep, pullout in clay backfill, and comparison of geogrid anchoring techniques were examined in the research program. The Tensar Corporation, Morrow, GA, and American Tenax, Ashtabula, OH, provided geogrids for the testing. Tensar supplied the SS2, a polypropylene grid with a mass per unit area of 0.3 kg/m^2 , and the SR2 and SR3 grids made with high density polyethylene of 0.85 kg/m^2 and 1.22 kg/m^2 mass per unit area respectively. Tenax provided the TT1 and TT2 grids, which are composed of high density polyethylene with mass per unit area of 0.79 kg/m^2 and 0.88 kg/m^2 respectively.

In order to develop maximum tensile stresses within the geogrids without imposing significant end effects, special clamps were fabricated to grip the geogrids during all phases of the testing. These clamps were designed to insure that stress concentrations were minimized at the point of "grabbing" the geogrid. A Riehle Model No. KA-120 testing machine was used for all testing. Geogrid samples were placed in a clamp at each end and slid into the grooves of the load cell assembly. Deformations were measured with an LVDT. Triplicate samples of each of five types of geogrids were tested.

Constant-rate-of-strain tensile tests on the SS2, SR2, SR3, TT1, and TT2 geogrids yielded load deformation data shown on Figure 1. A strain rate of 2 percent per minute was selected and a laboratory temperature of 26°C was maintained during the tensile testing. Each curve on Figure 1 represents the mean values of three replicate tests. The SR2 and SR3 geogrids were stronger than the other materials and developed smaller deformations prior to failure. The smaller deformations prior to failure, however, give little evidence that the failure state is approaching. The SS2, TT1, and TT2, while developing a lower peak strength, displayed large deformations that enable the onset of failure to be recognized.

The value of the information presented in Figure 1 is, therefore, not that particular products have different tensile strengths, but that large differences in deformation prior to reaching failure can result. Considerable differences in peak strength values and strain at failure can result when these materials are tested at different temperatures, strain rates, and clamping arrangements, Netlon Ltd. (4). McGown et al. (5) provide temperature and strain rate adjustment relationships for the Tensar products.

In order to investigate the geogrid properties due to sustained loading, a series of creep tests were performed on the same type of geogrids selected for the tensile testing. The testing was performed at three different stress levels. This

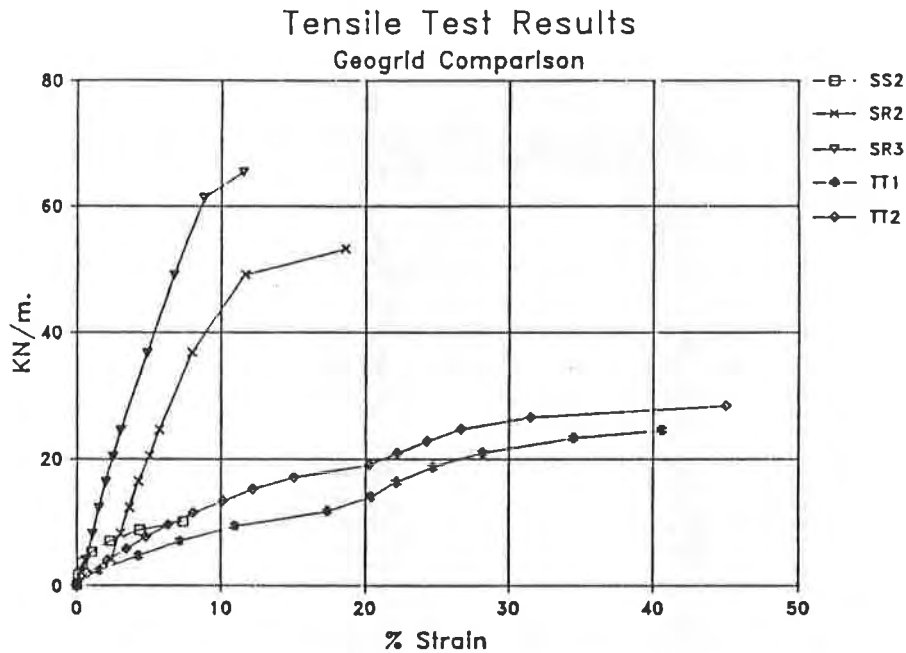


Figure 1. Tensile Strength of Geogrids

creep testing was conducted at 40, 50, and 60 percent of maximum load levels provided on Figure 1. The load was applied using dead weights to insure that the load remained constant during the duration of the test period. The test temperature was maintained at 23°C.

Once samples were cut to predetermined lengths they were placed in the clamps and initial sample lengths were established. The samples were then loaded by a dead weight hanger system, Figure 2. Deformations were measured at regular intervals during the creep portion of the test. When sample deformations were less than 0.01 mm per 24 hour period, the weight was removed and the "rebound" deformations measured. Sample strains were separated into recoverable and irrecoverable strain.

To determine the effects of sustained loading on the tensile behavior of the geogrids, tensile tests were performed on all creep samples after loading. Of particular interest were the tensile load and strains at failure which were compared to the tensile test results on specimens with no creep loading history.

The specimen performance at the 40 percent level is provided on Figure 3. It is apparent that at or below stress levels of 40 percent, and at laboratory temperatures of approximately 23°C, the geogrids reach essential equilibrium after 7 to 15 percent strain.

The geogrid response to sustained loading at 50 percent of the failure load is shown on Figure 4. At this higher stress level the deformations increase to the 12 to 25 percent range before apparent equilibrium is reached. Of the specimens tested, only TT1 provides an indication that deformation will continue if the test duration had been longer. McGown et al. (4) noticed creep continuing for SR2 and SS2 materials when the load levels were at 50 percent of maximum. Differences in test conditions, particularly temperature are believed to account for different creep observations.

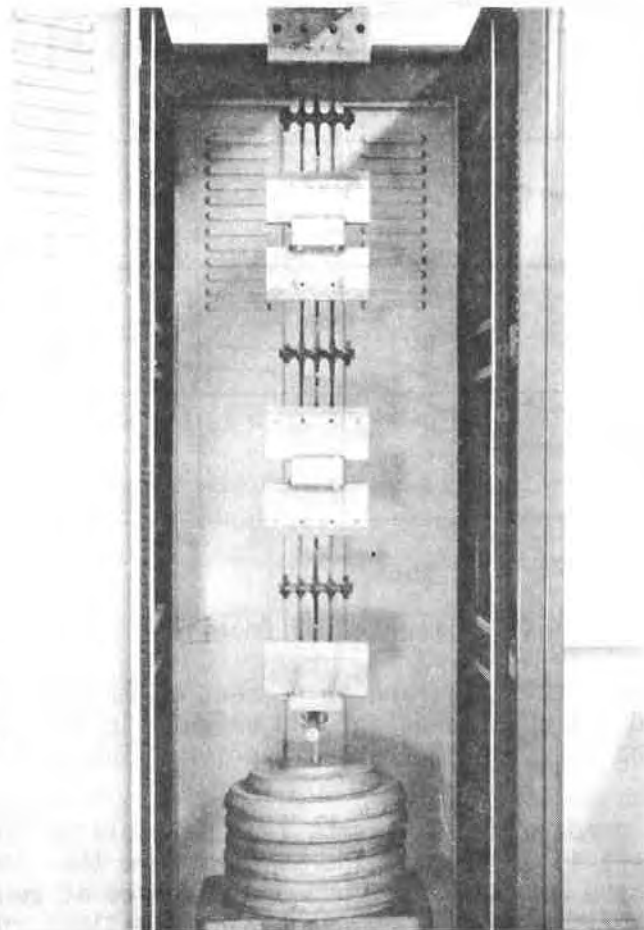


Figure 2. Creep Test Apparatus With Test in Progress

At the 60 percent loading level during the test period the strain had increased to a range of 19 to 31 percent, Figure 5. In addition to the large deformations, three of the five specimens were deforming at such a rate that it was apparent that failure was approaching.

The specimens were not allowed to deform to failure in order to examine the relative amounts of permanent versus recoverable strain at the completion of the creep test. At the completion of the sustained loading period the load was removed and the specimens allowed to deform. At the end of a 48 hour period the specimen lengths were measured and irrecoverable strain defined as the amount of strain still remaining after the 24 hour period. The amount of irrecoverable strain observed ranged from 2 to 14 percent, Figure 6. The elastic strain was defined as the recoverable deformations divided by the initial specimen length. Table 1 presents the "elastic" strains observed for the test geogrids. There are appreciable amounts of recoverable strain possible when the geogrids are free to relax.

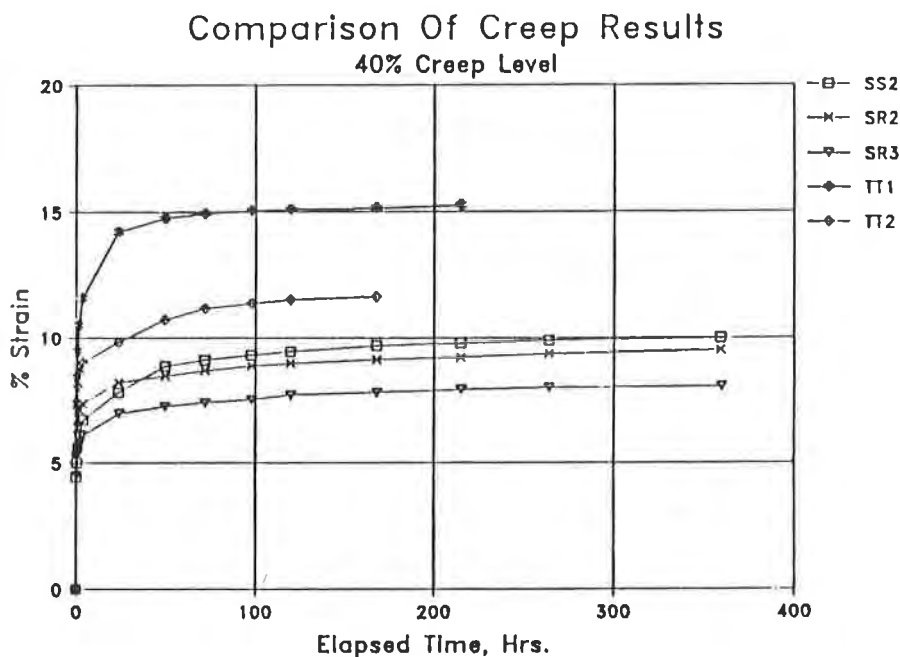


Figure 3. Creep Tensile Testing at 40 Percent of Maximum Tensile Load

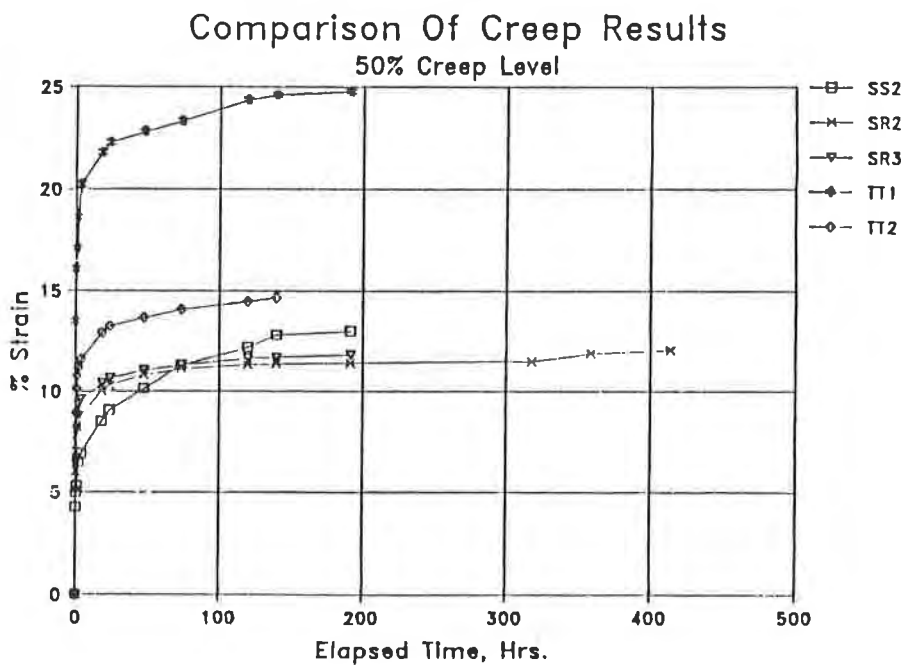


Figure 4. Creep Tensile Test at 50 Percent of Maximum Tensile Load

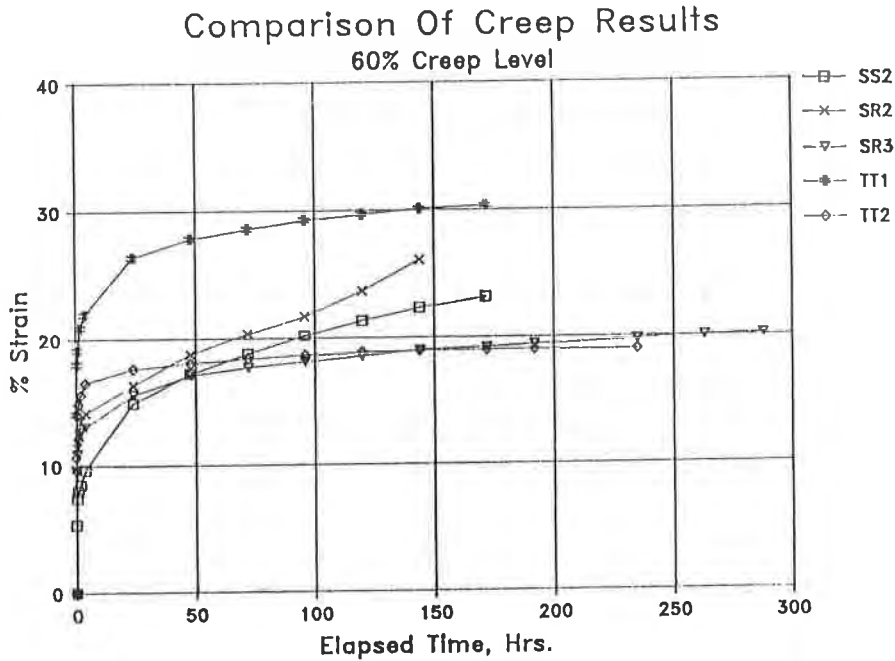


Figure 5. Creep Tensile Test at 60 Percent of Maximum Tensile Load

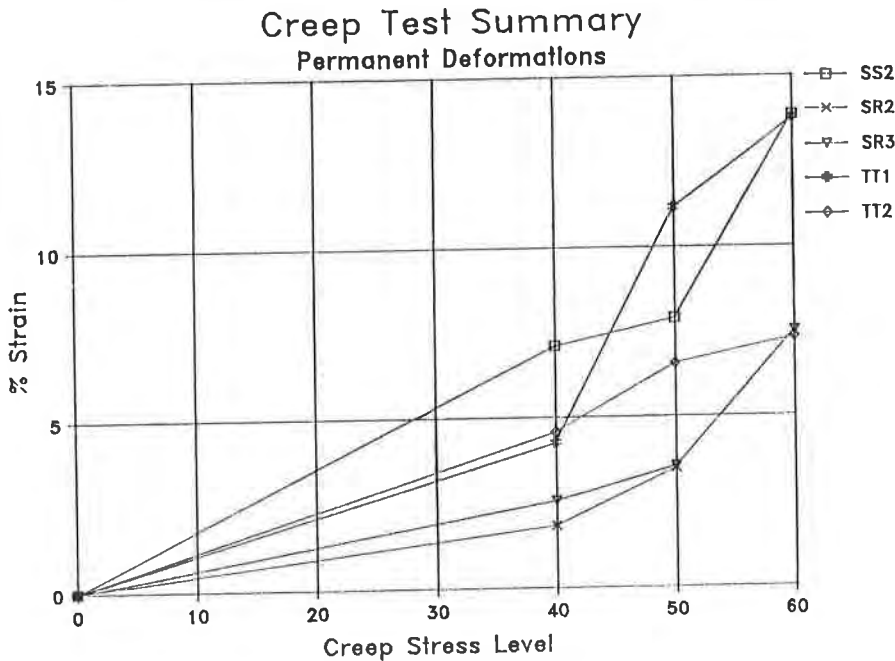


Figure 6. Creep Tensile Test Summary of Permanent Deformations Observed

Of interest was the strength that the geogrids possessed after being subjected to creep. The unloaded specimens were placed in the constant-rate-of-strain apparatus, and the initial length determined. The initial length included the irrecoverable deformations from the creep testing. The specimens were then loaded to failure at the same strain rate as was used in the tensile testing portion of the research. The results of this "strength after creep" testing are provided in Table 2.

Table 1. Summary of Elastic Strain Observed at the Completion of Creep Testing, in %

Specimen	Stress Level in % of Tensile Load		
	40	50	60
TT2	7.5	9.6	11.4
TT1	11.0	11.5	15.5
SR3	5.5	8.2	12.0
SR2	4.6	8.0	-
SS2	3.7	4.6	8.5

Table 2. Ratio of Tensile Strength After Creep Testing to the Maximum Tensile Strength Without Prior Loading

Specimen	No. of replicates	Creep Load as a Percent of Tensile Load		
		40%	50%	60%
SS2	2/3/2	0.98	1.19	1.13
SR2	2/2/-	1.24	1.26	-
SR3	3/3/3	1.08	1.09	0.65
TT1	3/3/3	1.31	1.33	1.19
TT2	3/3/3	1.17	1.12	1.09

There was a gain in tensile strength for twelve of the fourteen geogrid stress combinations tested after the creep testing portion of the program. Even for the SR3 samples, the after creep tensile strength was still 96 percent of the before creep strength. Only the SR3 specimens had a significant reduction in the average after creep strength and that was at the 60 percent stress level. There apparently continues to be an increase in tensile strength as the geogrids tested are stretched by an amount equal to the permanent deformations shown on Figure 6. The increase in strength following the creep testing is attributed to the increased orientation of the long-chain polymer molecules in the principal strain direction. The strain at failure, Figure 1, for the SR3 material suggests that differences in the manufacturing process may explain the differences between SR3 and SR2 specimens.

In order to examine the interaction between clays and geogrids, pullout tests were performed on four different types of geogrids, SR2, SR3, TT1, and SS2. A smectite

clay, Wyoming Bentonite LL = 515%, PI = 470% was used for the clay pullout tests. This potentially expansive clay was placed in a low moisture content state, approximately 10 percent, to simulate initial placement conditions.

An aluminum box with nominal dimensions of 30.5 cm per side with one open side and no top was fabricated for the clay pullout testing program. A hydraulic jack was used to apply a normal stress on one side of the clay and geogrid that was placed in the test box. The soil was placed around the 25.4 cm long by 25.4 cm wide geogrid specimen orientated vertically at a uniform density, 1.21 g/cc. The geogrid was then pulled from the soil at a constant deformation rate of approximately 0.01 cm/minute. Geogrid resistance to pullout was measured by load cell and displacements with an LVDT. The test apparatus is shown on Figure 7. Pullout tests were performed at normal stresses ranging from 11.97 KPa to 47.9 KPa. A total of four replicates was tested for each type of geogrid selected. A summary of pullout test results is provided by Figure 8. The pullout force versus normal force relationship is linear for each of the geogrids analyzed. In each test the deformations as the geogrid was pulled through the soil were large compared to the geogrid deformations observed for the same materials in the tensile test program.

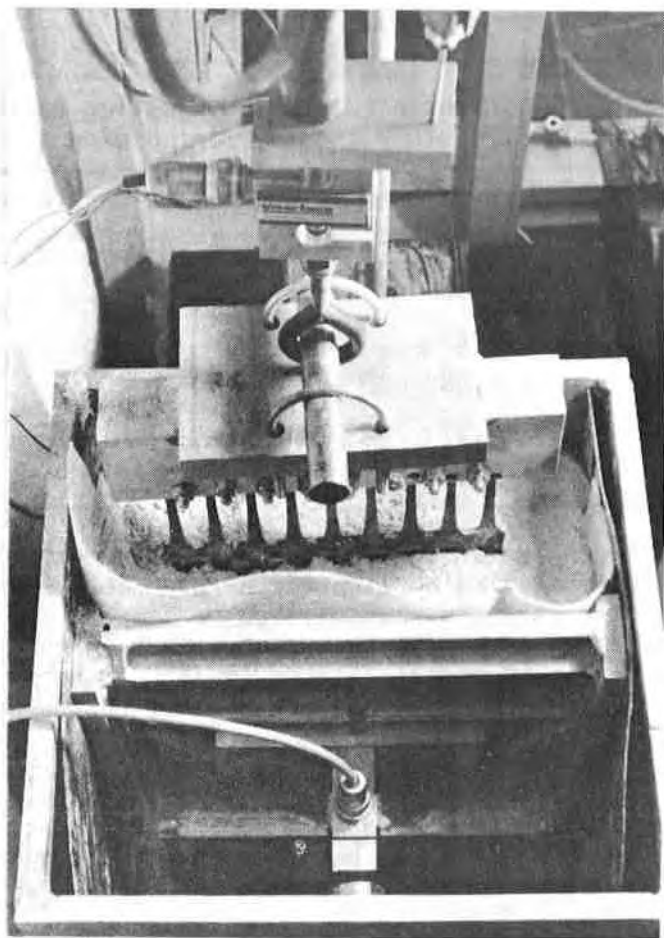


Figure 7. Pullout Test Apparatus

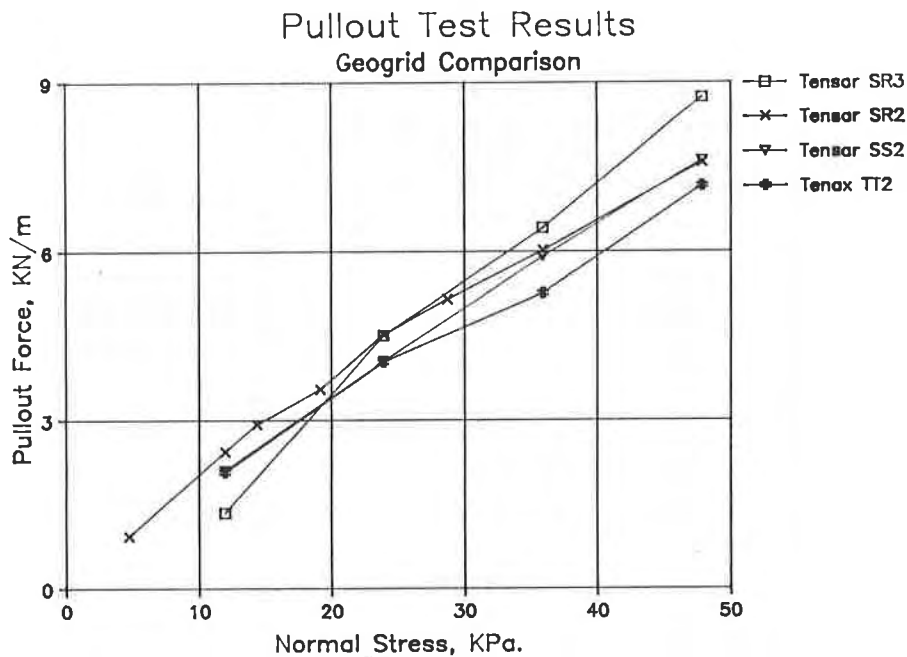


Figure 8. Summary of Pullout Test Results in Clay

The almost linear increase in pullout force with increasing normal stress is similar for each of the materials tested. The similar pullout resistance values indicates that it is the soil medium much more so than the geogrid which determines the pullout resistance that is available.

To assess the relationship between clay strength and the arching or stress transfer zone thickness around the geogrid, a sensitivity study was undertaken. Using the SR2 geogrids pullout testing was done while varying the thickness of clay on one side of the geogrid. As the thickness of clay increased the pullout force necessary to pull the geogrid through the clay decreased until a minimum force state was reached, Figure 9. For the SR2 material it is apparent that beyond 7.6 cm there is no significant transfer of stress from the geogrid to the platen applying the normal force. This technique would be used to establish the minimum spacing of geogrids in a soil embankment to maximize resistance to pullout.

In addition to pullout testing using clay soil, the same four geogrids were cast in concrete (approximate compressive strength of 10,300 KPa) and then pulled until tensile failure occurred. Typical load deformation curves for these tests were consistently greater for the samples tested in concrete compared to the clamped specimens, Table 3. The concrete imbedded specimens also had a more plastic load deformation curve than did their clamped counterparts.

All 16 specimens tested failed in tension, with none being pulled from the concrete, which had been allowed to cure approximately 10 days. The concrete anchored versus clamped tensile strength data provides insight into how important test conditions are to the tensile strength a specimen may deliver. Strength is clearly a function of test conditions which not only include deformation rate, laboratory

temperature, stress history, but method of "gripping" the specimen as well.

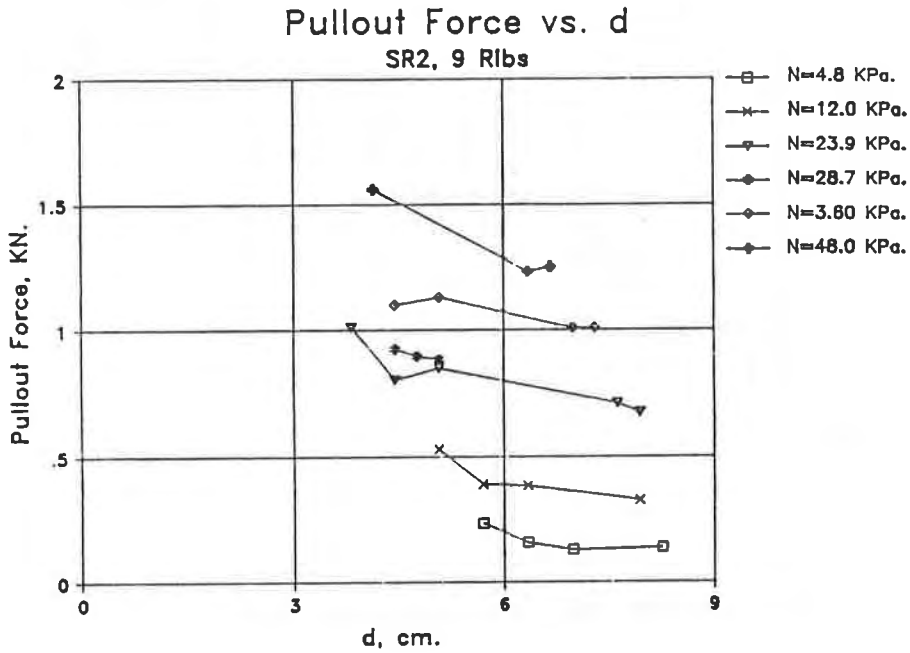


Figure 9. Summary of Pullout Force versus Thickness of Soil, d

Table 3. Comparison of Tensile Strength for Clamped and Concrete Embedded Specimens

Specimen	No. of Replicates	Clamped Strength (KN/m)	Concrete Strength (KN/m)
SS2	3/3	10.1	9.3
SR2	3/3	51.1	67.3
SR3	3/3	67.4	75.3
TT2	3/3	28.5	31.3

CONCLUSIONS

1. Tensile strength and magnitudes of strain to failure varies widely among geogrids and with test environmental conditions.
2. Creep deformations increase rapidly as the applied stress level increases above 50 percent of maximum tensile strength for the geogrids tested. Careful considerations of the environment in which the geogrids are to be placed, particularly temperature, must be made, since creep behavior is a function of temperature.
3. An increase in tensile strength after creep loading at less than 50 percent stress levels, was observed when the geogrid was first unloaded than loaded to failure. However, at creep stress levels greater than 50 percent of maximum load, a decrease in post creep tensile strength was observed for the SR3 specimens.
4. The method of fixing geogrid specimen ends prior to tensile testing has a significant increase on maximum tensile strength. Concrete embedded specimens consistently yielded greater tensile strengths than did aluminum clamped specimens. The observed differences in strength indicate that careful attention to how the geogrids are attached to structural elements can significantly affect performance.
5. Pullout resistance of geogrids in low moisture content clays is rather insensitive to geogrid strength or configuration at normal stress levels less than 48 KPa.

REFERENCES

- (1) Ingold, T.S., "Laboratory Pull-out testing of Grid Reinforcement in Sand," Geotechnical Testing Journal, GTJODJ, Vol. 6, Sept. 1983.
- (2) Jewell, R.A., Milligan, W.E., Sarsby, R.W., and DuBois, D., "Interaction Between Soil and Geogrids," Proc. Symp. Polymer Grid Reinforcement in Civil Engineering, ICE, London, Mar. 1984.
- (3) Jones, C.J.F.P., "Design and Construction," Proc. Symp. Polymer Grid Reinforcement in Civil Engineering, ICE, London, Mar. 1984.
- (4) Netlon Ltd., "Test Methods and Physical Properties of Tensar Geogrids," Netlon Ltd., Blackburn, UK, 1983.
- (5) McGown, A., Andrawes, K.Z., Yeo, K.C., and DuBois, D., "The Load-Strain-Time Behavior of Tensar Geogrids," Proc. Symp. Polymer Grid Reinforcement in Civil Engineering, ICE, London, Mar. 1984.

LESHCHINSKY, D.

University of Delaware, U.S.A.

FIELD, D.A.

CTC/GEOTEK, U.S.A.

In-Soil Load Elongation, Tensile Strength and Interface Friction of Nonwoven Geotextiles

INTRODUCTION

In recent years the use of geotextiles for reinforcement purposes in earth structures such as embankments, retaining walls, and road foundations has increased significantly. With the increasing acceptance of geotextiles has come a variety of design methods to include the effects of reinforcement contributed by the geotextile. These methods ignore the effect soil confinement has on geotextile behavior. The behavior of nonwoven geotextiles, however, has been shown ((1),(2)) to be affected by soil confinement; i.e., it becomes much stiffer and is able to carry higher tensile forces.

Another important property of confined geotextiles is the frictional interaction of the soil-geotextile interface. This friction is essential for preventing sliding and pullout failures of geotextile reinforced structures. The frictional property, however, has been studied extensively (e.g., ((3),(4),(5),(6)).

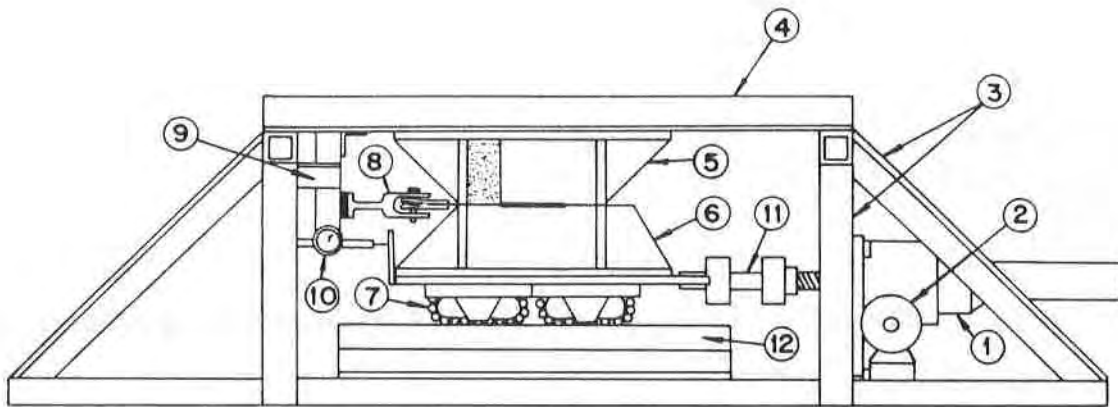
Apparently, there is no simple test that is capable of both determining the actual load-elongation of a confined geotextile, and simultaneously quantifying the frictional interaction between the soil and the geotextile. In this reported project it was desired to test an element of geotextile subjected to soil confinement and tensile stresses as would be encountered in a reinforced structure. The load-elongation behavior of the fabric, along with the frictional interaction and ultimate load at various soil pressures should be possible to estimate. Some form of direct shear device is the logical choice among standard soil laboratory equipment to adapt to simulate the field stress condition on the geotextile element.

EQUIPMENT AND TEST PROCEDURE

Description of Apparatus

A special apparatus was designed and constructed to simulate the in-soil conditions geotextile sheets are subject to when functioning as a reinforcing agent. The device is essentially a direct shear machine that has been modified to allow the inclusion of a membrane layer between the upper and lower shear boxes. The confining soil pressure is applied through an external loading frame. Fig. 1 illustrates the key elements of the modified direct shear machine. Numbers in the following discussion refer to items labeled in Fig. 1.

Shearing force is applied to the sample by a Duff-Norton Screw Jactuator (1), No. M-9809-06-1. This screw jack has a gear ratio of 56:1 and is capable of applying 10 tons of force. A Bodine electric motor (2), No. NSH-34RH, with a variable speed



- | | | |
|---------------------|--------------------------|---------------------------|
| (1) SCREW JACTUATOR | (5) UPPER BOX | (9) LOAD CELL FIXTURE |
| (2) ELECTRIC MOTOR | (6) LOWER BOX | (10) DIAL INDICATOR |
| (3) STEEL FRAME | (7) LINEAR BEARINGS | (11) SCREW JACK LOAD CELL |
| (4) TOP OF FRAME | (8) GEOTEXTILE LOAD CELL | (12) ROUNDWAY RAIL |

Figure 1. Modified Direct Shear Machine.

control, powers the screw jack. The screw jack is mounted to a welded steel frame consisting of square structural tubing, angle and channel sections (3). The top of the frame (4) is fastened by bolts to the lower section. The upper shear box (5) is bolted (clamped) to the top section of the stationary frame. Shims can be placed between the shear box and the frame or between the upper and lower frame elements to control the position of the upper box relative to the lower box.

The lower shear box (6) is mounted to four Thomson linear bearings (7), two RW16-S and two RW16-V. These bearings are each capable of supporting a load of 6000 lbs and have a frictional coefficient between 0.005 and 0.007. The two bearings in the V configuration keep the shear box aligned on the Roundway rails (12). The two rails are bolted directly to the channels which comprise the base of the loading frame. Shims were placed between the channels and the rail supports to achieve parallelism with the motion of the screw jack.

The lower box can be pushed or pulled by the screw jack to accomplish shearing. In order to test the geotextile specimens, the screw jack was run in a pulling mode. The fabric is anchored by its steel reinforcement to the front of the lower box by four bolts. Fig. 2 shows details of the geotextile sample anchoring. The opposite end of the sample is fixed and held by the geotextile load cell (8). This load cell is mounted in a fixture, comprised of angle sections, that bolts to the machine's frame at the opposite end from the screw jack (9). The end of the geotextile load cell consists of a threaded section to allow for adjustment in sample length.

The displacement of the lower box is measured with a static dial indicator (10). Forces applied to the lower box and developed in the geotextile were measured by the two load cells (8) and (11). The load cells are connected to the data acquisition system.

The sample is reinforced by thin sheet metal plates bonded by polyester resin on both ends of the fabric. One end of the fabric is bolted to the lower shear box. The other end is clamped with bolts to two aluminum plates which connect to the geotextile load cell with a pin. This pin allows the geotextile to rotate upon loading, minimizing nonuniform stresses across the sample width (see Fig. 2 for

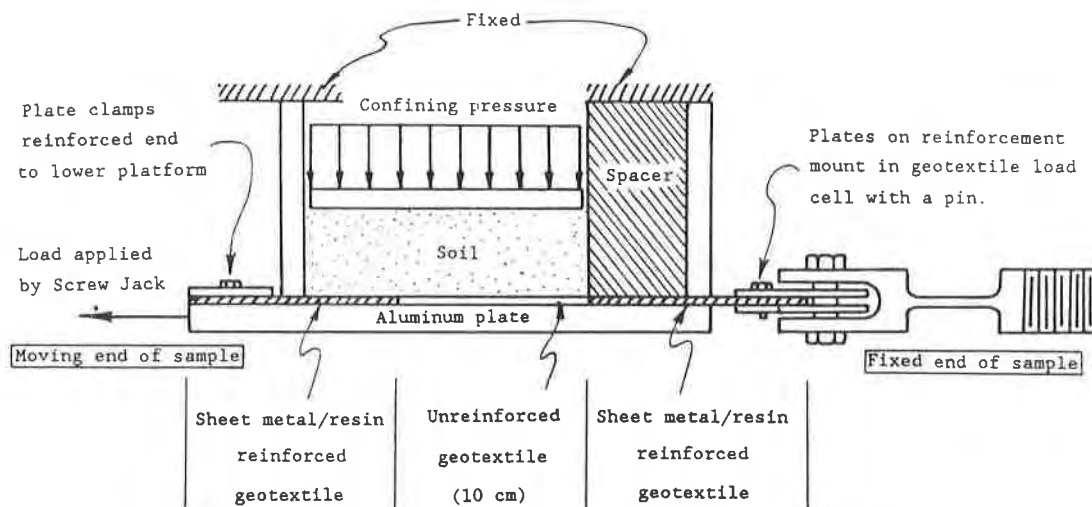


Figure 2. Details of Sample Anchoring and Position in Apparatus.

clarity). Post test investigation revealed that the resin bonding between the geotextile and the metal plates was solid and no relative slippage was detected.

Confining pressure is transmitted to the geotextile through a sand layer in the upper box that is loaded via a rigid plate with a loading frame. A spacer is installed in the upper box to ensure loading only the unreinforced area of the specimen and two inches of the metal reinforcement that is attached to the lower box (Fig. 2 details this). This is to prevent loading vertically the stationary sheet metal reinforced end of the sample which will have no support underneath it as the lower box moves.

The lower box is not filled with soil, rather it contains a metal platform which provides a smooth rigid surface for the geotextile to lay upon. This ensures that the geotextile sample remains exactly at the shear plane. To generate interaction between soil and geotextile only, friction between the elongating geotextile and the lower plate is minimized by placing a layer of grease covered by a latex membrane between the geotextile and the plate. To achieve maximum transmittal of confining pressure through the soil, a layer of grease covered with latex is also applied to the walls of the upper box. The friction developing between the upper surface of the sheet metal reinforcement and the soil at the free end of the sample was taken into account.

The soil used to confine the geotextile was Ottawa sand (Soiltest Density sand CN501). This soil was chosen for its uniform size, ease of compaction, and consistent frictional properties. The sand was placed on top of the geotextile at a relative density of 70%, prior to applying the confining pressure. The corresponding friction angle, determined from triaxial tests, is $\phi=37^\circ$.

Tensile Load at Moving End of Sample

The load applied by the screw jack is transmitted to the geotextile sample through the sheet metal/resin reinforced end. Note in Fig. 2 that initially a two inch portion of the reinforcement is subjected to the soil pressure. The load at the screw jack is not equal to the load at the moving end of the unreinforced geotextile due to friction between the reinforcement and cover soil. The recorded load, however, was at the screw jack end. It was necessary to correct this load to determine the net tensile force applied to the moving end of the sample. In contrast, the load at the fixed end of the geotextile is not subject to any frictional losses

as the reinforced area is not in contact with the cover sand and confining pressure.

Pullout tests were run with a continuous piece of sheet metal in place of the geotextile sample. One end of the sheet metal was clamped to the lower plate but it was not fixed at the other end. The sheet metal was covered with the same sand under identical pressures as used in the geotextile tests. The horizontal force necessary to cause displacement of the sheet metal quickly reached a constant value for each normal pressure. Consequently, the coefficient of friction between the sand and sheet metal was determined with confidence. During the testing of the confined geotextile samples, the force dissipated by sheet metal-soil friction at each increment of displacement was calculated using the friction coefficients as determined by the pullout tests. This frictional loss was subtracted from the screw jack load cell's reading.

Sample Description

An aspect ratio (width/length) of 2:1 was used resulting in an unreinforced sample size of 20 cm in width by 10 cm in length. Fig. 3 illustrates the final dimensions of the sample.

All tests were conducted with the axis of loading corresponding to the machine direction of the fabric. Two geotextiles were used in this investigation, both were nonwoven spunbound fabrics composed of polypropylene. They are marketed by Mirafi Inc. under the product designations 140-N and 900-N. In this paper, however, only the results regarding 140-N are reported. More information is available elsewhere (7).

It should be noted that the geotextile samples were subjected to a constant rate of strain of approximately 10% per minute (i.e., 10mm/min).

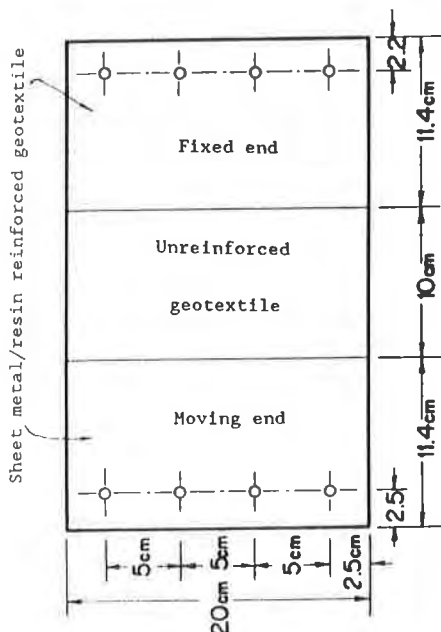


Figure 3. Dimensions of Reinforced Geotextile Sample.

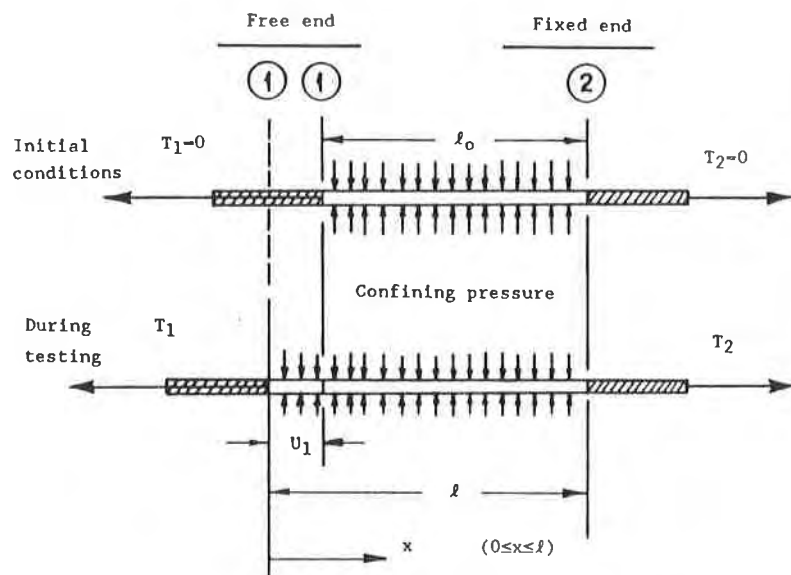


Figure 4. Schematic of Test Specimen.

RESULTS

Presentation of Data

The test specimen is shown schematically in Fig. 4. Point 1 refers to the moving end of the sample, the point of load application. Point 2 is the fixed end where displacement is zero. Upon loading the geotextile specimen, displacement of the moving end occurs, moving point 1 by a distance designated as U_1 . The tensile force causing U_1 and applied at point 1 is termed T_1 , while the tensile force developed at point 2 is termed T_2 .

For each confining pressure two tests were run to check their repeatability. Fig. 5 is a plot of tensile force vs. U_1 for the Mirafi 140-N geotextile at zero confining pressure. The two lines in this figure connect the data points from two tests. The tests were run until tear failure occurred. The tensile force along the sample is uniform since there is no frictional dissipation.

Fig. 6 shows a plot of T_1 and T_2 vs. U_1 for a confining pressure of 52 kPa (7.5 psi) for the same geotextile. It should be pointed out that T_1 is the net load applied to the moving end of the geotextile and its value is determined as explained before. Again two tests were run until failure with the resulting data points for each test being connected to distinguish the two experiments. With the application of confining pressure, T_2 is no longer equal to T_1 , as some of the load applied to

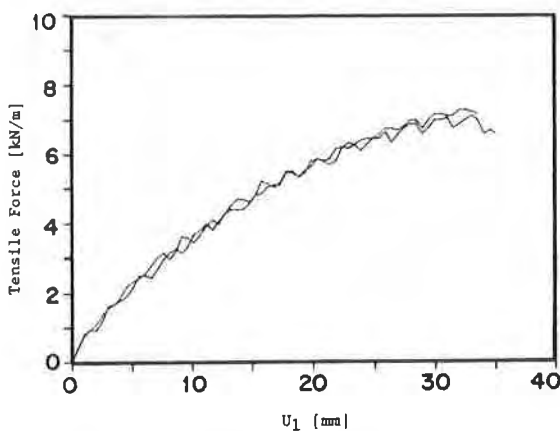


Figure 5. Applied Load vs. Displacement ($\sigma_v=0$ kPa).

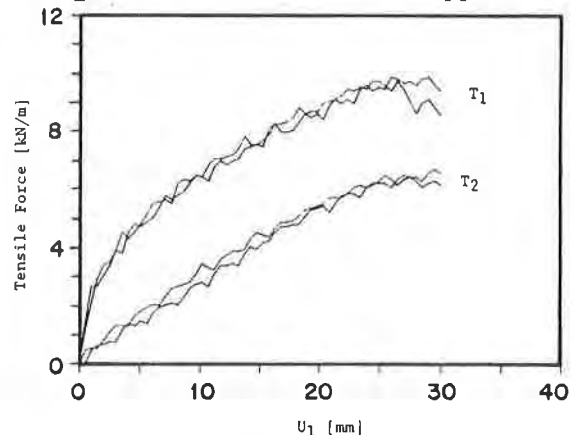


Figure 6. Applied Load vs. Displacement ($\sigma_v=52$ kPa).

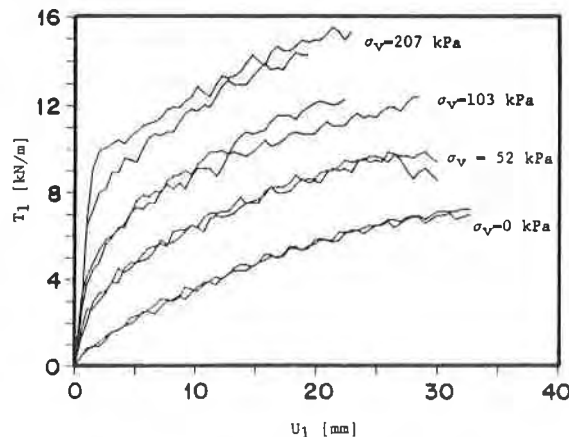


Figure 7. Summary of Load vs. Displacement.

the moving end of the geotextile is dissipated by frictional interaction with the soil along the length of the sample. Fig. 7 is a summary of T_1 vs. U_1 for all confining pressures for the Mirafi 140-N geotextile.

Observation of Failure

For unconfined specimens the failure could be observed visually. Failure occurred suddenly and was in the middle of the specimen. Necking was pronounced, resulting in a reduction in sample width of about 2.5 cm. Necking developed over the entire length of the sample.

With the application of confining pressure, failure developed gradually. Each test was performed until a significant drop in the load cell at the sample's fixed end occurred, indicating that the sample was no longer intact and transferring load. All failures in the confined samples occurred near the moving end of the geotextile sample in the area adjacent to the metal reinforcement. In this zone, maximum tensile load is carried by the geotextile (i.e., T_1). Necking in the region around the failure was evident in every sample. The amount of necking that occurred was dependent on the confining pressure. At low confining pressures the zone of necking was larger and extended further into the sample interior than at high confining pressures.

Determination of Interface Friction

The load applied at point 1 is transmitted along the length of the geotextile until it is apparent at point 2 (see Fig. 4). As the load is carried by the geotextile, friction between the elongating geotextile and the block of soil diminish the magnitude of the load.

The values of T_1 and T_2 for any displacement are measured; the difference ($T_1 - T_2$) is the amount of force dissipated by friction. By calculating the net normal force acting on the area of the geotextile only (excluding the portion of the confined metal reinforced at the moving end) at some displacement U_1 , the average interface frictional coefficient, μ , can be estimated as follows:

$$\mu = (T_1 - T_2)/N \quad (1)$$

or in terms of measured quantities, μ is defined by:

$$\mu = (T_1 - T_2)/[\sigma_v w(\ell_0 + U_1)] \quad (2)$$

where N is normal force on the geotextile; σ_v is confining pressure; ℓ_0 is initial length of sample; and w is width of sample (taken as constant).

Equation (2) is valid only when T_2 is measurable, that is when the tensile force has been transmitted along the entire unreinforced specimen length (along $\ell_0 + U_1$). Therefore, the results shown in Fig. 8 do not include values of μ calculated at small displacements when T_2 was not significant.

In calculating μ it was assumed that the difference between T_1 and T_2 is strictly due to friction developing between the deforming geotextile and the sand above it. Any friction which developed between the geotextile and the bottom plate, occurring over the lubricated latex sheet (see Description of Apparatus), was ignored. To verify the magnitude of this friction, however, two tests were run at confining pressures of 103 kPa and 207 kPa utilizing a sample with two latex sheets, heavily lubricated in between, on the top to remove the frictional effects of the sand. A latex membrane and grease were used beneath the sample as with the other tests. With this configuration any difference between T_1 and T_2 is due to the

frictional interaction between the latex sheets and the lubrication on top and bottom of the sample. Fig. 9 shows the results of these tests. Notice that μ is on the order of 0.02-0.03. This value is about 1/20 of the value of μ estimated to develop between the geotextile and the sand.

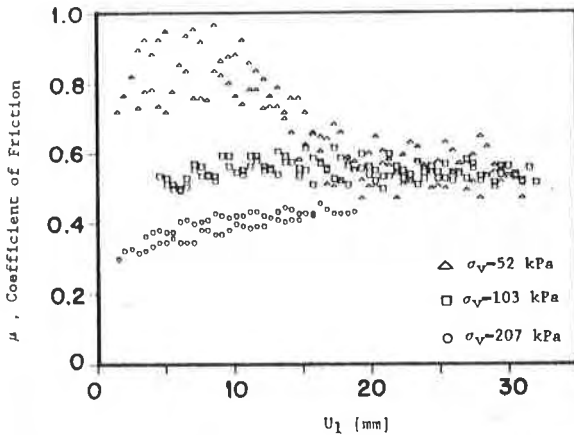


Figure 8. Development of Interface Friction.

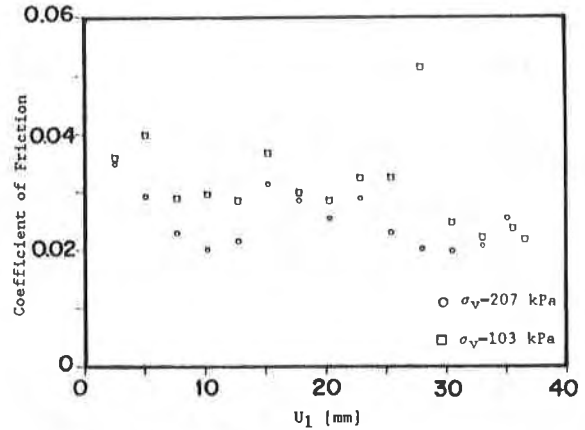


Figure 9. Friction of Greased Latex Membranes.

Interpretation of Data

To determine the load-elongation response of the geotextile specimen it was necessary to make an assumption of the displacement of each point along the length of the deforming geotextile. Referring to Fig. 4, an interpolation for $U(x)$ between $x=0$ and $x=l$ is needed; where $x=0$ at the moving end and $x=l$ at the fixed end of the sample ($0 \leq x \leq l$). Note from eq. (2) that $l = (l_0 + U_1)$.

It was assumed that a second degree polynomial could be used to describe the displacement along the length of the fabric:

$$U(x) = k_0 + k_1x + k_2x^2 \quad (3)$$

where k_0 , k_1 and k_2 are the polynomial coefficients. This function is subject to the following measured boundary conditions:

$$U(x = 0) = U_1 = k_0 \quad (4)$$

$$U(x = l) = 0 = k_0 + k_1l + k_2l^2 \quad (5)$$

By definition the elongation e along the geotextile sample is:

$$e = dU/dx = k_1 + 2k_2x \quad (6)$$

Note that $e(x)$ in eq. (6) is linearly distributed along the specimen. This, of course, is a consequence of the assumed interpolation function (i.e., eq. (3)).

From the previous section it follows that the coefficient of friction, μ , at the sand-geotextile interface remains approximately constant for a large range of U_1 (see Fig. 8). Since strain (or elongation) within the specimen increases as U_1 increases, it follows that μ is independent of e . Observing eq. (6), this independence implies that μ is also not a function of x . Subsequently, the net tensile force carried by the geotextile specimen (see also eq. (2)), at any location x , is:

$$T(x) = T_1 - \int_0^x \mu \sigma_v w dx = T_1 - \mu \sigma_v w x \quad (7)$$

Note that eq. (7) linearly relates T and x.

Since both T and e are linear functions of x (eqns. (6) and (7)) and since they both must be zero at the same location x (physically, when T equals zero e must equal zero too), the following can be stated: For any given x the ratio between T and e is constant. This statement becomes apparent when one observes Fig. 10. The ratio T/e is denoted by E and is termed the geotextile modulus. Subsequently, for any given U_1 , the following equation can be written:

$$T = E \cdot e \quad (8)$$

It should be emphasized that eq. (8) is a consequence of the assumed interpolation function (eq. (3)) and the observed independence of μ and x which enabled the assembly of eq. (7).

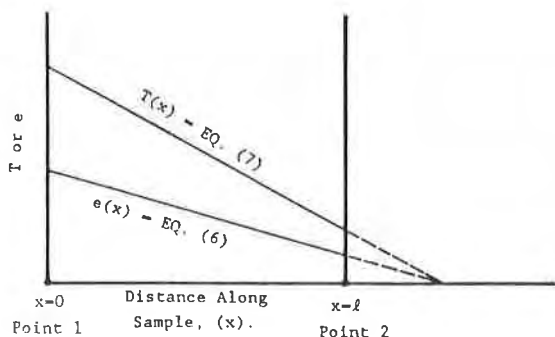


Figure 10. Schematic of T and e Distribution Along Sample.

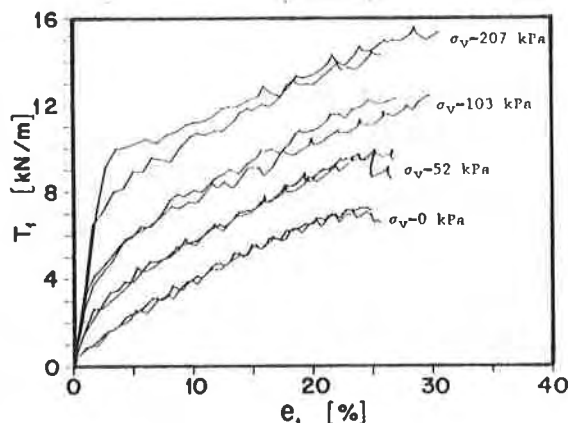


Figure 11. Load-Elongation Curves Summary.

Combining eqns. (6) and (8), the distribution of T along the length of the sample, at any given displacement U_1 , can be described by:

$$T(x) = E[k_1 + 2k_2x] \quad (9)$$

subject to the measured boundaries:

$$T(x = 0) = T_1 = E \cdot k_1 \quad (10)$$

$$T(x = l) = T_2 = E[k_1 + 2k_2l] \quad (11)$$

The system of equations (4,5,10 and 11) can be solved uniquely to yield the following:

$$k_0 = U_1 \quad (12)$$

$$k_1 = - 2U_1T_1/[\ell(T_1 + T_2)] \quad (13)$$

$$k_2 = [(T_1 - T_2)U_1]/[(T_1 + T_2)\ell^2] \quad (14)$$

$$E = [-\ell(T_1 + T_2)]/2U_1 \quad (15)$$

Thus, measuring U_1 , T_1 , T_2 and taking $\ell = \ell_0 + U_1$, one can determine k_0 , k_1 , k_2 and E solving eqns. 12 through 15. Consequently, $U(x)$ can be calculated using eq. (3). The elongation at any point along the sample is given by eq. (6).

Plots of T_1 vs. e_1 are presented in Fig. 11. These plots are derived from the results shown in Fig. 7. They correspond to the true load-elongation of point 1, provided the assumption of displacement is accurate.

DISCUSSION OF TEST RESULTS

Behavior of Confined Geotextile

It is interesting to get some insight into the nature of the assumed displacement distribution along the length of the sample as it deforms. Using the equations presented before, Fig. 12 shows typical U along the normalized sample length (x/ℓ) for the following selected values of displacement at the moving end (U_1): 2.5, 7.6, 12.7 and 20.3 mm. Only the results of one test per confining pressure was used to plot the displacement distribution. This was done for the sake of clarity.

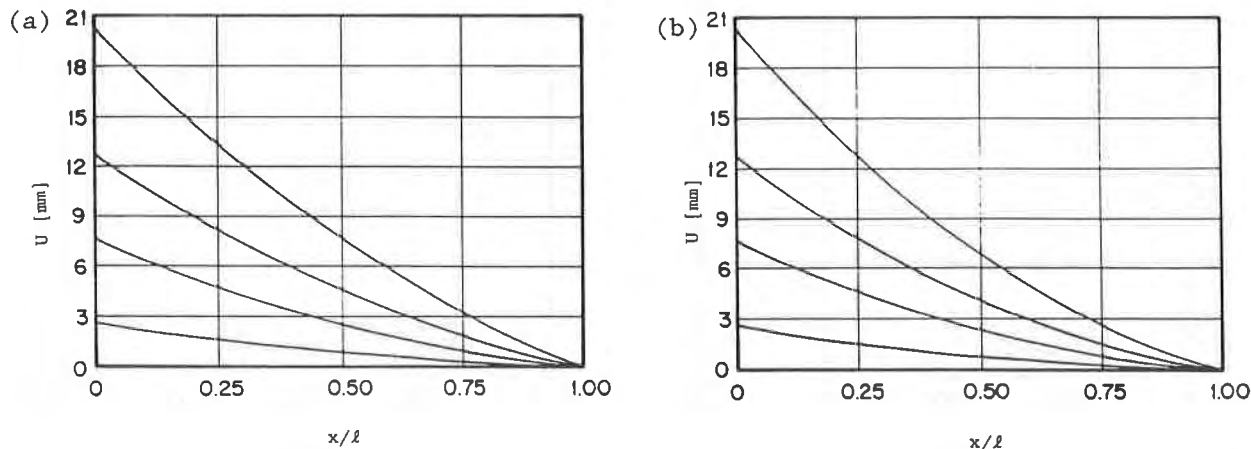


Figure 12. Displacement Distribution: (a) $\sigma_v = 103$ kPa, and (b) $\sigma_v = 207$ kPa.

Notice by comparing the plots of $U(x)$ that, as the confining pressure or U_1 increase, the curvature of the displacement distribution along the sample becomes more defined. It is known that in a boundary case where the confining pressure is zero, the elongation is uniform along the sample, implying that a linear distribution of $U(x)$ would exist. This boundary case seems to agree well with the assumed distribution trend.

The distributions of tensile force T and elongation e are linear along the sample's length (see eqns. (6) and (7)). Fig. 13 shows some typical distributions of $T(x)$. Fig. 14 illustrates distribution of $e(x)$.

Observing Fig. 13 one sees that higher tensile force is carried at the moving end of the sample as the confining pressure increases. Furthermore, a steeper tensile force gradient exists indicating that a higher force is dissipating due to friction between the geotextile and the soil as one would intuitively expect. For the boundary condition of zero confining pressure one can state a-priori that T is

uniform along the length of the sample. The trend seen in Fig. 13 agrees well with this known boundary.

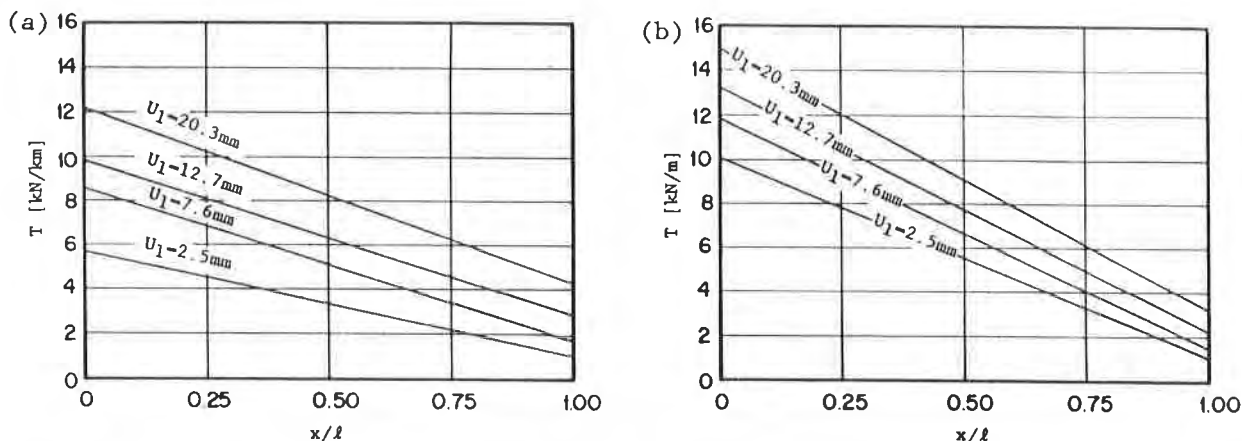


Figure 13. Tensile Force Distribution: (a) $\sigma_v=103$ kPa, and (b) $\sigma_v=207$ kPa.

One can see that the gradient of elongation along the sample increases with confining pressure (Fig. 14). This is expected as $e(x)$ is related to $T(x)$ by a constant multiplier E , the modulus of the geotextile (see eq. (8)). Once again for the boundary case of zero confining pressure, $e(x)$ is constant with zero gradient.

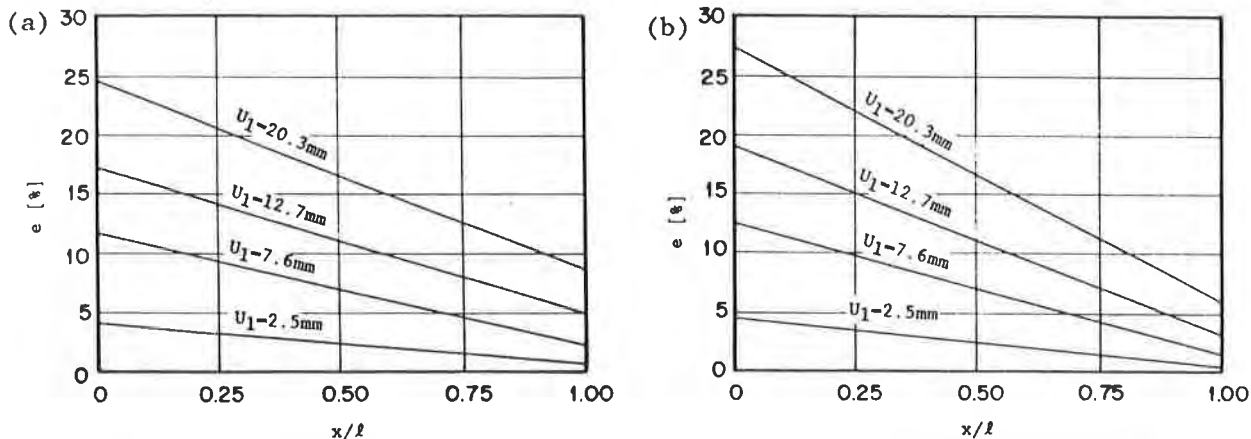


Figure 14. Elongation Distribution: (a) $\sigma_v=103$ kPa, and (b) $\sigma_v=207$ kPa.

The initial modulus (e.g., E at small e) has increased with an increase of confining pressure. With continued elongation, the value for the modulus E approached a constant value for all confining pressures. This trend is displayed in Fig. 15 which shows the calculated values of E vs. elongation based on eq. (15).

Frictional Interaction of Geotextile-Soil

It is important to note that regardless of confining pressure the soil-geotextile friction coefficient approached a narrow range of values (see Fig. 8 at large U_1). The values of calculated μ (0.45-0.65) correspond to a range of $(0.60-0.86) \cdot \tan\phi$ for the soil used (i.e., $\phi=37^\circ$).

Correlation of Tensile Strength with σ_v

There is a marked increase in the tensile strength with each increase in σ_v . The fabric, at a confining pressure of 207 kPa, was able to carry roughly two times the tensile force that caused failure at zero confining pressure (Fig. 8). The geotextile failed at about the same elongation regardless of the confining pressure (i.e., $e \approx 27\%$ --see Fig. 11). In each test the tear failure occurred at the moving end boundary of the geotextile. At this end the tensile load and corresponding elongation were maximum. Since tensile strength is an important parameter used in the design of reinforced earth structures, it is interesting to note the correlation of T_f with confining pressure. Fig. 16 presents the average value of T_f vs. σ_v . Clearly, a linear model for T_f as function of σ_v is adequate.

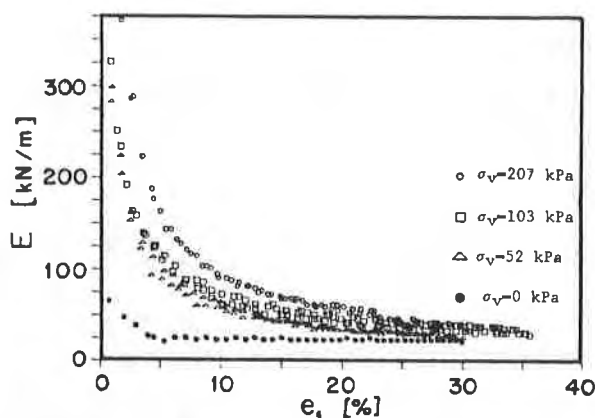


Figure 15. Modulus vs. Elongation.

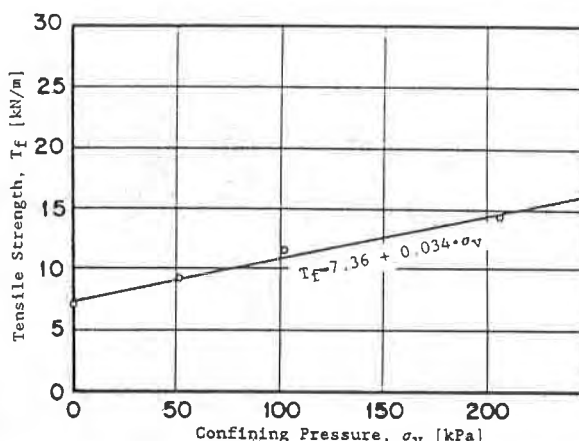


Figure 16. Tensile Strength vs. Confining Pressure.

CONCLUSION

An apparatus and testing procedure for determining the in-soil behavior of nonwoven geotextiles is presented. A method to describe the load-elongation behavior of the confined geotextile is developed. The method takes the soil-geotextile frictional interaction and resulting nonuniform elongation of the sample into account. Results of the test program show the effects of confining pressure on soil-geotextile friction, load-elongation behavior and ultimate tensile strength of the geotextile.

Some conclusions may be made about the tests and apparatus:

1. Individual tests are relatively simple to perform.
2. Test results can be repeated. Consistent results were achieved throughout the entire testing program.
3. The sheet metal/resin reinforcement of the sample ends provided a solid anchor to transfer loads to the geotextile.
4. A single test can provide information regarding the frictional interaction of the soil-geotextile, the load-elongation behavior and the ultimate tensile strength of a soil confined geotextile.
5. The developed apparatus has the additional advantage of being able to perform standard direct shear tests.
6. The frictional coefficient between the geotextile sheet and the soil which confines it stays within a narrow range of values regardless of confining pressure or geotextile deformation.

7. The modulus of a nonwoven geotextile becomes greater with increasing confining pressure up to an elongation of 10-15%. With further elongation, the modulus approaches a constant value similar for all confining pressures.
8. Failure occurred at about the same value of elongation ($e \approx 27\%$) regardless of confining pressure.
9. The ultimate tensile strength, or failure load, of the geotextile samples increased linearly with confining pressure.

The results of this research compare favorably with work done by other investigators. The results obtained, for example, by ((3),(4),(5)) support the values of μ calculated for the soil-geotextile interface. The load-elongation behavior of a soil confined geotextile described by ((1),(2)) is qualitatively very similar to the results of this research. Detailed comparison and correlation of results is given elsewhere (7).

ACKNOWLEDGMENT

The authors extend their thanks to Mirafi Inc. for donating the geotextiles used in this research.

REFERENCES

- (1) McGown, A., Andrawes, K.Z. and Kabir, M.H. "Load-Extension Testing of Geotextiles Confined In-Soil," Second International Conference on Geotextiles, Las Vegas, Nevada, 1982, pp. 793-798.
- (2) El-Fermaoui, A. and Nowatzki, E. "Effect of Confining Pressure on Performance of Geotextiles in Soils," Second International Conference on Geotextiles, Las Vegas, Nevada, 1982, pp. 799-804.
- (3) Myles, B. "Assessment of Soil Fabric Friction by Means of Shear," Second International Conference on Geotextiles, Las Vegas, Nevada, 1982, pp. 787-791.
- (4) Miyamori, T., Iwai, S. and Makiuchi, K. "Frictional Characteristics of Nonwoven Fabrics," Third International Conference on Geotextiles, Vienna Austria, 1986, pp. 701-705.
- (5) Collios, A., Delmas, P., Gourc, J.P. and Giroud, J.P. "Experiments On Soil Reinforcement with Geotextiles," The Use of Geotextiles for Soil Improvements, ASCE, Portland, Oregon, 1980, pp. 53-73.
- (6) Saxena, S.K. and Budiman, J.S. "Interface Response of Geotextiles," Eleventh International Conference on Soil Mechanics and Foundation Engineering, San Francisco, California, 1985, pp. 1801-1804.
- (7) Field, D.A., "In-Soil Load Elongation, Tensile Strength and Interface Friction of Nonwoven Geotextiles," a thesis submitted to the Faculty of the University of Delaware in partial fulfillment of the requirements for the degree of Master of Civil Engineering, 1986.

TZONG, W.H. and CHENG-KUANG, S.
University of Colorado at Denver, U.S.A.

Soil-Geotextile Interaction Mechanism in Pullout Test

ABSTRACT

The detailed mechanism of geotextile-reinforced earth have not been fully elucidated. A major factor, however, is that the geotextile, when deformed under applied loads, becomes stressed in tension. This, in turn, reacts with the surrounding soil, redistributes the compressive stress in the soil mass, and hence reduces or suppresses the strain rate of the earth structure.

In order to investigate the soil-geotextile interaction mechanism, a test was designed in which the geotextile was stressed in tension and was confined in soil. The soil bin was 48 inches by 24 inches in plane and 57 inches high. In the test, a large-size geotextile was embedded in the soil and incremental pulling forces were imposed on a sheet metal clamp which secured the geotextile specimen along its width. The displacement at the end of the geotextile where the load was applied as well as the displacements along the length of the geotextile were measured. A new procedure for placing the backfill was devised to ensure uniform density in the soil bin. One important aspect of the test is that the geotextile must be kept in the confinement of soil throughout the test. This will not only permit measurement of the displacement at the end of the geotextile where the load is applied, but also facilitate control of the pulling forces.

Displacement patterns of a test conducted until a failure condition was reached were evaluated to examine the soil-geotextile interaction mechanism for the imposed loading condition. Results of the test also provide invaluable controlled test data for verification of numerical models, which, upon establishing their reliability, can be used to investigate the soil-geotextile interaction mechanism in various geotextile-reinforced earth structures.

INTRODUCTION

The concept of reinforcing an earthfill by incorporating geotextiles which possess a much higher tensile strength than soil, and the capability to bond with soil through friction has begun to gain popularity in recent years. The technique of using geotextile as the reinforcing element has been applied to embankments

over soft foundation, retaining walls, slope reinforcement, and bearing capacity improvement of shallow foundations.

Geotextile-reinforced earth structures, however, suffer from a major problem -- there is a total lack of understanding as to the reinforcing mechanism. As a result, the design procedures are very empirical and not based on sound engineering research.

The interaction mechanism of geotextile-reinforced earth structures is complicated. As a general rule, when a geotextile-reinforced earth mass deforms under applied loads, the geotextile will be subjected to tension provided that there is adequate frictional resistance between the geotextile and soil. As a result, not only will the stresses in the soil mass be redistributed into a more favorable state, the geotextile will react along the surrounding soil, increasing its effective confinement and, hence its stiffness.

In order to gain better understanding of the soil geotextile interaction mechanism, a test apparatus was devised to investigate the geotextile behavior when it was stressed in tension and was confined in soil. The soil bin was 48 inches by 24 inches in plane and 57 inches high. In the test, a large-size geotextile was embedded in the soil and incremental pulling forces were imposed on a sheet metal clamp which secured the geotextile specimen along its width. The displacement at the end of the geotextile where the load was applied as well as the displacements along the length of the geotextile were measured. A new procedure for placing the backfill was developed to ensure uniform density in the soil bin. One important aspect of the test is that the geotextile must be kept in the confinement of soil throughout the test. This is necessary in order to avoid unrestrained stretching, hence necking, of the geotextile specimen when it becomes exposed to the air, to ensure uniform straining along the width of the test specimen, and to facilitate control of the applied forces.

It is to be noted that the test also provides invaluable controlled test data for verification of analytical models, which, upon establishing their reliability, can be used to investigate the soil-geotextile interaction mechanism in various geotextile-reinforced earth structures. The development of such an analytical model has recently been completed by Wu and his associates at the University of Colorado at Denver.

TEST SETUP AND INSTRUMENTATION

The pullout test setup consisted of a steel angle reinforced plywood soil bin and an assembly of steel tube loading frames with a hydraulic jack reacting against the bin to apply pulling forces. The pullout test setup is depicted in Figure 1.

The soil bin was constructed of 0.75 inch thick plywood panels on three sides, and on one side of a 0.75 inch thick acrylic sheet to allow for visual observation of the box interior. The box was 57 inches high with 48 inches by 24 inches in plane. The sides and bottom of the box were secured by using 0.25 inch thick steel angle sections. The four sides of the wall were reinforced by cross-ties at two levels with 0.5 inch diameter steel bars. There was a 0.5 inch wide slot on the front side of the bin to permit the geotextile to be attached to a pulling mechanism.

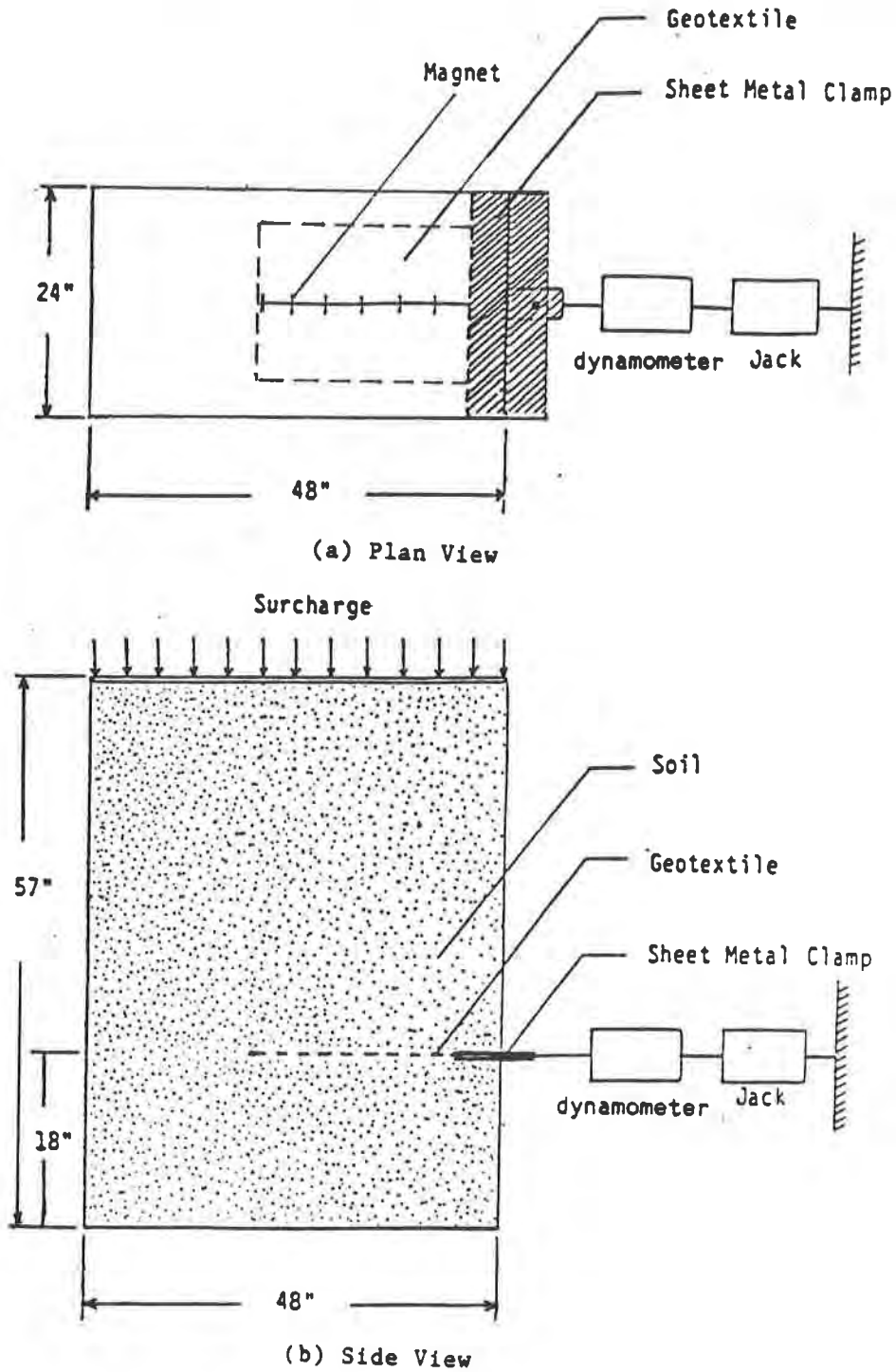


Figure 1. Large Pullout Test Setup
(a) Plan View (b) Side View

In order to minimize the side wall friction between the box and soil, the interior wall surface was lined with a layer of 1/16 inch thick smooth surface geomembrane.

In the test, a geotextile specimen was placed in the soil bin. The soil was prepared at a constant density and was subjected to a constant vertical load. Since the geotextile must be kept in the confinement of the soil throughout the test, one end of the geotextile specimen was glued between a set of steel sheet metal clamp which was partially embedded in the soil. The connection between the pulling mechanism and the sheet metal clamp was designed to allow for free rotation in the horizontal plane.

A new "uniform raining device" was developed to obtain uniform soil density in the bin. The device was a rectangular bin fitting the inside dimension of the soil bin. There were a screen and a two-piece door attached to the bottom of the bin. The door could be opened by releasing cables which were mounted above the soil bin. A series of tests were conducted with very consistent results obtained. Detailed procedure of its application was described by Su (2).

An electronic monitoring system including a hall generator probe, a X-Y recorder and a digital multimeter was used to measure displacements along the length of the geotextile. This was accomplished by measuring movements of magnets (0.06 inch thick and 1/16 inch in diameter), which were glued at 1.5 to 3 inches intervals long the length of the geotextile surface. The measurement was made by inserting a hall generator probe with a magnetic sensor into a glass tube which was embedded in the soil immediately above the center line of the geotextile. The movements of the magnets were recorded after each pulling force increment was applied to the geotextile. The displacement of the sheet metal clamp which indicated the movement at the clamped end of the geotextile was measured by a dial gage of 0.001 inch accuracy.

LARGE BOX PULLOUT TEST

The soil used in this study was a uniform Ottawa sand. The uniformity coefficient of the sand is 1.43. The sand has subrounded grain shape and a specific gravity of 2.65. The maximum and minimum dry densities determined in accordance with the Earth Manual (1) were 112.19 pcf and 97.52 pcf, respectively. In the test, the soil was prepared at a constant density of 107 pcf with an overburden pressure of 4.34 psi. Results of the triaxial compression tests indicated that the angle of internal friction was 37 degrees.

The geotextile used in the pullout test is a 100% polyester continuous spun needle punched fabric (Trevira 1127). The geotextile specimens used in the tests were 18 inches wide with variable lengths. In this paper only the one with 12 inch in length is presented.

Figure 2 shows the loading history and the relationship between applied pulling forces and the clamped end movements of the test. The left-hand-side of the figure shows the loading history. The loads were applied at a constant increment of 50 lb. As the movement of the geotextile occurred in response to a load increment, it was accompanied by a reduction in the force exerted by the hydraulic jack. The reductions are shown in the figure as dashed lines. The right-hand-side of the figure shows the applied load versus clamped-end movement. As a limiting load (approximately 600 lb.) was reached, the force dropped rapidly and it was not possible to maintain the loading level.

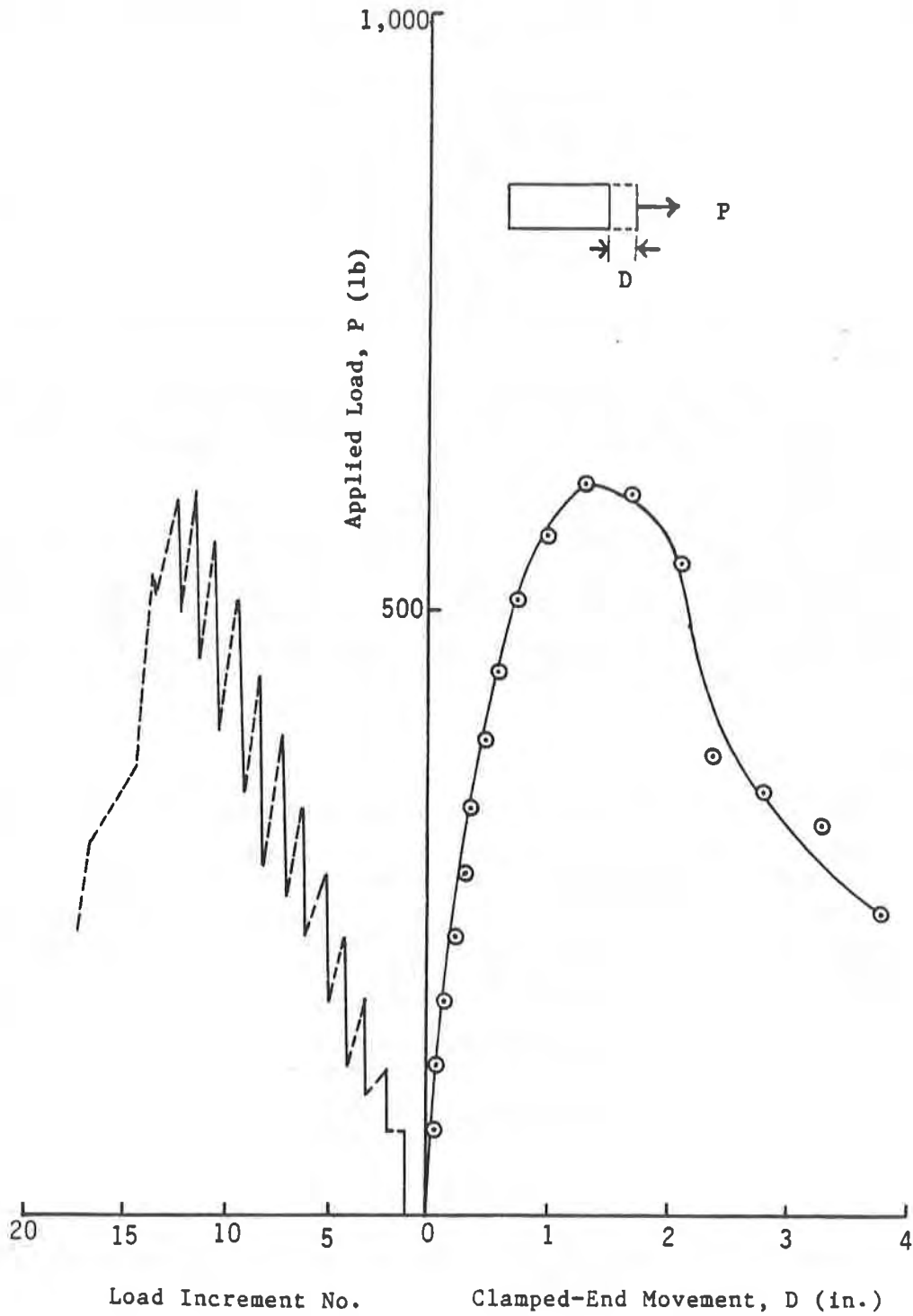


Figure 2. Applied Load Versus Clamped-End Movement

It should be noted that since the applied forces by the hydraulic jack were partially resisted by the friction between the metal clamp and the confining soil, the forces applied to the geotextile had to be corrected by subtracting the frictional forces over the embedded area of the metal clamp from the corresponding applied forces.

Geotextile is a "deformable" material. When a tension load increment is applied to one end of an embedded geotextile specimen, the movement of the geotextile is due entirely to stretching of the geotextile itself until a large enough load is reached so that sliding of the entire specimen against the soil begins to take place. Figure 3 illustrates the deformation (stretching) along the length of the geotextile in response to applied loads for the test. It is shown that the deformation initiates at the clamped-end and propagates toward the free-end as the load increases. The shaded area on the specimen shows the portion of the geotextile in which deformation has not developed before sliding of the specimen occurs.

Figure 4 depicts the deformations along the geotextiles at different load levels for the test. As a general rule, it is seen that the deformation along the geotextile reduces toward the free-end. The rate of reduction increases as the load level increases.

The tensile force distribution in the geotextile specimen at any given applied load can be determined from the strain distribution along the length of the geotextile and the load-deformation relationship of the geotextile under the same test conditions as the pullout test. For instance, the force distribution for an applied load of 450 lb. is shown in Figure 5. The in-soil load-deformation curve used in deducing the figure was obtained by employing a specially designed apparatus developed at the University of Colorado at Denver.

CONCLUSION

The findings and conclusions of this study are summarized in the following:

1. The large test setup devised in this study can be used to conduct pullout test satisfactorily and gives consistent test results.
2. In order to conduct pullout test of geotextiles, the specimen must be kept in the confinement of soil throughout the test. Using sheet metal clamp with the geotextile glued between the metal sheets fulfills this purpose and yields uniform straining across the width of the geotextile.
3. The uniform raining device developed in this study is a good approach for placing granular soil uniformly in a soil bin.
4. The hall generator probe-magnet system can measure the movements of the embedded geotextile along its length with an accuracy of ± 0.01 inch.
5. When a pulling force is applied to the geotextile specimen, the movement initiates at the clamped-end and gradually propagates toward the free-end as the force increases. The deformation of the geotextile is the largest at the clamped-end and becomes smaller toward the free-end. The rate of reduction in deformation increases as the force increases.
6. By combining the measured deformations with the in-soil stress-strain relationship of the geotextile, the tensile force distribution in the geotextile can be readily determined.

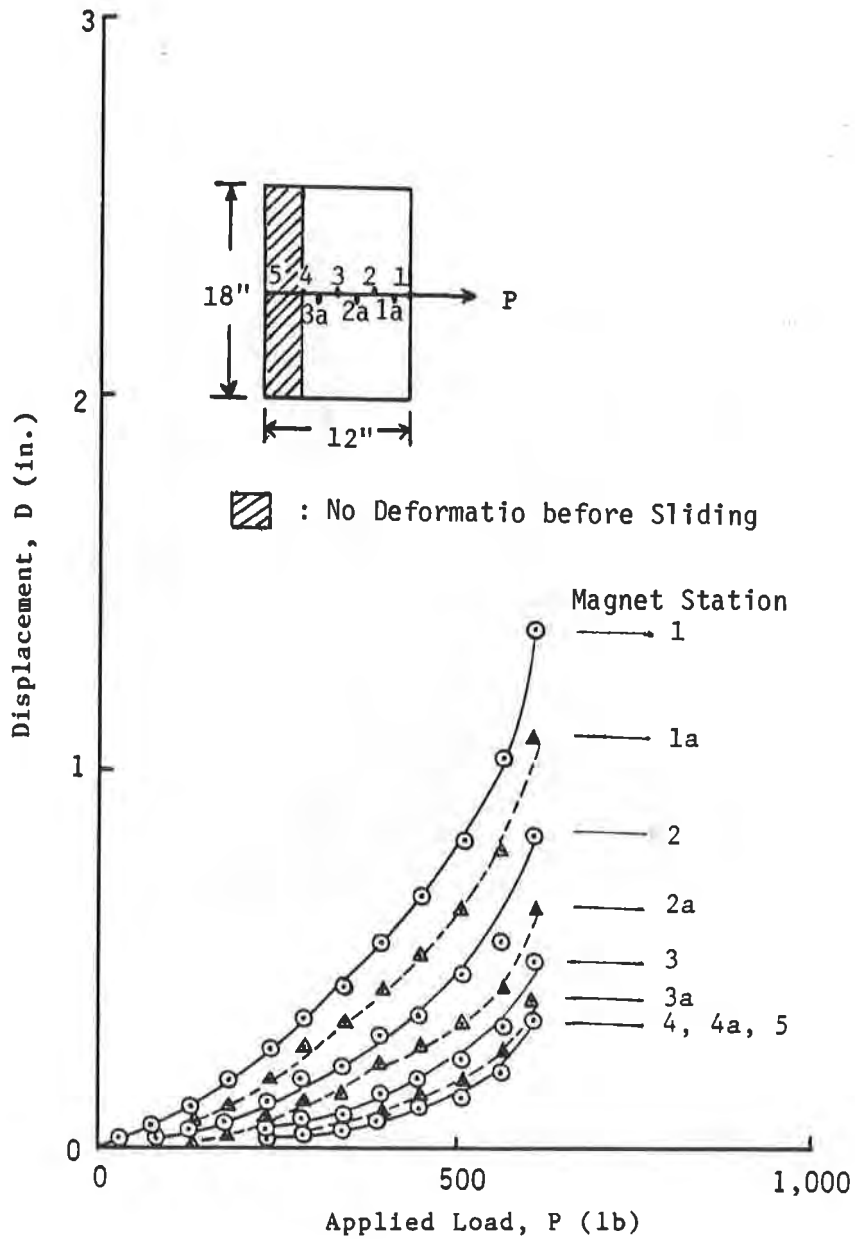


Figure 3. Applied Loads Versus Cumulative Displacements Along the Length of the Geotextile

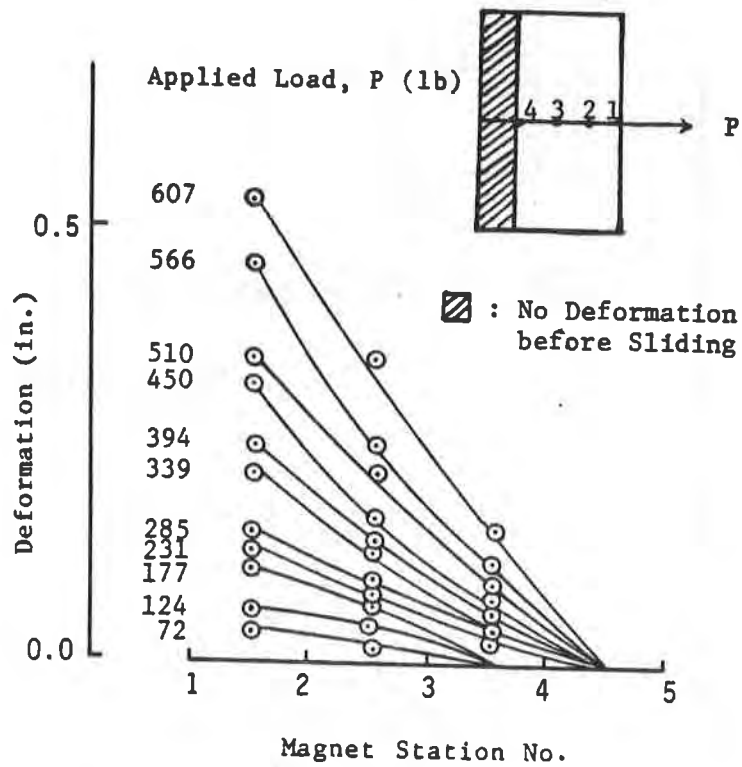


Figure 4. Deformations Along the Geotextile

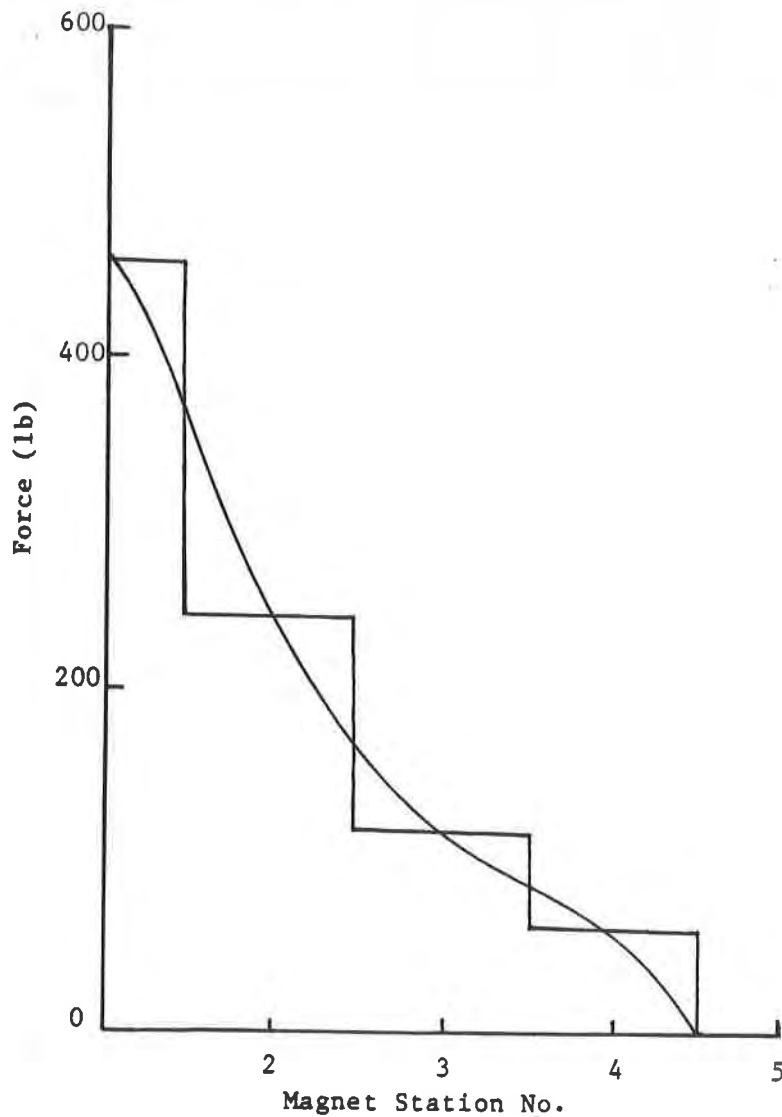


Figure 5. Tensile Force Distribution in the Geotextile for an Applied Load of 450 lb.

ACKNOWLEDGEMENT

Work described herein was supported by a research grant from the National Science Foundation, Grant No. CEE-8405110.

REFERENCES

1. Earth Manual, Bureau of Reclamation, Department of the internal, Second Edition, Denver, Colorado, 1974, 810 pp.
2. Su, C.K., "Investigating Soil-Geotextile Interaction Mechanism, "Master Thesis, Department of Civil Engineering, University of Colorado, Denver, July 1986.

SIEL, B.D.

ATEC Associates, U.S.A.

TZONG, W.H.

University of Colorado at Denver, U.S.A.

CHOU, N.N.S.

Colorado Department of Highways, U.S.A.

In-Soil Stress-Strain Behavior of Geotextile

ABSTRACT

The stress-strain behavior of geotextiles, under monotonic loadings, is dependent on the following factors: (1) the properties of the geotextile, (2) the overburden pressure imposed on the geotextile by the soil, (3) the interface frictional behavior between the soil and geotextile, and (4) the properties of soil surrounding the geotextile. To evaluate the in-soil geotextile stress-strain relationships, specially designed test apparatus must be employed.

This paper describes the detailed construction of a new test device for determination of in-soil geotextile stress-strain relationship in uniaxial tension, plane strain condition. In the test, a wide strip of geotextile embedded in a soil was subjected to incremental pulling forces at one end while fixed at the other end. The test setup can account for all the above-mentioned factors corresponding to the field condition.

Results of two sets of tests, conducted in two different soils under a range of overburden pressures, were presented.

INTRODUCTION

In recent years the concept of strengthening earth structures by incorporating geotextiles has begun to gain popularity. The technique has been applied to embankments over soft foundation (1, 3, 8, 9, 11, 13, 17), retaining walls (2, 4, 5), slope reinforcement (12, 15), and bearing capacity improvement of shallow foundations (10).

The stress-strain-strength properties of geotextiles used in design of geotextile-reinforced structures, usually supplied by the manufacturers, are often obtained by testing the geotextiles alone without regard to the soil. In this study a new test apparatus was manufactured and a series of tests were conducted to investigate the effects of soil type and overburden pressure on the stress-strain characteristics of geotextile. The geotextile used in the study was Trevira 1127, a nonwoven, needle punched, polyester material.

TEST APPARATUS

To investigate the stress-strain-strength characteristics of geotextiles in typical geotechnical environment, a testing box was designed and manufactured. The test box was designed to be used with a Wykeham Farrance direct shear loading frame. The test box was constructed of aluminum with a steel top loading cap. The test box was designed with a fixed clamp inside the box to hold the geotextile secure and a slot on the opposite side through which a movable clamp extended to securely grab the other side of the geotextile sample. The test was designed so that the geotextile sample was entirely within the test box and subject to the confining pressure throughout the test. The interior dimensions of the test box were 16.5 cm (6.5 inches) by 12.1 cm (4.75 inches) by 6.4 cm (2.5 inches) deep. The top loading cap was (6.5 inches) by 12.1 (4.75 inches) to distribute the normal load uniformly over the soil material contained in the test box, Figure 1.

IN-SOIL STRESS-STRAIN TESTS

Two soils were used in the tests, Ottawa #30 sand and Monterey #0/30 sand. The Ottawa #30 sand has a uniformity coefficient of 1.43 and a specific gravity of 2.65. The sand has subrounded grain shape and the maximum and minimum dry densities (ρ_d) are 17.62 KN/m^3 and 15.32 KN/m^3 respectively. The Monterey #0/30 sand has a uniformity coefficient of 1.60 and a specific gravity of 2.65. The grain shape of the sand is subangular to subrounded. The maximum and minimum dry densities are 16.62 KN/m^3 and 14.40 KN/m^3 , respectively. Both soils are classified as SP (poorly graded sand) by the Unified Soil Classification System.

For the tests, the Ottawa sand was placed at a density of 16.81 KN/m^3 (107.0 pcf), $D_r = 68\%$, and the Monterey sand was placed at a density of 15.83 KN/m^3 (100.8 pcf), $D_r = 68\%$. Two overburden pressures were employed: 57.6 KPa and 114.0 KPa. The exposed geotextile was 7.6 cm (3.0 inches) by 3.8 cm (1.5 inches). The geotextile sample was chosen to be this size for two reasons. First, to place it as far away from the sides of the box as possible, to minimize the side friction effects. Second, to maintain a plane strain configuration and avoid necking effects at small strain. In the field, geotextiles are usually strained less than 10%. This was the range of strain of greatest interest in this study, but the tests were continued to 20% strain. In-air stress-strain tests are usually carried out at 2% to 10% strain per minute. El-Fermaoui and Nowatzki (7) performed in-soil tests at 2.5% strain per minute and McGowen et al. (14) conducted in-soil tests at 2% strain per minute. The strain rate used in this study was 3.15% per minute or a deformation rate of 1.2 mm (0.3 inches) per minute.

It is to be noted that the shear stresses (friction) developed along the galvanized steel movable clamp due to the confining pressures were assumed by most researchers to be very small compared to the shear stresses developed on the soil-geotextile interface and were neglected. However, pullout tests with the test box and the galvanized steel movable clamp without geotextile showed that the shear stresses were significant, especially at small strains. The in-soil stress-strain test results were corrected for these shear stresses. In addition, an in-air test, using the same test apparatus, was performed for comparison.

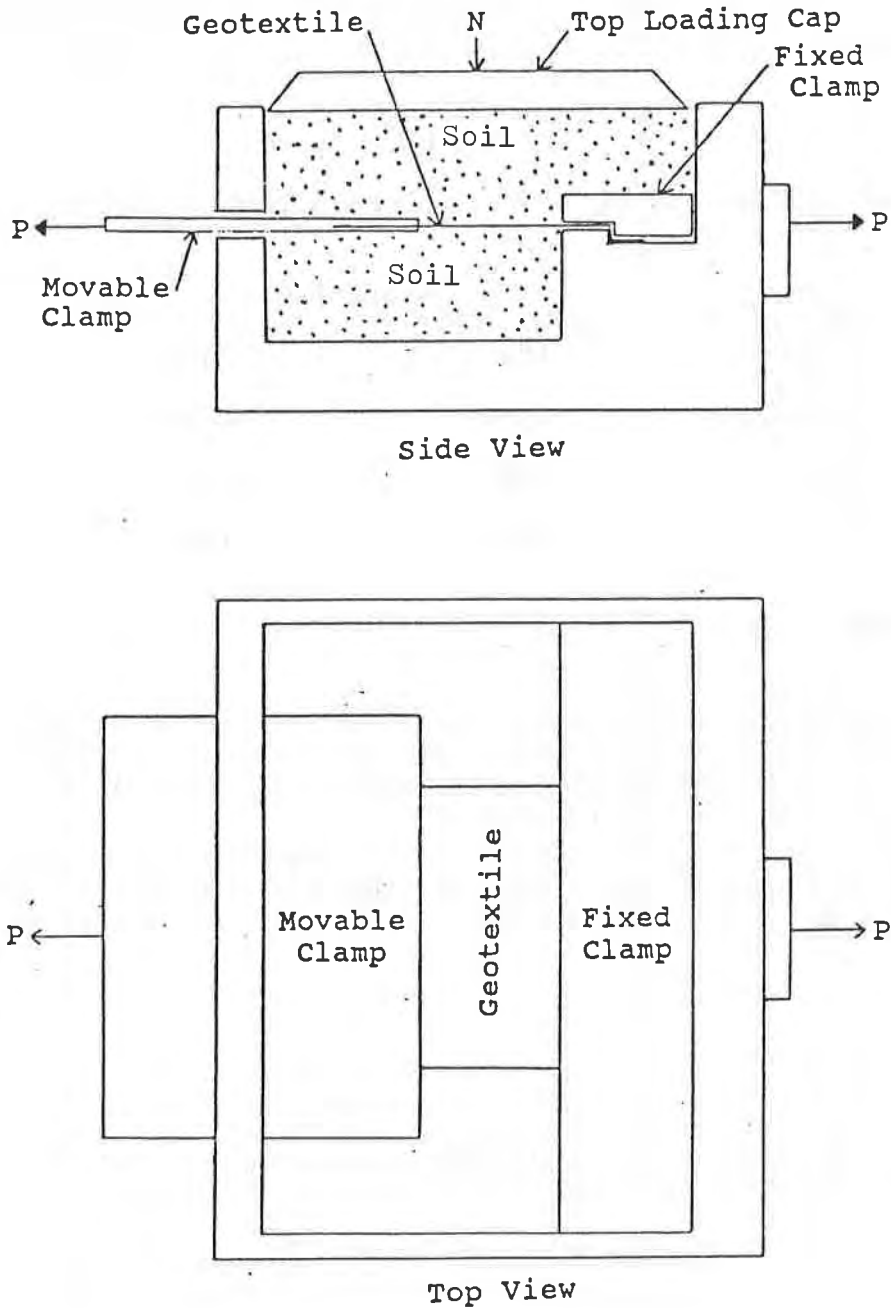


Figure 1. In-Soil Geotextile Stress-Strain Test Box

Figure 2 shows the load-deformation curves of Trevira 1127 geotextile with the two soils. It is seen that the geotextile has a much higher stiffness in the confinement of soil. The secant modulus of the geotextile at 2% strain was found to vary approximately linearly with overburden pressure, Table 1. The effect of soil type on the load-deformation relationship was found to be modest.

TABLE 1

Secant Moduli at 2% Strain for Trevira 1127 Geotextile

Confining Pressures (kPa)	Secant Moduli	
	Ottawa #30 (kPa)	Monterey #0/30 (kPa)
0 (in-air)	4,454	4,454
57.6	7,798	6,481
114.0	11,700	10,846

CONCLUDING REMARK

The test apparatus developed in this study provides a reliable means for determining the stress-strain-strength characteristics of geotextiles in the confinement of soils. Data reduction must account for the frictional resistance between the metal clamp and the confining soil.

The stiffness of the geotextile varied approximately linearly with overburden pressure. For the two sands, prepared at the same relative density, the effect of soil type on the stress-strain relationship of the geotextile is modest.

REFERENCES

- (1) Barsvary, A.K., MacLean, M.D., and Cragg, C.B.H., "Instrumented Case Histories of Fabric Reinforced Embankments over Peat Deposits," Proceedings of the Second International Conference on Geotextiles, Las Vegas, Vol. III, 1982, pp. 647-652.
- (2) Bell, J.R., and Steward, J.E., "Construction and Observation of Fabric Retained Soil Walls," Proceedings of the International Conference on the Use of Fabrics in Geotechnics, Paris, Vol. 1, 1977, pp. 123-128.
- (3) Bell, J.R., Greenway, D.R., and Vischer, W., "Construction and Analysis of a Fabric Reinforced Low Embankment," Proceedings of the International Conference on the use of Fabrics in Geotechnics, Paris, Vol. 1, 1977, pp. 71-75.

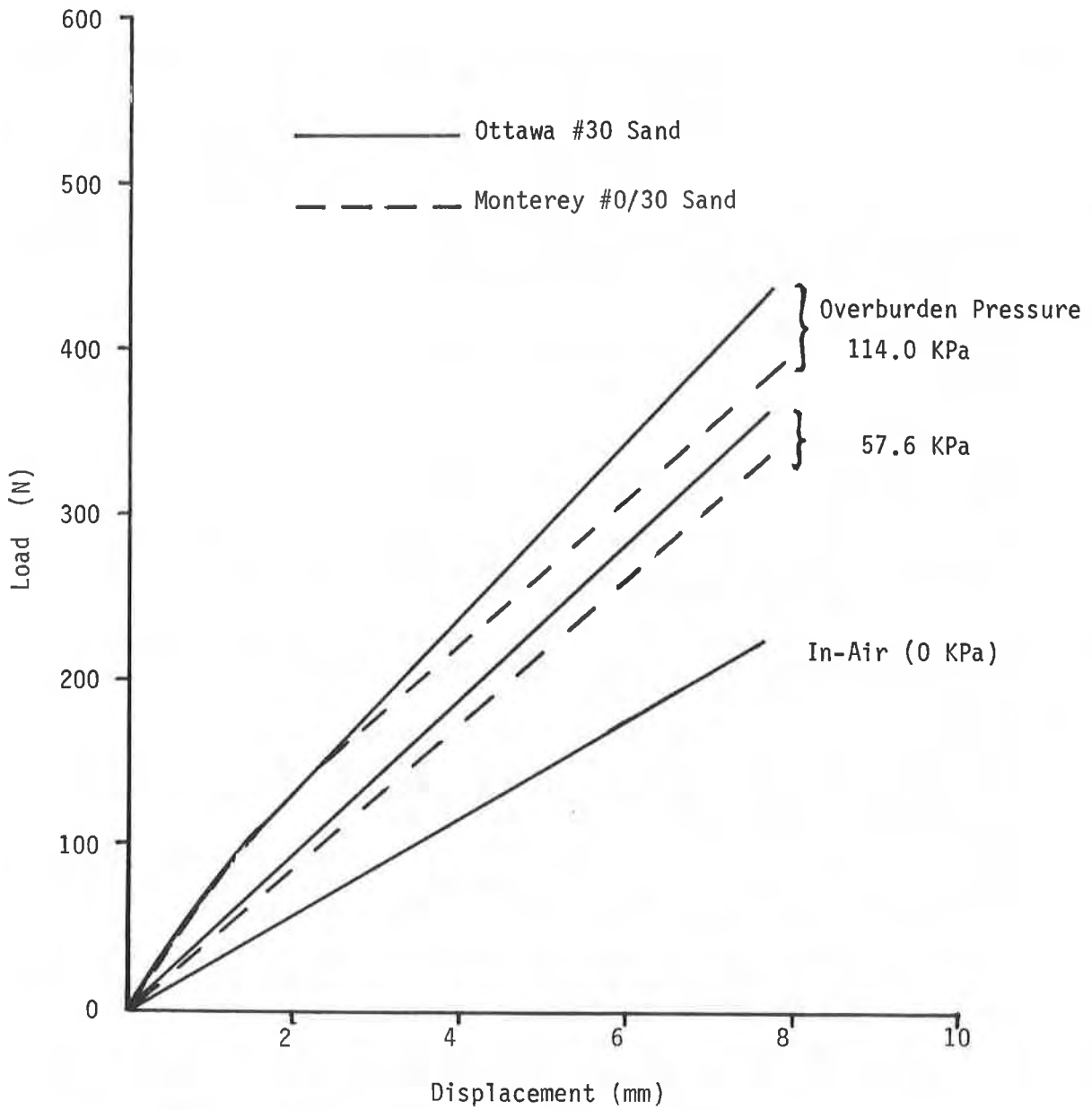


Figure 2. Load Versus Displacement Relations of the Geotextile

- (4) Bell, J.R., Barrett, R.K., and Ruckman, A.C., "Geotextile Earth Reinforced Retaining Walls Test, Glenwood Canyon, Colorado," Presented at the Annual Meeting, Transportation Research Records, 1983.
- (5) Douglas, G.E., "Design and Construction of Fabric Retaining Walls by New York State," Presented to the Annual Meeting, Transportation Research Board, 1982.
- (6) Earth Manual, Bureau of Reclamation, Department of the Interior, Second Edition, Denver, Colorado, 1974, 810 pp.
- (7) El-Fermaoui, A., and Nowatzki, E., "Effect of Confining Pressure on Performance of Geotextiles in Soils," Second International Conference on Geotextiles, Las Vegas, Nevada, Vol. 3, 1982, pp. 799-804.
- (8) Fowler, J., Haliburton, T.A., and Langan, J.P., "Design and Construction of Fabric Reinforced Embankment Test Section at Pinto Pass, Mobile Alabama," Transportation Research Record No. 749, 1980, pp. 27-33.
- (9) Fowler, J., "Design, Construction, and Analysis of Fabric-Reinforced Embankment Test Section at Pinto Pass, Mobile, Alabama," Technical Report EI-81-8, USAE Waterways Experiment Station, Vicksburg, Mississippi, 1981, 238 pp.
- (10) Guido, V.A., Biesiadecki, G.L., and Sullivan, M.I., "Bearing Capacity of a Geotextile Reinforced Foundation," Proc. 11th ICSMFE, San Francisco, Vol. 3, 1985, pp. 1777-1780.
- (11) Holtz, R.D., "Recent Developments in Reinforced Earth," Proceeding of the Seventh Scandinavian Geotechnic Meeting, Published by Polyteknisk Forlag, Copenhagen, Denmark, 1975, pp. 281-291.
- (12) Iwasaki, K. and Watanabi, S., "Reinforcement of Highway Embankments in Japan," Proceedings of the Symposium on Earth Reinforcement, ASCE, Pittsburgh, 1978, pp. 473-500.
- (13) Maagdenberg, A.C., "Fabrics Below Sand Embankment Over Weak Soils, Their Technical Specifications, and Their Applications in a Test Area," Proceedings of the International Conference on the Use of Fabrics in Geotechnics, Paris, Vol. 1, 1977, pp. 78-82.
- (14) McGowen, A., Andrawes, K.Z., and Kabir, M.H., "Load-Extension Testing of Geotextiles Confined In-soil," Second International Conference on Geotextiles, Las Vegas, Nevada, Vol. 3, 1982, pp. 783-798.
- (15) Murray, R.T., "Fabric Reinforcement of Embankments and Cuttings," Proceedings of the Second International Conference on Geotextiles, Las Vegas, Nevada, Vol. III, 1982, pp. 707-713.
- (16) Siel, B., "An Investigation of the Effectiveness of Tensile Reinforcement in Strengthening an Embankment over Soft Foundation," Master Thesis, Department of Civil Engineering, University of Colorado, Denver, 1986.
- (17) Wager, O., "Stabilitetsforbattrade Spontkonstruktion for Bankfyllningar," Swedish Geotechnical Institute, Reprint and Preliminary Report No. 28, Stockholm, 1968, pp. 21-24.

SESSION 2B

EMBANKMENTS OVER WEAK SOILS

ROWE, R.K. and SODERMAN, K.L.
The University of Western Ontario, Canada

Reinforcement of Embankments on Soils Whose Strength Increases With Depth

ABSTRACT

The results of a finite element study of the behaviour of geotextile reinforced embankments constructed on soils whose undrained strength increases with depth are reported. It is shown that practical failure of a reinforced embankment may occur prior to collapse as defined by classical plasticity. When the foundation strength increases with depth, the inclusion of high modulus geotextile reinforcement is shown to result in a substantial increase in embankment failure heights. Finally, the implications of these results with regard to modified limit equilibrium analysis of reinforced embankments are discussed.

INTRODUCTION

It has been established that under the right circumstances, geotextile reinforcement can substantially increase the stability of embankments constructed on weak relatively uniform foundations (e.g. (1), (2) and (3)). However, this research has also shown that for deposits where the foundation strength is relatively constant with depth, the effectiveness of reinforcement is highly dependent upon the geometry of the embankment relative to the layer depth. For layers with depths in excess of 0.5 times the embankment crest width, the contribution of even high modulus reinforcement to stability may be quite small.

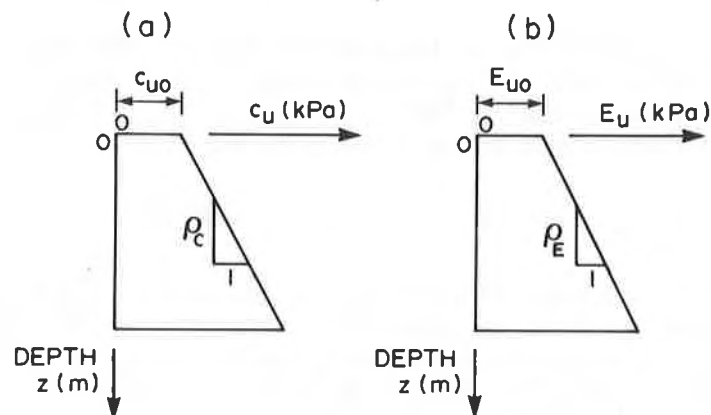


Figure 1. Typical foundation strength profile (a) and modulus profile (b)

Various investigators have considered the analysis of reinforced embankments (e.g. (4), (5), (6), (7), (8) and (9)). This present paper extends the authors' earlier research ((10), (11), (1), (2) and (3)) to the case where the soft foundation soil has undrained strength and Young's modulus which increase linearly with depth (see Fig. 1). Particular attention will be given to the effect of reinforcement upon the nature of the failure mechanism and hence the allowable height to which an embankment can be constructed on a given soft soil deposit. However, because of space limitations, it is only possible to present a few illustrative results for the case of a granular embankment with 2:1 side slopes and a crest width of 30 m.

ANALYSIS DETAILS

Small strain, elastic-plastic analyses were performed using the authors' finite element program. The soil model considered true elasto-plastic behaviour with a Mohr-Coulomb failure criterion and flow rule as proposed by Davis in 1968 (12) within the clay and fill as well as plastic failure at any point on the top and/or bottom of the geotextile-soil interface.

The analyses reported in this paper were performed for granular embankments with a crest width of 30 m resting on a 15 m deep soft clay deposit underlain by a rough rigid base. The embankment was constructed using up to 16 lifts and 250 load steps. The finite element mesh used involved 4620 degrees of freedom. The validity of the F.E. mesh was checked by performing analyses for the limiting cases of an unreinforced embankment and a perfectly rough rigid footing. Comparison of these F.E. results with the results from limit equilibrium analyses and from the plasticity solutions of Davis and Booker (13) indicated agreement to within 7% and 3% respectively for the worst cases examined.

The granular fill ($\phi = 32^\circ$, $\gamma = 20 \text{ kN/m}^3$, $\nu = 0.35$) was assumed to have a Young's modulus which is dependent on the minor principal stress and given by Janbu's equation (see (2)). For the results presented herein, the undrained modulus E_u of the clay was taken to be 125 times the undrained cohesion at any depth (i.e., $E_u/c_u = 125$, $\nu_u = 0.49$). The unit weight of the clay varied between 11 and 17 kN/m^3 depending on the soil strength and K'_0 was typically taken to be 0.6.

The geotextile was assumed to be located directly on the clay. The foundation-geotextile interface strength was assumed to be equal to the undrained shear strength of the clay at the surface of the clay (c_{u0} in Fig. 1). The fill-geotextile interface friction angle was assumed to be 32° .

FAILURE AND COLLAPSE

In any discussion concerned with reinforced embankment behaviour, it is essential to distinguish between the plasticity collapse height, and what constitutes the height at which the embankment could be regarded as having failed. Classical plasticity and limit equilibrium methods will only provide a direct indication of the potential collapse height/pressure at which the soil deformations become indeterminant. For example, in the case of a modified slip circle limit

equilibrium analysis, collapse corresponds to (a) the limit equilibrium strength being mobilized along the potential failure circle and (b) either breakage of the reinforcement or pullout of the reinforcement. Thus the collapse height is independent of the modulus of the soil or, more importantly, the modulus of the geotextile. It is, of course, well recognized that the collapse height calculated in this way may be overly optimistic and various investigators have recommended limiting the force in the geotextile to a value corresponding to some specified strain. In doing this, they are implicitly recognizing that the failure height may be less than the collapse height calculated for limiting equilibrium of the entire soil-geotextile system. This distinction may be particularly important for reinforced embankments on soft soils and can be illustrated by examination of the failure and collapse height deduced from careful finite element analyses.

Figure 2 shows the variation in the vertical displacement at point "a", beneath the shoulder of an embankment with a 30 m crest width, as the height h of the embankment is increased (i.e., as γh increases, where h is the total thickness of the fill above point a at any time). Results are given corresponding to fabric modulus values of 1000, 2000 and 4000 kN/m.

In each case, the deformations of the embankment became indeterminant and collapse occurred at an applied pressure of approximately 120 kPa. The collapse pressure was independent of the geotextile modulus and was in fact controlled by shear failure at the interface between the geotextile and the underlying clay foundation.

Inspection of Fig. 2 shows that the deformation of point "a" was also essentially independent of geotextile modulus up to a pressure of 60 kPa (i.e., half the collapse pressure) but beyond this pressure the geotextile modulus had a substantial effect on the deformations at point "a".

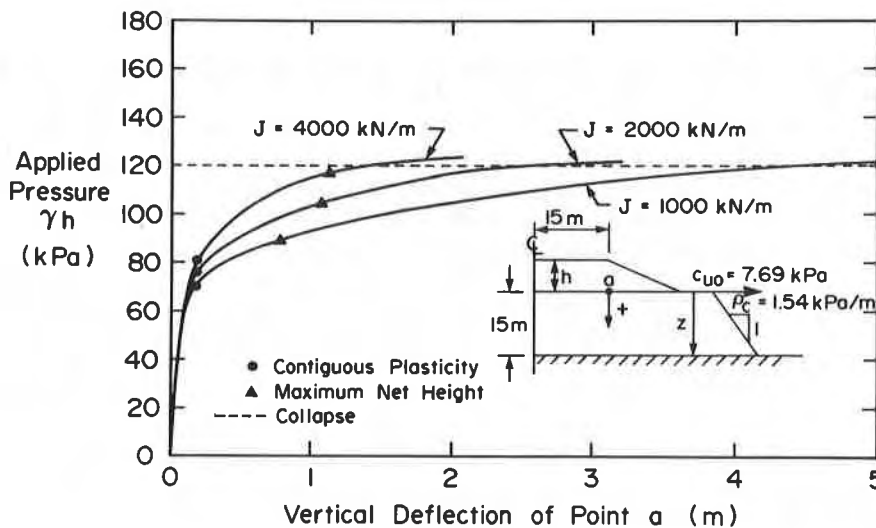


Figure 2. Applied pressure versus deflection for various reinforcement moduli

Contiguous plasticity corresponds to general plastic failure within the soil in the region of a potential collapse mechanism (i.e., the shear strength of the soil is mobilized along the potential collapse mechanism). For an unreinforced embankment, collapse and failure coincide with the development of contiguous plasticity and a corresponding collapse mechanism (in this case for a value of $\gamma h = 62$ kPa, see Fig. 3). However, for a reinforced embankment, the development of contiguous plasticity is only the first step towards failure and collapse. The height at which contiguous plasticity is developed is dependent upon the geotextile modulus as indicated in Fig. 2, but the effect is not large. The effect of the geotextile modulus is really only appreciable after the development of contiguous plasticity. Thus although the collapse pressure is the same for the three cases examined in Fig. 2, the deformations prior to collapse differ substantially.

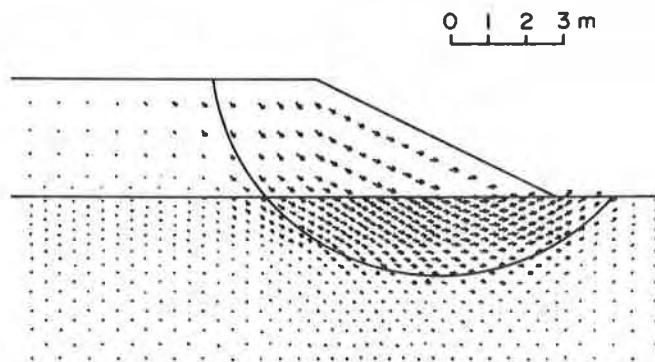


Figure 3. Velocity field at collapse for the case of $c_{u0}^* = 7.69$ kPa, $\rho_C^* = 1.54$ kPa/m and $J = 0$ (unreinforced)

The importance of considering deformations in any assessment of failure can be demonstrated by replotting the results given in Fig. 2 in the form of net fill height above original ground level (i.e., h - vertical deflection for that fill thickness) against the fill thickness h as shown in Fig. 4. For the unreinforced embankment, the maximum net fill height is about 3 m and occurs at the onset of contiguous plasticity. Notice that this also corresponds to the collapse height and in fact the net fill height at the onset of collapse is only slightly less than the fill thickness. For the reinforced embankments, it can be seen that the maximum net fill height does depend on the geotextile modulus. Any attempt to place additional fill after attaining this maximum height will result in the loss of net height. This corresponds to a controlled failure. In order to support the stresses imposed by the additional fill, large deformations of the geotextile and the soil must develop. This can continue in a controlled manner until collapse eventually occurs, however from a practical standpoint, the fill thickness of the embankment at failure should be considered to correspond to the fill thickness at the time the maximum net fill height is obtained and not the fill thickness required to achieve "true" (i.e., uncontrolled) collapse.

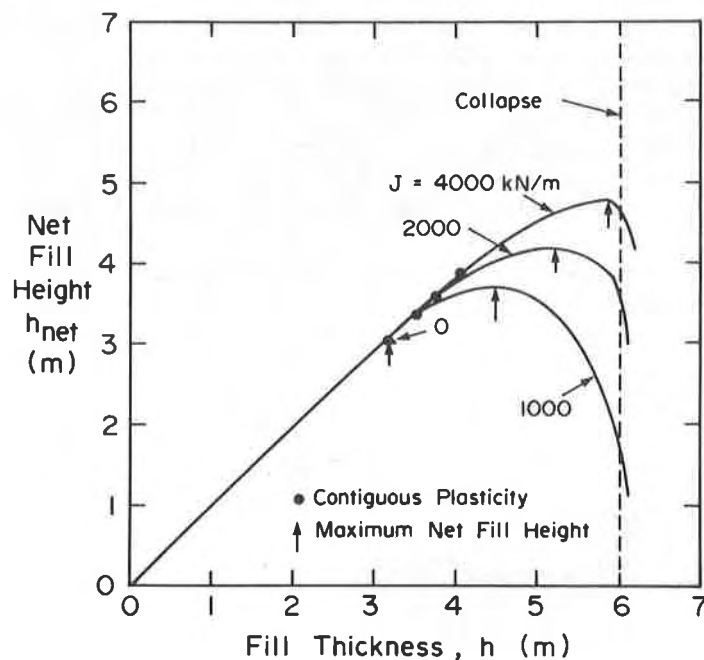


Figure 4. Net fill height vs fill thickness for various reinforcement moduli

The fill thicknesses, h , corresponding to failure (i.e., maximum net fill height) are shown as closed triangles in Fig. 2. Although failure was quite evident in Fig. 4, it is not obvious from Fig. 2; in fact, in Fig. 2 failure corresponds to a slope of the curve such that an increment in fill thickness yields an equal increment in vertical deflection.

From the foregoing it is evident that the failure height of an embankment on a given soil profile is directly related to the modulus of the geotextile. As might be expected, the maximum force mobilized in the geotextile at failure increases with increasing geotextile modulus, however because the collapse mechanism also changes with increasing geotextile modulus, these forces do not correspond to a unique strain for any given soil profile where the strength increases with depth. This change in mechanism will be discussed in the next section.

EFFECT OF REINFORCEMENT ON FAILURE MECHANISM

Figure 3 shows the velocity field at collapse for a typical case involving an unreinforced embankment. Also shown is the critical slip circle. Both the finite element analysis and the Bishop limit equilibrium analysis give a similar collapse height and mechanism. For deposits whose strength increases with depth, the mechanism is relatively shallow. For the cases examined in Fig. 3, the collapse mechanism is close to the shoulder and extends to a depth of about 2 m below the ground surface.

The inclusion of geotextile reinforcement significantly changes the collapse mechanism. For example, Fig. 5 shows the velocity field at collapse for an embankment reinforced with a "geotextile" having a modulus of 4000 kN/m. The collapse height for the reinforced case is approximately twice that for the unreinforced embankment (for a modulus of 4000 kN/m, the thickness of fill at failure is very close to that required for complete collapse--see Fig. 2). The reason for this substantial increase in collapse height is evident from a comparison of Figs. 3 and 5 which shows that the reinforcement forces the collapse mechanism down into the stronger soil at depth. In fact, increasing the modulus from 0 to 4000 kN/m moves the edge of the mechanism from near the shoulder to near the centreline of the embankment and forces it from a depth of about 2 m to a depth of about 8.5 m.

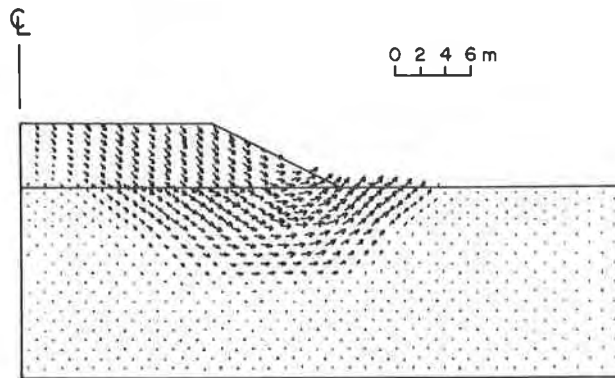


Figure 5. Velocity field at collapse for the case of $c_{uo}^* = 7.69$ kPa, $\rho_c^* = 1.54$ kPa/m and $J = 4000$ kN/m

ALLOWABLE PRESSURES

Figure 6 shows the effect of geotextile modulus on the allowable pressures (i.e., product of allowable height and fill unit weight) for a range of soil profiles assuming a factor of safety of 1.3 against failure. (In this context, the factor of safety is defined as the divisor necessary to reduce the soil strength to such a point that failure just occurs.)

For the embankments on a homogeneous deposit ($\rho_c=0$), the analyses showed that even a very high modulus reinforcement (i.e., 4000 kN/m) had relatively little effect on the allowable pressure. These results are consistent with the earlier findings of Rowe and Soderman (1) who showed that for deep uniform deposits, geotextile reinforcement had very little influence on the general stability of an embankment.

A substantially different result is observed when consideration is given to soil strength increase with depth as shown in Fig. 6. Indeed, for a strength increase with depth of 2 kPa/m, increases in the allowable pressure in excess of a factor of 2 were achieved in some cases. The potential increase in allowable fill thickness arising from an increase in geotextile modulus depends on both the rate of increase in strength with depth and the strength at the foundation-geotextile interface. Generally, the greater the increase in strength with depth, the more

effect increasing the geotextile modulus will have. However, an inspection of Fig. 6 also shows that the potential for achieving these increases is also controlled by the strength of soil-geotextile interface. For example, comparing the results given in Figs. 6a and 6c for a rate of increase in strength width depth (ρ_c) of 2 kPa/m, indicates that for a value of soil-geotextile interface cohesion of 5 kPa, most of the increase in allowable fill thickness due to geotextile reinforcement is realized for a modulus of 1000 kN/m and a four fold increase in modulus to 4000 kN/m only further increases the allowable pressure by about 6 kPa (i.e., approximately 0.3 m of fill). In this case, the force that can be carried by the higher modulus geotextile is severely limited by early failure at the clay-geotextile interface. When the strength of this interface is increased from 5 to 15 kPa (Fig. 6c), then for the same value of ρ_c ($\rho_c = 2$ kPa/m) increasing the geotextile modulus from 1000 kN/m to 4000 kN/m increased the allowable pressure by almost 40 kPa (i.e., approximately 2.0 m of fill).

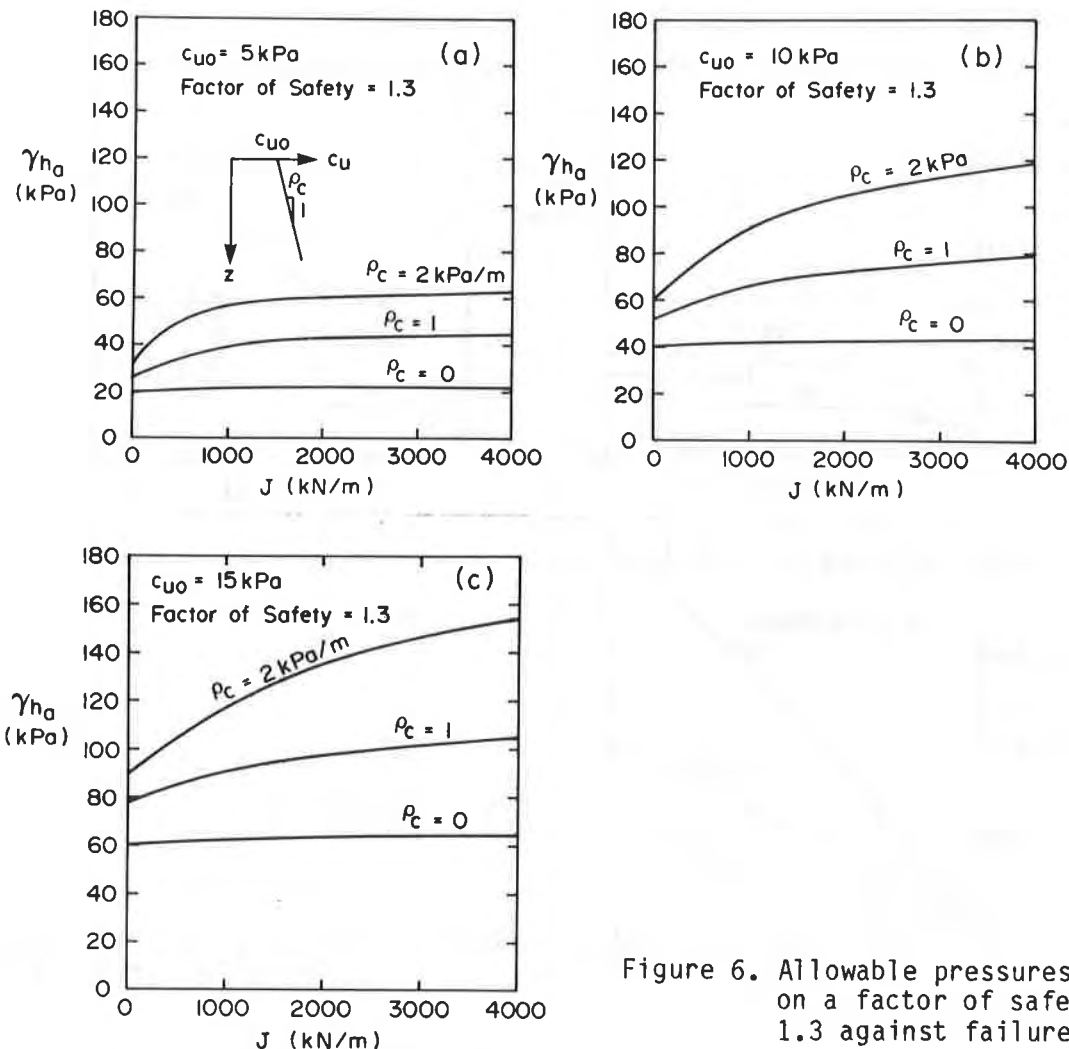


Figure 6. Allowable pressures based on a factor of safety of 1.3 against failure

The forces mobilized in the geotextiles at failure are shown in Fig. 7 for a number of cases. Note that the shear strengths adopted in Fig. 7 correspond to the nominal values given in Fig. 6 divided by the factor of safety $FS = 1.3$. Thus for an embankment on a foundation with nominal strengths of c_{u0} and ρ_c and a factor of safety $FS = 1.3$, factored strength values of $c_{u0}^* = c_{u0}/FS$ and $\rho_c^* = \rho_c/FS$ have been adopted for determining the failure pressures, γ_{h_u} and the geotextile force mobilized at failure. The failure pressure determined using the factored strength c_{u0}^*, ρ_c^* is taken to be the allowable pressure for an embankment on a foundation with nominal strength c_{u0}, ρ_c . It must, of course, be recognized that the forces given in Fig. 7 represent the forces at failure and not the forces expected under working conditions which will be substantially less.

As noted earlier, for low values of c_{u0} , the forces mobilized in high modulus geotextiles are relatively low and are controlled by the low soil-geotextile interface strength. For higher values of c_{u0} , the

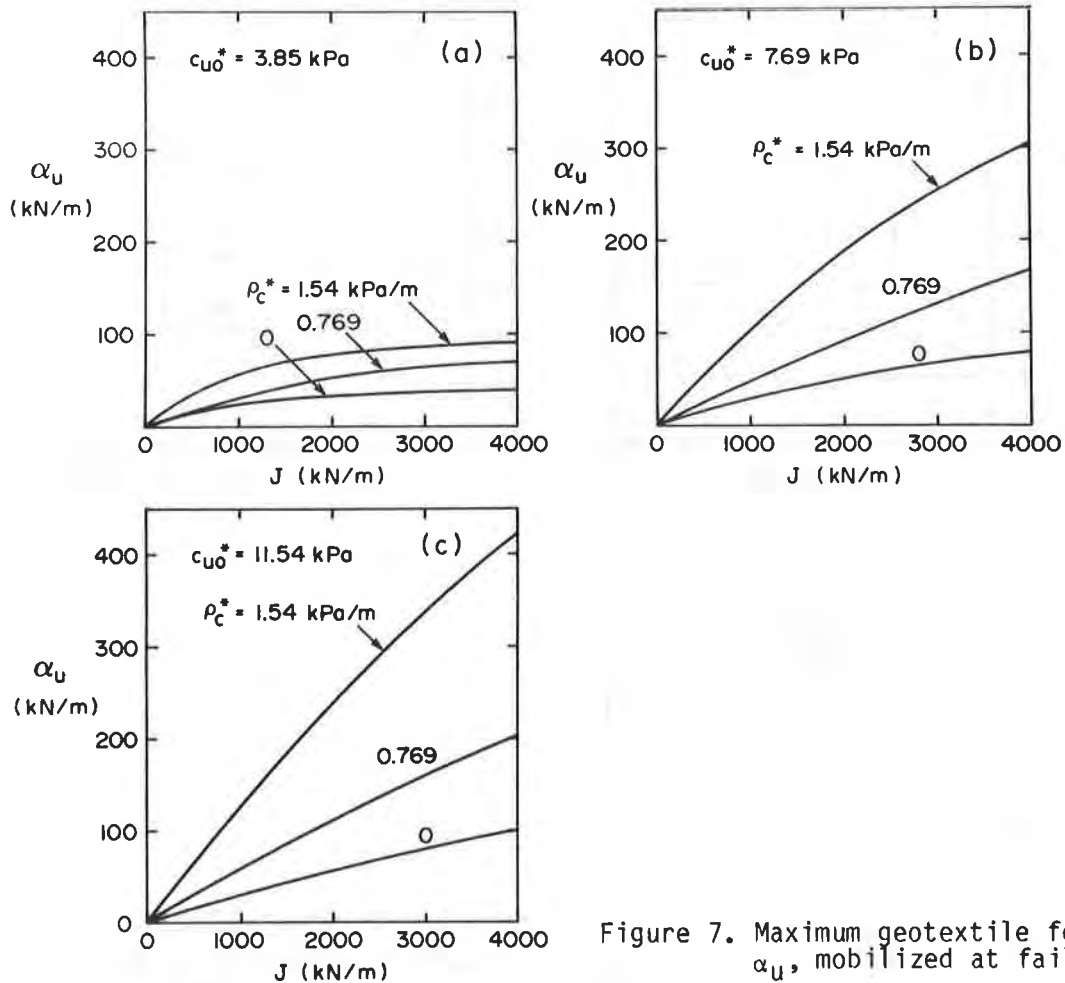


Figure 7. Maximum geotextile forces, α_u , mobilized at failure

soil-geotextile interface strength is sufficient to allow a substantial force to be developed in the geotextile at failure and so for profiles with significant strength increase with depth, it may be the permissible force in the geotextile (related to a specific geotextile's tensile strength) which will control the height to which an embankment could be constructed.

IMPLICATIONS FOR MODIFIED LIMIT EQUILIBRIUM ANALYSES

Comparison of the finite element results with the results from modified limit equilibrium analyses indicated good agreement provided that the geotextile force at failure determined from the finite element analysis was used as the geotextile force in the limit equilibrium calculations. While this finding is reassuring, it is not very helpful since it is necessary to have the results of the F.E. analysis in order to obtain reasonable results from limit equilibrium.

In an earlier publication (1), the authors proposed a modified limit equilibrium method for embankments on soil whose strength was constant with depth. In this approach, the force in the geotextile was limited to an allowable compatible strain which was deduced from the analysis of unreinforced embankments and was given by a simple expression. This approach worked well since the reinforced collapse mechanism was similar to the unreinforced collapse mechanism. However, as demonstrated earlier, this is not the case when embankments are constructed on a foundation where there is significant strength increase with depth. For these cases, the inclusion of significant geotextile reinforcement changes the strain pattern giving rise to a much deeper collapse mechanism passing through stronger and stiffer soil. Thus the "allowable compatible strain" which is determined for shallow mechanisms of the unreinforced case is not representative of the geotextile strains developed prior to failure for the reinforced embankments.

For similar reasons, limit equilibrium calculations performed assuming a blanket cutoff strain (be it 2%, 5%, 10% or whatever) to determine the geotextile force can not be expected to provide consistent results. For example, Fig. 8 shows a comparison of failure pressures obtained from finite element analysis, with those calculated using limit equilibrium for two different foundation strength profiles. The horizontal dashed lines indicate the collapse pressure obtained from the F.E. results while the asterisks refer to the F.E. failure pressures. The solid curves give the failure pressures obtained using a modified slip circle limit equilibrium analysis for the three values of allowable geotextile strain indicated. It is evident from Fig. 8 that for each different case, there is a specific allowable strain value which will result in agreement between the limit equilibrium and finite element failure pressures. However, this specific allowable strain value may vary depending on the foundation properties and geotextile modulus. For example, an allowable strain value of 5% seems to work reasonably well for the case in Fig. 8a provided the geotextile modulus is less than 2000 kN/m. However, if the geotextile modulus is 4000 kN/m, an allowable strain value of 5% yields a failure pressure which is 30% greater than the collapse pressure. Therefore, the allowable strain value of 5% which works well in some cases is grossly unconservative for others. Similar inconsistencies will result for any constant value of allowable geotextile strain which is adopted.

The authors' research suggests that modified limit equilibrium methods can yield reasonable results if the mobilized geotextile strain is known a priori either by instrumentation or by finite element analysis, however without such prior knowledge these methods can not be expected to provide consistently good results for soils whose strength increases significantly with depth.

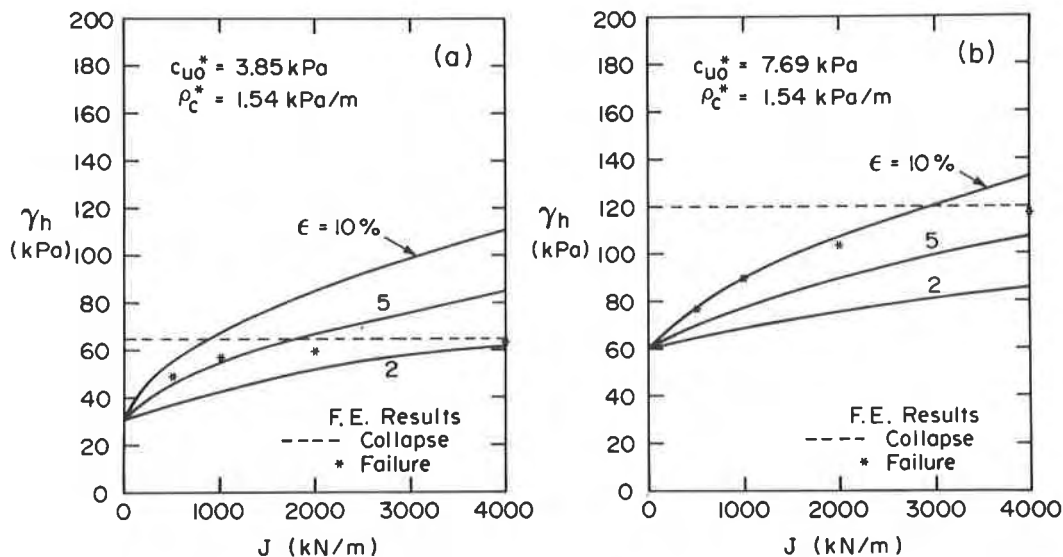


Figure 8. Comparison of limit equilibrium and finite element results.

CONCLUSIONS

The results of a finite element study of the behaviour of geotextile reinforced embankments on soils whose undrained strength increases with depth have been reported. It is shown that practical failure of a reinforced embankment may occur for fill thicknesses well below that required to cause collapse as defined by plasticity theory. Furthermore, it is shown that although the thickness of fill required to cause collapse may be relatively independent of geotextile modulus, the thickness of fill required to reach the maximum net embankment height may be substantially affected by the geotextile modulus.

The results presented demonstrate that the combination of geotextile reinforcement and strength increase with depth gives rise to a change in failure mechanism. As a result, provision of significant reinforcement may substantially increase the fill thickness which can be supported on soils whose strength increases with depth. This is shown to be true even on relatively deep deposits where the contribution of reinforcement would have been negligible if the strength had been assumed to be constant with depth.

The forces developed in a given geotextile at failure were found to depend on the shear strength of the geotextile-foundation interface. For soil profiles where the strength of the interface exceeds 10 kPa, quite large forces may be developed in the geotextile at failure for soils whose strength increases significantly with

depth (i.e., $\rho_c > 1.5$ kPa/m). In these cases, the strength of the geotextile may control the design height.

Finally, the implications of these results with regard to modified limit equilibrium analyses are discussed and it is indicated that while simple modified limit equilibrium methods work quite well for soils whose strength is constant with depth, these approaches do not provide consistently good results for soils whose strength increases with depth unless the actual force in the geotextile at failure is known either from a finite element analysis or field observation.

ACKNOWLEDGEMENT

The work described in this paper was supported by Grant A1007 from the Natural Sciences and Engineering Research Council of Canada.

REFERENCES

1. Rowe, R.K. and Soderman, K.L., "An Approximate Method for Estimating the Stability of Geotextile-Reinforced Embankments," Canadian Geotechnical Journal, Vol. 22, No. 3, 1985, p.p. 392-398.
2. Rowe, R.K. and Soderman, K.L., "Geotextile Reinforcement of Embankments on Peat," International Journal for Geotextiles and Geomembranes, Vol. 2, No. 4, 1985, p.p. 277-297.
3. Rowe, R.K. and Soderman, K.L., "Reinforced Embankments on Very Poor Foundations," International Journal for Geotextiles and Geomembranes, Vol. 4, No. 1, 1987 (to appear).
4. Fowler, J., "Theoretical Design Considerations for Fabric Reinforced Embankments," Proceedings, 2nd International Conference on Geotextiles, Las Vegas, Vol. 2, 1982, p.p. 665-670.
5. Ingold, T.S., "An Analytical Study of Geotextile Reinforced Embankments," Proceedings, 2nd International Conference on Geotextiles, Las Vegas, Vol. 2, 1982, p.p. 683-688.
6. Jewell, R.A., "A Limit Equilibrium Design Method for Reinforced Embankments on Soft Foundations," Proceedings, 2nd International Conference on Geotextiles, Las Vegas, Vol. 2, 1982, p.p. 671-676.
7. Boutrup, E. and Holtz, R.D., "Analysis of Embankments on Soft Ground Reinforced With Geotextiles," Proceedings, 8th European Conference on Soil Mechanics and Foundation Engineering, Helsinki, Vol. 2, 1983, p.p. 469-472.
8. Milligan, V. and La Rochelle, P., "Design Methods for Embankments Over Weak Soils," Proceedings of the Symposium on Polymer Grid Reinforcement in Civil Engineering, Institution of Civil Engineers, London, 1984, p.p. 95-102.
9. Gourc, J.P., Monnet, J. and Mommessin, M., "Reinforced Embankments on Weak Soil: Different Theoretical Approaches," Proceedings of 3rd International Conference on Geotextiles, Vienna, Vol. 4, 1986, p.p. 1043-1048.

10. Rowe, R.K., "The Analysis of an Embankment Constructed on a Geotextile," Proceedings, 2nd International Conference on Geotextiles, Las Vegas, Vol. 2, 1982, p.p. 677-682.
11. Rowe, R.K., "Reinforced Embankments: Analysis and Design," Journal of Geotechnical Engineering Division, ASCE, Vol. 110 (GT2), 1984, p.p. 231-246.
12. Davis, E.H., "Theories of Plasticity and Failure of Soil Masses," In: Soil Mechanics - Selected Topics, Ch. 6, Ed. by I.K. Lee, Butterworths, London, 1968.
13. Davis, E.H. and Booker, J.R., "The Effect of Increasing Strength With Depth on the Bearing Capacity of Clays," Geotechnique, Vol. 23, No. 4, 1973, p.p. 551-563.

HUMPHREY, D.N.

University of Maine, U.S.A.

HOLTZ, R.D.

Purdue University, U.S.A.

Use of Reinforcement for Embankment Widening

ABSTRACT

The effect of reinforcement on existing embankments constructed on soft ground that are widened and have their grade raised was investigated using a nonlinear finite element program with a cap type work hardening soil behavior model. The influence of existing embankment height, width of the widened section, and crust strength were examined and it was found that the reinforcement has a significant beneficial effect. Reinforcement was most beneficial for a 9.1-m widened section and a foundation with a weak crust. The benefit was less for 4.6-m and 13.7-m widened sections.

INTRODUCTION

Highway designers are often faced with the problem of widening and raising the grade of existing embankments constructed on soft ground. The low shear strength of the foundation may lead to loss of stability and excessive deformations. In a typical application, the foundation soils are fully consolidated under the weight of the existing embankment, so the undrained shear strength of the foundation is greater than that of the natural soil. The reinforcement (geotextile or geogrid) is usually placed over the crest and slope of the existing embankment and on the natural ground surface beneath the widened section, as shown on Fig. 1. Additional fill for the widened and raised section is then placed rapidly. Consequently, little dissipation of excess pore pressure occurs in the foundation during construction.

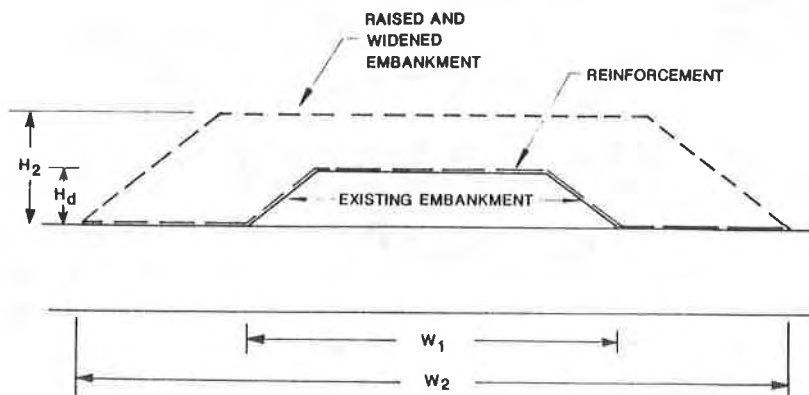


Fig. 1 Geometry for embankment widening.

Only three cases of embankment widening using geotextile reinforcement are reported in the literature (1,6,9). In each case apparently the reinforcement had a significant stabilizing effect. There have been no other systematic studies of the effectiveness of reinforcement in this application.

This paper presents the results of a finite element (FE) study on use of reinforcement to increase stability and reduce deformations when existing embankments are widened and have their grade raised. This work was part of a larger study of reinforced embankment behavior (2,3,4,7). The FE program uses a cap type work hardening soil plasticity model which is described below. Parameters for the model were determined from readily available soil properties using the procedure given in (2,4). The results of a comparative study of reinforced and unreinforced embankment behavior are presented herein, and the effect of reinforcement on displacements, embankment height at failure, and state of stress in the foundation and embankment fill are described. In addition, the forces developed in the reinforcement are examined. The influence of existing embankment height, width of the widened section, and strength of the surface crust on embankment behavior is presented.

ANALYSIS PROCEDURE

The effect of reinforcement on widened embankment behavior was studied using a plane strain finite element program PS-NFAP. Program operation is described in (5). Foundation soil behavior was represented by an elastic-plastic model with a strain hardening cap. The main features of the cap model are outlined in the next section. Further details are given in (2,7). The procedure used to represent embankment and foundation behavior is described in the subsequent section.

Cap Soil Model

The cap model used herein has a cone shaped Drucker-Prager ultimate failure surface and an elliptical work hardening cap (Fig. 2). They are expressed in terms

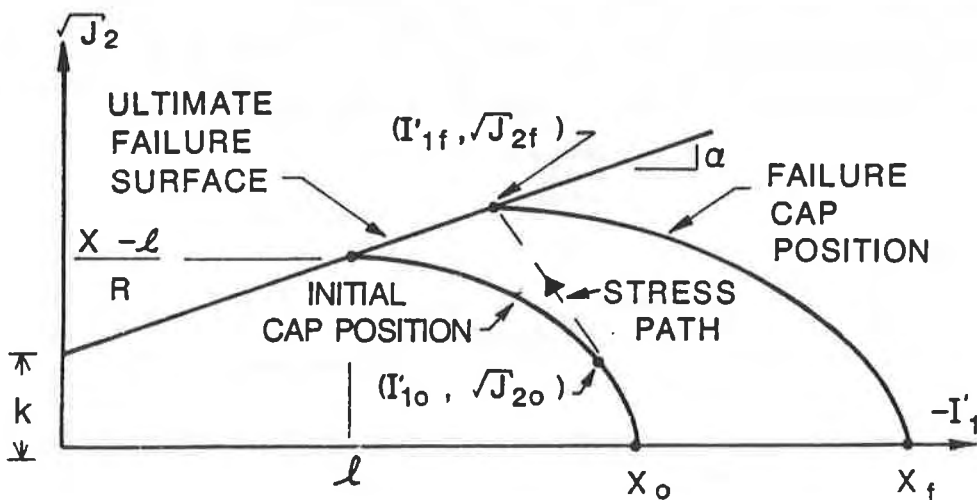


Fig. 2 Cap model in $I'_1 - J_2^{1/2}$ space.

of effective stresses by the first invariant of the stress tensor I'_1 and the second invariant of the stress deviator tensor J_2 . Compressive stresses and strains are taken as negative. The ultimate failure surface has a slope α and an intercept with the $J_2^{1/2}$ axis of κ (Fig. 2). The equation of this surface is

$$\alpha I'_1 + J_2^{1/2} - \kappa = 0 \quad (1)$$

The cap intersects the I'_1 axis at x and the ultimate failure surface at coordinates $[\ell, (x-\ell)/R]$ (Fig. 2). The aspect ratio R is the ratio of the major and minor radii. The cap's shape is described by the equation of an ellipse

$$(I'_1 - \ell)^2 + R^2 J_2 - (x - \ell)^2 = 0 \quad (2)$$

The position of the cap is coupled to the plastic volumetric strain ϵ_V^P by the relation

$$\epsilon_V^P = W[\exp(Dx) - 1] \quad (3)$$

where W and D are curve fitting parameters. A normal flow rule is assumed.

Elastic behavior is governed by the bulk (K) and shear (G) moduli which are given by

$$K = K_1 A_p [I'_1 / (3A_p)]^{K_2} \quad ; \quad G = G_2 + G_1 K \quad (4)$$

where K_1 , K_2 , G_1 , and G_2 are fitting parameters; A_p is atmospheric pressure and has the same units as the moduli. To avoid numerical difficulties it is necessary to specify a small minimum value of the bulk modulus K_{min} . For undrained loading the condition of no volume change is obtained by adding the apparent stiffness of the pore fluid-solid particle system to the stiffness of the soil skeleton (7).

Representation of Embankment and Foundation Behavior

The stress-strain behavior of the embankment fill was taken to be elastic-plastic with an ultimate failure surface of the Drucker-Prager type (2). A typical lift by lift embankment construction sequence was simulated using an incremental loading technique (7). Buoyant unit weight was used for fill that settled below the ground water table. No slip was allowed at the soil-reinforcement interfaces. This is reasonable provided the interface shear strength equals or exceeds the soil shear strength. In the field no forces develop in the reinforcement until fill is placed on it, and this development was simulated in the model.

The initial state of stress and shear strength in the foundation was obtained by simulating construction of the existing embankment with drained conditions in the foundation. This accounted for consolidation and increase in strength of the foundation soils under the existing embankment. Then, the widened and raised section was constructed with the foundation soils undrained. Further tendency for volumetric strain caused generation of excess pore pressure.

CASES ANALYZED

The cases analyzed had the basic geometry shown in Fig. 1. The existing embankment was 36.6 m (120 ft) wide at its base (W_1) with 2h:1v side slopes. The foundation was 9.1 m (30 ft) thick. Existing embankment heights (H_d) of 1.1 m (3.75 ft) and 2.3 m (7.5 ft) were examined. The widened section also had 2h:1v side slopes and fill widths $[(W_2 - W_1)/2]$ of 4.6, 9.1, and 13.7 m (15, 30, and 45 ft) were added to each side of the embankment. The reinforcement was located as shown in Fig. 1 and had a modulus of 880 kN/m (5000 lb/in) which represents a strong, high modulus geotextile or geogrid.

The embankment fill was granular. Effective strength parameters $\phi' = 32^\circ$ and $c' = 3.3$ kPa (68 psf) were assumed which correspond to $\alpha = 0.17$ and $\kappa = 2.4$ kPa for plane strain conditions (2,4). The small cohesion was used to avoid numerical difficulties. The bulk modulus fitting parameters were chosen to match nonlinear stress strain parameters given by (8). $K_1 = 190$ and $K_2 = 0.65$ provided a reasonable fit. A_p was 101.3 kPa. A minimum bulk modulus of 960 kPa (20,000 psf) was specified which corresponds to about 0.2 m of fill. Poisson's ratio was taken to be 0.35 resulting in $G_1 = 0.33$ and $G_2 = 0.0$. The fill had a unit weight of 18.9 kN/m^3 (120 pcf).

The foundation soils had the properties given in Table 1. The upper 2.3 m (7.5 ft) of the foundation was taken to be an overconsolidated crust. Two crust strengths were considered: 12 kPa (250 psf; strong crust) and 6 kPa (125 psf; weak crust). Soil underlying the crust was normally consolidated. The cap parameters of the foundation soils were determined using the procedures given in (2,4) and are summarized in Table 2.

BEHAVIOR OF REINFORCED EMBANKMENTS

The FE program was used to study the behavior of reinforced and unreinforced embankments with the geometry and soil properties given above. The height at failure, relative increase in embankment height (surcharge), and force in the reinforcement at failure for all cases is summarized in Table 3. The relative increase in embankment height is defined as the percent increase in height of the reinforced over the unreinforced embankment compared at the lesser of the two horizontal deformations at failure. Also shown in Table 3 for comparison are the results for a completely newly constructed embankment ("normal" embankment; i.e., existing embankment height of zero).

Comparison of Reinforced and Unreinforced Embankment Behavior

The effect of reinforcement was examined by comparing the behavior of reinforced and unreinforced embankments with a 9.1-m widened section on a foundation with a weak crust. The horizontal displacement at the toe and maximum settlement at the base of the embankment are compared in Fig. 3. The reinforcement increased the height at failure (expressed as a surcharge stress) and reduced deformations. The relative increase in height made possible by reinforcement was 12% for the 1.1-m high existing embankment and 40% for the 2.3-m high existing embankment.

Table 1. Foundation soil properties.

$\phi' = 28^\circ$	$C_r = 0.04$
$c' = 0.0$	$e_o = 0.7$
$s_u/\sigma'_{vo} = 0.32$	$v' = 0.3$
$C_c = 0.25$	$\gamma_{sat} = 18.1 \text{ kN/m}^3$

Table 2. Cap parameters for foundation soil.

Parameter	Normally consolidated	Strong crust	Weak crust
α	0.183	0.16	0.17
κ	0.005 kPa	0.005 kPa	0.005 kPa
K_1	98.0	98.0	98.0
K_2	1.0	1.0	1.0
K_{min}	48 kPa	48 kPa	48 kPa
A_p	101.3 kPa	101.3 kPa	101.3 kPa
G_1	0.46	0.46	0.46
G_2	0.0	0.0	0.0
Dx_o	-0.996	-0.996	-0.996
x_o	n.a.	-1.75	-0.83
W	0.146	0.146	0.146
R	0.75	0.75	0.75
K_o	1.0	0.6	0.47

Table 3. Summary of results of embankment widening analysis.

Existing embankment height (m)	Width of widened section (m)	Crust strength	-Ht. at failure-		Reinf. force at failure (kN/m)	Relative increase in height (%)
			Unreinf. (m)	Reinf. (m)		
2.3	4.6	Weak	3.8	5.2	35	17
2.3	9.1	Weak	3.1	4.1	57	40
2.3	13.7	Weak	2.7	3.1	34	25
2.3	9.1	Strong	3.8	4.0	31	10
1.1	9.1	Weak	2.7	3.1	34	12
1.1	9.1	Strong	2.3	3.9	26	13
0.0*	n.a.	Weak	2.3	2.6	19	22

*Normal embankment; completely newly constructed.

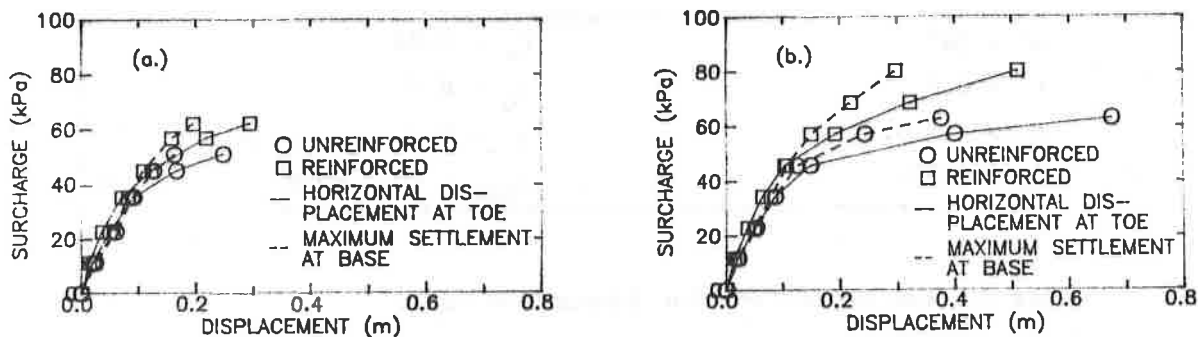


Fig. 3 Horizontal displacement at toe and maximum settlement at base for reinforced and unreinforced embankments, 9.1-m widened section, weak crust; (a) 1.1-m high existing embankment, (b) 2.3-m high existing embankment.

Displacement vectors caused by placing the widened section are shown in Fig. 4 for the reinforced embankment at its failure height of 4.1 m. The largest movements occur in the upper 4.6 m of the foundation beneath the widened section. Movements beneath the existing embankment are small.

Reinforcement alters the state of stress in the foundation. For a 2.3-m high existing embankment the state of stress for reinforced and unreinforced embankments at a height of 3.1 m are compared in Fig. 5. The unreinforced embankment failed at this height. Reinforcement reduces the extent of the failure, "corner", and "cap" states beyond the toe. The "corner" state corresponds to perfectly plastic behavior (i.e., ultimate undrained shear strength has been reached) and the failure and "cap" states correspond to elastic-plastic behavior (i.e., large plastic strains occurring but ultimate undrained shear strength has not been reached). In the embankment, reinforcement reduced the extent of soil in the tension state in the upper portion of the fill as seen by comparing Figs. 6a and 6b. This increases the available shear resistance in the fill, thereby increasing stability. Similar behavior was observed for the 1.1-m high existing embankment.

Forces in Reinforcement

The maximum force in the reinforcement versus applied surcharge is shown in Fig. 7 for a 9.1-m widened section and a foundation with a weak crust. The force increases with the applied load and the increase is quite rapid as failure is approached. The force at failure was 34 kN/m for the 1.1-m high existing embankment and 57 kN/m for the 2.3-m high existing embankment. The maximum force at failure for all cases is summarized in Table 3 and ranged from 26 to 57 kN/m. This is less than the tensile strength of many types of reinforcement materials.

The distribution of the reinforcing forces for the 2.3-m high existing embankment at several surcharges is shown in Fig. 8. The location of the maximum force moves from the mid-point of the widened section to near the toe of the existing embankment as the surcharge increases. The force near the center of the embankment and near the toe are small. The former suggests that it may not be necessary to

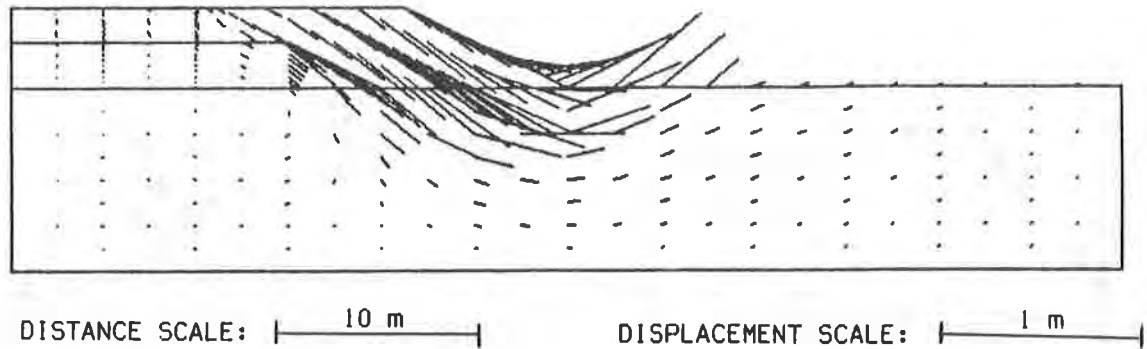


Fig. 4 Displacement vectors for due to placing widened section, 2.3-m high existing embankment, 9.1-m widened section, weak crust.

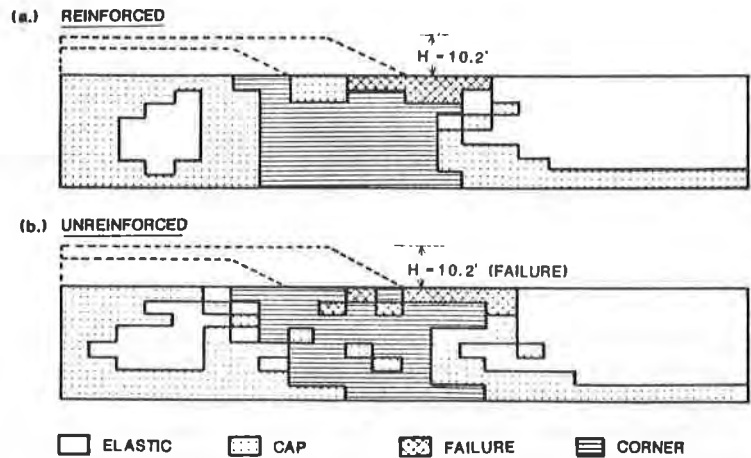


Fig. 5 State in foundation for reinforced and unreinforced embankments at height of 3.1 m, 2.3-m high existing embankment, 9.1-m widened section, weak crust (10.2' = 3.1 m).

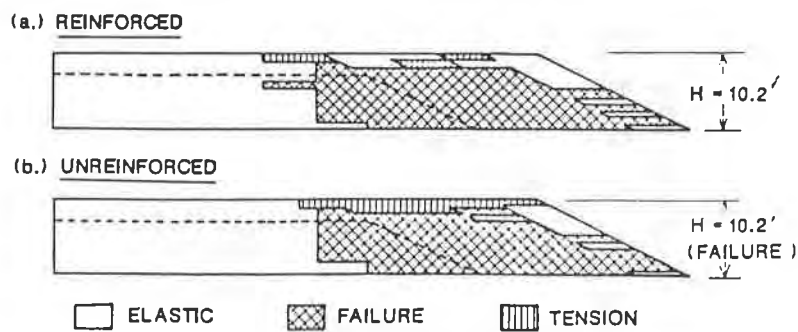


Fig. 6 State in embankment for reinforced and unreinforced embankments, 2.3-m high existing embankment, 9.1-m widened section, weak crust (10.2' = 3.1 m).

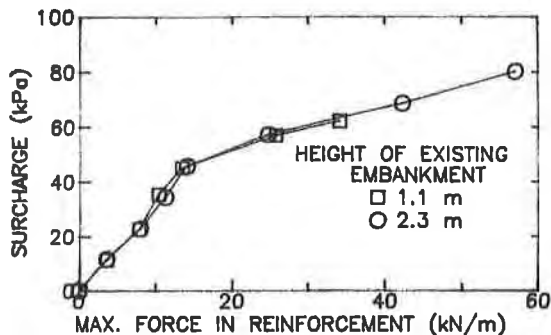


Fig. 7 Maximum reinforcement force vs. surcharge, 9.1-m widened section, weak crust.

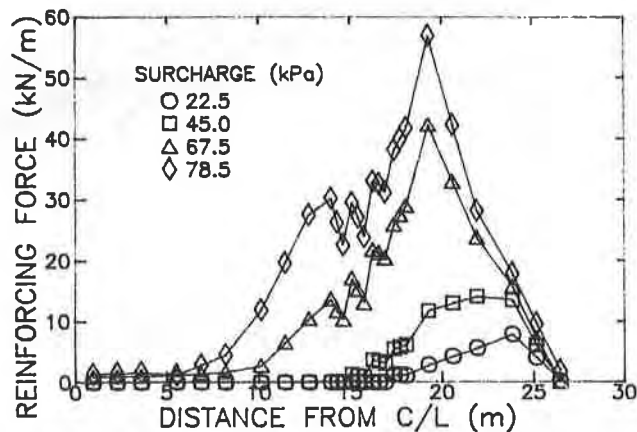


Fig. 8 Distribution of force in reinforcement vs. surcharge, 2.3-m high existing embankment, 9.1-m widened section, weak crust, reinforced.

place the reinforcement across the full width of the existing embankment crest. Significant reinforcing forces develop near the shoulder and on the slope of the existing embankment.

Effect of Existing Embankment Height

The effect of existing embankment height was examined. Horizontal displacement at the toe vs. surcharge for reinforced embankments with 1.1 and 2.3-m high existing embankments as well as a normal section are compared in Fig. 9 for the weak crust case. Similar behavior was observed for the strong crust case. For a given surcharge the displacement decreases as the existing embankment height increases. The relative increase in height made possible by reinforcement did not show a consistent relationship with existing embankment height (Table 3). The maximum force in the reinforcement versus surcharge for the two heights is shown in Fig. 7. This indicates that the height of the existing embankment has only a minor influence on reinforcement force.

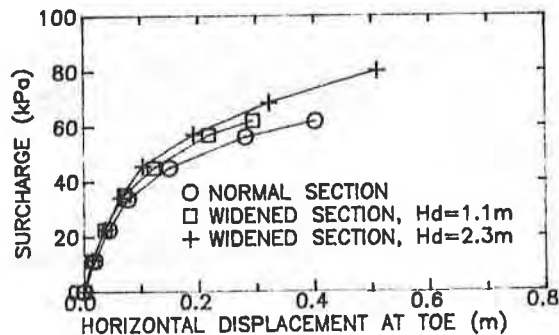


Fig. 9 Effect of existing embankment height on displacement at toe, 9.1-m widened section, weak crust, reinforced.

Effect of Width of Widened Section

The effect of width of the widened section on horizontal displacements at the toe is shown in Fig. 10 for a 2.3-m high existing embankment and a foundation with a weak crust. A normal section is also shown for comparison. Displacements increase as the width of the widened section increases and approach that of the normal section for the +13.7-m width. It is seen in Table 3 that the relative increase in height made possible by reinforcement is quite high for the +9.1-m width. The increase is about the same for the normal and +13.7-m widths suggesting that the influence of the existing embankment is small for wide widened sections.

The maximum force in the reinforcement versus the surcharge is also shown in Fig. 10. The curves for the normal, +9.1-m, and +13.7-m widths are very similar but it is quite different for the +4.6-m width. The reason for this is seen by examining the distribution of reinforcing force at failure (surcharge= 95 kPa) as shown in Fig. 11. The maximum reinforcing force occurs near the shoulder rather than the toe of the existing embankment as occurred for the +9.1-m and +13.7-m cases. This suggests that the critical slip surface passes near the shoulder of the existing embankment and the reinforcement on the original ground surface beneath the widened section does not directly contribute to stability. Considering a circular failure surface, the moment arm of a reinforcing force near the shoulder would be less than a force near the toe. This may account for the relative increase in height made possible by reinforcement being much less for the +4.6 m than for the +9.1 m or +13.7 m cases.

Effect of Crust Strength

The effect of crust strength on horizontal displacement at the toe and maximum settlement at the base for reinforced embankments with 9.1-m widened sections and 2.3-m high existing embankments is shown in Fig. 12. The displacements are greater for the weak than for the strong crust. Similar results were obtained for the 1.1-m high existing embankment. The relative increase in height made possible by reinforcement is summarized in Table 3. It shows that reinforcement is more effective for the weak crust, 2.3-m high case but are about the same for the 1.1-m high case. For a given surcharge the maximum force in the reinforcement is higher for the weak than the strong crust.

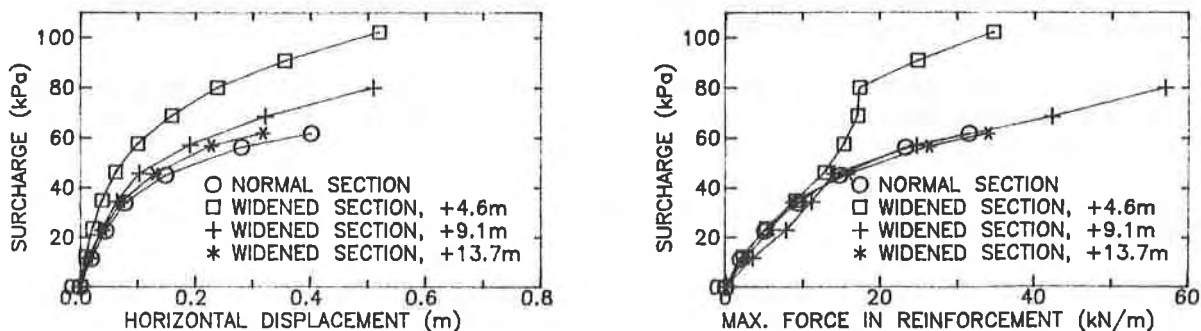


Fig. 10 Effect of width of widened section on displacement at toe and maximum force in reinforcement, 2.3-m high existing embankment, weak crust, reinforced.

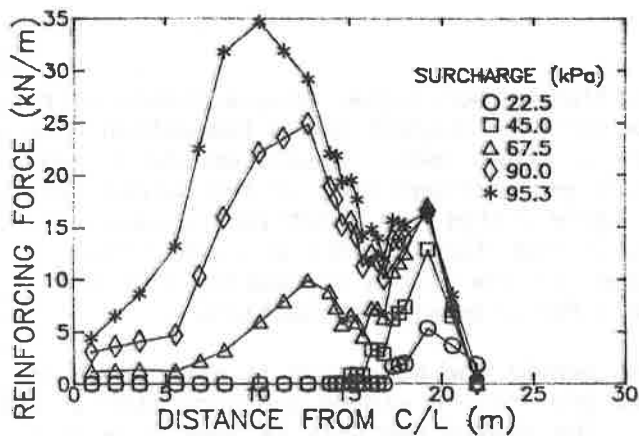


Fig. 11 Distribution of force in reinforcement vs. surcharge, 2.3-m high existing embankment, 4.6-m widened section, weak crust.

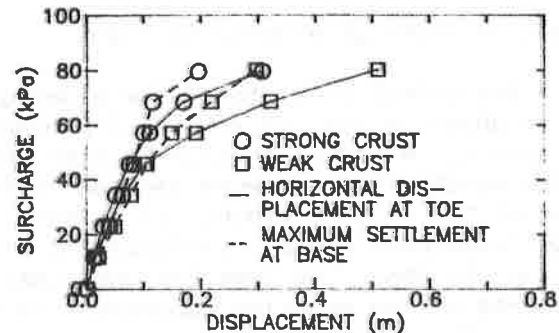


Fig. 12 Effect of crust strength on displacement at toe, 2.3-m high existing embankment, 9.1-m widened section, weak crust, reinforced.

CONCLUSIONS

Based on this study the following conclusions are made:

1. Reinforcement has a significant beneficial effect especially for some combinations of existing embankment height, width of the widened section, and crust strength.
2. Reinforcement was found to reduce horizontal deformations and increase stability. The highest relative increase in height made possible by reinforcement was 40%.
3. The effect of the reinforcement is to reduce the extent of the plastic and elastic-plastic zones in the foundation and to reduce the tensile zone in the embankment fill.
4. The behavior of embankments with wide widened sections approaches that of a completely newly constructed embankment.
5. The effect of reinforcement may be small for narrow widened sections because the critical failure surface passes through the existing embankment so there is little stabilizing effect provided by the reinforcement.
6. There may be little benefit to reinforcing the central portion of the existing embankment crest.
7. The maximum force in the reinforcement for most cases was less than the tensile strength of many strong geotextiles and geogrids.

ACKNOWLEDGEMENTS

Financial support for this research was provided by the Indiana Department of Highways and the Federal Highway Administration, through the Joint Highway Research Project at Purdue University. This support is gratefully acknowledged.

REFERENCES

- (1) Burwash, W.J., "A case history involving the use of a geotextile for a highway embankment on muskeg," Proceedings of the First Canadian Symposium on Geotextiles, The Canadian Geotechnical Society, Calgary, Alberta, September 23, 1980, pp. 225-235.
- (2) Humphrey, D.N., "Design of reinforced embankments," Joint Highway Research Project, School of Civil Engineering, Purdue University, West Lafayette, Indiana, Report No. FHWA/IN/JHRP-86/16, December, 1986, 423 pp.
- (3) Humphrey, D.N. and Holtz, R.D., "Reinforced Embankments -- A Review of Case Histories," Geotextiles and Geomembranes, Vol. 4, 1986 (to be published).
- (4) Humphrey, D.N. and Holtz, R.D. (1987), "A Procedure to Determine Cap Model Parameters," Proceedings of the Second International Conference on Constitutive Laws for Engineering Materials; Theory and Application, The University of Arizona, Tucson, Arizona, January, 1987, 8 pp. (to be published).
- (5) Humphrey, D.N., McCarron, W.O., Holtz, R.D., and Chen, W.F., "Finite element analysis of plane strain problems with PS-NFAP and the cap model -- User's manual," Joint Highway Research Project, School of Civil Engineering, Purdue University, West Lafayette, Indiana, Report No. FHWA/IN/JHRP-86/17, December, 1986, 184 pp.
- (6) Lukanen, E.O. and Teig, G., "Design and evaluation of roadway widening sections through swamps," Investigation No. 199 Initial Report, Research and Standards Section, Office of Materials, Research and Standards, Minnesota Department of Transportation, 1976, 40 pp.
- (7) McCarron, W.O., "Soil plasticity and finite element applications," Ph.D. Thesis, Purdue University, West Lafayette, Indiana, 1985, 265 pp.
- (8) Rowe, R.K., MacLean, M.D. and Soderman, K.L., "Analysis of a geotextile-reinforced embankment constructed on peat," Canadian Geotechnical Journal, Vol. 21, No. 3, August, 1984, pp. 563-576.
- (9) Volman, W., Krekt, L. and Risseuw, P., "Reinforcement with fabrics, a new technique to improve the stability of embankments on weak subsoils," (Originally in French, translated by D. N. Humphrey), Proceedings of the International Conference on the Use of Fabrics in Geotechnics, Ecole Nationale des Ponts et Chaussees, Paris, France, Vol. I, 1977, pp. 55-60.

FOWLER, J.

U.S. Army Corps of Engineers, U.S.A.

KOERNER, R.M.

Drexel University, U.S.A.

Stabilization of Very Soft Soils Using Geosynthetics

ABSTRACT

The introduction of high strength geosynthetic materials has allowed for construction on heretofore impossible sites. Saturated, fine-grained soils with in-situ unconsolidated-undrained strengths as low as 1.0 kPa (20.8 lb/ft²) have been successfully utilized for embankment foundations using geotextiles or geogrids for direct ground support. When rapid consolidation of the subsoil is desirable, the procedure sometimes calls for insertion of strip (wick) drains and, for lateral flow, could utilize drainage geocomposites as well.

This paper reviews and summarizes a number of soft soil stabilization projects. Drawing from these experiences, a five-part design methodology is presented to select and size the various geosynthetic material properties involved. The paper closes with recommendations for future research and development.

INTRODUCTION

A general category of in-situ foundation soils which has been extremely difficult for the geotechnical engineer to utilize is characterized by high water content and fine grained composition. High water content soils are too weak and compressible to build upon directly; because they are silts and clays, they drain too slowly for effective and economical utilization in a short time period. The usual remedies are to excavate and replace them with suitable soil or to install deep foundations through them to an adequate bearing stratum. Indeed, there have been many attempts made and techniques developed for using alternate methods of soil strengthening, e.g., electro-osmosis, deep dynamic compaction, chemical grouting, lime stabilization, stone columns, sand drains, etc., but all are site specific and relatively expensive to deploy.

In this paper, emphasis is on the basic use of a soil embankment or soil (surcharge) fill which is founded upon and which mobilizes consolidation of the in-situ soil. The unique part of this technique is its use on in-situ soils with shear strengths as low as 1 kPa (20.8 lb/ft²). However, such weak in-situ soil will simply not support the dead load of the soil fill much less the live loads from the construction placement equipment. Clearly, the in-situ soil needs help, which is precisely why a geosynthetic (usually a geotextile which will be referred to hereafter, although geogrids could also be used) is necessary. The function of the geotextile is tensile reinforcement for it initially must support the soil fill which is placed directly upon it. Subsequently, the consolidation process will

generate increased shear strength in the in-situ foundation soil allowing it to support part, or all, of the permanent load.

The soil fill which is placed on top of the geotextile, can take one of two geometric forms;

- (a) A linear soil fill, such as a dike or containment embankment, which is long relative to its width. This is the geometry often utilized by the U.S. Army Corps of Engineers when constructing containment dikes for dredged soil or levee embankment. In these cases the fill stays in place permanently and is upgraded as consolidation settlement occurs. Containment dike heights are in the 2-5 m (6' - 15') range with side slopes of 1-on-5 to as low as 1-on-20. Levees are often higher.
- (b) An areal soil fill, such as a temporary surcharge, which is large in both its length and width. This situation is one in which the entire site is necessary for subsequent construction and the fill is only placed temporarily. After sufficient consolidation settlement has occurred (along with its strengthening of the in-situ foundation soil) all, or part, of the surcharge fill is then removed. It is then replaced by the permanent facility which is now founded using a shallow foundation on a preconsolidated soil.

While both situations just described have great similarities, they are distinct enough to warrant certain differentiations in both design and construction.

CASE HISTORIES

Beginning in the late 1970's, the U.S. Army Corps of Engineers began experimenting with geotextiles placed over soft dredged soil to support containment dikes (1,2). The first major project was Pinto Pass at Mobile, Alabama, where a 160 kN/m (900 lb/in.) ultimate strength fabric was used (see Table 1). This project set the direction for a number of linear stabilization projects where high strength in the fabric's warp direction could be aligned perpendicular to the longitudinal axis of the dike. Full length rolls the entire width of the dike could be utilized without the necessity of seams. Seams were required, however, in the weft direction (i.e., along the long edges of each of the fabric rolls) which is also the direction of the minor principal stress. This is fortunate, because joining of high strength fabrics (usually by sewing) was still in an initial stage of development at the time. Required seam strengths were approximately 35 kN/m (200 lb/in.) which was considered (at the time) to be a high strength seam. A succession of linear stabilization projects followed; i.e., Minnesota DOT, three Corps of Engineers projects at Norfolk, Virginia and a Brunswick Pulp and Paper Co. project in Brunswick, Georgia (see Table 1).

More recently, projects involving areal stabilization have been undertaken. Washington National Airport in Washington, DC was the first in which length was approximately equal to width, but it was actually designed as two adjacent linear embankments. Thus the weft direction and its seams could be weaker than the fabric strength in the warp direction. The Corps of Engineers South Blakney Island project along with the Maryland Port Authority's Seagirt stabilization project, were true areal stabilization projects. In these cases, high strength in both warp and weft directions were required, along with a major increase in seam strength. Seam strengths of up to 140 kN/m (800 lb/in.) were now required. Today, seam strengths approaching 175 kN/m (1000 lb/in.) can successfully be made even under adverse field conditions of working on floating barges and on very soft soils (see projects

Table 1 (continued) - Review of Recent USA Reinforcement Embankment Project Using High Strength Geotextiles

Project No.	Geotextile			Dike Geometry			Soil Response		Fabric Distributor and Type
	Warp/Fill Ultimate Strength (kN/m)	Seam Ultimate Strength (kN/m)	Warp/Fill Secant Modulus (kN/m)	Height (m)	Width/Length (m)	Dike Slope H:V	Fill Material	Settlement (m)	
1	160/30	45	634/187 @ 30%	2	52/244	10:1	Sand	1	Nicolon 66475 Polypropylene
2	175/35	18	613/114 @ 30%	3	30/152	5:1	Glacial Till	0.3-1	Nicolon 1250 X Polypropylene
3	186/39	53	606/114 @ 30%	3	72/229	11:1	Sand	1	Nicolon 1250 Polypropylene
4	186/39	53	606/114 @ 30%	2	72/152	11:1	Sand	2	Nicolon 1250 Polypropylene
5	186/39	53	606/114 @ 30%	2	66/91	12.5:1	Sand	5	Nicolon 1250 Polypropylene
6	186/105	53	606/350 @ 30%/22%	3	72/	10:1	Sand	1-2	Nicolon 1250 X Polypropylene
7	186/53		606/350 @ 30%/22%	8	15/150	2:1	Salt	?	Nicolon 1250 Polypropylene
8	184/39	39	527/? @ 10%	5	183/213	5:1	Sand	1	Burlington
9	876/86	Not Required	21×10^8 kN/m ² Steel	7	55/366	3:1	Clayey Sand/Gravel	0.5	U. S. Steel
10	175/114	52	665/700 @ 10%	3	24/	4:1	Sand	2	Mirafi 2100 Polyester
11	175/114	52	665/700 @ 10%	3	24/	4:1	Sand & Clay	1	Mirafi 2100 Polyester
12	361/187	88	3940/1883 @ 11%/10%	2	15/300	2:1	varied	?	Nicolon Polyester
13	193/245	116/137	1786/? @ 10%/10%	1-5	671/488	-	Sand/Clay	1-2	Nicolon Polyester & Polypropylene
14	175/114	91	?	2	21/	5:1	Sand	1	Nicolon Polyester
15	361/187	88	3940/1883 @ 11%/10%	3	61/762	10:1	Sand	?	Nicolon Polyester
16	263/263	140	3415/2627 @ 10%/10%	5-6	122/213	12:1	Sand/Gravel	NA	Wellman/Quiline Polyester
17	506/105	105	59401 @ 5%	1.5-3	183/30	15:1	Sand/Silt	NA	Nicolon Polyester

Table 1 - Review of Recent USA Reinforcement Embankment Project Using High Strength Geotextiles

Project No.	Date Constructed	Owner	Name/Location	Foundation Conditions			
				Soil Type	Water Content (%)	Depth (m)	Shear Strength (kN/m ²)
1	1978	USAE COE Mobile District	Pinto Pass Mobile, AL	Organic Clay	70-150	12	2-5
2	1981	Minnesota DOT	St. Paul, MN Interstate 494	Peat	200-300	6	?
3	1982	USAE COE Norfolk Dist	Test Sect #1 Craney Is Norfolk, VA	Organic Clay	60-180	11	5
4	1982	USAE COE Norfolk Dist	Test Sect #2 Craney Is Norfolk, VA	Organic Clay	60-180	10	1-4
5	1982	USAE COE Norfolk Dist	Test Sect #3 Craney Is Norfolk, VA	Organic Clay	60-180	10	1-2
6	1983	USAE COE Norfolk Dist	Craney Division Dike Norfolk, VA	Organic Clay	60-180	11	1-5
7	1983	Brunswick Pulp & Paper	Brine Storage Facility Brunswick, GA	Marine Clay	50-100	10-12	1-2
8	1983	Washington, DC	Washington Airport Extension	Clayey Silt	75-100	5-6	2-5
9	1984	USAE COE Huntington, Dist	Dike #2 Mohicanville, OH	Peat & Clay	117-636 peat 29-180 clay	6-18	8 peat 9 clay
10	1985	USAE COE Mobile, AL	South Blakney Is Mobile, AL	Organic Clay	70-150	5	2-5
11	1985	USAE COE Mobile, AL	Greenwood Is Mobile, AL	Organic Clay	70-150	5-9	2-5
12	1986	Alaska DOT Nenana, AK	Parks Hwy	Glacial Till	50-100	4-8	1-3
13	1986	Maryland Port Adm.	Seagirt Surcharge Baltimore, MD	Organic Clay	50-100	9	2-5
14	1986	USAE COE Mobile, AL	North Blakney Is Mobile, AL	Organic Clay	70-150	5	4-5
15	1986	USAE COE Norfolk, VA	Craney Is South Perimeter Dike Norfolk, VA	Organic Clay	70-180	5	5
16	1986	USAE COE Philadelphia, PA	Wilmington Harbor South, Disposal Area Wilmington, DE	Organic Clay	70-160	9-12	2-5
17	1986	USAE COE New Orleans, LA	Reach A Test Plaquemines Parish, LA	Organic Clay	70-100	9-18	1-2

by the Corps of Engineers at Philadelphia, Pennsylvania and New Orleans, Louisiana, respectively, in Table 1).

While the above mentioned projects focused on the fabric's ultimate strength and elongation at failure (3), the Corps of Engineers, Huntington District project at Mohicanville, Ohio brought out the importance of the modulus of the reinforcement (4). Usually expressed as a secant modulus at a specific strain, this project required the use of a steel mesh to obtain the required stiffness. The use of this type of reinforcement should not be surprising, however, for there is a logical extension of the mechanical properties of plastic-to-glass-to-steel (5,6) as shown in Table 2. Note that these values are in stress units and to convert them to force per unit width as in Table 1, they would have to be multiplied by a suitable thickness. For a high strength fabric this would be approximately 2.5-5.0 mm (0.1-0.2 in.).

While proper design and careful construction should allow for initial stability of these dikes and surcharge fills, the time for primary consolidation to occur is often excessively long. Thus the use of strip drains has been employed on several of these projects. The Maryland Port Authority project had approximately one million linear meters (3 million feet) of strip drain placed through the surcharge, the fabric and the compressible foundation soil (7). The Corps of Engineers project in Wilmington, Delaware is somewhat similar and is currently ongoing. Both of these projects reflect the current state of the art in using geosynthetics to build upon and stabilize very soft foundation soils.

DESIGN CONCEPTS - REINFORCEMENT

While a generic design for all of the projects just described is essentially impossible to provide, some similarities have evolved and can be presented. In this regard there are five major concerns, each of which leads to a specific design parameter or property of the reinforcement geotextile or embankment.

a. Bearing Capacity (which leads to maximum height of embankment) - Overall bearing capacity of the site must be satisfied or a failure as shown in Figure 1(a) will occur. This is essentially the case with or without the reinforcing geotextile. Analysis follows along classical geotechnical engineering methods for infinitely long strip foundations and for undrained ($\phi = 0^\circ$) conditions; i.e.,

$$q = c N_c$$

and

$$q_{ave} = \gamma H$$

so

$$\begin{aligned} \gamma H &= c N_c \\ H_{ave} &= c N_c / \gamma \end{aligned}$$

where

- q = ultimate bearing capacity
- c = undrained shear strength
- N_c = bearing capacity factor (3.5 to 5.7)
- γ = unit weight
- H = height of embankment

For soils of low undrained shear strength (recall the values in Table 1), the height of the dike or embankment is greatly limited. It also forces wide and flat side

Table 2 - Intrinsic Properties of Polymeric Materials Contrasted to Glass and Steel,
after Lawson, 1982

Material Type	Tensile Strength		Elastic Modulus		Strain at Failure %
	MPa	kip/in ²	MPa	kip/in ²	
Polypropylene . monofilament	400	58	3230	471	17-19
. continuous filament	700	101	6500	942	17-19
Polyethylene-Monofilament . low density	80-120	12-17	800	116	25-50
. high density	350-500	51-72	4000	580	20-30
Polyester-Cont. Filament . medium tenacity	500-650	72-94	12,500-14,500	1810-2100	15-30
. high tenacity	750-1400	109-203	14,000-18,500	2030-2680	6-15
Polyester-Staple Fibers	500-700	72-101	4000-7500	580-1090	20-50
Nylon 6,6-Cont. Filament . medium tenacity	450-600	65-87	< 2500	< 362	20-30
. high tenacity	700-1000	101-145	3000-12,500	435-1810	12-15
Nylon 6,6-Staple Fibers	400-700	58-101	< 2000	< 290	20-35
Aramid-Cont. Filament . low tenacity	500-900	72-130	15,000-20,000	2180-2900	8-12
. high tenacity	2500-2900	362-420	55,000-130,000	8000-18,900	2-4
Glass . Type E	1750-3500	254-508	70,000-150,000	10,000-21,800	2-4
Steel . Prestressing	1450-2150	210-312	200,000	29,000	2

side slopes (again recall the values in Table 1). Even though the height and side slopes will be initially low, the foundation soil will consolidate and fill heights can be increased with time. If this time is too long, however, installation of strip drains will be necessary.

Regarding the design of strip drains, a considerable amount has been written (8). The simplified formula of Hansbo (9) appears to be adequate to obtain the proper spacing versus the time for consolidation to occur.

$$t = \frac{D^2}{8c_h} \left[\ln \frac{D}{d} - 0.75 \right] \left[\ln \frac{1}{1-U} \right]$$

where

- t = time for consolidation
- c_h = horizontal coefficient of consolidation of soil
- D = spacing of strip drain
- d = equivalent diameter of strip drain (circumference/ π)
- U = average degree of consolidation

Seen in the above equation is that by making the spacing D small, the time for consolidation under a given fill height can become as short as desired. For Maryland Port Authority's Seagirt project, the strip drain spacing was 1.5 m (60") which allowed for time for a 90% consolidation of approximately six months. Once consolidation is achieved, c increases and H may then be increased if desired.

b. Global Stability (which leads to fabric ultimate strength) - The next consideration one must assess is the determination of what ultimate strength is necessary vis-a-vis the applied loads (embankment plus live load) and the strength of the in-situ soil. Here one usually uses a limit equilibrium method as illustrated by the circular arc method shown in Figure 1(b). Taking moments about the origin results in a factor of safety equation as follows:

$$FS = \frac{(\tau_e L_e + \tau_f L_f) R + T_a a}{W x_s + L x_l}$$

where

- τ_e = shear strength of embankment soil (often neglected)
- τ_f = shear strength of in-situ soil
- L_e = arc length in the embankment soil
- L_f = arc length in the foundation soil
- T_a = allowable strength of geotextile
- a = moment arm about center of failure arc
- W = weight of soil mass
- x_s = moment arm of soil mass
- L = weight of live load
- x_l = moment arm of live load
- FS = factor of safety
- R = radius of the failure arc

For a given factor of safety (e.g., 1.1 to 1.3) one can solve for " T_a " as the unknown. This value of fabric allowable strength is related to the ultimate strength of the geotextile and, most directly, to its polymer type. In order to avoid tertiary creep, Lawson (5) recommends the following:

Table 3 - Allowable Strengths of Polymeric Geosynthetics to Avoid Tertiary Creep, after Lawson (5)

Polymer Type	Embankments* (% of Ultimate)	Walls and Slopes (% of Ultimate)
polypropylene	20-40	20
HDPE geogrid	30-40	30
polyester	40-60	40
aramid	45-60	45

*problems of the type described in this paper

Note that criteria for embankments founded on soils which will consolidate and gain in strength with time are less restrictive than permanent walls and slopes. Such calculations for embankments on very soft soils usually indicate geotextiles of 175 kN/m (1000 lb/in.) or greater ultimate strength.

The distinction between linear and areal fills can now be made. For linear fills the geotextile can be designed anisotropically. By knowing the direction of maximum stress, an unbalanced geotextile is possible. As noted previously, its stronger direction must be in the direction of maximum stress and its weaker direction perpendicular to that, in the direction of the minimum stress. Note that this really demands a three-dimensional slope stability analysis; a subject about which little is available and, when it is attempted, is quite complex. Lawson (5) recommends a longitudinal ultimate strength of 25% or more of the transverse ultimate strength.

For areal fills, however, the geosynthetic must be balanced in both the warp and weft (or machine and cross machine) directions and thus becomes essentially isotropic. This is because no preferential stress direction can be defined and all directions must be considered worst case situations. Obviously, the seams in both directions must be of a strength compatible with the fabric.

c. Elastic Deformation (which leads to fabric elastic modulus and strain at failure) - A decision as to allowable embankment deformation must be made in order to numerically define the elastic modulus and strain at failure (see Figure 1(c)). Finite element methods have been used (4) and empirical relationships based on experience have been developed. It appears as though a modulus of 5 to 25 times the ultimate strength allows for tolerable deformations for the projects described herein. Using this value and on the basis of a completely elastic material:

$$E_s = 5 \text{ to } 25 T_{ult}$$

$$\epsilon_f = \frac{T_{ult}}{E_s}$$

thus:

$$\begin{aligned}\epsilon_f &= 0.20 \text{ to } 0.04 \\ \epsilon_f (\%) &= 20\% \text{ to } 4\%\end{aligned}$$

where

$$\begin{aligned}E_s &= \text{elastic (secant) modulus} \\ T_{ult} &= \text{ultimate fabric strength} \\ \epsilon_f &= \text{strain at fabric at failure}\end{aligned}$$

Note from Table 2 that this consideration alone eliminates some of the potential polymeric materials listed. The amount of centerline deflection that such strain levels allow is quite large. Using an average value of 10% failure strain and assuming the deflected shape of the geotextile to be a parabola, i.e.,

$$S = 4w^2 + (B/2)^2 + \frac{(B/2)^2}{2w} \ln \frac{2w + \sqrt{4w^2 + (B/2)^2}}{B/2}$$

where

$$\begin{aligned}S &= \text{arc length} \\ W &= \text{centerline deflection} \\ B &= \text{base width}\end{aligned}$$

an embankment 30.5 m (100') wide (and an arc length S of 1.10 B) results in a centerline deflection of 6.1 m (20')! Such large deformations strongly suggest limiting the strain at failure to a minimum and making the elastic modulus a maximum.

d. Pullout (which leads to required anchorage length) - Once the embankment height and type of geotextile reinforcement have been selected, the anchorage distance must be determined. As seen in Figure 1(d), the anchorage zone extends behind the slip zone and back into the stable soil zone. It must be sufficiently long to mobilize the full strength of the geotextile. The analysis uses the following concept.

$$T_{ult} = 2\tau E L$$

where

$$\begin{aligned}T_{ult} &= \text{ultimate strength (therefore it includes the FS)} \\ \tau &= \text{shear strength of foundation soil} \\ E &= \text{efficiency factor for the particular soil/fabric combination} \\ L &= \text{the unknown length}\end{aligned}$$

Regarding the efficiency factor in the above equation, considerable research is ongoing. Geogrids appear to have the highest value with $E = 1.0$ to 2.0 ; rough geotextiles next with $E = 0.80$ to 1.2 ; and smooth geotextiles the lowest, with $E = 0.60$ to 0.8 . It must be recognized that in many situations using high strength geotextiles with soft soils, very long anchorage lengths will result from the above analysis.

e. Lateral Spreading (which leads to required fabric friction) - Utilizing techniques common to lateral earth pressure theory, one can obtain the required frictional characteristics of the geotextile. Using Figure 1(e) one can work with a factor of safety concept as follows:

$$FS = \frac{\text{Resisting Forces}}{\text{Driving Forces}}$$

$$FS = \frac{\tau L}{P_a}$$

$$FS = \frac{0.5 \gamma H \tan \delta L}{0.5 \delta H^2 K_a}$$

and,

$$\tan \delta = \frac{(FS) H K_a}{L}$$

where

- δ = angle of shearing resistance between the fabric and the embankment soil
- H = embankment height
- L = embankment length
- K_a = coefficient of active earth pressure = $\tan^2 (45 - \phi/2)$
- ϕ = angle of shearing resistance of soil
- P_a =

For the typical case of low slope conditions, (recall Table 1), the required "tan δ " values can usually be met by a reasonably competent embankment soil having good frictional characteristics. The calculation should be done incrementally from maximum height of embankment to the toe of the embankment, where conditions usually become more severe. It becomes a very critical problem when soft soils are used for the embankment above the reinforcing geotextile.

SUMMARY AND CONCLUSIONS

Presented in this paper are a number of case histories using geotextiles on extremely soft foundation soils. Distinctions were made; between linear embankments for containment dikes or barrier purposes and areal fills for stabilization purposes. Both situations are similar and each have tremendous areas for application, they are currently seeing intense activity.

The design aspects for both cases were outlined where the allowable fill height and slope conditions above the geotextile were first described. It is at this point where one decides about the use of a rapid consolidation technique. If considered to be desirable, then the use of strip drains should be implemented. Two case histories were discussed using this technique. At this point the design focuses on the calculation of the following required fabric properties;

- o ultimate strength in major stress direction
- o ultimate strength in minor stress direction
- o seam strength in minor stress direction
- o elastic modulus in both directions
- o strain at failure in both directions
- o anchorage length
- o friction

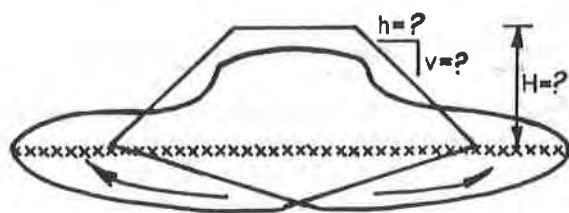
While the design methods presented are considered to be reasonable, the monitoring of the in-situ performance of the various systems has lagged behind the relatively large number of construction projects. The actual performance of the reinforcing geotextile material as determined by stress and/or strain monitoring will eventually tell of the appropriateness of these design methods. Work is also

ongoing in this regard and will be reported in the near future. At a minimum, it is considered that better insight is needed in the following areas;

- o actual stress levels immediately after construction versus the models proposed
- o long term stress levels to see if creep allowances are justified, (recall Table 3)
- o effect of punching holes in the geotextile when using strip drains
- o mechanism of load transfer over seams, particularly field seams
- o innovative, and possibly new, joining methods to transfer tensile stresses over 175 kN/m (1000 lb/in.)
- o verification of required values of elastic modulus and strain at failure
- o information on anchorage mechanisms, design and mobilization
- o information on friction behavior and mobilization along the length of the fabric

REFERENCES

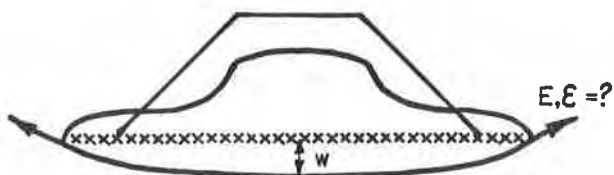
- (1) Fowler, J., "Analysis of Fabric-Reinforced Embankment Test Section at Pinto Pass, Mobile, Alabama," Ph.D. Thesis, Oklahoma State Univ., 1979.
- (2) Haliburton, T. A., Fowler, J. and Langan, J. P., "Design and Construction of a Fabric Reinforced Test Section at Pinto Pass, Mobile, Alabama," Trans. Res. Rec. 79, Washington, DC, 1980.
- (3) Fowler, J., "Theoretical Design Considerations for Fabric Reinforced Embankments," Proc. 2nd Intl. Conf. Geotex., Las Vegas, Nev., 1982, IFAI, pp. 665-676.
- (4) Fowler, J., Peters, J. and Franks, L., "Influence of Reinforcement Modulus on Design and Construction of Mohicanville Dike No. 2," Proc. 3rd Intl. Conf. Geotex., Vienna, Austria, 1986, pp. 267-271.
- (5) Lawson, C. R., "Geosynthetics for Soil Reinforcement," Notes for a Short Course, Ascam Institute of Technology, Bangkok, 1982.
- (6) Koerner, R. M. and Hausmann, M. R., "Strength Requirements of Geosynthetics for Soil Reinforcement," submitted for publication to Geotech. Fabrics Rept., IFAI, 1986.
- (7) Koerner, R. M., "Soft Soil Stabilization for Wilmington Harbor South Dredge Material Disposal Area," Report to USAE Waterways Experiment Station, Vicksburg, MS, June 28, 1986.
- (8) Koerner, R. M., "Designing with Geosynthetics," Prentice Hall Publ., Co., Englewood Cliffs, NJ, 1986.
- (9) Hansbo, S., "Consolidation of Clay by Band Shaped Prefabricated Drains," Ground Engineering, July, 1979, pp. 16-25.



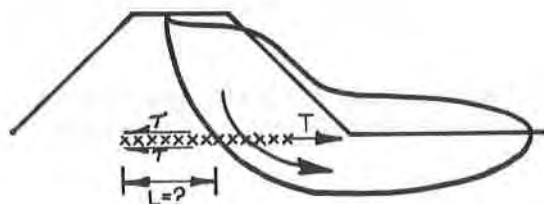
(a) BEARING CAPACITY



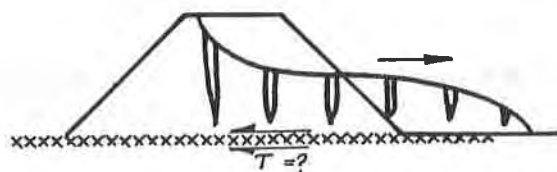
(b) GLOBAL STABILITY



(c) ELASTIC DEFORMATION



(d) PULLOUT OR ANCHORAGE



(e) LATERAL SPREADING

Fig. 1 - Geotextile Design Models for Use in Soft Soil Stabilization

WERNER, G. and RESL, S.
Chemie Linz AG, Austria
FROBEL, R.K.
Chemie Linz US Inc., U.S.A.

Stability Consideration of Embankments on Soft Soils Based on Improved Hydraulic Boundary Conditions

The stability of the 3-layer-system-embankment / geotextile / subsoil is strongly influenced by two geotextile parameters:

- a) horizontal and vertical permeability
- b) tensile strength

Whereas the tensile strength of a geotextile is generally of overrated importance for the stability of an embankment on soft saturated soils, the hydraulic boundary conditions are not or very seldom considered when looking at the major failure modes for stability analysis. The paper looks only at the separation and drainage function of a mechanically bonded non-woven geotextile installed inbetween embankment fill and soft subsoil, playing an important role for stability analysis in embankment construction due to its high vertical and horizontal permeability.

The design recommendations and charts as presented in this paper are based on sound engineering experience and extensive research. The design procedure follows the now widely accepted "Design by Function" geotextile design concept.

1. INTRODUCTION

During the filling of an embankment on soft soil part of the fill material will penetrate into the subsoil due to embankment construction and associated lift layer compaction. This penetration causes great plastic deformation of the soft soil, similar to the formation of the so-called "smear zone" known from the construction of vertical drains. As is generally known, the permeability of the drain-soil contact area exhibits a much lower permeability than the surrounding undisturbed soil. Assuming also a significant reduction of the permeability of the mix zone in the embankment base, then this much less permeable layer can be taken as the decisive hydraulic boundary condition for the consolidation of the undisturbed soft soil layer underneath.

As it can be shown by calculations using 3-dimensional consolidation theories, the development of shear stresses in the subgrade depends on the permeability of the embankment / subgrade interface. With an impermeable interface, shear stresses can greatly increase locally due to the Mandel-Cryer-Effect (1), and thus reduce the stability of the embankment. The Mandel-Cryer-Effect describes the rise of the porewater pressure over the initial value. This phenomenon has also been observed in experimental work where the maximum shear stress was found to be not constant with time which is contrary to the 1-D-theory (Terzaghi's Theory). Figure 2 shows the time dependent distribution of maximum shear stresses under an impermeable loading area.

Using calculations with 1-D-theory the Mandel-Cryer-Effect remains undiscovered. This effect

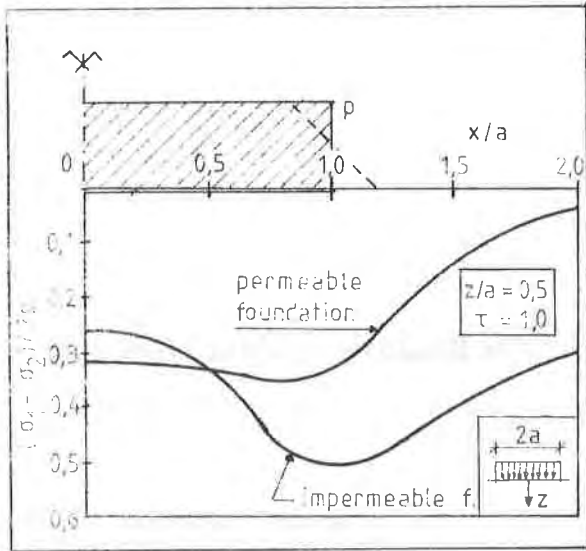


Figure 1: Distribution of the maximum shear stresses (1)

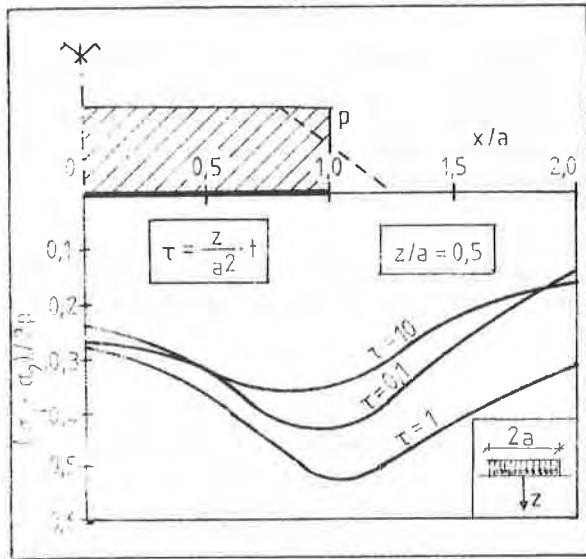


Figure 2: Time dependent distribution of the max shear stresses for an impermeable loading area (1)

can be greatly reduced when a permeable interface is assumed. Figure 1 shows the distribution of maximum shear stresses in the depth $z/a = 0,5$ underneath the area of loading for the case of a permeable and impermeable interface. Referring to Figure 1 it is especially interesting to see how sensitive the distribution of maximum shear stresses reacts on the hydraulic boundary conditions under the area of

loading, and how great the increase of shear stress is towards the edge of the loading area, if the loading area is impermeable. On the basis of these results, the importance of an effective drainage layer at the embankment base, such as provided by the high vertical and horizontal permeability of a needle-punched non-woven geotextile, becomes very evident.

2. TYPES OF FAILURE

In the following analyses (7), the stability of an embankment on a soft, homogenous soil layer with the thickness D is checked. The soil below the soft layer is assumed to be stiff. The embankment geometry on which stability calculations are based is illustrated in Figure 3.

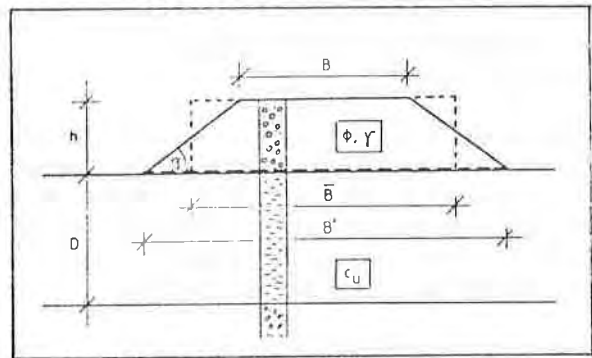


Figure 3: Embankment Geometry

Where:

- h = height of embankment (m)
- B = crest width (m)
- \bar{B} = width of rectangular replacement load (m)
 $\bar{B} = B + h \cdot \cotan \beta$
- B' = base width (m)
- β = inclination of slope ($^\circ$)
- ϕ = angle of internal friction of fill material ($^\circ$)
- γ = unit weight of fill material (kN/m^3)
- D = thickness of cohesive, soft layer (m)
- c_u = undrained shear strength of subgrade (kN/m^2)

Basically, there are three failure mechanisms that are possible and that are most often considered in stability analysis

- Base or overall bearing capacity failure
- Toe or slip surface failure
- Lateral sliding

For each of these three types of failure, the load bearing capacity factor k_c is calculated. The largest value of k_c is the governing factor for embankment stability:

$$k_c = \frac{c_u}{\gamma \cdot h}$$

An embankment cannot be constructed without resulting in large foundation displacement if the factor of safety is less than one. However, the displacement method of construction for unreinforced embankments is well known (6) and will result in the fill material sinking into the soft ground, displacing the foundation material. In this case, high elongation, low modulus continuous filament, nonwoven needle-punched geotextiles can be used for displacement applications to provide uniform sinking of the embankment (8).

2.1. Base or Overall Bearing Capacity Failure

Figure 4 below illustrates the types of base failure considered (2) (3). The forces and geometrical parameters which are necessary for stability calculations are shown in Figure 5 for base failure type "a".

Based on a numerical analysis, base failure type "a" yielded the lowest stability, and is

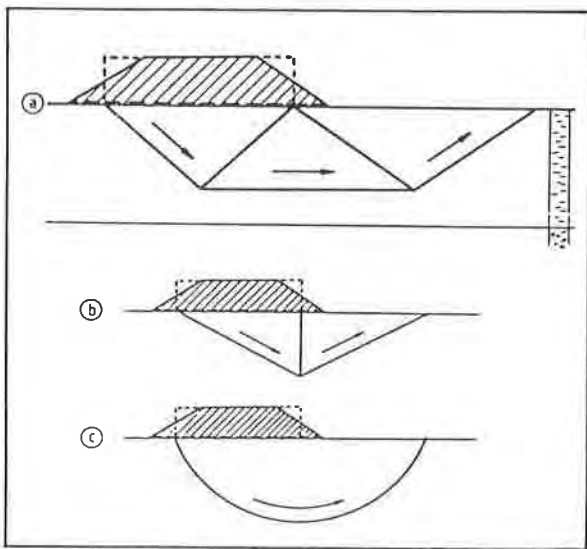


Figure 4: Types of Base Failure

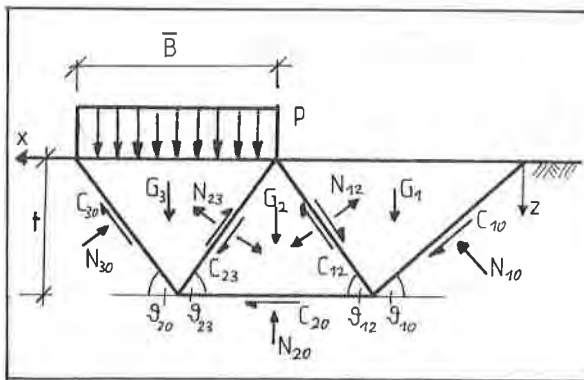


Figure 5: Calculation Parameters for Base Failure Type "a"

therefore relevant for establishing the design diagram shown in Figure 6. This diagram provides the required value for k_c as a function of the D/\bar{B} - ratio.

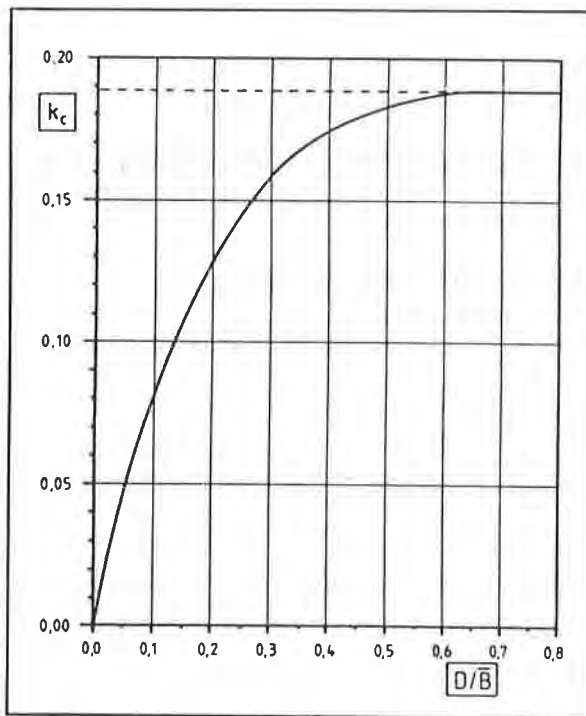


Figure 6: Determination of k_c Considering Base Failure of an Embankment (7), (9)

For $D/\bar{B} \geq 0,663$, k_c is constant with $k_c = 0,189$. This value correlates well with the static solution presented by Prandtl with $k_c = 1/(2 + \pi) = 0,194$, which is applicable for $D/\bar{B} \geq 0,71$.

2.2. Toe or Slip Surface Failure

Figure 7 shows the types of toe failure considered (2) (3) (4) (6), from which type "a" was again chosen based on lowest stability.

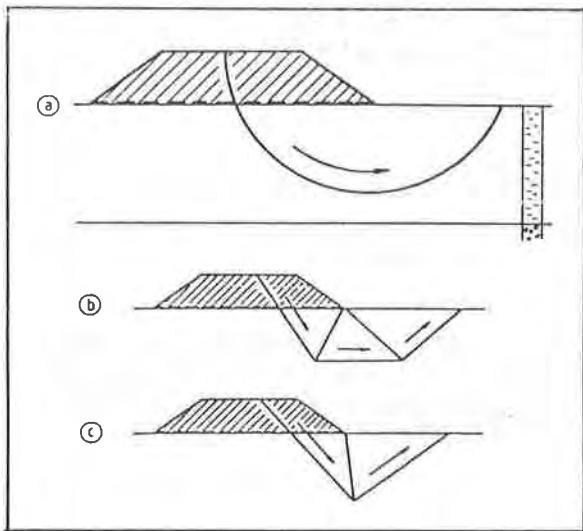


Figure 7: Types of Toe Failure

The free development of the relevant slip surface is restricted by two geometrical factors (see Figure 8):

- Thickness of soft layer D
- Crest width B

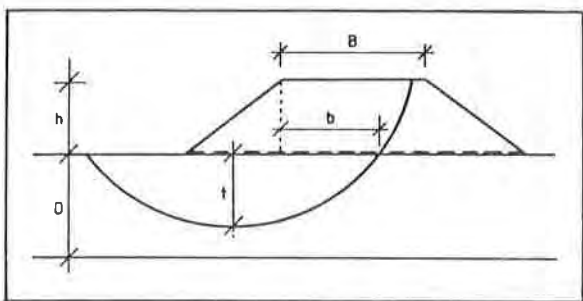


Figure 8: Geometry of Slip Surface

If the slip surface can develop freely, the value of k_c is constant with $k_c = 0,183$. However, if the depth of the slip surface t is greater than the thickness of the soft layer D , and/or the width b is greater than the crest width B , the geometry of the occurring slip surface than will be restricted by these two factors, and the k_c -value will be influenced significantly.

The following design scheme is based on a numerical analysis of toe failure type "a". Considering the geometrical restrictions mentioned above, the following flow chart gives the required steps for evaluating the k_c -value considering toe failure by using Figure 10 (see also Figure 9).

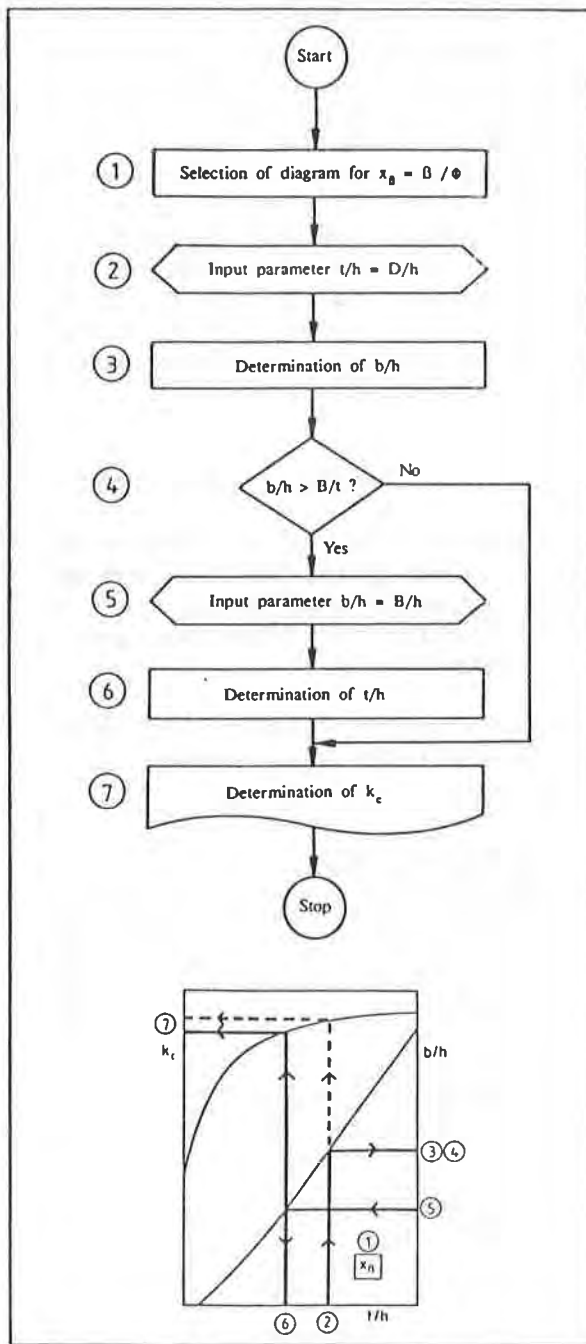


Figure 9: Schematic Showing the Use of the Diagrams for Toe Failure

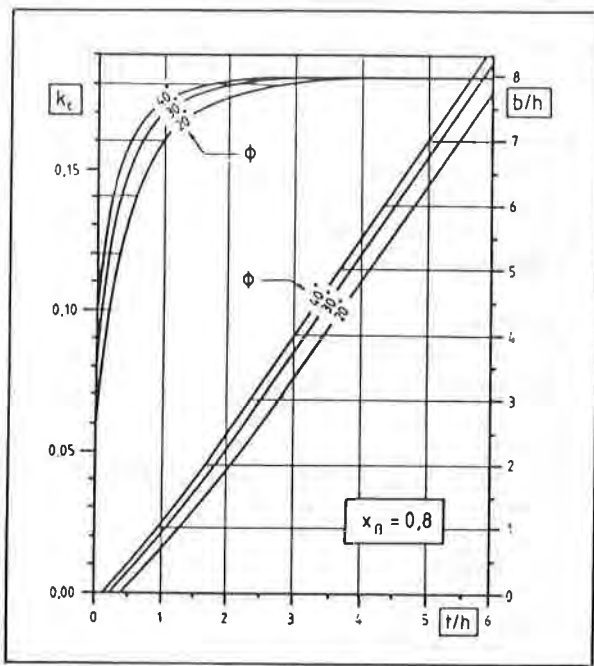


Figure 10: Determination of k_c Considering Toe Failure of an Embankment (One from a Series of 6 Diagrams) (7), (9)

2.3. Lateral Sliding

Earth pressure inside the embankment results in shear stresses in the embankment / subgrade-interface (see Figure 11) (5). For the present analysis that the embankment slides when the maximum shear stress is higher than the undrained shear strength c_u of the subgrade.

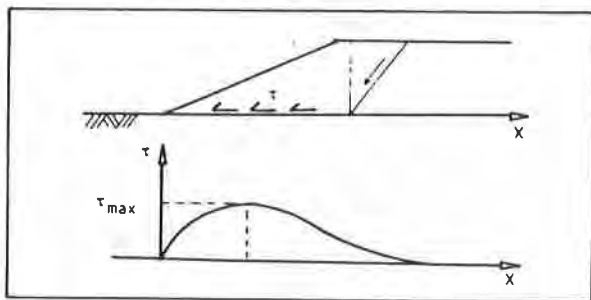


Figure 11: Distribution of Shear Stresses at the Embankment / Subgrade - Interface

The design diagram illustrated in figure 12 was established on the basis of numerical analysis. The k_c -value is therefore a function of friction angle ϕ and slope angle β .

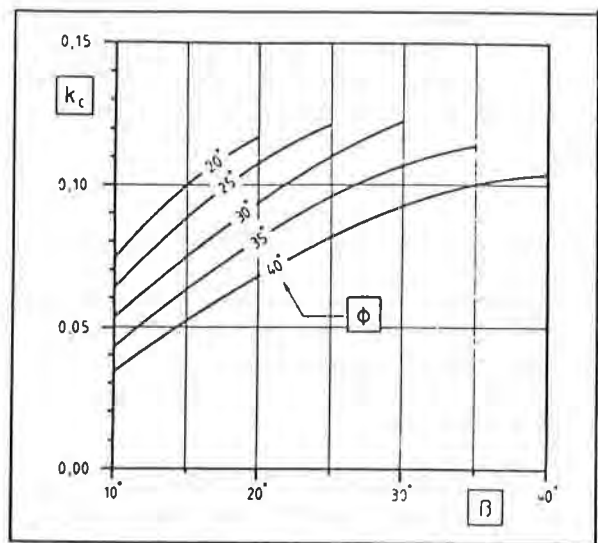


Figure 12: Determination of k_c for an Embankment Considering Lateral Sliding (7), (9).

2.4. Governing Type of Failure

For stability analysis, that type of failure governs which provides the greatest value for the load bearing capacity factor k_c .

When c_u is given, the allowable fill height of the first layer h_1 can be determined iteratively by assumption of h and comparison of required and actual c_u :

$$c_u \text{ required} = k_c \cdot \gamma \cdot h \leq c_u \text{ actual} / f_s$$

Where:

f_s = safety factor

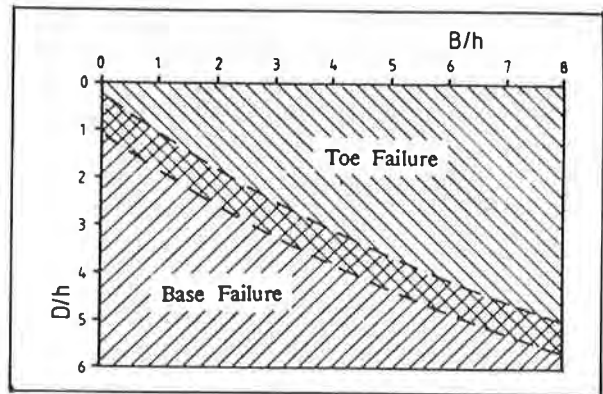


Figure 13: Governing Type of Failure of an Embankment

As a general rule, base failure is relevant for greater thickness of the soft layer D , whereas toe failure is relevant for greater embankment width B ; lateral sliding is only relevant in the case of very thin layer thickness D ($D/h < 0,3$).

2.5. Influence of Geotextile Tensile Strength

- During base failure, the entire embankment sinks down into the soft subsoil. At this time, tensile reinforcement in the embankment base line is not a consideration for the stability.
- Tensile reinforcement in the embankment base is particularly suited for the stability against sliding in the base due to active earth pressure. However, failure due to active earth pressure is only relevant to very thin layers of soft subsoil directly beneath an embankment, which very seldom occurs in practice.
- The factor of safety against slope failure can be improved theoretically by reinforcing the embankment base. However this improvement is considerably restricted by the above mentioned base failure, which still has to be considered. Therefore, the high strength fabrics also require the same or only slightly decreased consolidation periods as low strength fabrics with high elongation without allowing for significantly higher fill heights, even though the slope stability is increased by the reinforcing agent.

For this reason, the tensile strength of a geotextile is generally of overrated importance for the stability of an embankment on soft saturated soils. This can be easily proven by calculating the embankment stability using the design diagrams presented in this paper and published in (9).

3. DESIGN EXAMPLES

The following design example shows the use of the design diagrams.

- Given Data:

Embankment height $h = 6$ m
Crest width $B = 4$ m
Base width $B' = 30$ m
Slope angle $\beta = 25^\circ$

Fill material:

Friction angle $\phi = 30^\circ$
Unit weight $\gamma = 19$ kN/m³

Subsoil:

Undrained shear strength $c_u = 10$ kN/m²
Thickness of soft layer $D = 12$ m

- Base Failure:

$D/\bar{B} = 12 / 0,5 (4 + 30) = 0,70$
 $\rightarrow k_c = 0,189$

- Toe Failure:

$x_\beta = \beta / \phi = 25^\circ / 30^\circ = 0,8$
 $t/h = D/h = 12/6 = 2,0$
 $\rightarrow b/h = 2,25$

$2,25 > B/h = 4/6 = 0,67$

$\rightarrow b/h = 0,67 \rightarrow t/h = 0,8 \rightarrow k_c = 0,165$

- Lateral Sliding:

$\beta = 25^\circ, \phi = 30^\circ \rightarrow k_c = 0,110$

- Base failure is governing (max $k_c = 0,189$), and therefore stability of the embankment cannot be increased by a geotextile with high tensile strength.

- For the present case, Figure 14 illustrates the k_c -values as a function of the thickness of the soft layer D . As can be seen, the k_c -value can be reduced only in the case of thin layers ($D < 7$ m), and the

possible reduction will be very small. That means that in the present case there is no technical necessity for using a high strength geotextile.

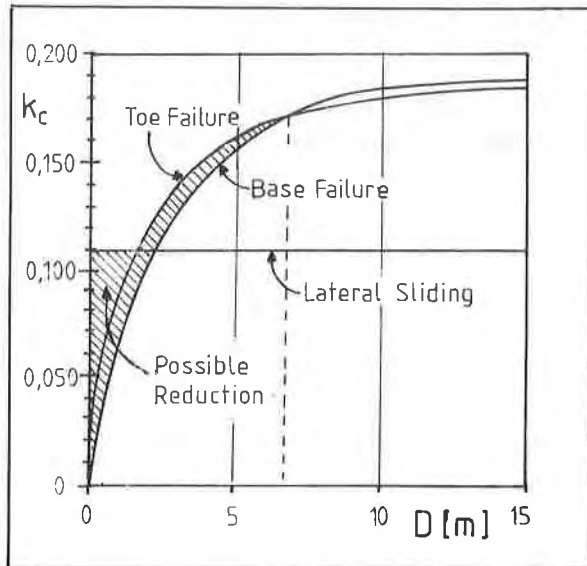


Figure 14: Bearing Capacity Factors k_c as a Function of Soft Layer Thickness D (Example)

Summary:

This paper has reviewed the three major failure mechanisms that have to be considered in embankment construction on soft saturated soils. These are

- Base or overall bearing capacity failure
- Toe or slip surface failure
- Lateral sliding

Unlike former stability analysis this study only considers the separation and drainage function of a geotextile, and the importance of a permeable embankment base for shear stress distribution in the subsoil.

The collapse of an embankment due to toe failure, which theoretically can be prevented by the proper design and use of a high strength fabric reinforcement is proven to be restricted

to a very narrow range of embankment / subsoil (D/h) geometry. This means, that in many cases high strength fabrics do not necessarily increase embankment stability as base failure also has to be considered. Based on this limited stability improvement it becomes evident that the available tensile strength of a relatively expensive high strength fabric is not used in many cases.

A design based on the "Design by Function" geotextile design concept always allows for consideration of worst case situations. In embankment construction it requires consideration of all major failure mechanisms together with the relevant geotextile parameters involved. Therefore in order to guarantee the required hydraulic boundary conditions of the embankment base a geotextile must provide high vertical and horizontal permeability to fulfill a drainage function and have sufficient tensile strength to guarantee long term separation.

References:

1. Schiffman / Albert / Chen / Jordan: "An Analysis of Consolidation Theories", ASCE, Vol. 95 (1969)
2. Gudehus, G.: "Bodenmechanik", Ferd. Enke-Verlag, Stuttgart, 1981
3. Goldscheider, M.: "Standortsicherheitsnachweis mit zusammengesetzten Starrkörper - Bruchmechanismen", Geotechnik Jahrgang 2, Heft 3 (1979)
4. Siedek, P. / Diesler, W.: "Die Standortsicherheit von Dämmen auf wenig tragfähigem Untergrund", Strassen- und Tiefbau 11 (1969)
5. Rendulic, L.: "Der Erddruck im Strassenbau und Brückenbau", Forschungsarbeiten aus dem Strassenwesen, Bd. 10 (1938), Forschungsgesellschaft für das Strassenwesen e. V.

6. Terzaghi, K., Peck, R. D.: "Soil Mechanics in Engineering Practice", John Wiley and Sons, Inc., New York, N. Y. (1967)
7. Graf, B. / Studer, J. (GSS-Zürich): "Damm-
untergrundverbesserung durch den Einsatz
von POLYFELT - Funktion und Bemess-
ungsdiagramme, 1985 (unpublished)
8. Fowler, J.: "Design, Construction and Ana-
lysis of Fabric-Reinforced Embankment Test
Sections at Pinto-Pass, Mobile, Alabama",
Techn. Report EL-81-8, USAE Waterways
Experiment Station, Vicksburg, Mississippi
(1981)
9. POLYFELT TS - Design and Practice; Pub-
lished by Chemie Linz AG (1986)

LOCKETT, L.

State of Alabama Highway Department, U.S.A.

MATTOX, R.M.

The Tensar Corporation, U.S.A.

Difficult Soil Problems on Cochrane Bridge Finessed With Geosynthetics

ABSTRACT

Construction of a 6.62 m (21.7 ft) high bridge approach embankment over weak marsh deposits in Mobile, Alabama was made possible through the use of five different geosynthetics resulting in an estimated savings of \$600,000. Lightweight polypropylene geogrids and a nonwoven polyester geotextile were used in tandem to permit the construction of a 0.61 m (2 ft) sand blanket across the marsh. The sand blanket served as a working platform for the installation of wick drains which were used to reduce the time required for settlement of the embankment to less than two months. High density polyethelene geogrids were employed to reinforce the embankment so that full embankment height could be constructed without incurring the time delays of stage construction. Polypropylene geogrids reinforced the base material of the east access road which maintained traffic across the marsh to the east bank of the Mobile river during construction of the mainline facility. The geotechnical design, construction procedure and the monitoring program are presented.

INTRODUCTION

The first bridge encountered on the recently completed Tennessee-Tombigbee Waterway is U. S. Alternate 90 which crosses the waterway on the north side of Mobile, Alabama from the mainland to Blakely Island where the highway runs due south along the edge of the Mobile River until it reaches an interchange with Interstate 10 immediately east of the twin tunnels under the river. This route is important in that hazardous or explosive materials are not allowed to be carried through tunnels and this route is the only east-west access to or from Mobile for these truck cargos. The bridge crossing the waterway is known as the Cochrane Bridge and the original structure was a lift span to allow clearance of river traffic under the bridge. In the early

1900's, travel from the eastern shore area of Mobile Bay to the city was by ferry which ran from Fairhope, Alabama to the Mobile city docks. The Cochrane Bridge Company was formed in the mid 1920's and was responsible for the design and construction of the bridge and a causeway which crossed the upper reaches of Mobile Bay to the eastern shore at Spanish Fort, Alabama. This private toll facility operated until the early 1940's when it was acquired by the Alabama Highway Department.

Due to the deterioration of the old structure and to the vertical clearance requirements for the Tennessee-Tombigbee Waterway, it was determined that the Cochrane Bridge would be demolished and replaced by a new bridge having a vertical clearance of 42.68 m (140 ft) and a main span length of 237.80 m (780 ft). In order to avoid the sharp curve on the east approach of the old bridge, the new facility was extended to a length of 2222.86 m (7291 ft) with a curving alignment that swung across a dredge disposal area and marshland on Blakely Island. This paper presents the design and construction of the south bridge approach embankment and the east access road which serves the eastern shore of the Tennessee-Tombigbee Waterway.

SITE CONDITIONS

Due to the extremely soft conditions in the marsh, borings were taken along the shoulder of existing U.S. 90. The surface of the marsh lies at approximately elevation +0.61 m (+2 ft). The borings revealed that the bottom of the existing embankment ranged from elevation -0.91 m (-3 ft) to -1.52 m (-5 ft). Beneath the embankment prism, a stratum of silty to sandy clay ran throughout the site. Grain size analyses showed that the sand fraction for this stratum held constant at approximately 33% with the silt and clay fractions varying considerably throughout the deposit. Accordingly, moisture contents varied from 45% to 105%. The thickness of this stratum ranged from 2.74 m (9 ft) to 5.18 m (17 ft) and liquid limits varied from a low of 32% to a high of 55% with P.I.'s ranging from 9 to 30. The results of unconfined compression tests showed shear strengths ranging from a low of 8.14 kPa (170 psf) to a high of 11.01 kPa (230 psf) near the bottom of the stratum. The standard penetration test results throughout this stratum were basically uniform and showed N-values of 2 blows per foot.

The second stratum ranged in thickness from 3.05 m (10 ft) to 6.71 m (22 ft) and consisted of silty sands to clayey sands. Standard penetration tests in this material showed N-values ranging from 2 to 6 with moisture contents ranging from 23 to 33%. The major fraction of this material was predominately sand and the majority of the Atterberg Limits showed the material to be nonplastic.

Beneath this layer, a stratum of medium dense to dense sand was found down to elevation -18.3 m (-60 ft). Standard penetration test results showed blow counts ranging from 14 up to 50 blows per foot.

Undisturbed samples taken from the first stratum of silty clay revealed a large variance in the material. Void ratios generally fell between 1.0 and 2.0, however, some samples revealed void ratios as high as 5.0 with a significant organic content. The dry unit weight for the material ranged from a low of 3.14 kN/m^3 (20 pcf) near the surface to 8.64 kN/m^3 (55 pcf) near the bottom of the stratum. The average coefficient of consolidation was $41.5 \text{ m}^2/\text{S}$ ($0.386 \text{ ft}^2/\text{day}$).

Since the borings were taken along the shoulder of the existing embankment, the results are indicative of a preconsolidated condition of the marsh deposits due to the imposed stresses of the existing highway. The surface of the marsh outside of the existing embankment was extremely soft and virtually impossible to traverse by foot. Based on the data obtained, the shear strength of the virgin marsh was estimated to vary linearly from 0 at the surface to 10.39 kPa (217 psf) at the bottom of the stratum.

DESIGN - BRIDGE APPROACH EMBANKMENT

Preliminary calculations showed that settlement from a combination of both foundation strains and consolidation could range from 1.22 m (4 ft) to 2.13 m (7 ft) beneath the design embankment and would require several years to achieve 90% consolidation. It was concluded, therefore, that the use of wick drains to accelerate the consolidation process would be mandatory. The use of wick drains coupled with a surcharge would eliminate post-construction settlements and negative skin friction on the abutment piling. The weak shear strengths of the marsh deposits, however, dictated that stage construction be used in order to avoid a deep seated shear failure. Calculations showed that the time required for each stage to reach a degree of consolidation where the gain in shear strength was capable of supporting the next embankment segment would stretch the construction schedule beyond acceptable limits for the completion of the project. It was concluded, therefore, that horizontal reinforcement would be required to achieve desired factors of safety during the interim period of consolidation. This approach enabled the embankment to be built at a controlled rate to full embankment and surcharge height without interim waiting periods.

The final embankment height at the bridge abutment was +5.09 m (+16.7 ft) and a 1.52 m (5 ft) surcharge brought the height of embankment at the bridge abutment to +6.62 m (+21.7

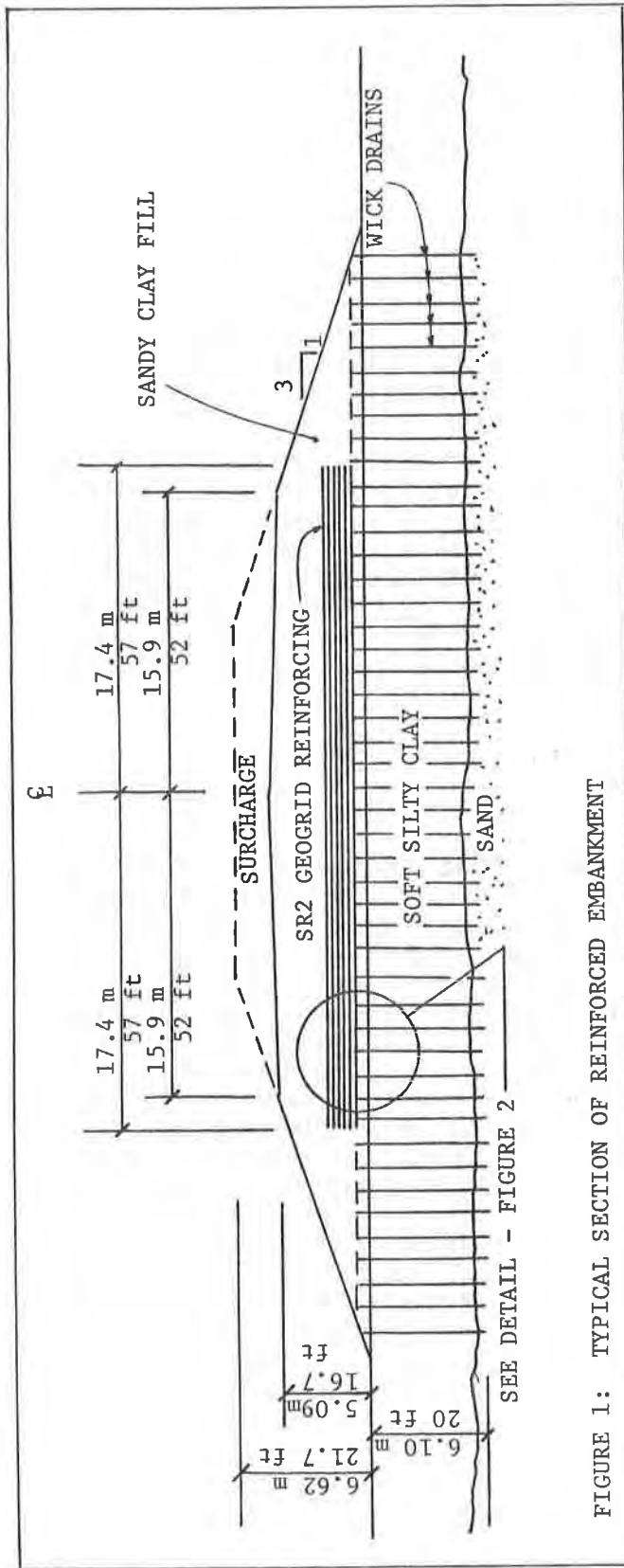


FIGURE 1: TYPICAL SECTION OF REINFORCED EMBANKMENT

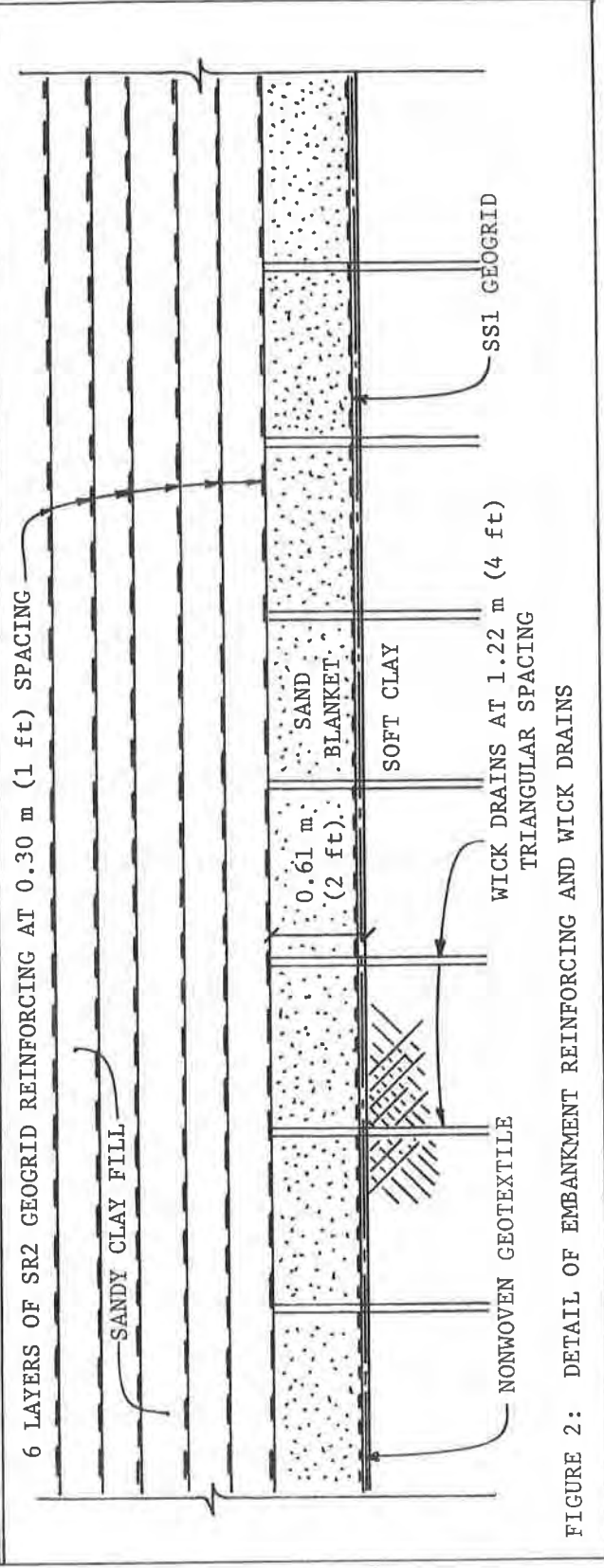


FIGURE 2: DETAIL OF EMBANKMENT REINFORCING AND WICK DRAINS

ft), (Figure 1).

It was determined that an embankment construction rate of 0.30 m/day (1.0 ft/day) coupled with a 1.22 m (4.0 ft) triangular spacing for the wick drains would produce a construction and surcharging period which fit the overall schedule for the project. Using this criteria, it was then possible to estimate the residual piezometric pressures which would exist within the marsh deposits at any time during the construction of the embankment (Figure 3). These estimates of the piezometric regime during construction enabled the shear strength of the underlying soft deposits to be calculated at various times during construction and stability analyses were conducted to ascertain the amount of horizontal reinforcing required to achieve a minimum factor of safety of 1.20. Using this approach, it was determined that six layers of Tensar SR2 geogrid would be required to achieve this minimum factor of safety at the bridge abutment. A profile of the embankment and the layout of the SR2 geogrid is presented in Figure 4. Decreasing embankment heights allowed truncation of the SR2 geogrid layers as the safety factors begin to rise with lower embankment heights.

The SR2 geogrid did not extend throughout the full width of the embankment (Figure 1). This reinforcing geometry was determined by stability analyses which showed that factors of safety could not drop below the specified minimum provided that reinforcing grid extended 7.62 m (25 ft) past the shoulder line of the embankment.

Further analyses also showed that the wick drain spacing could be spread to 1.52 m (5 ft) on center for embankment-surge heights up to 4.57 m (15 ft) and still achieve the desired degree of consolidation within the specified surcharging period. This was made possible due to the fact that this portion of the embankment would reach final surcharge height while the filling process was continuing on the higher portions of the embankment near the bridge abutment. Therefore, a longer period of consolidation time was available for this portion of the embankment thus allowing the increase in wick drain spacing.

DESIGN - EAST ACCESS ROAD

When the old Cochrane Bridge was demolished, it was necessary to establish a ferry crossing the Mobile River to carry the hazardous and explosive materials across the river. One of the requirements of the overall design of the project was to maintain this traffic during construction of the new facility. Therefore, it was necessary to plan the east access road as first order construction. The east access road is located parallel to and approximately 22.9 m (75 ft) west of the existing U.S. 90 roadway.

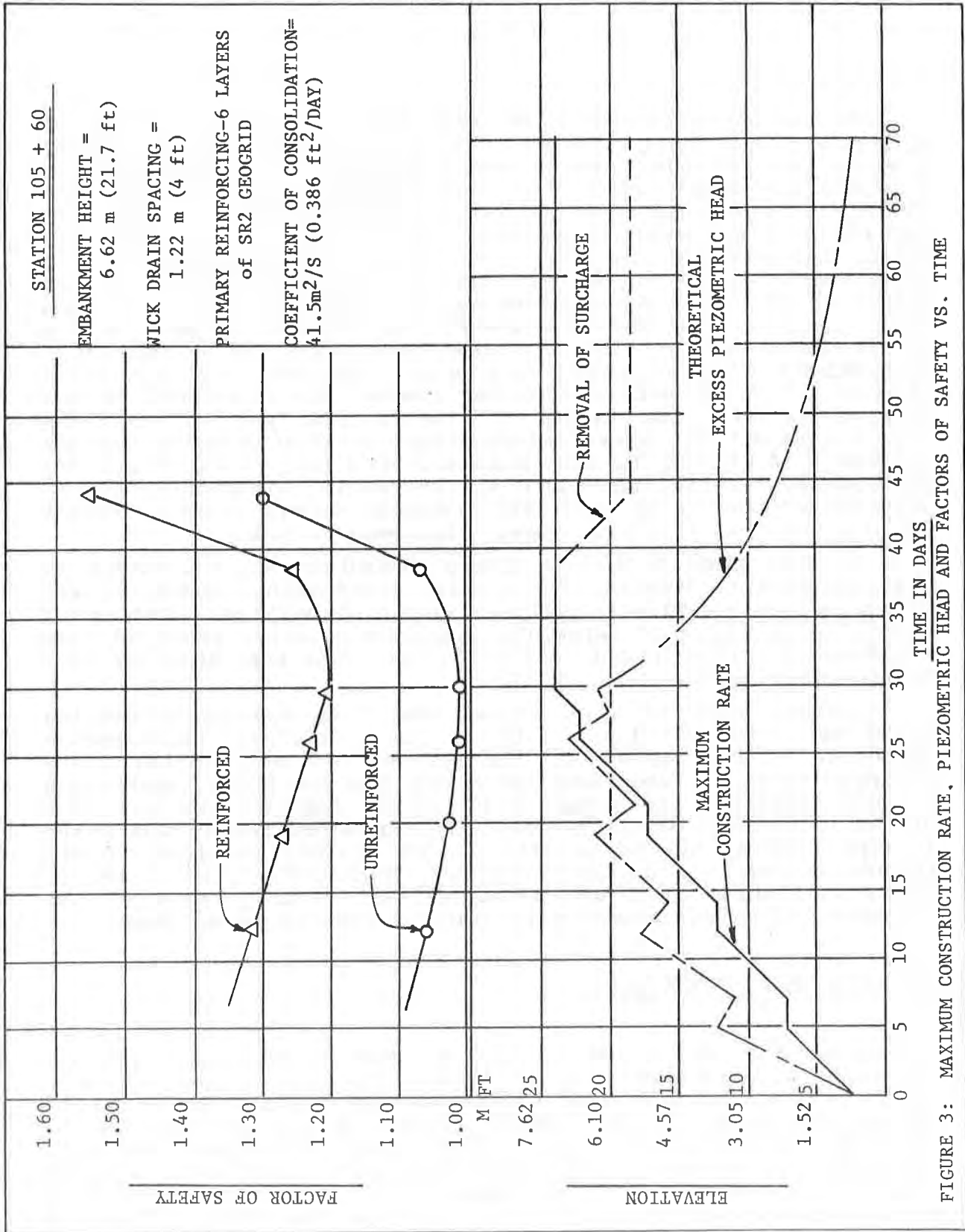


FIGURE 3: MAXIMUM CONSTRUCTION RATE, PIEZOMETRIC HEAD AND FACTORS OF SAFETY VS. TIME

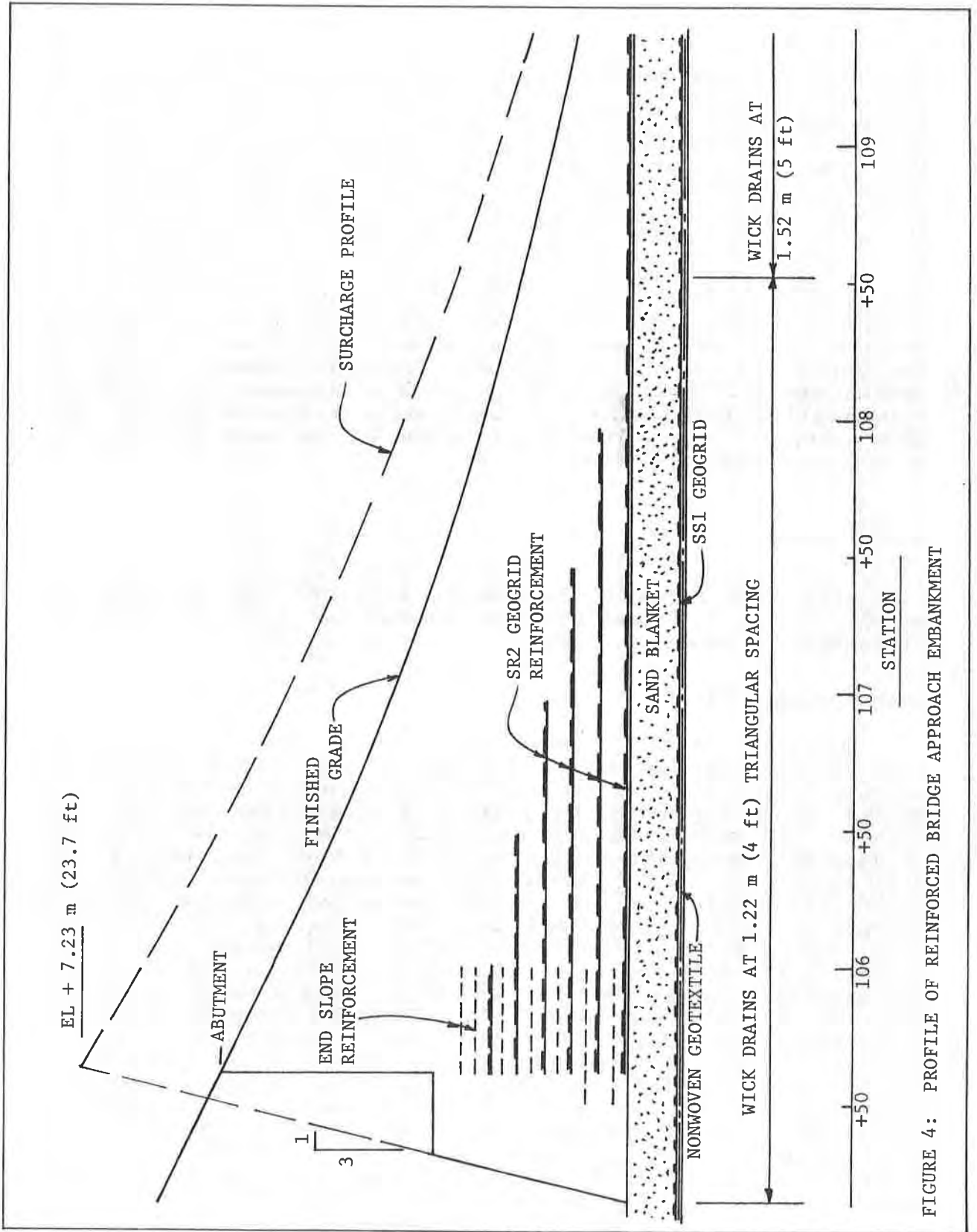


FIGURE 4: PROFILE OF REINFORCED BRIDGE APPROACH EMBANKMENT

This facility was designed using wick drains on a 1.52 m (5 ft) triangular spacing so that the amount of post construction settlement would be minimized. There was no time in the overall construction schedule, however, for surcharging of this facility. The final design called for a layer of nonwoven geotextile to be placed on the marsh surface followed by a layer of Tensar SS1 geogrid. These geosynthetics were to be covered by a 0.61m (2 ft) sand blanket which was to serve in a dual capacity as a drainage medium and as a working platform for the installation of the wick drains. Embankment material would then be placed on top of the sand blanket to final subgrade elevation. At that point, a layer of Tensar SS2 geogrid was required as base reinforcement for the 15 cm (6 in) soil aggregate base course and included in the design of the 25 cm (10 in) flexible pavement system to handle the high volume of truck traffic crossing on the ferry. Plans called for traffic to be routed on the completed east access road thus allowing construction of the mainline facility to commence along existing U.S. 90.

CONSTRUCTION

Bids were taken in September, 1985 and the contract was awarded to S. J. Groves and Sons Company in October. Construction began in February, 1986.

East Access Road

Construction of the east access road began in March, 1986 with the placement of the sand blanket. The first order of work was the installation of the lightweight nonwoven geotextile which served as a separator to prevent contamination of the sand blanket. The contractor had the option of sewing the geotextile or lapping the joints a minimum of 0.91 m (3 ft). Due to the difficulty of field sewing in the marsh environment, the contractor elected to use the lap procedure. Several rolls of geotextile were placed and unrolled parallel to centerline simultaneously for the full width of the east access road. This procedure was followed immediately by the unrolling of the Tensar SS1 geogrid directly over the geotextile, again using three foot laps at the side of the rolls. The SS1 geogrid served as reinforcing for the sand blanket which acted as a working platform for the wick drain equipment. The sand was truck hauled and placed parallel to centerline using small bulldozers. Throughout the 701.2 m (2300 ft) of east access road virtually no mudwaving or shear distortion occurred during placement of the sand blanket. The reinforced sand blanket provided excellent equipment support for the installation of the wick drains which were installed by Drainage and Ground Improvement, Inc. This

subcontractor used a hydraulic activated mandrel for the installation of wick drains to a depth of 6.10 m (20 ft). The wick drain equipment was mounted on a Cat 235 backhoe with the wick drain material being supplied to the installation equipment by truck. No mobilization difficulties were encountered during the wick drain installation. The subcontractor achieved a production rate of over 3048.7 m (10,000 ft) of drains installed per eight hour shift. The subcontractor chose Amerdrain for installation on this project.

Approximately 0.91 m (3 ft) of clay sand embankment material was added on top of the sand blanket to bring the east access road to final subgrade elevation. The readings from the settlement plates which had been installed throughout the east access road showed that the settlement ranged from 0.30 m (1 ft) to 0.72 m (2.35 ft) and occurred quite rapidly. Excess piezometric pressure dropped close to background levels within 35 days after completion of the fill to final subgrade elevation. It is estimated that approximately 80% of the settlement had occurred prior to paving of this facility. The east access road has been under traffic since June, 1986 and the performance has been excellent during this time frame with no major pavement distortions occurring.

MAINLINE FACILITY

Following the rerouting of traffic on the east access road, construction of the bridge approach embankment began. The first step was the installation of the sand blanket on the marsh surface on both the east and west sides of the existing facility. This was accomplished through the use of the lightweight nonwoven geotextile and the Tensar SS1 geogrid for reinforcement. The placement of the two foot sand blanket was achieved with virtually no mudwaving or shear distortions occurring either in front of or at the side of the filling operation. Wick drains were then installed using the same procedure and equipment as previously described throughout the area over the virgin marsh. While the wick drain installation was proceeding, the contractor began the removal of the pavement and base of the old U.S. 90 facility. This area was undercut 0.61 m (2 ft) and the sand blanket was continued across the old embankment prism. When this work was completed, the wick drain installation began in this area. The wick drain subcontractor immediately ran into penetration difficulties near the surface. It was discovered that two other old layers of asphalt existed below sea level. These old pavements had not been encountered in the original soil borings since they had been taken on the shoulders of the existing four lane facility. It became apparent that the ancient

pavements were initially constructed for a two lane roadway which subsequently settled, thus necessitating reconstruction over the marsh area in order that the surface of the roadway be maintained at an elevation above storm flood level.

It was determined that the most feasible approach to overcoming this obstacle to drain installation would be predrilling through the old pavement followed by installation of the drains. Approximately 1865 m (6,118 ft) of predrilled holes were required to penetrate the ancient pavement systems. The installation of 90,180 m (295,792 lf) of wick drains for the mainline facility was completed in mid October, 1986.

After the installation of the wick drains, the first layer of primary reinforcing was placed directly on top of the sand blanket from station 105+60 to station 110+00, (Figures 1 and 4). The truck hauled embankment material was then spread and compacted until the next prescribed elevation for reinforcing was reached. Each layer of geogrid was precut to the design length and field laydown was accomplished very quickly. The contractor reported that no difficulties were encountered with either the laydown operation or the spreading and compaction operation.

The fill reached final surcharge elevation on November 19, 1986. Four clusters of piezometers had been installed with each cluster having a piezometer located at elevations -1.52 m (-5 ft), -3.05 m (-10 ft) and -4.57 m (-15 ft). The rise in pore pressure has closely tracked the predictions (Figure 3) in the upper and center piezometers. Of these eight piezometers, seven gave residual heads at or below the predicted level, while one showed a head of 0.76 m (2.5 ft) above the predicted level. All of the piezometers located at elevation -4.57 m (-15 ft) are reading pore pressures consistent with the original ground water table at elevation +0.61 m (+2 ft), thus indicating that they were placed in the sand stratum which underlies the compressible soils.

The rate of dissipation of excess pore pressure has not been clearly established at the time of writing. Some piezometers are showing decay rates which closely track predictions while others are showing considerably slower rates, roughly one half of the predicted rate. All indications, however, point toward achieving the desired degree of consolidation under the surcharge load within the specified contractual time span.

The recorded settlement to date ranges from 0.61 m (2.0 ft.) to 0.85 m (2.8 ft.). The piezometric levels indicate that the compressible soil has reached approximately fifty percent of total consolidation. Therefore, the maximum settlement beneath full surcharge load should fall between 1.22 m (4.0 ft.) and 1.70 m (5.6 ft.).

There has been no evidence of embankment cracking, lateral spreading or shear displacements in the marsh either during or after embankment construction.

SUMMARY

The performance of all of the geosynthetics used in the construction of the east access road was excellent. Rapid dissipation of excess pore pressure was achieved through the use of wick drains and the sand blanket which was protected from contamination by the use of the lightweight nonwoven geotextile. The SS1 geogrid provided reinforcing for the sand blanket and excellent equipment support for the wick drain installation and subsequent filling operations. No lateral spreading of the embankment occurred under a vertical displacement of 50% of the height of the embankment. The asphalt pavement and base section reinforced with SS2 geogrid has shown excellent performance under a heavy volume of truck traffic.

The SS1 geogrid and the nonwoven geotextile showed the same performance for the bridge approach embankment. Excellent equipment support was provided throughout the marsh area during installation of the wick drains. To date no lateral spreading of the embankment has occurred and the primary reinforcing SR2 geogrids provided the desired stability during the critical time period of loading of the compressible marsh deposits. No evidence of embankment distress has been noted. Preliminary indications show that excess pore pressure should dissipate to desired levels within the contractual surcharge period.

PAGOTTO, A.

Comune di Modena, Italy

RIMOLDI, P.

RDB Plastotecnica, SPA, Italy

Design and Construction of a Geogrid Reinforced Embankment Over Waste Material

INTRODUCTION

This paper deal with the project of the execution of an earth dike to widen the present spoil bank of urban waste in Modena that is now completely filled up.

It is intended to build up, in successive stages, a series of landfills starting from the filling level of the existing spoil bank to obtain some concentric earth embankments, put in banks till a height of about 15 m on the ground level.

The trapeziform embankments, each 5m high, have a constant shape in their longitudinal development and for the successive levels: this is to allow either a uniformity of verification or the acquisition of an experience of installment useful for the various executive phases.

It is important to highlight that the project proposes a solution of rapid execution and moreover it is bound to use (for the customer's requirements) poor material like clay for the embankment execution, and urban solid waste as foundation soil; everything must be compatible with a good COST-PROFIT relation.

GEOMETRY OF THE LANDFILL

If someone want to define a section of an embankment (5m high) to be executed on a compacted soil, the minimal requirements to guarantee the stability must be listed as follow:

- to assign slope angles lower than the effective angle of internal friction;
- not to exceed the bearing capacity of the foundation soil;
- to consider and anticipate differential settlements causing friction cracks.

With reference to the first two points, for the actual embankment a isosceles trapeziform section 3.5 m wide on the top and 19m on the base with bank slope ratio 2/3 was derived; as to the third point the condition in which to operate are such to lead the planner to quit the simple compaction of the material and to choose more secure reinforced soil systems.

The high compressibility of the solid waste united with the

thickness variation can cause differential settlements which lead to cracks, and eventually to the instability of the realized landfills.

The only alternative is to improve the geotechnical characteristics of the fill providing it with reinforcements able to contrast the tensile stress caused by settlements.

We have chosen geogrid as reinforcement since it has very good mechanical characteristics ideal for this employment.

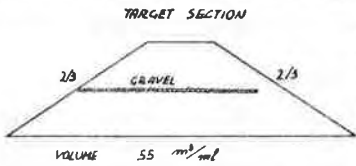
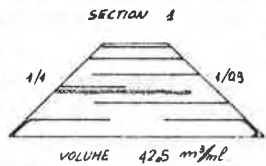
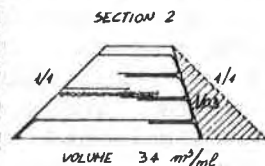
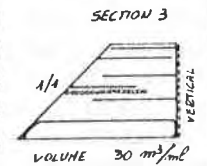
The use of geogrid allows to design the section of the dike with reduced dimensions, to improve the stability, to reduce the quantity of land needed, to increase the basin volume: this permits great money profits.

The reinforced embankment costs about 1.5 times more than a normally built one, but the volume gained by means of the former allows to cover - according to the present prices of waste market- from 0.6 to 0.8 times the cost itself of the work.

CHOICE OF THE SHAPE OF THE SECTION

The choice of the shape of the section is made according to a cost-profit ratio and keeping as a reference the cross section of a non-reinforced embankment whose cost is set at 100. In the following table the potential sections are reported, together with the items of comparison; all items refer to the basic cost 100 and without unexpected occurrences:

Tab. 1 - Costs for the possible alternatives

				
materials handling	+ 75	+ 60	+ 60	+ 42
formworks	0	0	+8	+50
geogrids	0	+56	+56	+50
accessory works	+25	+12	+12	+12
execution cost	+100	+128	+136	+154
profit volume saved	-0	-77	-112	-128
real section cost	100	51	24	26

As we can see from the analysis of the plain numbers the real cost of the section is almost identical for the solutions 2 and 3: if we consider the cost of execution of the two alternatives we would choose the solution number 2 instead of number 3. The comparison between the hypothesis 1 and 2 is favourable to the latter even if its cost of execution is slightly higher. Nevertheless, owing to financial and urgency factors, we have adopted the solution number 1 for the execution of first lot (200 metres long).

For this reason the following check out refers to this solution even if in future the solution number 2 will be adopted.

GEOTECHNICAL PARAMETERS

The landfill project can not leave out of consideration a precise knowledge of the geotechnical characteristics of the foundation soil and the material used for the work.

With regard to this, tests have been carried out, both on the place and in laboratory; the results obtained are the following:

-FOUNDATION SOIL - since it is formed by urban waste put in burrow and compacted, it wasn't possible to carry out laboratory tests because of the great eterogenity of the cluster and so the impossibility of drawing representative samples.

We have then chosen plate bearing tests carried out in a certain number of points on the burrow area.

The average of the obtained values compared to the studies executed on the same type of soil by (12), have given results similar to those related with organic soils:

specific weight of the waste	γ	= 10 (kN/mc)
cohesion	c'	= 30 (kpa)
internal friction angle	ϕ'	= 22 (degrees)
coef.primary consolidation	C_c	= .6 (-)
coef.secondary consolidation	C_a	= .1 (-)

-FILL SOIL FOR THE DIKE-

On a representative sample the following tests have been executed:

- particle-size analysis and specific weights
- Atterberg limits and soil classification
- compaction test according to AASHO modified
- triaxial test U.U. and triaxial test C.I.D. with back pressure
- permeability test by oedometer

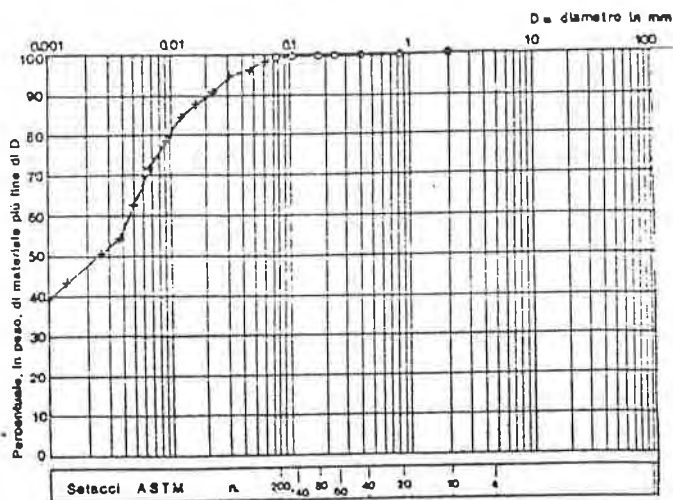
classification CNR-UNI 10006:

wl=65 ; wp=24 ; Ip=41 ; index group = 20 ;
group A7 ; under group A7-6

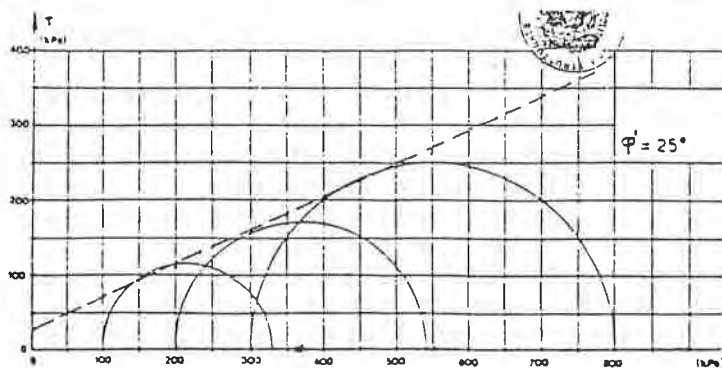
AASHO modified test:

γ = 18 (kN/mc) ; w = 13.5 (%) ; k = 3.0 E-11 (m/sec) ;

granulometry:



triaxial test C.I.D. :



The triaxial test U.U. has given a value of apparent cohesion $c_u = 7$ (kpa).

STABILITY OF THE SLOPES

The verifications are carried out in such a way as to compare the stability of the non-reinforced slopes with that of the reinforced ones.

The aim is to demonstrate that the safety factor is increased by using reinforcement.

All the verifications are executed by FELLENIUS method, on a sample section with unitary thickness.

The safety factor, as it's known, is obtained by the ratio between stabilizing forces and opposite ones, according to the relationships:

$$FS = \frac{\sum P \cos \alpha \cdot \operatorname{tg} \phi' + c' \cdot l}{\sum P \sin \alpha} \quad \text{for non-reinforced slopes}$$

$$FS = \frac{\sum (P \cos \alpha + T \sin \alpha) \cdot \operatorname{tg} \phi' + c' \cdot l + T \sin \alpha}{\sum P \sin \alpha} \quad \text{for reinforced slopes}$$

Using the geotechnical parameters presented in another part of this paper, the obtained results are as follows:

-SLOPE OF 45 DEGREES on the horizontal line

without reinforcement FS = 0.9
with reinforcement FS = 2.5

-SLOPE OF 70 DEGREES on the horizontal line

without reinforcement FS = 0.6
with reinforcement FS = 2.0

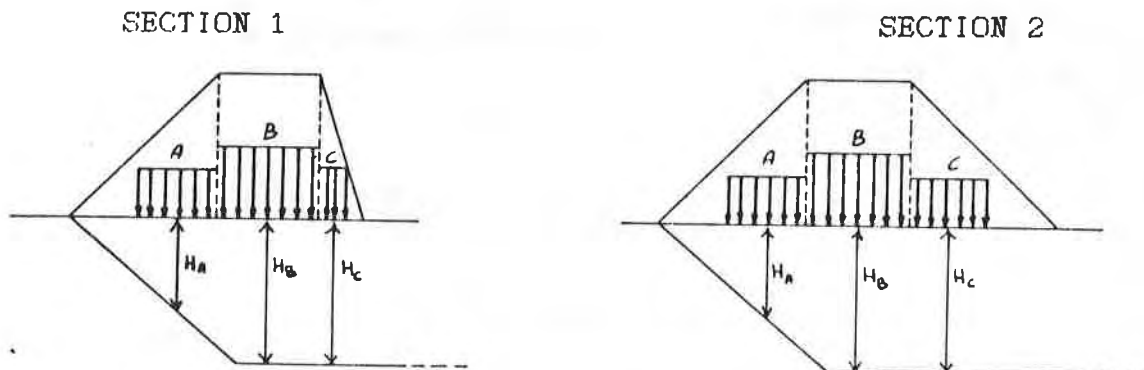
In the light of what has emerged, we underline the importance of the reinforcement as a sealing element along the slip surface. Practically the grids function as discrete reinforcing elements along the critical surface and they give two contributions: a force normal to the surface itself and a shear one.

The shear stress opposite to the slip surface functions as a further "cohesion" while the normal stress imposes an increase of pressure along the slip line; this causes a better soil to soil friction.

It is clear that this permits obtaining high safety factors; from two to three times more than those obtained without reinforcement.

ESTIMATE OF THE SETTLEMENTS WITHOUT GEOGRIDS

The embankment transmits, with its weight, some over-pressure to the foundation soil (very poor as above said): so it is necessary to divide the landfill target section into sectors of unitary thickness and to calculate for each of them the pressure bulb induced in the below soil; the curves of STEINBRENNER-FADUM were used for this purpose. In this specific case three load curves have been isolated that is a three sectors-scheme as follows:



At this point the geotechnical parameters and the load curve are known and so the settlements can be estimated using the oedometric theory of compaction.

In this phase it is to be remembered that all the calculations are related to the single sectors, without geogrid, and considering each at a time.

We determine as many settlements as the individualized sectors are, each of them responsible for the settlement calculated along the vertical line below with the formula:

$$s = H \frac{C_c}{(1 + e)} \log \frac{\sigma + d\sigma}{\sigma} \quad \text{where } C_c=0.6 (-).$$

The results obtained by the application of the method are reported in the following table:

Tab. 2 - Settlements without geogrids

settlements	sa[m]	sb[m]	sc[m]	sm[m]
section 1	0.32	0.40	0.34	0.35
section 2	0.32	0.40	0.24	0.33

These values will be used only for the calculation of the modulus of subgrade reaction of the soil.

DESIGN

The design was done on the basis of the indications included in the design manual of the geogrids producer (10).

The input data were as follows (see fig. 1):

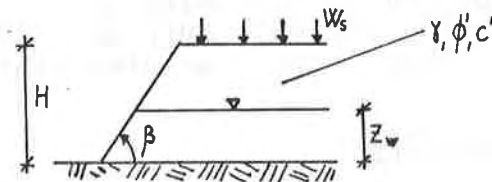


Fig. 1 - Design parameters

- height of the embankment: $H = 5.0 \text{ m}$;
- slope angle: $\beta = 55^\circ$;
- surcharge: $W_s = 10 \text{ kPa}$;
- unit weight of fill-soil: $\gamma = 18 \text{ kN/m}^3$;
- internal friction angle of fill-soil: $\phi' = 25^\circ$;
- cohesion of fill-soil: $c' = 0$;
- maximum tensile strength of TENAX TT1 geogrids: $\alpha_{\max} = 66 \text{ kN/m}$.

The assumed Factor of Safety were:

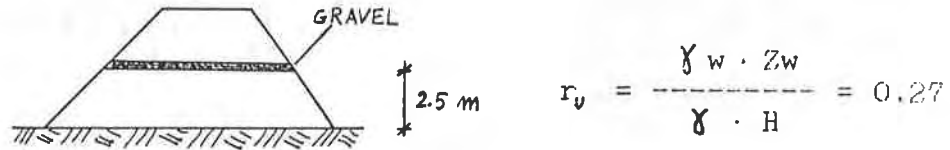
- $FS_{\text{global}} = 1.1$ (well known geotechnical parameters);
- $FS_{\text{time}} = 1.35$ (mean difficulty and duration for the work);
- $FS_{\text{construction}} = 1.35$ (used clay not good for earth dikes);
- $FS_{\text{grid}} = FS_{\text{global}} \times FS_{\text{time}} \times FS_{\text{construction}} = 2.0$

The design parameters were reduced as follows:

$$\phi'^* = \arctg(\text{tg } \phi' / FS_{\text{global}}) = 23^\circ;$$

$$\alpha_a = \alpha_{\max} / FS_{\text{grid}} = 33 \text{ kN/m}.$$

The pore pressure parameter r_u was evaluated with the hypothesis that the worst condition is the embankment being "submerged" at an height of 2.5m from base plan, that is just under the draining gravel layer:



For the calculations it was then used the value: $r_u = 0.25$. The calculation, made on the basis of the above data, allowed to design the final configuration of the reinforced embankment, as shown in fig. 2. It's important to note that, with these calculations, the average tensile resistance requested for the reinforcing layers is: $\bar{\alpha} = 22.8 \text{ kN/m}$.

The average Factor of Safety against geogrids failure is then:

$$FS_{\text{grid}} = \bar{\alpha} / \alpha_{\text{max}} = 22.8 / 66 = 2.9$$

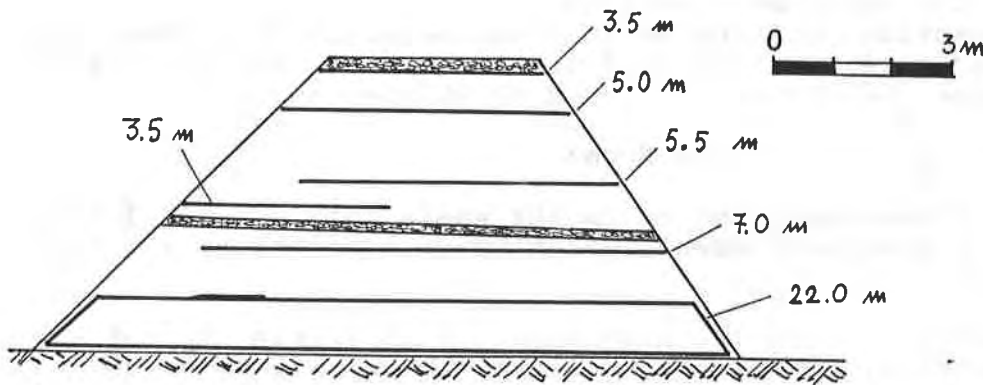


Fig. 2 - Final configuration of the embankment section

STABILITY CHECK

SETTLEMENTS OF WASTE AND TENSILE FORCE IN THE BASE GEOGRID

Since the reinforced embankment doesn't stay on a solid base, settlements in the waste mass are expected, so that the base geogrid will be bent and put in traction. It is very important to forecast the distribution of settlements and of tensile forces in the geogrid along the section of the dike.

For this prediction, it was developed a model based on a Winkler-like scheme: that is, it was made the hypothesis that the inferior layer of compacted fill-soil, contained in the base geogrid close onto itself, acts as a beam on a Winkler soil, characterized by the soil reaction constant K_s , as shown in Fig.3. In fact, the compacted clay into the base geogrid, is enough rigid, omogeneous and compact that it will seem judicious the hypothesis that it acts as a foundation beam.

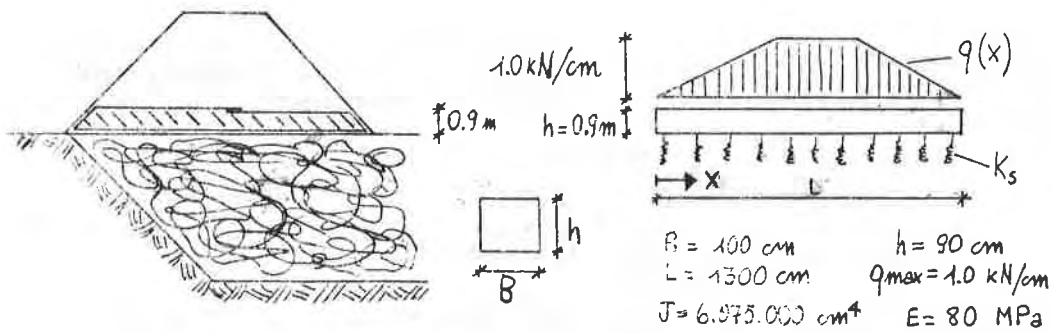


Fig. 3 - Scheme for the Winkler model

So, the beam length is assumed equal to the embankment width; the beam width equal to 1m of embankment length; in this way it isn't taken into account the stiffness given from the remaining length of the earthwork; a possible plate working was not considered, in favour of safety. The beam has a thickness of 0.9m, equal to the base layer one, as shown in Fig. 3, where it can also be seen that the beam is loaded with a trapezoidal surcharge given from the shape of the embankment section.

The soil reaction constant K_s is a parameter which takes into account the average compliance of the waste layer which makes the embankment base. Consequently, it is calculated as:

$$K_s = \frac{q_{\max}}{\bar{s}} F_g = 0.33 \text{ N/cm}^3$$

where: q_{\max} = maximum pressure on the waste mass; $\bar{s} = \frac{\sum s_i L_i}{L_i}$
 \bar{s} = mean settlement, weighted on the lengths = $\frac{\sum s_i L_i}{L_i}$
 $F_g = 1.08 - 1.13$

The settlements s_i under each portion, with length L_i , of the embankment section, considered without reinforcing geogrids, are the same already calculated, as stated before.

The F_g factor takes into account the stiffening given by the geogrid, thanks to which the soil acts as it has a greater reaction constant. The value of F_g was fixed with loading tests with plates and concrete bags, with which it was possible to evaluate the elastic answer of the soil constituted by the actual compacted trash, with and without a geogrid under the load.

With the above values of L , B , h , K_s , and taking into account an elastic modulus E of the clay equal to 80 MPa, the settlements and the moments along the beam axle were calculated, using a standard computer program for beams on Winkler soil.

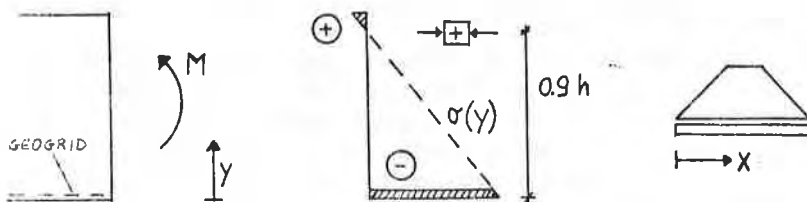


Fig. 4 - Distribution of σ on the beam section

In order to obtain the entity of the tensile force in the base geogrid, it is necessary to make an hypothesis on the distribution of the normal stress σ on the beam section, as shown in Fig. 4.

With this hypothesis the tensile stress σ_g in correnspondence of the geogrid is given by:

$$\sigma_g(x) = \frac{M(x) \cdot 0.9 h}{J}$$

The tensile force in the geogrid is now given by the equation:

$$F_g(x) = \sigma_g(x) \cdot A_g = \sigma_g(x) \cdot T_g \cdot B$$

where: A_g = area of the section of the geogrid;

T_g = equivalent average thickness of the geogrid = 2 mm.

B is calculated as the total solid area of the geogrid section divided by the width of the section.

The above formulas allowed to obtain the values of the forces $F_g(x)$ and of the settlements $s(x)$, as plotted in Fig. 5.

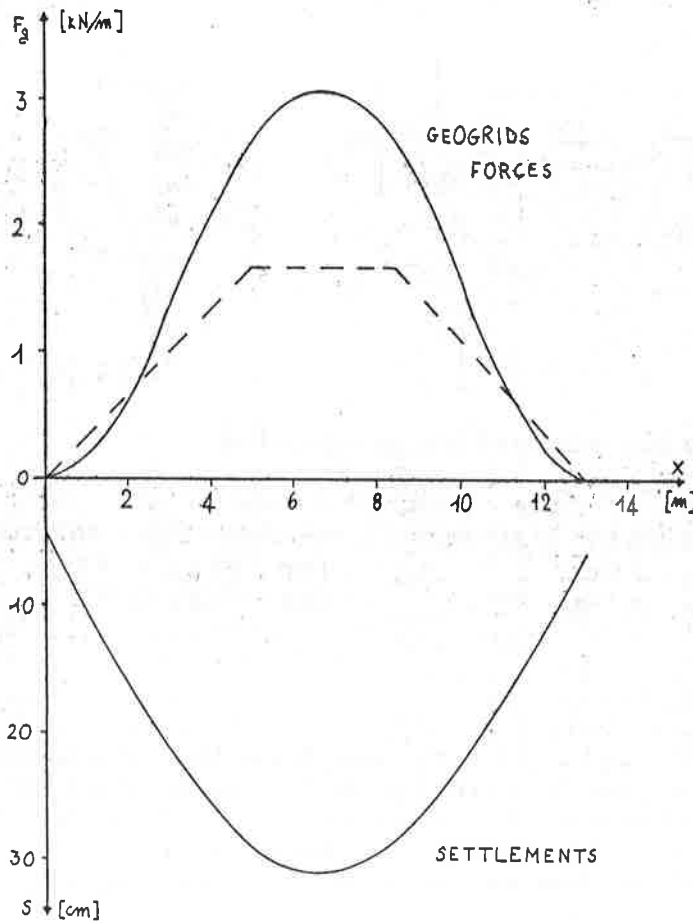
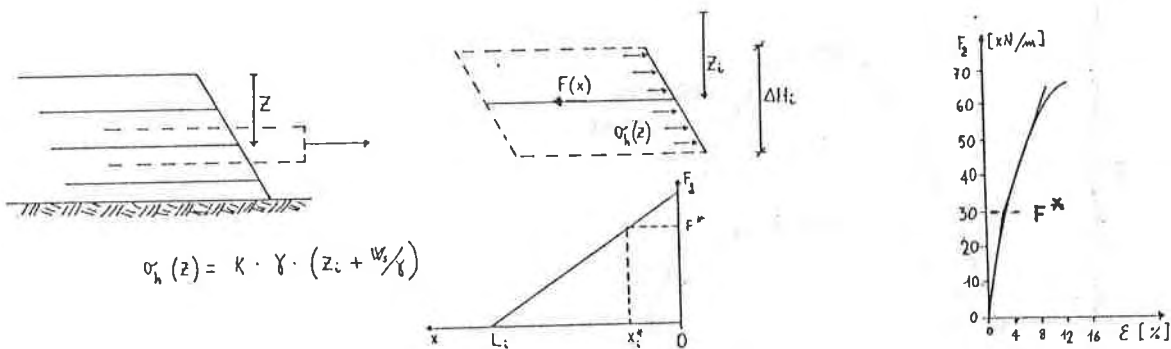


Fig. 5 - Results of the Winkler model

With the obtained results, it seems that the tensile force which the geogrid will have to resist to, is relatively small; therefore in this case the rather small settlements cause only weak tensile forces of flexional nature. The geogrid seems anyway to be indispensable, in order to distribute the load and to omogeneize the settlements, taking into account the etherogeneity of elastic behaviour from point to point of the waste mass base.

GEOGRIDS ELONGATIONS.

For the stability of the embankment it's important that excessive horizontal displacements along the slope don't occur. Thus a prediction was done on the maximum elongation in the various layers of reinforcement, assumed equal to those of the adjacent fill-soil, due only to the thrusts along the slope. The calculation is made imposing the local equilibrium of each reinforcing layer and of the adjacent soil, in conditions of limit equilibrium, as shown in Fig. 6.



$$\sigma_h(z) = K \cdot \gamma \cdot (z_i + w_s/\gamma)$$

Fig. 6 - Scheme for geogrids elongation prediction

The stress-strain curve of the geogrid (see Fig. 6) was schematized with two straight line and it assumes the following analytical form:

$$\begin{aligned} \epsilon &= a_1 \cdot F(x) && \text{for } F(x) < F^* \\ \epsilon &= \epsilon_0 + a_2 \cdot F(x) && \text{for } F(x) > F^* \end{aligned}$$

where: $a_1 = 0.0010 \text{ m/kN};$
 $a_2 = 0.0018 \text{ m/kN};$
 $\epsilon_0 = - 0.024;$
 $F^* = 30 \text{ kN/m}.$

For the calculation of elongations, it was done the simplifying hypothesis that the maximum tensile force for each reinforcing layer were in correspondence of the slope edge and that the tensile force reduces in linear way along each layer (13), as shown in Fig. 6. Said K the earth pressure parameter, the analytical form of F(x) is therefore:

$$F(x) = \gamma \cdot z_i^* \cdot K \cdot \Delta H_i \cdot (1 - x/L_i)$$

with: $z_i^* = z_i + w_s/\gamma .$

The maximum tensile force in each layer is given, on this hypothesis, by:

$$(F_i)_{\max} = \gamma \cdot Z_i^* \cdot K \cdot \Delta H_i$$

If $(F_i)_{\max} > F^*$, it's possible to determine the abscissa X_i^* , where $F(x) = F^*$:

$$X_i^* = \left(1 - \frac{F^*}{\gamma \cdot Z_i^* \cdot K \cdot \Delta H_i}\right) \cdot L_i$$

The elongation in each layer is then given by:

$$\Delta i = \int_{X_i^*}^{L_i} a_1 \cdot \gamma \cdot Z_i^* \cdot K \cdot \Delta H_i \cdot (1 - x/L_i) dx + \int_0^{X_i^*} [\epsilon_0 + a_2 \cdot \gamma \cdot Z_i^* \cdot K \cdot \Delta H_i \cdot (1 - x/L_i)] dx = \gamma \cdot Z_i^* \cdot K \cdot \Delta H_i \cdot [a_1 (L_i/2 - X_i^* + X_i^{*2}/2L_i) + a_2 (X_i^* - X_i^{*2}/2L_i)] + \epsilon_0 X_i^*$$

The values obtained with these equations are reported in Tab. 3 : the maximum elongation, in correspondence to the second layer from the base, is equal to 0.120 m and it is judged as fully compatible with the functionality of the earthwork.

Anyway, the greatest stresses for the geogrid seems to come from the lateral thrusts of the fill-soil, rather than from the flexure caused by the base settlements.

Tab. 3 - Horizontal elongations of the geogrids

Layer n.	Z_i^* [m]	H_i [m]	L_i [m]	$(F_i)_{\max}$ [kN/m]	X_i^* [m]	[cm]
1	5.5	0.45	7.9	18.26	0	0.072
2	4.6	0.90	7.9	30.55	0.14	0.120
3	3.7	1.05	5.5	28.67	0	0.079
4	2.5	1.20	5.0	22.14	0	0.055
5	1.3	1.40	3.5	13.43	0	0.024

FINAL CONTROLS AND CONCLUSIONS

In spite of the initial difficulty of the problem, different stability checks have shown the feasibility of the project and the effectiveness of geogrids; particularly, geogrids are absolutely needed in this case to avoid breaks for sliding on circular surfaces, as the stability analysis has shown.

The embankment was then realized, for a length of 200 m, with a working speed only a little lower than that required for a not reinforced one. The placing of geogrids is simple and quick; little problems are born because of dry clay clusters, which tend a lot the grid in restricted areas, causing concentrated forces. However, the geogrid has resisted very well and it seems that also the direct passing of heavy trucks doesn't cause apparent dangers.

After two months from the end of the works, the collected maximum settlements vary between 30 and 40 cm, with an average value of

about 33 cm, a little greater than the predicted ones. The proposed model seems anyway able to give satisfactory answers for design needs.

The second part of the embankment, 600 m long, will be realized in spring 1987: it's already foreseen to install gauge devices in order to measure the settlements and the forces in the geogrids with a certain precision, in order to make possible to adjust the calculation method with a back-analysis process.

ACKNOWLEDGEMENTS

The authors wish to thanks: A.M.I.U., the committent of the work, and Mr Mario Beretta of RDB, geogrids producer, for the information given; dott.sa Luisa Marino for the assistance in the stability calculations; miss Luisa Valli for the translation.

REFERENCES

- (1) Binnie & Partners, "WAGGLE - A computer program for the stability analysis of reinforced soil slopes and embankments" - Program Manual, London, U.K., 1982.
- (2) Department of Transport, "Reinforced soil retaining walls and bridge abutments", Technical Memorandum BE3/78, London, U.K., 1978.
- (3) Jewell, R.A., "Some effects of reinforcement on the mechanical behaviour of soils", PhD Thesis, University of Cambridge, U.K., 1980.
- (4) Jewell, R.A., Milligan, G.W.E., Sarby, R.W., Dubois, D., "Interaction between soil and geogrids", Proc. Symp. Polymer Grid Reinf. in Civil Engg., London, U.K., 1984.
- (5) Mc Gown, A., Paine, N., Dubois, D., "The use of geogrid properties in design", Proc. Symp. Polymer Grid Reinf. in Civil Engg., London, U.K., 1984.
- (6) Ministere des Transports, "Les ouvrages en Terre Armee. Recommandation et regles de l'art", LCPC, France, 1979.
- (7) Schlosser, F., Jacobsen, H.M., Juran, I., "Soil reinforcement. General Report", Proc. 8th Eur. Conf. Soil Mech. Fndn Engg., Vol. 3, Helsinki, Finland, 1983.
- (8) Schlosser, F., Juran, I., "Design parameters for artificially improved soils. General report", Proc. 7th Eur. Conf. Soil Mech. Fndn Engg., Vol.5, Brighton, U.K., 1979.
- (9) Whitman, R.V., Bailey, W.A., "The use of computers for slope stability analysis", ASCE J. Soil Mech. Fndns. Div., Vol. 93, SM4, July, 1967, pp. 475-498.
- (10) Rimoldi, P., "Il progetto dei pendii ripidi rinforzati", Collana Tecnica RDB-1, RDB Plastotecnica, Milano, Italy, 1986.
- (11) Cancelli, A., "Appunti di geotecnica", CUSL, Milano, Italy, 1982.
- (12) Cancelli, A., Cossu, R., "Problemi di stabilita' negli scarichi controllati - aspetti geotecnici e degradazioni biochimiche", Atti del XXX Corso di Aggiornamento in Ingegneria Sanitaria, Politecnico di Milano, Italy, 1985.
- (13) Cazzuffi, D., "L'impiego dei geotessili nelle opere di sostegno: criteri di progettazione e indagini sperimentali", ENEL-CRIS, Milano, Italy, 1982.

CHOU, N.S.S.

Colorado Department of Highways, U.S.A.

TZONG, W.H.

University of Colorado at Denver, U.S.A.

SIEL, B.D.

ATEC Associates Inc., U.S.A.

The Effectiveness of Tensile Reinforcement in Strengthening an Embankment Over Soft Foundation

ABSTRACT

A study was undertaken to investigate the effectiveness of placing a single layer of tensile reinforcement at the base of an embankment construction on a soft foundation in order to strengthen the embankment and reduce detrimental settlement. The embankment was constructed by the Colorado Department of Highways. The reinforcement was Tensar SS-2, a polypropylene geogrid.

The study was conducted by use of the finite element analysis. Nonlinear soil behavior and incremental construction sequence were accounted for in the analyses. Field measured data of vertical and horizontal movements in the foundation were used to calibrate the soil parameters. Simulation of the tensile reinforcement was accomplished in two different manners. The first was to use the stress-strain properties of the geogrid with bar elements. The second was to incorporate the geogrid-soil composite properties with quadrilateral elements.

Using the calibrated parameters, it was shown that the analysis procedure predicted very well the performance of the embankment as additional fill was placed. The results also indicated that the use of the tensile reinforcement did not appreciably reduce the differential settlement of the embankment, compared to using no tensile reinforcement. This is primarily because the deformation of the embankment is predominately in the vertical direction.

INTRODUCTION

This is the first embankment stabilization project using polymer geogrid as soil reinforcement in the Rocky Mountain Area. The project consist of approximately 750 linear feet of up to 28 feet high embankment over a very weak foundation materials situated between Sheridan Boulevard and Tennyson Street, Denver on Interstate Highway 76. The foundation soils include: (1) concrete waste (cement wash) materials, similar to fly-ash in texture. A summary of laboratory test results of the material is listed in Table 1. (2) trash, ranging from paper, plastic to auto body. (3) natural soil, including gravel pit and bedrock (shale). A stratigraphic cross-section of the embankment/foundation is shown in Figure 1.

Two major concerns with this embankment constructed on soft foundation have been slope stability and settlement. The proposed embankment slopes range from 3:1 to 4:1, depending on the location. Slope stability analysis was performed using

TABLE 1

Summary of Lab Test Result for
Concrete Waste Materials

Summary of laboratory test results

Concrete Waste Material (Cement Wash)

(1) Physical Properties:

- (a) Description: Sandy silt, very soft, white
- (b) AASHTP Classification = A-4(0)
- (c) Specific Gravity = 3.11
- (d) Density: Wet = 73-80 PCF; Dry = 19-33 PCF
- (e) Void Ratio = 4.7-9.3
- (f) Plastic Index = 0
- (g) Moisture Content = 39 to 93%
- (h) Chemical Component: Silicon (>10%), Calcium (10%), Aluminum (5%), Iron (2%), Sodium (1%); Sulfate (.148%), Chlorides (0.015%), PH = 8.1, CR level = 1

(2) Triaxial Tests

<u>Type of Test</u>	<u>Cohesion (PSF)</u>	<u>Friction Angle (Degree)</u>
(a) Consolidated Drained (CD)	$C' = 0$	$\Phi' = 41$
(b) Consolidated Undrained (CU)	$C' = 0$ $C = 0$	$\Phi' = 41$ $\Phi = 22$
(c) Unconsolidated Undrained (UU)	$C = 130$ to 460	$\Phi = 0$

(3) Consolidation Tests

- Compression Index (C_c) = 3.6
- Recompression Index = 0.1
- Coef. of Consolidation (C_v) = .0152 - .0235 in²/min.
- Maximum Pre-Consolidation Pressure (P_c) = 0.8 TSF
- Immediate Settlement = 50% of Total Settlement
- Primary Consolidation = 40% of Total Settlement
- Secondary Compression = 10% of Total Settlement

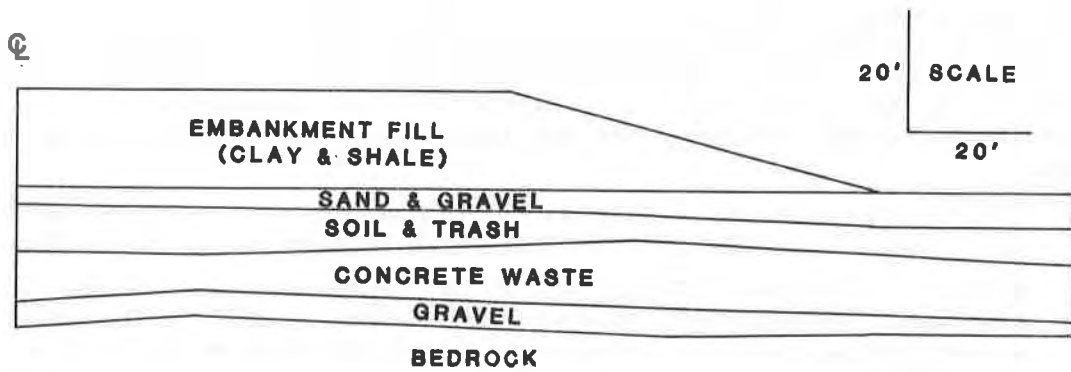
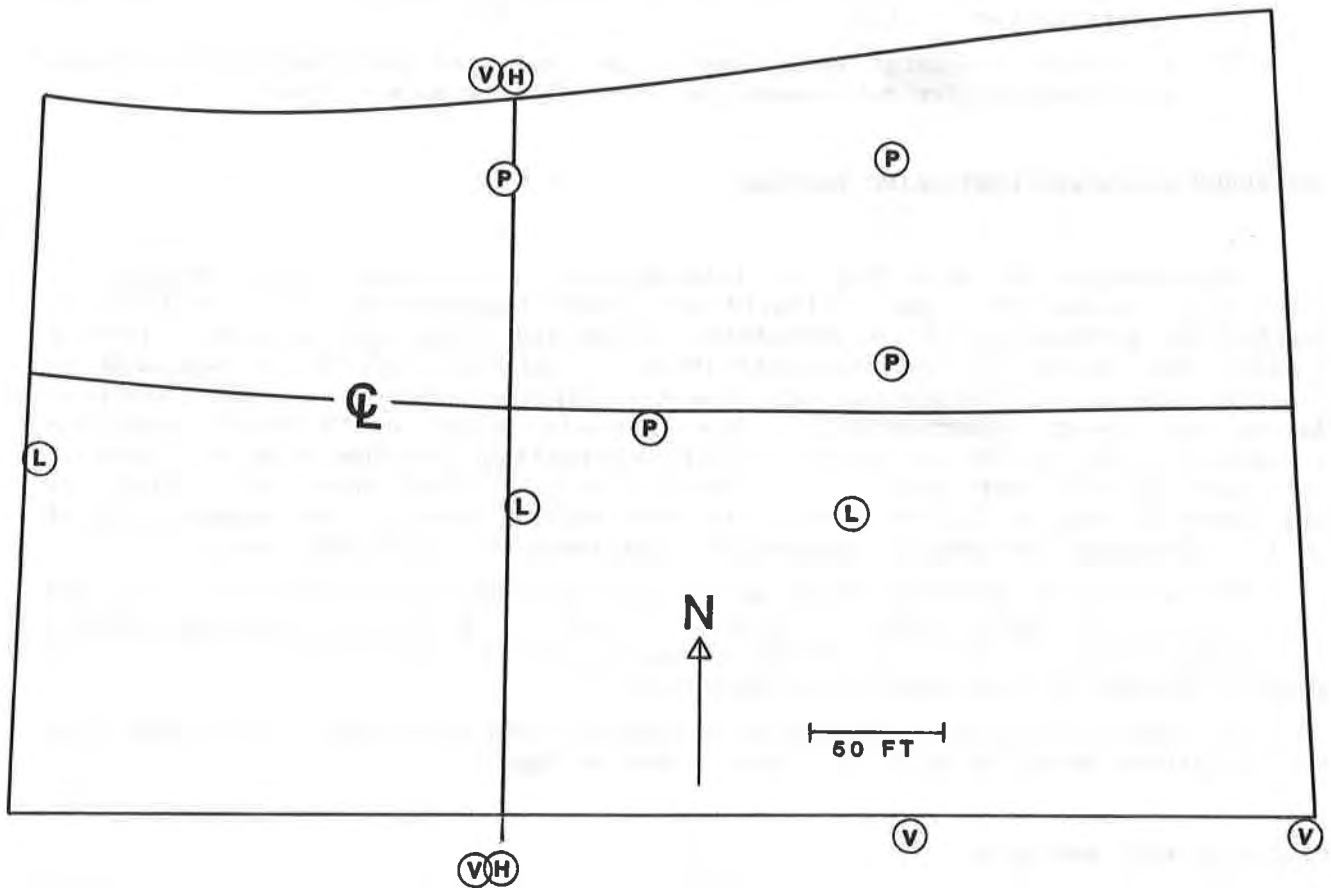


FIG. 1: STRATIGRAPHIC CROSS-SECTION



- H - HORIZONTAL INCLINOMETER
- V - VERTICAL INCLINOMETER
- P - PIEZOMETER
- L - LIQUID SETTLEMENT TRANSDUCER

FIG. 2: INSTRUMENTATION PLAN

the conventional Modified Bishop method. A marginal safety factor was obtained for an undrained condition, which simulated immediately after construction condition with rapid placement of the embankment fill. It was estimated that significant settlement of up to 0.5 m might occur after the full embankment is placed. To alleviate the potential stability and settlement problems, the following measures were taken:

- (1) Staged construction: Two phases construction each consists of half of the total fill height, with a four month waiting period in between.
- (2) A layer of Tensar SS-2 geogrid was installed at the base of the embankment before the placement of embankment fill. The geogrid was chosen over geotextiles because of its higher tensile stiffness and yield strength.

The geogrid was sandwiched between two 8-inch thick layers of granular base coarse material to optimize grid interlock. The geogrid mat extends across the entire base width of the embankment where the weak foundation materials are located.

- (3) A two-foot surcharge was placed on the completed embankment to reduce the post construction settlement due to traffic loads and creep.

INSTRUMENTATION AND MONITORING PROGRAM

Instrumentations including 6 piezometers, 3 vertical inclinometers, 1 horizontal inclinometer, and 3 liquid settlement transducers, were installed to monitor the performance of the embankment during and after construction. Figure 2 depicts the layout of the instrumentations. All the instruments appeared to function properly. The piezometers showed negligible porewater pressure increase during embankment construction. This indicates that a "drained" condition prevailed in the foundation soil. Lateral deformations obtained from the vertical inclinometers are very small, less than .02 m (1"), which also reveal that the embankment is very stable throughout the construction period. The measurements of liquid settlement transducers agreed well with those of the inclinometers.

The settlement profiles along the horizontal inclinometer for the first and second phases of construction are shown in Figure 3. To eliminate geology related discrepancy, only an "average" settlement curve obtained from both the northern and southern halves of cross-section is presented.

The average horizontal deformations measured from both ends of the embankment for the second phase of construction is shown in Figure 4.

FINITE ELEMENT ANALYSES

A finite element code SSTIP, developed at the University of California at Berkeley, was used for the analysis. In the analysis, field measurement data were used to calibrate the most representative soil and geogrid parameters. The parameters were then used to investigate the effectiveness of the tensile reinforcement. The finite element discretization of the embankment foundation system is shown in Figure 5.

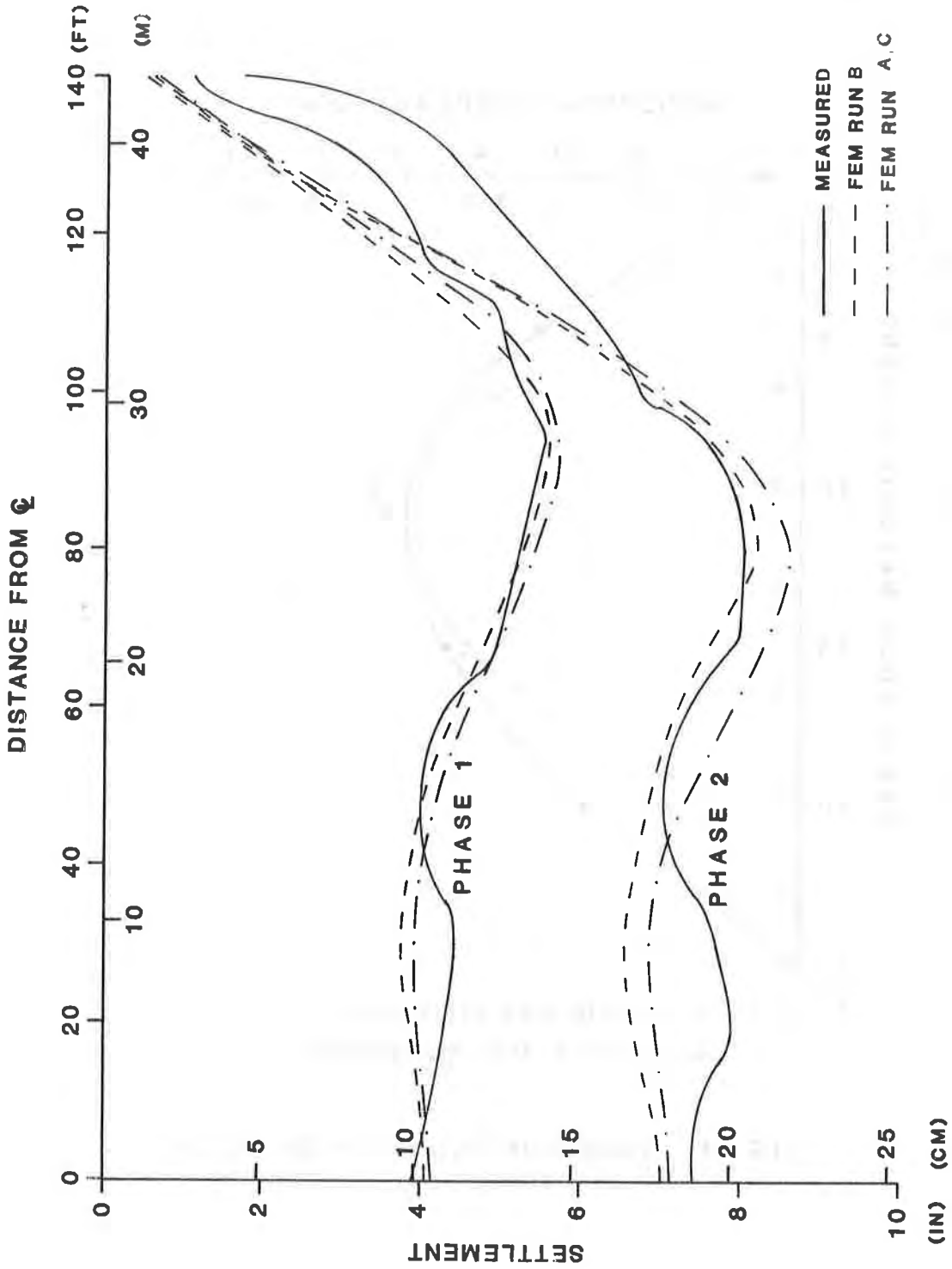


FIG. 3: SETTLEMENT PROFILE ALONG THE HORIZONTAL INCLINOMETER

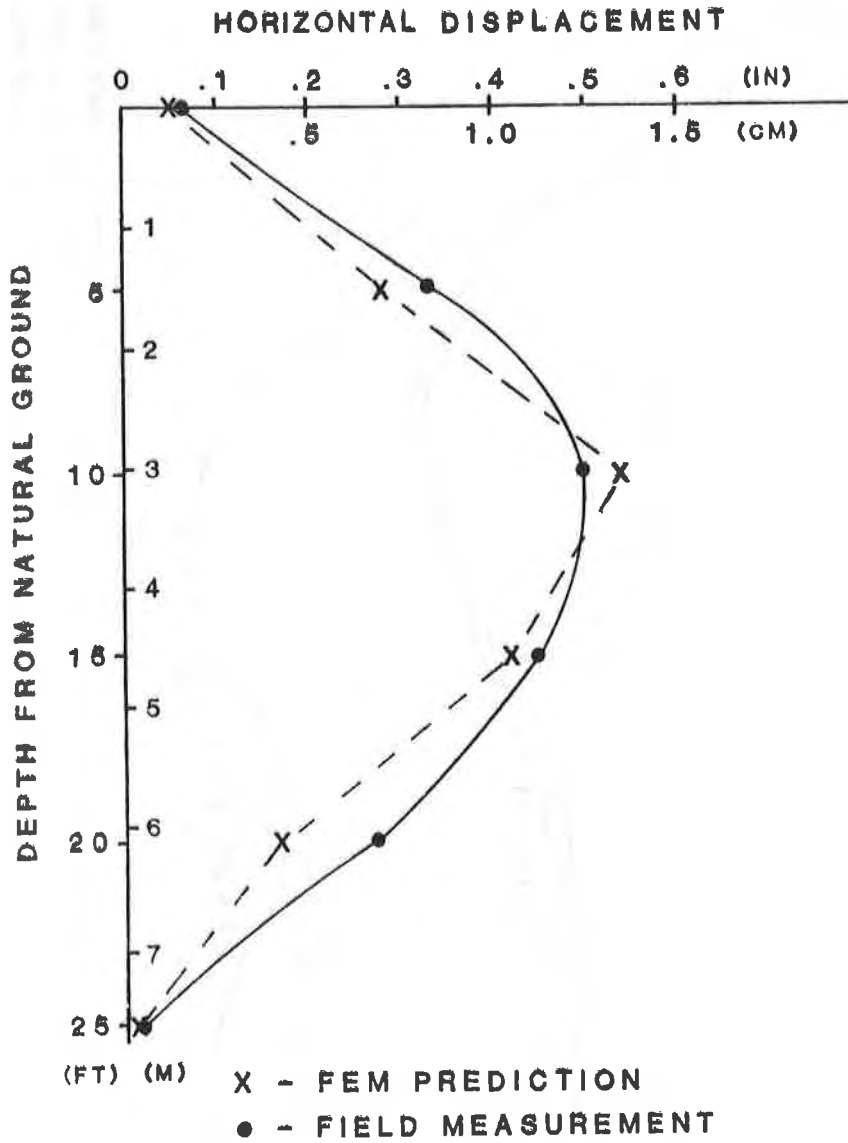


FIG. 4: HORIZONTAL DEFORMATION

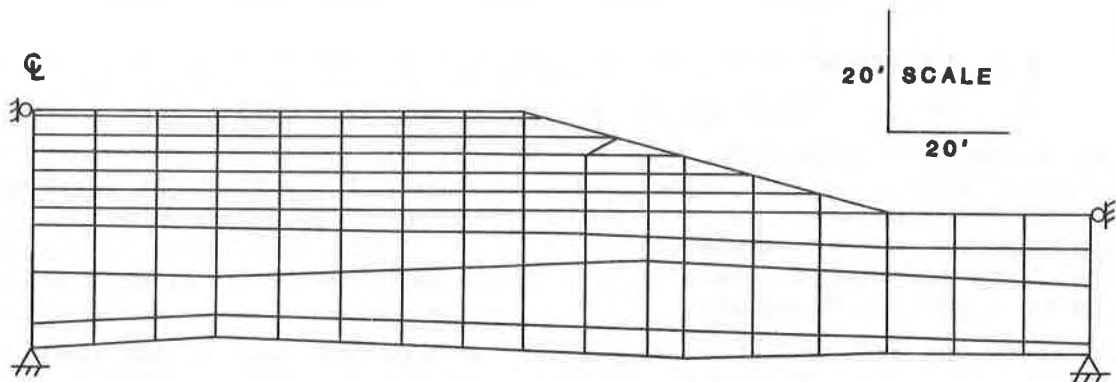


FIG. 5: FEM DISCRETIZATION

The hyperbolic soil model developed by Duncan and Chang (1) was used in the finite element analysis, because the loading is monotonically increased, nonlinear stress dependent soil behavior and incremental construction sequence can be accounted for in a realistic manner.

The Duncan-Chang soil model requires 5 parameters, (i.e., K , n , R_f , C , Φ) to describe the stiffness and strength characteristics, and three parameters, (i.e., G , D , F) to describe the volume change characteristics. A wide range of soil parameters was used in the analysis in order to obtain a set of representative parameters, except for the stiffness-strength parameters of the concrete waste material, which were obtained from Triaxial CD & 1-D consolidation tests.

The most representative soil parameters of the Duncan-Chang model for the concrete waste material were determined as:

$$\gamma = 11.47 \text{ KN/m}^3 \text{ (73 pcf)}, K = 20, n = 0.22, D = 0, G = 0.27,$$

$$F = 0.03, C = 0, \Phi = 41^\circ, R_f = 0.50$$

To simulate the field behavior of the geogrid, two methods were adopted in the analysis:

- (1) Use a series of bar elements with linear elastic constitutive law to represent the characteristics of the geogrid since no bending resistance is available for geogrid.
- (2) Use quadrilateral elements with Duncan-Chang model to simulate the composite of the geogrid and the surrounding soil. The composite properties were determined from triaxial CD tests. In the tests, one layer of geogrid was placed at the middle of 0.15 m (6") diameter sample of the same material used in field. This is to simulate the fact that the soil above and below the geogrid is subject to shear stress while the geogrid is subject to tension, and its deformation is restrained by grid interlockings.

The following parameters for composite materials were deduced from triaxial CD tests:

$$\begin{aligned}\gamma &= 18.85 \text{ KN/m}^3 \text{ (120 pcf)}, K = 454, n = 0.4, D = 7.1, G = 0.33 \\ F &= 0.07, C = 75.83 \text{ kPa (11 psi)}, \Phi = 35^\circ, R_f = 0.73\end{aligned}$$

The settlements calculated from methods (1) and (2) were reflected by curves designated as Runs A and B, respectively, in Figure 3. Method (2) seems to be a better way for simulation of the field behavior of geogrid since the in-soil geogrid behavior was accommodated in the test. The settlements obtained from method (2) are somewhat smaller, as method (1) employed in-air geogrid properties supplied by the Tensar Corporation.

To study the effectiveness of geogrid, an analysis (Run C) was performed by removing the bar elements from the finite element mesh. The results are depicted in Figure 3 for the two phase construction.

The results of Runs A and B are plotted in Figure 3 which agreed well with the measured settlements for the first phase construction. Figure 3 also shows the predicted and measured settlements for the second phase construction using the material properties deduced from the first-phase construction. The predicted settlement from Runs A and B demonstrated good agreement between predicted and measured settlements for the second construction phase.

Figure 4 shows the measured and predicted horizontal deformations along the vertical inclinometer for the second phase construction. Again, the predicted deformations agreed very well to those measured.

Based on the above three sets of settlement/deformation data, it may be concluded that the parameters determined in Runs A and B are rather reliable. It is to be noted that the settlement/deformation difference between Runs A and C (with and without a layer of geogrid) was surprisingly insignificant. It was believed that this was because the settlement was essentially one-dimensional. Since the lateral displacement of the concrete wash material was rather small, the overall (average) strain of the geogrid was trivial. The tensile stresses developed in the geogrid were thereby insignificant.

CONCLUSIONS

The above study was undertaken to investigate the performance of an embankment situated on concrete waste material by the finite element analysis. The findings of the study are summarized in the following:

- (1) Using material parameters calibrated from settlement measurements of the first phase construction the finite element analysis procedure predicted very well the field settlements, in both vertical and horizontal directions.
- (2) The use of geogrid did not show much benefit in reducing the differential settlement. It is because the settlement is essentially one dimensional therefore the tensile strength of the geogrid was not mobilized.

The conclusions had been verified by an independent study conducted by Siel (3) using a different finite element code CANDE (2).

REFERENCES

1. Duncan, J. M., and C. Y. Chang, "Nonlinear Analysis of Stress and Strain in Soils," Journal of the Soil Mechanics and Foundation Division, ASCE, Vol. 96, No. SM9, Proceedings Paper 7513, 1970, pp. 1635-1653.
2. Katona, M. G., Smith, J. M., Odell, R. S., and Allgood, J.R. "CANDE - A Modern Approach for the Structural Design and Analysis of Buried Culverts," Report No. FHWA-RD-77-5, Washington, D.C., 1976.
3. Siel, B. D., "An Investigation of the Effectiveness of Tensile Reinforcement in Strengthening an Embankment over Soft Foundation," Master Thesis, Department of Civil Engineering, University of Colorado at Denver, April 1986.

ACKNOWLEDGEMENTS

The authors gratefully acknowledge the geotechnical staff of the Colorado Department of Highways for their assistance in establishing the field instrumentation program. Special thanks are due Messrs. John B. Gilmore and Ed Balknap for their fruitful discussions.

SEAWELL, H.

Thompson Engineering, Testing, U.S.A.

MATTOX, R.M.

The Tensar Corporation, U.S.A.

An Economical Solution to Increasing the Capacity of an Industrial Waste Facility with a Geogrid Reinforced DikeIntroduction

An international chemical manufacturing corporation with a facility in Mobile County Alabama, recognized the necessity in late 1984 to provide additional storage capacity for its industrial process waste. The existing 7.69 hectare (19 acre) earthen diked containment basin which had successfully functioned as the primary storage facility for the iron oxide sludge material since 1974 was determined to have less than six months of useable life and, at the time, had less than 0.61 meters (2 feet) of freeboard. Operational needs dictated the provision of an additional 2.5 meters (8 feet) of storage over the entire 7.69 hectare (19 acre) basin. A secondary "tailings pond" designed and constructed in 1983 to receive the industrial by-product after the original pond reached capacity had been restricted from its intended use for an indefinite period of time. The deposition and recovery of waste material liquids within the storage basins was central to the production process and function of the manufacturing plant. Aware of this problem, an accelerated feasibility study and engineering design was ordered by the facility owner.

Solution techniques and feasible construction options available to the designer were severely limited by operational and physical constraints. Existing environmental and mechanical systems peripheral to the pond facility, coupled with property boundary limitations escalated the cost of conventional outboard earthen berm and "flat slope" construction as a dike raising option. The considerable costs of constructing an entirely new containment basin remote to the existing slurry delivery and return systems - notwithstanding the difficulties in regulatory agency approval - rendered this option untenable. Remaining construction alternatives involved increasing the storage capacities by constructing dikes inboard of the narrow existing dike crest and directly upon the sludge. The extraordinarily weak deposits of iron oxide sludge would have dictated slopes flattened to a degree such that significant loss in containment area and storage would have resulted. Further, the cost of this approach was considered excessive.

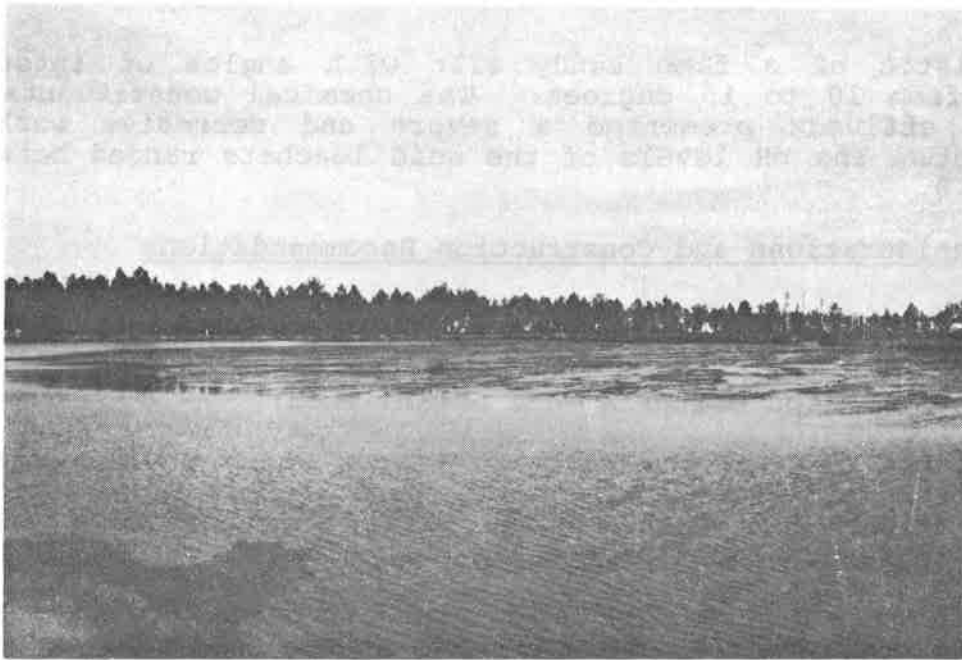
Previous geotechnical study opinions secured by the owner indicated that weak subsurface soils and corresponding slope stability problems precluded conventional increases in dike heights for additional storage. An independent geotechnical investigation and analysis concurred that factors of safety against shallow inboard slope failure of less than unity and deep seated outboard failure factors approaching unity were to be expected. Cost estimates and time studies clearly indicated, however, that the most favorable solution to the waste capacity problem would be to construct an unconventional containment system with steepened slopes and improved stability through specialized geotechniques.

This solution involved the design and construction of a geosynthetic reinforced dike section with slopes positioned strategically upon both the pre-existing dike embankments and contained waste sludge.

Subsurface and Environmental Conditions

Generally, the industrial storage facility was constructed over extremely weak alluvial marine deposits in the coastal plains of south Alabama. Underlying a shallow 3.1 meter (10 foot) thick surficial layer of loose saturated silty sands is a dominant layer of very soft compressible organic laden silty clay with shear strength ranging from around 9.57 to 23.9 kPa (200 to 500 psf). This critical substratum extending to depths of 16.8 meters (55 feet) overlies a clayey and silty sand deposit of medium density and strength. The original containment dike, which had been elevated to +31.0 ft-NGVD (approximately 4.6 meters (15 feet) above exterior grade), was constructed of native site soils with 3H:1V inboard and outboard slopes. Total settlements in the range of 15.2 to 30.5 cm (6 to 12 inches) had been observed after construction of the original dike.

The deposits of iron oxide sludge existed in a viscous, underconsolidated, saturated state. The plant discharge of oxide slurry remained constant during the entire construction process with weir controlled levels of fluid at or above the sludge surface. The oxide sludge had the characteristic of a very soft silty clay with measured shear strengths of between 2.39 and 4.79 kPa (50 and 100 psf) increasing with depth. Notably, however, the indices of consolidation were relatively high and the consolidated drained materials assumed the



VIEW OF IRON OXIDE POND PRIOR TO MODIFICATION



VIEW OF PRE-SEWN GEOTEXTILE LAYER APPLICATION

characteristic of a fine sandy silt with angles of internal friction from 10 to 15 degrees. The chemical constituents in the pond effluent presented a severe and corrosive working environment. The pH levels of the acid leachate ranged between 1.0 and 2.0.

Design Considerations and Construction Recommendations

After assessing all project needs and construction constraints, the following design criteria were established:

Steepened inboard and outboard slopes which would minimize encroachment into difficult pond conditions, reduce quantities of earthen dike fill, and improve slope stabilities of both inboard and outboard.

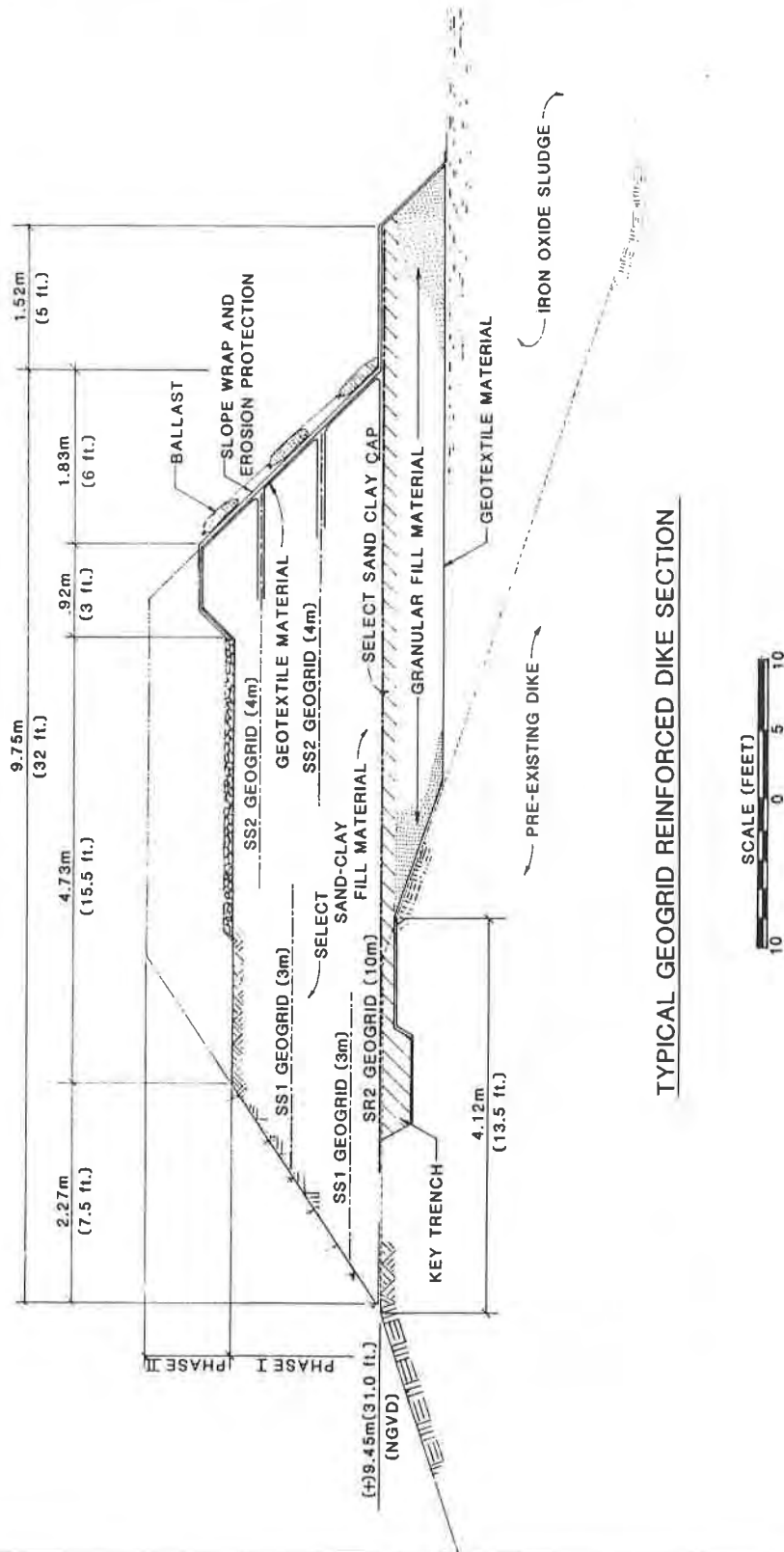
Specified geosynthetics which would provide the necessary ground improvement during each stage of construction, provide strain compatibility with earthen fill and adequately resist site environmental conditions. Notably, the design of construction materials resistant and inert to the acid environment at the site included clay mineralogical analyses and the selection of soil fill types comparably resistant to long term deterioration.

A design scheme which would allow for construction of dikes by conventional earth hauling, moving and shaping equipment.

A design scheme which would optimize strength gain as a result of consolidation of both the contained sludge material and weak foundation soils.

A design scheme would require that the accelerated construction time schedule be satisfied.

Figure No. 1 depicts the selected dike section which was designed to meet all of the established criteria. The design was based on the results of computerized slope stability analyses which included the placement of horizontal reinforced elements, worst case conditions of phreatic surfaces and neutral stress development. Figure No. 2 graphically depicts the critical failure plans and corresponding factors of safety for both internal and external conditions.



TYPICAL GEOGRID REINFORCED DIKE SECTION



FIGURE NO. 1

SLOPE STABILITY GRAPHIC

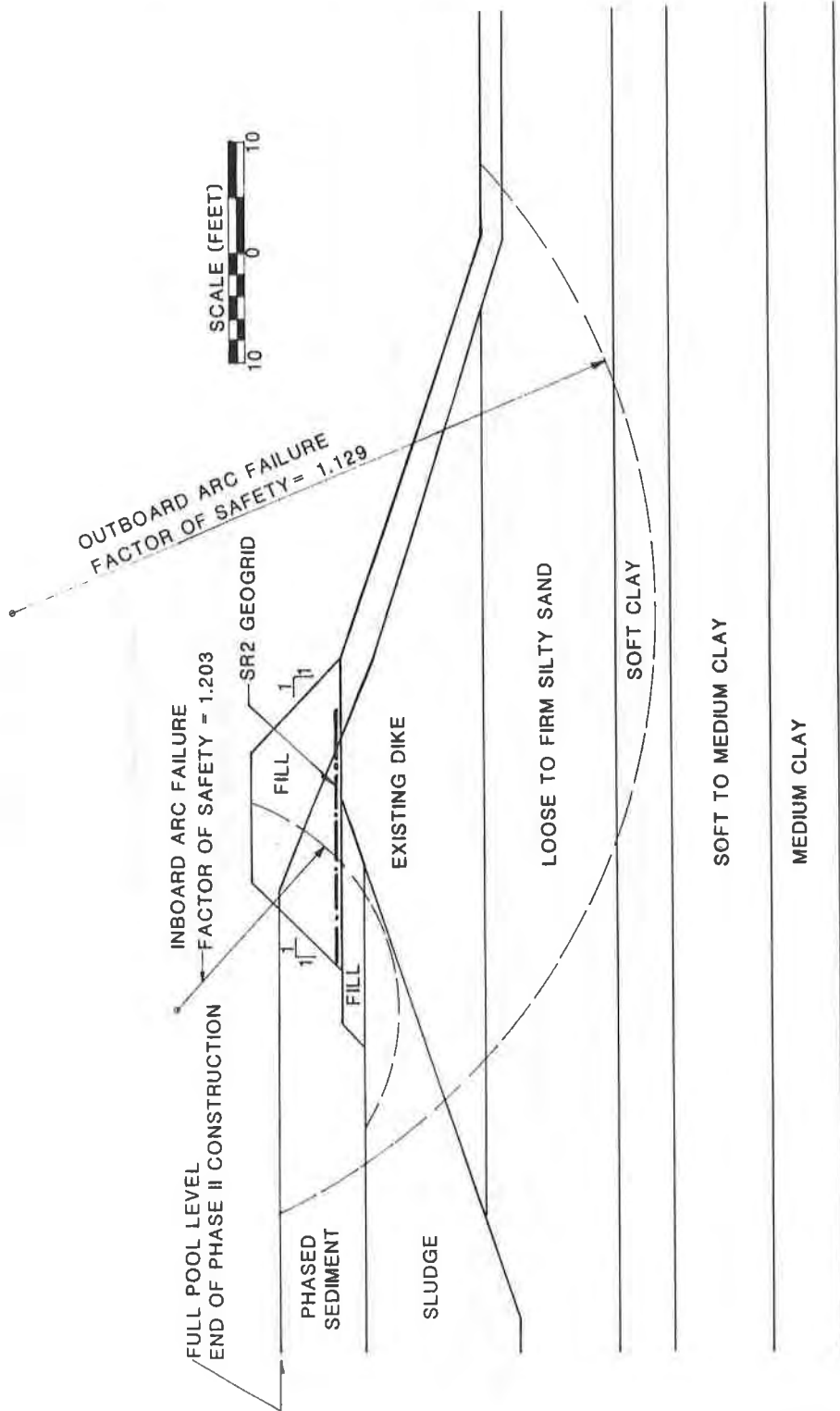


FIGURE NO. 2

The construction of the elevated dike sections was accomplished in four primary phases:

The existing dike surfaces were prepared by shaping to the design section and cutting a trapezoidal key along the centerline for anchorage of inboard geotextile layers and receipt of a seepage abatement clay core. Concurrent with the initial site activities, instrumentation was installed at eight critical stations and included inclinometers, piezometers, and settlement plates for performance monitoring of the stressed earthen embankment.

An intermediate strength woven polypropylene geotextile ("fabric") with design Grab Tensile strength of 52.5 KN/m (300 lb/inch) at a maximum elongation at rupture of 25% was specified to provide the initial separation and short term support of a granular earth working surface. Criteria for resistance to ultraviolet deterioration and loss of dimension within the acid environment was specified. The general contractor selected Terratex HD geotextile, a product of Webtec, Inc. A minimum 30.48 cm (12 inch) layer of sand fill was placed and leveled to existing dike crest elevations by back-dragging and spreading. Low ground pressure, wide-tracked equipment was used to place the granular fill over the fabric covered surface. A select fill topping (composed of specified low permeability sandy clay soil) was placed and loosely compacted over the entire earthen platform width. As expected, settlements and elastic distortions on the order of 30.48 to 45.72 cm (12 to 18 inches) occurred during this early phase construction.

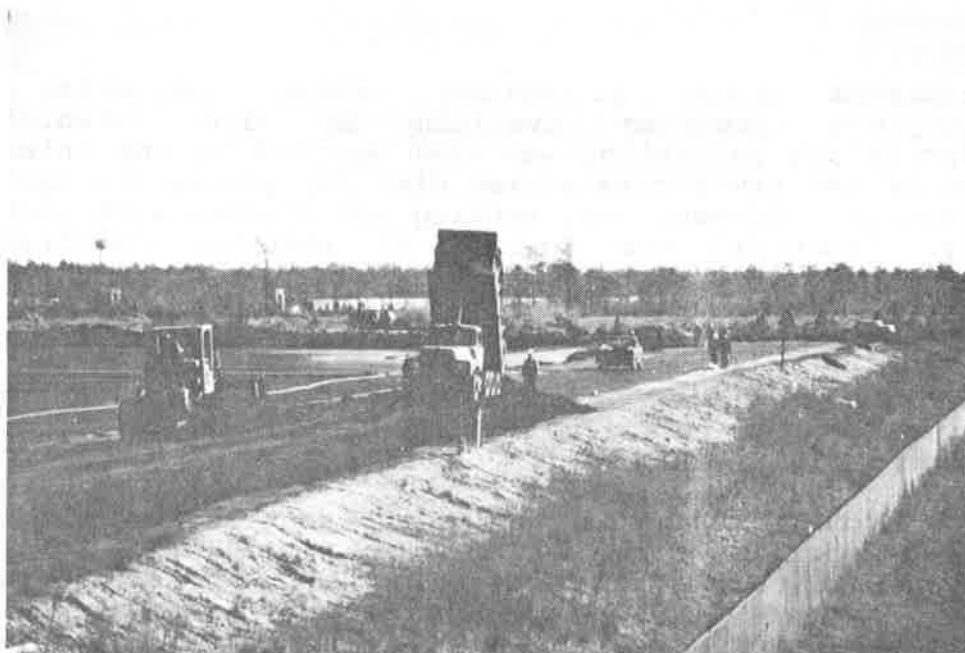
The primary geosynthetic reinforcement layer was then installed over the entire width of the embankment to prevent bearing capacity failure into the pond and deep seated failure outboard of the pond. SR2 Geogrid manufactured by The Tensar Corporation was selected based on its soil structure interlocking action, high modulus, and ease of installation. The SR2 Geogrid was installed perpendicular to the dike axis about the entire pond perimeter. The specified sand clay fill was then placed in a layered depth of 0.3 meters (1 foot) and compacted. Lightweight SS1 and SS2 geogrids were then placed horizontally at appropriate vertical spacings as the dike construction continued, to reinforce steep slopes of 1.5H:1.0V outboard and 1.0H:1.0V inboard. To protect the steep exposed inboard slopes against erosion and incidental sloughing, a "face wrap" of lightweight Terratex GS-150 fabric was constructed at each Geogrid level (60.8 cm (24 inches) on-center) for layered anchorage.



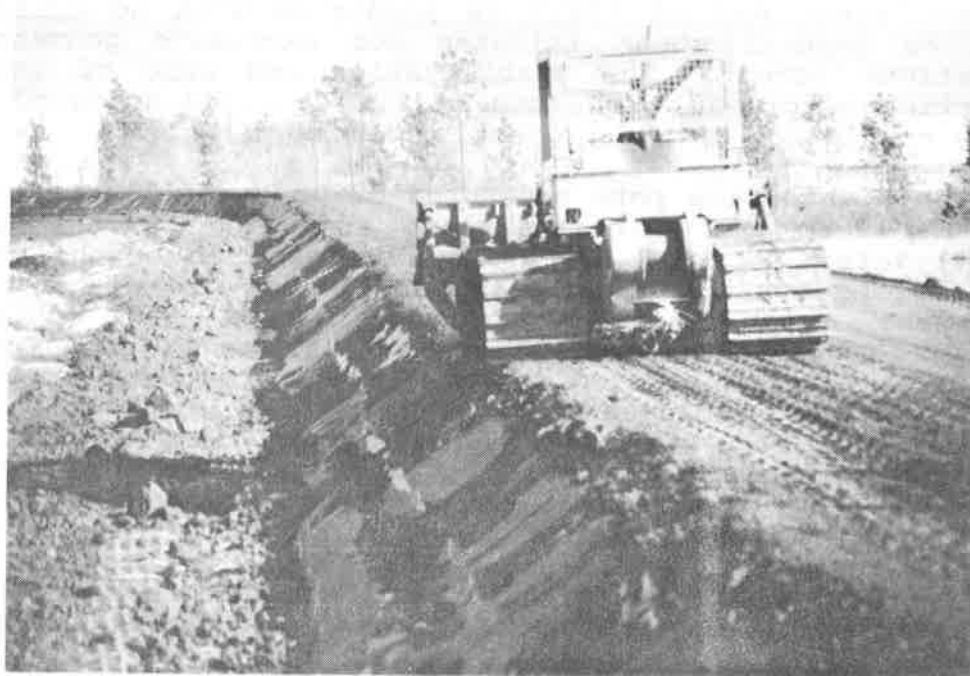
**GEOGRID SR2 APPLICATION AT COMMON DIKE
(PLACED TRANSVERSE TO DIKE CENTERLINE)**



**GEOGRID SS1 APPLICATION AT COMMON DIKE
(PLACED PARALLEL TO DIKE CENTERLINE)**



TYPICAL EARTHMOVING OPERATIONS AT SOUTH DIKE



EARTH MOVING AND COMPACTION OPERATIONS
ALONG STEEP (1H:1V) SLOPE

A finished slope protection scheme consisting of polyethylene sheeting overlain by U.V. stabilized geotextile and ballasting was then applied to the internal slopes of the newly constructed dike for protection against wave action. Conventional sodding and seeding with erosion control "netting" was applied to exterior constructed slopes.

Design and Construction Performance

A post construction review verified that all of the established project criteria were fulfilled by the design and construction techniques employed at the site.

The geotextile separated "floating" section provided the intended working surface for the installation of the reinforced earthen dike section. Although considerable distortions and "mudwaving" occurred during placement of the "sand platform", no failure of the geosynthetic layer nor associated ground shear occurred. Furthermore, no related construction delays were encountered.

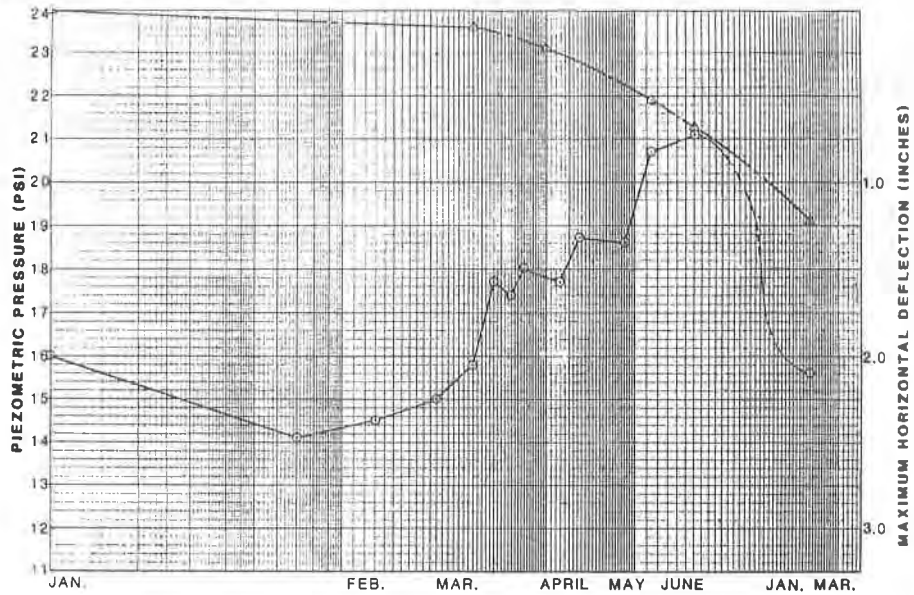
The Geogrid reinforced earthen dike has continued to perform (since May of 1985) as predicted with no related local or general shear failures nor excessive geometric distortions noted. The stabilization and ease of earth compaction afforded by the use of the Geogrids assisted in timely completion of the project.

Although high excess pore pressures of up to 37.93 kPa (5.5 psi) and deep seated deformations exceeding 5.1 cm (2.0 inches) laterally at 9.14 meters (30 feet) in depth) were noted during construction, such magnitudes were within the allowances established by the monitoring and control program. Pore pressure dissipations and embankment rheologies have stabilized satisfactorily following project completion and subsequent filling of the storage pond. Reference is made to the representative instrumentation graphics shown on Figure No. 3. Logarithmic pore pressure build-up and dissipation, with corresponding maximum lateral deformation patterns within the soft foundation soils are evident. It is noted that the later stage rates of horizontal deformation (re: inclinometer graphic) have stabilized and are consistent with long term consolidation.

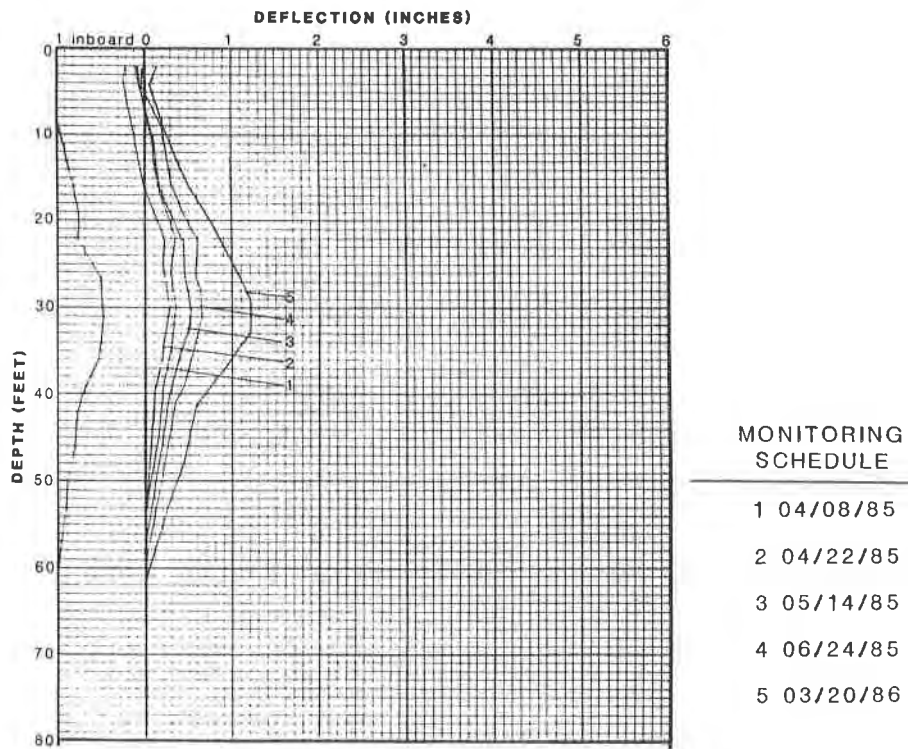
Economics and Time Savings of the Design

The waste facility modification project involved the construction of approximately 1,219 meters (4000 lineal feet) of dike, utilizing 45875 cubic meters (60,000 cubic yards) of fill

TYPICAL INSTRUMENTATION RESPONSE GRAPHICS



TIME VS. PIEZOMETRIC/INCLINOMETRIC RESPONSE



DEPTH VS. INCLINOMETER DEFLECTION

and over 58,520 square meters (70,000 square yards) of geosynthetics. It was completed in less than 60 days at a cost of under \$600,000.00. The cost savings based on the value of the nearest feasible option exceeded \$1,000,000.00. Furthermore, plant operations and waste discharge activities were not interrupted by the project construction. Finally, allowances were made in the design for future dike height increases of up to 0.9 meters (3 feet) and plans are presently being prepared for this additional storage capacity at the iron oxide storage site.

GEOSYNTHETICS '87

CONFERENCE PROCEEDINGS

Geosynthetics Conference '87

**Clarion Hotel, New Orleans, LA
February 24 & 25, 1987**

VOLUME 2

GEOSYNTHETICS '87

CONFERENCE PROCEEDINGS

Geosynthetics Conference '87

**Clarion Hotel, New Orleans, LA
February 24 & 25, 1987**

VOLUME 2

GEOSYNTHETICS '87 CONFERENCE

SPONSORED BY:

THE INDUSTRIAL FABRICS ASSOCIATION INTERNATIONAL

UNDER THE AUSPICES OF:

AMERICAN SOCIETY ON GEOSYNTHETICS

AND

INTERNATIONAL GEOTEXTILE SOCIETY

GEOSYNTHETICS '87 CONFERENCE

ORGANIZING COMMITTEE

CHAIRMAN

JOSEPH E. FLUET, JR. President, American Society on Geosynthetics; Former Secretary/Treasurer, International Geotextile Society; Former Chairman, Geotextile Division, IFAI; Organizing Committee Member, 2nd International Conference on Geotextiles and 1st International Conference on Geomembranes; Former Committee Member Geotechnical Fabrics Conference '85.

COMMITTEE MEMBERS

RUDOLF BONAPARTE Charter Member of American Society on Geosynthetics.

RICHARD CAIN Chairman, Geomembrane Division, IFAI; Organizing Committee Member, Geotechnical Fabrics Conference '85.

KRISTI LEE JOHNSON Editor of Geotechnical Fabrics Report.

ROBERT M. KOERNER President Elect, American Society on Geosynthetics; Former Chairman, Geotechnical Fabrics Conference '85.

WILLARD PUFFER Chairman, Geotextile Division, IFAI; Organizing Committee Member, Geotechnical Fabrics Conference '85.

JUDY SHIMON Staff Director of Geomembrane and Geotextile Divisions, IFAI.

ROBERT WALLACE Chairman, Canadian General Standard Board, Subcommittee on Geotextile Test Methods; Former Chairman, Second Canadian Symposium on Geotextiles and Geomembranes; Former Chairman, Alberta Symposium on Geotextiles; Former Council Member, International Geotextile Society.

STEPHEN WARNER Executive Vice President, IFAI; Secretary General, American Society on Geosynthetics; Former Secretary General, 2nd International Conference on Geotextiles.

These papers are published by:
Industrial Fabrics Association International
345 Cedar Building, Suite 450
St. Paul, MN 55101
(612)222-2508
TWX: 910-563-3622

©Industrial Fabrics Association International

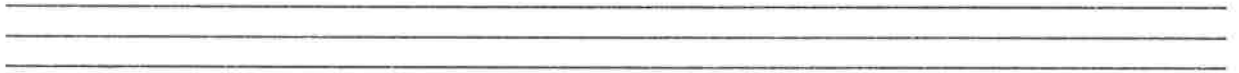


TABLE OF CONTENTS

T A B L E O F C O N T E N T S

V O L U M E 1

OPENING AND KEYNOTE ADDRESSES

Opening Address	1
FLUET, J.E., Jr., Chairman, Organizing Committee, Geosynthetic '87 Conference GeoServices Inc. Consulting Engineers, U.S.A.	
Keynote Address	4
GIROUD, J.P., President, International Geotextile Society GeoServices Inc. Consulting Engineers, U.S.A.	

SESSION 1A: UNPAVED AND PAVED ROADS

Co-Leaders: J.S. Freese, Mirafi, Inc., U.S.A. J.D. Scott, University of Alberta, Canada	
Field Tests on the Use of Geosynthetics to Support Paved Roads Over Voids-Preliminary Conclusions	6
T.C. KINNEY University of Alaska, U.S.A.	
A Geosynthetics Post-Construction Assessment.	14
R.B. WALLACE and J.F. BEECH GeoServices Inc. Consulting Engineers, U.S.A. R.J. GRAHAM EBA Engineering, Canada	
The Behavior of Geotextiles as Separating Membranes on Glacial Till Subgrades	26
D.T. GLYNN, and S.R. COCHRANE The Queen's University of Belfast, United Kingdom	
Railroad Ballast Reinforcement Using Geogrids	38
J.C. WALLS The Tensar Corporation, U.S.A. L.L. GALBREATH CSX Transportation, U.S.A.	
Granular Base Reinforcement of Flexible Pavements Using Geogrids.	46
R.G. CARROLL, and J.C. WALLS The Tensar Corporation, U.S.A. R. HAAS University of Waterloo, Canada	

Polymer Grid Cell Reinforcement in Construction of Pavement Structures	58
B. KAZERANI and G.H. JAMNEJAD Sunderland Polytechnic, England	
AC Overlay Strategies for PCCP Pavement Using Asphalt Saturated Textiles.	69
J. HANNON California Department of Transportation, U.S.A. J. MINER and M. DONAHUE Phillips Fibers Corporation, U.S.A.	
New Mexico Study of Interlayers Used in Reflective Crack Control.	82
V.M. LORENZ New Mexico State Highway Department, U.S.A.	
<u>SESSION 1B: SLOPES AND WALLS</u>	
Co-Leaders: W.C.B. Villet, Dames & Moore, U.S.A. W.L. Deutsch, Roy F. Weston	
A Design Procedure for Geotextile-Reinforced Walls.	95
D. LESHCHINSKY University of Delaware, U.S.A. E.B. PERRY U.S. Army Engineer, U.S.A.	
Design Charts for Geogrid-Reinforced Soil Slopes.	108
G.R. SCHMERTMANN, V.E. CHOUERY-CURTIS and R.D. JOHNSON The Tensar Corporation, U.S.A. R. BONAPARTE GeoServices Inc. Consulting Engineers, U.S.A.	
Slope Reinforcement Using Geogrids.	121
R.B. WALLACE and J.E. FLUET JR. GeoServices Inc. Consulting Engineers, U.S.A.	
The Importance of Stress-Strain Relationships in Reinforced Soil System Design	133
J.F. BEECH GeoServices Inc. Consulting Engineers, U.S.A.	
Geogrid Reinforced Soil Retaining Wall to Widen an Earth Dam and Support High Live Loads	145
B.R. CHRISTOPHER STS Consultants, Ltd., U.S.A.	

Design of the Devon Geogrid Test Fill	157
J.D. SCOTT, D.C. SEGO and B.A. HOFMANN Dept. of Civil Engineering, University of Alberta, Canada	
E.A. RICHARDS Dept. of Clothing and Textiles, University of Alberta, Canada	
E.R. BURCH Alberta Transportation, Canada	
Strain Development in Anchorage Zones	169
P.M. JARRETT and R.J. BATHURST Royal Military College of Canada, Canada	
Long-Term Allowable Tension for Geosynthetic Reinforcement.	181
R. BONAPARTE GeoServices Inc. Consulting Engineers, U.S.A	
R. BERG The Tensar Corporation, U.S.A	
SESSION 2A: <u>LABORATORY AND MODEL EVALUATION</u>	
Co-Leaders: W.G. Puffer, Puffer & Associates, U.S.A. B.L. Jeffery, Foss Manufacturing Company, U.S.A.	
Stitchbonded Composites	193
J.N. PAULSON and M.C. LANGSTON Exxon Chemical Company, U.S.A.	
Frictional Characteristics of Geotextiles With Compacted Lateritic Gravels and Clays	205
J. LAFLEUR, M.S. SALL and A. DUCHARME Ecole Polytechnique de Montreal, Canada	
Plate Loading Tests on Geogrid-Reinforced Earth Slabs.	216
V.A. GUIDO and J.D. KNUEPPEL The Cooper Union School of Engineering, U.S.A.	
M.A. SWEENEY Mueser Rutledge Consulting Engineers, U.S.A.	
Strength and Pullout Testing of Geogrids	226
S.R. BRAND Black and Veatch, U.S.A	
D.M. DUFFY Arizona State University, U.S.A.	
In-Soil Load Elongation, Tensile Strength and Interface Friction of Nonwoven Geotextiles.	238
D. LESHCHINSKY University of Delaware, U.S.A.	
D.A. FIELD CTC/GEOTEK, U.S.A.	

Soil-Geotextile Interaction Mechanism in Pullout Test 250
W.H. TZONG and S. CHENG-KUANG
University of Colorado at Denver, U.S.A.

In-Soil Stress-Strain Behavior of Geotextile. 260
B.D. SIEL
ATEC Associates, U.S.A.
W.H. TZONG
University of Colorado at Denver, U.S.A.
N.N.S. CHOU
Colorado Department of Highways, U.S.A.

SESSION 2B: EMBANKMENTS OVER WEAK SOILS

Co-Leaders: G.N. Richardson, Soil and Material Engineers, U.S.A
P. Lucia, Woodward-Clyde Consultants

Reinforcement of Embankments on Soils Whose
Strength Increases With Depth 266
R.K. ROWE and K.L. SODERMAN
The University of Western Ontario, Canada

Use of Reinforcement for Embankment Widening 278
D.N. HUMPHREY
University of Maine, U.S.A.
R.D. HOLTZ
Purdue University, U.S.A.

Stabilization of Very Soft Soils Using Geosynthetics 289
J. FOWLER
U.S. Army Corps of Engineers, U.S.A
R.M. KOERNER
Drexel University, U.S.A.

Stability Consideration of Embankments on Soft Soils
Based on Improved Hydraulic Boundary Conditions 301
G. WERNER and S. RESL
Chemie Linz AG, Austria
R.K. FROBEL
Chemie Linz US Inc., U.S.A.

Difficult Soil Problems on Cochrane Bridge Finessed
With Geosynthetics. 309
L. LOCKETT
State of Alabama Highway Department, U.S.A
R.M. MATTOX
The Tensar Corporation, U.S.A

Design and Construction of a Geogrid Reinforced Embankment Over Waste Material.320
A. PAGOTTO Comune di Modena, Italy	
P. RIMOLDI RDB Plastotecnica, SPA, Italy	
The Effectiveness of Tensile Reinforcement in Strengthening an Embankment Over Soft Foundation.332
N.N.S. CHOU Colorado Department of Highways, U.S.A.	
W.H. TZONG University of Colorado at Denver, U.S.A	
B.D. SIEL ATEC Associates Inc., U.S.A.	
An Economical Solution to Increasing the Capacity of an Industrial Waste Facility with a Geogrid Reinforced Dike.341
H. SEAWELL Thompson Engineering, Testing, U.S.A.	
R.M. MATTOX The Tensar Corporation, U.S.A.	

V O L U M E 2

SESSION 3A: DESIGN/CONSTRUCTION

Co-Leaders: N. Schomaker, U.S. EPA, U.S.A. C. Ryan, GEO-CON, U.S.A.	
Design and Construction of a Hazardous Waste Landfill.353
L.O. YAMAMOTO International Technology Corporation, U.S.A.	
Current Practice in the Use of Geosynthetics in the Heap Leach Industry365
J.A. LEACH, T.G. HARPER, and R.T. TAPE Klohn Leonoff Consultants, Canada	
Geomembrane-Soil Composite Lining Systems Design, Construction Problems, and Solutions.375
D. BURANEK and J. PACEY Emcon Associates, U.S.A.	
Preventing Geomembrane Failures.385
A.A. MCCREADY Harding Lawson Associates, U.S.A.	

SESSION 3B: TRANSMISSION

Co-Leaders: M.J. Cowell, The Tensar Corporation, U.S.A.
I. Peggs, GeoSyntec Inc., U.S.A.

Geocomposite Drainage Systems: Mechanical Properties
and Discharge Capacity Evaluation. 393
A. CANCELLI
University of Milano, Italy
D. CAZZUFFI
ENEL's Research Centre for Hydraulics and Structures, Italy
P. RIMOLDI
Politecnico di Milano, Italy

Transient In-Plane Flow of Liquids in Fibrous Networks. 405
K.L. ADAMS and L. REBENFELD
Princeton University, U.S.A.

The Use of Geosynthetics in Conjunction With
Three-Dimensional Drainage Cores 417
J.O. SNYDER
GeoTech Systems Corporation, U.S.A.

Creep of Geocomposite Drains. 422
A.D. SMITH and S.R. KRAEMER
Haley & Aldrich, Inc., U.S.A.

SESSION 4A: DURABILITY

Co-Leaders: N. Schomaker, U.S. EPA, U.S.A.
C. Ryan, GEO-CON, U.S.A.

An Analysis of the Durability Problems of Geotextiles. 434
H. SCHNEIDER
Chemie Linz, Austria
M. GROH
Polyfelt Inc., U.S.A.

Long-Term Durability of Geosynthetics Soil Reinforcement. 442
W.S. WHELTON
The Tensar Corporation, U.S.A.
N.E. WRIGLEY
Netlon Limited, United Kingdom

SESSION 4B: FILTRATION

Co-Leaders: M.J. Cowell, The Tensar Corporation, U.S.A.
I. Peggs, GeoSyntec, U.S.A.

Geosynthetic Filtration in Landfill Design. 456
A.L. ROLLIN
Ecole Polytechnique de Montreal, Canada
R. DENIS
Solmers Internationale, Canada

Permittivity of Geotextiles in Presence of Water
and Pollutant Fluids 471
A. CANCELLI
University of Milano, Italy
D. CAZZUFFI
ENEL's Research Centre for Hydraulics and Structures, Italy

Filtration Behavior Analysis of Thin Heat-Bonded Geotextiles. 482
G. LOMBARD and A. ROLLIN
Ecole Polytechnique, Canada

SESSION 5A: QUALITY ASSURANCE/QUALITY CONTROL

Co-Leaders: N.D. Williams, Georgia Institute of Technology, U.S.A.
J. Luna, Hoechst Fibers Industries

Geomembrane Seam Inspection Using the Ultrasonic Shadow Method. 493
R.M. KOERNER, A.E. LORD JR., and R.B. CRAWFORD
Drexel University, U.S.A.
M. CADWALLADER
Gundle Lining Systems, Inc., U.S.A.

Evaluating Polyethylene Geomembrane Seams 505
I.D. PEGGS
GeoSyntec, Inc., U.S.A

Construction Quality Assurance/Quality Control
for Land Disposal Facilities 519
T. HEBERT
Hebert Engineering Corp., U.S.A.

Geosynthetic Lining Systems and Quality Assurance-State of
Practice and State of the Art 530
J.E. FLUET JR.
GeoServices Inc. Consulting Engineers, U.S.A.

SESSION 5B: MATERIAL SELECTION

Co-Leaders: G. Kolbasuk, Precision Laboratories, U.S.A.
R. Carriker, Amoco Fabrics Company, U.S.A.

Selection of Geosynthetic Materials for Canal Liner 542
L.O. TIMBLIN JR.
Bureau of Reclamation, U.S.A.

High Density Polyethylene Liners: A Users Experience 554
I.L. PFALSER
Phillips Petroleum Co., U.S.A.

The Composite Advantage in the Mechanical Protection of
Polyethylene Geomembranes: A Laboratory Study 565
R. FROBEL
Polyfelt Inc., U.S.A.
W. YOUNGBLOOD and J. VANDERVOORT
PolyAmerica, Inc., U.S.A.

SESSION 6A: TESTING

Co-Leaders: N.D. Williams, Georgia Institute of Technology, U.S.A.
J. Luna, Hoechst Fibers Industries, U.S.A.

Laboratory Testing of Geosynthetics and Plastic
Pipe for Double-Liner Systems. 577
H.E. HAXO JR. and M.J. WALLER
Matrecon, Inc., U.S.A.

Performance of a Comprehensive Liner System
Compatability Testing Program. 595
M.F. COIA
Roy F. Weston, Inc., U.S.A.
L. SHERMAN
Fondessy Enterprises, Inc., U.S.A.
H.E. HAXO JR.
Matrecon, Inc., U.S.A.

The EPA Testing Program for Components of Treatment,
Storage, and Disposal Facilities 609
R.E. LANDRETH
United States Environmental Protection Agency, U.S.A.

SESSION 6B: OTHER GEOSYNTHETIC APPLICATION

Co-Leaders: G. Kolbasuk, Precision Laboratories, U.S.A.
R. Carriker, Amoco Fabrics Company, U.S.A.

Evaluation of Interface Friction Properties
Between Geosynthetics and Soils. 616
N.D. WILLIAMS
Georgia Institute of Technology, U.S.A.
M.F. HOULIHAN
Law Environmental Services, U.S.A.

Geoboard Reduces Lateral Earth Pressures. 628
A.M. PARTOS and P.M. KAZANIWSKY
SITE Engineers, U.S.A.

SESSION 3A

DESIGN/CONSTRUCTION

SPONSORED BY



SOLMAX

YAMAMOTO, L.O.

International Technology Corporation, U.S.A.

Design and Construction of a Hazardous Waste Landfill

The design considerations and the construction quality control program for a hazardous waste landfill located in southern California are discussed. The liner system is composed of a compacted clay liner, two geomembranes, a leachate collection system, and a leak detection system. A field and laboratory testing and inspection program formed the basis of the quality control program which documented and verified the quality of construction.

INTRODUCTION

A hazardous waste landfill was constructed at the International Technology Corporation facility in southern California. This paper describes the design of the landfill and the monitoring of construction. The design was started in November 1984 and the construction was completed in January 1986. The design of the landfill was based on the then current U.S. Environmental Protection Agency Minimum Technology Guidance (1984) [1], issued in accordance with the Hazardous and Solid Waste Amendment (HSWA) of 1984, and the California Administrative Code, Title 23, Subchapter 15 [2].

GENERAL DESCRIPTION OF LANDFILL

The 2.8 hectare (7 acre) landfill was constructed within two existing surface impoundments. The plan configuration of the landfill was dictated by the state and federal regulations requiring 61 m (200 feet) minimum setback from Holocene faults. This necessitated the construction of new embankments on both the east and west sides of the landfill (Figure 1). New embankments were constructed with interior side slopes of 2H:1V. The existing pond embankments were incorporated into the new landfill at the north and south ends. These existing embankments were maintained at a 3H:1V interior slope to make use of their existing clay liners. The landfill bottom, which is constructed directly over natural clays, is designed with a high point flow line near its center. A slope is provided to sumps located at the ends of the landfill to allow collection and removal of waste leachate.

SITING INVESTIGATION

The siting of the landfill and its conformance with applicable regulations were accomplished by reviewing available reports and implementing a field program

which included trenching and drilling. The trenching defined the location of faults, and the drilling program defined the location and extent of underlying clays and provided soil samples for laboratory testing.

EARTHWORK

In general, the earthwork included excavation of native soils and placement of select fill to construct embankments and clay liner. Approximately 37,000 m³ (48,000 cubic yards) was excavated from within the existing ponds in which the landfill was constructed. This was used to construct the new embankments. An additional 15,000 m³ (20,000 cubic yards) was removed and placed back again as compacted fill to construct the clay liner in the landfill bottom.

The clay soils were tested prior to construction to determine suitability. Among the tests performed were hydrometer; Atterberg limits; compaction; unconsolidated, undrained triaxial compression; and permeability. The clays were classified as an inorganic, medium to high plasticity clay with U.S.C.S. classification of CL and CH.

The in-situ moisture content of the clay borrow was high. Therefore, the clays required drying to achieve the specified compaction. The clay was excavated by dozer and scraper and then was spread to dry either in areas requiring fill or in drying areas outside of the landfill. After spreading, the borrow materials were disced to hasten the drying and to break down the size of clods. Compaction was achieved using a sheepsfoot compactor. The clay was spread in 225 cm (8 inch) maximum loose lifts (150 cm compacted lifts). The embankments and clay liner were constructed of the same clay materials using the same construction methods.

LINER SYSTEM

The liner system is composed of a compacted clay liner, two geomembranes, a leachate collection system, and a leak detection system. A generalized cross section of the liner system is shown in Figure 2.



Figure 1. Aerial View of Landfill Looking East

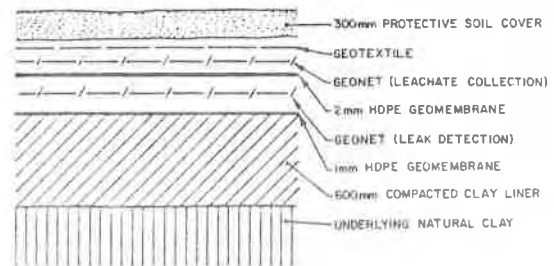


Figure 2. Generalized Cross Section of Liner System

The liner system components, in ascending order (following the construction sequence), are as follows:

- Clay Liner. This liner consists of a minimum of 600 mm (2 feet) thick compacted clay with a permeability less than 1×10^{-7} cm/s.
- Secondary Geomembrane. This geomembrane is 1 mm (40 mil) thick high density polyethylene.
- Leak Detection System. This system is composed of geonet with drainage to a collection sump.
- Primary Geomembrane. This geomembrane is 2 mm (80 mil) thick high density polyethylene.
- Leachate Collection System. This system is composed of geonet with drainage to a collection sump (over landfill bottom only).
- Geotextile. This fabric separates the overlying soil cover from the underlying drainage layer to prevent clogging due to fines (over landfill bottom only).
- Protective Soil Cover. This cover consists of a minimum of 300 mm (1 foot) thick soil (over landfill bottom only).

Clay Liner

As discussed previously, the clay liner was constructed in maximum compacted lifts of 150 mm (6 inch) to a total minimum thickness of 600 mm (2 feet). The clay was compacted to no lower than 90 percent of maximum dry density at a moisture content of at least one percent wet of optimum as determined by ASTM D 1557. The surface of the clay liner was rolled with a smooth-drum roller prior to placing the overlying geomembrane.

The compatibility of the clay material to waste leachate was evaluated through long-term permeability tests of remolded clay samples. The leachate used was manufactured from wastes expected to be received at the landfill. The permeability testing, in accordance with EPA Method 9100, indicated no significant effects of the leachate on the clay. The testing was accomplished by determining the permeability of a sample using a standard permeant ($0.01N \text{ CaSO}_4$) and then switching to the leachate after a stable permeability had been achieved.

Primary and Secondary Geomembranes

The primary and secondary geomembranes are 2 mm (80 mil) and 1 mm (40 mil) high density polyethylene (HDPE), respectively. HDPE was selected over other available materials because of its wide range of chemical resistance and its good weathering characteristics. The HDPE was manufactured by Gundle Lining Systems, Inc., Houston, Texas and was installed by the Serrot Corporation, Huntington Beach, California.

Laboratory chemical compatibility testing of the HDPE with the waste leachate was conducted in accordance with EPA Method 9090. The 120 day test resulted in no apparent trends in the values of the parameters tested which indicated the lack of reaction between the geomembrane and the waste. However, it should be noted that there was wide scatter in the values of tensile stress at break and elongation at break which was likely due to the poor reproducibility of these tests for HDPE geomembranes. These values are sensitive to the surface condition of the geomembrane, the condition of the die, and minor imperfections in the liner. Because there were no obvious trends over the test period, the fluctuations in the values were unlikely to have resulted from an effect due to a reaction with the waste.

The 1 mm HDPE and 2 mm HDPE geomembranes were supplied in rolls of sheets 6.9 m (22.5 feet) wide by 198 m (650 ft) long and 98 m (320 feet) long, respectively. The sheets were cut to required lengths in the field. The sheets were joined in the field by first tack welding the sheets together with a Leister welder (Figure 3). A Gundle extrusion welding machine was then used to provide the actual seal (Figure 4). The welding machine supplied molten HDPE to the upper edge of the 100 mm (4 inch) overlap resulting in a fusing of the two geomembranes.

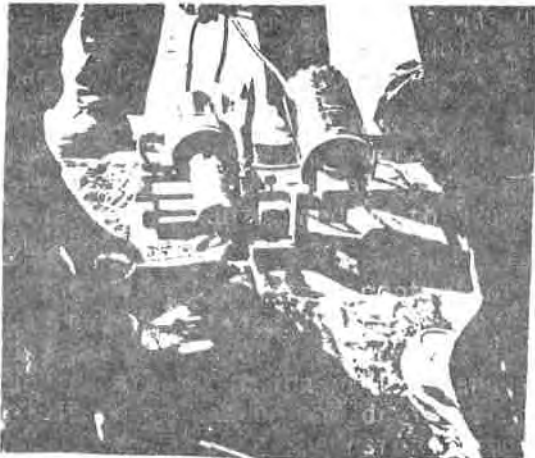


Figure 3. Leister Tack Welding (Copper Wire in Foreground is for Spark Testing)

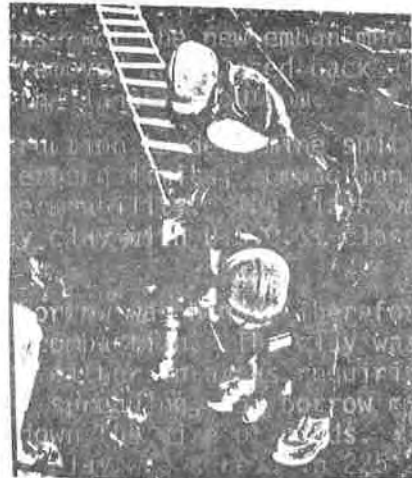


Figure 4. Extrusion Welding

The 1 mm HDPE was installed during the summer when temperatures reached highs of 43°C (110°F). Because of the relatively high thermal expansion that is characteristic of HDPE geomembranes, the installation techniques for the 1 mm liner were modified to minimize the effects of the high temperatures. The construction methods included the following:

- Final backfilling of the anchor trench was not performed during the heat of the day when the geomembrane was at its greatest thermal expansion but rather at night or in the early morning.
- Welding of the geomembrane sheets on slope in the four corners of the landfill was performed at night or in the early morning. If all seaming were to have been accomplished during the heat of the day, excessive bridging of the geomembrane would have resulted during cooler temperatures. Similarly, the final seaming of the panels on the bottom was not completed in the heat of the day.

In addition to the high temperatures, gusty winds and thunder showers also affected the installation. On two separate occasions, winds dislodged sandbagged sheets which required repositioning of the panels and repairs to "creases" caused by sharp folds in the sheet. Some panels were repaired by applying a bead of extrudate over the creases using the extrusion welding machine. Other panels with numerous creases were simply replaced. Thundershowers occurred on two different occasions during the 1 mm liner installation which caused the work to be suspended at those times.

The 2 mm HDPE geomembrane was installed during the cooler winter months which eliminated much of the problems that were encountered during the 1 mm HDPE installation. However, the installation was suspended three different times because of rain. The rain not only forced stoppage of the liner installation, it created pools of water within the sumps at either end of the landfill. Water was pumped from the sumps using vacuum trucks. The welding system used for joining the 2 mm HDPE sheets was the same as used for the 1 mm sheets.

During the geomembrane installation, a question was raised by the state regulatory agencies regarding the necessity of welding the sheets completely to their ends within the anchor trench. The welds were being terminated about 300 mm (1 foot) into the trench. There was concern that an incomplete seam could result in stress concentrations which could lead to failure at the seam. To appease the concerns, 150 mm (6 inch) diameter patches of HDPE of the same thickness as the parent material were welded over each seam at the top of slope. These patches served as reinforcements to each seam. Laboratory testing performed showed that the strength of seam samples with a patch had approximately double the strength of a seam welded to the ends of the sheet. The testing also showed little difference in strength between seams welded to the end and those not welded to the end. The testing was conducted using an off-center peel test. The two sheets of liner were pulled in opposite directions at a separation rate of 12.7 cm/min (5 in/min). The highest peak in pounds to tear the liner was recorded.

Leachate Collection and Leak Detection Systems

The leachate collection and leak detection systems are designed to ensure that the leachate depth over the underlying geomembranes does not exceed 300 mm (1 foot) and that the systems are capable of carrying twice the maximum expected volume of leachate. The expected volume of leachate to be generated was calculated by performing a water balance analysis [3]. The results of the analysis predicted zero leachate generation because of the low rainfall and high evaporation rates at the site.

The leak detection system was installed between the primary and secondary geomembranes and the leachate collection system was installed on top of the primary geomembrane. Both the leak detection and leachate collection systems were similarly designed. Each system is composed of a geonet with a two percent minimum slope to a sump located at each end of the landfill.

Each sump is approximately 3 m (10 feet) square, 0.6 m (2 feet) deep and filled with drain rock. The rock was a hard, sound, noncalcareous, subrounded, river-run gravel and sand generally graded between U.S. standard sieve sizes 3/4 inch and No. 10. Prior to installing the drain rock, the sumps were lined with Crown Zellerbach Grade 300, a polypropylene, needle-punched geotextile. The geotextile served as a cushion to protect the geomembrane from the overlying rock. And because the geotextile totally encapsulated the layer of rock, it also served as a filter, minimizing the transport of fines into the sump (Figure 5).

Liquid is detected and collected through 225 mm (8 inch) diameter PVC pipes that extend from each sump to the dike crest. The pipes are located within trenches on the landfill side slopes eliminating penetrations through the liners. This not only eliminates the potential for leakage around pipe seals, but also eliminates the potential for loss of liquid due to a damaged or improperly jointed pipe because all piping is contained within the liner system.

The geonet installed was Gundle G-3. It was supplied in rolls of sheets 1.6 m (5.3 feet) wide by 25m (82 feet) long. The geonet on side slopes were installed lengthwise downslope and anchored in the geomembrane anchor trench. Sides and ends of adjoining sheets were butted or overlapped approximately 1/4-inch and secured with plastic ties. The ties were installed approximately 2 m (6.5 feet) on center and as necessary to result in a flat and uniform layer. The underlying geomembrane was swept of wind-blown dirt and debris prior to installing the geonet.

The geonet, sandwiched between a geomembrane and geotextile, had a specified minimum transmissivity of $1 \times 10^{-4} \text{ m}^2/\text{s}$ at a normal load of 240 kPa (5,000 psf) and hydraulic gradient of 0.5. The geonet was specified instead of a conventional sand layer for the following reasons:

- The geonet has a higher transmissivity than a 300 mm (12 inch) sand layer that has a permeability of $1 \times 10^{-2} \text{ cm/s}$.
- The velocity of flow in the geonet is two orders of magnitude higher than the sand layer described previously.
- The geonet is easily and quickly installed by hand with no heavy equipment required.
- The geonet is easily installed on slope and will not slough.

Geotextile

The geotextile on top of the leachate collection system serves as a separator between the overlying soil cover and the geonet. The geotextile also serves as a filter minimizing the potential for clogging of the drainage layer. The geotextile specified was Mirafi 140N, a nonwoven, polypropylene fabric, heat-treated on one side. A nonwoven fabric was selected because of its generally better filtering capability compared to woven fabrics. The heat treatment of the geotextile provides a surface that is smoother and less fibrous compared to non-heat-treated nonwoven geotextiles. Therefore, the heat treated side of the geotextile in contact with the geonet provides less of an impedance to flow.

The installation of the geotextile closely followed the installation of the geonet. This minimized the amount of wind-blown debris caught in the drainage layer. The geotextile was supplied in rolls of sheets 4.6 m (15 feet) wide by 110 m (360 feet) long. Adjacent panels of geotextile were overlapped a minimum of 300 mm (1 foot) (Figure 6).

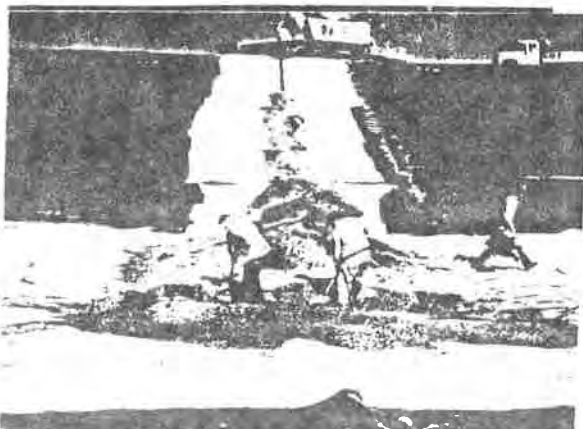


Figure 5. Installation of Drain Rock



Figure 6. Installation of Geotextile

Protective Soil Cover

The material for the protective soil cover was sandy silt obtained on site. The soil was a fine grained material with no rocks or debris that could harm the liner system. Ribbons of sand ($k > 1 \times 10^{-3}$ cm/s) were installed within the soil cover to provide a free draining layer (Figure 7).

The soil cover installation was started in one corner of the landfill. A ramp was constructed and the soil was pushed outward over the bottom with dozers. As the soil cover progressed, a wrinkle in the liner system developed at the leading edge of the soil. Its cause was due to the accumulation of small wrinkles in the geomembranes as the soil cover advanced. The wrinkle was trapped so it could not move by depositing soil on the opposite side of the wrinkle using the bucket of a wheel loader. Once trapped, soil was placed over the wrinkle. Trapping the wrinkle in this manner also prevented it from folding over on itself.

Placement of the geotextile closely preceded the installation of the soil cover so that no geotextile was left exposed for more than 24 hours. The placement of the soil cover was done primarily with wheel loaders which allowed the trapping of even the smallest wrinkles without propagating into larger ones. The soil cover was installed in widths of approximately 12 m (40 feet) to allow the installation of the sand ribbons. As soon as a sufficient area had been covered on the bottom, the trailer dump trucks were allowed inside the landfill to deposit the soil near the advancing edge of the cover. The soil cover was installed starting at one end of the landfill and proceeded to the opposite end. When the leading edge of the cover advanced passed the high point of the bottom, it was wrapped with geotextile at the end of each day to minimize the effect of rain and wind. Fortunately, during the entire soil cover installation, there was no rain, and the winds were relatively calm. However, on four separate occasions, during the installation of the soil cover, the underlying drainage layer(s) and/or geomembrane(s) had to be repaired due to operator error. The damaged areas were caused by the dozer blade being too low, the bucket of the front end loader being too low, or the spinning track of a dozer.

CONSTRUCTION QUALITY CONTROL PROGRAM

Although the overall quality control (QC) program for the project included both design activities and construction activities, this paper will focus only on those related to the construction phase. The construction quality control program was conducted to document that regulatory and design requirements were properly incorporated into the landfill construction. Specific field controls were monitored or performed throughout the construction. These controls can be characterized into the following types:

- Field inspections performed by QC Monitors. The inspections were primarily visual examinations but also included measurements of materials and type of equipment being used, techniques employed, and the final product. Inspections were performed to verify that a specification or procedure for the activity was successfully completed. The results of visual inspections when non conformances were detected were documented in a daily log.
- Field testing was performed by the QC Monitor or by construction personnel in the presence of a QC Monitor, according to specified procedures. Field testing was performed to determine conformance with project requirements.

- Laboratory testing performed by on-site or off-site laboratories on samples of materials used in the landfill. Laboratory testing was performed to characterize materials and assess performance.
- Surveying including establishment of horizontal and/or vertical position, as appropriate.
- Receiving inspections performed by the QC Monitors. The inspections included, as necessary, a visual examination and measurements of materials obtained from suppliers. They were performed to verify that the materials used met specifications.
- Manufacturer's certificates obtained from suppliers for selected shipments of materials received. They entailed a statement that the materials met specifications.

Field tests were performed as soon as possible after material receipt or completion of the portion of the constructed work to provide prompt confirmation or rejection of the material or constructed work. This minimized the possibility of removing satisfactory work added over defective material or work.

A minimum of two QC Monitors and as many as four (composed of geologists, technicians or engineers, depending on the phase of work) plus the Resident Engineer were on site to serve as the QC team. The quality control activities and requirements for the various construction items are discussed below.

Earthwork (Including Clay Liner) Quality Control Activities and Requirements

- Inspection and logging, as necessary, by on-site geologists of excavated keyways and finished subgrade.
- Inspection by on-site geologists and field technicians of materials used for general fill and for the clay liner.
- Laboratory testing of fill materials. These tests were performed to document the engineering properties of the fill materials including clay liner material.
- Documenting the type and quantity of earthwork equipment used.
- Surveying of lines and grade of subgrade prior to installation of the compacted clay liner.
- Field density and moisture testing of the embankments and clay liner.
- Inspecting lift thickness.
- Observing coverage and number of passes made by compaction equipment.
- Surveying lines and grade of completed clay liner and embankments.

In addition to the tests described above and in an attempt to comply with regulatory-mandated field testing, two different field permeability test methods were used to evaluate the clay liner. The tests included the BAT porous probe and the sealed double ring infiltrometer (SDRI). The BAT system consists of a plastic tip containing a cylindrical porous filter driven into the clay liner. The filter is connected to a container partly filled with water and partly filled with compressed gas. The rate of flow of liquid through the porous filter is computed by measuring the gas pressure change in the container and then applying Boyle's law. Analysis of the time pressure record utilizing the falling head method yields the coefficient of permeability. A detailed description of the BAT system is reported by Petsonk [4]. The SDRI was installed in a clay liner test fill outside of the landfill using the same materials and method of construction as the landfill clay liner. The SDRI is evolved from the double-ring infiltrometer (ASTM D 3385). The

SDRI's improvement includes a sealed, dome-shaped inner ring which is submerged within the ponded water of the outer ring [5]. This reduces the effects of evaporation and temperature fluctuations. The results of the two test methods showed the clay liner to have a permeability less than 1×10^{-7} cm/s. A detailed description of the test procedures and results is reported elsewhere [6].

Primary and Secondary Geomembrane Quality Control Activities and Requirements

- Manufacturer's material certification regarding physical properties of HDPE sheet and resin. Included are the quality control certificates which list the test values measured for each batch number and/or roll number tested.
- Geomembrane/waste compatibility testing in accordance with EPA Method 9090.
- Inspection of material upon receipt. In addition to damage, the thickness of the rolls of geomembrane were randomly measured with a hand dial gage.
- Inspection of proper storage.
- Inspection of subgrade prior to geomembrane installation. The subgrade was inspected for smoothness, lack of sharp discontinuities, and lack of loose clods or debris.
- Inspection of location and dimensions of anchor trench.
- Inspection of liner panels after unrolling.
- Observation of start-up seams. Field-fabricated start-up seams were required at the beginning of each work day and when climatic conditions changed. The start-up seams were tested in a field tensometer for both peel and shear strength (Figure 8). No welding unit was used until it produced seams that, when put into peel or shear, failed outside of the seam area and in the parent material. However, it should be cautioned that failure within the parent material but without elongation is an unacceptable weld. Tearing without elongation is likely due to a welding unit that is too hot and/or an operator moving the welding unit too slow.

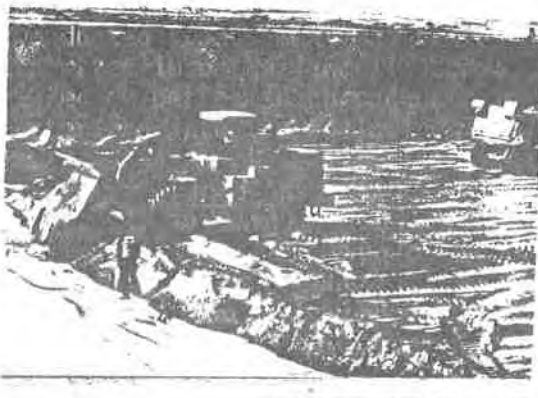


Figure 7. Installation of Protective Soil Cover



Figure 8. Testing of Start-Up Seams with Field Tensometer

- Observation of the temperature of the seam welding unit.
- Inspection of seam overlap for the specified 100 cm (4-inch).
- Visual inspection of welds for noticeable discontinuities in the extrusion, offsets of the extrusion from the edge of the liner, fish-mouths, and excessive grinding of the liner material.
- Monitoring and observation of seam field testing. Spark testing and vacuum-testing of the seams was performed by the contractor under the continual observation of a QC Monitor (Figures 9 and 10). No field seam testing was allowed unless a monitor was present to observe the testing and mark all defects for repair.



Figure 9. Vacuum Testing of Seams



Figure 10. Spark Testing of Seams

The project specifications called for vacuum testing as the field method for testing tightness of seams. The contractor, however, preferred spark testing. To satisfy his own preference and the specifications, both methods were used. Spark testing was accomplished by placing a continuous copper wire between the overlap of the two geomembranes prior to extrusion welding. A charged wand of about 20,000 volts was connected to one end of the wire and slowly moved over the length of the seam. A pinhole in the seam or any defect which allowed arcing between the wand and the copper wire resulted in an audible alarm from the unit. In addition, a readily discernible crackling sound was apparent when arcing occurred. Vacuum testing was performed by placing a gasketed box with a clear top over a seam that has a soap solution applied. A vacuum of 20.5 to 41 kPa (3 to 6 psi) was induced and held as long as necessary to mark any locations of leaks as evidenced by the formation of bubbles. All seams were both spark tested and vacuum tested. An interesting finding of this dual testing was the fact that the vacuum test invariably detected defects that the spark test missed. As a check, the spark test followed the vacuum test to determine if the reverse were true. It was not; the spark test did not detect any additional defects after following the vacuum tester. The spark test is a very quick and clean test method but it should not be the sole test method based on our experience.

- Laboratory testing of seam samples to determine the following three properties:
 - Bonded seam strength in shear in accordance with ASTM D 3083. The minimum acceptable value is 90 percent of the material tensile strength at yield.
 - Bonded seam strength in peel in accordance with ASTM D 413. The acceptable failure mode is for the seam to tear in one of the sheets (film tearing bond) rather than parting at the seam (overlap) and to elongate when tearing.
 - Thickness in accordance with ASTM D 1593, paragraph 9.1.3. The measured values shall conform to the specified thickness which is the nominal thickness (specified thickness \pm 10 percent).
- Random seam samples were taken from the installation at a rate of one per 500 feet of field seam. The samples were random but were also taken in such a way that a sample was obtained from as many different liner rolls as possible. Samples were also taken in areas where the QC Monitor may suspect something may be wrong. Seam samples welded from scrap material was not used. Experience on previous geomembrane installations has indicated that seam samples made from scrap are not be as representative of true field seams. The workers are extra careful in the construction of samples they know will be tested. Therefore, only samples taken from the installation were tested. Each seam sample was numbered as it was obtained and the location plotted on a working drawing.
- Walk-through inspection of each geomembrane after its completion.
 - Preparation of as-built liner panel layout.

Geonet, Geotextile, PVC Pipe, and Drain Rock Quality Control Activities and Requirements

- Manufacturer's material certifications.
- Geonet/waste, geotextile/waste, and PVC pipe/waste compatibility testing in accordance with a modified EPA Method 9090.
- Grain size analyses of drain rock.
- Inspection of materials upon receipt.
- Inspection of proper storage.
- Inspection of cleanliness of materials prior to installation. (The drain rock was stockpiled on top of sheets of geotextile to minimize mixing with soil.)
- Inspection of material defects during and after installation.
- Inspection of overlap in the geonet, and geotextile, and joints in the PVC pipe.
- Observation of method of installation for occurrences of damage to the underlying synthetic materials.

Protective Soil Cover Quality Control Activities and Requirements

- Inspection of soil material to verify it is free from large angular rocks, rubbish and other deleterious material.
- Prior to placement of the soil cover, a test pad was constructed outside of the landfill. The pad consisted of 2 mm HDPE geomembrane over a prepared subgrade, followed by geonet, geotextile, and 300 mm (1 foot) of soil cover. The equipment to be used for the soil cover

- installation was driven over the pad to determine the adequacy of the cover to protect the underlying synthetic materials. The test showed the soil cover to be more than adequate to provide protection from the front end loader, loaded end dump trucks, and track mounted dozers.
- Observation of the method of cover placement and the effect upon the underlying synthetic materials. Inspection for displacement or damage to the materials.
- Inspection of soil cover thickness.

SUMMARY

The successful completion of the landfill was the result of both proper engineering, and the strict adherence to a detailed construction quality control program. The QC program documented the materials of construction and the quality of construction of the entire project. The QC program was responsible for the detection of construction defects as well as the documentation of their repair.

In conclusion, the following is provided as a list of items that will be considered in our future designs, based on the experience of this project.

- Test unexposed samples of materials at each test period rather than just at the beginning of the EPA 9090 compatibility test. This will show the variations in the test results that are due to the variability in the material and test methods themselves, and not due to any effect from the waste.
- Use the geocomposites now available (e.g., geotextile fused to geonet) to minimize the movement and wrinkling of the synthetic materials, especially during soil cover placement.
- Do not use the spark test as the sole seam field test for testing for leak paths.
- Use the thicker HDPE geomembranes. There was a far greater number of seam defects (leak paths) found in the 1 mm HDPE installation than the 2 mm HDPE installation. The 1 mm HDPE geomembrane is apparently more difficult to seam compared to the 2 mm HDPE.

REFERENCES

- [1] U.S. Environmental Protection Agency, "Draft Minimum Technology Guidance on Double Liner Systems for Landfills and Surface Impoundments - Design, Construction and Operation," December 1984.
- [2] "California Administrative Code, Title 23, Water Resources Control Board, Subchapter 15," adopted October 18, 1984.
- [3] U.S. Environmental Protection Agency, "Use of the Water Balance Method for Predicting Leachate Generation from Solid Waste Disposal Sites," SW-168, October 1975.
- [4] Petsonk, A.M., "The BAT Method for In Situ Measurement of Hydraulic Conductivity in Saturated Soils," M.S. Thesis in Hydrogeology, University of Uppsala, Sweden, 1984.
- [5] Daniel, D.E., and S.J. Trautwein, "Field Permeability Test for Earthen Liners," Proceedings of In Situ '86, ASCE specialty conference, Blacksburg, Virginia, June 23-25, 1986, pp. 146-160.
- [6] Chen, H.W., and L.O. Yamamoto, "Permeability Tests for Hazardous Waste Management Unit Clay Liners, Ninth Annual Symposium on Waste Management, Colorado State University, Fort Collins, Colorado, February 1987.

LEACH, J.A., HARPER, T.G., and TAPE, R.T.
Klohn Leonoff Consultants, Canada

Current Practice in the Use of Geosynthetics in the Heap Leach Industry

ABSTRACT

Heap leaching accounts for a large proportion of U.S. gold production. Geomembranes and geotextiles are widely used in the construction of the liner system for leach pads and solution ponds. Aspects of liner selection and design are presented with recommendations for future developments in liner design technology.

INTRODUCTION

During the 1970's increasing metal prices gave rise to renewed interest in gold and silver mining. The heap leach process in particular has attracted much interest because it provides a method of economically processing oxidized ores with gold grades as low as 1 gm/tonne (.025 oz/ton) which are uneconomic for conventional milling and extraction. The process has modest capital costs which make heap leach projects within the financial capability of junior mining companies.

A heap leach operation typically consists of four stages; mining, crushing, leaching and extraction. For some mines crushing is not necessary. The ore is mined by the open pit method which allows the movement of large volumes of ore at low cost. The run of mine ore is crushed to a predetermined size in a multi-stage crushing operation. The crushed ore may sometimes require agglomeration using cement and water to enhance percolation and hence leaching. The ore is stacked in horizontal lifts, typically 3 to 10 m thick on prepared leach pads. Leaching is achieved by sprinkling the ore heap with a weak sodium cyanide solution using sprinklers or wobblers to evenly distribute the solution. Sprinkling is carried out at a predetermined rate, typically 23 ml/m²/sec (.004 g/ft²/min) and the solution percolates through the ore leaching out the gold and silver. The leach pad is covered with a low permeability liner which intercepts the gold bearing pregnant solution preventing loss of the gold and escape of toxic solutions. Pregnant solution is drained from the leach pad and stored in the pregnant solution storage pond before passing to the process plant where the gold and silver are extracted. The barren solution, stripped of the gold and silver is stored in the barren solution pond where the cyanide content and pH are adjusted before recycling to the sprinklers. A schematic flow diagram for a heap leach operation is shown in figure 1.

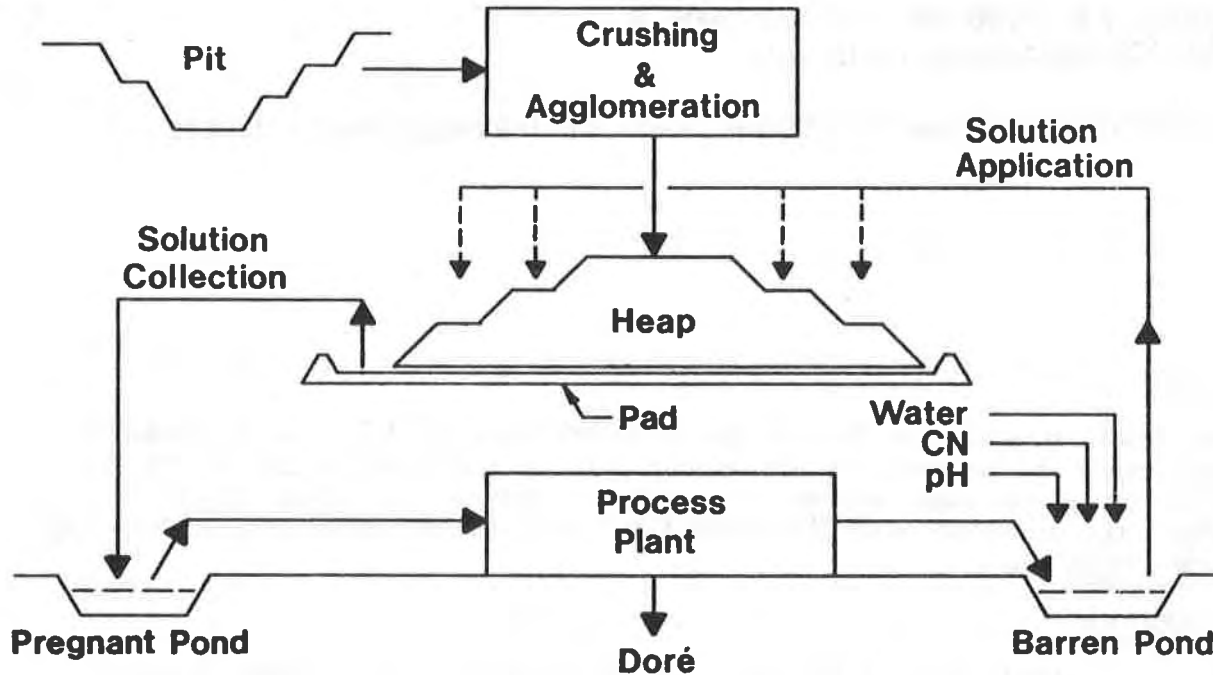


Fig. 1
Schematic of Heap Leach Process

This paper discusses recent experiences in the design of leach pad and solution pond liner systems in the western U.S. using geomembranes, geotextiles and geonets.

LEACH PAD DESIGN

The leach pad is required to hold large quantities of crushed ore during the leaching process and requires foundations capable of withstanding the applied loads from an ore pile that could be as high as 100 m (330 ft.). At the base of the heap a low permeability liner system is constructed to prevent loss of toxic solutions and to permit recovery of the gold and silver. Three types of leach pad designs are in use at the present time, the reusable pad, the permanent expandable pad and the valley fill pad.

Reusable Leach Pad

Reusable leach pads were commonly used in early heap leach mines and are still favored where the ore is fast leaching and high grade. The reusable leach pad comprises four or more pad areas which are alternately loaded with 3 to 6 m of ore, leached and unloaded. The spent ore is detoxified to destroy the

residual cyanide, and hauled to a waste dump. Reusable pads are generally constructed on flat or gently sloping ground with a cross fall of approximately 1% to 5%. Although geosynthetics are used in the construction of reusable pads, a more durable and abrasion resistant liner such as asphalt or concrete is usually preferred to permit easy unloading of the spent ore. As an alternative, a geomembrane covered with a permanent granular cover of about 1 m thickness can be employed.

Permanent Expandable Leach Pad

Permanent expandable leach pads involve the construction of pads where the area of the leach pad is increased with time to accommodate increasing quantities of ore. When leaching is complete the ore is left in place, detoxified and the heap reclaimed.

Permanent expandable leach pads are generally constructed on flat ground. At some operations, large quantities of mine waste are used as structural fill to create the necessary flat sites for pad construction.

This type of leach pad is used when ore volumes are large and the ore grade is insufficient to support the rehandling costs. The permanent expandable pad is also especially favorable for slow leaching ores. Leach pads of this type up to 40 ha (100 ac.) with heaps up to 80 m (265 ft.) high are in operation or under construction in the western U.S.

Valley Fill Leach Pad

The valley fill leach pad is a variant of the permanent expandable leach pad. A valley site is lined and filled with ore over a number of years. A dike of waste material may be constructed to confine and stabilize the heap. If a retaining dike is constructed, the basin created may be used to store operating solution and excess precipitation, thereby eliminating or reducing the need for outside solution ponds. At abandonment the ore is detoxified and the liner punctured to allow free drainage of the heap.

Various types of valley fill pads are shown in figure 2. The choice of pad style is governed by site topography, availability of waste rock for fill, the maximum height at which the ore will continue to leach, the desirability of storing solution in the voids of the ore, and stability of the ore. Generally, pad slopes in the range of 1% to 30% are used, the lower end to ensure drainage and the maximum set to provide reasonable construction techniques over large acreages.

Without a toe berm there is potential in storm conditions for excess water and solution to spill over the collection trench. A small dike along the lower edge can control the potential for overflow, and also enhance overall stability of the ore. Some pads are constructed with large dikes which allow storage of solution in the ore and provide significant contributions to stability. Storage of solution in the voids of the ore is only feasible for ores that are structurally sound and do not degrade on leaching. Liner design must take into account the potential hydraulic head on the liner of many tens of meters.

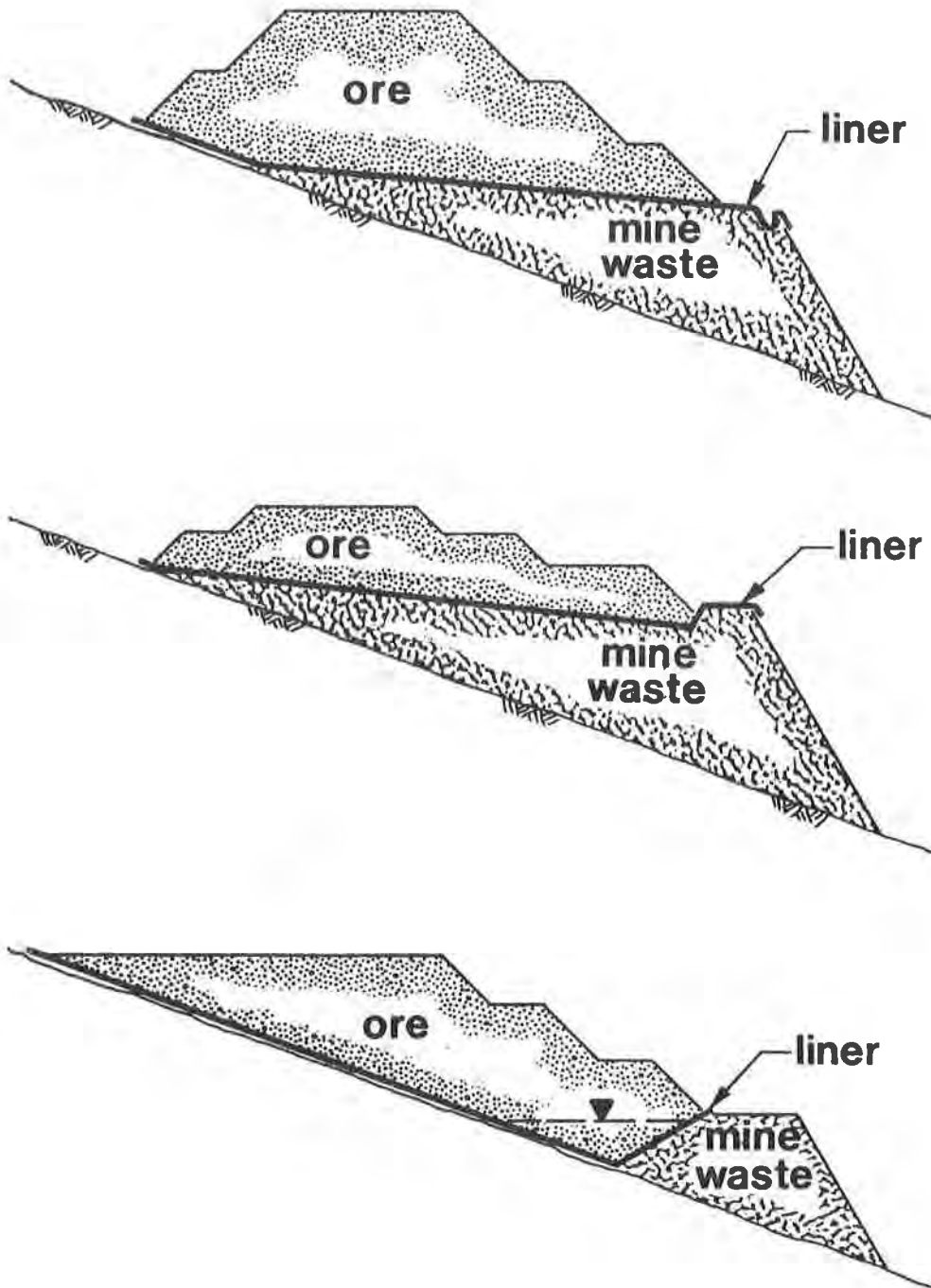


Fig. 2
Valley Fill
Leach Pad Types

LEACH PAD LINERS

The liner system comprises one or more low permeability materials, sometimes separated by a drainage medium. The liner system must be capable of with standing the weight of the ore placed on it and have low permeability under the applied hydraulic heads. Liner systems generally have a design life of five to fifteen years and are selected on the basis of engineering performance and economics. Examples of commonly used liner systems are shown on figure 3.

Liner Selection

Double liners are required by many regulatory agencies and are commonly specified by leach pad designers. The lower liner is generally a natural material with a coefficient of permeability lower than 1×10^{-6} cm/sec. Some material such as clays, weathered shale, or weathered granitic rock are suitable as is; others, such as tailings silt and sand, or silty clays may require modifications such as added bentonite or proprietary soil sealant to attain the required permeability.

The upper liner is normally a geomembrane. Polyvinyl Chloride (PVC) and High Density Polyethylene (HDPE) are the most frequently used geomembranes, although others such as Chlorinated Polyethylene (CPE) and Chlorosulfonated Polyethylene (CSPE) are also used.

The selection of geomembrane is made on an individual leach pad basis, taking into account a number of factors including the availability and type of natural liner construction materials, the stresses and hydraulic head to which the liner system will be subjected, and the temperatures at which liner will be installed.

Friction Angles

Generally interface friction angles along geomembrane contacts are lower than individual material strengths, and thereby control heap stability. Geomembrane interface peak and residual strength friction angles taken from Klohn Leonoff projects and Koerner (1986) are presented below:

TABLE 1
TYPICAL CONTACT FRICTION ANGLES

<u>Materials</u>	<u>Friction Angle (°)</u>
PVC rough/Clay	9.6*-26.2
smooth/Clay	6.1*-25
PVC rough/Sand	25-27
smooth/Sand	21-25
PVC/Ore	33
PVC rough/Geotextile	23
smooth/Geotextile	21
HDPE/Clay	13
HDPE/Sand	17-27
HDPE/Ore	26-29
HDPE/Geotextile	7.3*-11.3

* Residual Value

Peak strength represents the shearing resistance available the first time that the interfacing materials are forced to move relative to one another. As movement progresses, the shearing resistance decreases to its residual strength. Laboratory stress/strain data indicate that there is a substantial difference between peak and residual strengths for interfaces involving geomembranes and that very little movement, perhaps only a few millimeters is necessary to cause a drop from peak to residual strength. Laboratory tests indicate, however, that interface strengths are higher for PVC than for HDPE against clay or geotextile. As a result, some PVC leach pads may either be built at steeper angles or accommodate more ore than HDPE lined pads.

Puncture Resistance

Geomembranes, designed for fluid containment, are prone to puncture when used for leach pad liners. The susceptibility of geomembranes to puncture is a site specific problem involving ore size, fines content and sharpness of the ore.

Puncture resistance is determined using a laboratory compression test procedure to simulate field conditions. A disc of geomembrane is placed in a steel mold on bedding material. The geomembrane is covered with crushed ore of the appropriate size. A steel platen is placed on the ore and a normal stress equivalent to 125% of the maximum ore height is applied. The load is applied for 24 hours at which time the geomembrane is removed and examined. The sample is considered acceptable if no punctures, major depressions or gouges are observed.

The need for a protective cushion above the geomembrane is evaluated on the basis of the puncture tests. Protective cushions are discussed below.

Protective Cushions

Protective cushions are required when the tests show that the unprotected membrane is punctured by the ore. Puncturing is most likely to occur when the ore comprises large sharp angular particles and when the ore has a low fines content. Geotextile or sand may be used as a protective cushion. Use of geotextile allows rapid placement without serious risk of damage to the underlying geomembrane. As shown in Table 1 the friction angle between geomembrane and geotextile can be very low, and in order to maintain overall heap stability it may be necessary to place a very thin friction layer of sand between the geotextile and geomembrane. A cushion of sand 150 mm (6 in.) thick will adequately protect the geomembrane from puncturing by ore. For construction purposes, however, the cushion layer is often increased to 450 mm (18 in.) to provide support for tracked construction equipment spreading and placing the sand. For mine trucks a minimum of 1 m (3 ft.) is recommended for trucks up to 50 tonne capacity.

At some heaps the ore is crushed to 10 mm (3/8 in.) maximum size and the ore can be placed directly on a thick geomembrane without the need for a cushioning layer. With this sized ore under high heaps puncturing will tend to occur if the ore segregates allowing single sized particles to come in contact with the geomembrane. Care has to be taken to place an initial lift of ore without segregation.

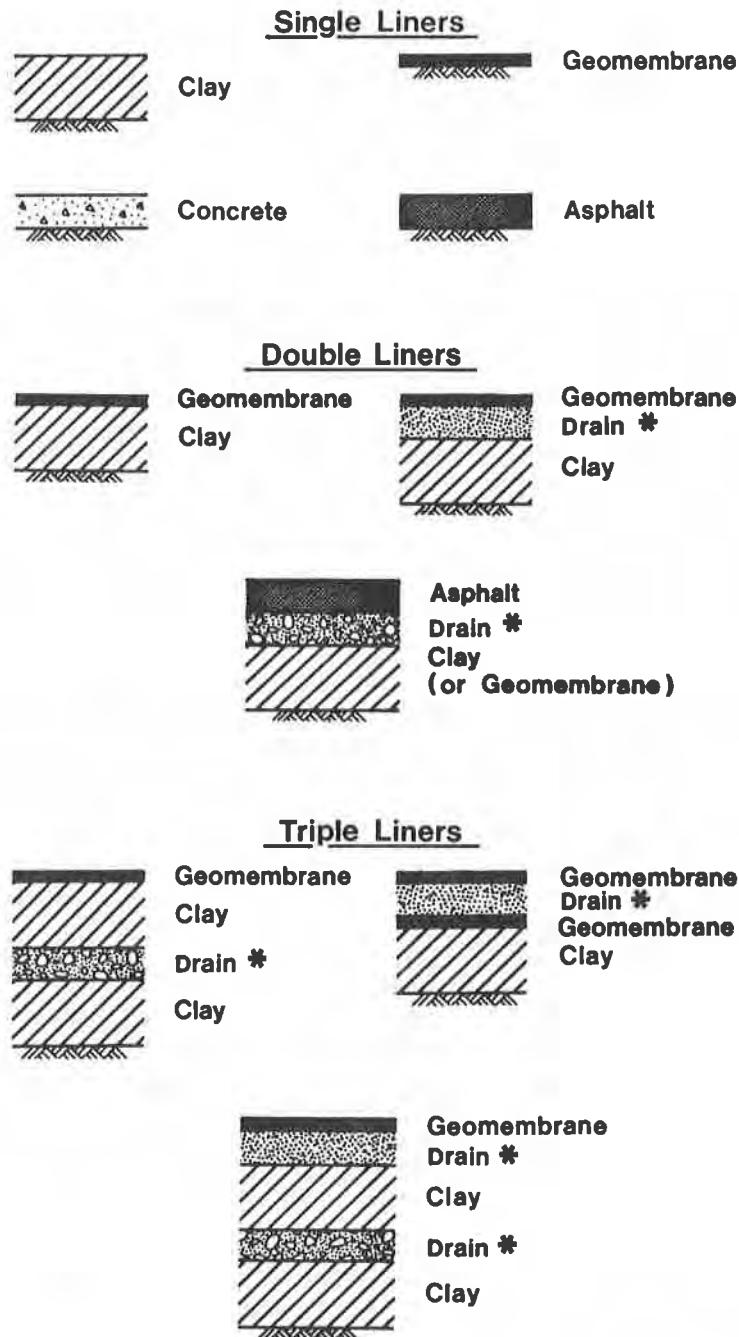


**Fig. 3
Liner Systems**

* Filters may be required between clay liner and drain materials

Drains

Drainage layers are sometimes installed between the two low permeability members of a double liner. The function of the drain is to permit monitoring of the geomembrane to determine if leaks are occurring and also to provide a means of recovering escaping solutions. The drainage layer should have high transmissivity in order to ensure that the hydraulic head on the upper surface of the lower liner is maintained at a low level.

The drainage medium should be selected taking into account the ultimate size of the heap. Laboratory tests indicate that under low heaps the transmissivity of a geotextile drain or a geonet drain will remain adequate. Under moderately high heaps a geonet drain protected against the underlying clay liner by a geotextile will provide adequate drainage. Under the high loads associated with large valley fill heaps the transmissivity of geotextile is inadequate. Under high loads PVC may become overstressed and split if placed in contact with a geonet and therefore under large heaps sand drains are required. Sand drains have modest transmissivity which does not drop greatly as loading increases. Sand drains are typically 50 to 450 mm (2 to 18 in.) thick and may support pipes which reduce reporting time and aid the recovery of fugitive solution. Thin sand drains are placed by hand. The pipes may be arranged in such a manner that the approximate location of a leak in the geomembrane may be identified, and controlled by limiting the area being sprinkled.

Usual practice is to install the drain between the geomembrane and the natural liner. In order that the drain be capable of conducting leaking solution away quickly enough to minimize the head on the lower liner, the drain must have a high permeability. This means use of a coarse granular material which raises the threat of membrane puncturing, in turn requiring a protective geotextile between the drain and the membrane, thereby lowering friction and raising the question of stability along the contact. Using geonet for the drain also can result in problems from low interface friction angles. An alternative is use of a sand drain which will have limited transmissivity but will not reduce stability. Sand may also tend to plug a leak in the lower liner, acting to reduce the rate of solution loss while still providing drainage. A sand drain will allow head to build above the lower liner, but only over a limited area surrounding the membrane defect. Considering overall liner system integrity it may prove more advantageous to place the geomembrane directly in contact with the natural material liner. This has the advantages that a puncture in the geomembrane will have limited capacity for solution flow because of the immediate backup of the lower liner, and no drain to laterally distribute high head solution to a significant area of the lower liner.

A drain between the liners will react when a leak through the upper liner occurs leaving the lower liner to contain the leak. A detection system below the bottom liner will react only to a leak through the entire system, requiring some method of handling the seepage below the liner system. In areas where there is groundwater flowing to the surface it can be argued that seepage through the liner system is prevented from entering the groundwater and can be intercepted at a downstream location.

POND DESIGN

Solution ponds are required to store pregnant and barren solution and act as surge ponds for the mineral recovery plant. The barren pond is used for storage of solution prior to adjustment of pH and cyanide content before recycling the solution back to the heap. Pond capacity is typically up to 20,000 m³ (5 million gallons) each. Valley fill leach pads may provide on-pad storage of pregnant solution, thereby eliminating the need for the pregnant pond. The need for additional storage is determined by water balance calculations.

Stresses on the pond liner system are normally low and therefore pond design is less complex than leach pad liner design. Slopes of 3:1 (H:V) are favored to facilitate liner placement and to reduce the risk of accidents during operations. From the geotechnical viewpoint the excavation must be stable when the pond is full and also after the solution level has been drawn down.

Pond Liner Selection

Pond designs usually utilize a double liner comprising a natural liner and a geomembrane, separated by a leak detection and recovery system.

The natural liner is normally the same material used for the leach pad liner construction. Geomembrane selection must take into account the long term exposure of the liner to sun light, and therefore HDPE or CSPE is generally preferred.

Pond Drains

Pond drains are used to monitor the geomembrane for solution loss and permit the recovery of solution. Normal stresses on the liner system are rarely greater than 120 kPa (2500 psf) compared with the 1500 kPa (30,000 psf) on leach pad liners. At these lower normal stresses, geotextiles and geonets have sufficient transmissivity for use as solution recovery drains.

CONCLUSIONS

On the basis of experience with several heap leach projects a number of conclusions have been reached regarding leach pad and pond liner system design.

Geosynthetics provide an economic solution to liner system design challenges which arise out of short supply of suitable natural materials and/or high cost of borrowing the large volumes of material required.

A liner system comprising strictly geosynthetics is not generally considered for a heap liner as a multi-liner system concept holds true only if the separation of the geomembranes is sufficient to prevent a single puncture event from penetrating both membranes. The separation of membranes would need to be at least 50 mm (2 in.) in most cases, requiring a sand layer for economical construction.

The selection of the liner system must take account of the stresses to which it will be subjected in terms of the anticipated heap height and potential for movement from settlement. Hydraulic head must be considered as this will vary from a few 300 mm (12 in.) in a reusable pad to tens of meters in a valley fill heap.

Considerable care is taken to protect the geomembrane from damage by cushion layers and careful construction practices. When a double liner is used, equal care should be taken to ensure the integrity of the natural liner. A leak in the geomembrane underlain by a drain layer in a valley fill leach pad will result in a high hydraulic gradient across the natural liner which could lead to a piping failure in the natural liner. Designs for natural liners should ensure that the liner material is adequately filtered against any grading fill or other coarse material underlying the liner.

Future Developments

Geocomposites are becoming more readily available and the use of these products for heap leach application is expected to increase in the near future. The materials presently available comprise thin geomembranes bonded to geotextiles. These materials can be used for pond construction where low stresses are involved and the risk of puncture is small. Geocomposites with thicker geomembranes and thicker geotextiles will have applications in leach pad liners, geotextile side providing the geocomposite does not delaminate under the applied stresses.

HDPE geomembrane has low interface friction angles against geotextiles and clay materials. Considerable improvements in interface friction could be achieved by providing textured surfaces to the sheet in the way that PVC is currently produced.

Presently, sand size particles are generally recognized as producing acceptable cushion material to protect geomembranes from puncture by ore. However, sand is not always readily available and coarser materials have to be considered. Although laboratory compression test data indicate that certain sand-gravel size mixtures may adequately cushion some geomembranes at relatively high load applications, the results are considered inconclusive. Some improvements in evaluating the cushioning performance of fine gravel and sand mixtures placed over geomembranes of varying thicknesses and subjected to variable loads would be helpful in heap leach pad design. Further work is required to define acceptability criteria for geomembranes partially penetrated by ore particles.

References

- (1) Koerner, R.M. Designing with Geosynthetics, Prentice Hall, New Jersey, 1986, p.p. 232-233.

BURANEK, D. and PACEY, J.
Emcon Associates, U.S.A.

Geomembrane-Soil Composite Lining Systems Design, Construction Problems, and Solutions

GEOMEMBRANE-SOIL COMPOSITE LINING SYSTEMS
DESIGN, CONSTRUCTION PROBLEMS, AND SOLUTIONS
DENNIS BURANEK AND JOHN PACEY
EMCON ASSOCIATES

ABSTRACT

The advantages of using geomembrane-soil composite lining systems to reduce seepage losses due to defects in the geomembrane liner have been well documented.

Double composite lining systems with leachate collection layers can provide a greater degree of confidence regarding seepage mitigation. However, construction of multiple composite systems can present several difficulties, most of which are associated with placement of the claysoil liner over the underlying geomembrane-geonet-geotextile secondary liner and leachate collection system. These problems are discussed and construction techniques for solving these problems are presented.

INTRODUCTION

Geomembrane liners (also known as synthetic liners or flexible membrane liners) have been used increasingly since the early 1970s to contain chemical and hazardous wastes because of their low permeability and potential high resistance to chemical degradation when in contact with these wastes. The use of geomembrane liners for containment of wastes received a significant boost from the U.S. Environmental Protection Agency (EPA) in 1976 as a consequence of the Resource Conservation and Recovery Act (RCRA). The ensuing 40 CFR 264 regulation established a preference for geomembranes as a primary liner which would "prevent" waste from passing into the liner during the active life of the facility."

The lining system recommended for hazardous waste facilities by the EPA in Minimum Technology Guidance on Double Liner Systems for Landfills and Surface Impoundments (1) consists of a primary leachate collection and removal system (for landfills), a primary geomembrane liner, a secondary leachate collection and removal system, and a secondary liner, which is comprised of a geomembrane overlying a minimum of 3 feet of compacted clay soil (permeability of less than 1×10^{-7} cm/sec or less). A typical liner section complying with these requirements is presented on Figure 1. This paper addresses the additional use of a composite liner for the primary liner system.

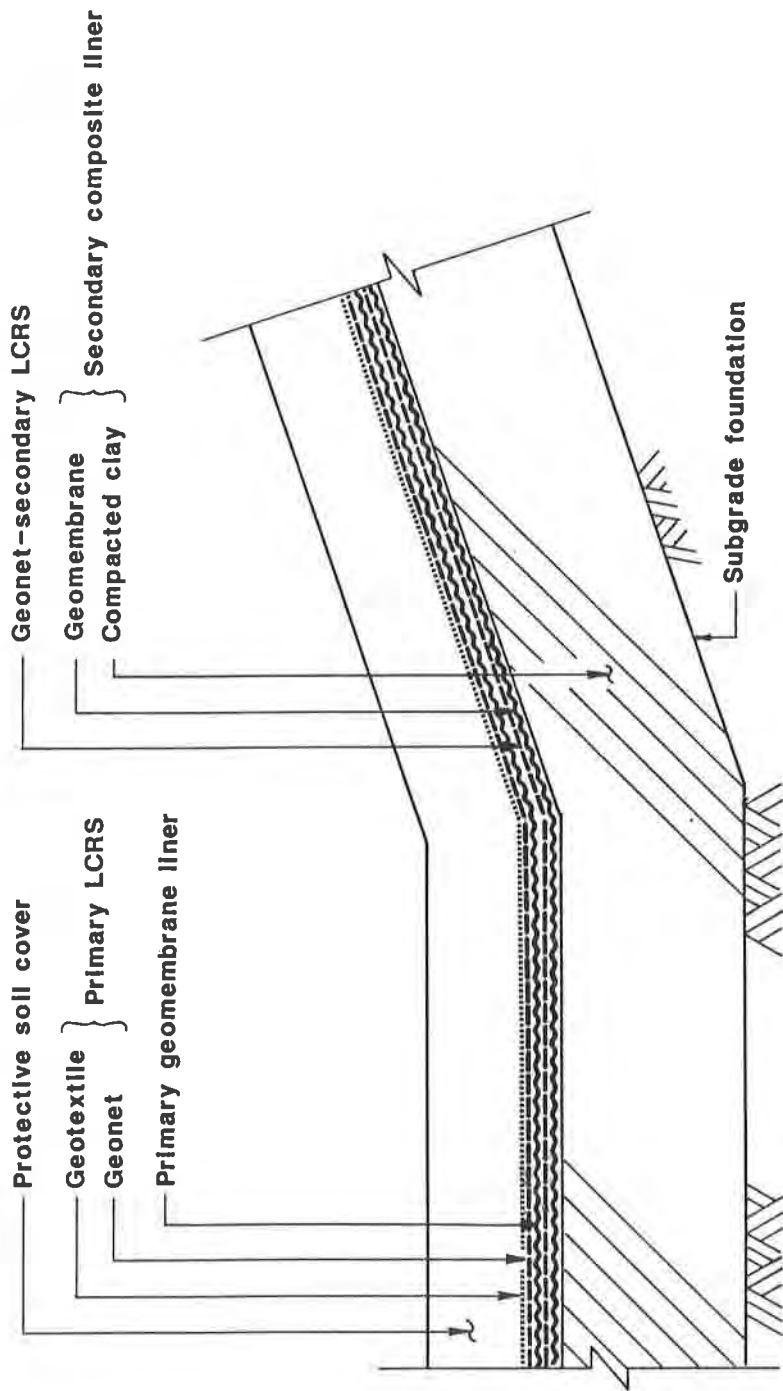
There are several different types of geomembrane material available for use in hazardous waste containment units. The most frequently used geomembrane materials are the semicrystalline, linear low-density polyethylene (LLDPE) and the more crystalline, high-density polyethylene (HDPE). These materials have achieved acceptance because of their excellent chemical resistance to a broad range of wastes. Because of the predominance of HDPE and LLDPE in hazardous waste facilities, we will consider only these materials when discussing geomembranes in this paper.

The EPA has specified a maximum allowable leakage rate (MLR) for hazardous waste facilities. The MLR is a very small quantity, originally defined as 1 gallon per acre per day. In the past, the MLR was known as the "de minimus" leakage rate. The EPA is presently considering that the MLR for composite liners should be in the range of 1 to 20 gallons per acre per day. Minor flaws in a geomembrane or its seams will probably result in a leakage rate that falls within the range of 5 to 20 gallons per acre per day.

Intuitive reasoning and empirical data in Quantify Leak Rates Through Holes in Landfill Liners (2) suggests that leakage through a defect in a geomembrane will be significantly reduced if the geomembrane is in contact with an underlying low permeability soil. Data from the above study indicates that flow rates through small holes in a geomembrane are approximately five orders of magnitude lower when the geomembrane is underlain by a low permeability soil than when a geomembrane with the same size hole is underlain by gravel. Therefore, there is a tremendous advantage in use of composite liners (geomembrane overlying a low permeability clay).

DOUBLE COMPOSITE LINERS

The advantages of a composite primary liner include the following: (1) it maximizes leachate collection in the primary leachate collection and removal system (LCRS) of a landfill; (2) it reduces the seepage loss through the primary geomembrane liner if there is a defect in the liner; and (3) it will allow the secondary LCRS to continue to function as intended even if it has become partially blocked because of the slower leakage through the primary liner.



- NOTES:**
1. The primary LCRS componets are not applicble for surface Impoundments.
 2. The primary and secondary LCRS may be granular material.
 3. Protective soil cover may be optional for surface Impoundments.

FIGURE 1 DOUBLE-LINED WASTE UNIT

The disadvantages of the composite primary liners include: (1) a leak in the primary geomembrane liner will not be detected rapidly as the waste must pass through the clay component of the liner; (2) the primary liner system cost is increased by the addition of the clay element; and (3) the construction of a primary composite liner significantly complicates the construction of the facility.

In recognition of the advantages of using composite liners to reduce leakage through the primary and secondary liners, double composite liners have been considered as a desirable option by the EPA for hazardous waste facilities. With a double composite liner, the primary geomembrane liner is immediately underlain by a layer of compacted, low permeability soil, such as clay. Since the minimum technology guidance document for double-lined systems essentially requires a secondary composite liner, a double composite lining system will frequently be highly regarded for design. A section of a typical double composite liner is shown on Figure 2.

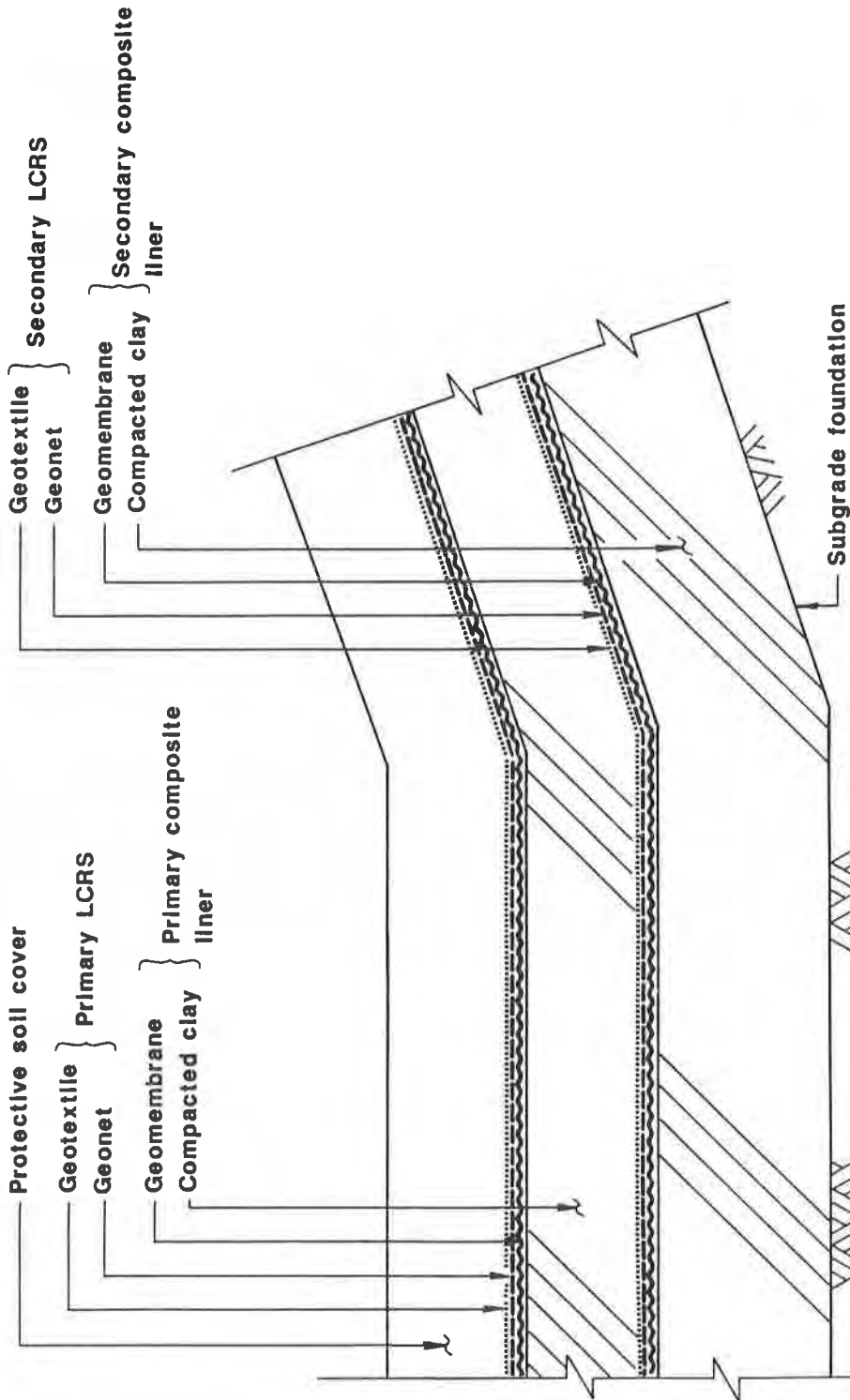
There are several conditions and considerations unique to the construction of double composite liners that must be recognized. To minimize and solve problems in construction, all parties involved in the project must first recognize the potential difficulties. To solve these problems, there must be cooperation between the facility owner, the design engineer, the construction quality assurance (CQA) organization(s), the earthwork contractor, the geosynthetic installation contractor, and the regulatory agencies.

The conditions that must be considered in construction of a double composite liner can be divided into the following groups: (1) earthwork construction and construction equipment, (2) construction monitoring and control activities, and (3) weather conditions. Many of the potential construction problems are associated with the interrelationships of all these groups. Potential problems and their solutions are discussed in the following sections.

Earthwork Construction and Construction Equipment

The most significant consideration in the construction of a double composite liner is the protection of the geosynthetic materials from damage. These materials can be easily damaged by construction equipment. For example, the geosynthetics in the secondary liner can be damaged when the overlying soil layer of the primary liner is placed. Damage can include puncture, tearing, folding and creasing, or excessive elongation of the underlying geosynthetics.

The potential for damage was recognized early in the use of geosynthetics. Thus cover materials or granular drainage layers placed over geomembranes were placed in relatively thick lifts (12- to 18-inches thick) and then spread and compacted with relatively low-contact pressure equipment. Placement of the protective soil prevents direct contact between the geosynthetics, and the thick lifts and



NOTES: 1. Primary LCRS components are not applicable for surface impoundments.

2. Primary and secondary LCRS may be granular material.

3. Protective soil cover may be optional for surface impoundments.

FIGURE 2 DOUBLE COMPOSITE LINER

low-contact pressure equipment mitigates the potential for damage to the underlying geosynthetics from installation stresses. Placement and compaction of "clay" liners encourages thin lifts (generally 6- to 8-inch-thick loose lifts) and high contact-pressure compaction equipment.

A solution to this dilemma is to recognize the problem and place the soil liner in a thicker lift or in several thick lifts. Since the purpose of the clay liner is to provide a low permeability barrier, the clay should be placed at a very high moisture content, well above the Standard Proctor optimum moisture content. At these high moisture contents, it becomes easier to obtain the density and fabric of the clay liner needed to meet the permeability criteria. It also allows placement of thick lifts (12 to 18 inches) using heavy, rubber-tired compaction equipment. The use of sheeps-foot compactors should be discouraged because the small contact area of the feet of this equipment increases the potential for unseen damage of underlying geosynthetics.

By utilizing the thicker lift, the lower part of the lift will probably likely not be as well compacted as the rest. This should be recognized, accepted, and considered in the initial design and specifications; the designer should recognize that permeability, not density, is the control criteria. Therefore, the specifications should reflect that the acceptance of the compaction soil is based on the moisture-density-permeability relationship, as determined by laboratory analyses and interpreted by the CQA monitor. The determination of acceptable compaction may not be a specified relative compaction.

The induced stresses on the geosynthetics from placement, spreading, and compacting cohesive soils (such as clay) are greater than with noncohesive soils (such as sand). Since typically a geotextile serving as a separator and filter is in direct contact with the overlying soil, the geotextile and the geotextile seams must be strong enough to withstand the installation stresses. The underlying geonet will generally move in unison with the geotextile because the two become interlocked. To limit difficulties with these two materials, the following criteria should be considered:

- There should preferably be no horizontal seams in the geotextile, the geonet, or the geomembrane on the slopes of the facility.
- The geotextile should have adequate strength to withstand the installation stresses, especially on the slopes of the facility.
- Geotextile seams in contact with soil should be sewn, not heat seamed. Heat seaming tends to burn the geotextile resulting in holes, which reduce its ability to function as a separator and filter and also causes a weak seam.

- Soil placement should be in the geosynthetic's machine direction and from the toe of slopes to the top so that the stresses on seams are limited.
- Placement of the clay liner should be as close to the point of its deposition as possible to minimize pushing of the clay.
- Compaction and placing equipment should not make quick stops or sharp turns because this might cause the underlying geosynthetics to move and fold.
- Construction equipment entrance and exit points, ramps, and access roads should have relatively flat slopes to limit stresses in these areas. These access features should be part of the facility design. An additional sacrificial geotextile should also be considered for these ramps to add protection for the geosynthetics during construction.
- Close survey and grade control should be maintained during the placing and compacting of the primary soil liner. The dozer or compactor operators should not be relied upon to know if the equipment is operating on 1 foot of material or 3 inches. This is especially critical in corners and near the toe of slopes.
- Continuous, close-range monitoring and observation of the primary soil liner placement and compaction operations are mandatory. Such monitoring is particularly important for preventing direct equipment contact with the geosynthetics, excessive elongation, tears, rips, or punctures of the geosynthetics, and development of folds and creases in the geosynthetics, especially the geomembrane. If damage to the geosynthetics is observed or folding and creasing of the geomembrane is noted, earthwork construction activities in the area of the problem should be stopped until appropriate repairs to the geosynthetics can be accomplished.

Construction Monitoring and Control Activities

Intensive and extensive construction quality assurance (CQA) programs are required by the EPA for hazardous waste facilities. The organizations and personnel conducting these programs and the agencies reviewing and approving the programs should be aware of the unique conditions presented by double composite liners, such as the activities associated with sampling, testing, and survey-grade control.

- CQA plans typically require that a specified number of field moisture and density tests be performed on each lift of the soil liner. Additionally, a specified number of relatively undisturbed tube samples of the soil liner material are required for laboratory testing of the in-place liner. Field density testing involves a piece of construction equipment scraping surficial material from the test area (reducing soil thickness over the secondary geosynthetics) and performing a sand cone or nuclear densitometer test. The nuclear densitometer tests are often preferred because of the speed of the testing. Both methods typically involve either excavating a hole (sand cone test) or driving a steel spike, into the soil, withdrawing the spike, and then lowering a probe into the hole (nuclear densitometer). With both methods there is the possibility of puncturing or damaging the underlying geosynthetics. The same potential for damaging the underlying geosynthetics exists when obtaining tube samples. A proposed solution to this potential problem is to not test the lower part of the clay liner unless absolutely necessary, and then it should be performed with extreme caution.
- Close survey and construction grade control is obviously required for hazardous waste facilities for many of the reasons already discussed. However, particular care is required so that temporary survey monuments, hubs, and grade staking do not puncture or damage the geomembrane during installation and that they are not left in-place to subsequently damage overlying geomembranes.

Weather Considerations

Nearly all earthwork construction activities can be affected by the weather. This is especially true when constructing composite liners because of the properties of HDPE (and LLDPE). The principal weather-related considerations include wrinkles in the geomembrane, excessive tightness (trampolining) in the geomembrane, drying and desiccation of soil components, and rainfall or excessive construction water.

- Some of the more common and significant problems associated with HDPE geomembranes are associated with the thermal expansion and shrinking properties of the geosynthetic material. For composite liners to be effective in reducing leakage rates through flaws in the geomembrane, the geomembrane must be in contact with, or at least very close to, the underlying low permeability soil. HDPE geomembranes installed during relatively cool periods will develop significant expansion wrinkles as the geomembrane warms. Correspondingly, if the geomembrane is installed in a taut condition during a relatively warm period, it will contract to the point of

lifting off the subgrade (trampolining) upon cooling. This condition is unacceptable because of the stresses induced in the geomembranes, especially on the seams. There are other problems associated with the thermal properties of HDPE geomembranes that are well recognized by the liner industry. There must be a compromise regarding installation temperature, which is not overly restrictive to the liner installer. Temperature extremes should be avoided if possible. When installation occurs in hot weather, the development of significant wrinkles in the geomembrane should be avoided during the placement and spreading of soil over the geosynthetics. The development of significant wrinkles can be minimized if the initial placement of the primary clay liner takes place during the early morning hours when the geomembrane is contracted but not trampolining. If wrinkles develop that can not be "walked out," the soil placement must stop and the wrinkle removed by cutting the liner, overlapping, welding, and then cap stripping. This condition is not desirable because the seaming adds another potential area of weakness, and seam tests are usually not available before the clay is placed over the new seams. If the seam tests are not acceptable, then it may be very difficult to relocate and repair this defect.

- The affect of dry, hot, and windy conditions on the clay component of composite liners can be significant. Desiccation cracking, if allowed to occur, can significantly increase the hydraulic conductivity of the clay component of the liner. Thus it is desirable to cover the clay as soon as possible with the geomembrane. However, CQA programs require that laboratory permeability tests be performed on undisturbed samples of constructed clay liners. The sampling, transportation to the laboratory, and proper testing generally takes several days. Thus, when desiccation is likely to present problems, other provisions such as temporarily covering the clay with a very thin geomembrane, controlled water sprays, or surface sealants should be utilized.
- If significant rainfall occurs during geomembrane installation before the landfill or pond is completely covered with geomembrane, water will invariably get beneath the geomembrane. This will also occur on large facilities if water spray for desiccation-crack control is excessive. Water under the liner will cause the geomembrane to float and prevent adequate seaming if the seaming has not been completed. If this occurs during construction, the geomembrane must be cut, the water pumped out, the subgraded dried and repaired, and the geomembrane patched.

The use of double composite liners can be a significant step towards meeting the goals and guidelines for hazardous waste disposal. To have a successful installation, all parties involved must recognize the interrelationships between the various components and cooperate to overcome the conditions and constraints imposed when constructing composite liners.

REFERENCES

(1) EPA, Minimum Technology Guidance on Double Liner Systems for Landfills and Surface Impoundments - Design, Construction, and Operation (Draft), U.S. Environmental Protection Agency, 1985.

(2) Brown, K.W., et al., Quantify Leak Rates Through Holes in Landfill Liners, (Draft), U.S. Environmental Protection Agency, Grant No. CR10940, 1985.

MCCREADY, A.A.

Harding Lawson Associates, U.S.A.

Preventing Geomembrane Failures

INTRODUCTION

Geomembrane failures can be prevented by considering 1) factors which lead to successful installations, 2) misconceptions about geomembranes, 3) types of failures, and 4) how to prevent failures.

It's hard to believe that, as long as geomembranes have been used to contain products and wastes, failures still frequently occur. Not all failures are spectacular; in fact, very few are visibly detectable. Yet the economic impact of even minor releases can be significant.

Many of the early geomembranes were used to contain non-hazardous and unregulated materials, commonly treated drinking water. As the major concern during construction was the economic impact of losing treated water, these geomembrane systems were rarely leak-proofed. One gallon per minute per million gallons of storage was an acceptable construction objective.

Today geomembranes are used to contain hazardous materials controlled and regulated by the U. S. EPA and state and local agencies. Regulations prohibit any leakage from waste containment systems. These new standards require greater awareness of construction and maintenance techniques.

SUCCESSFUL INSTALLATIONS

For successful installations, the strength, compatibility, thickness and intended use of geomembranes must be considered when designing a project. Knowing what a geomembrane can and cannot do is essential. Current knowledge on this subject is expanding and becoming readily available to designers and would-be users. Figure 1 shows the building blocks which make up a successful geomembrane system. The absence of one or more components can increase the likelihood of or cause failure.

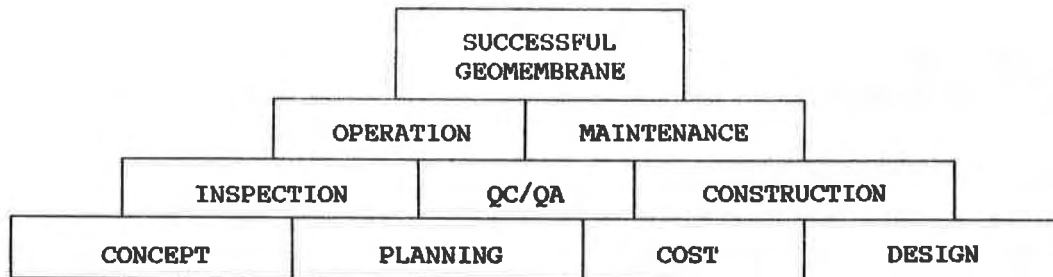


FIGURE 1

MISCONCEPTIONS

A number of misconceptions about geomembranes should be cleared up:

1. "Geomembranes do not leak." This is hardly an accurate statement. The material itself has a permeability coefficient and, with its many seams and repairs, certainly allows minor leakage. When "zero" discharge is required, a double geomembrane system is needed.
2. "Third party QC/QA is unnecessary and is only an extra cost." This concept has prevailed since the start of geomembrane useage. This writer's field experience in Quality Control/Quality Assurance (QC/QA) programs indicates that the geomembrane installer who attempts to provide QC/QA often overlooks needed repairs. The installer's first and foremost objective is to complete the job on time and within budget. These are hardly factors that will lead to a thorough QC/QA program.
3. "Geomembranes require no maintenance." Of course they require maintenance. A lack of maintenance can and often does lead to failure. This need for maintenance must be conveyed to the user; and the maintenance program included in a written operation and maintenance plan.
4. "Geomembranes are sometimes designed as structural elements of an overall system." This misconception can have serious consequences. For example, the case where a single geomembrane system is intended to prevent an embankment or dam from becoming saturated to maintain the stability of the soil structure. The stability of a soil structure should not depend entirely on the performance of a single geomembrane. Multiple geomembranes with liquid collection and removal systems may be considered to prevent saturation under certain circumstances.

Other misconceptions about geomembranes exist, but are not as significant as the above four.

TYPES OF FAILURE

For the purposes of this paper, we have defined failure and mode as below:

Failure - Costs incurred by the geomembrane user which are beyond installation and normal maintenance costs.

Mode - The process through which failures occur.

To understand how, when, where, and why a failure occurred, it is important to understand the mode of failure. Four categories of failures are discussed in the following paragraphs.

A. Chemical Compatibility

Geomembranes used to store and dispose of regulated hazardous materials must undergo a chemical compatibility test program. The most widely used test method is EPA 9090, which involves a series of physical tests performed before, during and after exposure to liquids and solids to be contained.

Most manufacturers have a general compatibility guide in their literature. These lists are useful in identifying extreme compatibility problems, but should not be relied on for varied waste streams and different concentrations of chemicals.

Compatibility damage may occur over wide areas or in isolated areas. Degradation in isolated areas is usually caused by a phase liquid representing a minor-fraction of the waste stream. The phase liquid will either float on the liquid surface or collect in globs on the liner surface in low areas of the containment. When concentrated, these compounds may dissolve the liner material and cause holes.

B. Material

Material failures are normally a result of deficiencies in the formulation and/or production of geomembranes. If adequate QC and QA procedures are maintained by the manufacturer and the user of the geomembrane, material deficiencies are detected prior to or during installation. Material failures include pinholes, poorly dispersed mix components, delamination and a membrane thickness less than specified.

C. Design Deficiencies

Design deficiencies are the result of the designer's lack of understanding the limitations of geomembranes. The deficiencies include a wide range of conditions. A good example is distortion of the earth subgrade slopes in ponds containing liquids where a thin geomembrane is exposed. As shown in Figure 2, the geomembrane may be disturbed at any liquid level.

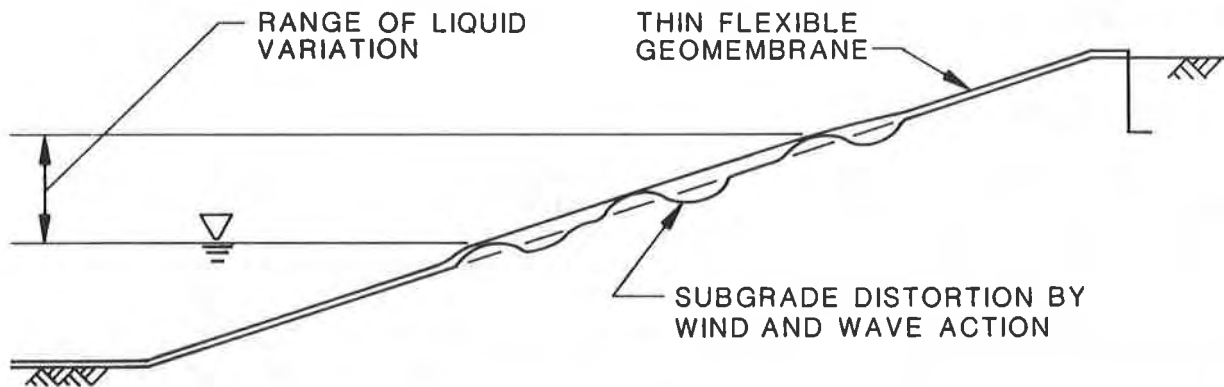


Figure 2

The voids and humps in the subgrade beneath the liner stresses the liner on the slope. In extreme cases water pressure against a non-uniform subgrade can cause large tears in the liners.

Problems of this sort have been known in the Liner Industry for many years. It is generally agreed that the condition occurs when wind and waves buffet an exposed liner against the subgrade. Knowledge of this potential problem permits a designer to include necessary design precautions. Otherwise, the unsuspecting designer (and owner) may have to learn the hard way.

Other important design deficiencies include inadequate seals at geomembrane penetrations, lack of protection during operation, foundation settlement, and incompatible construction materials.

D. Installation

In a liner installation of several acres, there are thousands of points where failure may occur. The major installation tasks where problems may result in failure are presented in Table 1.

Table 1
INSTALLATION PROBLEMS

- o Shipping and handling
- o Storage on site
- o Subgrade preparation
- o Unrolling or unfolding
- o Final positioning
- o Temporary securing with sand bags
- o Dirt, mud and moisture in seam area
- o Adhesive or welding procedures
- o Welding equipment
- o Seam testing
- o Liner damage away from seams
- o Weather conditions
- o Repairs not made
- o Cover layers contain debris and rocks
- o Equipment on liner or not enough cover
- o Equipment spreading and grading
- o Damage not repaired
- o Lack of liner contractor QC
- o Lack of owner QC/QA

The importance of QC/QA cannot be overstated. If your liner installation was a hot air balloon that must carry you over the Pacific Ocean to Hawaii, what level of QC/QA would you apply to assemble the balloon from 10-foot-square pieces of fabric?

E. Operation and Maintenance

What can possibly go wrong after you have successfully installed your liner? Everything! The operations people may not understand the strength limitations of geomembranes. Dragging hoses, driving over geomembranes with equipment, welding, raising embankments, disposing of materials not intended, and a lack of maintenance can all cause failures.

PREVENTIVE MEASURES

A. Responsibility

Who bears the ultimate responsibility for a geomembrane during its operating life and in some instances the closure period? The owner. Although responsibility may be transferred by the owner to designers, consultants, and contractors, the transfer is only as good as the third party's ability to assume the responsibility. The owner should deal with financially capable subcontractors and consultants that hold appropriate insurance coverage.

The owner of a proposed geomembrane system must know enough about geomembranes to make rational choices of specialists needed to design, construct, and inspect the system. As there are a number of misconceptions about geomembranes, particularly the difficulty to install a leak-proof system, a competent specialist is needed to provide a liner for which the owner will be initially, if not ultimately, responsible. Geomembranes are not products that you simply remove from a shelf, unfold and walk away.

So, in the simplest terms, responsibility begins and ends with the owner.

B. Regulatory Control

EPA, state, and local regulations regarding the use of geomembranes for containment of hazardous materials will greatly reduce the number of unnecessary geomembrane failures. The regulations require owners to follow procedures that lead them through design, construction and operation. The majority of these procedures were previously ignored, but are now minimum requirements. It is to the owner's advantage to follow the minimum requirements and to even use higher standards if it will prevent later economic hardship.

C. Role of QC/QA

Until recently, one of the most significant missing links in successful geomembrane installations has been the lack of quality control (QC) and quality assurance (QA) during installation. Owners have generally viewed such activity by independent third parties as an unnecessary extra cost. They have relied entirely on the installer's QC program which may be highly sophisticated or nonexistent.

In the hazardous waste field, nothing short of a complete and thorough QC/QA program will do. The regulations now require a thorough QC/QA program. It is to the benefit of the owner to see that it is properly carried out. Between enforcement by regulators and increased awareness of users, the number of common failures should diminish.

D. Geomembrane User Checklist

Prospective geomembrane users should refer to the checklist in Table 2 to determine if they have considered all major factors that will lead to a successful liner installation.

Table 2
GEOMEMBRANE USER CHECKLIST

- ___ Containment concept is sound.
- ___ Schedules and logistics reasonable.
- ___ Preliminary and final costing is complete.
- ___ Funding is available.
- ___ Designer is experienced in geomembranes.
- ___ Field inspectors are experienced.
- ___ QC/QA program is included.
- ___ Installation contractor is financially responsible and experienced on similar installations.
- ___ Operation procedures are written and available to staff.
- ___ Maintenance program has been prepared and a commitment made to carry it out.

CANCELLI, A.

University of Milano, Italy

CAZZUFFI, D.

ENEL's Research Centre for Hydraulics and Structures, Italy

RIMOLDI, P.

Politecnico di Milano, Italy

Geocomposite Drainage Systems: Mechanical Properties and Discharge Capacity Evaluation

1. FOREWORD

The use of geosynthetics to make high capacity drainage systems seems an interesting way of conveying large quantities of liquids in important civil engineering applications. Therefore, a great number of different high drainage composite prefabricated materials (usually called "geocomposites") is commercially available.

Design engineers need some valuable information regarding mechanical properties and discharge capacity behaviour of geocomposite products. The most part of the data presently available is concerning the characteristics of the single components (as geotextiles, geogrids, geomats, geomembranes, and so on). A laboratory study (1) on different products (geotextiles, 3-D geosynthetics and geomembranes) forming a sort of geocomposite, was recently carried out in order to design a particular waterproofing and drainage system inside an ENEL power station.

It seems now important to concentrate the attention of researchers on the properties of the whole geocomposite system: this study deals in fact with a comparison of different characteristics obtained on different prefabricated geocomposites, that are, presently, commercially available in Italy.

2. DESCRIPTION OF TESTED GEOCOMPOSITES

Six different products from three different manufacturers were considered in this experimental study:

- Tenax TN, TNT and MNT, from RDB Plastotecnica (Italy)
- Filtram 1B1, from I.C.I. (United Kingdom)
- Enkadrain TP and St, from Enka (Netherlands)

Filtram 1B1, Enkadrain TP and St and Tenax TNT are formed by a polymeric drainage core, coupled on both sides with geotextile filters. Tenax TN presents the geotextile filter only on one side, while Tenax MNT has geotextile filter on one side and geomembrane on the other side.

In order to evaluate the physico-chemical characteristics of the intrinsic components, a DSC (differential scanning calorimetry) analysis was made in Special Materials Laboratory of ENEL's Research Centre on Hydraulics and Structures in Milano. The results are shown in Table 1.

Table 1. Results from DSC analysis on geocomposites (av. values on 3 specimens).

Type of geocomposite	Core characteristics		Geotextile filter characteristics		
	Type of polymer (%)	Melting point (°C)	Type of polymer (%)	Melting point (°C)	
Tenax TN	HDPE 100.0	130.5	PP 100.0	161.2	
Tenax TNT	HDPE 100.0	131.5	PP 100.0	161.9	
Tenax MNT	HDPE 100.0	131.7	PP 100.0	161.4	
Filtram 1B1	LDPE 100.0	112.3	PP 74.7	163.5	
			PE 25.3	110.9	
Enkadrain TP	PA 100.0	220.6	PES 74.0	251.3	
			PA 26.0	219.1	
Enkadrain St	PA 100.0	220.3	PES 74.5	250.5	
			PA 25.5	218.3	

PA: polyamide PES: polyester PP: polypropylene PE: polyethylene
 HDPE: high-density polyethylene LDPE: low-density polyethylene

3. MECHANICAL PROPERTIES

In order to evaluate the mechanical behaviour of tested geocomposites, two different types of tests were planned: tensile tests as index tests and compression-creep tests, useful in order to obtain valuable information for design.

3.1 Tensile behaviour

Tensile tests were carried out at ENEL-CRIS in Milano on 5 geocomposites (namely, Tenax TN, Tenax TNT, Tenax MNT, Filtram 1B1 and Enkadrain TP): it was in fact impossible to put the Enkadrain St specimen inside the tensile clamps, because of the important thickness of this product. Considering the very similar physico-chemical characteristics it seems reasonable to assume for Enkadrain St the same tensile characteristics exhibited by Enkadrain TP.

The tensile test curves, in terms of force and strain, are shown in Fig. 1.

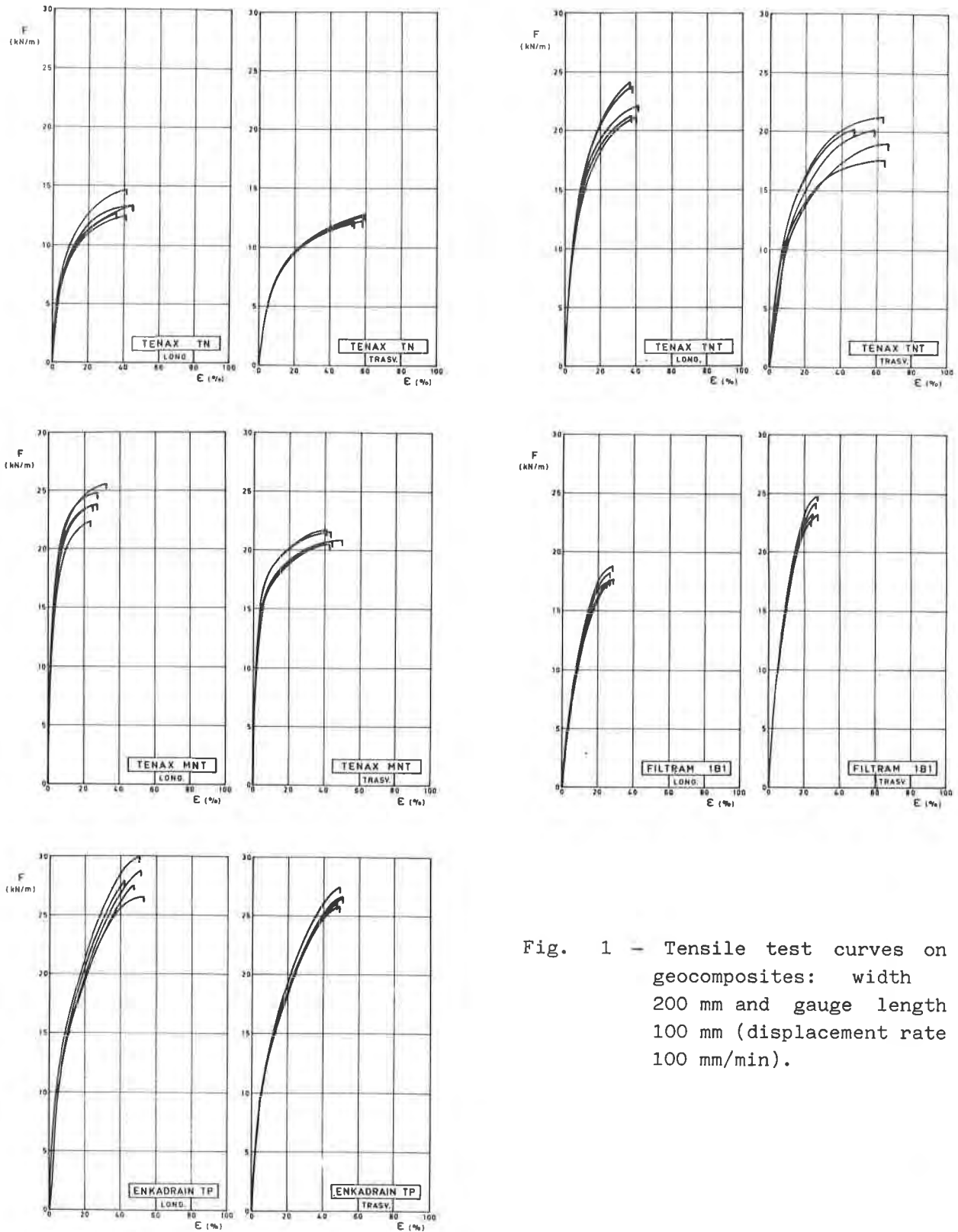


Fig. 1 - Tensile test curves on geocomposites: width 200 mm and gauge length 100 mm (displacement rate 100 mm/min).

The specimen dimensions of geocomposites used for the tensile test were: width 200 mm and gauge length 100 mm; the displacement rate was 100 mm/min. The tensile test results are summarized in Table 2, together with the measured values of mass per unit area and nominal thickness (obtained under 2 kPa).

Table 2. Results from tensile tests on geocomposites (average values on 5 specimens for each direction: L = longitudinal and T = transversal).

Type of geocomposite	Mass per unit area (g/m^2)	Nominal thickness under 2 kPa (mm)		Force at failure (kN/m)	Strain at failure (%)
Tenax TN	936	5.7	L	13.07	41.6
			T	12.21	56.0
Tenax TNT	1372	6.6	L	22.01	38.6
			T	19.26	59.6
Tenax MNT	1296	4.5	L	23.57	27.6
			T	20.69	44.4
Filtram 1B1	968	6.1	L	17.60	27.4
			T	23.19	26.4
Enkadrain TP	960	9.7	L	27.75	48.6
			T	26.02	49.2
Enkadrain St	950	21.0	L	-	-
			T	-	-

3.2 Compression-Creep Behaviour

Compression tests were carried out in the Soil Mechanics Laboratory, Politecnico di Milano, on 3 geocomposites (namely, Tenax TNT, Filtram 1B1 and Enkadrain St), in order to investigate stress-strain relationships and long-term creep behaviour. Classical, increment-load, oedometer devices were adopted for tests, with small modifications due to the different heights of tested specimens. For each selected geocomposite, 100 mm-diameter specimens were cut, then laterally revetted with polythene film and silicone grease, and finally placed inside testing boxes, the bottom and top porous stones having been previously saturated with water. Complete saturation of specimens, protection from shocks and vibrations, quasi-constant air humidity (60-70%) and room temperature (18-22°C) were ensured and maintained.

Static loads were applied by successive increments, giving average normal stresses σ equal to 10 - 25 - 50 - 100 - 200 kPa, the duration of each step being 1 hour. The stress-strain plots, reported in fig. 2, were drawn; the relationship between axial strain ϵ and the logarithm of normal stress σ (fig. 2-left) resulted approximately linear, concave downward, or concave upward, depending on the internal structure and the nominal thickness of geocomposites; therefore, ϵ vs. σ plots in arithmetic scale (fig. 2-right) resulted more significant and comparable each to other, all showing initial upward concavity and a linear relationship beyond about 25-50 kPa, reading:

$$\epsilon (\%) = a + b \cdot \sigma \text{ (kPa)} \quad (1)$$

For tested geocomposites, the values of parameters a,b reported in table 3 were evaluated. The high deformation wire web core of Enkadrain is responsible for the exceptionally high value of parameter a; as for as parameter b, it seems to be representative both of core and geotextile filter deformabilities: the highest value was measured for Filtram.

In each compression test, the maximum, final applied load ($\sigma = 200$ kPa) was kept constant for about 2 months, in order to evaluate long-term creep properties of the same geocomposites. The variation of axial strain with time is represented in fig. 3; from each plot, after an initial, transient (primary) creep, a quasi-steady state (secondary) creep can be recognized, that can be interpreted by a simple linear relationship (axial strain rate $\dot{\epsilon} = \text{constant} = \text{see fig. 3}$).

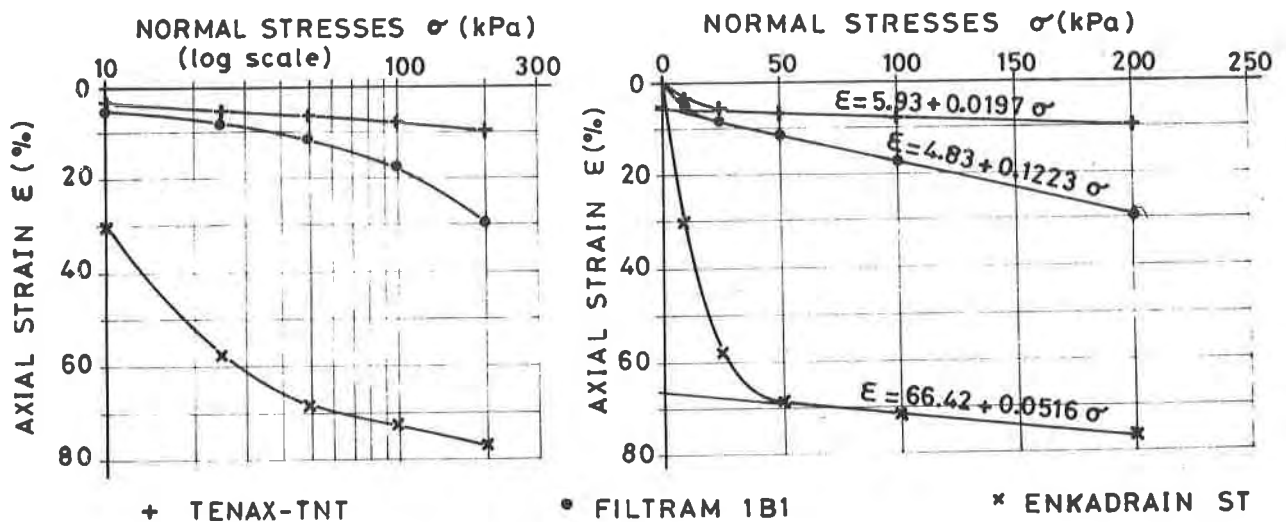


Fig. 2 - Oedometric stress-strain curves on geocomposites.

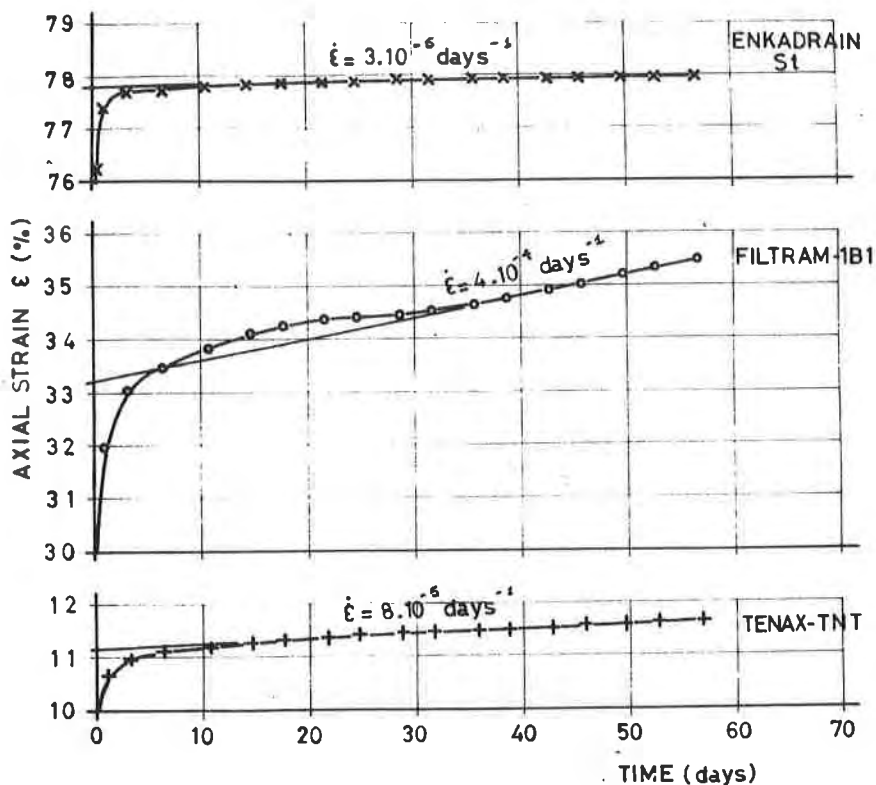


Fig. 3 - Compression-creep behaviour of geocomposites.

According to Koerner et al. (2), the creep behaviour of geocomposites could be analyzed in the light of the 3-parameters creep model formerly proposed for soils by Mitchell (3). The strain rate is expressed by the equation:

$$\dot{\epsilon} = A e^{\alpha D} (t_1 / t)^m \quad (2)$$

- where: D = stress level;
- t = elapsed time;
- t₁ = reference unit time;
- m = absolute value of the slope of the straight line on the log $\dot{\epsilon}$ vs. log t plot;
- α = slope of the linear part of the log $\dot{\epsilon}$ vs. σ plot;
- A = value of the strain rate for D = 0, evaluated from the log $\dot{\epsilon}$ vs. σ plot.

The values of parameters m, α , A, determined for a stress level D = 200 kPa on the same tested geocomposites, are reported in table 3.

As a general comment, values of m close to 1, common to all tested samples, mean a substantially straight line in the ϵ vs. log t plot. Concerning the other creep constants, the high value of A is consistent with the high deformability of Enkadrain core, even for low stress levels; the lowest values of both α and A seem to indicate Tenax TNT as the least creep sensitive among all tested materials.

Table 3. Values of stress-strain parameters (eq. 1) and secondary creep parameters (eq. 2) determined on 3 geocomposites.

Type of geocomposite	Stress-strain parameters		Secondary creep parameters		
	a (kPa)	b (-)	m (-)	α^{-1} (kPa ⁻¹)	A (hours ⁻¹)
Tenax TNT	5.93	0.0197	0.98	$0.99 \cdot 10^{-5}$	0.062
Filtram 1B1	4.83	0.1223	0.97	$2.42 \cdot 10^{-5}$	0.095
Enkadrain St	66.42	0.0516	0.99	$2.36 \cdot 10^{-5}$	0.650

4. HYDRAULIC PROPERTIES

Hydraulic properties have a fundamental importance, since the specific function of geocomposites is just to collect and carry a fluid, usually water, toward a prefixed point.

The hydraulic properties which are of interest in practice are the following: the filtration behaviour of the geotextile filter and the transmissivity of the whole geocomposite. The filtration behaviour of the geotextile filter was already the object of various other studies, for example by Bertacchi and Cazzuffi (4). Therefore this paper deals particularly with the transmissivity of the whole geocomposite.

In practice, in order to design a drainage system, it is needed to know the discharge which every geocomposite can carry, under specified conditions of applied pressure and of hydraulic gradient: transmissivity is defined as the discharge per unit width of the considered geocomposite, and for unity of hydraulic gradient.

The transmissivity can be calculated on the hypothesis that the fluid flow is laminar and, on the base of the Darcy's law for which $v = k i$, it can be measured in m^2/s and expressed as:

$$\phi = (q/B)/i \quad (3)$$

where: q = discharge (m^3/s);

B = width of the geocomposite (m);

i = hydraulic gradient (m/m).

Since in reality, as it was verified during the present study by means of velocity measurements, the water flow in the geocomposite is generally not laminar, but transitional, the test results₂ should be expressed in terms of flowrate, that is the discharge per unit width (m^2/s), for each value of hydraulic gradient:

$$Q = q/b \quad (4)$$

In order to better show the dependence of the flowrate from the hydraulic gradient i , a sequence of diagrams of Q versus the applied pressure σ , one for each value of i , is needed.

The apparatus generally used to measure the transmissivity, described for example in (5)(6)(7), follows the scheme of that originally used by Darcy to measure the permeability of sands: it consists of two water reservoirs which allow to maintain a constant head and of a central housing for the tested geocomposite, upon which it is laid a plate applying a constant predefined pressure, and of a system for the measure of the passing flow.

The Bernoulli's theorem shows that the water discharge carried by the geocomposite during the tests is a function both of the characteristics of the product, upon which the loss of pressure due to friction only depends, and of the geometry of the testing apparatus, upon which the losses at the inlet and at the outlet depend.

By means of two piezometers, the former downstream the inlet loss and the latter upstream the outlet loss, it's possible to get a more precise measure of the hydraulic gradient i , but anyway the discharge is always a function of the geometry. In this way transmissivity measurements got with different devices are not exactly comparable: therefore it's needed to reach a precise standardization of the testing apparatus and not only of the executive modalities. In any case, measures on different geocomposites got with the same apparatus allow for a relative measurement of the transmissivity (or flowrate) of various products.

Taking into account the above limitations, a testing apparatus for the flowrate evaluation of different geocomposites was developed: the apparatus used is shown in Fig. 4. As it can be seen, it is possible to get measurement under 4 values of the hydraulic gradient: $i = 0,5 - 1,0 - 1,5 - 2,0$. The electronic controlled loading machine allows to program and maintain a prefixed load, up to 200 kN. The tests were carried out with loads giving the following serie of applied pressures: 5, 25, 50, 100, 200, 350, 500, 1000, 100 kPa. The specimen sizes were: 305 mm x 305 mm.

It was also possible to measure the average velocity of the water: a small tank of red coloured water was connected to a small tube, closed by a tap, which arrived just at the inlet of the sample of geocomposite; suddenly opening the tap, and measuring the time needed for red water to reach the downstream reservoir, the water velocity can be obtained. These measures allowed to control that the water flow was not laminar, because Darcy's law wasn't respected, and therefore formula (3) was not applicable for the transmissivity computation.

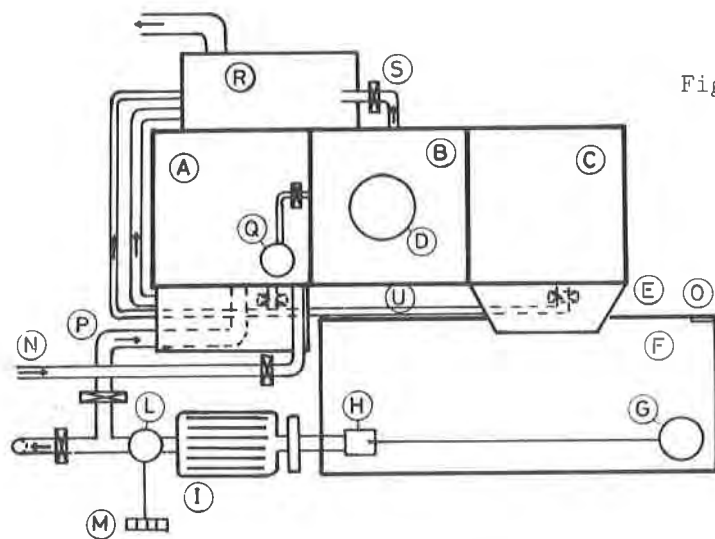
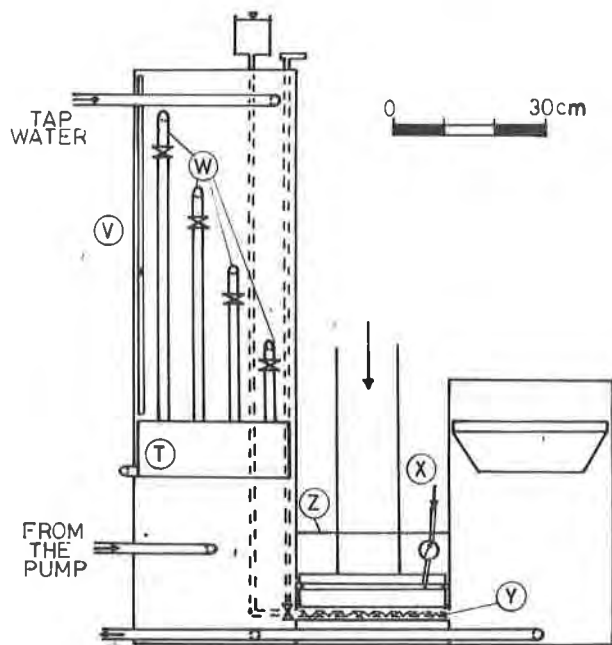


Fig. 4 - Scheme of the transmissivity test apparatus: plant and lateral view.

- A = UPSTREAM CHAMBER
- B = HOUSING FOR THE SAMPLE
- C = DOWNSTREAM CHAMBER
- D = PISTON OF THE ELECTRONIC CONTROLLED PRESS
- E = SPILLWAY
- F = TANK OF THE PUMP
- G = FLOATING SPHERE
- H = REGULATING PISTON
- I = PUMP
- L = ELECTRONIC LITER-COUNTER
- M = DIGITAL DISPLAY
- N = TAP WATER INLET
- O = MILLIMETRIC BAR
- P = RECIRCULATION FROM THE PUMP
- Q = TANK FOR COLOURED WATER WITH CLOSING TAP
- R = WATER COLLECTING TANK
- S = TAP FOR THE CONTROL OF WATER LOSSES ALONG THE PLATE
- T = WATER COLLECTING TANK
- U = WATER FINAL OUTLET
- V = PIEZOMETER
- W = SPILLWAY TUBES FOR THE CONTROL OF THE HYDRAULIC GRADIENT
- X = PRESSURIZED AIR INLET FOR THE SEALING OF THE PLATE WITH A RUBBER TUBE
- Y = SAMPLE OF GEOCOMPOSITE UNDER TEST
- Z = LOADING PLATE



The most original parts of the apparatus consist in the system for discharge measurement and in the system of hydraulic seal of the loading plate. The former is made as follows: from the spillway the water falls in the tank from which the pump sucks; the pump puts the water in the upstream reservoir; a digital litercounter with digital display is inserted on the delivery tube of the pump. The suction tube of the pump has the inlet regulated from a piston joined to a floating sphere: in this way the system automatically finds a regulation, after few minutes of transient flow, in such a way that the discharge of the pump becomes equal to that entering the tank. When the water level in the pump reservoir becomes constant, the

discharge measured by the litercounter is exactly equal to that passing through the geocomposite. A millimetric bar allows to evaluate when the system is in steady-state conditions. The sealing system of the loading plate is of pneumatic type: a rubber tube, which is inflated and maintained at a pressure of 550 kPa, is placed in a small groove of the plate: the thrust against the lateral wall guarantees the hydraulic seal even during the movements of the plate.

The testing procedures were the following:

- preparation of the specimen and putting it in the testing apparatus;
- preparation of the loading plate, positioning under the loading piston, inflation of the pneumatic sealing;
- water inflow and measure of its temperature;
- application of a pressure and measurement of the steady-state discharge for the selected values of hydraulic gradient;
- measurement of the water velocity with coloured flume, with $i = 1.0$;
- increase of the pressure and new series of measurement;
- after the measurements at 1000 kPa, this pressure was maintained for 1.5 hours and then a set of measurements under 100 kPa was taken.

The values of measured discharge were reported to a standard temperature of 20°C with the formula:

$$q_{20} = q_T \left(\frac{\eta_T}{\eta_{20}} \right) \quad (5)$$

where: q_{20} , q_T = measured discharge at 20°C and at T°C;
 η_{20} , η_T = dynamic viscosity of water at 20°C and at T°C.

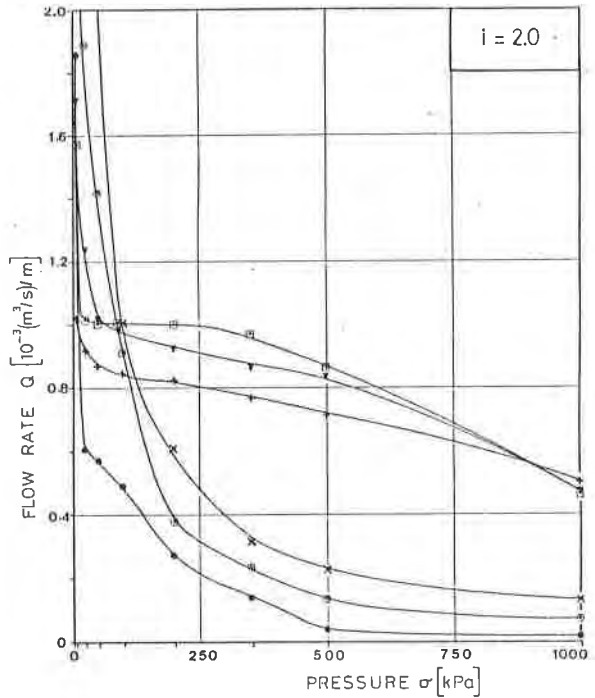
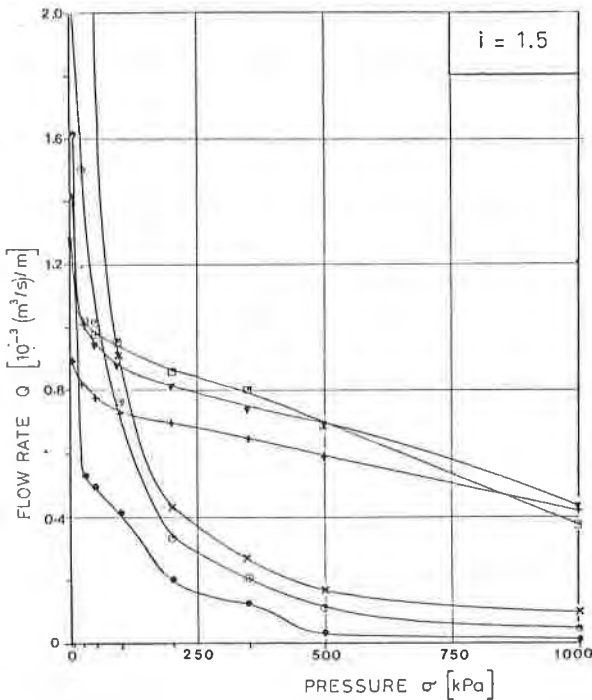
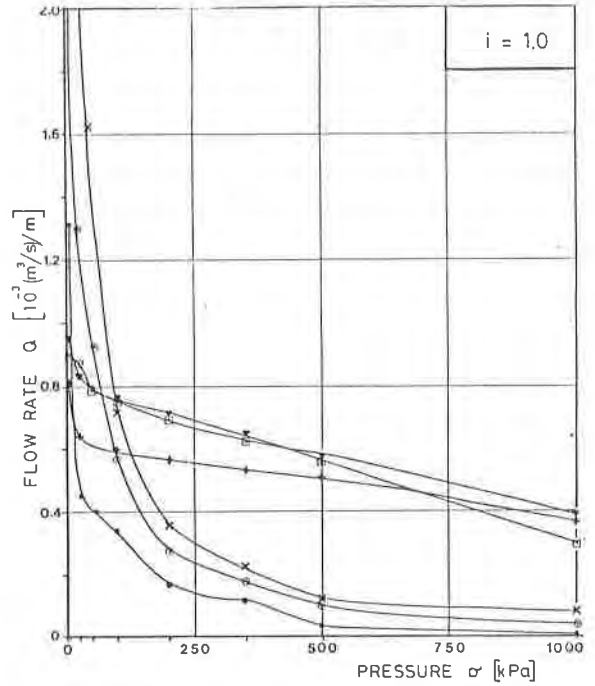
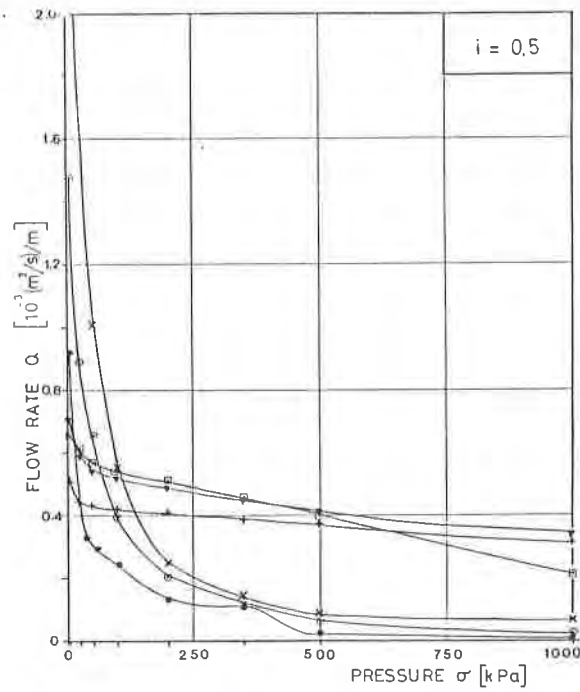
The obtained results (average values on 2 specimens) are plotted in Figg. 5 and 6.

From this experimental study, the following considerations can be drawn. Both Enkadrain products present the greatest values of flowrate, when the applied pressure is lower than 100-150 kPa; beyond this value the flowrate drops rapidly because of the high deformability of the core. For pressures greater than 100-150 kPa, Tenax products have the greatest flowrate values among the 6 tested geocomposites, thanks to the low deformability of the core (fig. 5); they exhibit also the greatest capacity of elastic return (fig. 6).

Filtram 1B1 seems to present two instability phenomena: to the Authors' opinion, this fact could be due, respectively, to the geotextile penetration into the core channels, and to the tilting of the upper strands of the net on the side of the lower ones, with a sudden closure of the openings for the water flow.

5. CONCLUSIONS

The paper presents some preliminary results concerning mechanical and hydraulic behaviour of a number of geocomposite products commercially available in Italy. Particularly, the experimental study has concerned tensile tests, compression-creep tests and transmissivity tests. To the Authors' opinion, the modalities of the different tests here presented could be taken into account in view of the development of an International Standardization for geocomposite products.



- FILTRAM 1B1
- x ENKADRAIN ST
- ⊙ ENKADRAIN TP
- + TENAX TNT
- ▼ TENAX TN
- TENAX MNT

Fig. 5 - Flow-rate vs. normal stress for different values of the hydraulic gradient

The results obtained from this co-ordinated research program emphasize the great influence of the core material and structure, particularly on compression-creep and transmissivity behaviour of the whole geocomposite.

In conclusion, it seems important to plan a further research effort, extending the tests presented in this paper to a wider series of geocomposites, also in order to achieve a lot of data inside each family of products (i.e. geotextile-core, geotextile-core-geotextile and geotextile-core-geomembrane).

ACKNOWLEDGEMENTS

The materials were supplied by RDB Plastotecnica (Mr. Beretta), ICI Italia (Mr. Nanni) and SEIC-Italian distributor of Enka (Mr. Fantini).

The tests were carried out by Mr. Bonfanti, Mr. Biella and Mr. De Feo (transmissivity tests), Mr. Fede (DSC analysis), Mr. Villa (tensile tests) and Mr. F. Iscandri, Mr. E. Iscandri and Mr. Rinaldi (compression-creep tests).

The typing was ensured by Mrs. Rocco.

REFERENCES

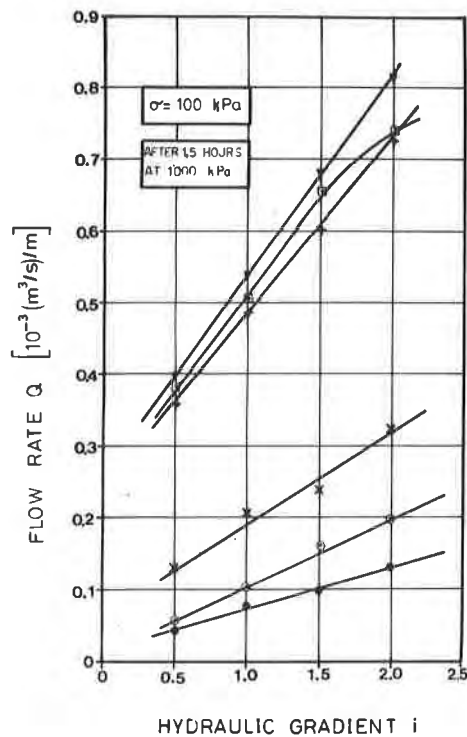


Fig. 6 - Flow-rate vs. hydraulic gradient of geocomposites.

- (1) CAZZUFFI, D. - FERRARA, G. - VENESIA, S. - D'ISCHIA, A. - SILVESTRI, T., "Transmissivity of geotextiles and related products: laboratory tests and practical applications", Proc. Third Int.Conf. on Geotextiles, Vienna, 1986, 879-884.
- (2) KOERNER, R.M. - LUCIANI, V.A. - FREESE, J.St. - CARROLL, R.G., "Prefabricated drainage composites: evaluation and design guidelines", Proc. Third Int.Conf. on Geotextiles, Vienna, 1986, 551-556.
- (3) MITCHELL, J.K., Fundamentals of Soil Behaviour, J.Wiley, New York, 1976.
- (4) BERTACCHI, P. - CAZZUFFI, D., "Geotextile filters for embankment dams", Water Power and Dam Construction, Dec. 1985.
- (5) KOERNER, R.M. - CARROLL, R.G. - LUCIANI, V.A., "Drainage geocomposites", Proc. Geotech.Fabrics Conf., Cincinnati, 1985.
- (6) VAN DEN BERG, C. - MYLES, B., Geotextile Testing: an inventory of current geotextile test methods and standards, IGS, 1986.
- (7) WILLIAMS, N. - GIROUD, J.P. - BONAPARTE, R., "Properties of Plastic Nets for Liquid and Gas Drainage Associated with Geomembranes", Proc. Int.Conf. on Geomembranes, Denver, 399-404.

ADAMS, K.L. and REBENFELD, L.
Princeton University, U.S.A.

Transient In-Plane Flow of Liquids in Fibrous Networks

INTRODUCTION

Among the many functions of geotextiles, none is more important than that of drainage. In such applications the permeability of the fibrous network is the critical physical property, although other properties such as strength, durability and stability are also of importance. Permeability is a material property that is dependent primarily on the pore structure of the network. In view of structure anisotropies that invariably exist in textile fabrics and other fiber networks, it can be expected that permeability will differ depending on the direction of fluid flow. A perfectly isotropic network with no preferred fiber orientation would have equal values of permeability in the three orthogonal principal flow directions. In view of the geometric dimensions of fibers, particularly the high aspect ratio (length to diameter ratio), and the common methods of fabric manufacture, complete three dimensional structural isotropy is rarely if ever achieved. Even two dimensional planar structural isotropy is difficult to achieve. For example, even in randomly air-laid nonwovens there is usually some degree of preferred fiber orientation corresponding to the machine or processing direction. Thus, typical fabrics (woven or nonwoven) can be expected to have three permeability values depending on the direction of fluid flow. One permeability would be associated with transverse flow (normal to the plane of the fabric), and two values would be associated with in-plane flow corresponding to the principal in-plane flow directions.

Transverse fluid flow in fiber networks has been rather extensively studied since this mode of flow is important in many end uses of fabrics, particularly as filter media. In-plane fluid flow, on the other hand, has not been accorded as much attention even though it is of great importance in geotextile applications and also in the formation of certain types of fiber reinforced composite systems. Several workers have studied in-plane flow of geotextiles under conditions intended to simulate use [1-3]. Particular attention has been given to the effects of lateral compressive stresses since geotextiles can be expected to be subjected to such deformations under typical end use conditions. Previous studies of in-plane flow related to geotextiles have focused on steady-state flow as a means of quantifying fabric permeability, expressed in terms of transmissivity (defined as the product of fabric permeability and thickness). The disadvantage of steady-state permeability measurements is that they do not provide an opportunity to detect and quantify in-plane directional permeabilities and in-plane flow anisotropies.

We wish to report a method whereby we are able to measure transient in-plane flow in fiber networks from which we can calculate directional permeabilities and a flow anisotropy index by appropriate analyses. While our method has been applied primarily to model woven fabrics, we feel that it has great potential for geotextiles and other planar porous materials. For reasons that will become obvious, our method relies on the use of high viscosity liquids. However, since permeability is an inherent material property reflecting pore structure, fluid properties (viscosity) and external variables such as driving pressure and temperature should have no influence.

EXPERIMENTAL

Materials

An epoxy resin, Shell Epon[®] 828 (Miller-Stephenson), was used as one of the experimental fluids. The viscosity of the resin is 145 poise at 25°C, as measured by a Cannon-Fenske capillary viscometer, and the fluid viscosity exhibits no shear rate dependence over the range of interest. A Dow Corning[®] 200 silicone fluid with a viscosity of 9.69 poise at 25°C was used in some of the measurements. Materials used in this study were a series of biaxially woven monofilament screening fabrics (Tetko), as described in Table I, and several typical nonwoven materials described in Table II.

TABLE I
STRUCTURAL PROPERTIES OF WOVEN TEST FABRICS

<u>Fabric</u>	<u>Type</u>	<u>Filament diameter</u> <u>μm</u>	<u>Mesh size</u> <u>μm</u>	<u>SETT (fil/in)</u>	
				<u>Machine</u>	<u>Cross</u>
3-50-297	Nylon, plain weave	200	297	52	51
HC 3-335	Nylon, " "	160	335	54	53
5-280	Polypropylene, " "	160	280	59	63
7-50-297	Polyester, 2/1 twill	200	297	51	52

TABLE II
STRUCTURAL PROPERTIES OF NONWOVEN TEST FABRICS

<u>Fabric</u>	<u>Type</u>	<u>Areal density</u> <u>(g/m²)</u>
Typar [®]	Polypropylene, spun bonded	116
Reemay [®]	Polyester, spun bonded	39
Geotextile I	Polypropylene, air-laid	158
Geotextile II	Polypropylene, air-laid	244

Apparatus

The experimental apparatus is illustrated in Figure 1. Two 15 cm square plates form the upper and lower boundaries of a radial flow region. The lower glass plate enables observation of the in-plane flow process, while the upper aluminum plate provides strength and excellent heat transfer. A 1 cm diameter inlet hole is centered in the upper plate, and a Teflon® shutter valve in the plate separates the flow region from a 6 cm diameter inner glass cylinder. This cylinder serves as a container for the fluid and is connected by flexible PVC tubing to a tank of pressurized nitrogen. The entire inner cylinder is surrounded by a 12 cm diameter polycarbonate outer cylinder. Thermostated water is passed continuously through the annular shell between the two cylinders to maintain a constant temperature, typically $25 \pm 0.5^\circ\text{C}$. A mirror is positioned just below the apparatus to enable either visual observation or photographic recording through the lower glass plate.

Procedure

One or more preweighed fabric layers of known dimensions, and with a precut hole in each layer, are aligned with the inlet hole of the aluminum plate and sandwiched between the aluminum and glass plates. The entire sandwich is secured with four c-clamps. After thermal equilibrium is attained, the sandwich thickness is measured with a micrometer, in four locations, and spacing deviations between locations are eliminated by readjusting the clamps. The desired driving pressure (in the 50-500 mm Hg range) is set by pressurizing the space above the fluid with compressed nitrogen, and the experiment is initiated by opening the shutter valve in the aluminum plate and allowing fluid to spread radially in the plane of the fibrous network. When the fluid front has advanced 0.5 cm, a stopwatch is started and the radial position and shape of the advancing front are monitored as a function of time. Two types of moving fronts are generally observed: circular isotropic fronts, and ellipse-like anisotropic fronts. In the general anisotropic case illustrated in Figure 2, the temporal advancement of the moving fluid front is recorded at 0.5 cm intervals, in the directions of maximum and minimum flow. θ , the angular displacement of the maximum flow direction relative to the machine direction of the fabric, is also noted. In the isotropic case, there is no unique θ value and data are only recorded in a single flow direction. The experiment is usually terminated when the advancing front exceeds a radial distance of 5.5 cm in all in-plane flow directions. At least three specimens are used to characterize a fabric assembly and the experimental results averaged. The data on a given fabric are normally reproducible to within 5% of the mean.

THEORY

The most general flow case, depicted in Figure 2, is the radial penetration of liquid into a homogeneous, anisotropic fibrous medium. At $t = 0$, liquid enters the porous material from a cylindrical boundary of radius R_0 . The liquid pressure at this position is P_0 . At a later time, t , the moving front is ellipse-like in shape and is characterized by its maximum and minimum radial extents, R_{f1} and R_{f2} , as well as the angular displacement, θ . The pressure at the moving front is P_f . The characteristic properties of the medium are the porosity, ϵ , and the thickness, h , which is large enough to neglect any flow resistance due to the boundaries yet small enough to minimize gravitational effects. Furthermore, the spreading process is considered pseudo-steady state.

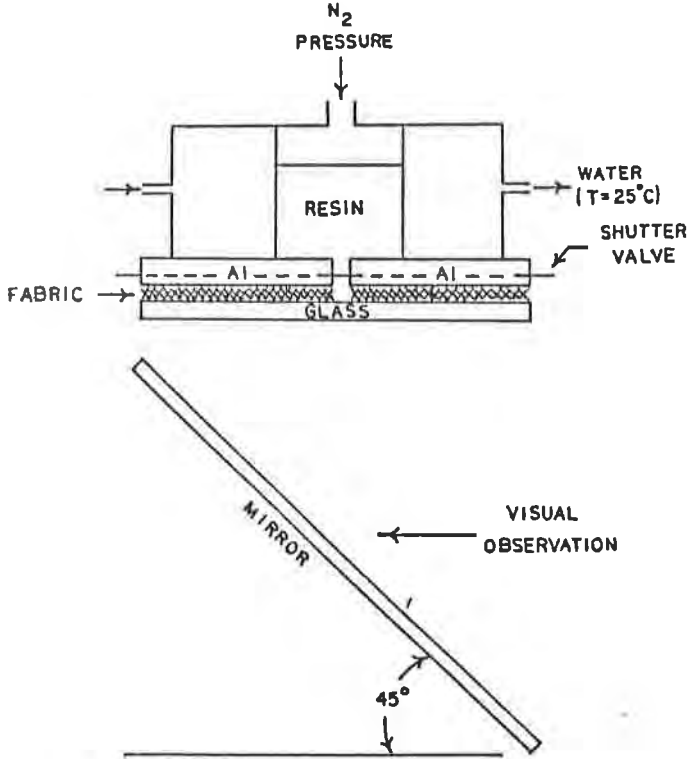


Figure 1

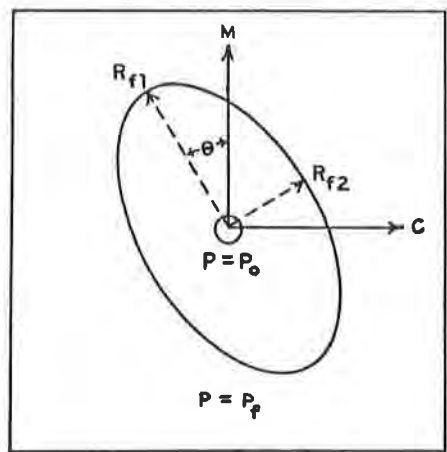
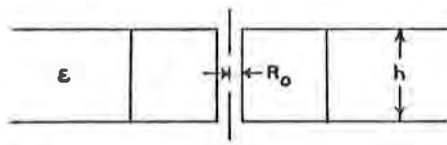


Figure 2

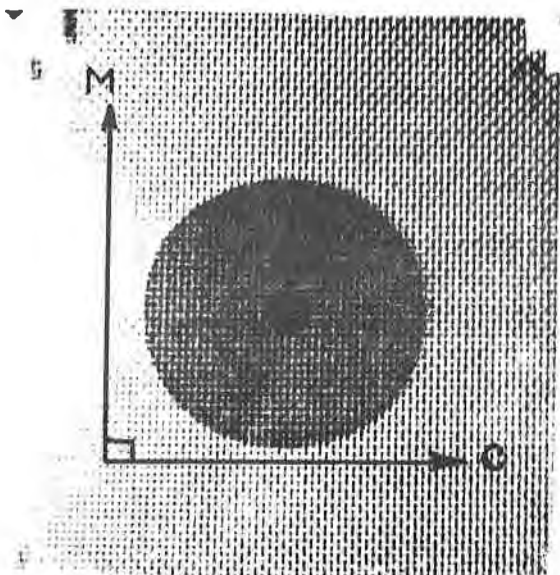


Figure 3 An isotropic flow front.

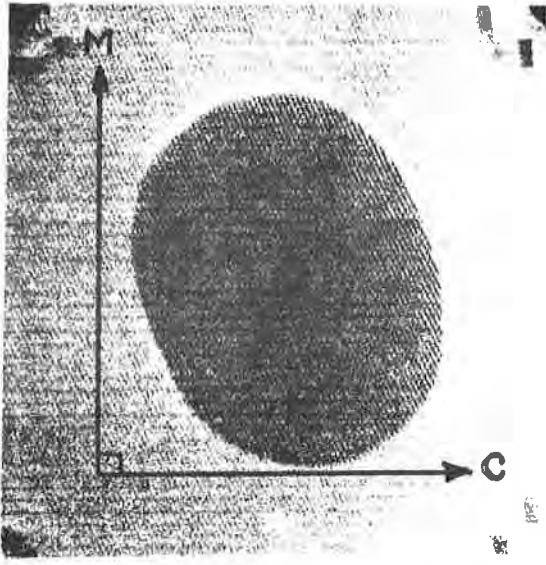


Figure 4 An anisotropic flow front.

The basic equations describing the fluid motion are the continuity equation for incompressible flow,

$$\nabla \cdot \underline{v}_0 = 0 \quad (1)$$

and Darcy's law,

$$\underline{v}_0 = \frac{-\underline{k} \cdot \nabla P}{\mu} \quad (2)$$

\underline{v}_0 is the superficial velocity vector, \underline{k} is the permeability tensor of the medium, and μ is the viscosity of the penetrating liquid. Combining Equations 1 and 2 in a rectangular coordinate system, x_1 - x_2 , corresponding to the principal flow directions of the medium gives

$$\frac{\partial^2 P}{\partial x_1^2} + \left(\frac{k_2}{k_1}\right) \frac{\partial^2 P}{\partial x_2^2} = 0 \quad (3)$$

Principal directions 1 and 2 are orthogonal and assumed to lie in the plane of the fibrous material. k_1 and k_2 are the in-plane principal permeabilities, and $\alpha = k_2/k_1$ is a measure of the degree of anisotropy of the medium. The boundary conditions associated with Equation 3 are the constant pressure requirements at the inlet hole and moving front. A final condition imposed at the moving front requires that the boundary propagate with the local fluid velocity at that surface,

$$\underline{v}_f = \frac{dx_f}{dt} = \frac{v_0}{\epsilon} \Big|_{R_f} \quad (4)$$

In Equation 4, the porosity is needed to convert the superficial velocity to a pore velocity.

Equations 2, 3, and 4 constitute a system of coupled equations that must be solved to predict the radial movement of a liquid front in an anisotropic fibrous network. The solution strategy involves solving Equation 3 for the pressure distribution, substituting this distribution into Equation 2 to yield the superficial velocity, and evaluating this result at the moving front in accordance with Equation 4. This procedure generates one or more ordinary differential equations which predict the temporal advancement of the liquid boundary. With the exception of the special isotropic case in which $\alpha = k_2/k_1 = 1$, the solution of this system of equations is nontrivial and will be reported elsewhere. For the purposes of this paper the isotropic and anisotropic data analyses will begin with the differential equations obtained from Equation 4.

Isotropic Data Analysis

For fabrics exhibiting circular fronts, such as that shown in Figure 3, the differential equation obtained from Equation 4, describing the motion of the boundary is

$$\frac{d(R_f^2)}{dt} = \frac{2k\Delta P}{\epsilon\mu} \frac{1}{\ln(R_f/R_0)} \quad (5)$$

where $k = k_1 = k_2$ and ΔP is the difference between the pressure at the inlet hole and the liquid front. The porosity, ϵ , is determined from properties of the fibrous network,

$$\epsilon = 1 - \frac{W}{\rho h A} \quad (6)$$

where W is the total mass of the test assembly, ρ is the material solid phase (fiber) density, h is the total in-plane flow thickness, and A is the area of the fibrous flow plane. The thickness is determined from the difference between the total sandwich thickness and the thickness of a no-fabric blank. Since ΔP is specified experimentally and μ is a known property of the fluid, discrete $R_f(t)$ data may be plotted in the form of $d(R_f^2)/dt$ vs. $1/\ln(R_f/R_0)$ as suggested by Equation 5. From the slope of the least squares line through the origin, m , one can obtain the isotropic in-plane permeability,

$$k = \frac{m\epsilon\mu}{2\Delta P} \quad (7)$$

Anisotropic Data Analysis

For fiber networks exhibiting ellipse-like moving boundaries, such as that shown in Figure 4, the differential equation obtained from Equation 4 describing motion in the maximum flow direction is

$$\frac{d\xi_{f1}}{dt} = \frac{k_1\Delta P}{\epsilon\mu R_0^2} \left(\frac{\alpha}{1-\alpha} \right) \cdot \frac{1}{(\xi_{f1} - \xi_0)(\cosh^2 \xi_{f1})} \quad (8)$$

and that describing motion in the minimum flow direction is

$$\frac{d\xi_{f2}}{dt} = \frac{k_2\Delta P}{\epsilon\mu R_0^2} \left(\frac{\alpha}{1-\alpha} \right) \cdot \frac{1}{(\xi_{f2} - \xi_0)(\cosh^2 \xi_{f2} - 1)} \quad (9)$$

ξ_{f1} and ξ_{f2} are equivalent elliptical extents in the principal flow directions and are related to the radial extents by

$$\xi_{f1} = \sinh^{-1} \left(\frac{R_{f1}}{R_0} \left(\frac{1}{\alpha} - 1 \right)^{-1/2} \right) \quad (10)$$

and

$$\xi_{f2} = \cosh^{-1} \left(\frac{R_{f2}}{R_0} (1 - \alpha)^{-1/2} \right) \quad (11)$$

In addition, ξ_0 is the elliptical equivalent of the inlet hole radius and is given by

$$\xi_0 = \ln \left(\frac{1 + \alpha^{1/2}}{(1 - \alpha)^{1/2}} \right) \quad (12)$$

The anisotropic data analysis is iterative in the degree of anisotropy, $\alpha = k_2/k_1$. First, α is guessed and the experimental data are converted to equivalent elliptical extents using Equations 10 and 11. Analogous to the isotropic case, these discrete directional extents are then plotted as suggested by Equations 8 and 9. If α is chosen correctly, the slopes of the least squares lines through the two sets of directional data will be equal and given by

$$m_{\xi} = \frac{k_1 \Delta P}{\epsilon \mu R_0^2} \left(\frac{\alpha}{1 - \alpha} \right) \quad (13)$$

Knowledge of the experimental variables (ΔP , ϵ , μ) permit quantification of k_1 , the principal permeability of the 1 direction. Subsequently, k_2 is determined directly from α . If α is not chosen correctly, the algorithm must be repeated until the slopes converge. The entire procedure is conveniently performed on a microcomputer.

As a first order approximation to this complex anisotropic data analysis, the isotropic working equation (Equation 5) may be applied to directional flow data. Although numerically inaccurate, this method would provide a quick means of establishing trends in experimental data and assessing approximate degrees of anisotropy.

RESULTS AND DISCUSSION

Woven Test Fabrics

A first test of the theoretical analyses is the degree to which experimental data adhere to the isotropic and anisotropic working equations. Typical experimental data for the three isotropic fabrics are shown in Figure 5, plotted as

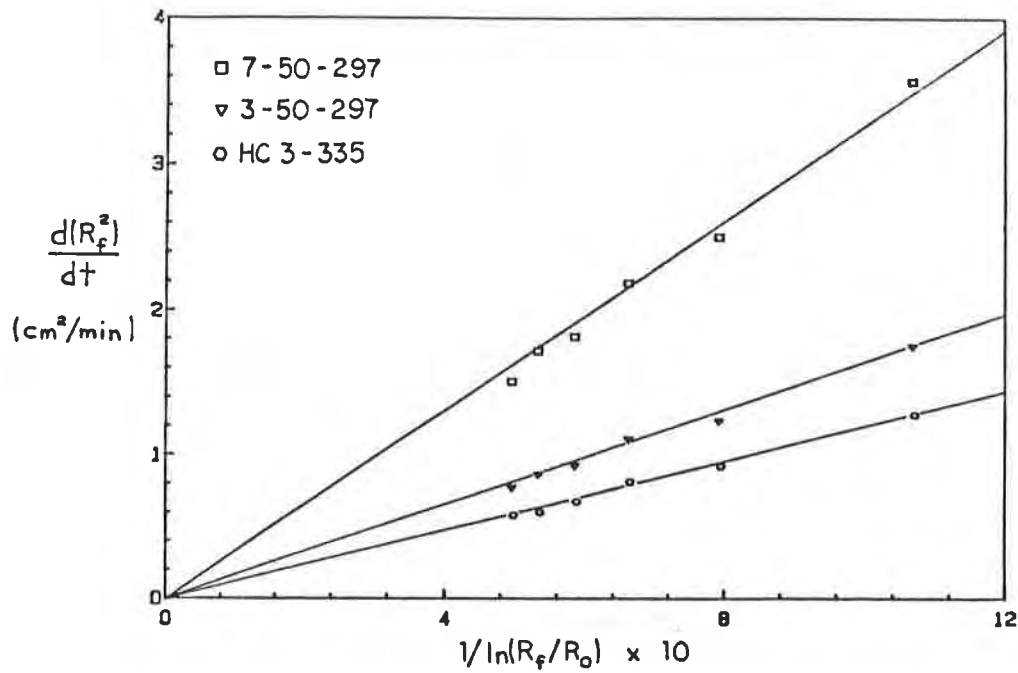


Figure 5 Typical data for isotropic flow plotted according to equation 5.

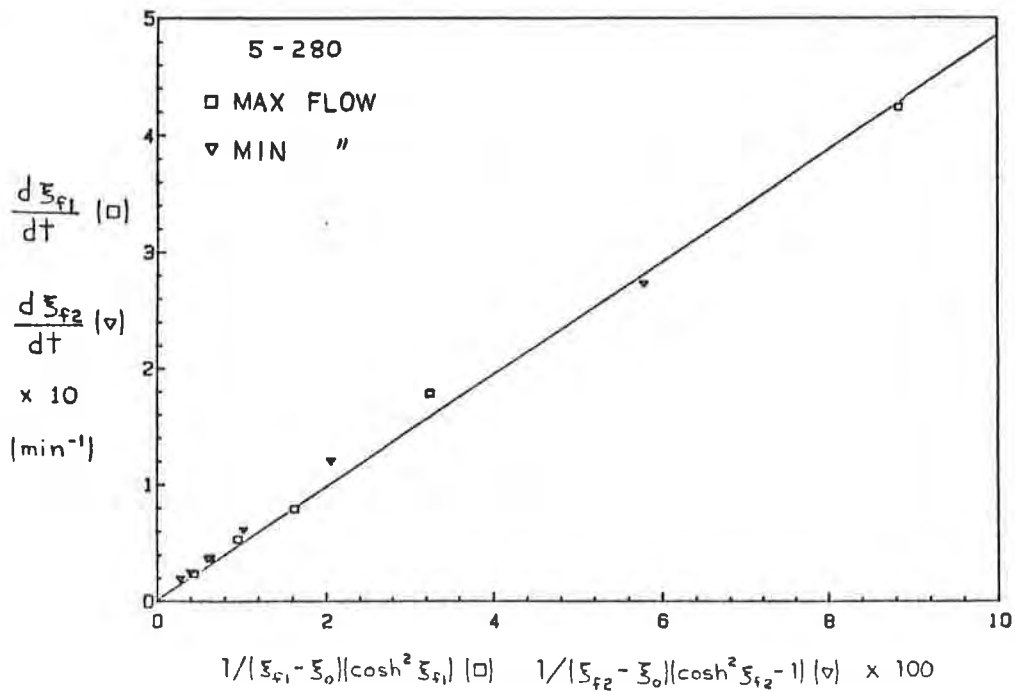


Figure 6 Typical data for anisotropic flow plotted according to equations 8 and 9.

$d(R_f^2)/dt$ vs. $1/\ln(R_f/R_0)$. In all three cases, the data correlate well with least squares lines forced through the origin. Good agreement between theory and experiment is also seen for anisotropic flow data. As illustrated in Figure 6, experimental data taken in the directions of maximum and minimum flow for anisotropic fabric 5-280 agree with the functional dependencies of Equations 8 and 9. The directional data lie on a single line forced through the origin only when α , the degree of anisotropy, is chosen correctly. Permeability values (k) and anisotropy indexes (α) calculated from the slopes of the lines in Figures 5 and 6 according to Equations 7 and 13, respectively, are shown in Table III. The differences among the permeabilities of the woven test fabrics can be explained in terms of the varying pore structures created by the different weaves and mesh sizes of the fabrics (see Table I) as discussed in our earlier publication [4]. The in-plane flow anisotropy exhibited by fabric 5-280 is due to the imbalance of the sett.

TABLE III

IN-PLANE FLOW PROPERTIES OF WOVEN TEST FABRICS

<u>Fabric</u>	<u>Permeabilities</u> (darcy)		<u>Anisotropy</u> index $\alpha = k_2/k_1$
	<u>k₁</u>	<u>k₂</u>	
3-50-297	463	463	1.0
HC-3-335	541	541	1.0
5-280	453	309	0.7
7-50-297	817	817	1.0

The permeabilities obtained from the slopes of the isotropic and anisotropic data plots are property constants of the fibrous material, independent of the flowing fluid. This is demonstrated by the fact that varying the fluid viscosity (from 62 to 200 poise by varying temperature from 22 to 30°C), and varying the driving pressure (from 50 to 200 mm Hg) had no effect on the permeability values.

Furthermore, according to the present analysis, two fabrics with identical structural features (pore structure) will have identical in-plane permeabilities, regardless of fiber type. This is because the experimental driving pressure is large enough to ignore capillary pressures in the system, i.e., fiber surface wettability effects are not significant. As a means of demonstrating this fact the fiber surface properties of the test fabrics were altered by treatment with an aerosol mold release agent (MS-122 Miller-Stephenson) containing polyfluoroethylene solids. In-plane flow characteristics of the treated and untreated fabrics were evaluated, and there were no appreciable differences in in-plane permeabilities resulting from the fiber surface treatment.

Nonwoven Test Fabrics

The results of in-plane flow studies of the nonwoven fabrics are summarized in Table IV.

TABLE IV
IN-PLANE FLOW PROPERTIES OF NONWOVEN TEST FABRICS

<u>Fabric</u>	Permeabilities (darcy)		Anisotropy index
	<u>k₁</u>	<u>k₂</u>	<u>α</u>
Typar®	165	165	1.0
Reemay®	403	287	0.71
Geotextile I	173	173	1.0
Geotextile II	243	243	1.0

Nonwoven fabrics do not possess an obvious set of principal flow directions, and the flow patterns can be expected to reflect the fiber orientation distributions in the material. Isotropic flow patterns for nonwovens can usually be associated with a completely random distribution of fiber orientations in the plane of the fabric, while flow anisotropies can be expected if the distribution of fiber orientations is not random. The direction of maximum flow can most likely be associated with the preferred fiber orientation of the material. Typar®, a spunbonded polypropylene, exhibited flow isotropy, while an in-plane flow anisotropy was observed for the Reemay®, a spunbonded polyester fabric. The geotextile I material produced uniform isotropic fluid fronts from which average permeability values of 173 darcy in the two principal in-plane flow directions could be readily derived. On the other hand, the geotextile II material produced nonuniform and irregular fluid front shapes, although these shapes still correspond to circular rather than elliptical patterns. Permeability values for geotextile II in both principal in-plane flow directions were estimated to be equal, corresponding to $\alpha = 1.0$, and somewhat higher than for geotextile I. However, the irregular shape of the fluid front for geotextile II indicates a high degree of localized structural nonuniformity. This feature of a fibrous material is easily detectable from our transient in-plane flow experiment, and we are now developing a suitable means of quantifying this important characteristic utilizing computerized image and edge analyses.

Multilayer Assemblies

In many applications, fibrous networks are used in the form of multilayer assemblies of either similar or dissimilar materials. In the case of heterogeneous assemblies, where the layers are composed of different fabrics, the effective in-plane flow characteristics of such assemblies are likely to be a complicated function of the flow properties of their constituent layers. Initial experiments have been undertaken to study these systems.

The two materials used in this study were the isotropic model fabrics, 3-50-297 and 7-50-297. Table V gives in-plane permeability data for two-layer assemblies constructed from these fabrics. In the assembly column, L (low permeability) denotes a 3-50-297 layer, H (high permeability) denotes a 7-50-297 layer, and the sequence reflects their order.

TABLE V
PERMEABILITY DATA FOR 3-50-297/7-50-297 ASSEMBLIES

	<u>Assembly</u>	<u>ϵ</u>	<u>k (darcy)</u>
2-layer homogeneous	LL	0.553	525
	HH	0.654	1051
2-layer heterogeneous	HL	0.604	1011
	LH	0.605	912
	average	0.604	962

The results in Table V indicate that the heterogeneous assembly has a permeability almost as high as the high permeability layer itself. In other words, it appears that the permeability of a two-layer assembly is governed by the high permeability layer. This is at first not obvious and it might have been expected that the permeability of the two-layer assembly would be dictated by the low permeability component. We have evidence that the same observation holds for three- and four-layer combinations. This aspect of our work is continuing and will be reported in a future publication where we propose that a transverse flow mechanism is responsible for filling the low permeability layers and keeping the macroscopic liquid front uniform.

Conclusion

The in-plane flow characteristics of fibrous networks are not only important properties of these materials but are also very sensitive indicators of fabric structure. The in-plane flow apparatus and data analysis described in this paper provides an effective means of quantifying these properties for isotropic and anisotropic fabrics. Directional permeability values, independent of driving pressure, fluid viscosity, and surface wettability, are obtained using this technique and may be used to compare structurally different fibrous networks. The technique is also most effective in demonstrating flow and structural anisotropies and in detecting localized nonuniformities and irregularities.

Acknowledgement

The authors are pleased to acknowledge the assistance and cooperation of Ms. Susan M. Montgomery, TRI Research Fellow, in connection with the data on the geotextile materials.

REFERENCES

1. Koerner, R. M., Bove, J. A., and Martin, J. P., Water and Air Transmissivity of Geotextiles, Geotextiles and Geomembranes, 1, pp 57-73 (1984).
2. Raumann, G., In-Plane Permeability of Compressed Geotextiles, Proceedings Second International Conference on Geotextiles, Las Vegas, NE, USA, August 1982, pp 55-60, Industrial Fabric Association International, St. Paul, MN.
3. Bucher, F., Jeger, P., and Sterba, I., Results of Permeameter Tests on Statically Loaded Geotextiles, Proceedings Second International Conference on Geotextiles, Las Vegas, NE, USA, August 1982, pp 845-850, Industrial Fabric Association International, St. Paul, MN.
4. Adams, K. L., Miller, B., and Rebenfeld, L., Forced In-Plane Flow of an Epoxy Resin in Fibrous Networks, Polym. Eng. Sci., 26, pp 1434-1441 (1986).

SNYDER, J.O.

GeoTech Systems Corporation, U.S.A.

The Use of Geosynthetics in Conjunction With Three-Dimensional Drainage Cores

Paralleling the steady increase in the use of geosynthetics in recent years has been the equally expanding market for geocomposites; products which are significantly dependent upon their incorporation of geotextiles. Geocomposites, which may be defined more accurately as prefabricated drainage structures, have established themselves as a significant market for geosynthetic materials. Indeed, most of these products depend entirely on the integrity of a geotextile for their ability to function. Because of this integral relation of geotextile to geocomposite, and realizing the rapidly increasing number of new such products in the marketplace, a brief examination of the relative design and performance of these drainage products becomes desirable. It is the intention of this paper, therefore, to review the more prevalent forms of geocomposites in an effort to report on this comparatively new avenue for the use of geotextiles.

Although prefabricated drainage structures have seen widespread acceptance and use mainly within the last two to three years, they are, in fact, a concept which has been established for some time. One product, made of a core of molded plastic, was first developed in the United States approximately fifteen years ago. Another design, using beads of expanded polystyrene, is a West German concept which has been used extensively in Europe for nearly twenty years. Like most new developments in construction techniques, these products have experienced a slowly increasing acceptance as a replacement for more historically conventional methods of dealing with drainage. Increasingly, however, geocomposites are becoming an accepted standard in construction design and specification.

The primary function of the geocomposite is to provide a consistent medium for the flow of groundwater down and away from below-grade walls, to some form of perimeter drain system. Placement of geocomposite sheets or panels over a below-grade structure will thus help to relieve the potential for hydrostatic pressure build-up, and helps prevent the failure of waterproofing systems. In this way potential damage to the structure as a result of pressure or leakage can be reduced. In the past, the only method for providing a similar drainage medium was through the use of granular backfills. A layer of gravel or coarse sand would be placed around the foundation, which would improve upon the drainage capacity of the soil which was removed. Though this has been an accepted practice, it nonetheless has proven to be time consuming, complicated, and costly. The movement and placement of large quantities of granular fill obviously requires significant effort in regard to equipment and manpower; and

placement of such layers in reasonably even, consistent dimensions requires excessive time and labor.

In Europe, where gravel is far less easily available than in some areas of the United States, and site conditions often limit available storage and work areas, a new concept in providing drainage was developed in the late 1960's. Using a porous panel composed of expanded polystyrene beads, affixed directly to the foundation's waterproofing layer, it was possible to achieve excellent flow rates in a lightweight and easily installed product. Today, a wide variety of related products is available, but all of them are based on the principle of providing a drainage core in a lightweight, easy to use product.

At present there are three basic designs for geocomposites, and they may be generally classified as either single-function products (providing drainage capabilities only) or multi-function products (offering additional product characteristics to drainage). One product is comprised of a core of waffle-shape molded plastic, one side of which has been covered with a geotextile. Recently, a wide variety of variations on this waffle-core have appeared. These include plastic core products which are of a thin corrugated or diamond grid configuration, which act more as wicks in providing drainage. As the waffle-core product was the original concept - and remains the most prevalent of these forms - we will refer only to this one form in subsequent discussions. A second geocomposite design is constructed of a sheet or roll of rigid nylon meshed fibers. This product also has a filter fabric attached to one side. Both of these forms of prefabricated drainage structures are marketed solely as products providing below-grade drainage capabilities. Like granular backfills, and due to their often sharp surfaces, they must be installed over some form of protection board, to prevent damage of the waterproofing membrane, (although a one-sided variation of the waffle form has recently appeared which has limited acceptance against some waterproofing membranes). Also, due to their respective configurations, the geotextile facing plays a primary part in their performance. Maintaining the strength and integrity of the filter fabric is critical, as sagging or tearing of the fabric would render the product useless. At present, the aforementioned products are offered with only one grade of geotextile facing; a factor which should be considered for projects involving soil conditions which may not be compatible with the fabric facing provided. Examination of backfill materials and consultation with a soils engineer would thus be recommended. The third design - the original West German concept - involves a panel composed of large beads of expanded polystyrene (EPS) which have been radially bonded with a bituminous emulsion. Although solid in appearance in comparison to the other structures, this configuration provides a panel with excellent porosity. Also, because of its EPS composition, (EPS being a superior insulation), this product provides significant additional insulation values. Lastly, because of its smoother surfaces and the resiliency of EPS, the panel serves as its own protection board for the waterproofing membrane, preventing damage during backfill and compaction. Although available as a plain panel, this product is offered with a variety of geotextile facings, providing protection from soil fines infiltration. A fourth product, made of fiberglass panels with oriented strands, has also recently appeared. It serves primarily as a protection and insulation board, but has been shown to provide wick-action

drainage capabilities as well.

The primary use for geocomposites has been, as indicated, as a drainage medium for building foundations. They are all intended for use only in conjunction with a perimeter hydrostatic pressure relief system, regardless of the application. In below-grade building areas, the standard application in open-wall construction is to install a perforated drain pipe along the foundation footing, held in place with a small amount of gravel. The geocomposite is then installed on the foundation wall, with protection board as required over the waterproofing, running from the footing to within a few inches of groundlevel. Some of these products may also be incorporated into below-grade projects involving property line construction (versus open-wall construction). In this instance the geocomposite is attached to the wooden lagging, a geotextile or polyethylene slipsheet is placed over it to prevent concrete infiltration, and the concrete wall is then poured directly against the drainage product. Groundwater would then be channeled down through the geocomposite to a system of weepholes around the building perimeter, which would permit water flow into the interior drain system for discharge.

Whereas most geocomposites are specified for use in commercial building foundations, some are finding steadily increasing markets in residential construction. And prefabricated drainage products are not limited to building applications alone. Virtually any form of retaining wall - from building foundation, to highway retaining wall, to garden wall - requires some method of hydrostatic pressure relief. In retaining walls, when applied in conjunction with a system of weepholes, geocomposites provide the same function as in building foundations. Some of the drainage products also function well in landscaping applications. By lining either exterior or interior planters with certain of these geocomposites, a consistent soil environment for plants can be maintained; and root systems can be kept out of standing water. Certain designs provide additional functions unique to their product design or composition. The aforementioned wire mesh product, for example, is actually a geosynthetic itself. This product originally was developed for soil retention applications, and is widely used for this. The EPS panel, which was first developed specifically for use on buildings, is now seeing use in a variety of other applications. Because this product is molded in large blocks, it is possible to cut it in thicknesses from 2.54cm to 60.96cm (1" - 24"). This makes it particularly desirable as a means for providing a lightweight, porous fill in areas where weight is of concern. In landscaped roof applications, for example, this material may be used to replace numerous inches of soil in planters, thus greatly reducing weight loads. This is equally true for any form of below-grade roof structure, as a drainage channel of significant thickness can be provided, reducing earth loads. As noted before, the insulation and protection value of this product is unique as well; and the product is, in fact, marketed not solely as a drainage medium, but as a combination of its performance characteristics.

Factors determining the selection and application of specific geocomposites are numerous, as the products vary greatly. If it has been determined that a hydrostatic pressure relief system is recommended for dealing with groundwater, (as it is for the vast majority of buildings), two factors are then of primary

consideration: groundwater flowrate and soil pressure. As a geocomposite normally will not be specified in cases involving excessive flowrates, almost any of the available products are designed to more than accommodate for typical groundwater conditions. However, foundation depth and the resultant pressures encountered at greater depths must be closely considered, due to the compressibility or physical structure of the various products. The waffle-core design, for example, retains its rigidity at significant depths; however, its performance under such pressures is entirely dependent upon the ability of the filter fabric facing to resist the same pressures, while bridging large open areas of the core matrix. Should soil pressure be great enough to cause sagging or tearing of the geotextile, the performance of the product could be seriously affected. The nylon wire mesh product, on the other hand, is highly compressible, and would obviously experience a marked decrease in flowrate as soil pressures increase. The EPS bead panel also is susceptible to deflection under significant soil pressures. However, this may be compensated for quite easily by increasing the recommended product thickness, as the depth increases.

Application techniques should be a final and equally important consideration in reviewing the variety of available geocomposite drainage designs, particularly in the way that a product's installation will affect the waterproofing membrane already in place. In installing most of the plastic waffle-core products, a 1.22m by 2.44m (48" x 96") sheet is mechanically attached to the foundation wall. This may involve significant damage to the waterproofing membrane, which can be of significant concern. The sheet is installed obviously, with the geotextile facing outward, and the sheets are overlapped by several inches to cover seams. This factor should be considered when calculating required amounts of material, as the surface area of each sheet will be reduced by a notable percentage. Backfilling against the sheet - generally to the full height of the installed row of sheets - should preferably be accomplished quickly, to avoid exposing the material to possible construction site damage. Application practices for the wire mesh product are virtually the same as for the plastic core. It is possible, however, to purchase this product in long rolls, if desired. This permits fastening of a roll at the top of the foundation, and can provide a single sheet of geocomposite from there to the footing. This is helpful if the structure is to be backfilled in the near future, but installation in rows of small sheets is more practical if backfilling is to be done in lifts. The EPS product requires no mechanical fasteners, and will not affect the waterproofing in any way. This product is offered in 1.22 by 1.22m (48" x 48") panels (although the material may be factory cut to any size smaller than this), generally in a 5.08cm (2") thickness (again, however, available in any thickness to 60.96 cm). The panels are abutted edge to edge, with a selvedge strip on the geotextile facing serving as a protection for the seams. Attachment is with an adhesive, available from the manufacturer, which is applied in dabs. After application of the adhesive, the panel is pressed onto the waterproofing, and backfill is suggested after installation as well.

Although they are diverse in both design and performance, the increasingly popular concept of the geocomposite is rooted in a single, common quality: the ability to effectively protect below-grade walls and roofs from exposure to, and

pressure from, groundwater. In so doing, these products have greatly improved upon the effectiveness of basement walls, and actually help to increase usable building space by making below-grade spaces more inhabitable. The insulating EPS product, in particular, can help to control mildew and dampness, as well as reduce heating costs for these areas, thus actually providing a return on investment. All, however, offer far greater security against building leaks; and that alone makes inclusion of a geocomposite in any building project below-grade both a sensible and desirable addition.

SMITH, A.D. and KRAEMER, S.R.
Haley & Aldrich, Inc., U.S.A.

Creep of Geocomposite Drains

ABSTRACT

Geocomposite drains are one of the newest geosynthetics to be applied to civil engineering projects. Proper application of the diverse products requires a thorough understanding of the performance characteristics of the drain system. However, only limited information is available on the tendency of the products to creep when exposed to long term stresses. In addition most of the published data regarding creep have been developed using apparatus with boundary conditions which differ significantly from in-situ conditions.

A testing program was conducted to study the tendency of geocomposite drains to creep and to evaluate test methods for quantifying creep behavior. The program included compression tests, two types of creep tests, and in-plane flow tests. The results have been analyzed to provide a comparison of test methods and product performance, and design guidance with respect to the anticipated long term creep performance of the tested drains. The analysis of the test results was concentrated on creep behavior since signs of creep were observed in all of the test types, and because important performance characteristics of the drains can be overlooked without a better understanding of creep behavior.

INTRODUCTION

The use of prefabricated drainage systems (referred to hereafter as geocomposite drains) for geotechnical applications is increasing rapidly. Their proper use is complicated because the products and technology are being introduced to the marketplace faster than design engineers can gain adequate and reliable information on the products, appropriate useage and design criteria. Only recently have detailed relevant information on geocomposite drain products, testing of critical characteristics, and design considerations including specifications been available (6, 7).

Geocomposite drains, also referred to as in-plane drains, are specially fabricated for subsurface drainage applications and are typically constructed of a geotextile and a semi-rigid plastic core. The major function of the drain system is to collect and transport subsurface water with each of the components serving different functions in the drainage process. The system design of the drain

product requires consideration of the component properties, but the system characteristics relative to the service conditions determine whether or not the geocomposite drain will function satisfactorily (i.e., collect and transmit subsurface water adequately).

The major function of the drainage core is to transmit water which passes through the geotextile with as little head loss as possible. Accordingly, the hydraulic flow resistance properties of the core under confining stress are important. The potential effect of confining stresses to reduce the core cross-sectional area and therefore increase the hydraulic resistance can be critical to the drain design and performance.

An important characteristic for satisfactory performance is the ability of the drain to resist the imposed stresses without detrimental deformation with time. Creep, deformation under constant stress over time, is a major consideration when evaluating a geocomposite drain application and/or drain product. Creep of concrete, soil, plastics, and other engineering materials is a well documented phenomenon (8), which is normally subdivided into three stages - primary, secondary, and tertiary creep (see Figure 1). Primary creep occurs just after the initial instantaneous deformation and prior to secondary creep, which is identified by a constant rate of deformation. After a period of secondary creep and depending on the stress level, tertiary creep, identified by an steadily increasing creep rate, may occur until failure.

Various theories have been proposed to predict the creep behavior of materials including polymers (8); however, many of the models that have been developed consist of mechanical spring/dashpot elements which can model the behavior of simple systems reasonably, but can not accurately predict the performance of a relatively complex system like geocomposite drains. Therefore, designers are currently forced to utilize limited available creep test results and considerable engineering judgement when considering creep tendency of geocomposite drains.

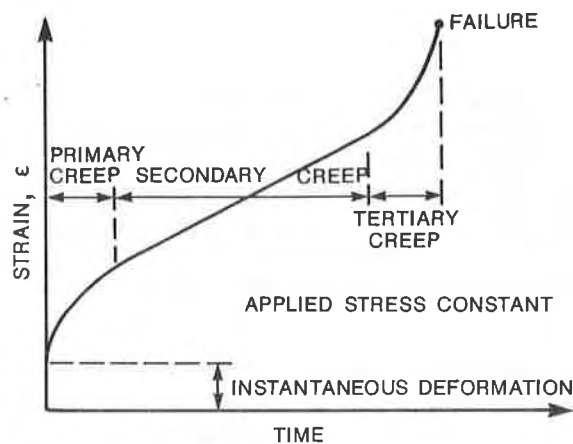


Figure 1 Typical stages of creep.

The reduction in cross-sectional area available to transport water, due to deformation of the geotextile and/or drainage core, may occur with time under constant stress due to creep of the drain system components. The potential for significant creep effects is an important concern especially for drain applications with a long design service life, with a relatively high applied confining stress compared to the drain ultimate strength, or when there are significant adverse consequences of poor drain performance.

Satisfactory drain performance depends on the service conditions (applied stresses, soil and groundwater, etc.) and interdependent characteristics of the drain system components. Four characteristics of geocomposite drain systems which were studied during the subject research include: 1) compressive strength, 2) in-plane flow capacity, 3) hydraulic properties of the geotextile, and 4) creep characteristics of the system.

Compressive strength is one measure of a drain's short-term ability to withstand the stresses imposed on the drain by the adjacent soil and other sources including transient loads due to vehicular traffic or construction traffic. The in-plane flow capacity of the drain is also an important characteristic. In-plane flow capacity is a function of the drain geometry and materials, the magnitude and duration of the applied stresses, and the influence of the adjacent soil or confining medium. The hydraulic properties of the geotextile include filtering and clogging (1, 2).

Prior to this research, published information on laboratory testing of geocomposite drain products has concentrated on testing of systems (geotextiles and drainage cores) and on the hydraulic transmissivity (i.e., flow capacity within the plane of the drainage core) of the systems in a confined state (3, 9). Although most of the testing suggested substantial creep effects, the magnitude of creep and its possible consequences had not been directly addressed.

TESTING PROGRAM

The scope of the testing program was to review previous geocomposite testing and to develop simple test methods for comparing the performance of different products. The subject testing was focused on the system or core for three reasons: 1) There is a continuing need for comprehensive comparative test results on drain systems; 2) Design engineers interested in a specific project will most likely test systems; and 3) There are a multitude of geotextiles that might be used in a geocomposite drain and therefore, any geotextile-dependent testing (i.e., permeability and clogging testing) would pertain only to the soil/geotextile selected for testing.

The program of testing consisted of four different types of tests: compression tests, core creep tests, system creep tests, and in-plane flow tests. A description of each test type, and a complete record of data are available in the final reports (5, 6). For illustration, the tests and the results for three specific products are described briefly below. Inclusion of the test results for the three products is not intended to be a comparison of their relative performance. The products discussed here include:

<u>Product Name*</u>	<u>Core</u>	<u>Geotextile</u>	<u>Total Thickness</u>
HITEK™ Cordrain™	high density polyethylene	Typar 3401 (spun bonded polypropylene)	2.1 cm (0.82 in.)
Miradrain™ 4000	high impact polystyrene	Mirafi 140N (needle punched polypropylene)	1.9 cm (0.75 in.)
Stripdrain 75	high density polyethylene	Trevira S61170 (polyester)	1.9 cm (0.75 in.)

*Manufactured or distributed by Burcan Manufacturing, Inc.; Mirafi, Inc.; and Armco, Inc. respectively.

These products were selected for inclusion in this paper because they all have cusped waffle cores of similar thickness and wavelength, and the cores in the HITEK™ Cordrain™ and Stripdrain 75 are identical in composition. Other products were tested in the study and the results are presented in the final reports (5, 6).

"Quick" Compression Tests:

Compression tests were performed because the test is a simple yet useful procedure which is performed on a wide variety of engineering materials, and the equipment for performing the test is readily-available in most geotechnical and materials testing laboratories. The products were loaded to failure in compression between flat metal plates oriented parallel to the plane of the core in a standard compression machine at a strain rate of approximately 10 % per minute. The 10.8 cm (4.3 in.) square samples were tested dry at room temperature. The results of the "quick" compression tests (see Figure 2) indicate that all three products exhibit definite yielding at stresses ranging from about 172 to 276 kPa (25 to 40 psi) at strain levels of about 10%. The performance after initial

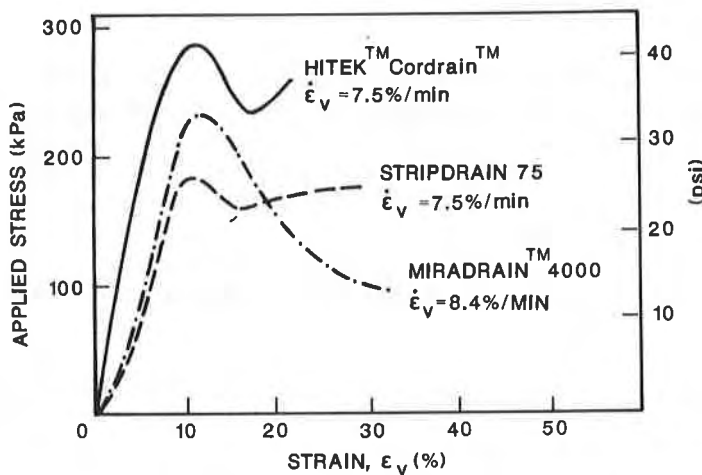


Figure 2 Compression test results for three geocomposite drain samples.

yielding differed considerably. The Miradrain™ 4000 sample exhibited a significant drop in residual strength which is characteristic of polystyrene (8). The HITEK™ Cordrain™ and Stripdrain 75 exhibited greater residual strengths. The "quick" compression test was found to be a good index test to differentiate among and compare products, but it has limited applicability for determining design parameters due to the significant differences between the testing configuration and service conditions.

Core Creep Tests:

All of the available geocomposite drain products known to the authors have cores formed of thermoplastic polymers. Such polymer materials are viscoelastic, that is, exhibit elastic deformation during relatively rapid increasing stress and creep under constant stress. As a result of creep strain, the available flow area in the core, and possibly the effectiveness of the drain, can be reduced with time under constant stress conditions. To evaluate the potential for creep deformation of the polymer cores, constant stress creep tests similar to those performed by Luciani (7) were performed by loading samples of the geocomposite cores between rigid plates and measuring the resulting deflection under constant stress. Since the applied stress is carried primarily by the core due to the rigid boundary conditions, these tests were referred to as core creep tests.

The core creep tests were performed by placing 10.8 cm (4.3 in.) square drain samples in a close fitting metal box with rigid plates on all sides of the sample to achieve a plane strain condition. A stress was applied by means of a lever arm soil consolidometer. Assuming that the plate was rigid, the applied load results in a uniform displacement of the plate with a non-uniform stress transferred to the sample. The resulting displacement was measured as time progressed using a dial gauge. After the desired data were recorded (up to three days elapsed time), the applied load was increased and the process repeated.

Results of the core creep tests indicate that the polymer cores creep under stress with time. The magnitude depended on the drain product, the nominal stress level and duration of load, as can be seen in the examples in Figure 3. Upward curvature of the strain-time curves indicates possible tertiary creep and impending creep failure. In general, the higher the applied stress, the greater the creep rate and the shorter time to failure. A threshold stress below which "failure" due to creep will not occur exists for most geocomposite drains (i.e., secondary creep will continue without excessive deformation), but the thresholds were not determined during the testing.

Although the test equipment for core creep tests is convenient, the rigid plates have very limited applicability for determining design parameters due to the unrepresentative boundary conditions imposed on the samples. As with the "quick" compression test, the rigid plates contact the core at the nodes only, and thus induce stress concentrations in the cores far beyond the range of normal working stresses. Other than the rate of loading the core creep and the "quick" compression tests differ only slightly, and as demonstrated in Figure 4, the results may not be significantly different.

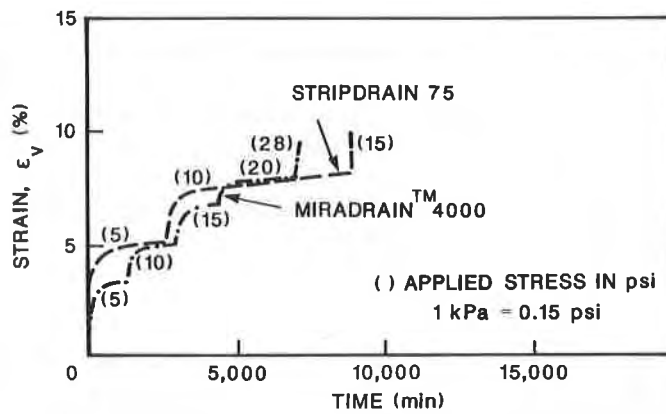


Figure 3 Core creep test results for two geocomposite drain samples.

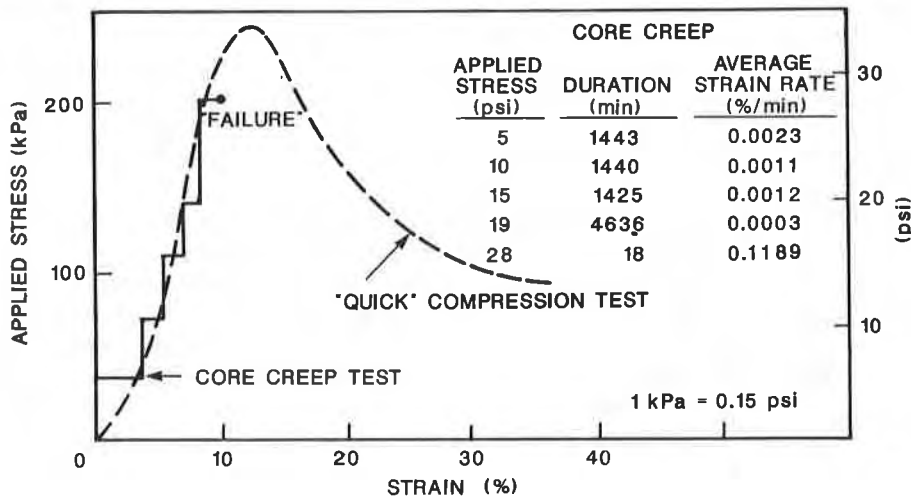


Figure 4 Comparison of "quick" compression and core creep tests on Miradrain™ 4000.

System Creep Tests:

Because the stress concentrations in the "quick" compression and core creep tests do not represent service conditions, a system creep device was developed (see Figure 5) which uses a flexible membrane to apply uniform stress (normal stress only) on the side of the drain geotextile with a rigid plate on the other side while applying backpressure. The apparatus can be easily modified to have soil on one or both sides of the sample. The stresses induced in the sample under this loading better represent service conditions. The creep of the system (geotextile and core) is measured as volumetric strain. The system creep test was designed to aid in quantifying the intrusion of the geotextile into the open spaces of the core, and the deformation of the core itself, which in service could cause a significant decrease of the available flow volume in the core.

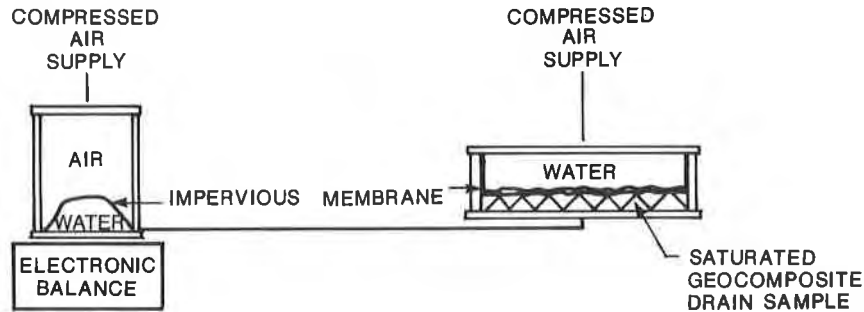


Figure 5 System creep test device.

The test used 27.9 cm (11.0 in.) diameter drain samples placed in a confining chamber with the geotextile side up. After soaking the sample with distilled, deaired water, a flexible impermeable membrane was placed on top of the sample and secured. Hydraulic pressure was applied to the flexible membrane after saturating the sample using backpressure, and the resulting volume change was recorded to measure volumetric strain with time. Volumetric strain was defined as change in volume divided by the total sample volume. Once the rate of volume change had stabilized, the stress was increased and the process repeated.

Results of the system creep tests (see Figure 6) indicate higher volumetric strains for the same stress level and duration than with the core creep test which measures linear strain only (see Figure 3). This is due in part to the deflection of the geotextile into the openings in the core, as well as the effects of the different boundary conditions. Examination of the test samples after testing indicated that the geotextile had often molded itself to the shape of the core.

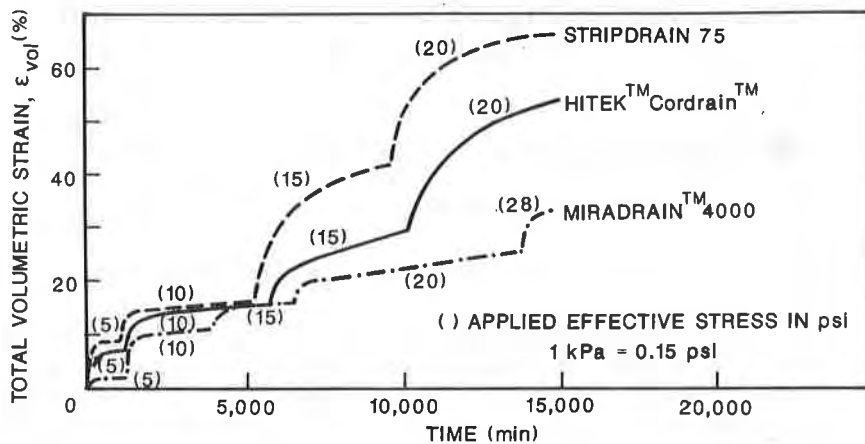


Figure 6 System creep test results for three geocomposite drains.

The results of the system creep test on Stripdrain 75 and HITEK™ Cordrain™ are believed to demonstrate an influence of the geotextile on the system creep.

At the lower stress levels (34 and 69 kPa (5 and 10 psi)) the volumetric strains recorded for the two products were nearly identical. At 103 and 138 kPa (15 and 20 psi), the volumetric strains and the strain rate were considerably higher for the Stripdrain 75 with the polyester geotextile than for the HITEK™ Cordrain™ with a spun-bonded polypropylene geotextile. Since the cores are identical, the higher creep tendency in the Stripdrain 75 was attributed to greater creep in the geotextile.

The creep of the geotextile into the core has been identified to be a significant factor in the deformation behavior of the products. The consequences of extreme creep in the geotextile are potentially severe. In service, this could result in a nearly complete shutdown of the drainage function of the drain, and possible failure of the system.

In-plane Flow Capacity Tests:

ASTM is currently developing a standard method to measure the in-plane flow capacity or hydraulic transmissivity of geocomposite drains. Results of in-plane flow capacity tests on geocomposite drains including Miradrain™ 4000 have been reported by others (3, 7, 9). In the tests the stresses have been applied for periods up to 200 hours. The consistent trend is for the in-plane flow capacity to decrease with increasing confining stress and duration of stress application.

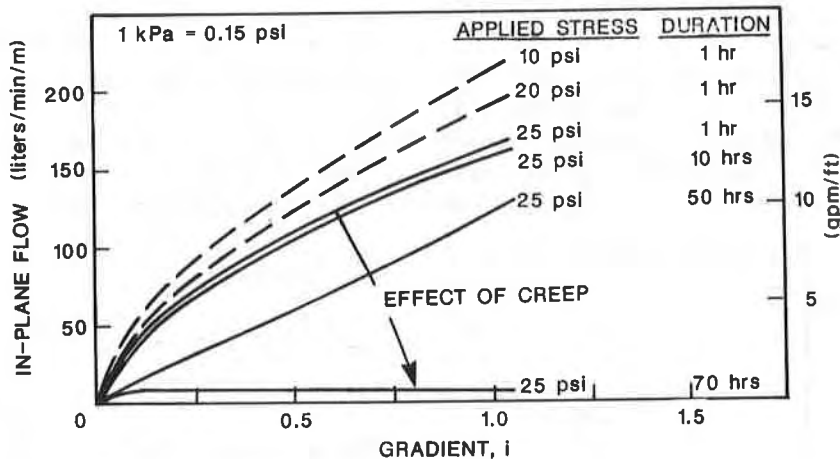


Figure 7 In-plane flow rate vs. gradient and time for Miradrain™ 4000.

Figure 7 illustrates such effects of creep on the critical property of in-plane flow rate from testing conducted during the subject research. A similar example of the effects of creep, shown in Figure 8, was obtained by performing falling head in-plane flow tests on a sample of Miradrain™ 4000 confined under 172 kPa (25 psi).

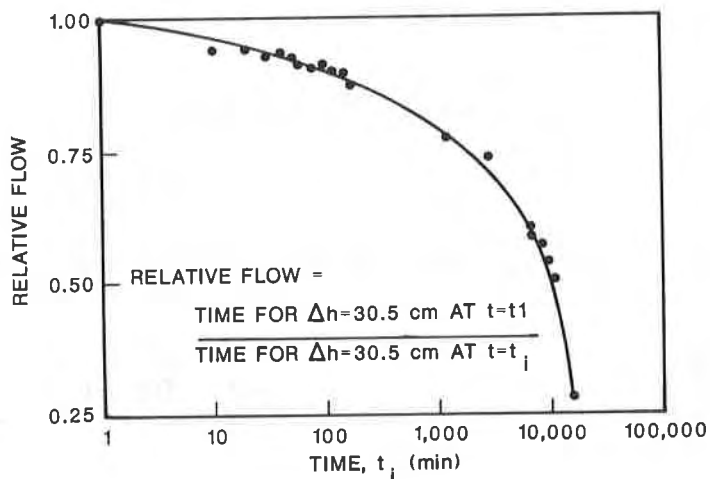


Figure 8 Falling head in-plane flow tests on Miradrain™ 4000.

CONCLUSIONS

Based on the analysis of laboratory tests performed by others and by the authors, it is concluded that creep behavior can be observed for each of the geocomposite drain products in each of the test types. The magnitude of volumetric strain due to creep can be sufficient to adversely affect the performance capabilities of the drain. Therefore, it is important for researchers and engineers to develop a greater understanding of creep behavior and the influence of creep on the measured test results before using the results for design purposes. It is also important for design of drain applications to predict the potential magnitude of creep and effects of creep on performance under field conditions.

Additional conclusions are summarized as follows:

- Based on previous tests and tests from this research, it has been demonstrated that creep can reduce the drain in-plane flow capacity significantly (to the point of collapse or closure of the drain).
- The developed system creep test can be used to quantitatively evaluate creep performance of the drain system (core and geotextile).
- The duration of creep tests reported to date, typically less than 1 month, is inadequate to reasonably predict performance throughout design lives of 10 years or more.
- The existing test results demonstrate that creep failures, with potentially severe consequences to drain performance, can occur under confining stresses as low as about 1/2 of the "quick" compressive yield stress.

Methods are needed to extrapolate creep behavior from relatively short duration tests to the much longer design lives of drain applications. An example

presentation of some available data which might aid in developing such methods is shown on Figure 9.

Figure 9 was developed for the Miradrain™ 4000 product using the "quick" compressive test yield stress as a normalizing stress. The figure is intended to illustrate combinations of time and magnitude of applied stress for tests resulting in "failure" and "no failure." As more data are developed for individual products, for longer test durations, it may be possible to identify "failure" thresholds or envelopes which could be used for selection of allowable stress levels for drain application design.

For the data in Figure 9, failure in the core creep and system creep tests was defined as a sudden collapse of the core structure. For the in-plane flow tests, failure was defined as a reduction in the in-plane flow capacity to less than 20% of the initial value for the given confining stress.

Figure 9 was developed for illustration purposes only and is not intended to be used for design. For presentations such as in Figure 9, it should be recognized that test conditions may invalidate direct comparison of creep data from different tests and definitions of failure must be defined somewhat arbitrarily. In the future, data to be used and evaluated together for design purposes should be developed from testing under one set of test conditions.

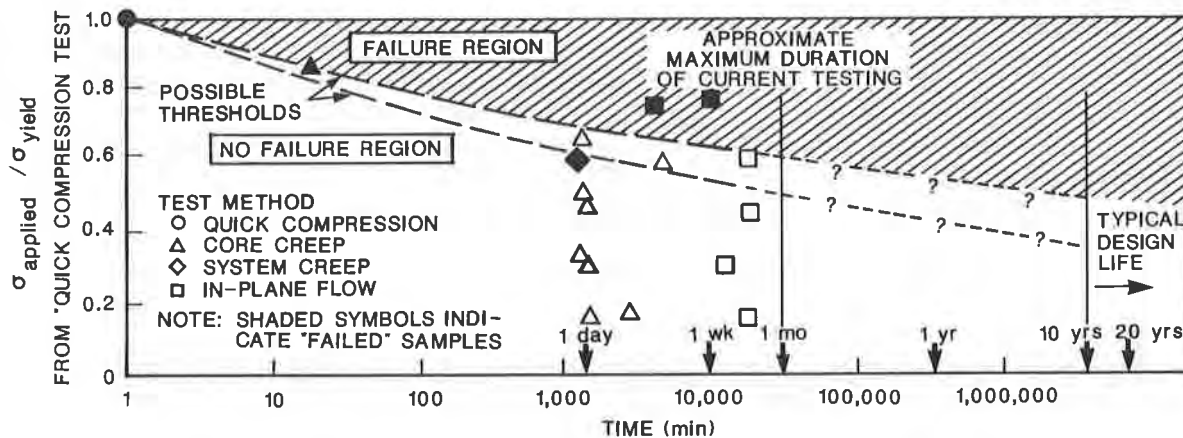


Figure 9 Normalized stress vs. time to failure for Miradrain™ 4000 (data from References 6 and 7).

Although others may develop different definitions of failure for the given tests, an important overall conclusion is that an acceptable stress threshold for the product can be interpolated using data such as in Figure 9 but only within the time frame of the test durations and by realizing the limitations of the test conditions. In the authors' opinion, extrapolation of the threshold stress level to the design life of most geocomposite drain applications (usually 10 years or more) is not feasible from the available data.

It is believed that the behavior characteristics of geocomposite drains under near-service conditions need to be more thoroughly studied and determined before the products can be used with confidence in applications where long-term drain performance is critical. Manufacturers, researchers, and designers have begun to realize the need for more extensive and more standardized testing of these products. Unfortunately, most of the testing that has been completed and that is known to be underway is not standardized with respect to scope, method or purpose. Consequently, test information that is available, and being developed, can be misleading if used by persons unfamiliar with the details and assumptions of the tests.

Based on the limited information available at this time and the testing program described above, considerations with respect to future geocomposite drain testing are as follows:

Compression Tests: Compression test results are useful primarily as an index test for the preliminary comparison and screening of products. Compression tests should be performed using ASTM D 1621 (Compressive Properties of Rigid Cellular Plastics) as a general guide. The tests should be performed at strain rates of about 10 % per minute. Such "quick" compression tests can limit and standardize possible effects of loading rate or creep on measured compressive strength.

Core Creep Tests: Core creep tests performed using rigid plates are often performed because the tests are relatively easy. However, the use of rigid plates does not simulate service boundary conditions. Therefore, if core creep tests are performed, the results should be used cautiously and preferably as an index indicator of the core creep properties only. Due to the lack of substantial difference in the results, it appears that core creep tests could be discontinued in favor of "quick" compression tests for most purposes.

System Creep Tests: The system creep test measures the volumetric strain of the system (geotextile and core). Since the system creep test is more realistic with respect to typical in-situ conditions than the core creep test, system creep tests are preferable for determination of design creep properties. Two recommendations concerning the performance of system creep tests are as follows:

- The sample size should be as large as practical. Samples at least 27.9 cm (11 in.) in diameter are probably reasonable for most drain products. With a relatively large sample the possible effects of number and location of nodes are reduced.
- The sample should be prepared and tested with the geotextile attached to the core (normal manufactured condition) using realistic loading sequences and boundary materials.

In-plane Flow Tests: More extensive in-plane flow tests with a better measurement of the effects of creep over extended periods of time are required in order to use drains in critical applications with any reasonable confidence. A concerted effort should be made to coordinate future in-plane flow tests with parallel or simultaneous system creep testing.

ACKNOWLEDGEMENTS

The research for this paper was partially funded by the Federal Highway Administration under contract DTFH61-83-C-00101. The authors also wish to acknowledge the cooperation of the drain manufacturers who supplied samples, test data, and general comments in an effort to assist with the development of a better understanding of geocomposite drain behavior.

REFERENCES

- 1) Bell, J.R., Hicks, R.G., et. al., "Evaluation of Test Methods and Use Criteria for Geotechnical Fabrics in Highway Applications," Interim Report No. FHWA/RD-80/021, Federal Highway Administration, Offices of Research and Development, Structures and Applied Mechanics Division, Washington, D.C., 1980.
- 2) Christopher, B.R. and Holtz, R.D., Geotextile Engineering Manual, prepared under Contract No. DTFH61-80-C-00094, Federal Highway Administration, Washington, D.C., 1984.
- 3) Koerner, R.M., Carroll, R.G., Jr., and Luciani, V.A., "Drainage Geocomposites," Geotechnical Fabrics Conference '85, Industrial Fabrics Association International, Cincinnati, June, 1985.
- 4) Koerner, R.M., Designing with Geosynthetics, Prentice-Hall, Englewood Cliffs, New Jersey, 1986, 424 p.
- 5) Kraemer, S. R., and Smith, A. D., "Geocomposite Drains: Volume I-Engineering Assessment and Preliminary Guidelines," prepared under Contract No. DTFH61-83-C-00101, Federal Highway Administration, Washington, D. C., 1986.
- 6) Kraemer, S. R., and Smith, A. D., "Geocomposite Drains: Volume II-Laboratory Data Report," prepared under Contract No. DTFH61-83-C-00101, Federal Highway Administration, Washington, D. C., 1986.
- 7) Luciani, V.A., "Characteristics and Behavior of High Drainage Geocomposites," MSCE Thesis, Drexel University, Dept. of Civil Engineering, 1985.
- 8) Merritt, F.S., ed., Standard Handbook for Civil Engineers, McGraw Hill Book Co., New York, 1983.
- 9) Williams, N., Giroud, J.P. and Bonaparte, R., "Properties of Plastic Nets for Liquid and Gas Drainage Associated with Geomembranes," International Conference on Geomembranes, Denver, Colorado, June, 1984, pp. 399-404.

SESSION 4A
DURABILITY

SCHNEIDER, H.
Chemie Linz AG, Austria
GROH, M.
Polyfelt, U.S.A.

An Analysis of the Durability Problems of Geotextiles

1. INTRODUCTION

Most geotextiles consist of synthetic polymers. Like other materials - iron, wood, concrete, asphalt, glass - all polymers change somewhat with time. In addition to the changes in the polymer forming the base of the geotextile, structural changes due to stresses and strains may also alter its properties.

An examination of geotextiles exposed to static and dynamic stresses for 20 years has shown that with but a few exceptions the geotextiles had remained functional although their mechanical properties had somewhat declined. The observation and examination of geotextiles installed for several years under highly diverse conditions and serving a variety of functions in building applications yields important information and indicates trends of change to be considered in cases of long-term exposure to stresses.

An analysis of the samples taken provided information concerning

- chemical changes
- physical changes
- structural changes and
- the relationship between changes in individual components and fabric properties.

At the same time important insights can be gained as to possible modifications of the products with regard to

- stabilisation
- fibre structure
- geotextile construction.

While long-term in-situ and exposed weathering tests are indispensable and useful they have a number of disadvantages:

- long duration (decades)
- differences in test conditions due to different climates and geographic zones
- poor reproducibility
- high cost.

For this reason short-term tests simulating practical conditions have again and again been tried but also found to be problematic: While in practical applications the various changes occur slowly and are due to relatively weak influences, short-term tests are based on more intensive action over a short period and do not allow a recovery of the geotextile in between. What is more, stresses encountered in practice usually consist of several components acting simultaneously.

For most long-term changes it has not been possible so far to establish a satisfactory correlation between short-term laboratory tests and practical in-situ studies. Indeed, short-term tests that are not properly designed occasionally produce misleading results.

A number of experiments have been carried out in order to determine the reasons for this unsatisfactory correlation between short-term tests and practical applications.

2. UV RESISTANCE OF GEOTEXTILES
(UV = ultraviolet radiation)

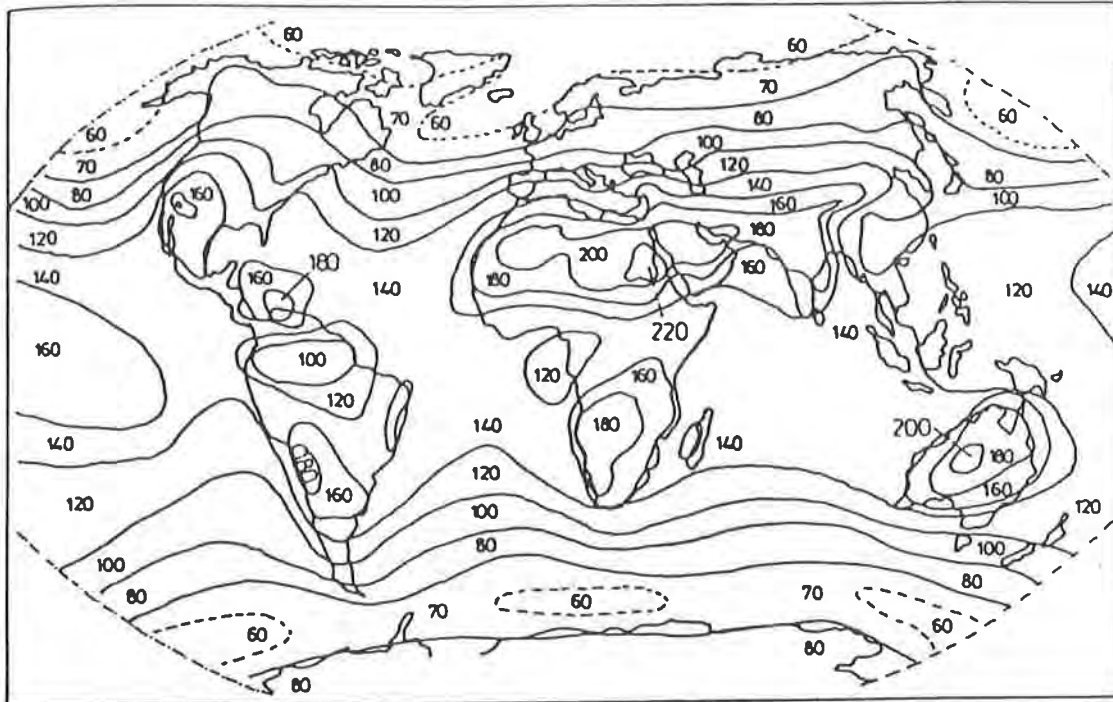


Figure 1: Generalised isolines of global radiation

Radiation intensity varies worldwide according to geographic reasons (Fig. 1 [1]) from 60 to 220 kcal/cm²/year. At the same time, radiation intensities tend to change over the years in one and the same geographic zone in most parts of the world.

Weathering tests performed in various geographic regions - Australia, Austria, South Africa - on the same product, a mechanically bonded polypropylene continuous fibre non-woven (Polyfelt TS 700) under identical weathering conditions (45° angle of inclination, North and South, respectively) yielded results that were in no way directly related to the radiation intensity at the location in question. At the same time, no correlation was found between laboratory findings and field tests.

In order to understand why no such correlation was found we have to consider the principle of UV-radiation stresses:

A molecule absorbing light is raised to an energy-rich or excited state. The energy that

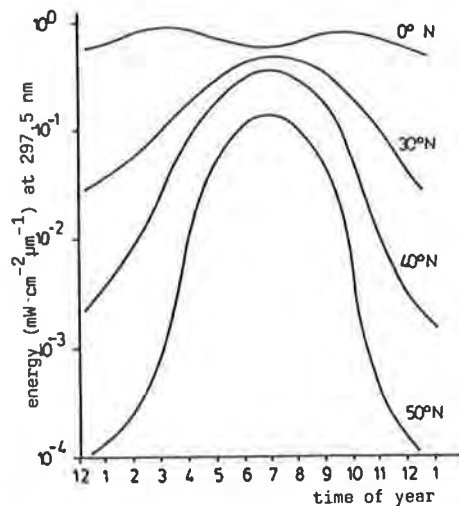


Figure 2: Daily total solar radiation over the year

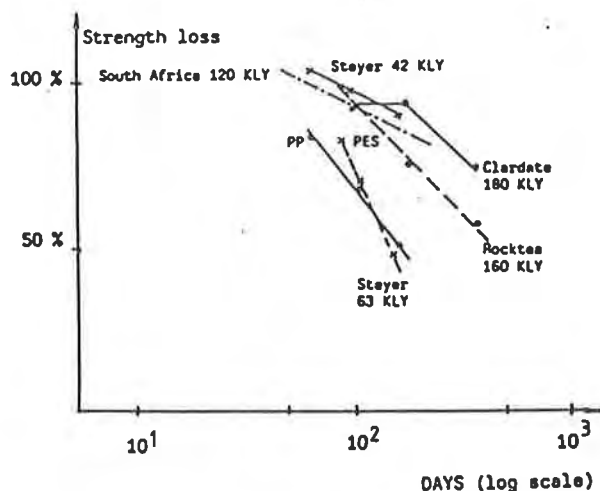
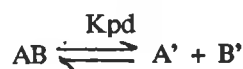


Figure 3: Results of weathering tests on a PP continuous-fibre non-woven in geographic zones with different radiation intensity

has to be absorbed in order for the molecule to react is called activation energy (E_a).

The reaction produces free radicals ultimately leading to chain fracture, which in turn, reduces the molecular weight of the polymer and produces structural changes.



K_{pd} = rate constant for photodissociation

On the basis of K_{pd} we can predict the extent of dissociation (intrinsic quantum yield), which depends on the reaction rate and all factors counteracting it.

$$\Phi_{\text{intrinsic}} = \frac{K_{pd}}{K_f + K_{ic} + K_{isc} + K_{qQ} + K_{pd}}$$

The extent of dissociation is independent of the intensity of radiation.

According to the equation of Arrhenius

$$K_p = A \cdot e^{-E_a/RT} \quad (1)$$

where

- A = a constant
- E_a = the activation energy
- R = the gas constant
- T = absolute temperature

The rate constant depends on two parameters:

- the activation energy E_a
- and the temperature T

since $A = \frac{eKT}{h} \cdot e^{s/R}$

Under certain conditions, at 25° C,

$$A = 10^{-13}$$

where

- K = Boltzman's constant
- h = Planck's constant
- s = activation entropy
- T = absolute temperature
- R = gas constant

In this case equation (1) becomes

$$K_{pd} = 10^{-13} \cdot e^{-E_a/RT} \quad (2)$$

This indicates that the temperature of the product has a major effect on photo-oxidative stresses, which is confirmed by degradation of the material in a Xenotest 450 apparatus at different test temperatures. Fig. 4.

One problem is the determination of the temperature in rapid weathering devices. Normally two temperatures are given, viz.

- interior room temperature
- black panel temperature,

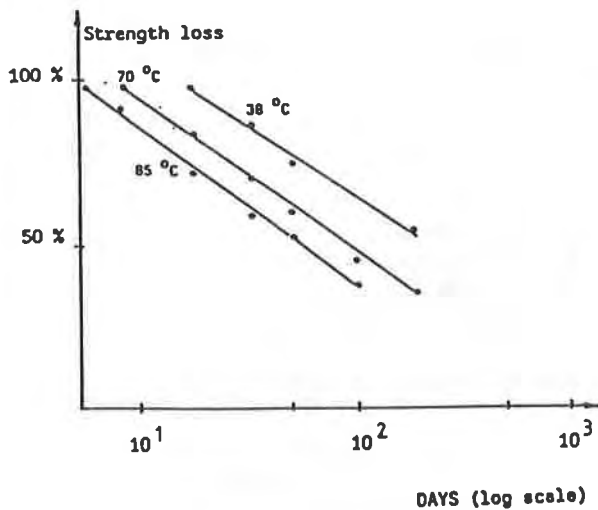


Figure 4: Degradation of a PP continuous-fibre non-woven in a Xenotest 450 at different temperatures

which have, however, been found to be irrelevant (3).

Results that can be properly evaluated can be obtained only by temperature measurements on the sample surface and inside the sample.

Note that depending on the material on which the sample is placed the temperature rise in the sample may be different: insulating materials may lead to an additional increase in temperature. In the same way the sample thickness may have an effect on the temperature rise.

For this reason the type of stabilisation of polypropylene is of special importance.

Fig. 5 demonstrates the effect of temperature on half-life.

While at lower temperatures the two products behave in more or less the same way, they show considerable differences (2 to 4-fold) at higher temperatures. This explains why the long-term durability of one and the same product is often assessed quite differently.

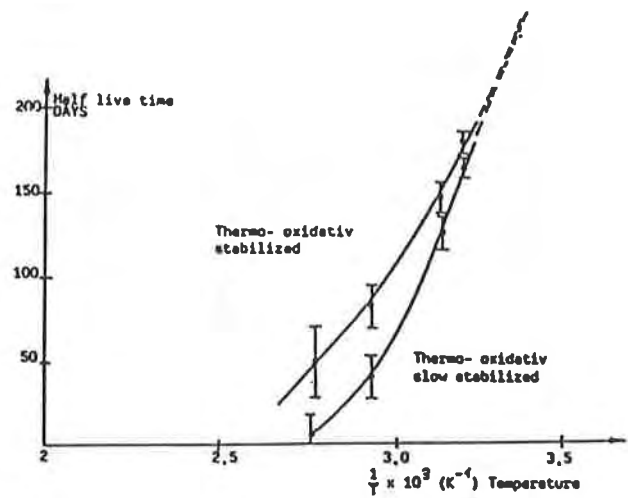


Figure 5: Half-life/temperature ratio ($\frac{1}{T}$) K°.

These studies have shown that temperature greatly influences the photo-oxidative degradation of polymers and thus their long-term properties. Studies have also shown that at the same radiation intensity the surface temperature depends on the angle of incidence. In an open-air weathering test this phenomenon was used for testing two products with known stabilisation at different surface temperatures in one and the same location. The geotextile samples were placed at angles of 0° and 45° with the ground. A theoretical curve was calculated from the curves shown in Fig. 4 and 5 as well as those obtained in tests at higher temperatures, and compared with the measured results (Fig. 6).

The mean daytime sample temperatures were 50° C and 35° C, respectively. Agreement with theoretical curve E was found to be better.

If all sources of error such as mean temperature calculation, exposure time, property variation within the sample, influences of other factors, are taken into consideration this test approximates the conditions prevailing in long-term stresses by photo-oxidative degradation more realistically than other tests.

In addition, there are a number of other

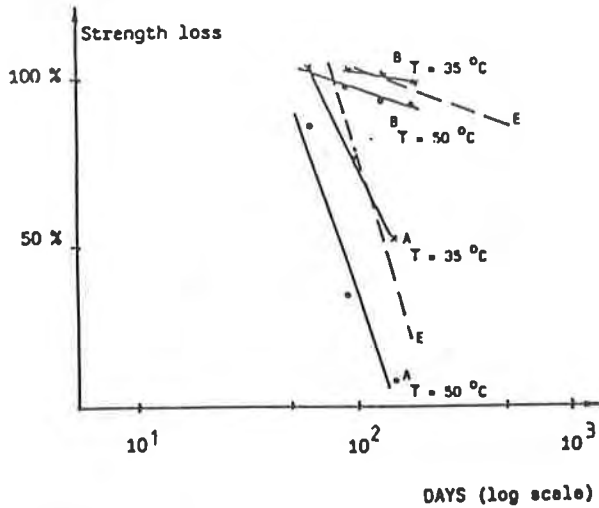


Figure 6: Comparison of open-air weathering tests at different temperatures

factors that render assesment difficult. The samples are subjected to greater stresses on the exposed side than on the unexposed one. (Fig. 7). Different forms of stabilisation also add to the inhomogeneity of results.

3. THE RESISTANCE OF GEOTEXTILES TO HYDROLYSIS

The action of water, temperature, alkalis and acids on geotextiles produces even more widely different results than UV radiation. Fig. 8 attempts to summarise practical results published about polyester and polypropylene geotextiles (5,6,7). While these data are apparently unrelated, the differences noted in different publications can be explained and may be considered to be realistic if due consideration is given to the chemical principles of hydraulic degradation and to the factors that enable or facilitate it. The one mistake to be avoided is to extrapolate from each individual result the overall behaviour of the geotextile as such.

Hydrolysis can take place only after water has been adsorbed and diffused into the polymer. The rate of hydrolysis is invariably directly related to the water concentration (8); the reaction takes place much faster in an acid or alkaline medium (9).

Products	Exposure Xenotest 450 - hours	Intrinsic viscosity		
		full exposure	back of exposed part	back of covered part
Polyfelt TS 400 ₂ 350g/m ² PP spun- bonded non-woven	5000	0.76 / 10 000	1.36 / 150 000	1.58 / 180 000
Polyfelt TS 700 ₂ 280g/m ² PP spun- bonded non-woven	5000	1.21 / 121 000	1.56 / 18 000	1.59 / 180 000

Figure 7: Stress differences within the sample

The influence of a variety of factors - water, water vapour, alkalis - on the hydrolytic degradation of polyethylene terephthalate geotextiles is shown in Fig. 9. The differences in reactions under different conditions may at least in part explain the different results obtained in practical tests.

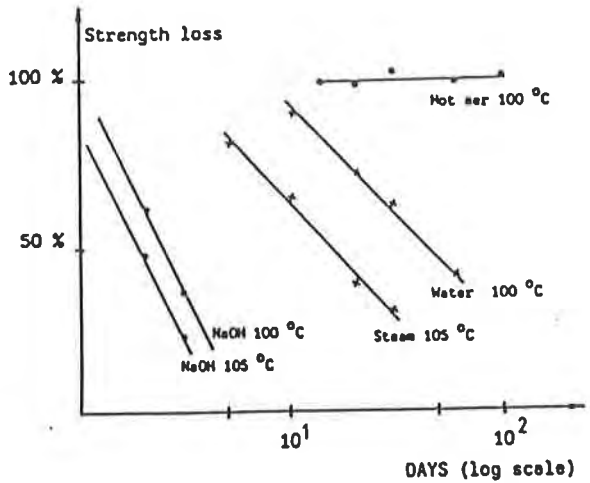


Figure 9: Hydrolytic degradation of a polyethylene terephthalate (polyester) geotextile

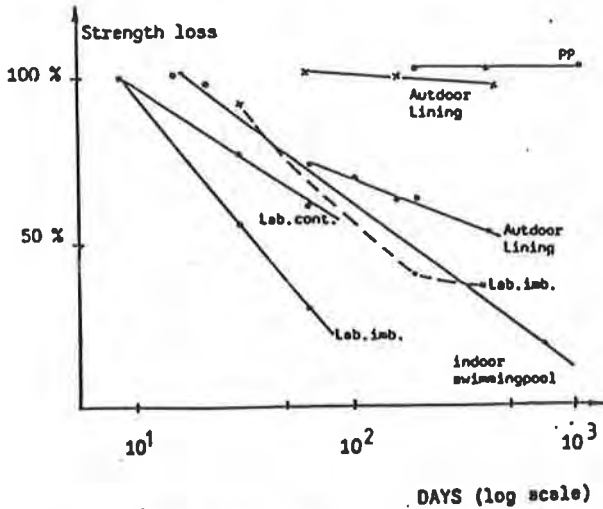


Figure 8: Practical results on the hydrolytic degradation of polypropylene and polyester geotextiles

As in the case of photo-oxidative decomposition, the reaction rate depends largely on temperature, and the law governing this type of reaction is again.

$$\ln K = A + E_a/RT,$$

the one major difference being that in the case of polyesters this reaction is kinetically 10 times faster than thermal decomposition and 5 x 10 faster than oxidative degradation. (10)

The influence of the temperature on the degradation of polyethylene terephthalate (PETP) is shown in Fig. 10. It will be seen that the rate of degradation is minimal at 20° C, since the attack is mostly restricted to the surface. The carboxylate ions and the low dielectric constant prevent the hydroxyl ions from penetrating. In this way the hydrolysis is prevented from propagating (11).

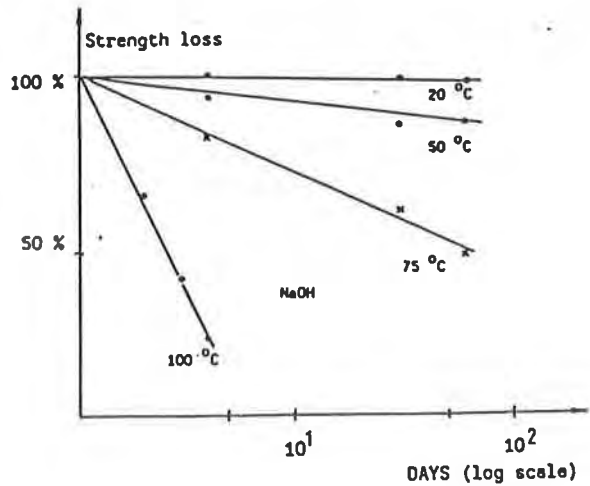


Figure 10: Hydrolytic degradation at different Temperature

However, merely indicating the pH of a chemical stress says little about how aggressive the substance in question actually is with regard to the geotextile under consideration, since it fails to say anything about the electrolytic

conditions prevailing in the system polymer/alkali/water, nor about the mobility of the ions or the reaction rate.

Tests performed at 22° C showed that the pH of a sodium hydroxide (NaOH) solution had very little effect on the hydrolytic decomposition of PETP. If NaOH is replaced by $\text{Ca}(\text{OH})_2$ (calcium hydroxide) degradation is greatly accelerated. (Fig. 11). This acceleration might be explained by a change in electrolytic structure. In any case, it is a phenomenon that must be taken into account when assessing the long-term properties of the material.

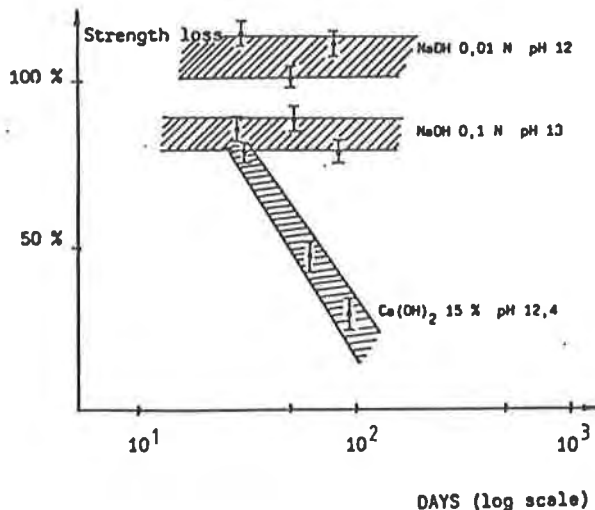


Figure 11: Hydrolytic degradation of PETP in alkaline media

Further studies were designed to determine the temperatures likely to occur in practical applications. In these tests, the use of geotextiles as protective layers for synthetic plastic sheets was simulated. The tests were carried out in Linz/Austria. On a normal sunny day (in June) the temperature in the shade

was found to be 25° C,
the temperature in the sun 39° C,
the temperature of the film 50° C
and the temperature beneath the film was 60° C.

A further measurement was taken in October and the temperatures found were

22° C in the sun and
35° C beneath the film.

In tropical climates temperatures around 100° C may well occur and it is not difficult to imagine their effect on hydrolytic degradation. Cases of considerable decomposition of PETP have been reported in the literature (5,12).

One factor that is disregarded in ageing studies is the aminolysis (influence of ammonia) of PETP, which may result in a 20 - 30% reduction in strength within a month at a concentration of only 2% and a temperature of 60° C.

4. CONCLUSION

1. When studying and assessing ageing processes in polymers the nature and laws of material decomposition have to be taken into account.
2. The temperature to which a geotextile is exposed considerably influences the reaction rate and has to be taken into consideration when developing and evaluating geotextiles.
3. Due consideration of these principles permit the development of geotextiles fully satisfying the requirements of civil engineering.
4. In evaluating hydrolytic decomposition attention has to be paid to water concentration, temperature, presence of acid or alkaline media and the kind of alkaline media.
5. If these principles are observed better rapid tests can be developed permitting, within limits, a prediction of long-term behaviour.
6. Temperatures of 50 - 70° C (in temperate zones) and around 100° C (in tropical areas) can be expected to occur on the surface of geotextiles and must be considered.

References:

- (1) Collman, W.: "Diagramme zum Strahlenklima der Erde", Ber. DWD 42, (1958)
- (2) Henderson, S.T.: "Daylight and its spectrum", Adam Hilger Ltd., London, (1970)
- (3) Schneider, H. / Hüttner, G.: Allg. Vliesstoffreport 6/1982 238-240
- (4) Schneider, H.: "Durability of Geotextiles" Conf. on Geotextiles, 13-14 May 1985, Singapore
- (5) Schneider, H. / Supanz, P.: "Einsatz von Bodenbelägen in der Automobilindustrie", Intercarpet 81, Baden
- (6) Luenenschloss, Albrecht W., Vliesstoffe G. Thieme Verlag 1982/324
- (7) Schneider, H.: "Durability of Geotextiles" 20. Intern. Man made fibres conf., Dornbirn, (1981)
- (8) Hoechst Technical Information F0002, (1979)
- (9) Ravens, P.A. Warrd, Foraday Soc. 57, 150, (1961)
- (10) Rudakova, T., Moissev, Yu., Vysoko mol/ Soe-din SerA 1974 16(6) 1356/63 + 1972 14(2) 449/53
- (11) Buxbaum, L.N.: "Angew. Chemie", 80 225/233, (1968)
- (12) Von Falkai, B.: "Synthesefasern" Verlag Chemie, (1981)
- (13) Sotton, M.: Index 81, Amsterdam, May 1981, Vol. 7, 118

WHELTON, W.S.

The Tensar Corporation, U.S.A.

WRIGLEY, N.E.

Netlon Limited, United Kingdom

Long-Term Durability of Geosynthetics Soil Reinforcement

INTRODUCTION

"Does it deteriorate?" is one of the most obvious and pertinent questions asked about polymer geosynthetics when used in permanent, critical structures such as mechanically stabilized highway embankments. An exact response to this question is difficult due to the many factors that affect long-term, in-ground geosynthetic performance. Resin type and properties, additive packages, product geometry, and product processing all affect long-term behavior.

This paper examines the possible causes of deterioration of geosynthetics products, including 1) ultra-violet degradation, 2) thermal and oxidative degradation, 3) chemical attack, 4) microbial attack, and 5) environmental stress cracking. These five possible causes are then evaluated for one specific geosynthetic product, TENSAR® SR2 Geogrid.

Geotechnical products can be developed to resist deterioration through use of a properly "engineered" resin and processing recipe. Crucial to this recipe is the selection of the proper 1) resin, 2) additive package, 3) processing conditions and 4) product geometry. This paper shows how each of these factors has been considered and evaluated in the production of TENSAR SR2 Geogrids. Independent research and test results addressing each factor are presented.

This paper will serve as a source of explanation to geotechnical engineers on the factors that may cause geosynthetic deterioration and will provide guidance for evaluation of the effects of these possible causes.

ULTRA-VIOLET DEGRADATION PROTECTION

Polyolefins such as polyethylene and polypropylene in an unprotected state have poor resistance to sunlight with brittleness developing in thin sections in less than six months. This brittleness or loss of flexibility, resulting from oxidation energized by the ultra-violet component of ordinary sunlight, is accompanied by physical changes, principally chain scission or shortening. This results in lowered molecular weight, together with cross-linking. The net result of these changes is a brittle material having little strength.

®Registered Trademark

Since the deterioration of polyolefins observed in outdoor exposure is produced by short wave length radiation, barriers or screens which would prevent such energy from being absorbed have been developed. Of these, carbon black has been determined to be the most effective barrier to UV absorbance by polyethylene. The carbon black type and dispersion characteristics are crucial to extended life. The resistance to aging of any given polyolefin-carbon black compound depends upon three factors:

- 1) Type and particle size of the carbon black.
- 2) Concentration of the carbon black.
- 3) Dispersion of the carbon black.

In order to ensure extended UV protection the carbon black must 1) be a channel type with a particle size of less than or equal to 20 nanometers (20×10^{-9} meter), 2) must be concentrated at 2% minimum, and 3) must be well dispersed in the polyolefin.

From work by Wallder (1) of Bell Telephone Labs in comparing natural versus accelerated aging of high density polyethylene at varying concentrations of 25 nanometer Paris grade carbon black, 100 hours of accelerated aging equals 1 year of outdoor exposure (Figure 1 and Table II). Wallder used a bare carbon arc with water spray accelerator system which was found to give good correlation with outdoor behavior. Figure 2 shows the effect of carbon black type on accelerated aging of polyethylene for 1 per cent concentrations of five commercial carbon blacks. Polyethylene resistance to aging increases with decreasing carbon black particle size. This is shown in Figure 3 where aging resistance is plotted against the particle size of the carbon black. The dependence of aging on carbon black concentration is shown in Figure 4 where aging resistance is shown to increase with increasing Vulcan P or Kosmos BB carbon black concentration until a concentration of 2.0% is reached.

Figure 5 is taken from work performed by J. B. Howard and H. M. Gilroy of Bell Telephone Laboratories, Inc. (2) again reinforcing the aging resistance of polyethylene when properly protected with fine grade carbon blacks.

The wire and cable market has done extensive research defining the UV resistance afforded by carbon black through accelerated and actual field installations (1). Overhead cable exposed for >20 years when protected with a fine grade, well dispersed carbon black has actually shown insignificant loss in any original design characteristics.

The DuPont Company has supplied tons of HDPE to the cable and pipe industry. Per W. F. Jensen and J. N. Jones paper on "Weatherability of Black Polyethylene--Predictable?" (3), when 2% well dispersed fine grade carbon black is added, "Along with accelerated aging tests, actual field experience was being generated over the past 30 years. Rural telephone wire hung on a pole in Florida for 20 years was still capable of being tied in knots without crazing or cracking."

Per V. T. Wallder of Bell Telephone Laboratories, Inc., from Weathering Studies on Polyethylene; (4)

"Unprotected polyethylene deteriorates rapidly when exposed to weather. The addition of channel carbon black having a particle size below ~25 milli-microns, when dispersed in a suitable polyethylene to give a minimum of agglomerates at a concentration of 1% or greater, will produce a compound having a resistance to outdoor weathering adequate for most normal applications. On the basis of accelerated tests a life of 20 years or more appears to be reasonable."

TENSAR uniaxially drawn UX1200 (SR2), (Figure 1A) is produced from a copolymer grade of high density polyethylene (HDPE) with molecular orientation continuous through the longitudinal ribs and transverse bars. This geogrid contains a Vulcan P (Cabot) grade carbon black additive with an average particle size of 20 nanometers at a concentration of 2.5% \pm 0.5%.

The exposure of polyolefin materials similar in scale to the geogrids discussed in this paper have been reported (5), (6). In both cases no significant loss of strength was detected after 20 years exposure in temperate climates. These results have given credence to the theory that carbon black protects against U.V. degradation by shading all but the surface layer of molecules from the light. Therefore degradation takes place only at the very surface and cannot penetrate further until the surface has gone. Thus in constant light and weather conditions a model process that could be envisaged is a very slow but constant rate of attrition (7).

This model rate of attrition can be estimated from performance data on 50 micron tapes. The time for such tapes incorporating 2.5% carbon black to lose 50% of strength is in excess of 10 years in a temperate climate, and this effect is independent of whether the tape is molecularly oriented or not (5). It can therefore be said that half the thickness of the tape (25 microns) has been degraded in 10 years, i.e. a model rate of attrition of 2.5 microns/annum. The geogrid considered in this paper has carbon black and a minimum rib thickness of 1.2-1.3 mm. Therefore using this model, these products could retain 90% of initial strength when exposed for approximately 50 years.

THERMAL AND OXIDATIVE DEGRADATION

Controlling oxidation of polyolefins is a well developed science, with long term experience in a variety of applications--pipe, telecommunications and cable insulation.

Oxidation and thermal degradation cause embrittlement of polyethylene. Natural polyethylene oxidizes due to the formation of carbonyl end groups at increased temperatures and high oxygen concentrations. The combination of a thermal additive package (Irganox 1010 and BHT), channel grade carbon black at 2.0% concentration, and increased order of the molecular structure through orientation inhibits oxidative degradation.

Effect of Increased Order of Molecular Structure

In examining the orientation effect on oxidation resistance let's look closer. Bulk HDPE and PP are 50-60% crystalline with fine lamellar crystallites separated by thin amorphous zones and the crystallites branch intricately to form three-dimensional spherulites. The major change which is then made to this structure in the manufacture of TENSAR Geogrids is that of molecular orientation. In this process the spherulites are transformed into microfibrils and the crystallites and molecular chains within the amorphous matrix are drawn into alignment (10). Studies have shown (11) that with HDPE this alignment within the amorphous zones can be sufficient for crystalline bridges to form between crystallites. There is a direct relationship between the degree of draw (orientation) applied to a material and its improvement in mechanical properties (11), (12).

The micro-structure of HDPE has very low permeability to aqueous solutions. Uniaxial orientation, as in all TENSAR Geogrid ribs, has been shown to give significant reduction in permeability by several researchers (13), (14), (15).

It is concluded that as HDPE is oriented, the degree of crystallinity increases, leading to reduced molecular segmental mobility and less solubility of gas in the polymer (9). TENSAR HDPE Geogrids have degrees of orientation in the load carrying portion of the grid which are well ordered in structure, thus resisting oxidation.

Effect of Additive Inhibitors

The ability of carbon black to inhibit thermal oxidation of polyolefins has been known for more than 30 years. Most studies concerned with the thermo-oxidative stability of carbon black reinforced polyolefins are basically qualitative. However, in the work of Pleshanov (8) the ability of carbon black to terminate kinetic chains was studied and quantified by the initiated oxidation of PE at temperatures higher than the melting point. During oxidation, bonds are formed between PE molecules and the surface carbon black, which hinders molecular motion at temperatures higher than the polymer melting point.

Research by W. L. Hawkins (16) "has shown that photooxidation is practically stopped by incorporating about 3% of weight of the carbon black of a particle diameter below 50 milli-microns." This need is reduced to 2% carbon black by weight of particle size diameters at 20 milli-microns. "Such blacks also act as mild thermal anti-oxidants." It was shown by Hawkins and co-workers that carbon black may act as a trap for propagating radicals, as a result of the free radical quenching action of the surface groups on black at temperatures up to 140°C.

Finally, Hawkins determined that carbon blacks act to catalytically decompose peroxides participating in the thermal oxidation of polyethylene, thus contributing to inhibition of thermal oxidation.

Among the anti-oxidants, Irganox 1010 is added to TENSAR HDPE Geogrids for high temperature processing. Over 1000 ppm Irganox is added to absorb free oxygen interaction with PE. The underground cable industry has confirmed that insignificant leaching of the anti-oxidant occurs (17). Research at exposed temperatures

up to 78°C has shown no loss in HDPE properties after 29 years when an adequate anti-oxidant package was added (16).

CHEMICAL RESISTANCE

The chemical resistance of both HDPE and PP is typified by the statement made by Herms, et. al. in discussing the design of apparatus (18): "For experiments ... in hot Sodium Hypochlorite, which is extremely corrosive to most metals, the materials that were not attacked were gold, platinum, glass, polyethylene, polypropylene, polyvinylidene chloride and the fluoropolymers". HDPE has been used in buried applications even longer than PP, in particular in the critical applications of potable water and gas distribution where for some sizes it has now been the prime material for up to 30 years. For gas distribution HDPE gas pipe is supplied on a prognosis of a 50 year minimum life--the critical element is the risk of internal softening due to occluded gas condensate--the risk of attack from the buried soil environment is considered to be not critical (19). In addition the chemical resistance of HDPE is increased with density (20) and thus the performance of the grades used for geogrids at 0.947 density will exceed that of the pipe grades at 0.935 - 0.945 density.

The manufacturers of polyolefin resins have carried out a wide range of tests on the resistance of these materials to chemical attack as they are now frequently specified for the storage of aggressive chemicals. Information on this resistance is freely available and a study of this literature confirms that these polymers are inert to all chemicals likely to be found in soils. There is no solvent for either PP or HDPE at ambient temperatures (21), (22).

MICROBIAL ATTACK (BIOLOGICAL RESISTANCE)

Polyethylene and Polypropylene are both resistant to biodegradation. Early experiments confirming this for Low Density Polyethylene were reported by Dolezel in 1967 (23). An extensive research programme on HDPE was carried out by Albertson in the late 1970's (24), (25), (26). In these experiments HDPE samples were incubated at 25°C for 800 days in aerated cultures of various organisms. The HDPE was in the forms of anti-oxidant free unoriented film and powder to accelerate testing. Two effects were identified--abiotic auto-oxidation and a biological effect.

It was found that there was no possible biological mechanism of degradation. The only effect found from the micro-organisms was the consumption by them of the very low molecular weight, and therefore non-structural, 'extractable' fraction of the polymer. This effect was proportional to the surface/volume ratio and after two years was consuming less than 0.1% per annum of a powder with a surface/volume ratio of 10.5 m²/g. As TENSAR Geogrids have a maximum surface/volume ratio of circa 5 x 10⁻³ m²/g, this effect would be barely measurable even over 100 years. In addition, even this effect was reduced in rate by a factor of 3 by the inclusion of an anti-oxidant in the polymer.

Further work by Albertson states that average chain length straight HDPE molecules above weight average 1000 Mw are inert to microbial attack because of the lack of suitable enzymes that split the C-C bond (26). TENSAR HDPE Geogrids are produced from resins with molecular weight averages between 150,000-200,000.

The biological resistance of polyolefins has in fact led to serious concern about the effect on the environment of the longevity of the vast quantity of these materials used in the modern packaging industry. Research has therefore been carried out to try and increase their biodegradability. This work was summarized by Griffin in 1983 (27). The only method found to encourage the biological breakdown of such products was the incorporation of a high proportion (up to 40%) of a nutrient filler such as starch.

The resistance of HDPE to attack by larger organisms was confirmed by 15-year marine exposure tests carried out from 1956 to 1970 (28). No significant attack occurred on HDPE from even marine borers, the most aggressive organisms. Also resistance to termite attack was confirmed by tests commissioned by B. P. Chemicals Ltd. (29).

Finally, the biological resistance of the particular polymer systems, including stabilizers and carbon black, used in TENSAR Geogrids is confirmed by the approval given for similar compounds to be used for potable water conveyance (5), (30). One of the prime criteria in this approval by the British National Water Council is that a material must not support biological growth.

ENVIRONMENTAL STRESS CRACKING

Environmental stress cracking (ESC) is the term used to describe the premature failure that can occur in some materials, without chemical change, when they are subjected to concurrent stress and a particular environment. Though not chemically the same, it is similar in effect to the environmental stress corrosion failure that can occur in an incorrectly specified 'stainless steel' in a chloride environment (e.g. sea water).

With polyethylene, the fact that less extreme environments can cause ESC on some grades has been known since 1946. There is now such a wide body of research knowledge available that it is possible to select appropriate grades of HDPE for the manufacture of geogrids to eliminate concern about ESC.

The relationship between molecular weight and ESCR (environmental stress crack resistance) has been known and understood since the 1950's. Extensive research by V. T. Wallder of Bell Telephone Laboratories, Inc. in 1955 (31) showed polyethylene with an average molecular weight of >30,000 resists environmental cracking when exposed or submerged to alcohols, soaps, surfactants such as Igepal and other wetting agents.

Wallders' work showed that for U.S. manufactured low molecular weight polyethylene, cracking occurred almost instantaneously in a 10% Igepal environment. In this work, Igepal CA was employed as a cracking environment because of its stability and cracking activity. Further, Wallder found that high molecular weight resin, with 2% fine grade carbon black and 0.07% anti-oxidant showed 0% cracking vs 93% cracking for the lower molecular weight resins. Figure 6 summarizes clearly the findings of Wallder.

Supportive research by Christ, Leong-Lacarva and Carr (32) shows that HDPE crack propagation is a function of HDPE average molecular weight and density; the higher, the less crack propagation.

Further work by J. M. Crissman and L. J. Zapas (33) of the US National Bureau of Standards supports the effects of polymer make up characteristics on environmental stress crack resistance. Crissman and Zapas examined two HDPE's; 1) a linear polyethylene having an average molecular weight (Mw) of 99,000 and a nominal density of 0.966 g/cm^3 , and 2) an ethylene-hexene copolymer which is slightly branched, and had a Mw of 211,000 and a nominal density of 0.955 g/cm^3 . One mm amorphous dumb bell sheets were stressed at varying levels in a highly active and aggressive surface stress cracking agent (10% solution in water of nonylphenoxypoly ethonal). Both resins were stressed and monitored for time to failure in air and the cracking agent at two temperatures (296K and 330K, i.e. 73°F and 135°F).

Figures 7 and 8 are plots from the above work of the linear homopolymer and copolymer HDPE fracture performance at varying stresses in air and cracking agent. These show the very significant improvement made by moving to higher molecular weight and co-polymerization.

TENSAR HDPE Geogrids are produced from a copolymer resin, with a Mw of 150,000-200,000 and slight branching. This resin is in line with the copolymer resin used by Crissman and Zapas.

As a result of the above knowledge, it was possible, when developing TENSAR Geogrids, to choose in consultation with the manufacturers, grades of HDPE that would ensure a freedom from problems of ESC.

The most appropriate test for engineering design purposes is the constant load test developed by Lander in 1960 (34). For such purposes this test was now been adopted in ASTM D-2552-69 [reapproved 1980] (35). In this latter standard, Clause 4.3 states "... by evaluating the material over a suitable range of initial stresses or temperatures, or both, using this method, information useful for predicting end-use performance may be obtained". Therefore, tests of this form were carried out by BP LTD when TENSAR SR Geogrids were first developed in 1979. These tests showed that the load bearing capacity of these grids is not affected by ESC (7).

The less oriented region of TENSAR UX1200 (SR2) is perhaps more susceptible to ESC. In simply looking at the design strength of SR2, 30 kN/m (2055 lbs/ft) divided by a safety margin of 1.5 results in a design load of 20 kN/m (1370 lbs/ft). converting the cross-sectional area 1 meter wide by 180 mils thick, the effective stress per area becomes: 4.4 MN/m^2 .

Examination of Figure 8 indicates that TENSAR UX1200 (SR2) Geogrids produced from high Mw Copolymers submerged in 10°C soil environments containing highly active ESC agents can actually be designed conservatively without making allowance for the improvements due to orientation at applied stresses of 7.5 MN/m^2 . This converts to 34.3 kN/m width.

CONCLUSIONS

There are many situations where polymeric materials are used for load-bearing in buried situations. A broad ranging bank of data exists on the durability of these materials, particularly high density polyethylene. In selecting a polymeric material for long term load-bearing application in buried situations, detailed consideration must be given to resin selection, the resin additive package, controlled processing, and product geometry.

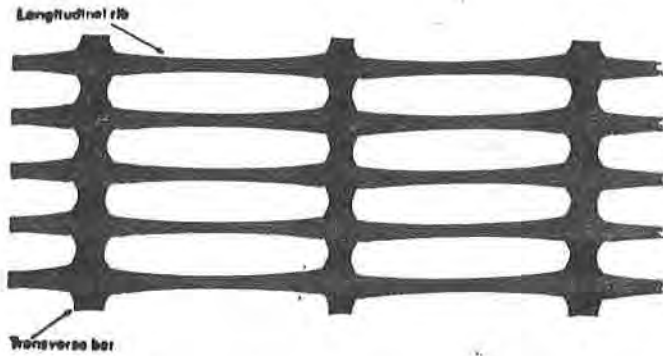


Figure 1A

Natural vs Accelerated Aging of Polyethylene Compounds

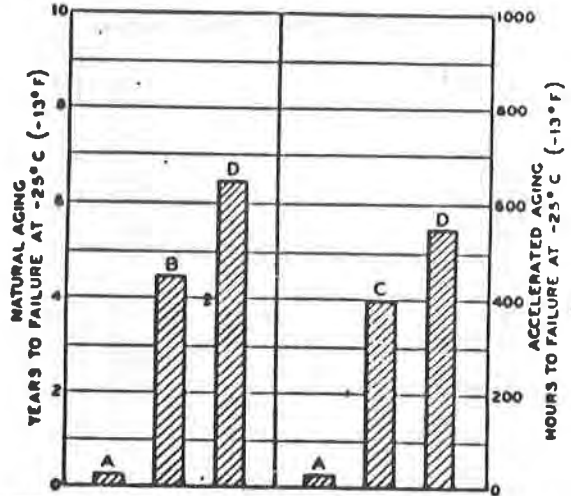


Figure 1

Table II. Composition of Polyethylene Compounds

	A	B	C	D
Polyethylene resin	100.00	94.34	94.34	98.00
Carbon black - Paris		0.94	0.94	2.00
Polyimideylene		2.36	2.36	
Hydrocarbon wax		2.36	2.36	
	100.00	100.00	100.00	100.00
Form of sample	molded sheet	wire insulation	molded sheet	molded sheet
Exposure location	Northern N. J.	Miami, Fla.	Northern N. J.	Northern N. J.
Types of resin	American	British	American	British

1% CONCENTRATIONS OF FIVE CARBON BLACKS

Effects On Accelerated Aging of Polyethylene

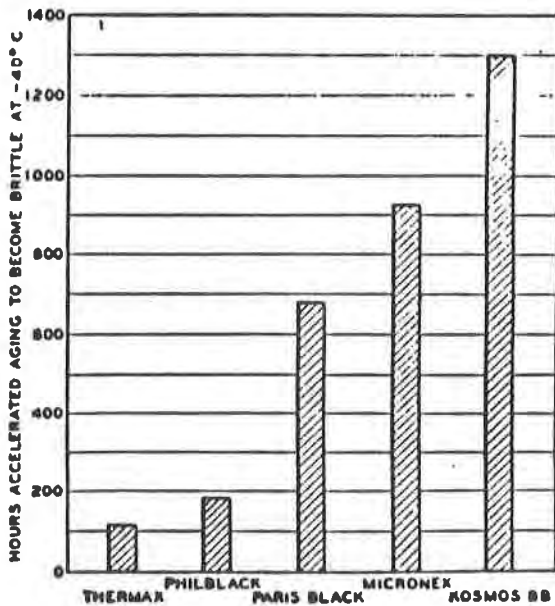


Figure 2

CARBON BLACK PARTICLE SIZE

Effect on Accelerated Aging of Polyethylene

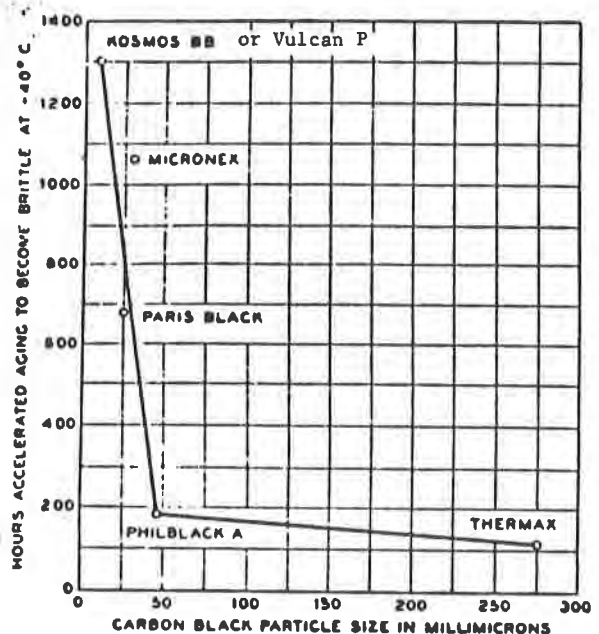


Figure 3

CARBON BLACK CONCENTRATIONS

Effect On Accelerated Aging of Polyethylene

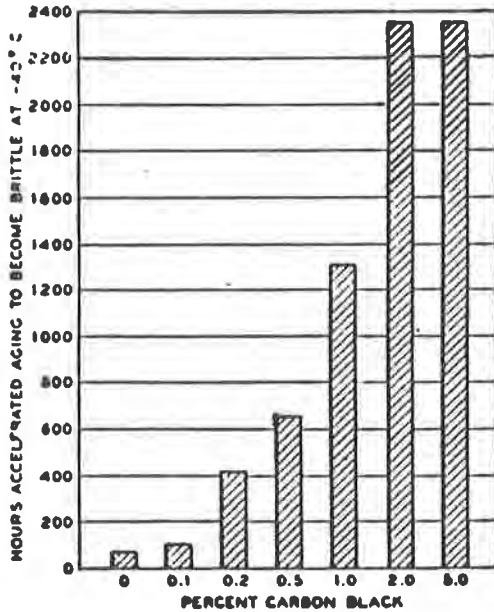


Figure 4

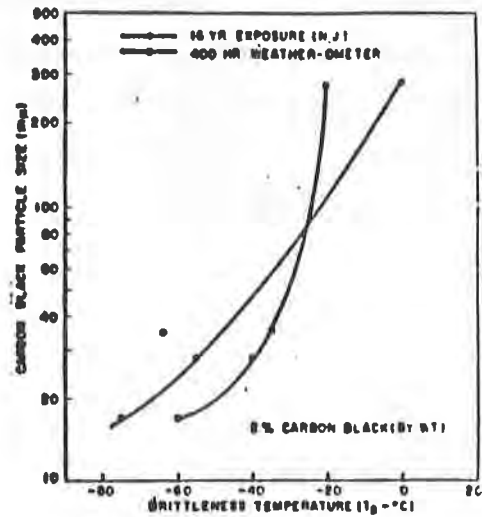


Figure 5
EFFECT OF CARBON PARTICLE SIZE ON WEATHER RESISTANCE OF BLACK POLYETHYLENE

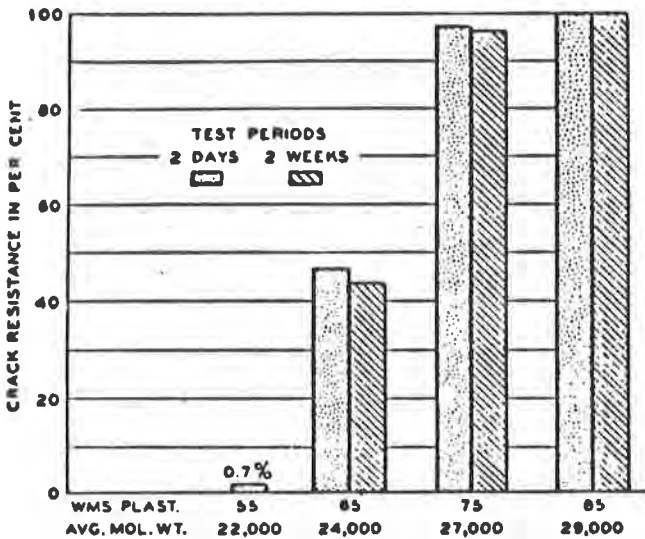


Figure 6 Effect of molecular weight on crack resistance

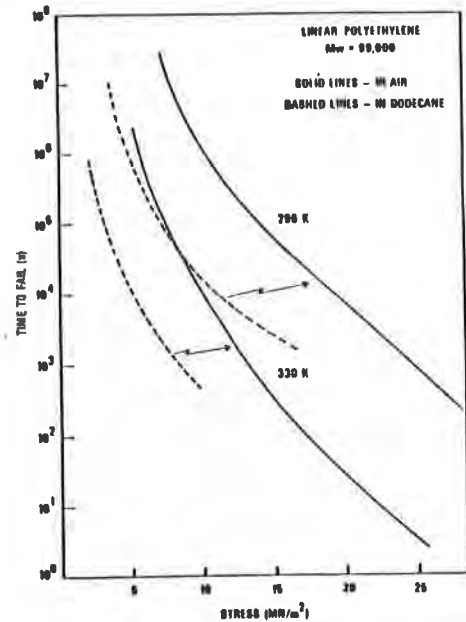


Figure 7 Log time to fail vs. applied stress for Sample 13: (—), in air; (---), in the solvent dodecane.

Bell Telephone Laboratories cracking test. Compounds contain 2-per-cent carbon black and 0.07-per-cent antioxidant

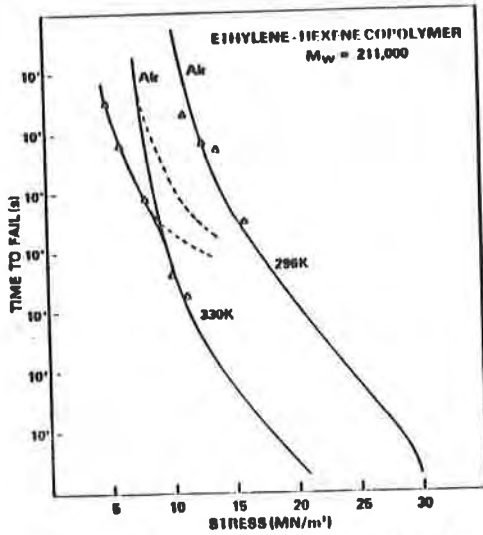


Figure 8 Log time to fail vs. applied stress for Sample E; (—), the time to fail in air; (- - Δ - -), the time to fail in stress-cracking agent; (- - -), the extension to higher stresses of the crack growth mechanism which obeys equation 1.

ACKNOWLEDGEMENTS

In a review of this nature the prime work has always been completed by the wide range of authors and researchers quoted in the text and table of references, without which the review would not have been possible. In addition, in the particular case of this paper, the help given by many of these authors and researchers directly, in particular Sir Hugh Ford, Professor I.M. Ward and members of the staff of ICI Plc and BP Chemicals Limited, was of great assistance. Also Dr. F.B. Mercer, Mr. K.F. Martin, Dr. D.I. Bush and Mr. R. I. Robinson of Netlon Limited and Mr. D.B.G. Swan, Teaching Company Associate, and Ms. Janet Rivett of The Tensar Corporation have provided invaluable advice and a significant contribution to the preparation of the paper. Thanks are also due to Sandy Waddell for typing this paper.

REFERENCES

1. Wallder, V.T., "Polyethylene for Wire and Cable". Bell Telephone Laboratories, Inc., Murray Hill, New Jersey, 1955.
2. Gilroy, H.M. and J.B. Howard, "Natural and Artificial Weathering of Polyethylene, Bell Telephone Laboratories, Inc., Murray Hill, New Jersey, Volume 9.
3. Jensen, W.F., Jr., and J.N. Jones, "Weatherability of Black Polyethylene--Predictable?", E.I. DuPont de Nemours & Co., Plastic Products and Resins Department, Wilmington, Delaware, 1969.
4. Wallder, V.T., W. J. Clarke, J.B. DeCoste, and J.B. Howard, "Weathering Studies on Polyethylene", Bell Telephone Laboratories, Inc., Murray Hill, New Jersey.
5. ICI plc, : Technical Report No. TS/P/A/14/86 : Petrochemicals & Plastics Division, April 1986.
6. Walker, D.M. & Juzkow, M.W., : PE/Carbon-Black Survives 20 Years of Weathering in Canada : Modern Plastics International 13 (6) 36-69 (June 1983).
7. Wrigley, N.E., "The Durability of TENSAR Geogrids, Materials Science and Technology", to be published, 1987.
8. Pleshanov, Berlyant, and Burukhina, "Study of Kinetics of Inhibition of Thermo-Oxidation of Polyethylene by Carbon Black", 1982.
9. Popov, Blinov, Krisyuk, Karpova, Peverov, and Zaikov, "Oxidative Degradation of Polymers Under Load. Ozone-Oxygen Action on Oriented Polyethylene", Chemical Physics Institute, U.S.S.R. Academy of Sciences, April 1980.
10. Capaccio, G., T.A. Crompton, I.M. Ward : The Drawing Behaviour of Linear Polyethylene I : Journal of Polymer Science, Polymer Physics Edition, Volume 14, 1641-1658 (1976).

11. Cappacio, G., & I.M. Ward : Structural Studies of Ultrahigh-Modulus Linear Polyethylene Using Nitric Acid Etching and Gel Permeation Chromatography, I & II : Journal of Polymer Science, Polymer Physics Edition, Volume 20, 1107-1128 (1982).
12. Glenz, W., A. Peterlin : Crystal Size in Highly Drawn Polyethylene : Journal of Polymer Science, Part A2, Volume 9, 1243-1254 (1971).
13. Marshall, J.M., P.S. Hope, I. M. Ward : Sorption and Diffusion of Solvents in Highly Oriented Polyethylene Polymer, 1982, Volume 23, January, 142-143.
14. Ward, I.M., A.M. Selwood, B. Parsons, A. Gray : The Production and Properties of Die-Drawn P.E. Pipe : Proc. 6th.
15. Paulos, J.P., L. Thomas : Effect of Post Drawing on the Permeability of Gases in Blown Polyethylene Film : Journal of Applied Polymer Science, Volume 25, 15-23 (1980).
16. Hawkins, W.L., "The Role of Carbon Blacks in the Thermal Oxidation of Polyolefins", Journal of Applied Polymer Science, 1959.
17. Palermo and Deblieu, "Ageing of Polyethylene Pipe in Gas Distribution Service, A.G.A. Distribution Conference, 1983.
18. Herms, J., L.H. Peebles Jr., D.R. Uhlmann : Chemical Stress Cracking of Acrylic Fibres : Journal of Materials Science 18 (1983) 2517-2530.
19. I.S.O. : Buried Polyethylene Pipes for the Supply of Gaseous Fuels, Draft International Standard ISO/DIS 4437.2, 1984.
20. Downes, G. : Polyolefins : Physical Properties : Vinyl and Allied Polymers, Volume I, Iliffe Books 1968, p. 140 et. seq.
21. BP Chemicals Ltd. : Chemical Resistance of Rigidex : Technigram T800/1.
22. ICI Plc, : Technical Report No. TS/P/A/50/85 : Petrochemicals & Plastics Division.
23. Dolezel, B. " The Resistance of Plastics to Micro-Organisms : British Plastics, October 1967, 105-112.
24. Albertson, A-C., : Biodegradation of Synthetic Polymers II : Journal of Applied Polymer Science, Volume 22, 3419-3433 (1978).
25. Albertson, A-C. : Biodegradation of Synthetic Polymers III : Journal of Applied Polymer Science, Volume 22, 3435-3477 (1978).
26. Albertson, A-C., Z.G. Banhidi : Microbial and Oxidative Effects in Degradation of Polyethene : Journal of Applied Polymer Science, Volume 25, 1655-1670 (1980).

27. Griffin, G.J.L. : Degradable Polyethylene in the Packaging Field : Polyethylenes 1933-1983. C.4.8.1-C.4.8.9.
28. Connonly, R.A., J.B. DeCoste, H.L. Gaupp : Marine Exposure of Polymeric Materials and Cables after 15 Years : Journal of Mat., JM LSA, Vol. 5, No. 2, June 1970, 339-362.
29. Dinsey, M. : A Test of Polythene Pipes for their Resistance to Termite Attack : Bulding & Road Research Institute, Kumasi, 1981, Available from B.P. Chemicals Ltd., Grangemouth.
30. B.P. Chemicals Ltd. : Data Sheet TDS 54.
31. Wallder, V.T., "Polyethylene for Wire and Cable", Bell Telephone Laboratories, Inc., Murray Hill, New Jersey.
32. Christ, B.K. Leong-Lacava, and S.H. Carr (Northwestern University), "Crack Propagation in Model Polyethylenes" Ninth Plastics Fuel Gas Pipe Symposium, pp. 242-248, November, 1985.
33. Zapas and Crissman, "Static Fatigue of Polyethylene in Uniaxial Creep In the Presence of Stress-Cracking Agents and Solvents", National Bureau of Standards, Washington, D.C.
34. Brown, R.P. : Testing Plastics for Resistance to Environmental Stress Cracking : Polymer Testing 1, (1980) 267-282.
35. ASTM Standard Test Method D 2552-69 (Reapproved 1980) : Environmental Stress Rupture of Type III Polyethylenes Under Constant Tensile Load.



SESSION 4B
FILTRATION

The first part of the document discusses the importance of maintaining accurate records of all transactions. It emphasizes that every entry, no matter how small, should be recorded to ensure the integrity of the financial statements. This includes not only sales and purchases but also expenses, income, and transfers. The text suggests that a systematic approach to record-keeping is essential for identifying trends and potential areas of concern.

In the second section, the author addresses the common challenge of reconciling bank statements with the company's internal records. It provides a step-by-step guide to identifying discrepancies, such as timing differences or errors in recording. The importance of regular reconciliation is highlighted to prevent small errors from accumulating and causing significant issues at the end of the period.

The third part of the document focuses on budgeting and financial forecasting. It explains how a well-defined budget can serve as a roadmap for the organization's financial goals. By comparing actual performance against the budget, management can make informed decisions about resource allocation and identify areas where costs are being exceeded. The text also touches upon the importance of reviewing and adjusting the budget as circumstances change.

Finally, the document concludes with a discussion on the role of financial statements in providing a clear picture of the organization's financial health. It stresses that these statements are not just for internal use but are also crucial for communicating with stakeholders, including investors, lenders, and regulatory bodies. The author encourages a transparent and accurate approach to financial reporting to build trust and ensure long-term success.

ROLLIN, A.L.
Ecole Polytechnique de Montreal, Canada
DENIS, R.
Solmers Internationale, Canada

Geosynthetic Filtration in Landfill Design

INTRODUCTION

Following the same footsteps as the industry at large, geosynthetics are now extensively used in landfill design. Synthetic products such as geomembranes, geonets and geotextiles are not only being specified out of preference for such projects, they are indeed compulsory in answer to regulations, proper design, reliability and constructability.

Although numerous references, case histories and design procedures are readily available from both governmental and industrial sources, specific information concerning drainage consideration of these secure landfills are somewhat often overlooked. It is very important to keep in mind that a landfill is considered **SECURE** or **impervious** if its **intrinsic drainage system** is throughly operational.

This corollary implies that all landfill elements must be properly selected and installed. They must function as expected and that includes all filtration and drainage geotextiles unfortunately often eclipsed by the overwhelming impervious necessities of the liner itself. Accurate design and construction procedures pertaining to geotextiles used in this specific context have been traditionally handled with a relatively liberal approach. In fact, geotextiles have been known to clog once in a while or worst yet, not to filter at all on account of incompatibilities between soil granulometry and fabric opening size. Realizing the potential problems at a landfill level, the purpose of this paper is to expose those related concerns and to propose a design approach.

HYDRAULIC PROPERTIES OF GEOTEXTILES

The hydraulic properties of geotextiles are considered for separation, filtration and drainage functions. These properties (presented in Table-1) are governed by the textile structure comprised of synthetic fibres or filaments whether knitted, woven, needle-punched or thermally bonded.

normal permeability or permittivity
transverse permeability or transmissivity
filtration opening size (FOS)
apparent opening size (AOS)
wettability

TABLE-1: HYDRAULIC PROPERTIES OF GEOTEXTILES

Standard test procedures are used to determine property values of virgin geotextiles. Since these properties may vary during their utilization in earth structures by clogging or blocking, a decrease in permittivity and transmissivity can jeopardize the entire design.

Many investigations pertaining to geotextile clogging mechanisms in drainage applications have been reported (1,3,6,7,22,23,25,26,27,28), where a great number of clogging factors have been identified (see Table-2). Furthermore it is very likely that a number of factors acting together are responsible for the clogging mechanism.

hydraulic conditions
soil conditions
structural characteristics of the geotextiles
microorganisms
quality of the drained water
nature and size of waste particles to retain

TABLE-2: FACTORS INFLUENCING CLOGGING OF GEOTEXTILES

FILTRATION MECHANISMS

Two distinct types of filtration are recognized: a) soil in contact with the geotextile ; and b) soil particles in suspension.

1) SOIL IN CONTACT WITH GEOTEXTILE

Geotextiles are often used to drain soils to stabilize earth structures by retaining soil particles in place while allowing excess pore pressure to be relieved. To perform this function, the fabric must act as a synthetic barrier suitable to the formation of a natural filter by one of the following mechanisms: a) bridge network formation ; or b) vault network formation.

A) bridge network formation

As shown by Carroll (2) and since then supported by many investigators (4,20,24), geotextiles to be used in relatively well graded soils should be selected to stop the larger size particles (d_{65} or d_{75}). Under a hydraulic gradient, small particles located initially at the soil-geotextile interface will be carried into the fabric structure by the flowing water. These particles may be trapped inside the geotextile or entrained through the filter. As a consequence, the larger size particles will migrate to the filter interface and will eventually retain smaller and smaller particles upstream (as shown schematically on Figure-1). After a while, a natural granular filter is formed and soil movement is halted.

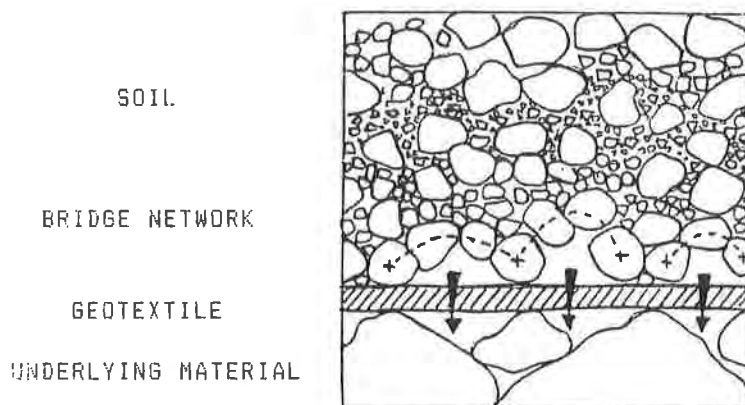


FIGURE-1: BRIDGE NETWORK FORMATION

B) vault network formation

Vault formation may occur in well graded soils with an appreciable clay content. The adhesion of soil particles and geotextile fibres can be promoted by a proper choice of fibre coating and by special geotextile surface characteristics such as free fibres buffer layers (22). Such a geotextile behaves more like a conventional natural granular filter.

As schematically presented on Figure-2, a cross section of a geotextile with its adjacent soil layer displays formation of vaults. This mechanism enables to stop particles smaller than the opening size of the filter (defined as the FOS or AOS). In fact it was shown by Faure et al (11) and others (15,21,23) that the size of the larger retained particles can be as much as three times smaller than the opening size of the geotextile (the ratio of the FOS to the d_{65} of the soil decreasing as the soil uniformity coefficient decreases).

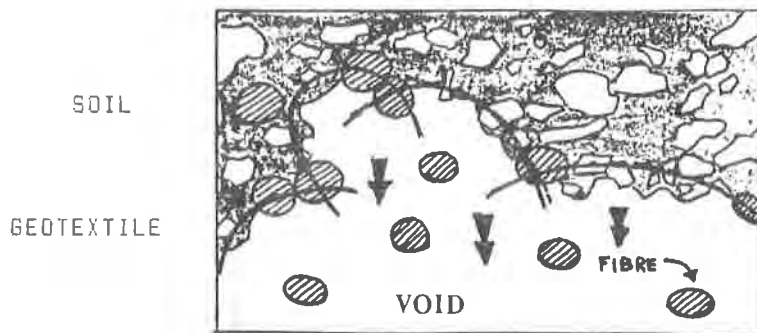


FIGURE-2: VAULT NETWORK FORMATION

2) SOIL PARTICLES IN SUSPENSION

In many applications such as silt fencing, sea barriers, tailing pads, landfills and others works, a geotextile is used to retain particles in suspension in a liquid. Often during construction, soil particles may be carried by rain water or particles can easily be carried by water in a saturated environment. Delays of covering or lack of contact between the soil and the geotextile constitutes inciting conditions stimulating particles to reach freely the filter as shown in Figure-4. Under these conditions clogging risk is very high.

The filtration mechanism is similar to industrial filtration and must be differentiated from the previous described mechanisms. The life expectancy of the filters is short and the geotextile must be serviced at regular intervals or be used for a rigorously evaluated period of time prior to its selection.

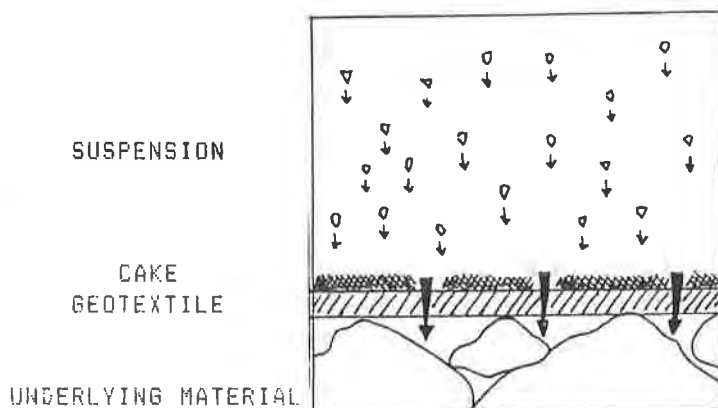


FIGURE-4: SOIL PARTICLES IN SUSPENSION

FILTRATION CRITERIA

Many filtration criteria for geotextiles have been proposed (17). Four widely used criteria for formation of a natural filter and one for the stopping of particles in suspension are gathered in this paper.

A) CFG CRITERION

The French Committee on Geotextiles (CFG) has adopted the following criterion (4):

$$FOS < C_1 \times C_2 \times C_3 \times C_4 \times d_{85} \dots\dots [1]$$

where FOS = the Filtration Opening Size of the filter measured by hydrodynamic sieving (9,12,13).

C₁ = coefficients as presented in Table-3.

d₈₅ = the diameter of soil particles at which 85% of the soil particles are, by dry weight, finer than that grain size. Care must be taken when using the d₈₅ of the fine fraction for a curve of type B as shown on Figure-3.

coeff.	value	condition
C ₁	1.00	for continuous and well graded soils
	0.80	for continuous and uniform soils
C ₂	1.25	for confined and dense soils
	0.80	for unconfined and loose soils
C ₃	1.00	for hydraulic gradient i < 5
	0.80	for hydraulic gradient 5 < i < 20
	0.60	for hydraulic gradient 20 < i < 40
C ₄	1.00	for filtration function only
	0.30	for filtration and drainage functions

TABLE-3: COEFFICIENTS TO USED IN CFG FILTRATION CRITERION

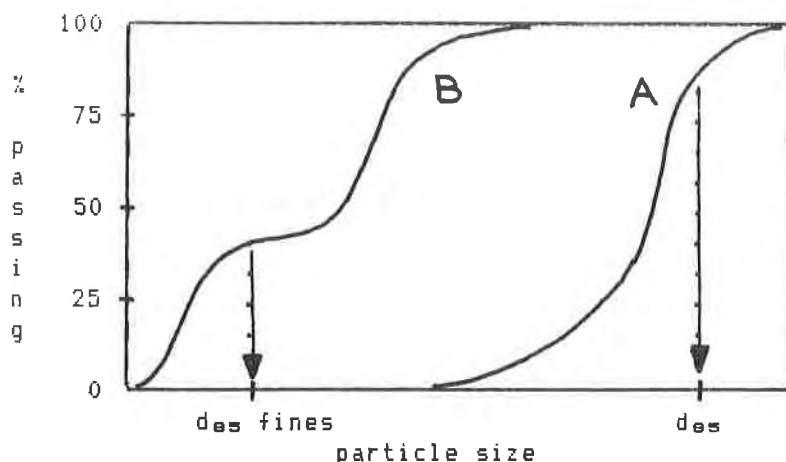


FIGURE-3: DETERMINATION OF d_{65} FROM GRANULOMETRIC CURVES

B) GIROUD CRITERION

The Giroud (15) criterion is based on the density index (I_D), the normalized uniformity coefficient (C_U) of the soil, the apparent opening size (AOS) of the geotextile and the average particle size (d_{50}). This criterion should not be used with soil having a granulometric soil as type B in Figure-3 nor for a two directional flow. This criterion is summarized in Table-4.

	$1 < C_U < 3$	$C_U > 3$
$I_D < 35\%$	$AOS < 1.0 C_U d_{50}$	$AOS < 9.0 d_{50} / C_U$
$35\% < I_D < 65\%$	$AOS < 1.5 C_U d_{50}$	$AOS < 13.5 d_{50} / C_U$
$I_D > 65\%$	$AOS < 2.0 C_U d_{50}$	$AOS < 18.0 d_{50} / C_U$

TABLE-4: GIROUD CRITERION

C) FHA CRITERION

The Federal Highway Administration criterion (5,19) is based on Equivalent Opening Size (EOS), the d_{65} of the soil and the gradient ratio (G.R.) (18). This criterion is divided into clogging and filtration criteria as presented in Table-5.

D) IRIGM/EPM CRITERION

The criterion developed by the Institut de Recherche Interdisciplinaire de Geotechnique et Mecanique, University de Grenoble in collaboration with Ecole Polytechnique de Montreal (11) is based on the filtration opening size (FOS) and the d_{65} of the soil as summarized in Table-6.

FILTRATION	$0.149 \text{ mm} < E_{OS} < d_{es}$	for soils with 50% or less particles passing sieve no. 200.
	$0.211 \text{ mm} > E_{OS} > 0.149 \text{ mm}$	for soils with greater than 50% of particles passing sieve no. 200
CLOGGING	non-woven G.R. < 3.0	for severe applications
	woven open area > 4%	
	fabric $K > 10 \times \text{soil } K$ $K = \text{normal permeability}$	for other applications

TABLE-5: FHA FILTRATION CRITERIA

for uniform soils	$FOS < 1.5 d_{es}$
for continuous graded soils	$1.5 < FOS / d_{es} < 3.0$

TABLE-6: IRIGM/EPM FILTRATION CRITERION

E) STOPPING OF PARTICLES IN SUSPENSION CRITERION

The only proposed criterion to be used for suspension of particles has been proposed by the French Committee on Geotextiles (4).

$$4 \times d_{15} < FOS < C_1 \times C_2 \times C_3 \times C_4 \times d_{es} \dots \dots \dots [2]$$

where C_1 = coefficients from Table-3

GEOTEXTILE USES FOR LANDFILL DESIGN

Three of the four major functions as originally identified by Giroud (16) may be assumed by geotextiles in landfill design: A) filtration; B) drainage; and C) separation.

In order to clearly visualize this three-way involvement, a landfill cross-section is presented in Figure-5. This schematic cross-section should not be considered as corresponding to an exhaustive case nor to minimum design

requirements. It's only purpose is to assemble into one view the different geosynthetics liable to be found in state-of-the-art landfill design. As shown, the different layers are grouped into three major design elements (indicated by roman numerals):

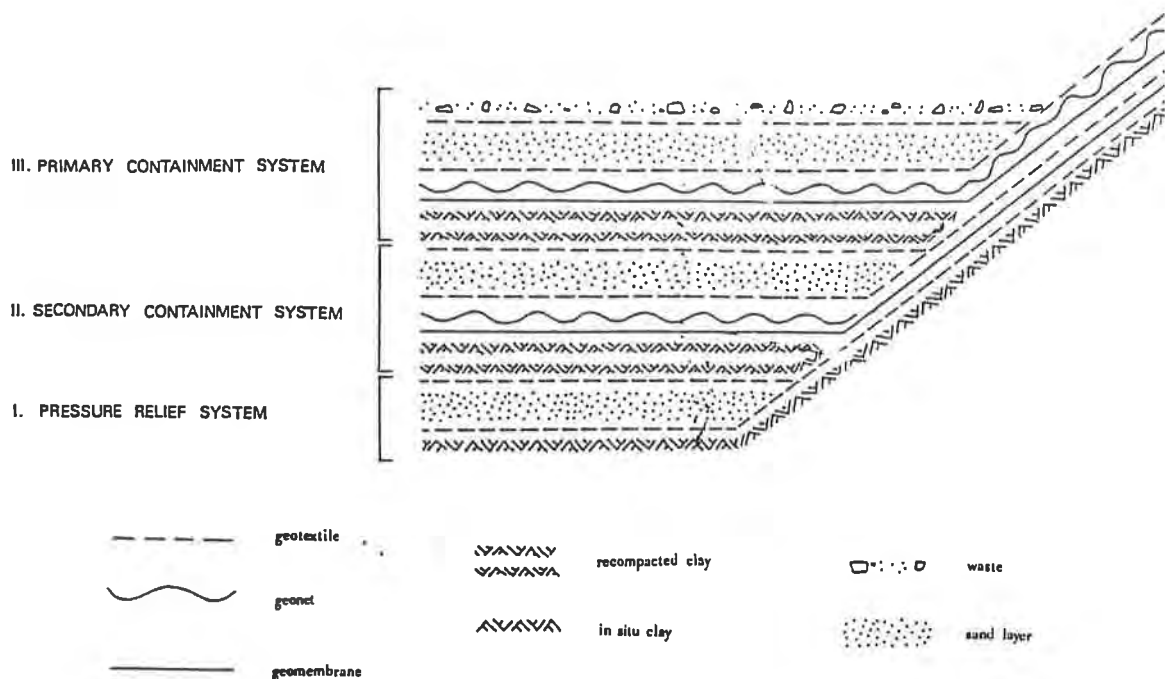


FIGURE-5: CROSS SECTION OF A LANDFILL

I) PRESSURE RELIEF SYSTEM

Should a pressure relief system be required for the site-specific design to prevent hydrostatic uplift from the in-situ clay pore pressure, a separation geotextile (GX-1) (see Table-7) might be required to prevent contamination of the collecting sand layer by the underlying in-situ clay layer's fines. It is usually desirable to insert such a geotextile since construction might be seriously impaired by the corresponding high water content of the in-situ clay.

Additionally, since placement of natural granular material on steep slopes is a feat by itself, thick non-woven geotextiles or geonets (GX-2) will be utilized to drain off excessive slope pore pressure towards the lower collecting sand layer.

Finally, since a maximum thickness re-compacted clay layer is usually required prior to installing the secondary membrane (GM-1), a second separation geotextile (GX-3) might also be needed on top of the collecting sand layer for anti-contamination purposes. This latter geotextile will obviously not run on the slope area since sand would only be placed on the near-horizontal bottom portion of the cell.

II) SECONDARY CONTAINMENT SYSTEM

In addition to the secondary containment system's role of primarily assuring a second impervious barrier, a leak detection responsibility will also be assumed. This detection task will again necessitate the use of geosynthetics. Since by definition **DETECTION is associated with accuracy and swiftness**, the selection of materials can not be over-stressed. In practice, a high flow/velocity medium will be installed on top of the secondary membrane (GM-1) and will comprise both geonets and geotextiles in addition to a sand layer.

A geotextile (GX-4) will thus be placed between the sand layer and the geonet (GN-1) as a separator to prevent contamination and insure the high velocity characteristics of the geonet layer on the bottom portion of the cell.

On the slope areas, if geonets are not used, a thick non-woven geotextile (GX-5) will be installed to provide drainage towards the bottom of the cell.

Finally, since a re-compacted clay layer is often required below the primary geomembrane (GM-2), a geotextile separator (GX-6) will be called for and installed between this clay layer and the sand layer to prevent contamination.

III) PRIMARY CONTAINMENT SYSTEM

The primary containment system also assumes two functions: it obviously offers the main leachate carrier, but it also carries a leak collection responsibility in answer to regulatory guidelines pertaining to maximum depth of collected leachate. This collection task will again necessitate the use of geosynthetics in a very similar secondary containment system fashion.

A geotextile (GX-7) will thus be installed between the collection sand layer and the high/velocity geonet layer (GN-2) as a separator on the bottom of the cell.

On slope areas where geonets are almost always utilized in a collection context, a geotextile (GX-8) will also be used and placed above the geonet to prevent it's contamination from the waste itself. This geotextile will then assume two functions: separation and filtration.

Finally, a geotextile (GX-9) will be installed additionally to provide separation and filtration in the bottom of the cell between the waste and the sand collection layer.

To recapitulate, as shown in Table-7, nine geotextiles might be used in a landfill to fulfill separation, filtration and drainage functions. Geotextiles may also be used for numerous other applications in landfill design such as a much needed protective cushion in sump areas and around appurtenances. Geotextiles are also extremely handy during the actual landfill construction where they are often used for silt fencing thus assuming another

filtration role. Those additional uses are nevertheless beyond the scope of this paper.

SYSTEM	GEOTEX.	BETWEEN	FUNCTIONS	CLOGGING RISK
I	GX-1	in-situ clay sand layer	S	very high
I	GX-2	in-situ clay geomembrane GM-1	S - F - D	high
I	GX-3	sand layer recompacted clay	S	low
II	GX-4	sand layer geonet GN-1	S	very low
II	GX-5	geomembrane GM-1 geomembrane GM-2	D	very low
II	GX-6	recompacted clay sand layer	S	low
III	GX-7	sand layer geonet GN-2	S	very low
III	GX-8	waste geonet GN-2	S - F	very high
III	GX-9	waste sand layer	S - F	very high

where S = separation, F = filtration and D = drainage

TABLE-7: GEOTEXTILES USED IN LANDFILL DESIGN

IMPORTANCE OF FILTRATION CONSIDERATIONS

As originally stated in the introduction, the main purpose of this paper is to caution design engineers against neglecting the filtration characteristics of all geotextiles used in a landfill. Without going in details with the consequences of all individual geotextile filtration deficiencies, one can clearly understand that the anticipated performance of a landfill can seriously be jeopardized by a single filtration non-conformance.

To illustrate this concern, the following scenario is presented: assuming that insufficient care has been taken when specifying the waste/sand collection layer geotextile (GX-9) so that clogging occurs at the interface on account of the filtration incompatibility of the geotextile with the waste's granulometry. The resulting situation can be quite pathetic for the following reasons:

1) the leachate will obviously pond on top of the collection system and will undoubtedly do so in excess of the maximum permitted depth (one foot (8)) since it simply has nowhere to go. The problems associated with such a situation can reasonably be deduced as follows:

- a) the bottom portion of the waste is always saturated preventing any meaningful compaction.
- b) leachate overflow towards unprotected areas is very prone to happen if the landfill was designed with some temporary berms (usual method used in multi-phase cell construction).
- c) the landfill does not conform to regulations.

2) the collection system will always be dry and this condition constitutes the only indication of the faulty system. Consequently the detection system will also always be dry and this condition will not yield any meaningful conclusions.

It is quite obvious that a situation as the one previously described would translate into a major headache just to mention the forensic investigations, liabilities, and most important, the proposed solution keeping in mind that probably Mega-tons of waste may have already been buried.

The functions performed by each geotextile used in a landfill and the clogging risks involved are presented in Table-7.

GEOTEXTILE DESIGN PROPOSED METHOD

As previously demonstrated in numerous references (4,10,15) , geotextile filtration performance is mainly dictated by two parameters: the geotextile inner structure and the nature and granulometry of the soil or waste in contact. Unfortunately this latter parameter currently constitutes the thorn in one's side for whomever is faced with a landfill design. As a matter of fact, a design engineer can consider himself very fortunate in possessing any valuable data related to the anticipated waste nature, let alone it's granulometry. As a consequence, the selection of geotextiles GX-8 and GX-9 becomes very problematic.

To accurately apply the filtration criteria already presented, compulsory waste samples of the anticipated first lift would have to be submitted and tested prior to any design conclusions. The procedure would be similar to geomembrane chemical compatibility testing methodology where landfill permit-seekers are requested to supply leachate samples for analysis. In the absence of knowledge of the waste nature and granulometry, proper selection of geotextile becomes unrealistic (in fact it is important to note that landfill faulty drainage may also be caused by impervious waste lifts, but this constitutes a topic beyond the scope of this paper).

Since clean sands do not usually constitute a problem when in contact with a geotextile, this design procedure is meant to be utilized for either clay soil or waste interfaces. Looking back at Table-7 yields the following six identified geotextiles: GX-1, GX-2, GX-3, GX-6, GX-8 and GX-9.

To insure satisfactory filtration performance, proposed characteristics of geotextiles used in landfill are presented in Table-8. The type of geotextile to use, their Filtration Opening Size (FOS) and their normal permeability (K) are specified taking into account the nature of the material to retain. The FOS has been selected over ADS or EOS since the test method used to evaluate it is not limited to geotextile of opening size greater than 100 μm . Characteristic granulometries of compacted clay and clean sand were used to establish values for geotextiles GX-3 to GX-7. On the other hand, characteristic granulometry of in-situ clays and pore pressure conditions were taken into account in determining geotextiles GX-1 and GX-2 parameters. As already mentioned, the characteristics of geotextiles GX-8 and GX-9 can be selected only if the waste left to be placed in the bottom of the cell has been characterized. Exact values of FOS and permeability of all geotextiles can be obtained by using one of the established selection criteria.

GEOTEX	TYPE	FOS	PERMEABILITY
GX-1	non-woven	< 75 μm	low
GX-2	thick non-woven or geonet	> 75 μm	low
GX-3	non-woven	< 140 μm	intermediate
GX-4	non-woven	< 140 μm	high
GX-5	thick non-woven or geonet	> 75 μm	high
GX-6	non-woven	< 140 μm	intermediate
GX-7	non-woven	< 140 μm	high
GX-8	thick non-woven	?	intermediate
GX-9	non-woven with open structure or free fibre buffer layer	?	?

TABLE-8: SUGGESTED CHARACTERISTICS RANGE OF GEOTEXTILES IN LANDFILL DESIGN

QUALITY ASSURANCE PROGRAM CONSIDERATIONS

Realizing the fact that expected design efficiency is directly proportional to construction controls, landfill geotextile quality controls should not be considered lightly. Unfortunately although extensive severe quality assurance programs have reached industry standard levels, not enough consideration has been devoted to geotextiles, truly one of the backbones of landfill performance.

All quality controls should obviously be oriented toward ensuring that all factors that influence clogging of geotextiles as previously identified in Table-2, are minimized. As a result, controls will be needed at all project stages to ensure the expected efficiency;

A) DESIGN STAGE

- expected waste granulometry (first lift)
- all granular materials granulometry
- expected leachate quantities and flows
- leachate/geotextile chemical compatibility
- proposed geotextile FOS

B) CONSTRUCTION STAGE

- conformance testing of all filtrating and filtrated elements
- proper installation of all filtrating elements

C) OPERATIONAL STAGE

- proper placement of first waste lift
- on-going detection system monitoring
- on-going collection system monitoring
- on-going over-all site stabilization monitoring

D) POST-CLOSURE STAGE

- on-going detection system monitoring
- on-going collection system monitoring
- on-going over-all site stabilization monitoring
- on-going spill monitoring

CONCLUSION

Design considerations and controls of geotextile filtration parameters are of paramount importance in landfill design. Although numerous types of geotextiles are readily available on the market presently, the design engineer is cautioned to rely on established selection criteria for his ultimate choice realizing that this process may call for yet-to-be-seen type of product that would specifically apply to the waste industry.

BIBLIOGRAPHY

- 1- BROUGHTON R.S., Damant C., Ami S. and English B., "The Soil Retention and Water Flow Performance of Some Drain Tube Filter Materials", CPTA annual meeting, Pointe Clear, Alabama (1976).
- 2- CARROLL R.G., "The Study of Fabric Variance in the Development of Design Criteria for Fabric Filter", Master thesis, University of Tennessee (1975).
- 3- CESTRE T., "Revue des criteres d'appréciation des risques de colmatage mineral des drains agricoles", CEMAGREF, bulletin information no 325 (1985).
- 4- COMITE FRANCAIS DES GEOTEXTILES, "Recommandations pour l'utilisation des geotextiles en filtration et drainage", brochure CFG (1986).
- 5- CORPS OF ENGINEERS, "Civil Works Construction Guide Specification for Plastic Filter Fabrics", specification no CW-02215, US Army Corps of Engineers, Washington (1977).
- 6- DIERICKX W. and Yuncuogly H., "Factors Affecting the Performance of Drainage Envelope Materials in Structural Unstable Soils", Agric. Water Management, vol 5, 215 (1982).
- 7- DIERICKX W., "Field Experience and Laboratory Research on Drainage Envelopes", proceedings int. sem. on Land Drainage, 51, Helsinki (1986).
- 8- EPA, "Minimum Technology Guidance Document on Double Liner System for Landfills and Surface Impoundments; Design, Construction and Operation", EPA-530-SW-85-014 (1985).
- 9- FALYSE E., Rollin A.L., Rigo J.M. and Gourc J.P., "Study of the Different Techniques used to Determine the Filtration Opening Size of Geotextiles", proceedings 2nd Canadian symposium on Geotextiles and Geomembranes, 45-50, Edmonton (1985).
- 10- FAURE Y., Gourc J.P. and Sundias E., "Influence of the Filtration Opening Size on Soil Retention Capacity of Geotextiles", proceedings of the int. conf. on flexible armoured revetments incorporating geotextiles, London (1984).
- 11- FAURE Y., Gourc J.P., Brochier P. and Rollin A.L., "Interaction sol-geotextiles en filtration", proceedings 3rd int. conf. on Geotextiles, 1207, Vienna (1986).
- 12- FAYOUX D., "Filtration hydrodynamique des sols par les geotextiles", proceedings int. symp. of the used of geotextiles in geotechnical structures, vol 2, 329, Paris (1977).

- 13- FAYOUX D., "Porometrie, permeabilite et drainage", Jordana Hispana Francesa sobre Geotextiles, Barcelone (1981).
- 14- GIROUD J.P., "Designing with Geotextiles", Materiaux et Constructions, RILEM, vol 82 (1981).
- 15- GIROUD J.P., "Filter Criteria for Geotextiles", proceedings 2nd int. conf. on geotextiles, vol 1, 103-108, Las Vegas (1982).
- 16- GIROUD J.P., "Introduction to Geotextiles and their Applications", geotextiles and geomembranes definitions, properties and design, selected papers, IFIA (1984).
- 17- GOURC J.P., "Quelques aspects du comportement des geotextiles en mecanique des sols", PhD thesis, University of Grenoble (1983).
- 18- HALLIBURTON T.A. and Wood P.D., "Evaluation of the US Army Corps of Engineers Gradient Ratio Test for Geotextiles Performance", proceedings of the 2nd int. conf. on geotextiles, vol 1, 97-101, Las Vegas (1982).
- 19- HALLIBURTON T.A., Lawmaster and McGuffey, "Use of Engineering Fabrics in Transportation", FHA instruction manual (1982).
- 20- KOERNER R.M. and Welsh J.P., "Construction and Geotechnical Engineering using Synthetic Fabrics", John Wiley and Sons (1980).
- 21- LEFLAIVE E. and Puig J., "L'emploi des textiles dans les travaux de terrassement et de drainage", bulletin de liaison, laboratoires ponts et chaussees, vol 69 (1974).
- 22- ROLLIN A.L., "Les mecanismes de colmatage des geotextiles non-tisses: analyse de structures colmatees", revue association suisse des professionnels de geotextiles, Zurich (1983).
- 23- ROLLIN A.L., Broughton R.S. and Bolduc G., "Synthetic Envelope Materials for Subsurface Drainage Tubes", CPTA annual meeting, Fort Lauderdale (1985).
- 24- ROLLIN A.L., "Mecanismes de colmatage des geotextiles", proceedings conf. on long term behaviour of Geotextiles, RILEM, Paris (1986).
- 25- SOTTON M. "Le vieillissement et la durabilite des geotextiles", congres INDEX, session 7 (1981).
- 26- SOTTON M., Leclercq B., Fedoroff N., Fayoux D. and Pauté J.L., "Contribution a l'etude du colmatage des geotextiles: approche morphologique", 2nd int. conf. on geotextiles, Las Vegas (1982).
- 27- STUYT L.C.P.M., "A Non-Destructive Morphological Study of Mineral Clogging of Drains", proceedings int. sem. on land drainage, 90, Helsinki (1986).
- 28- WILLARDSON L.S., "Exit Gradients at Drain Openings", proceedings 2nd int. drain workshop, 198, Washington (1982).

CANCELLI, A.

University of Milano, Italy

CAZZUFFI, D.

ENEL's Research Centre for Hydraulics and Structures, Italy

Permittivity of Geotextiles in Presence of Water and Pollutant Fluids

1. INTRODUCTION

The use of geotextiles has been increasing during the last 20 years in multifarious fields of civil engineering, and it's still increasing today. These materials can perform different, mechanical and hydraulic functions, depending on the specific application area.

When used in sanitary landfills, geotextiles generally perform hydraulic functions (filtration and drainage), and also of mechanical protection for the synthetic liner (1). In most cases, geotextiles are not supposed to come into contact with leachate, and interactions can be occasionally originated from putting-in-place defects, or from long-term deterioration of the geomembrane. On the other hand, there are some design solutions, in which a geotextile is used as filter and drainage for leachate collection systems (see sketches in fig. 1 a-b); thus, geotextiles come directly into contact with leachate since the beginning of sanitary landfilling operations, and they should be properly selected and designed for such working conditions.

Interactions between leachate and geotextiles can include both physical (hydraulic) and chemical phenomena. However, chemical aspects are not considered in this preliminary research work, and only the influence of leachate on permittivity of geotextiles is investigated.

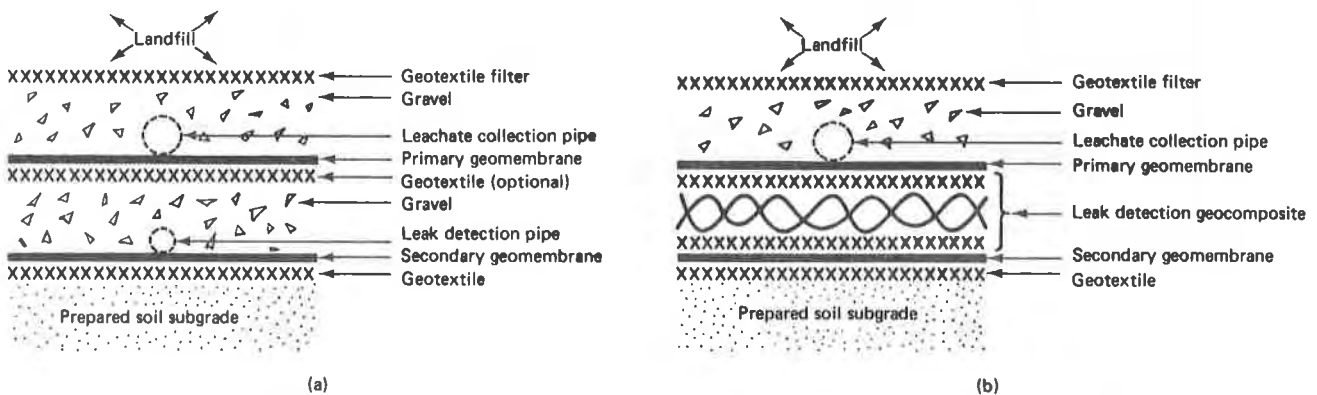


Fig. 1. Examples of technical solutions for double-lined landfills with leachate collection systems (from (1)).

2. EXPERIMENTAL WORK

The testing program included permittivity tests on several kinds of geotextiles, selected among the most commercially available in Italy. Two sets of tests were performed, accordingly to the type of fluid: demineralized water, and leachate.

2.1. The Testing Apparatus

All tests were carried out by means of a permeameter, that was purposely designed for geotextiles and realized at ENEL-CRIS laboratories in Milan (2) (3). Most parts are made with plexiglass: in this way, a direct observation of all phenomena rising during permeability tests is possible. The apparatus hydraulic scheme is shown in fig. 2; the basic elements are:

- the permeameter;
- the feeding group;
- the flow measuring group.

The permeameter is formed by 3 coaxial cylinders, having internal diameter of 284, 124 and 51 mm, respectively. The internal cylinder houses, at its base, the geotextile specimen to be tested, and, at the same time, it is the feeding cylinder for the permeability test. The intermediate cylinder acts as a constant level cylinder; the water exceeding the spillway is sent, by an overflow pipe, to the feeding tank.

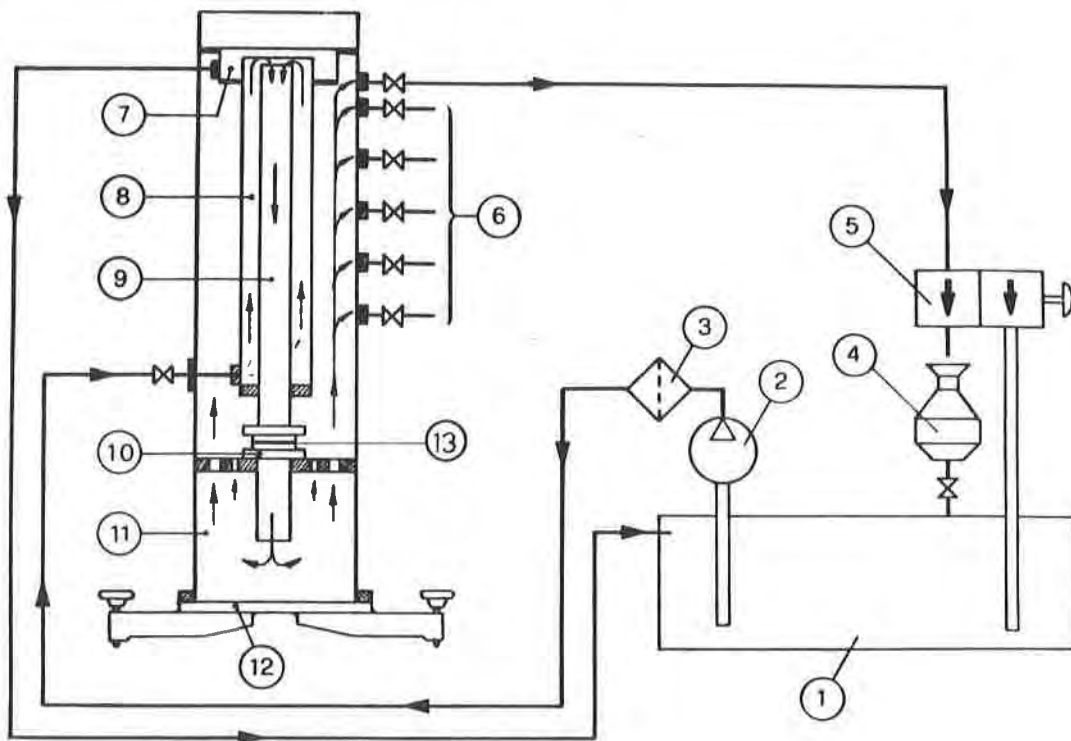


Fig. 2. Hydraulic scheme of the closed circuit, constant head permeameter for permittivity tests: (1) backwater tank; (2) feed pump; (3) filter; (4) calibrated container; (5) two-way valve; (6) outlets (6 positions for 6 different levels); (7) overflow system; (8) constant level cylinder; (9) feed cylinder; (10) specimen bearing; (11) external cylinder; (12) base; (13) geotextile specimen (from (2), (6)).

The external cylinder is the support of the entire apparatus; it has 6 openings, at 6 different levels, so that 6 different values of the hydrostatic load h can be applied (h is given by the difference between the spillway level and the selected outlet, and is maintained constant during a single test). Each opening has a cross section of 100 mm by 12 mm.

The feeding apparatus is formed by a pump, sucking water from a feeding tank; this tank is also the backwater tank at the end of the test circuit. The flow measuring group is essentially formed by a calibrated reservoir, that can be feeded, or excluded, by a two-way valve.

This constant head permeameter has a closed hydraulic circuit, so that the same permeability test can be performed by using the same, small quantity of demineralized, disaerated water (or, alternatively, leachate).

When performing normal permeability tests on geotextiles, a particular problem is given by the validity limits of Darcy-Ritter's law. In this view, an upper limit value was computed for the apparent water velocity, resulting $v_{\max} = 0.035$ m/s (3)(5). This means that a minimum value of the specimen thickness H , in turn function of the hydrostatic load h , should be kept. For this research work, the minimum value of H was obtained by superimposing different layers of the same geotextile; the number of layers was ranging from 3 to 6, depending on the thickness T_g of the geotextile to be tested (3).

The coefficient of normal permeability k_n and the permittivity Ψ of the geotextile are computed by the formulas

$$k_n = \frac{V \cdot H}{A \cdot h \cdot t} = \frac{V \cdot x \cdot T_g}{A \cdot h \cdot t} \quad (1)$$

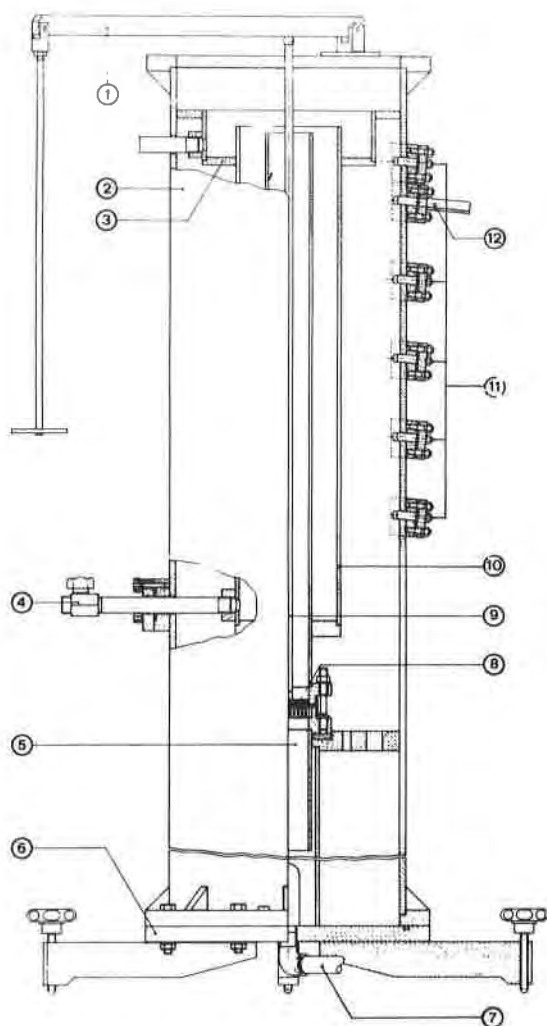
and

$$\Psi = \frac{V \cdot x}{A \cdot h \cdot t} \quad (2)$$

where: V = calibrated volume = $1450 \cdot 10^{-6}$ m³;
 A = specimen surface = $2043 \cdot 10^{-6}$ m²;
 H = specimen thickness (m);
 x = number of geotextile layers forming a specimen;
 h = hydrostatic load (m);
 t = required time to fill calibrated volume V during a single test (s).

The permeameter, as described above, allows for tests in the absence of normal stresses on the specimen surface. In order to perform permittivity tests under compressive normal stresses, the permeameter was modified as shown in fig. 3.

A synthetic porous stone (formed by monogranular, siliceous sand bonded by small quantities of polyester resin, and having permeability higher than tested geotextiles) is placed on the specimen surface, and overlaid by a PVC perforated element (bearing a spherical seat for the loading steel rod). The static load is applied by a lever system; values of the average normal stress σ up to 0.2 MPa were adopted in this testing program. The loading device is completed by a dial gauge, allowing to measure the variations of T_g versus the applied normal stress σ .



LEGEND

1. Loading system
2. External cylinder
3. Overflow system
4. Feed valve
5. Specimen support system
6. Base flange
7. Outflow valve
8. Geotextile specimen
9. Loading rod
10. Constant level cylinder
11. Outlets
12. To the flowrate measurement

Fig. 3. Scheme of the permeameter with the loading device, for permittivity tests in the presence of normal stresses (from (2)).

2.2. Characteristics of Tested Geotextiles

The complete list of tested geotextiles is reported in table 1, together with the most significant physical properties. For some materials, different thicknesses and masses per unit area were available, so that for most of them water and/or leachate was used as fluid for permittivity tests (see numbers or letters in table 1).

The list includes only nonwoven geotextiles: mostly monofilament, both needled and thermobonded, and some staple-type Italian products. The mass per unit area is ranging from 240 to 370 g/m², and the nominal thickness (as measured under $\sigma = 2$ kPa) from 2.1 to 9.2 mm.

Where possible, data about the opening size O_{95} were inserted into the table, as drawn from literature (4): these data are referred to the hydrodynamic filtration procedure, that is commonly adopted in Italy, France, and Belgium.

Table 1 - General characteristics and type of permittivity test developed on the considered geotextiles.

Commercial name and manufacturer	Polymer and process	Type	μ_2 (g/m ²)	Tg (mm)	O ₉₅ (μ m)	Permittivity test	
						Water	Leachate
BIDIM - Rhône-Poulenc(F)	PES NP CF	U 34	290	2.9	120	2	A
TREVIRA - Hoechst (D)	PES NP CF	11/300	300	2.8	120	1	
DRENOTEX - Politex (I)	PES NP SF	TFP	320	1.7	82	4	
SINTER - Ovatex (I)	PES NP SF	300	300	3.0	52	3	
DREFON - Man.Fontana (I)	PES NP SF	S-45	200	2.2	48		B
TECNOFELT - Tecnofibra (I)	PES NP SF	FAG	300	3.4	-		C
GEODREN - Edilfloor (I)	PES NP SF	PE/S	300	2.8	-		D
SODOSPUN - Sodoca (F)	PP NP CF	AS 420	320	3.1	-	5	
POLYFELT - Chemie Linz (A)	PP NP CF	TS 750	370	3.0	125	6	E
DREFON - Man.Fontana (I)	PP NP SF	SIA-200	200	2.9	-		F
STRATUM - Viganò Pav. (I)	PP NF SF	SIA-400	400	5.2	-		I
TYPAR - Du Pont (LUX)	PP TB CF	3807	280	0.7	37	8	H
TERRAM - I.C.I. (UK)	PP-PE TB CF	1000	140	0.8	100		G
		2000	240	1.1	80	7	

PES : polyester	PP : polypropylene	PE : polyethylene
NP : needle-punched	TB : thermo-bonded	
CF : continuous-filament	SF : staple-fibre	

2.3. Testing with Water

Permittivity tests on geotextiles have been concerned by several investigations, at least for $\sigma = 0$, and tentative standard methods were proposed in the most recent years (see e.g. (5)). Therefore, without entering in details of testing procedure, the following main points were kept present in this research work:

- a) all tests were carried out by using water that had been previously demineralized (by treatment with cationic and anionic resins), and disaerated by a vacuum pump; special care was used to eliminate air bubbles from the whole hydraulic circuit;
- b) for $\sigma = 0$ tests, in order to fulfill the aforementioned requirements for the validity of Darcy's formula ($v_{\max} = 0.035$ m/s), the specimen thickness was obtained by superimposition of 3 geotextile layers;
- c) for tests under normal stresses $\sigma \neq 0$, the same criterion required to double the number of layers, so to neglect the head loss due to the presence of porous stones in adjacency to the specimen;
- d) the water temperature was maintained approximately constant (about 20°C) for all tests;
- e) for $\sigma = 0$ tests, the time required to attain a steady state flow through the specimen was only 10 minutes;
- f) for $\sigma \neq 0$ tests, a complete stabilization was needed both for water flow and for the specimen compression under the datum load increment; therefore, times of 30 minutes about were necessary, and some tests were pursued for 24 hours or more (the program of loading steps was 0.002 - 0.026 - 0.05 - 0.075 - 0.100 - 0.125 - 0.150 - 0.175 - 0.200 MPa).

The results of tests on 8 different geotextiles are shown in fig. 4, where both the coefficient of normal permeability k_n and the permittivity Ψ are reported versus the normal stress σ . For each testing condition, the values of k_n and Ψ were obtained as mean values of 3 successive measurements. Concerning these results, the following observations can be made:

- a) in the absence of normal stresses ($\sigma = 0$), the values of k_n are ranging from $1.4 \cdot 10^{-4}$ m/s to $6.28 \cdot 10^{-3}$ m/s; accordingly, the values of Ψ vary from 0.2 to 2.22 s^{-1} ; these values are consistent with the range of values found by other researchers (1);
- b) for all geotextiles, k_n and Ψ decrease with increasing σ , but the rate of decrease is different from a geotextile to another, depending on nature of fibers and bonding processes;
- c) among monofilament, needled products, and for comparable values of mass per unit area μ and thickness T_g , PP geotextiles show values of k_n lower than PES ones; this fact is explained by the lower density of PP filaments and, consequently, by the lower porosity of PP geotextiles; anyway, the difference tends to be reduced with increasing σ ;
- d) as it's well known, thermobonded geotextiles show lower values of k_n and Ψ , with only a slight decrease with increasing σ , as a consequence of lower porosity and higher cohesion;
- e) staple - fibre products show intermediate values of k_n and Ψ between monofilament needled and thermobonded ones; they also show a more rapid decrease of k_n with increasing σ .

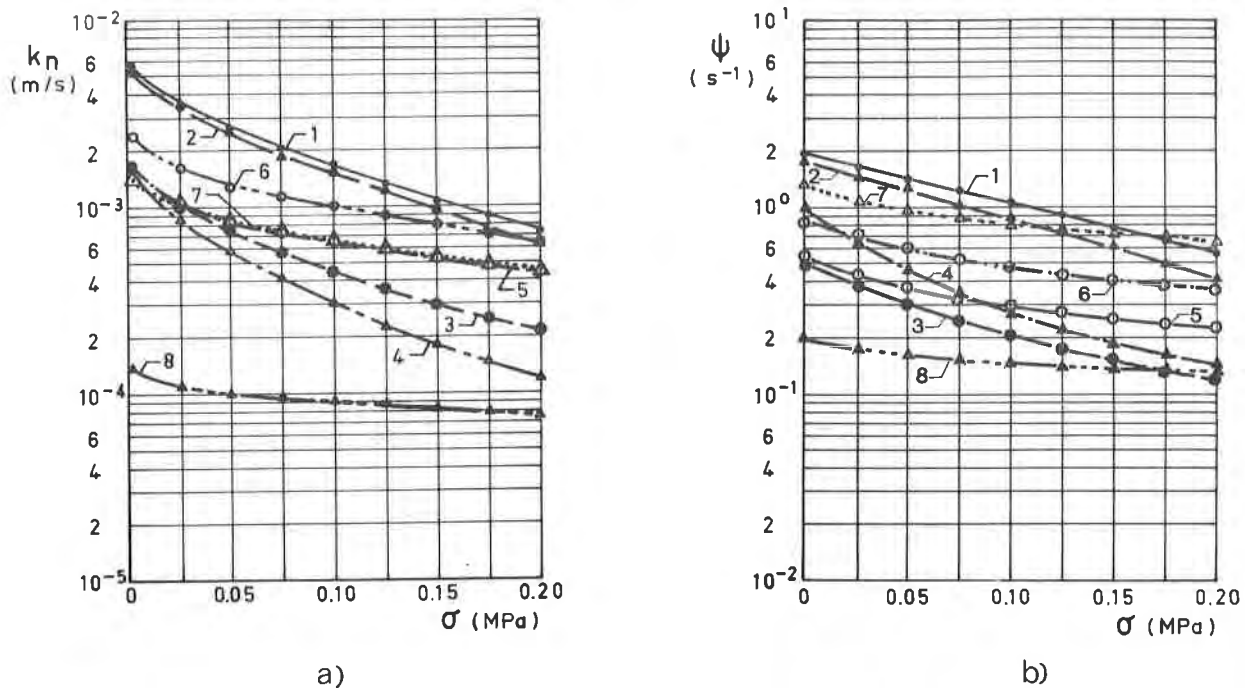


Fig. 4. Results of permittivity tests to water: a) k_n vs. σ ; b) ψ vs. σ (the numbers refer to geotextiles listed in table 1).

2.4. Testing with Leachate

In order to investigate the permittivity of geotextiles to contaminant fluids, a second series of tests was programmed and carried out. In general, the geotextiles were not the same of the former set of permittivity tests to water, and a real comparison was possible only for BIDIM U34, POLYFELT TS/750 and TYPAR 3807 (see table 1).

The contaminant fluid was sampled from the outlet of leachate collecting system of a sanitary landfill in Guanzate (Province of Como, Northern Italy). As permittivity tests were carried out in 2 groups at 2 different times, 2 separate samples had to be taken: sample A was used for testing BIDIM and POLYFELT, while sample B was used for all the other geotextiles (see table 1). The chemico-physical characterization of the two leachate samples is reported in table 2.

In defect of previous experiences with permittivity tests to leachate, the testing procedures were modified in the course of the research work. Owing to the (feared) high clogging capacity of leachate, testing specimens formed by a single geotextile layer were adopted (anyway, the major obstacle to seepage was proved to be due not to the clogging of pores into the geotextile, but to the deposition of suspended material on the geotextile surface).

As told above, the testing apparatus has a closed hydraulic circuit, and the same pure water could be utilized indefinitely for different materials (at least in theory). Of course, this procedure is not possible with leachate, because of deposition of suspended solid material on geotextile specimens, and every geotextile should be tested with "fresh" fluid; on the other hand, the fluid volume that is needed to

Table 2. Composition of leachates used for tests (analyses by Institute of Sanitary Engineering, Politecnico di Milano).

Parameter (°)	Leachate 'A'	Leachate 'B'
pH	6.3	6.0
Chemical oxygen demand (COD)	28060	38520
Biological oxygen demand (BOD)	10400	3000
Alkalinity (CaCO ₃)	4250	5125
Volatile acids	435	1575
Organic nitrogen (N NH ₄)	554	60
Ammonia (NH ₃)	1203	1293
Chlorine (Cl)	1868	2231
Sulfate (SO ₄)	1860	1600
Calcium (Ca)	995	175
Magnesium (Mg)	827	1469
Iron (Fe)	330	47
Manganese (Mn)	27	42
Zinc (Zn)	5	7
Sodium (Na)	1300	1400
Potassium (K)	1200	1200

(°) All values in milligrams per liter, except pH

fill the whole permeameter is about 100 liters, and only limited quantities of leachate were available for this research. Therefore, a compromise solution was adopted, consisting in changing the fluid every two geotextiles, so that only five materials could be tested with fresh leachate, while the remaining ones were tested with filtered leachate.

As a consequence:

- the results obtained for the former group (BIDIM U34, GEODREN PE/S, TECNOFELT FAG, DREFON S1A-200, and TERRAM 1000) can be considered valid and comparable each to other;
- for the latter group of geotextiles (POLYFELT TS/750, STRATUM, DREFON S1A-400, DREFON S45-200, TYPAR 3807), the measured values are only indicative, and should be considered with extreme caution (it has to be remembered that, in field applications, geotextiles do not come into contact with pre-filtered leachate).

Permittivity tests to leachate were performed only for $\sigma = 0$ conditions. For most materials, tests were interrupted after 50 ± 100 minutes; in two cases (staple-fibre geotextiles, having high thickness and mass per unit area, indicated with letters I and L in table 1), the duration of the test was prolonged to about 3 hours. The results of all tests, expressed by k_n vs. time and Ψ vs. time plots, are reported in figs. 5 and 6.

On the basis of all results, the following considerations can be made:

- a) all tested materials show a marked decrease of the coefficient of permeability k_n (and, accordingly, of the permittivity Ψ) with the time t elapsed from start-

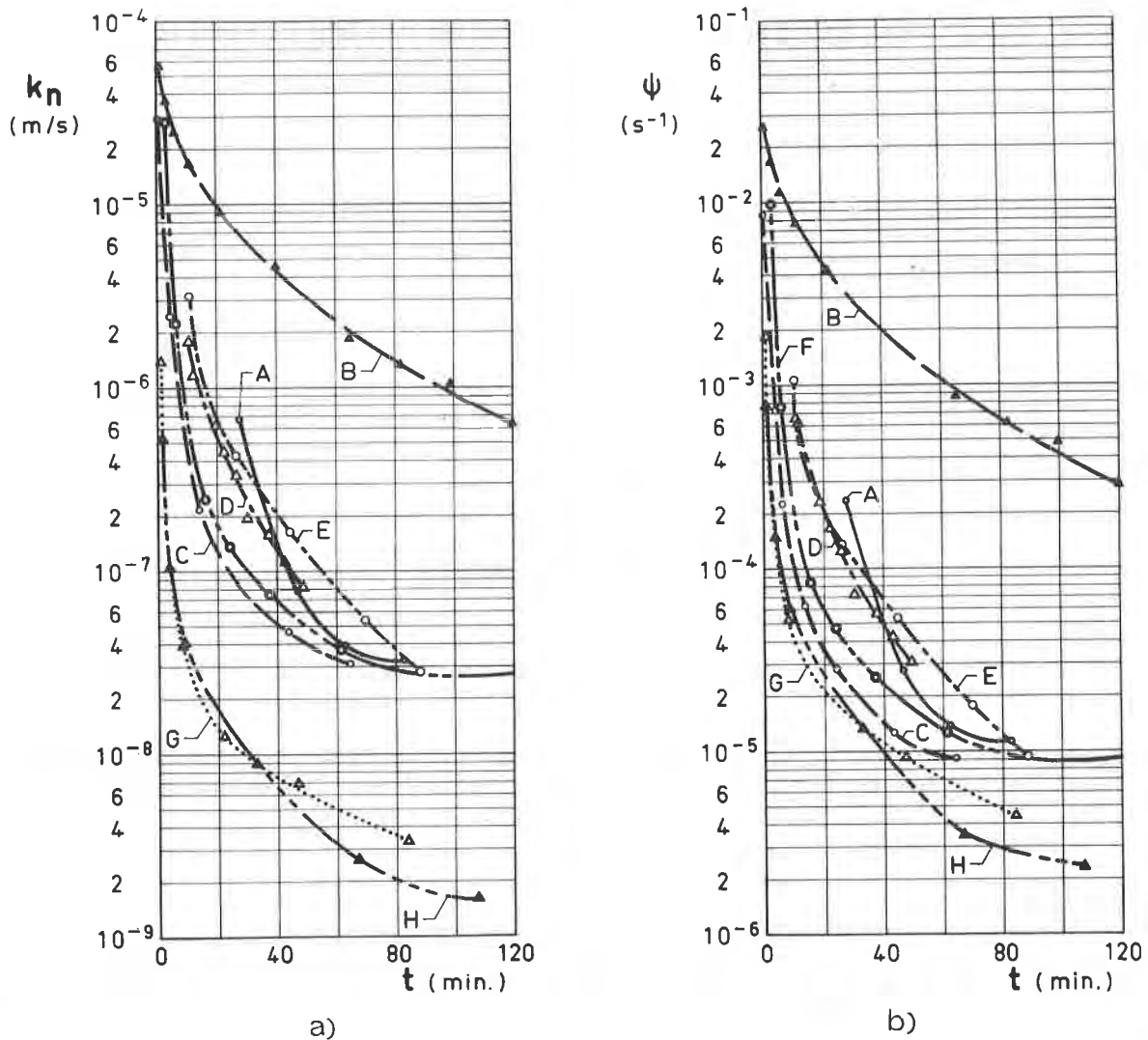


Fig. 5. Results of permittivity tests to leachate on 8 materials: a) k_n vs. time; b) ψ vs. time (the letters refer to geotextiles listed in table 1).

ing the test (figs. 5 and 6); the ratio between initial and final permeability is about 100 times; 1 ÷ 2 hours are generally required for a rough stabilization of the flowrate;

- b) likely, the decrease has to be ascribed essentially to the deposition of solid substances, that were suspended into leachates, prevalently on the geotextile surface, and partly also into the pores of the geotextile itself;
- c) if only the three materials tested both to water and to leachate (i.e., BIDIM U34, POLYFELT TS/750, and TYPAR 3807) are considered, with reference to the values measured for $\sigma = 0$ (fig. 4) and for $t = 80 \div 120$ minutes (fig. 5), it can be seen that the effect of leachate is to reduce normal permeability to less than 1 / 100,000 of the original value; anyway, the rating between different classes

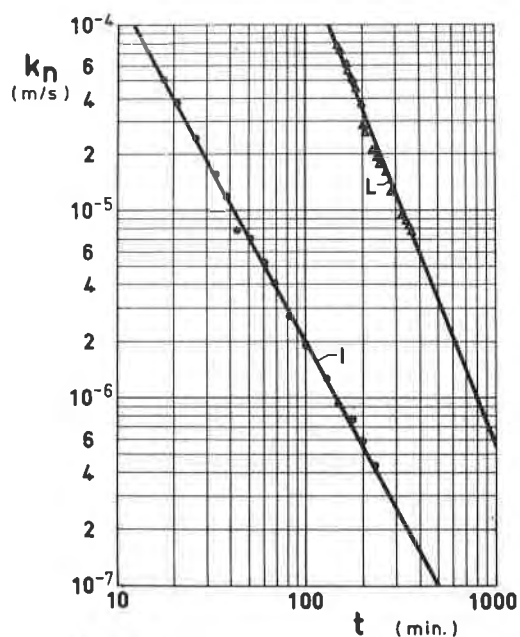


Fig. 6. Results of long duration permittivity tests to leachate on 2 staple-fibre, needle-punched geotextiles: k_n vs. time (I = DREFON S1A-400; L = STRATUM).

of geotextiles (monofilament to staple; needled to thermobonded) seems to remain approximately the same;

- d) a linear relationship (in bilog scale) seems to exist between k_n and t (fig. 6); anyway, this hypothesis should find confirmation in a more extended laboratory investigation.

3. CONCLUSIONS

The paper presents the results of two laboratory investigations on geotextiles, that have been carried out by means of a new, constant head, closed circuit permeameter, adapted to perform permittivity tests both in the absence and in the presence of normal stresses on the geotextile specimen.

The apparatus, and testing procedures, gave fairly good, repetitive results; the values measured by permittivity tests to water are in good agreement with other published data.

The results of a preliminary research on permittivity tests to leachate coming from a sanitary landfill show that leachate causes a strong decrease of permeability, under the combined effects of surface deposition and internal clogging; as the flow-rate attained stabilization, the coefficient of permeability is reduced to that of a silty soil.

When a geotextile is used as a filter on the bottom of a sanitary landfill, the decrease of permittivity (and, likely, of transmissivity), can produce two opposite effects:

- detrimental decrease of draining performances;
- beneficial increase of watertightness and safer conditions for the groundwater.

Obviously, a correct design and a proper application of the geomembrane system has, in any case, a preminent importance.

Further developments of researches about leachate / geotextile interactions should include:

- analysis of retained material;
- chemical effects on the geotextile permittivity;
- study of the behaviour of the whole geotextile filter - geomembrane system, in the presence of leachate.

ACKNOWLEDGEMENTS

The laboratory tests were carried out by Mr. L. Francia and Mr. D. Pessina, respectively on water and leachate, in the course of their thesis work for graduating in civil engineering; the valid cooperation by all technicians of ENEL-CRIS, Special Materials Laboratory, is kindly acknowledged. Chemical analyses on leachate were carried out by courtesy of Prof. Giugliano, Institute of Sanitary Engineering, Politecnico di Milano. Leachate samples from sanitary landfill in Guanzate (Como), were supplied by I.G.M.

REFERENCES

- (1) Koerner, R.M., Designing with Geosynthetics, Prentice-Hall, Englewood Cliffs, NJ, 1986.
- (2) Bacci, R., Apparecchiatura per la prova di permeabilità su nontessuti, ENEL - CRIS, internal report, 1983.
- (3) Francia, L., Studi sperimentali sui geotessili per applicazioni in campo geotecnico ed idraulico, unpublished thesis, Faculty of Engineering, University of Bologna, 1983.
- (4) Fayoux, D., Cazzuffi, D., & Faure, Y., "La détermination des caractéristiques de filtration des géotextiles: comparaison des resultats de différent laboratoires", Proc. Materials for Dams 84, Monte Carlo, Monaco, 1984.
- (5) Gourc, J.P., Faure, Y., Rollin, A., & La Fleur, J., "Standard Test of Permittivity and Application of Darcy's Formula", Proc. 2nd Int. Conf. on Geotextiles, I, pp. 149-154, Las Vegas, 1982.
- (6) Gourc, J.P., Telliez, Ch., Sotton, M., & Leclercq, B., "Perméabilité des géotextiles et perméamètres", Matériaux et Constructions, No. 82, 1981.

LOMBARD, G. and ROLLIN, A.
Ecole Polytechnique, Canada

Filtration Behavior Analysis of Thin Heat-Bonded Geotextiles

1. INTRODUCTION

Geosynthetics represent a very large range of products available on the market: geotextiles (woven, knitted, non-woven), geomembranes, geogrids, geodrains, geonets, geomeshes, agrotextiles (17), Texsol (11), geocomposites. Each one has its own structure and applications. For example, heat-bonded fabrics, a type of non-woven geotextiles, are well used for separation and filtration applications.

In spite of their wide utilization, the filtration behaviour, and particularly the soil particle retention, of these materials has not been related to their structure parameters. Classical approaches are not well adapted for description of these very complex structures. Particularly, they do not take into account the randomness of the elements (fibres or filaments) in the structure.

As filtration criteria are generally expressed by ratio of soil and filter characteristic sizes, it is necessary to obtain these characteristic dimensions. For soils, these informations are given by the well known granulometric analysis.

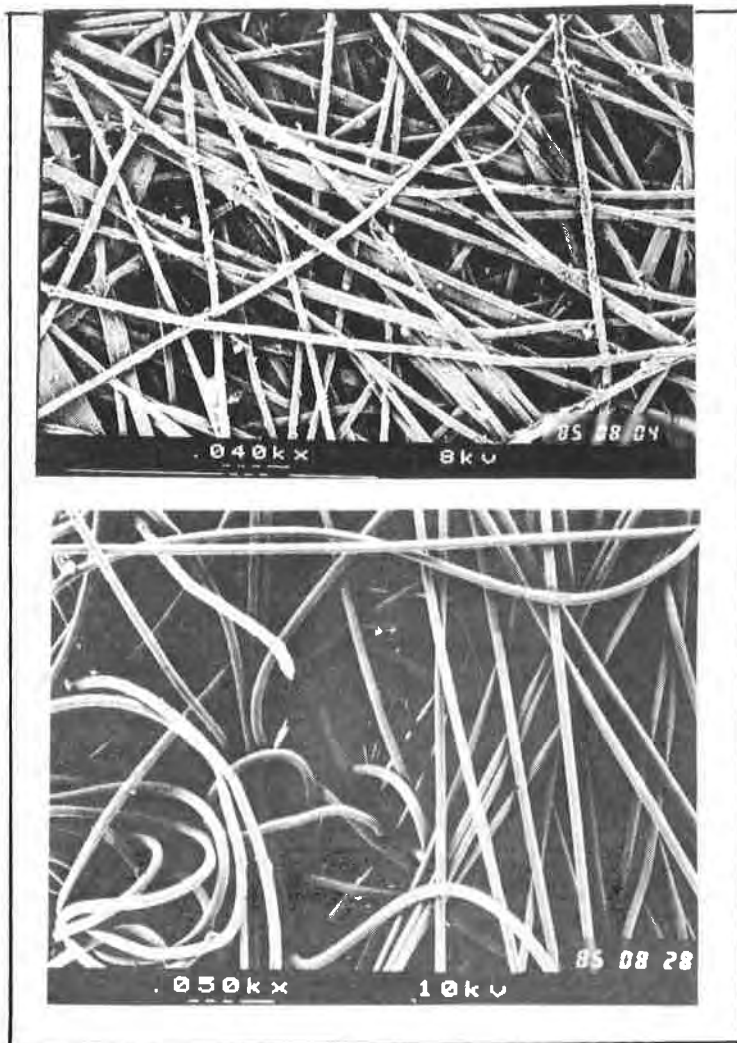
On the contrary, for geotextiles few different methods are proposed for determination of their pore size characteristics. As they are based on different principles, it remains difficult to compare results obtained by each method.

As a contribution to the development of filtration criteria for geotextiles, the filtration behaviour of non-woven heat-bonded fabrics is analysed. A theoretical model and two experimental techniques used for filtration opening size determination are evaluated and filtration tests run in laboratory are analysed.

2. STRUCTURAL ANALYSIS

Heat-bonded geotextiles are calendered fabrics with a resulting thin and stiff structure quite different from needle-punched textiles (Figure 1).

From observation of these structures, it is assumed that these fabrics are made up of layers of infinite randomly distributed filaments with their axis lying in the plane perpendicular to the bulk flow direction.



Heat-bonded fabric

Needle-punched fabric

Figure 1: Top views of non-woven geotextiles

Using a theory based on geometrical probabilities (13, 14), the Poisson polyhedron theory, an expression of the cumulative probability for a filter pore diameter to be equal or smaller than " d_f " has been developed (8, 9, 10):

$$F(d_f) = 1 - [(\sigma d/2 + 1)^{T_g/D_f} \exp(-\sigma d T_g/2D_f)]$$

where σ is the ratio of the total length of deposited filaments to the filter area (mm^{-1}), usually called specific length.

The specific length expression can be obtained from basic manufacturing parameters (9, 13):

$$\sigma = 8 \mu / (\pi T_g D_f \rho_f)$$

where μ is the mass per unit area of the geotextile (g/m^2), T_g the fabric thickness (mm) and ρ_f the polymer density (kg/m^3).

The calculated opening diameter distribution $F(d_f)$ is finally:

$$[3] \quad F(d_f) = 1 - [(4 \mu d / (\pi T_g D_f \rho_f + 1))^{T_g/D_f} \exp(-4 \mu d / \pi D_f^2 \rho_f)]$$

The theoretical pore size distribution $F(d_f)$ is plotted in Figure 2 for the A5 fabric (Table 1) showed in Figure 1 and corresponding to a fabric with a mass per unit area of a 260 g/m^2 . In order to compare experimental and calculated results, the diameter corresponding to $F(d_f) = 95\%$ (Equation 3) has been considered and called the Calculated Opening Size (COS). The curve $F(d)$ corresponds to the pore size distribution of an elementary layer of filaments (9).

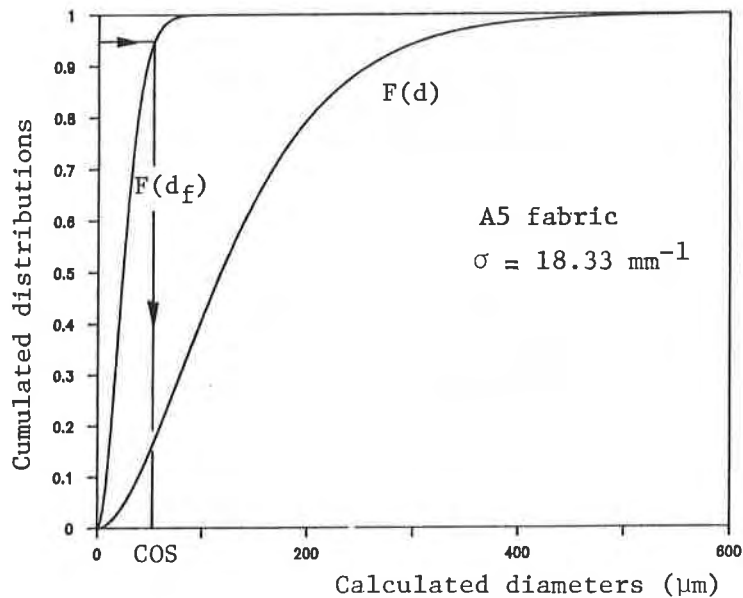


Figure 2: Theoretical pore size distributions

3. EXPERIMENTAL FILTRATION OPENING MEASUREMENTS

As already mentioned, different methods are proposed for opening size measurement of geotextiles. In this paper, two of the most used techniques for this evaluation are compared: dry sieving of glass beads (1) and hydrodynamic sieving (4).

In the first method, different size classes of glass beads are sieved through a geotextile test specimen using a shaker. The percentage of retained beads is plotted versus the bead diameter. The Apparent Opening Size (AOS) is the bead diameter where 95% are retained on the specimen.

The second method consists in sieving a well graded soil (silica powder for example) through the geotextile specimen under alternating water flow. The Filtration Opening Size (FOS) is taken equal the d_{95} of the passing soil.

Analysis of these methods have already been discussed (2, 5, 15). The dry sieving is a rapid test but presents some limitations: sensitivity to the shaker type, to the bead size (AOS determination is limited for openings lower than $100\mu\text{m}$ and particularly for needle-punched fabrics), to the test atmosphere conditions. On the other hand, hydrodynamic sieving does not present these previous limitations but is a time-consuming procedure.

4. FILTRATION TESTS

The significance of all opening size determinations (AOS, FOS, COS) has been analysed by conducting filtration tests in laboratory.

4.1 Selected geotextiles

Nine different heat-bonded geotextiles, made of continuous filaments of polypropylene and polyethylene ($\rho_f = 910 \text{ kg/m}^3$) have been tested. They represent a fair large range of mass per unit area μ (76 to 308 g/m^2) and the thicknesses T_g vary from 0.49 to 1.25 mm (Table 1). As shown in Figure 5, where the porosity n and the specific length σ are plotted versus the mass per unit area μ , two types of heat-bonded geotextiles can be considered: A and B fabrics ($n = 1 - \mu/\rho_f T_g$).

4.2 Selected soils

Five different uniform soils have been used for the filtration tests. They cover a particle size range comprised between 1 and $200\mu\text{m}$, with uniformity coefficients, $C_u = d_{60}/d_{10}$, smaller than 3 . Their characteristic values are presented in Table 2 and their granulometric curves in Figure 3.

4.3 Testing program

More than 40 filtration tests were performed in a permeameter designed and built at Ecole Polytechnique (Figure 4). More details on the apparatus can be found elsewhere (8).

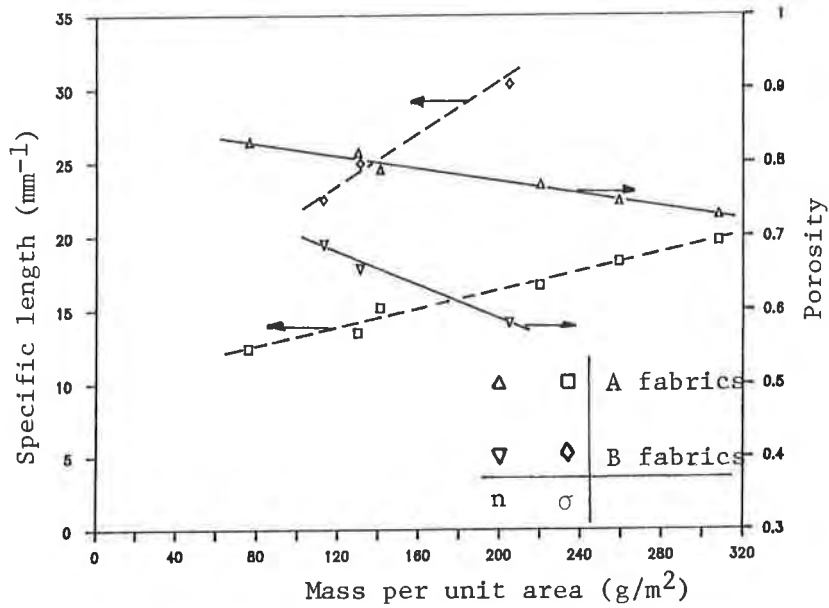


Figure 5: Specific length and porosity versus mass per unit area

Table 1: Geotextile characteristics

Sample	μ (g/m ²)	T _g (mm)	D _f (μ m)	n (%)	σ (mm ⁻¹)	COS (μ m)	AOS (μ m)	FOS (μ m)	O ₉₀ (μ m)
A1	76	0.49	35	82.9	12.44	130	340	195	327
A2	130	0.77	39	81.4	13.53	109	150	—	127
A3	141	0.74	35	79.1	15.21	83	140	115	122
A4	220	1.05	35	77.0	16.73	62	74	50	61
A5	259	1.13	35	74.8	18.33	54	62	47	54
A6	308	1.25	39	72.9	19.72	56	74	—	64
B1	113	0.40	39	69.0	22.55	96	209	160	178
B2	131	0.42	39	65.7	24.95	84	150	110	124
B3	205	0.54	39	58.3	30.34	60	69	47	54

The filtration conditions were:

- hydraulic head: 320 mm
- soil thickness: 40 mm
- hydraulic gradient: $\frac{8}{2}$
- flow area: 507 mm²
- uncompacted soil.

The system, shown in Figure 4, was saturated with deaerated water until the water rises above the geotextile sample. The soil was then poured in the inner cylinder and saturated by the rising water. Finally, a hydraulic head was established and the water flow through the soil-geotextile system initiated.

During the test, volumetric flux and water temperature are regularly measured, thus monitoring the evolution of the system permeability. The filtration test was stopped when the permeability coefficient variations were less than 6×10^{-9} m/s/h.

Particles carried through the fabric are recovered downstream in a recovery container. At the end of the test, entrained particles are dried and weighted in order to obtain the passing particle mass.

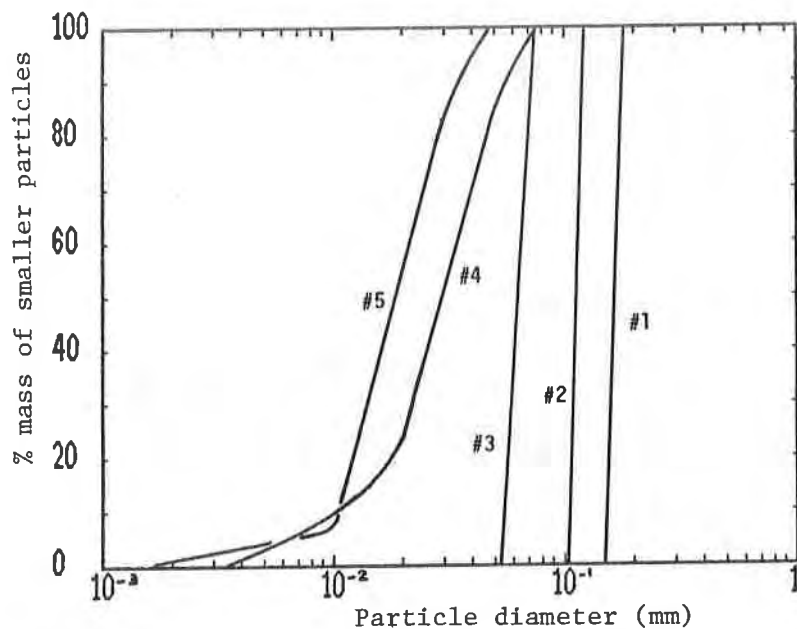


Table 2: Soil characteristics

Figure 3: Granulometric curves of soils

Soil	d ₁₀ (μm)	d ₆₀ (μm)	Cu	d ₅₀ (μm)	d ₈₅ (μm)	d ₉₀ (μm)
1	150	170	1.1	165	175	180
2	107	115	1.1	115	120	122
3	55	65	1.2	57	70	72
4	12	35	2.9	31	50	53
5	12	22	1.8	19	30	35

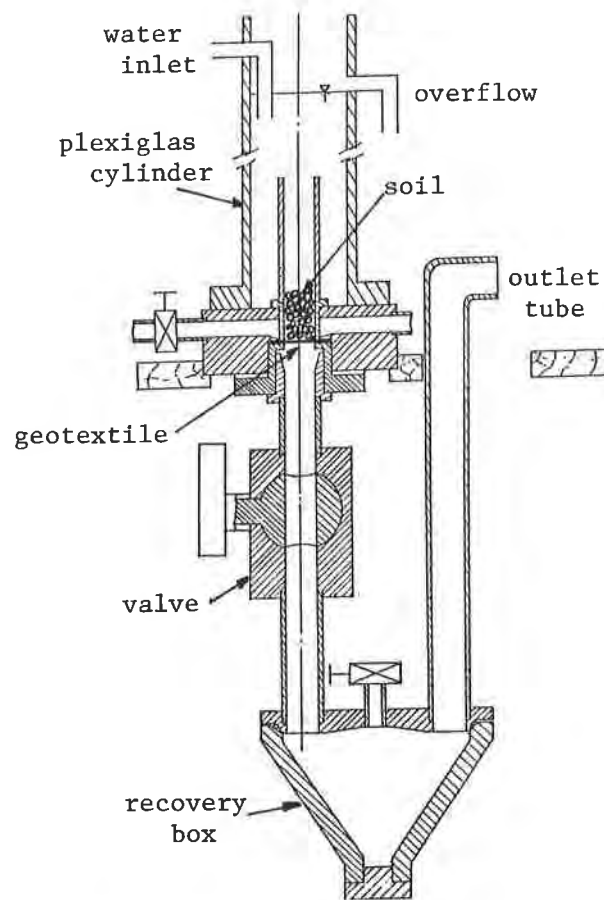


Figure 4: Filtration test apparatus

5. RESULTS AND DISCUSSION

5.1 Opening sizes

The opening sizes obtained are plotted versus the mass per unit area in Figure 6. Whatever the test method used, the opening size decreases with an increase of the mass per unit area. In fact, the probability for a particle to be stopped by the geotextile increases with the fibre layer number, so with the fabric thickness. And, as shown in Figure 5, the specific length σ increases with the mass per unit area.

It is evident, from Figure 6, that openings obtained by the dry sieving technique are larger than those obtained by hydrodynamic sieving technique. At this stage, some explanations are plausible:

- The quantity of particles involved in each case is quite different: 1.45 kg of beads per square meter of filter is required for the dry sieving and 7 kg/m² for hydrodynamic sieving. Blinding mechanism is possible in this second case. Rose (16) demonstrated that the greater is the quantity of particles used, the larger is the quantity of retained particles, during a sieving test.

- For the dry sieving, tests are performed with uniform bead fractions as compared to a graded soil for hydrodynamic sieving. An auto-filtration can take place during the test: large particles stop the smaller ones which stop smaller and smaller particles.

Openings calculated using the proposed model, COS, are smaller than the values measured, the lower is the mass per unit area, the greater are these differences. In development of the structure model, a particle going through the simulated filter can not move laterally between fibres. In a filtration test, this possibility really exists, and could explain the larger values of FOS compared to COS. As values of the specific length σ are larger for larger mass per unit area (Figure 5), for heavy heat-bonded geotextiles fibres are closer in the structure. Lateral displacements of the particles are then reduced. This is showed by similar values of FOS and COS in the case of filters with large mass per unit area.

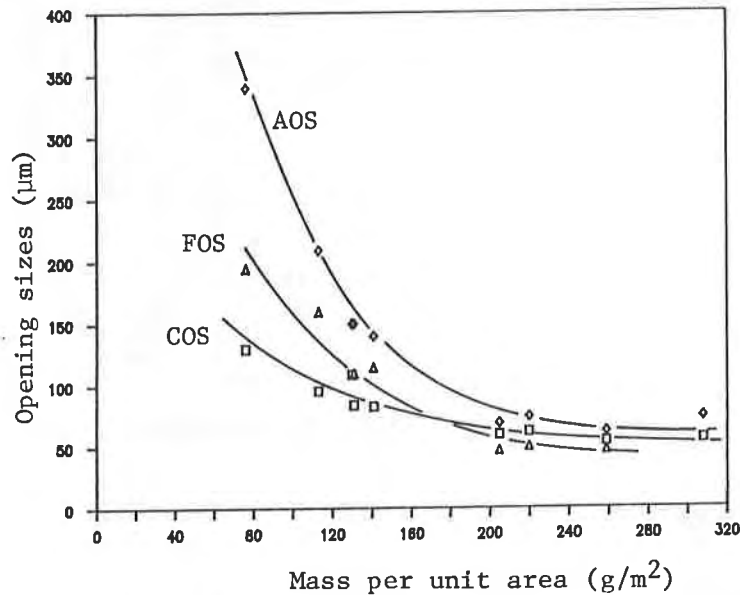


Figure 6: Opening sizes versus mass per unit area

5.2 Filtration tests

To analyse the retention performance of heat-bonded geotextiles (under the filtration conditions explained in paragraph 4.3), passing particle mass per unit area of filter is plotted versus the ratio COS of the geotextile to d_{85} of the soil in Figure 7.

As expected, the mass of particles entrained through the geotextile increases with the ratio COS/d_{85} . A significant change in the filtration behaviour occurs at ratio value equal to 1.65. For ratios larger than 1.65, the mass of passing soil becomes too great and the filtration behaviour can be look at as instable. This type of behaviour has already been pointed out by Faure and al (3) for woven and needle-punched fabrics associated with uniform soils.

A minimum quantity of particles can be released from a soil during the initial stage of a filtration application. But as suggested by the results, this quantity should be kept very low. To avoid the lost of a too large amount of particles, the ratio COS/d_{85} should be kept lower than 1.65.

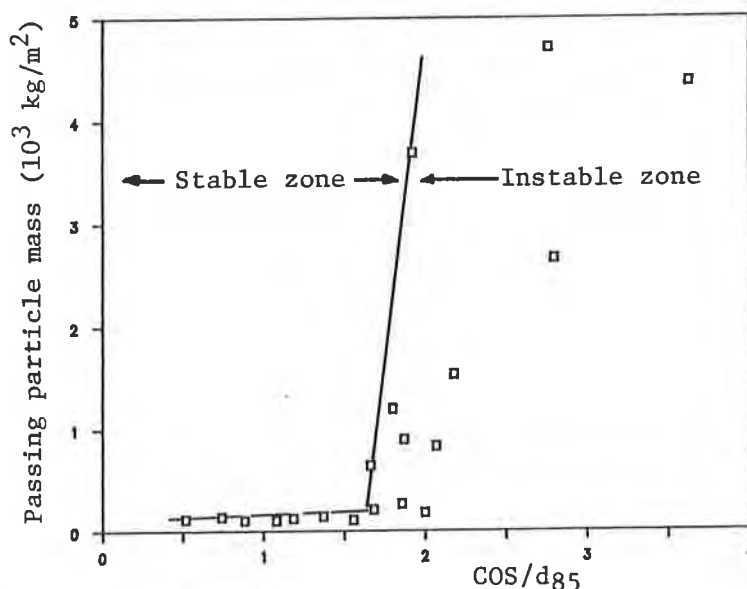


Figure 7: Filtration test results

5.3 Filtration criteria

Finally, using results obtained in this filtration program, three of recognized geotextile selection criteria are checked. All geotextile-soil systems with a passing mass lower than 250 g/m^2 were considered as stable (Figure 7). The opening size determined according specified technique has been associated to corresponding criterion. For example, the AOS was used for Giroud criterion. Results of this analysis are presented in Table 3. The O_{90} opening is obtained in the same way as AOS, but is the diameter where 90% of beads are retained.

The selection criteria seem to be conservative (ratios FOS/d_{50} , $AOS/C_u d_{50}$ or O_{90}/d_{90} are higher than suggested for instable behaviour), even if the filtration tests were conducted under relatively critical conditions:

- the tested soils are uniform ($C_u < 3$).
- the soil was deposited loose on the fabric without subsequent compaction.

Table 3: Retention criteria proof

References			Loudière (1982)	Giroud (1982)	Heerten (1982)
Criteria			$\frac{FOS}{d_{50}} \leq 0.8$	$\frac{AOS}{C_u d_{50}} < 1.5$	$\frac{O_{90}}{d_{90}} \leq 1$
Soil	Filter	Stability Stable Instable	$\frac{FOS}{d_{50}}$	$\frac{AOS}{C_u d_{50}}$	$\frac{O_{90}}{d_{90}}$
2	A1	S	1.7	2.7	2.7
	A4	S	0.4	0.6	0.5
3	A1	I	3.4	5.0	4.5
	A3	S	2.0	2.0	1.4
	B1	S	2.8	3.1	2.5
4	A1	I	6.3	3.8	6.2
	A3	I	3.7	1.6	2.3
	B1	I	2.8	2.3	3.4
	B2	S	3.5	1.7	2.3
5	A3	I	6.0	4.1	3.5
	A4	I	2.6	2.2	1.7
	A5	I	2.5	1.8	1.5
	B1	I	8.4	6.1	5.1
	B2	I	5.8	4.4	3.5
	B3	S	2.5	2.0	1.5

6. CONCLUSION

An analytical approach based on geometrical probabilities was used to support a model developed for non-woven heat-bonded geotextiles. An expression for the pore size distribution of these products was obtained from the basic manufacturing parameters (thickness, mass per unit area, fibres diameter and polymer density). The approach is unique since it is using the formation of polygons from the filament network obtained for elementary layers.

Two methods were compared (dry sieving of glass beads and hydrodynamic filtration) to determine the filtration opening size of these geotextiles. Results indicated that opening sizes obtained with dry sieving method (AOS) are larger than that obtained with hydrodynamic sieving (FOS), especially for light fabrics. Calculated Opening Sizes (COS) obtained from the analytical model are comparable to the Filtration Opening Sizes (FOS).

Filtration tests run in laboratory yield a critical ratio COS/d₈₅ of 1.65. For ratio values higher than 1.65, instable behaviour of soil-geotextile system was observed. Using the filtration test results, some retention criteria proposed in litterature are showed to be relatively conservative.

REFERENCES

1. CALHOUN, C.C., "Development of Design Criteria and Acceptance Specifications for Plastic Filter Cloths", Technical Report S.72.7, U.S. Army Engineer Waterways Experiment Station, Vicksburg Mississippi (June 1972).
2. FALYSE, E., ROLLIN, A., RIGO, J.M., GOURC, J.P., "Study of the Different Techniques Used to Determine the Filtration Opening on Geotextiles", Proceedings of the 2nd Canadian Symposium of Geotextiles and Geomembranes, 45-50, Edmonton (September 1985).
3. FAURE, Y., GOURC, J.P., BROCHIER, P., ROLLIN, A., F., "Soil-Geotextile Interaction in Filter Systems", Proceedings of the 3rd International Conference on Geotextiles, 4, 1207-1212, Vienna (April 1986).
4. FAYOUX, D., "Filtration hydrodynamique des sols par les textiles", Comptes rendus du Colloque International sur l'Emploi des Textiles en Géotechnique, 2, 329-332, Paris (1977).
5. FAYOUX, D., CAZUFFI, D., FAURE, Y., "The determination of Filtration Characteristics of Geotextiles: Comparison of the Results of Different Laboratories", Proceedings of Materials for Dams, Monte-Carlo (1984).
6. GIROUD, J.P., "Filter Criteria for Geotextiles", Proceedings of the 2nd International Conference on Geotextiles, 1, 103-108, Las Vegas (August 1982).
7. HEERTEN, G., "Dimensioning the Filtration Properties of Geotextiles Considering Long-Term Conditions", Proceedings of the 2nd International Conference on Geotextiles, 1, 115-120, Las Vegas (August 1982).
8. LOMBARD, G., "Analyse et comportement hydraulique des géotextiles thermoliés et thermosoudés", Ph.D. Thesis, Ecole Polytechnique, Montréal (1985).
9. LOMBARD, G., ROLLIN, A., WOLFF, C., "Theoretical and Experimental Filtration Opening Sizes of Heat-Bonded Geotextiles", to be published in Geotextiles and Geomembranes.
10. LOMBARD, G., ROLLIN, A., WOLFF, C., "Analysis and Hydraulic Behaviour of Thin Heat-Bonded Geotextiles: Structure and Flow Models", Proceedings of the 3rd International Conference on Geotextiles, 2, 615-620, Vienna (April 1986).
11. LEFLAIVE, E., LIAUSU, P., "Le renforcement des sols par fils continus", Comptes rendus du 3^e Congrès International des Géotextiles, 2, 523-528, Vienne (Avril 1986).
12. LOUDIERE, D., FAYOUX, D., "Filtration et drainage au moyen de géotextiles: essais et spécifications", Comptes rendus du 2^e Congrès International des Géotextiles, 1, 61-66, Las Vegas (Août 1982).
13. MATHERON, G., "Les polyèdres poissonniens isotropes", Cahier interne du Centre de Morphologie Mathématique, Fontainebleau (1971).
14. MATHERON, G., "Ensembles fermés aléatoires, ensembles semi-markoviens et polyèdres poissonniens", Advanced in Applied Probability, 4, 508-541, (1972).
15. ROLLIN, A., "Filtration Opening Size of Geotextiles", A.S.T.M. News, 50-52 (May 1986).
16. ROSE, H.E., ENGLISH, J.E., "The Influence of Blinding Material on the Results of Test Sieving", Transactions of the Institution of Chemical Engineers, 51, 14-21 (1973).
17. SOTTON, M., "Caractérisation des agrotextiles", Bulletin Scientifique de l'Institut Textile de France, 14, N^o 55, 45-51 (3^e trimestre 1985).

SESSION 5A

QUALITY ASSURANCE/QUALITY CONTROL

KOERNER, R.M., LORD, A.E., Jr., and CRAWFORD, R.B.

Drexel University, U.S.A.

CADWALLADER, M.

Gundle Lining Systems, Inc., U.S.A.

Geomembrane Seam Inspection Using the Ultrasonic Shadow Method

Abstract

The ultrasonic shadow method is described and illustrated by use on geomembrane samples and a statistical correlation with the same samples tested mechanically. Then a series of specific studies are presented on the effects of UV aging, water and soil contamination during welding, seam cooling temperature, and delamination. We currently feel that technical feasibility of the shadow method has been positively indicated and that full scale field trials should be made for further development and utilization of the method.

Overview

It is generally recognized that the geomembrane industry's current ability to manufacture near flawless sheets far surpasses its ability to seam separate sheets together. Furthermore, it is also recognized that the ability to make factory seams is significantly better than the ability to make field seams. Field seams owe this difficulty to a number of reasons:

- nonhorizontal (sloped) preparation surfaces
- nonuniform (or yielding) preparation surfaces
- nonconforming sheets to the subsurface (air pockets)
- slippery liners made of low friction materials
- wind-blown dirt in the areas to be seamed
- moisture and dampness in the areas to be seamed
- penetrations, connections and appurtenances
- wind fluttering the sheets out of position
- ambient temperature variations during seaming
- uncomfortably high (and sometimes low) temperatures for careful working
- expansion and/or contraction of sheets during seaming

With so many potential problems it is natural that emphasis on high quality field seams and on subsequent seam inspection is commonly referenced.^(1,2) This need grows progressively more important depending upon the implications of the contained material (usually liquid) escaping. Thus hazardous and radioactive waste facilities have the highest priority, while recreational reservoirs and aesthetic ponds have a much lower priority.

Various types of seam tests and seam inspection methods are available ^(3,4) however the authors feel that the ultrasonic methods are potentially of greatest value. Furthermore, emphasis will be on a specific ultrasonic method, called the "shadow

method". It will be described in detail along with correlation to destructive test results and then further illustrated by a number of specific studies.

Ultrasonic Test Methods

Ultrasonic methods are the newest of the methods used to evaluate seam integrity. (5) The ultrasonic pulse echo technique is basically a thickness measurement technique and is only for use with nonreinforced geomembranes. Here a very short, high-frequency pulse (center frequency in the MHz range) is sent into the upper geomembrane and (in the case of a good seam) reflects off of the bottom of the lower one. If, however, an unbonded area is present, the reflection will occur at the unbonded surface interface. The use of two transducers (usually coupled into one housing, thus termed a transceiver), a pulse generator, and a CRT monitor are required. The ultrasonic impedance plane method works on the principle of acoustic impedance. A continuous wave of 160 to 185 kHz is sent into the seamed liner and a characteristic dot pattern (representing the end of the acoustic impedance vector) is displayed on a CRT screen. Calibration of the dot pattern is required to signify a good seam. The method has potential for all types of geomembranes but still needs additional development work. The ultrasonic shadow method uses a very long pulse with center frequency between 0.5 and 5.0 MHz which enters through a transducer (i.e., the transmitter) on one side of the seam and is received by a second transducer (i.e., the receiver) on the other side of the seam. The amount of energy received, relative to that initially transmitted, is indicative of the quality of the seamed region between the two transducers.

The Ultrasonic Shadow Method

The shadow method is the ultrasonic technique most applicable, in the author's opinion, to NDT of geomembrane seams. The technique has several advantages over other ultrasonic methods in current use:

- it has the potential to be used on virtually all geomembrane types.
- it has the potential to be used on virtually all geomembrane seam types.
- it is potentially capable of assessing complex seam regions, e.g., appurtenances and connections.
- it requires no couplant media between the transducers and the geomembrane under test.
- it is faster than the other ultrasonic methods since it questions the full width of the seam as it travels along.

The ultrasonic shadow system used for this study is a Balteau Sonatest Model UFD-S Dryscan Ultrasonic Flaw Detector®. The system consists of two roller mounted, spring loaded, transducers (one transmitter and one receiver) wired to a signal generator/CRT display unit. One transducer is placed on the near side of the seam, the other is placed on the far side in line with the near side transducer. In this configuration, the transducers straddle the seam itself making the method insensitive to the seam type or geometry. Throughout this study, transducer spacing was kept constant at 6.67 cm (2.63 in.), however, the spacing may be varied to accommodate wider seams. A long ultrasonic energy pulse (50-100 μ sec long of center frequency about 1 MHz) is sent from the transmitter, through the seam region, to the receiver. A good seam will convey most of the energy, while a poor seam will convey little or none of it. By comparing the received signals on the system's CRT screen, a qualitative assessment of the seam integrity can be made. Figure 1 shows a schematic diagram of the shadow method and a representation of the results for a "good", "questionable" and "poor" seam. Figure 2 shows actual

data for extrusion fillet welded seam samples of 0.75 mm (30 mil) and 1.5 mm (60 mil) thickness. The varying amplitudes of response indicate varying seam quality.

Few studies using the shadow method have been reported in the literature probably due to the newness of the technique. Only three reports using the shadow method were found. The first deals with assessing the bonds in plastic pipes (6), the second on the inspection of joints on inflatable boats (7) and the third deals directly with NDT of geomembrane seams (8). This last reference by Peggs, et al., provided the background for this particular effort.

Shadow Method Results and Correlation with Destructive Tests

Testing was done on three, 45.7 cm (18.0 in.) long seam sections. Each geomembrane section was 1.5 mm (60 mil) thick HDPE seamed by extrusion fillet welding. Two of the sections were seamed under normal welding conditions to produce good quality seams. The third section was seamed with surface water being placed directly in front of the extrusion welder to produce an inferior seam. All three sections were then evaluated by the ultrasonic shadow method in 2.5 cm (1.0 in.) increments. The shadow amplitude, as percent full screen height (FSH), for each 2.5 cm (1.0 in.) increment was then recorded. The seam sections were then cut into 54, 2.5 cm (1.0 in.) wide, destructive test specimens along the lines used to separate the individual samples for ultrasonic evaluation. Approximately 85% (i.e. 47) of the samples were randomly selected for mechanical testing in peel. The remainder of specimens were retained for more detailed analyses to be performed subsequently (i.e., SEM, polarized light analysis, etc.). The 47 samples tested in peel were then categorized according to their failure type. Table 1 presents the results of correlating the number of acceptable (i.e. Sheet Failure) and nonacceptable (Non Sheet Failures or Fillet Failures) destructively tested peel specimens to each range of shadow amplitude (expressed as % FSH).

As seen, a good correlation was obtained with respect to "good" or "bad" failure mode prediction. The exception is the 3 specimens at the top of the table which exhibited an off-screen (>100%) shadow amplitude. This phenomena was unanticipated, as standard, unseamed 1.5 mm (60 mil) HDPE can simply not transmit this high an amount of ultrasonic energy. Therefore, this particular phenomena requires more detailed study. Disregarding those three specimens, however, the results are extremely promising. From 100% FSH to 50% FSH all the tested peel specimens were acceptable with respect to their failure mode. From 50% FSH to 20% FSH the specimens were in a questionable range (i.e. a 1:3 ratio of unacceptable to acceptable). Finally, below 20% FSH almost all the specimens failed in an unacceptable mode (i.e. a 5:1 ratio of unacceptable to acceptable).

Individual Special Studies

The following special studies were performed to illustrate the ultrasonic shadow method on a wide range of problems of practical interest. Each study is a self contained unit.

(a) Effect of Seam Exposure to Ultraviolet Light - Seam samples taken from a 1.5 mm (60 mil) HDPE liner which had been exposed to Arizona sunlight for 3 1/2 years, were evaluated with the ultrasonic shadow method. The seaming technique which had been used was a thermal fusion method, and more specifically, a dual hot wedge.

Table 1 - Statistical Correlation Between Shadow Method Display Amplitude and Mechanical Peel Test Failure Mode for 1.5 mm (60 mil) Extrusion Welded HDPE

Shadow Method (% FSH)	Sheet Failure Samples	Non-Sheet Failure Samples	
> 100%	0	3	} unlikely to occur
90% - 100%	4	0	
80% - 90%	4	0	} good seams
70% - 80%	5	0	
60% - 70%	3	0	
50% - 60%	4	0	} questionable seams
40% - 50%	4	1	
30% - 40%	2	0	} poor seams
20% - 30%	3	2	
10% - 20%	1	4	
0% - 10%	1	6	

In order to ultrasonically test both fusion portions of the double seam, two passes with the shadow transducers were required; the first scanning both portions and the second scanning only the inner portion (i.e. the portion of the dual seam closest to the edge of the top sheet). A lower amplitude was obtained for the double fusion portion scan due to the high attenuation around the air channel. Typically, a 30% FSH amplitude is the maximum attainable transmission with double fusion portion scans (i.e., when the single fusion portion scan is calibrated to 100% FSH).

Standard samples were taken and evaluated with the ultrasonic shadow method in the manner previously described. Then the specimens were taken and tested mechanically in peel; first in standard peel to evaluate the outer fusion portion and secondly in back peel to evaluate the inner fusion portion of the seam. All samples tested were then categorized according to the failure mode they exhibited during peel testing. Table 2 presents the results for the specimens. Here, a good correlation is seen between specimens with high shadow amplitude and no fusion zone peel and between specimens with low shadow amplitude and partial fusion zone peel.

(b) Effect of Seams Exposed to Water During Seaming - A section of 1.5 mm (60 mil) HDPE was seamed in the laboratory using an extrusion fillet welder. One half of the total seam distance was welded under normal conditions. The remaining distance was seamed with surface water being placed directly in front of the welding device. The water vaporized during welding and resulted in large air bubbles randomly appearing in the fillet rib of the water exposed section. Each section was then evaluated in 2.5 cm (1.0 in.) increments using the ultrasonic shadow method. Virtually all the water exposed specimens exhibited shadow amplitudes 2 to 3 times less than those exhibited by the normal condition specimens.

Table 2 - Correlation Between Ultrasonic Shadow Amplitude and Percent of Intact Seam Remaining (Unpeeled) for Thermally Fused, 1.5 mm (60 mil) HDPE Exposed to 3 1/2 Years Ultraviolet Radiation

Spec. No.	Double Seam Shadow Amplitude (% FSH)	Inner Seam Only Shadow Amplitude (% FSH)	Failure Mode (% Seam Remaining)	
			Outer Seam	Inner Seam
1	30	100	SF-NAL (100%)	SF-NAL (100%)
2	30	65	SF-NAL (100%)	SF-PAL (80%)
3	10	70	SF-PAL (50%)	SF-PAL (80%)
4	20	20	SF-PAL (80%)	SF-PAL (30%)

Note:

FSH = Full Screen Height

SF-NAL = Sheet Failure - No Adhesion Loss

SF-PAL = Sheet Failure (%) - Partial Adhesion Loss w/ percent of intact, unpeeled seam remaining at failure.

The specimens were then taken and tested mechanically in peel. All the water exposed samples failed the mechanical evaluation for failure mode in peel, i.e., all were Non-Sheet Failures. Shown in Table 3 is a statistical breakdown of the data obtained. As seen, the shadow method clearly detected all the inferior samples. Of practical importance is that although air voids were throughout the fillet rib of the water exposed sample, not all the voids were visible on the rib surface. As such, visual inspection, air lance, or mechanical point stress tests would not have detected all the inferior specimens as the shadow method technique did.

Table 3 - Result of Shadow Method on Seams Exposed to Water During Seaming

Criteria	Water Exposed Specimens	Normally Prepared Specimens
Max. Shadow Amp. (% FSH)	30%	100%
Min. Shadow Amp. (% FSH)	0%	30%
Avg. Shadow Amp. (% FSH)	12%	68%
No. of Sheet Failures	0	12
No. of Nonsheet Failures	12	0
No. of Fillet Failures	0	0

Total No. of Samples 24

No. of Normally Prepared 12

No. of Water Exposed 12

FSH = Full Screen Height

(c) Samples Exposed to Soil Contamination During Seaming - A 1.5 mm (60 mil) sample of HDPE was thermally fused in the laboratory using the dual hot wedge technique. One half of the seam distance was prepared under normal conditions, the remaining distance prepared with a thick bentonite slurry being placed between the

overlapped geomembrane sheets directly in front of the seaming device.

After cooling, both seam sections were evaluated in 2.5 cm (1.0 in.) increments using the ultrasonic shadow method. Surprisingly, each section exhibited approximately the same shadow amplitude, regardless of the preparation method. Each incremental specimen was then taken and tested mechanically in both standard peel and back peel. Little variation appeared between the normally prepared seam specimens and the bentonite slurry exposed seam specimens. The quantitative results for this section of testing are shown in Table 4.

Table 4 - Results of Shadow Method on Seams Exposed to Soil Contamination During Seaming

Spec. No.	Preparation	Shadow Amp. (% FSH)		Standard Peel		Back Peel	
		Double	Single	Mode	Yield Load (kN/m)	Mode	Yield Load (kN/m)
1	Normal	30	80	SF-NAL	20.4	SF-NAL	20.7
2	Normal	25	80	SF-NAL	19.7	SF-NAL	20.9
3	Normal	20	70	SF-PAL (90%)	19.2	SF-PAL (90%)	19.6
4	Clay	25	80	SF-NAL	20.3	SF-NAL	20.2
5	Clay	30	90	SF-NAL	18.9	SF-NAL	20.2
6	Clay	20	100	SF-NAL	20.9	SF-NAL (90%)	19.7

Note:

SF-NAL - Sheet Failure - No Adhesion Loss

SF-PAL (%) - Sheet Failure - Partial Adhesion Loss w/percent of intact, unpeeled seam remaining at failure.

FSH - Full Screen Height

(d) Effect of Seam Cooling Temperature - A section of 1.5 mm (60 mil) HDPE was seamed in the laboratory using a hot air thermal fusion technique. Blown air temperature was held constant at 260°C (500°F). Immediately after seaming, a specific section of seam was ultrasonically monitored with time to evaluate the effect of seam cooling on the ultrasonic amplitude. Shown in Figure 3 is a plot of the ultrasonic shadow amplitude versus log time after seaming (i.e., the effect of cooling time). As seen, immediately after seaming, no ultrasonic energy was conveyed through the seam region. Approximately three minutes after seaming, some ultrasonic energy began to be transmitted. After 15 minutes, the seam was cool enough to touch and approximately 82% of the ultrasonic energy was being transmitted. Finally, after 60 minutes, nearly all of the ultimate energy was being conveyed. Irrespective of the mechanistic phenomenon which causes this behavior (which is probably related to the varying ultrasonic attenuation of the material during phase change), one aspect of practical importance is demonstrated. That is, the technique cannot be used immediately following the seaming operation. There must be a time lag before inspection can properly commence. As indicated here, for this type of seam, the time is approximately one hour.

(e) Delamination (Unbonding) Study - Specimens of 1.5 mm (60 mil) HDPE were thermally fused with a hot air welding device in the laboratory to produce three dif-

ferent qualities of HDPE seams:

- Those which could not be penetrated with a pick (i.e., a mechanical point stress device) on the exposed edge.
- Those which could be penetrated with a pick on the exposed edge approximately 40% through the fusion zone (i.e., approx. 2.3 cm (0.9 in.) on a 5.7 cm (2.3 in.) seam).
- Those which could be penetrated completely through the fusion zone with a pick (thus unbonded).

The three specimen groups of varying seam quality were then tested with the ultrasonic shadow method. The resulting shadow amplitudes for each different quality seam were then compared to their corresponding pick test penetration. Typical results are shown in Figure 4. As seen, the shadow method detected both the "good" (total bonding) and "bad" (little or no bonding) seams consistently. However, the "questionable" seams (partial bonding) conveyed more energy than either of the previous seam qualities. At present, no attempts have been made to analyze and explain this phenomenon, however, it is a topic that must be pursued at greater length.

Summary and Conclusion

Widely recognized among all segments of the geomembrane industry is the need for nondestructive testing of seams. This is particularly the case for geomembranes used in solid waste containment. Furthermore, when dealing with hazardous or radioactive waste, 100% seam quality assurance is essential. This paper has briefly reviewed the available methods, emphasized the ultrasonic methods, and furthermore, focused on the ultrasonic shadow method.

The ultrasonic shadow method uses a separate transmitting and receiving transducer on opposite sides of a seam and questions its full width as it travels along. The response from the 50 to 100 μ sec energy pulse is shown on a CRT screen and compared to that of a known good seam via its full screen height (FSH) or amplitude.

The major study in this paper evaluated 1.5 mm (60 mil) thick HDPE geomembranes seamed by extrusion fillet welding. It was found via destructive tests in peel that (a) greater than 50% FSH resulted in good seams, (b) between 50% and 20% FSH resulted in questionable seams and (c) less than 20% FSH related in unacceptable seams. Thus, the beginnings of a data base have been established. Clearly, this type of analysis could be extended to other types of seams and other types of geomembranes.

To further illustrate and demonstrate the method a set of separate studies were conducted. Briefly, they were the following:

- effect of ultraviolet light - showing reasonable correlation to destructive tests
- effect of water during seaming - showing excellent correlation to destructive tests
- effect of soil contamination during seaming - showing no adverse effect (which was somewhat surprising)
- effect of seam cooling temperature - indicating that testing cannot commence for one hour after seaming
- effect of delamination - illustrating questionable correlation with other tests

In conclusion we feel that technical feasibility of ultrasonic shadow method testing on a wide variety of situations has been illustrated. The method is straightforward to use, relatively free of operator dependence, quite fast in its deployment and correlates well with destructive tests. It is also capable of being quantified and of producing hard copy for authentication and record keeping. The next step in the method's development is field evaluation. Here a number of geomembrane types, seam types, subsurface and ambient conditions will be required before firmer conclusions can be reached.

References

- (1) U. S. EPA, "Hazardous Waste Management System: Permitting Requirements for Land Disposal Facilities," Federal Register 47 (143) : 32273-32373, July 26, 1982.
- (2) U. S. EPA, Minimum Technology Guidance on Single Liner Systems for Landfills, Surface Impoundments and Waste Piles - Design, Construction and Operation, EPA/530-SW-85-013, May 24, 1985.
- (3) Frobel, R. K., "Methods of Constructing and Evaluating Geomembrane Seams," Proc. Intl. Conf. Geomembranes, Denver, Colo., 1984, IFAI, pp. 359-364.
- (4) Koerner, R. M., Designing with Geosynthetics, Prentice Hall Publ. Co., Englewood Cliffs, NJ, 1986.
- (5) Lord, A. E. Jr., Koerner, R. M. and Crawford, R. B., "NDT Techniques to Assess Geomembrane Seam Quality," Proc. Mgmt. Uncontrolled Hazardous Waste, Washington, DC, HMRCI, 1986.
- (6) Badgerow, D. L., "New Developments in Ultrasonic Joint Inspection for Polyethylene Systems," Am. Gas Assn. Dist. Conf., Houston, Texas, May 16-18, 1983.
- (7) Dickson, J. K., "Investigation into the Inspection of Bonded Joints on Inflatable Boats," Balteau Sonatest Ltd., North Bucks, England, August, 1980.
- (8) Peggs, I. D., Briggs, R. and Little, D., "Developments in Ultrasonics for Geomembrane Seam Inspection," Proc. Canadian Geotextile Conf., Edmonton, Canada, 1985.

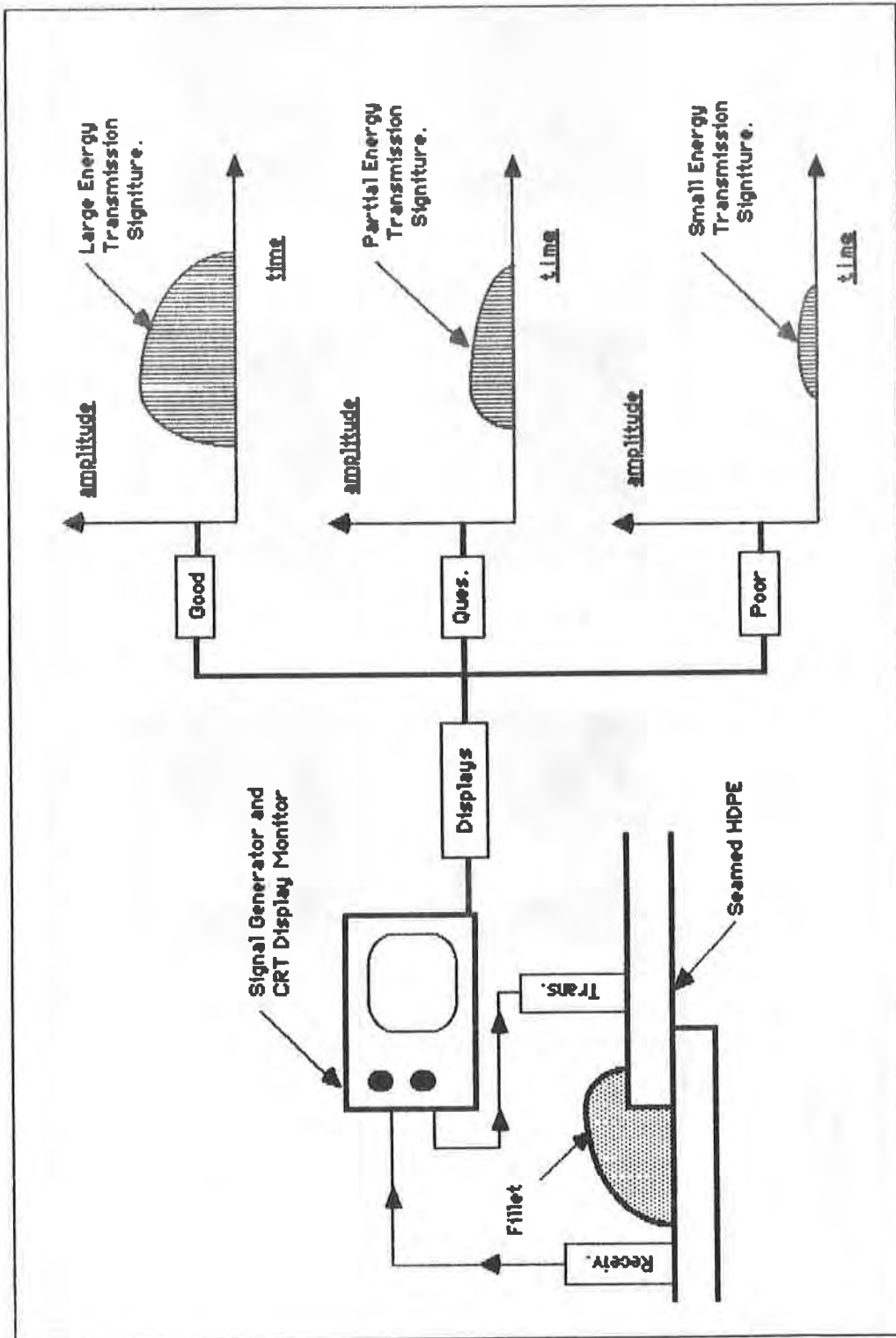


Figure 1 - Schematic Diagram of Operational Concepts of
Ultrasonic Shadow Method

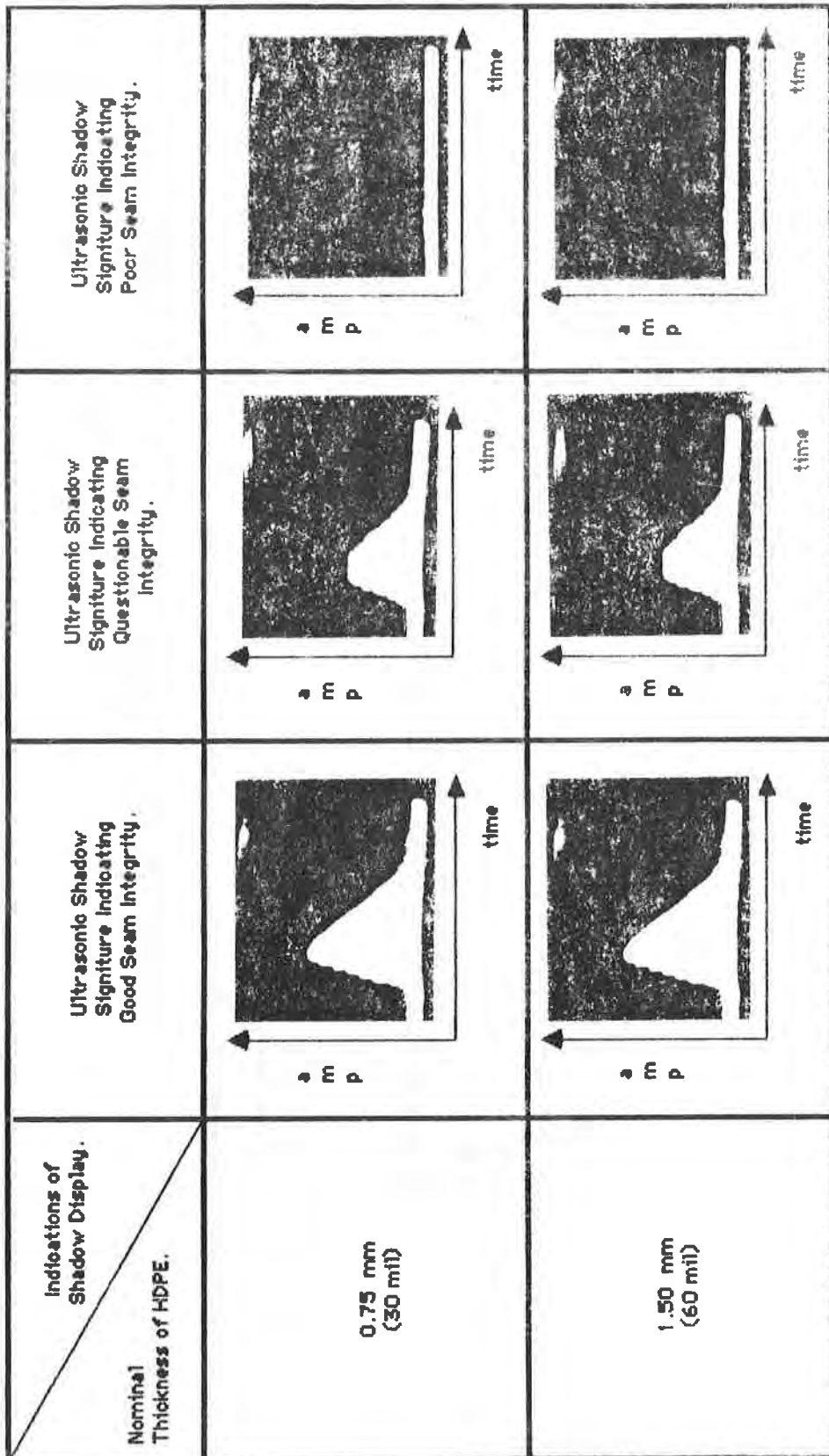


Figure 2 - Typical Ultrasonic Shadow Results for Extrusion Welded HDPE Seams of Various Thicknesses

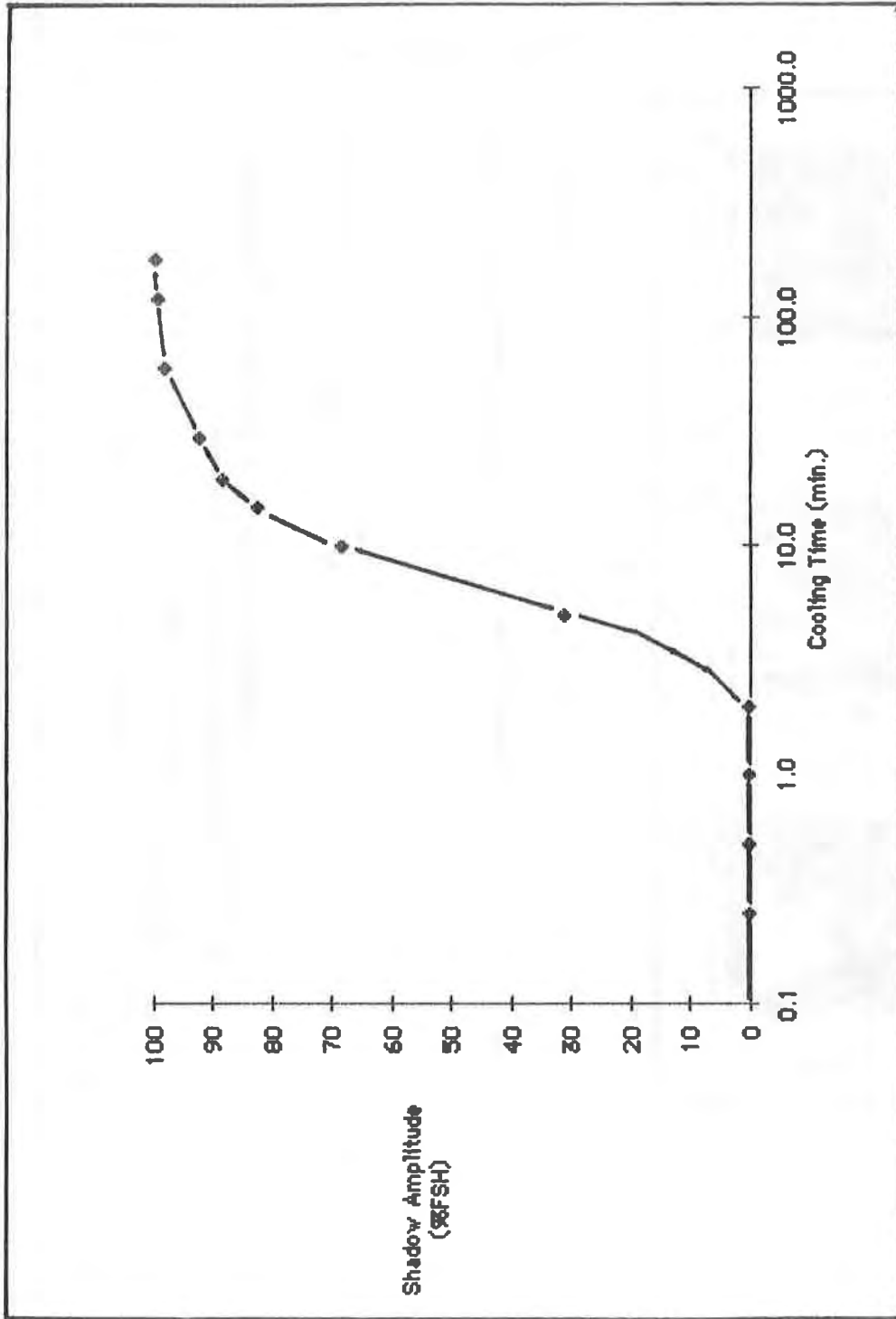


Figure 3 - Response of Shadow Amplitude with Cooling Time
for 1.5 mm (60 mil), Thermally Fused HDPE

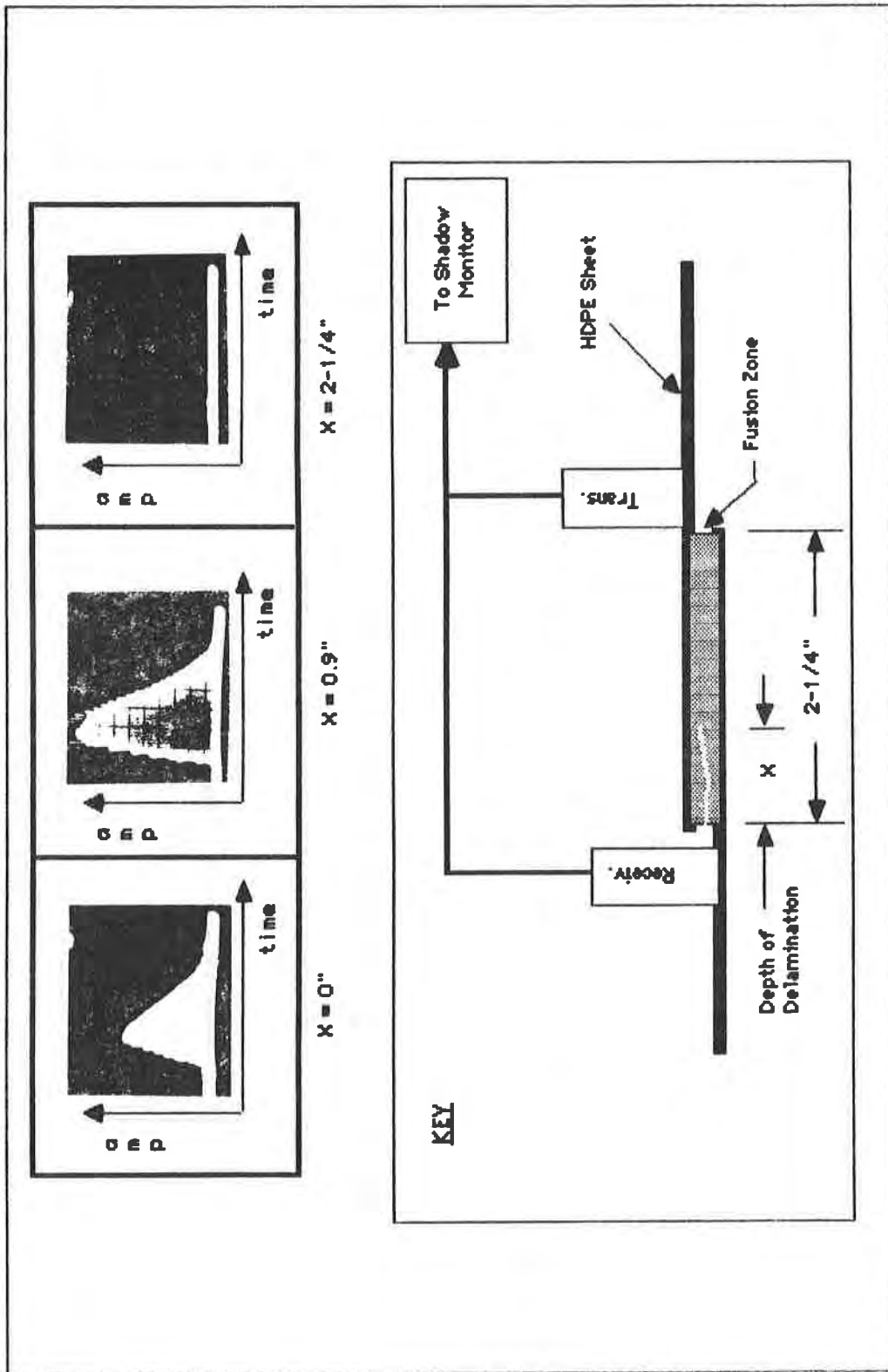


Figure 4 - Ultrasonic Shadow Results for 1.5 mm (60 mil),
Thermally Fused HDPE Showing Typical Results
for Varying Amounts of Seam Delamination

I.D. PEGGS

GeoSyntec, Inc., U.S.A.

Evaluating Polyethylene Geomembrane Seams

INTRODUCTION

The use of polyethylene (PE) geomembranes in lining systems for hazardous waste landfills, municipal solid waste landfills, sewage lagoons and chemical storage ponds is increasing at a rapid rate, to the extent that PE is almost the geomembrane material of universal choice. It is essential that installation quality control test procedures keep pace with geomembrane technology to ensure that failures do not occur, not only during installation, but also during the projected service life of the installation. Unfortunately, but not surprisingly, some failures are occurring.

The most common failure mode of PE geomembranes, other than seam separation due to poor seaming practice, is brittle cracking both in, and adjacent to, the seam. Such cracking has been observed in geomembranes located in both cold and warm environments and in seams produced by extrusion, hot wedge, and hot air techniques.

While seam test procedures and acceptance criteria have been developed, most seam test procedures do not presently evaluate parameters which contribute to brittle fractures.

FRACTURE BEHAVIOR

Figures 1 and 2 show cracking within the seam and in the geomembrane. Cracking across an extruded seam has been observed (Figure 3). This phenomenon is thus not limited to geomembrane produced by a single manufacturer, one specific resin type, one specific seaming procedure, nor any particular environmental conditions.



Figure 1
Brittle fracture adjacent to an extruded lap seam
prepared in the plant

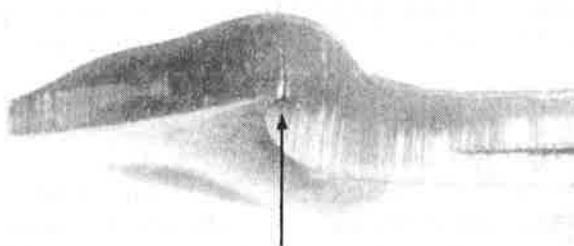


Figure 2
Crack (arrowed) propagating upwards through the
cross-section of an extruded lap seam prepared in the field

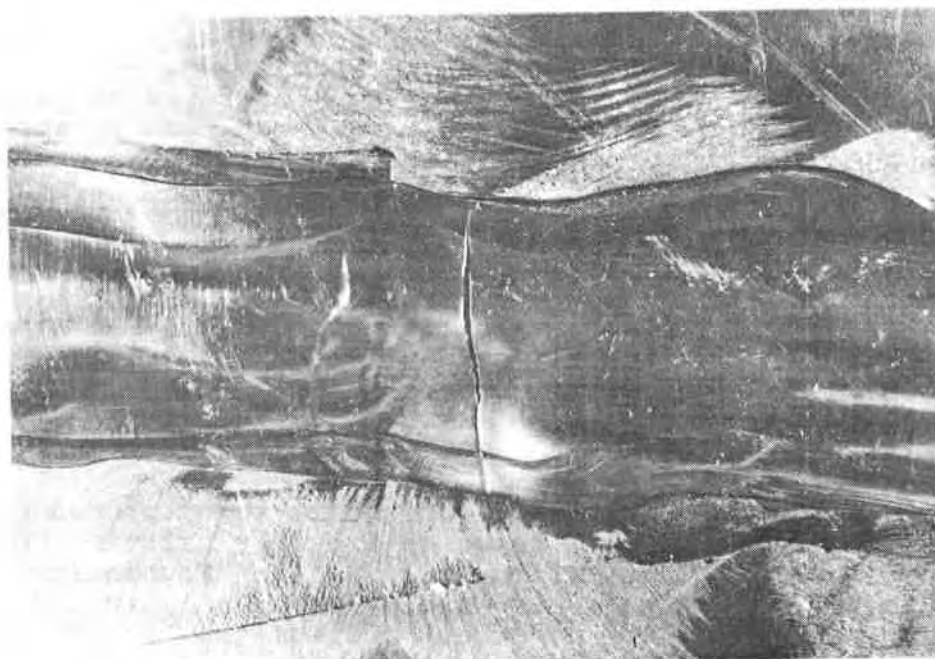


Figure 3
Brittle fracture across an extruded fillet seam
initiated by melt cavities on the underside surface

Brittle fractures have been observed in plant seamed geomembrane before installation, within two weeks of installation prior to filling the containment facility, and after two or three years of satisfactory service (1). In the final case, several fractures were observed on the exposed slope of an installation in the spring of the second year of operation. The cracks were repaired, and no further cracking occurred until the high amplitude temperature cycles characteristic of a northern Canadian spring occurred the following year. Since the growth and development of visual cracks is a time dependent function it is apparent that, at any instant, for every obvious through-geomembrane crack, there are probably many additional non-penetrating cracks actively propagating or ready to propagate when stress conditions are appropriate (at springtime). There are remedies to alleviate the springtime cracking in the above example but it may still be expected that some cracking will continue to occur each spring until existing cracks have propagated to a stable configuration. Such a configuration may continue to include complete geomembrane penetration.

The slow crack growth (SCG) phenomenon is similar to the phenomenon which resulted in many failures in the high density polyethylene (HDPE) pipe natural gas distribution industry a few years ago (2) and which is presently receiving a great deal of research attention (3). A more detailed review of the phenomenon, as it applies to HDPE geomembranes, will be published shortly (4). The cracks are initiated at notch-type stress concentrating features and may propagate under the influence of a constant stress. This process may be likened to a non-cyclic, monotonic fatigue process.

It is vital that quality assurance test procedures be initiated which, in some way, identify the susceptibility of field produced seams to the slow crack growth process.

REVIEW OF EXISTING QUALITY CONTROL TEST PROCEDURES

There are many proprietary sets of seam test procedures and acceptance criteria. All are based on the only existing national standard, produced by the National Sanitation Foundation (NSF), Standard Number 54 entitled "Flexible Membrane Liners" (FML). Unfortunately this standard does not address the parameters and criteria which could be used to evaluate the long term service behavior of geomembranes.* Although provision is made for constant load and elevated temperature seam testing, the scope of the standard is primarily limited to the immediate properties of the seam at the time of testing. Consequently, most seam evaluation procedures leave considerable room for improvement. Thus, service failures such as brittle cracking will continue to occur unless additional test parameters are monitored.

Most seam qualification procedures are based solely on shear and peel testing (5) using 25 mm wide strip specimens. Under no circumstances should ASTM D638 Type IV, or D638M Type III "dogbone" specimens be used to evaluate seams over 15 mm wide, as the seam width may equal or exceed the gauge length of the specimen and produce inapplicable results.

The NSF 54 standard identifies minimum requirements for Bonded Seam Strength, or the maximum load recorded during the shear test. Theoretically, since the shear strength of most materials is approximately one-half of the tensile strength, a welded interface only twice as wide as the geomembrane thickness is required to transfer tensile loads from sheet to sheet. Generally, seam widths exceed 10 mm, thus it is very rare that the minimum shear strength criterion is not met - even in seams which may be of inferior quality, and peel to complete detachment (6). In addition, when shear test failures occur in the geomembrane they may do so at adequate loads whether or not that fracture occurs in a ductile or

* "Geomembrane" will be used throughout this paper instead of FML. It is considered to be a more appropriate term.

brittle manner. The latter is not desirable, as the surface gouging and other defect features which cause its occurrence are among the features which may initiate the brittle SCG phenomenon. It is evident that seam shear strength alone is not an adequate acceptance criterion for seam quality.

The sole NSF peel criterion for PE geomembrane seams is that the specimen should demonstrate a Film Tearing Bond (FTB) failure. The intent of the FTB definition is that the geomembrane must fail before the welded interface "separates" but it is not clear whether the geomembrane should fail before any peel separation occurs or whether, for instance, 80% separation is permissible provided that the weld displays some integrity, and the geomembrane itself ultimately breaks. At first glance, it may appear that the latter behavior is acceptable since some of the seam still has enough strength to cause the geomembrane itself to fail. However, research has shown (7) that when a substandard weld interface separates, considerable surface damage occurs. Crazes, which may extend through 30% of the thickness of the geomembrane, are induced in the separated surfaces. Such crazes may eventually become cracks and propagate to cause ultimate failure of the geomembrane. Such crazes initiated at stress concentrating surface geometrical defects were the cause of the brittle springtime failures noted earlier.

The NSF 54 standard requires that shear test specimens be tested at a crosshead speed of 20 in/min. (500 mm/min). However, it has become conventional practice for all polyethylene shear tests to be stressed at a rate of 50 mm/min (2 in/min).

Some proprietary specifications have rejected FTB as the sole acceptance criterion for seam peel behavior (in fact they reject the use of the term FTB altogether) and instead use a minimum peel strength criterion. However, even a peel strength criterion does not consistently evaluate seams in geomembranes of all thicknesses. The bond strength of one body of PE to another should be a unique value. However, peel specimens can only be stressed to a maximum value determined by the thickness of the geomembrane because the geomembrane will fail before the seam separates in peel. Thus, the seam in a 2.5 mm thick geomembrane will be loaded to 2.5 times the load of a 1.0 mm thick geomembrane when geomembrane failure occurs. The seam in the thicker geomembrane has been much more severely tested than the thinner one. For instance, if a minimum peel load of 50 kN is specified, a (thick) geomembrane will be rejected if the measured peel load is only 40 kN. However, a peel specimen of the thinner geomembrane will be accepted if the peel load exceeds only 20 kN. It is thus possible that the thinner geomembrane may not have been adequately tested.

It is important that the ramifications of a peel strength criterion be considered if such a criterion is put in place. The use of a peel strength criterion is an improvement over the FTB criterion but it does define the necessity for a modified peel test, perhaps performed as a sharp wedge penetration test (7, 8), as shown in Figure 4, or as a Z-axis tear test (9). However, this topic will not be pursued further in this paper.

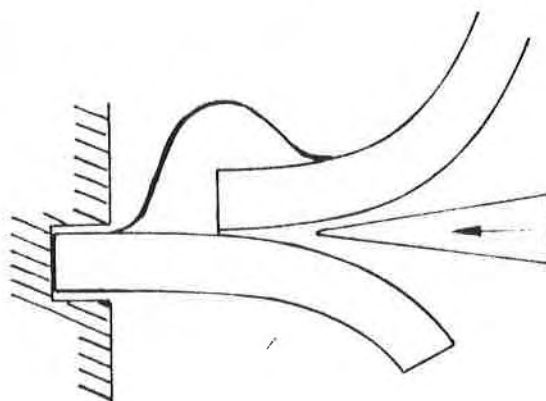


Figure 4
Outline of proposed wedge peel test

It is vital that seam testing procedures be expanded to incorporate the measurement of parameters which will define the long term serviceability of geomembrane seams. Then, having performed the tests it is necessary to have an adequate set of acceptance criteria for the complete cut-out seam sample. Such criteria do not presently exist, but a prototypical set of criteria will be proposed in this paper.

EXISTING SAMPLE TEST ACCEPTANCE CRITERIA

The previous discussion has identified the presently existing basic peel and shear test acceptance parameters. However, these criteria apply only to individual specimens. Instances in which acceptance criteria exist for the total sample, which consists of five individual peel and five individual shear tests, are rare. In the majority of cases, the number of individual specimen failures permitted before the sample is considered a failure is undefined.

Is it adequate to perform tests on two peel and shear specimens, and only if one or both fail to perform tests on a further three specimens? This is presently a common practice. Are peel and shear specimens to be considered in pairs or are all five peel specimens to be considered a separate group from the shear specimens? What is Film Tearing Bond?

PROPOSED SEAM TEST PROCEDURES

All seam evaluation tests, whether performed on trial weld samples at the beginning of each shift or on samples cut out from production seams, should be performed with five peel and five shear specimens cut in an alternating fashion (shear, peel, shear, peel, etc.) from the sample. It may be informative to test the specimens in the order of cutting to define any trend in seam quality along the length of the sample.

All specimens should be cut as 25 mm (1 in) wide strips to ensure that the seam does not exceed the test gauge length of the specimen. Loads measured in the test may be immediately expressed as a unit tension in Imperial units. These unit tension values may be quickly converted to stress values by dividing by the thickness of the geomembrane in which break occurred.

Shear Test

Specimens should be inserted in the machine with gauge lengths of 50 mm (2 in) between each edge of the seam and the adjacent grip. The crosshead speed should be 50 mm/min (2 in/min) for conventional medium and high density PE and 500 mm/min (20 in/min) for linear low and linear medium density PE. These speeds are generally used for quality control and conformance tensile tests on the basic geomembrane.

The parameters monitored during the test should be load and crosshead displacement. The test may be terminated when the crosshead has moved 50 mm (2 in).

If the geomembranes were tack-welded before joining with the designed weld the specimens should be tested across both welds unless the tack weld can be separated manually. If the tack weld cannot be separated manually, allowing the designed weld to be properly tested, the tack weld should be considered to be a part of the seam and must meet all acceptance criteria.

Peel Test

Peel specimens shall be inserted in the tensile machine so the grips are no closer than 25 mm (1 in.) to the edge of the seam. The grips may be closer than 25 mm only if there is insufficient material to allow insertion at this setting. All seam peel specimens from HDPE, MDPE, and LLDPE should be tested at 50 mm/min. (2 in./min.). The load and amount of peel separation (area) should be monitored. As in the shear test, if the tack weld cannot be manually separated it should be included in the peel test.

Both tracks of a double track fusion seam must be tested in peel. Wide, single track fusion seams and wide extruded lap seams should be subjected to peel tests from the exposed (to the contained solids or fluid) edge of the seam and meet the same acceptance criteria as the conventional peel test performed on the unexposed edge of the seam.

PROPOSED SAMPLE TEST ACCEPTANCE CRITERIA

The following parameters for each specimen should be determined:

Shear Specimens:

- . ultimate unit tension (N/m) or stress (MPa). Both may be referred to as the shear strength.
- . elongation at break (%). This should be recorded as; "greater than 100%", or the actual value if less than 100%.

Peel Specimens:

- . ultimate unit tension (N/m) or stress (MPa). Both may be referred to as the peel strength.
- . area of peel separation (%). This should be recorded as a percentage of the original weld interface which is being stressed, i.e. one track of a double track seam; one-half of the total width of an extruded fillet seam.

The sample acceptance criteria will be based on a unit tension or stress value identified in the project specifications. This value could, in turn, be based on one of the following:

- . minimum bonded seam strength (NSF 54);
- . minimum geomembrane Yield Stress (NSF 54);
- . a typical mean geomembrane yield strength, as quoted in manufacturers' brochures;
- . a typical minimum geomembrane yield strength specified by manufacturers; or
- . the measured mean geomembrane yield strength.

Having defined this specified strength value, the criteria of acceptance of the seam sample will be:

- . the mean shear strength of the five specimens shall exceed the specified value;
- . no shear specimen strength value shall be less than 80% of the mean shear strength;
- . no shear specimen elongation value shall be less than 50%;
- . the mean peel strength of all five specimens shall exceed 80% of the specified strength value; and
- . no peel specimen strength value shall be less than 80% of the mean peel strength.
- . no peel specimen separation value shall exceed 10%.

All of the above criteria must be met for the complete sample to be considered acceptable.

DISCUSSION

The selection of the specified strength value is of critical importance, and the value selected will be a function of the nature of the installation and the knowledge of the lining system designer or specifications contractor.

Test data have shown that a 20% tolerance on individual specimen minimum strength values exceeds two standard deviations in a normal Gaussian distribution of peel strength values measured on 1.5 and 2.0 mm thick PE geomembrane which has been adequately seamed (10). It may thus be necessary that the specified strength value relate to a minimum material property, rather than a mean material property in order that the few strength values outside two standard deviations do not result in the unnecessary rejection of a few seam samples.

For guidance purposes a survey of recently generated test data is shown in Table 1.

TABLE 1
COMPARISON OF PEEL STRENGTH WITH OTHER
STRENGTH PARAMETERS FOR DIFFERENT
GEOMEMBRANE/SEAM COMBINATIONS

GEOMEMBRANE	SEAM TYPE	MEAN PEEL STRENGTH (MPa)	GEOMEMBRANE YIELD STRENGTH (MPa)		MEAN SEAM SHEAR STRENGTH (MPa)
			Minimum Specified	Measured	
LLDPE	Double wedge	13.8	(<13.8)	19.0	16.9
HDPE	Fillet Mfr. A	14.6	16.1	-	18.3
HDPE	Fillet Mfr. A	13.2	16.1	18.6	17.6
HDPE	Fillet Mfr. B	14.5	17.3	19.4	17.8

Only an insignificant number of specimens used to generate the data for Table 1 showed more than 10% peel separation.

Table 1 shows that mean peel strength values vary between:

- . 84 and 100% of the minimum specified geomembrane yield strength,
- . 71 and 84% of the measured mean geomembrane yield strength, and
- . 75 and 82% of the measured seam shear strength.

Table 2 lists sample peel strength values from a typical set of test data and shows that the lowest sample mean peel strength can be within 20% of the mean peel strength.

TABLE 2
MEAN PEEL STRENGTH PARAMETERS

GEOMEMBRANE	SEAM TYPE	PEEL STRENGTH, (MPa)			S.D.
		Minimum	Meam	Maximum	
HDPE	Fillet Mfr. A	12.9	14.6	17.6	1.6
HDPE	Fillet Mfr. A	11.5	13.2	15.4	1.3
HDPE	Fillet Mfr. B	11.6	14.5	16.3	1.2

The information provided in Tables 1 and 2 shows that the proposed criteria may be met if an appropriate specified strength value is selected.

The inclusion of shear elongation and peel separation in the criteria provide a basic contribution to the required guide to the long term behavior of the geomembrane seams.

Low elongation values result from surface damage (gouges, overgrinding) in the geomembrane (6). Such damage produces stress concentrations which are known to be capable of initiating the previously discussed slow crack growth fractures.

The separation of inadequately fused seams has been observed (Figure 5) to initiate crazing in separated surfaces. Such crazes may eventually open up into cracks which propogate in a brittle manner.

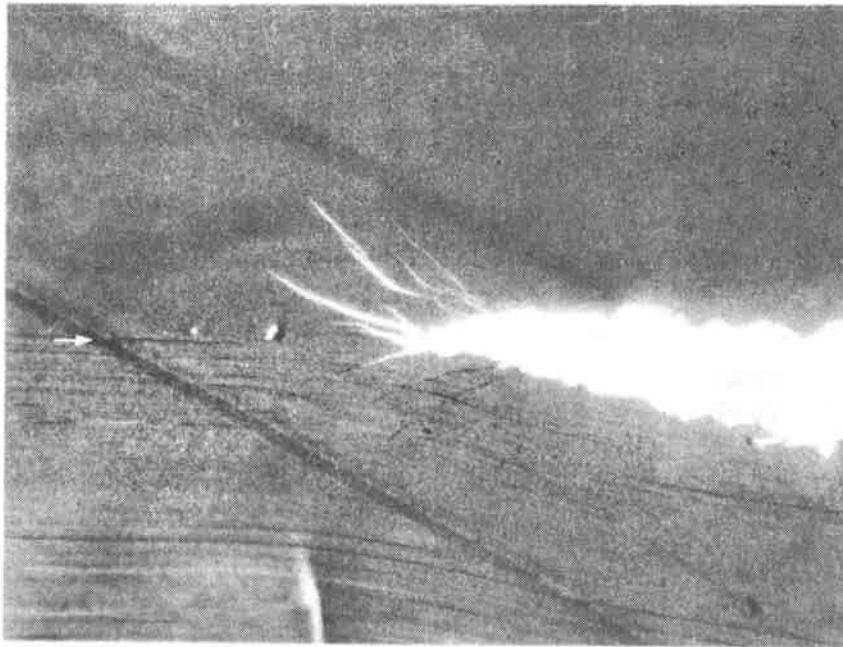


Figure 5
Seam peel specimen showing crazing induced in peel
separated surfaces. Magnification x 50

There are other qualifying factors which could be written into a set of seam acceptance criteria but which need to be the subject of further discussion prior to their incorporation. These factors include:

- . Failure in the fillet weld bead during a peel test.

A weld which fractures through the weld bead but which displays adequate strength may be deemed to be acceptable. However, a seam which fractures through the weld bead after separation of the bead from the edge of the top sheet may be deemed unacceptable.

. Tack Welds

If the tack weld is considered part of the seam (i.e. the tack weld cannot be manually separated) it should behave as part of the seam on all tested specimens. If it is intended to be an integral part of the seam there should be no lack of fusion between it and the extruded fillet seam. Alternatively, if there is lack of fusion there must be a sufficient amount that the lower geomembrane can be cut through to this lack of fusion so that a peel test can be performed on the fillet weld. The tack weld is, or is not, a part of the seam system. It must not be allowed to interfere with testing the designed weld.

SUMMARY

This paper has discussed the necessity for polyethylene geomembrane seam testing protocols which provide information on the long term behavior of seams.

With minor modifications, some appropriate data indicating long term seam serviceability may be generated from existing test protocols. The data include values for:

- . seam shear elongation
- . seam peel strength
- . seam peel separation

This paper has presented acceptance criteria for seam cut-out samples.

REFERENCES:

- (1) Peggs, I.D., Unpublished consulting reports. 1982-1986.
- (2) Gual, J.F., "Field-Life Study - An Assessment of Residual Long Term Suitability of In-Service PE Piping". Proceedings of Ninth Plastic Fuel Gas Pipe Symposium, New Orleans, 1985 pp. 194-201.
- (3) Brown, N., "Relationship Between Slow Crack Growth and Ultimate Failure of Polyethylene". Ibid. pp. 283-290.
- (4) Peggs, I.D., "Brittle Fractures in HDPE Geomembranes". To be published in Geotextiles and Geomembranes.

- (5) "Flexible Membrane Liners" National Sanitation Foundation
Standard Number 54. 1985 p. 5.
- (6) Peggs, I.D., Rose, S., "Practical Aspects of Polyethylene
Geomembrane Seam Welding". Geotechnical Fabrics Report
1985, February.
- (7) Peggs, I.D., "The Effectiveness of Peel and Shear Tests in
Evaluating HDPE Geomembrane Seams". Proceedings of Second
Canadian Symposium on Geotextiles and Geomembranes, Edmonton,
1985 pp. 141-146.
- (8) Lupton, D.C., Joneja, S.J., "Parametric Evaluation of the
OCF Wedge Test". Proceedings 42nd. Annual Conference
Reinforced Plastic/Composites Institute, 1987.
- (9) Fruck, B., "Review and Development of Physical Test Methods
for Polyethylene Geomembranes". Alberta Environmental
Research Trust, Grant #T01104, 1986.
- (10) Peggs, I.D., Unpublished consulting reports, 1982-1986.

HEBERT, T.

Hebert Engineering Corp., U.S.A.

Construction Quality Assurance/Quality Control for Land Disposal Facilities

INTRODUCTION

This presentation for construction quality assurance/quality control of a land disposal facility is for a double liner facility constructed per the RCRA 1984 amendments.

CONSTRUCTION QA/QC PLAN

The objective of the construction QA/QC plan is to ensure the constructed land disposal facility complies with the design.

The construction QA/QC officer has responsibilities in the design, construction, documentation, and certification of the project. The officer must review the design for constructability and clarity. He directs the inspection and documentation of the construction. Corrective actions for problems arising in construction are developed with the design engineer and construction management team. The QC officer assists the design engineer certifying the facility was built per the design after review of the construction QA/QC documentation.

The contents of the construction QA/QC plan include:

- # Responsibility and Authority
- # CQA Personnel Qualifications
- # Inspection Activities
- # Sampling Activities
- # Documentation.

This paper addresses the inspection and sampling activities, as the other items are similar on most construction projects.

INSPECTION

The inspection objective is to determine if materials, properties, composition, and performance comply with the design.

The items presented here for inspection requirements include:

- # Foundations
- # Dikes
- # Clay Liners
- # Geomembrane Liners
- # Leachate Collection System

The cross section shown here of the liners and leachate systems shows the components.

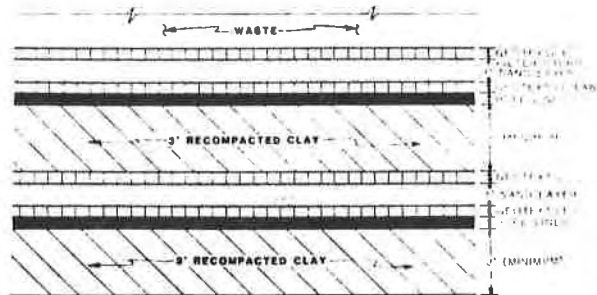


FIGURE 1 - Liners and Leachate Systems Cross Section

FOUNDATION INSPECTION

The foundation is the bottom and side slopes of the completed excavation. The bottom clay liner is placed on this excavation bottom and slopes. In South Louisiana the bottom of the land disposal facility is usually much deeper than the water table. The high water table requires providing a pressure relief system below the bottom clay liner to prevent heave or blow out of the liner. The pressure relief system would consist of a drainage layer and a method of removing the water from the drainage system.

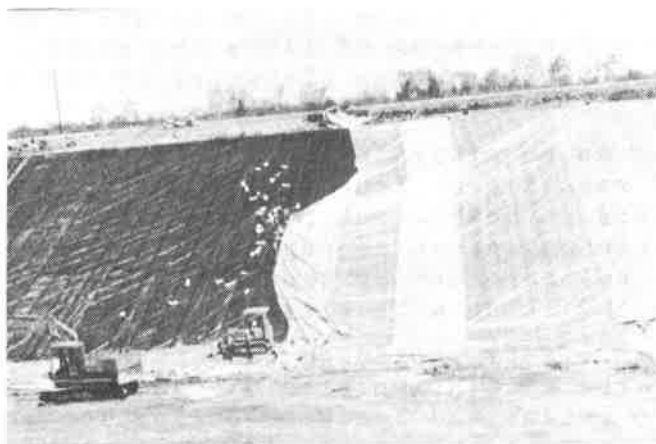


FIGURE 2 - Pressure Relief System -
Installation of Slope Drainage



FIGURE 3 - Pressure Relief System -
Installation of Gravel Collection Laterals

The primary foundation preconstruction activity is to review the site information in detail.

Subsurface information such as boring logs and geotechnical test results should be studied to understand the anticipated conditions. Site topography, drainage, and layout should be reviewed.

The foundation construction inspection activities include survey control and density/moisture content control for any compacted fill.

Survey control requires a 15 meter (50 foot) areal grid and elevation benchmarks for control of lines and grades. The same controls may be used for recording placement of the waste after construction.

Potential problems can be mitigated by proper quality control. Slope failures may result from improper survey control. Also, silt lenses and other permeable outcroppings on the slopes below the water table may cause seepage and localized slope failure. This may be corrected by excavating a bench into the seepage zone and backfilling with clay.

Seepage may be drawn off by providing for drainage at the bottom and side slopes of the excavation with ditches draining to a sump. The pressure relief and leachate collection drainage systems may be used during construction for dewatering. Foundation settlement may be mitigated by proof rolling the completed foundation. Permeable materials can be removed and backfilled with clay to provide an impermeable base.

DIKES INSPECTION

The two criteria for a dike are that it be structural stable and impermeable. These objectives and the construction and inspection methods are the same as for a clay liner. Therefore, the following discussion of clay liners is also applicable to dikes.

CLAY LINERS INSPECTION

The objectives of the clay liner include:

- * Prevent leaks
- * Protective base for geomembrane.
- * Structurally stable base.

The clay liner preconstruction inspection activities include testing the material. Liquid and Plastic Limits tests identify the material to be used is the specified material. The moisture content is tested to determine if it is within the range that can achieve the specified density, permability, and strength.

The relationship of the permeability to the type of soil, as defined by the Liquid and Plastic Limits, and density, moisture content, and strength should be established during the design phase by sufficient testing of site samples. The specified permeability and strength should define a range of density and moisture contents that can achieve the specified permeability and strength. The specified density and moisture content for construction QC should be at a point within this

range. The actual moisture content of the soil at the time of borrow excavation may be greater or less than specified. This will require aerating the soil if too wet and watering if too dry before stockpiling.

The stockpiling of material must be properly planned and managed. This is particularly true in South Louisiana if onsite clay is to be used for the liner due to the presence of silt layers interspersed in the clay.

The clay must be uniformly spread and compacted to achieve a uniform thickness and the specified density. The thickness should be measured on 15 meter (50 foot) centers at the completion of each lift.



FIGURE 4 - Clay Liner -
Initial Placement and Spreading



FIGURE 5 - Clay Liner -
Placement, Compaction, Fine Grading, and Testing

Testing includes calculating the degree of saturation as a relation of moisture content and density to permeability.

Traffic should be minimized on the accepted lift. Material should be placed at the edge of the liner and dozers used to spread it in front of the dozer.

Potential problems that may be encountered during construction of the clay liner include lift separation, liner penetrations, and erosion or desiccation. Lift separation can be avoided by maintaining the surface of each lift at the specified moisture content and rough enough to provide sufficient bonding between lifts. Aeration may be required if the surface is too wet, and scarifying and watering may be required if the surface is too dry. Liner penetrations should be hand compacted like other voids. Erosion and desiccation can be reduced by seal rolling the surface at the end of each day or placing a temporary cover if the liner is to be exposed for a longer period.

Clay Liners Inspection - Acceptance Criteria

Acceptance testing consist of strength and permeability testing as well as the same test conducted during construction.

The finished liner should be surveyed for line and grade and visually inspected for defects.

Documentation requires preparing a block evaluation report. The report should contain all daily records prepared for the liner and summarize the construction activities and test results for the clay liner.

GEOMEMBRANE LINER INSPECTION

The objective of the geomembrane liner is to prevent leachate migration. The liner characteristics include resistance to waste liquid constituents and sufficient strength and thickness to withstand construction and operation forces.

The geomembrane material specification should be thorough. A good reference is the National Sanitary Foundation Standard Number 54, "Standards for Flexible Membrane Liners."

GEOMEMBRANE LINER INSPECTION

FINISH PRODUCT SPECIFICATIONS

- o THICKNESS - Nominal \pm 10%
- o MODULUS OF ELASTICITY - 110,00 psi
- o TENSILE STRENGTH AT BREAK - 4 pounds/inch width/mil of thickness
- o ELONGATION AT BREAK - 700 percent
- o TEAR RESISTANCE - 0.75 pounds/mil of thickness
- o PUNCTURE RESISTANCE - 4.25 pounds/mil of thickness
- o DENSITY - 0.94 grams/cc
- o OZONE RESISTANCE - no cracks at 7 magnification
- o PERCENT CARBON BLACK - 2-3 percent by weight
- o VOLATILITY LOSS - 0.1 percent by weight

FIGURE 6 - Geomembrane Product Specification

Geomembrane Liner Inspection - Shipping Label

Each roll of geomembrane should contain a shipping label with pertinent identification information and instructions.

GEOMEMBRANE LINER INSPECTION

SHIPPING LABEL

- o NAME OF MANUFACTURER/FABRICATOR
- o PRODUCT TYPE
- o PRODUCT THICKNESS
- o MANUFACTURING BATCH CODE
- o DATE OF MANUFACTURE
- o PHYSICAL DIMENSIONS (LENGTH AND WIDTH)
- o PANEL NUMBER OR PLACEMENT ACCORDING TO THE DESIGN LAYOUT PATTERN
- o DIRECTION FOR UNROLLING OR UNFOLDING THE MEMBRANE

FIGURE 7 - Geomembrane Liner Shipping Label

Geomembrane Liner Inspection - Construction

Geomembrane liner placement inspection should include these items.

- * Penetrations should be inspected closely to be sure the seal materials and construction are correct.

- * Layout should be in accordance with the panel layout drawing and the shipping label. Record the layout position.
- * The entire panel should be inspected for tears, punctures, and defects, particularly along edges and at penetrations.



FIGURE 8 - Geomembrane Liner Placement -
Slope and Bottom



FIGURE 9 - Geomembrane Liner Placment -
Anchor Trench

Proper seaming is the key to obtaining an impervious liner. Seaming inspection includes the following items:

- * Clean, dry membrane
- * Seaming material and equipment
- * Base
- * Weather conditions
- * Seaming temperature, pressure and speed
- * Membrane damage prevention.

Except for the base and weather conditions, these items can be controlled by the liner contractor. The clay liner base should be fine graded and seal rolled prior to placing the geomembrane to provide a smooth, uniform seam base.

Nondestructive testing, NDT, of the seams should be conducted on 100 percent of the welds. Failures are repaired and retested. Destructive seam testing should be conducted at planned locations and frequencies. Coupons are taken and tested in peel and shear. Failures can be reconstructed to the adjacent pass test locations on both sides or retested closer to the failure to reduce the length of reconstruction. All repairs are NDT'd. All testing and rework should be well documented.

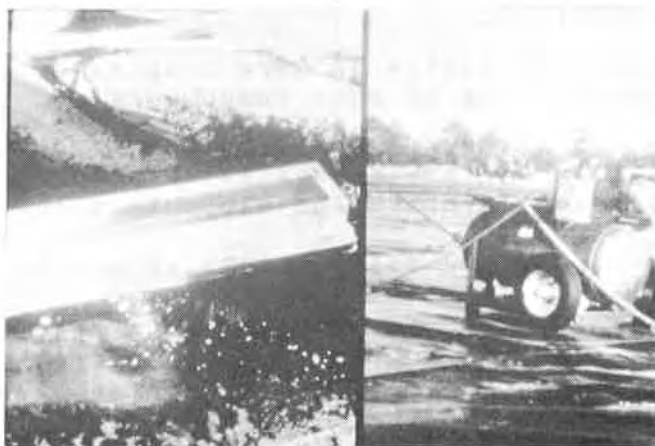


FIGURE 10 - Geomembrane Seam NDT -
Vacuum Box and Vacuum Pump

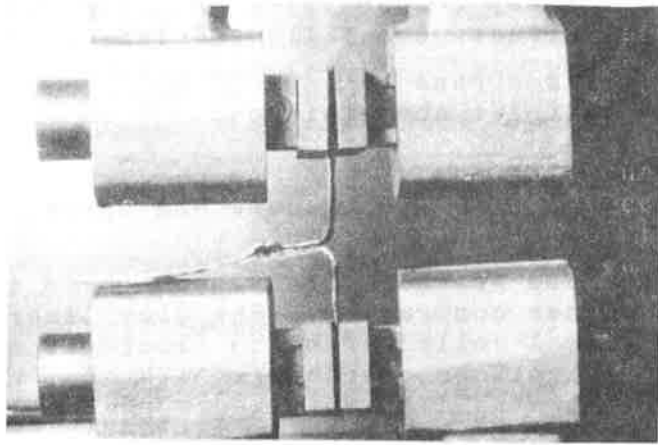


FIGURE 11 - Geomembrane Seam
Destructive Peel Seam Test

LEACHATE COLLECTION SYSTEM INSPECTION

The objectives of the leachate collection system are to minimize leachate head on the impervious geomembrane liner and remove liquid from the landfill.

The leachate collection system is more complex in that it is a drainage system consisting of many components:

- * Piping key items are the type and grade of material, the quality of the perforations for drainage collection, proper location and slope to allow drainage, and tight joints.
- * Soil drainage and filter media should be tested for gradation.
- * Geosynthetics should be verified as the material specified. Placement and seams must be inspected.
- * Prefabricated structures are inspected and tested during offsite construction. Construction methods for installation should be reviewed with the contractor.
- * Equipment consists of pumps, power supply and instrumentation for removal of the leachate from the landfill. The inspection of equipment installation and testing should be done in conformance with the manufacturer's instruction as a minimum.

A word of caution needs to be provided for the use of geosynthetics for leachate collection system. Actually, this applies to any system in which two or more geosynthetics are placed adjacent each other on a slope. The problem is the friction factor between the geosynthetics is much lower than the friction factor provided by the vendors for a soil/geosynthetic interface. This lack of stability on slopes due to low friction factors may result in placing the layered geosynthetics in tension and can tear the fabrics on long or steep slopes. The tension may not be noticeable in placement because it has no weight on top to cause tension. But after the material is covered, particularly with a heavy clay liner and the heavy loads of actual waste placement, the tension would increase. Normally this tension can be seen during placement of a clay liner over the layered synthetics before the clay liner covers the entire slope.

The author suggests that several things be considered to address this lack of friction between geosynthetics on slopes.

1. Leachate collection or pressure relief drainage composites should be sufficiently bonded to provide the required shear strength. The result would be a unified composite drainage system.
2. Geomembranes should not be directly interfaced with another geosynthetic. The common practice is to place a protective fabric atop the geomembrane. Instead a layered of soil should be placed atop the geomembrane to provide sufficient friction and the required protection.

The completed leachate collection system should be inspected for acceptance. The system should be inspected that all components are properly located, fitted together, and not damaged. Consideration should be given to conducting a performance test to confirm each component and the system functions properly. The EPA guidance document for construction QA/QC proposes a performance and capacity test.

REFERENCE

- (1) Herrmann, J. G., "Construction Quality Assurance for Hazardous Waste Land Disposal Facilities," EPA Document No. 530-SW-85-021, Cincinnati, Ohio, 1985.

FLUET, J.E., Jr.

GeoServices Inc. Consulting Engineers, U.S.A.

Geosynthetic Lining Systems and Quality Assurance—State of Practice and State of the Art

Although the use of geosynthetics is clearly well established in the waste disposal industry, the current state of practice may well be considered primitive by designers of future lining systems. In this paper, the historical development of the installation and quality assurance of geosynthetic lining systems is reviewed, the current state of practice as well as the state of the art are described, and recommendations are made for future requirements and developments.

1. INTRODUCTION

Geosynthetics have arrived. Waste disposal lining systems in the United States now commonly incorporate geosynthetics. The geosynthetic and waste disposal industries are now interdependent, and it appears they will so remain for years to come. Geosynthetics are now used in virtually every aspect of landfill and surface impoundment construction. In particular:

- Primary leachate collection systems (LCS) utilize geotextiles as filters, and they utilize geonets, geotextiles, or geocomposites as drainage media.
- Primary and secondary liners utilize geomembranes either alone as the entire liner or in combination with low permeability soils to form composite liners, and they utilize geotextiles as cushions.
- Secondary leachate collection systems, now usually referred to as leak detection systems (LDS), utilize geonets, geocomposites, and occasionally geotextiles as drainage media, and they utilize geotextiles as filters.
- Pressure relief systems constructed beneath lining systems utilize geotextiles as filters, and they utilize geonets, geocomposites or geotextiles as drainage media.
- Gas collection and distribution systems utilize geotextiles as filters, and they utilize geonets, geocomposites or geotextiles as drainage media.
- Closure systems utilize geomembranes as caps/covers, they utilize geotextiles as cushions and filters, they utilize geonets, geocomposites or

geotextiles as drainage media, and they utilize geogrids and high modulus geotextiles as subgrade support.

- Slope stabilization systems utilize geogrids or high modulus geotextiles as reinforcement to prevent sliding of cover soil on internal slopes as well as on the exterior slopes of closure systems.
- Subgrade support systems utilize geogrids and high modulus geotextiles to minimize differential settlement beneath lining systems.

This paper is based on the experience gained by the author and his firm in the design, quality assurance, and forensic analysis of many waste disposal geosynthetic lining systems during the past several years. Additionally, the author's understanding of the subject has increased substantially in the process of teaching several short courses on geosynthetic lining systems to various EPA regions as well as continuing education courses on behalf of several universities.

2. HISTORICAL DEVELOPMENT

The predecessors to the current usage of geosynthetics in the waste disposal industry included the many installations of geomembranes as pond and canal liners from the 1950's to the present time, as well as the use of geotextiles as filters, cushions, and separators from the 1960's to the present time in other aspects of civil engineering such as highway construction, erosion control, and railroads. During the late 1970's and early 1980's, geomembranes and geotextiles were experimentally installed in a few landfills and surface impoundments. Relatively few, if any, of these early waste disposal installations enjoyed the benefits of comprehensive conceptual and detailed design by qualified geosynthetic engineers - for the most part, they were simply "designed" based on recommendations of the geosynthetic manufacturers. However well intentioned, such manufacturer recommendations typically failed to incorporate fundamental civil, geotechnical, and environmental engineering principles, and consequently experienced varying degrees of success. These early problems notwithstanding, it is to these early pioneers that we owe the development of today's technology. In the evolution of any technology, criticism of early efforts is based on the wisdom of hindsight and often fails to credit the foresight exhibited by the pioneers.

It was in the early 1980's that the first fully-engineered geosynthetic lining systems began to appear in the waste disposal industry. Much of the success of these efforts must be credited to two men, a designer and a researcher:

- Dr. J.P. Giroud, who developed design methods and pioneered geosynthetic double liner systems, geotextiles combined with geomembranes (both in the early 1970's), and the use of geonets for leakage detection; and
- Dr. Henry Haxo, who was and continues to be regarded as the leading expert on the chemical compatibility of geomembranes and waste products, and whose research gave credibility to the use of geomembranes in waste disposal applications.

Much of the developmental research into the use of geomembranes was sponsored by the U.S. Environmental Protection Agency (EPA) and the U.S. Bureau of Reclamation (USBR). The EPA and the USBR thus provided the financial and legislative impetus which caused the geosynthetic liner system technology to bridge the gap between early trial and error experiments and today's engineered systems.

Several conclusions may be drawn from a review of the development of lining system technology:

- the development of geosynthetic lining system technology has changed in character from a relatively slow evolution prior to 1980 to a technological revolution in the past few years;
- the success of the technology has been critically dependent on the careful application of fundamental principles from all related engineering and scientific disciplines, i.e., civil, geotechnical, environmental (in the development of new design methods and applications), chemical, polymer, plastics, and textiles (in the development of new materials); and
- full acceptance of the technology has been predicated by the development of a body of supporting data, analytical methods, and construction methodology, as well as completion of laboratory and full-scale tests.

3. CURRENT GEOSYNTHETIC LINING SYSTEMS

The geosynthetic lining systems which are typically in use currently do not represent the state of the art in geosynthetic lining system design; i.e., as is common in civil engineering, the state of practice lags behind the state of the art. Nonetheless, the state of practice in geosynthetic lining systems is moving much faster than the geosynthetic state of the art in many other civil engineering applications. Currently, the lining systems state of practice is probably no more than a few years behind the state of the art.

Because of the more severe environmental threat of hazardous waste, the design of hazardous waste containment facilities (as opposed to Municipal Solid Waste (MSW) facilities) has led the way in the development of both the state of the art and the state of practice of waste disposal lining systems. As a consequence, the majority of the previously published literature on this subject has specifically addressed hazardous waste facilities. In the past few years, however, geosynthetic lining systems have been used increasingly in MSW applications. Several states have now enacted legislation which requires one or more geomembranes in MSW facilities and many states encourage the use of other geosynthetics as well. In the past year, for example, the author's firm has been involved in the design of several double composite geosynthetic lining systems for MSW sites. Recognizing that the concentrations of undesirable chemicals in MSW are certainly lower than in hazardous waste, it is nonetheless true that some hazardous chemicals are occasionally inadvertently disposed of as (or in) MSW. Although the subsequent leachate concentrations of these chemicals are very low, they are nonetheless of great concern to designers because they may pose some threat to the groundwater if released. Consequently, prudent designers now often apply state-of-the-art geosynthetic lining system technology to MSW sites which are not otherwise isolated from sole source aquifers.

3.1 Best, Available Technology (BAT)

The author has often been asked (particularly during the conduct of lining system short courses) whether today's state-of-practice geosynthetic lining systems represent the ultimate solution to waste disposal. The answer is always the same:

- first, today's state of practice will probably be considered primitive by designers of future lining systems, i.e., lining system technology continues to develop at an astounding rate;
- even in the presence of very good and ever-improving lining system technology, the author hopes and prays for infinitely better ultimate solutions, e.g., waste vitrification, shooting waste into the sun, or some other futuristic wonderful solution; and
- in the meantime, the best technology we currently have available to protect our environment from our own solid and hazardous waste is land disposal in units encapsulated by well engineered geosynthetic lining and closure systems.

It is also true that the lining system technology we are now developing will almost surely continue to be applied to interim waste storage facilities even once we do develop better permanent disposal technology. Therefore, our current efforts should not be viewed simply as developing stop-gap measures. The technology itself will be applicable into the distant future - only the end-use will change. Furthermore, the technology we are now developing will certainly be applicable to other important civil engineering applications such as large dams and irrigation systems.

3.2 Current Practices and Guidelines

This section describes the current practices and guidelines for installation and quality assurance of geosynthetic lining systems. These are described in great detail in [1, 2, 3, 4]. In order to successfully design and construct a BAT lining system, the following are required: (i) careful design of the lining system, (ii) careful installation of the lining system, and (iii) careful quality assurance of the lining system.

Currently, the only design guidelines which are available are broad and somewhat incomplete. As a consequence, designers must scour legislative guidelines and technical publications in order to develop a basis for their design methods. They must then develop their own comprehensive conceptual and detailed design methods and procedures. Since such design approaches are usually independently developed and are therefore unverified, it is very important that all designs undergo independent quality assurance review. Unfortunately, few designs are current reviewed by an outside party other than regulators who are often too busy or insufficiently trained to conduct a comprehensive engineering review. Future legislation will undoubtedly address this issue.

Giroud and Fluet [1] list eleven separate operations which must be performed in order to install the geosynthetics in a double composite liner system. Each of these operations must be conducted by a qualified, experienced crew (or at least

crew leader) if there is to be any expectation of a high quality lining system.

When all the operations listed by Giroud and Fluet [1] occur simultaneously, one quality assurance monitor would be required for each operation in order to fully document the installation. In addition to those monitors, another monitor would be required to measure and accurately located each panel's position on the site and then to transfer the information onto the record drawing. (Remember when we were allowed by the insurance industry to call them "As-Built" drawings and to use the term "inspector"?) The record drawing should also include patches and other repairs. This monitor also would be the one responsible for observing the condition of the panels themselves (as opposed to the seams) for factory defects and handling damage. These monitors plus the quality assurance manager would therefore be required on the project if the owner wished to have 100% documentation and certification. If, on the other hand, financial or other constraints were to dictate a fewer number of monitors, then the result would be a proportionate decrease in level of documentation and certification. In typical projects, the installer coordinates his work such that six or seven crews are performing simultaneous work. Accordingly, six or seven monitors are therefore required if the owner wishes to have 100% documentation and certification.

As with all rapidly evolving technical disciplines, today's waste disposal lining system state of the art will soon become the state of practice. In fact, waste disposal lining system technology is changing so rapidly that the dividing line between state of practice and state of the art is unclear, and varies from locale to locale, and even from design firm to design firm. Recognizing that differences of opinion will exist, the author proposes that many experienced lining system engineers would offer the following comments on the current state of practice:

- Double Composite Liner Systems are the BAT, but few designers understand the concept, much less the design methods or construction procedures.
- HDPE/LLDPE is the most commonly used liner material, but designers and contractors dislike some of its properties.
- Welding is the preferred seaming method, but the technology is still quite primitive.
- Vacuum testing is almost universally used to non-destructively test seams, but it is awkward, slow, and primitive.
- Destructive seam testing and conformance testing are not currently standardized and are rarely well documented.
- Most designers believe that leachate collection and leak detection systems are a good idea, but very few designers are familiar with the formulations and methods required to properly design them.
- Quality Assurance (QA) is usually underfunded, undermanned, and underplanned.
- QA personnel are often unqualified and the resulting QA documentation is unsatisfactory.

4. STATE OF THE ART

Fortunately, all of the above criticism is not in vain, because many of the points have already been addressed and the answers are already being implemented as state-of-the-art technology, and some other points are currently in the research stage. (The fact that a few points have not been addressed at all will serve as job security for lining system researchers.)

4.1 Liners: Concepts and Materials

The EPA is currently in the process of preparing several documents which address the conceptual and detailed analytical design methods and procedures associated with composite liners, double liner systems, and double composite liner systems. These documents include several computer programs which are directly related to liner system design. Additionally, several short courses are currently being taught by the EPA, major university continuing education departments, and private concerns, all of which address various aspects of liner system design. Furthermore, several books have already been published on the subject, and at least one more is currently being written. In summary, the information, data, and analytical procedures required to design state-of-the-art liner systems is currently developed, and the ease of obtaining the information is increasing rapidly. It is therefore the responsibility of every prudent designer to take the steps necessary to educate himself accordingly.

The construction methods associated with double composite liner systems have not been adequately described in the literature, probably because the lessons learned have been painful and expensive and the contractors are not therefore anxious to share the knowledge. Suffice it to say that the construction methods associated with double composite liner systems are reasonably well established and improving rapidly, with the following areas being of key concern:

- means of protecting clay components from desiccation and/or excessive exposure to moisture prior to being covered by geomembrane components;
- means of preventing rutting of clay components by the equipment used to distribute and place overlying components; and
- means of placing the clay component of the primary (top) composite liner without damaging the secondary composite liner and/or the LDS.

At least one other paper in these proceedings (Buranek and Pacey) [6] addresses many of these issues.

The choice of liner system materials continues to be very limited. HDPE and LLDPE have excellent durability, chemical/biological resistance, and weldability; however, their mechanical properties leave much to be desired. Specifically: they are too stiff and therefore very difficult to handle in the field; their sensitivity to notches and scratches limits design strains to 5-8% in spite of their ability to elongate 500-700% in the un-notched state; and they have relatively high coefficients of thermal expansion/contraction and consequently are very difficult to place in varying temperature conditions (it is common for an exposed HDPE/LLDPE geomembrane to be taut and perfectly wrinkle-free after a

cool night, and completed "cross-hatched" with large wrinkles by that afternoon). As a consequence, a number of manufacturers are currently attempting to modify their current HDPE/LLDPE products to address some of the above problems. Some manufacturers are also working to develop new products which will combine the durability, chemical/biological resistance, and weldability of HDPE/LLDPE with the excellent mechanical properties of other materials, say PVC. In the meantime, means and methods have been developed to design and construct excellent liner systems which compensate for the known problems of HDPE/LLDPE (several such methods are described in these proceedings); therefore, it is the responsibility of designers, owner/operators, contractors, and regulators to ensure that the best available technology is indeed being used on their project.

No discussion of liner system concepts and materials would be complete without a comment on welding equipment technology. Although both direct fusion and extrusion welding equipment have improved significantly in the past few years, much improvement is still needed. In particular:

- equipment should be automated such that there is less dependence on operator finesse and skill;
- equipment should be equipped with gauges, readouts, and alarms to aid the operator in determining the quality of his work; and
- current methods of grinding the surface of the geomembrane prior to extrusion welding are primitive and archaic, and are the cause of a very high percentage of geomembrane liner flaws - this equipment must be automated and controlled (perhaps by lasers) using modern technology.

Recognizing the already large and growing nature of the waste disposal liner system market, manufacturers are hereby challenged to address these issues and develop liner materials and seaming technology which are consistent with this rapidly evolving technology.

4.2 Leachate Collection and Leak Detection Systems

Well designed leachate collection and leak detection systems are key components of double and double composite liner systems. It is a well established fact [2,5] that our present technology is not able to deliver a large scale geomembrane or clay liner that is not in some way flawed and does not therefore leak. More importantly, it is extremely unlikely that this situation will improve in the foreseeable future. As a consequence, designers must do all in their power to deal with leakage through flaws (i.e., minimize leakage through flaws, and then intercept and remove whatever leakage does still occur). We must design lining systems which do not measurably leak in spite of the fact that individual liners do leak.

To this end, designers must consider that there are three factors which control the leakage through a given flaw in a geomembrane:

- the hydraulic head which is the driving force of the leak;
- the residence time of the liquid over the flaw; and

- the interface conditions between the geomembrane and the material underlying the geomembrane.

Having made the unavoidable assumption that there will be flaws in both the primary and secondary geomembrane liners/components, then the designer must therefore minimize system leakage by applying the above three principles as follows:

1. Minimize the hydraulic head on the primary (top) liner by designing the flow characteristics of the LCS such that the liquid depth will be limited to a maximum of approximately 0.3 m (smaller design heads are of course desirable but are typically not cost effective).
2. Minimize both the hydraulic head and the residence time on the secondary (lower) liner by designing the LDS to have very high flow velocities (an important additional feature of this design is a greatly reduced leakage detection time and subsequent response).
3. Design the interface conditions between the geomembrane and the underlying material such that the underlying material will have as low a permeability as is economically feasible, i.e., use composite liners (note that the thickness of this low permeability lower component is not nearly as important as its permeability).

Following these three steps will generally result in an LCS comprised of clean gravel, clean sand, or equivalent material, and an LDS comprised of clean gravel, geonet, or equivalent material. Simply stated, the state-of-the-art system is a double composite liner system with an LCS whose primary design consideration is to limit hydraulic heads and an LDS whose primary design consideration is the highest possible velocity.

4.3 Testing Requirements

It is critical that both field and laboratory testing be conducted with the best equipment and by highly qualified technicians.

Field testing currently refers primarily to testing of seams for continuity, i.e., the presence, but not the strength of the seam. Although it would be desirable to test seams in the field for both continuity and integrity (strength), current field testing equipment is only capable of determining continuity. Perhaps the most promising state-of-the-art development in this regard is ultrasonic seam testing. Currently, ultrasonic testing equipment is hampered by high operator skill requirements, rapid operator fatigue, lack of automated visual/audible flaw detection signals, lack of automatic documentation of flaws, and an insufficient data base to accurately define and classify flaws. None of these drawbacks appears to be insurmountable, and one may expect practical ultrasonic seam testing equipment to appear on the market in the future.

Laboratory testing must include seam strength testing (peel and shear), conformance testing of all materials to ensure conformance with specifications, and chemical compatibility testing of all materials. Naturally, all of these

must be performed by independent laboratories. Seam strength testing is well established and the state-of-the-art equipment includes computer interfaces to produce automated results and thereby minimize operator error. Conformance testing is equally well established, but those responsible for selecting laboratories should ensure that the laboratory is qualified and experienced in the specific testing methods associated with geosynthetics. Chemical compatibility testing procedures are well documented in EPA method 9090; however, many knowledgeable laboratory scientists and engineers agree that method 9090 should be extensively revised in light of data and experience acquired since its publication.

4.4 Quality Assurance

QA methods and procedures have greatly improved and have become well accepted in the past year or so. A number of EPA publications [3,4] as well as technical papers [1,2] have addressed the issue in considerable detail. As a consequence, the time is clearly opportune to move on to the next step - second generation quality assurance. This next step should address the following three areas:

- QA personnel training and qualifications;
- documentation of QA activities; and
- extension of QA to non-construction aspects of the lining system, i.e., design, manufacturing, fabrication, post-construction operations, and post closure.

Currently, many (if not most) QA personnel are either relatively inexperienced regarding geosynthetics or relatively inexperienced regarding other lining system components. Both situations are dangerous and could be addressed by requiring certification of QA personnel. As a beginning, such certification could be based on a combination of experience, education and on-the-job training in addition to completion of approved training courses in the procedures, techniques, and documentation associated with both lining system construction and quality assurance.

Recognizing that detailed and comprehensive documentation are the heart of quality assurance, QA contractors should be required to develop standard logs and forms which document all facets of the installation and which are included as appendices to the quality assurance final report. The final report itself should be very detailed and include:

- a description of the scope and activities of the QA effort;
- a discussion of any problems and non-conformances;
- all logs, forms, and reports completed by QA personnel; and
- detailed record drawings to include all panel dimensions in each layer of the system, locations of flaws and repairs, and required cross sections and details.

In accordance with state laws, all QA activities must be conducted under the auspices of a registered professional engineer. Similarly, the final report, certification, and record drawings should be signed and sealed by a registered professional engineer.

Finally, and perhaps most importantly, QA should be extended to non-construction related activities. QA should begin at the beginning - with the design. This is especially critical in light of the lack of experience of many designers. It is understandable that designers are reluctant to share their hard-earned expertise with potential competition; nonetheless, we must arrive at a compromise which will ensure BAT designs. One strong possibility for such a compromise is for regulatory agencies to act as design reviewers. Note that design review implies detailed engineering expertise and efforts, and not simply a cursory checklist for completeness. Recognizing that many regulatory agencies at the state and federal levels do not have the time, expertise, or personnel availability to conduct design reviews, the design reviews could be contracted out to qualified engineering firms. Such a procedure would have the dual advantages of providing funding (by the agency) for the design review, and providing for regulatory agency approval of reviewing firms, thus ensuring that reviewers are both competent and qualified. Another benefit of this approach is that these same approved firms could be used to review final QA reports prior to agency issuance of a permit to operate. Currently, these final reports, however good or bad, are only minimally reviewed by agencies.

QA should also include a review of manufacturer methods and quality control, as well as on site monitoring of all fabrication. The activities are thoroughly described in [1].

QA should also extend through the post-construction landfill operation period, and even into post-closure in some cases. In cases where chemical compatibility is in doubt, samples (coupons) of all materials used in the lining system may be continuously immersed in leachate collected from the containment unit, and these samples can be periodically tested by an independent laboratory for deterioration. In this way, the owner/operator will receive advance warning of potential problems and will be able to react accordingly to prevent damage to the environment. Similarly, flow rates in leachate collection and leak detection systems can be monitored to determine the level of exposure to leachate of the various materials in the lining system, as well as to identify the time and possibly the approximate location of breaches in the top liner. QA personnel can also be used to conduct periodic site visits to ensure compliance with permitted operating procedures.

All of these QA activities are of course very expensive, and the cost must be borne by someone. The cost of QA was described in considerable detail by Giroud and Fluet [1]. That paper concluded that the vast majority of the cost was in construction quality assurance, and that the other QA costs were small in comparison. As a consequence, no matter whether the increased cost of increasing the scope of QA beyond construction is borne by the owner/operator, or by the regulatory agency, the cost is small in comparison to the benefits received. The following table shows the order of magnitude of funds which should be budgeted for QA of lining systems.

Table A: Cost of Quality Assurance

<u>Phase</u>	<u>Percent of Cost of Installed Lining System</u>
Design	1 - 3
Manufacturing	1 - 2
Fabrication	1 - 3
Lining System Construction	20 - 30
Final Report Review	1 - 2
Operations	< 1 per year
Closure System Construction	5 - 10
Post Closure	< 1 per year

The cost percentages shown are for complete (100%) QA documentation. The actual cost percentage for a particular site will depend on the degree of QA desired (partial or full), the size of the project, the quality of the design and the construction work, site-specific conditions, and problems encountered.

4.5 Geosynthetic Soil Reinforcement

One state-of-the-art concept which has recently gained increasing acceptance in the design of both MSW and hazardous waste landfills is geosynthetic soil reinforcement. Geogrids and/or high modulus geotextiles provide a means of stabilizing cover soils which are placed above geosynthetic lining systems; i.e., without the geosynthetic reinforcement, the cover soil would slide off the underlying geosynthetic (mostly because of the low coefficient of friction of some geomembranes). Another application of geosynthetic reinforcement is the use of geogrids or high modulus geotextiles to minimize the effects of differential settlement of subgrades. This concept is especially useful when designing new lining systems to be constructed over the slopes of existing landfills, as well as when designing cover systems over landfills and impoundments.

4.6 Future Developments

This paper would not be complete without some acknowledgement that major changes in the concepts, materials, and techniques associated with waste disposal lining systems are almost certain to occur as a result of research and development efforts which are currently under way. Triple liner systems, pressurized systems, reverse gradient systems, and other notions not even yet conceived are likely to dot the landscape in the not too distant future.

5. ACKNOWLEDGEMENTS

No paper on geosynthetic lining systems could be written without significant reliance on the extensive pioneering work conducted by Dr. J.P. Giroud, and the author is especially indebted to him for his support and guidance. The author also wishes to thank Dr. J.F. Beech and Ms. C.A. Pearce for their help in reviewing this paper, and Mrs. Grace Saunders for typing the manuscript.

6. REFERENCES

1. Giroud, J.P., and Fluet, J.E., Jr., "Quality Assurance of Geosynthetic Lining Systems", Geotextiles and Geomembranes, 3(4), (1986) 249-287.
2. Fluet, J.E., Jr., "Geosynthetic Lining Systems: Installation and Quality Assurance", Proceedings of the National Liner/Leachate Conference, St. Louis, (1986) 40-49.
3. "Minimum Technology Guidance on Double Liner Systems for Landfills and Surface Impoundments--Design, Construction and Operation", U.S. Environmental Protection Agency, Washington, DC, (1985) 71 pp.
4. "Construction Quality Assurance for Hazardous Waste Land Disposal Facilities", U.S. Environmental Protection Agency 530-SW-86-031, Washington, DC, (1986) 88 pp.
5. Giroud, J.P., "Impermeability: The Myth and a Rational Approach", Proceedings of the International Conference on Geomembranes, Denver, 1 (1984) 157-162.
6. Buranek, D., and Pacey, J., "Geomembrane-Soil Composite Lining Systems Design, Construction Problems, and Solutions", Proceedings of the Geosynthetics '87 Conference, New Orleans, (1987).

SESSION 5B

MATERIAL SELECTION

TIMBLIN, L.O., Jr.
Bureau of Reclamation, U.S.A.

Selection of Geosynthetic Materials for Canal Liner

Proper selection of geosynthetics for canals involves many factors relating to the purpose, design, construction, operation, and costs of the canal. This paper concentrates on major canals and laterals for conveyance of water for irrigation, municipal, and industrial users.

PURPOSE OF A CANAL

The purpose of a water supply canal is to convey the water from one point to another in a cost effective, environmentally acceptable manner. Water is a nonhazardous, nontoxic substance, universally accepted as essential for life and supporting a desirable lifestyle. To do this, it must be available in large quantities at comparatively low cost. As such, the considerations are different when transporting potable water than for transporting, storage, or containment of other materials such as toxic wastes or expensive industrial fluids. Water supplies normally are to meet long-term needs so that long-term high level performance and easy maintenance are important considerations. In summary, the canal needs to be low cost, comparatively watertight, able to function for many years with minimum maintenance, and without impairing the water quality. These requirements all influence the selection of the lining system.

When a geomembrane canal-lining system is referred to in this paper, it will be a buried geomembrane lining system. For long canals with prospect of windblown sediment, some mechanical cleaning is normally expected. It has been considered infeasible to mechanically clean canals lined with an exposed geomembrane without mechanically damaging the lining. Limited field tests have supported this position. Therefore, the paper will emphasize buried geomembrane lining systems.

DESIGN AND CONSTRUCTION CONSIDERATIONS

The selection of the canal lining system and any geomembrane which is to be used is, overall, a design decision. This includes the specific design and construction factors as well as the associated considerations which have been given. The specific design and construction factors can include:

- Hydraulic design
- Climatic conditions
- Ground-water conditions
- Available earth materials for lining or geomembrane earth cover
- Special seepage conditions

Hydraulic design is one of the major factors in selection of a lining system. For a buried geomembrane canal lining system to function satisfactorily, the velocity must be high enough to prevent deposition of silt and low enough to avoid washing away the cover material (1). * Experience has shown that a velocity of 0.6 to 0.9 m/s (2 to 3 ft/s) is normally acceptable.

The velocity is determined by the slope of the canal, the roughness of the lining surface, and the shape of the canal cross section. To determine if a buried geomembrane lining system may be feasible, the following procedure may be used:

1. Determine from the project requirements the maximum discharge, Q, required
2. Determine the maximum and minimum slopes of the canal from the proposed canal profile
3. Find the preferred-design maximum velocity, V_m, for an earth-lined canal with a 2:1 side slope using figure 1
4. Find the preferred-design hydraulic radius for an earth-lined canal with maximum velocity and a 2:1 slope using figure 2
5. Using the maximum and minimum slopes of the canal from step 2, compute the maximum acceptable velocity for the preferred-design geometry for an earth-lined canal using Manning's equation:

$$V_c = \frac{(1.0)(r)^{2/3} (S)^{1/2}}{n} \quad (V_c = \frac{(1.49)(r)^{2/3} (S)^{1/2}}{n})$$

where V_c = computed velocity in m/s (ft/s)
 S = slope of energy gradient in m/m (ft/ft)
 r = hydraulic radius in m (ft) (step 4)
 n = coefficient of roughness 0.0225

If $2 < V_c \leq V_m$, the flow in the canal would probably be acceptable, and further design could be initiated.

If $V_c > V_m$, the velocity would be too large and the cover material would not be stable and probably would wash away.

If a different cross section were attempted to reduce the velocity, a shallow, wide canal would be required which would result in higher rights-of-way, excavation, geomembrane materials and cover, and construction costs. For buried geomembrane lining, a different canal profile with smaller canal slope could be investigated. Otherwise, a hard surface lining such as concrete would be required.

Climatic and ground-water conditions can make the use of geomembrane linings more feasible than concrete linings. If the summer/winter temperatures involve severe fluctuations between warm and very low temperatures, frost heave forces will develop which cause serious cracking and slab displacement of concrete canal lining. An earth lining or geomembrane lining will function much more satisfactorily under these conditions.

Climatic factors can also seriously influence requirements for extreme temperatures during construction. Often construction in northern latitudes involves low temperatures. This may require special requirements in materials specifications. This was recognized in the large geomembrane lining project in Canada (2). After much study, a specification was prepared for cold-temperated PVC.

* References are listed at the end of this paper.

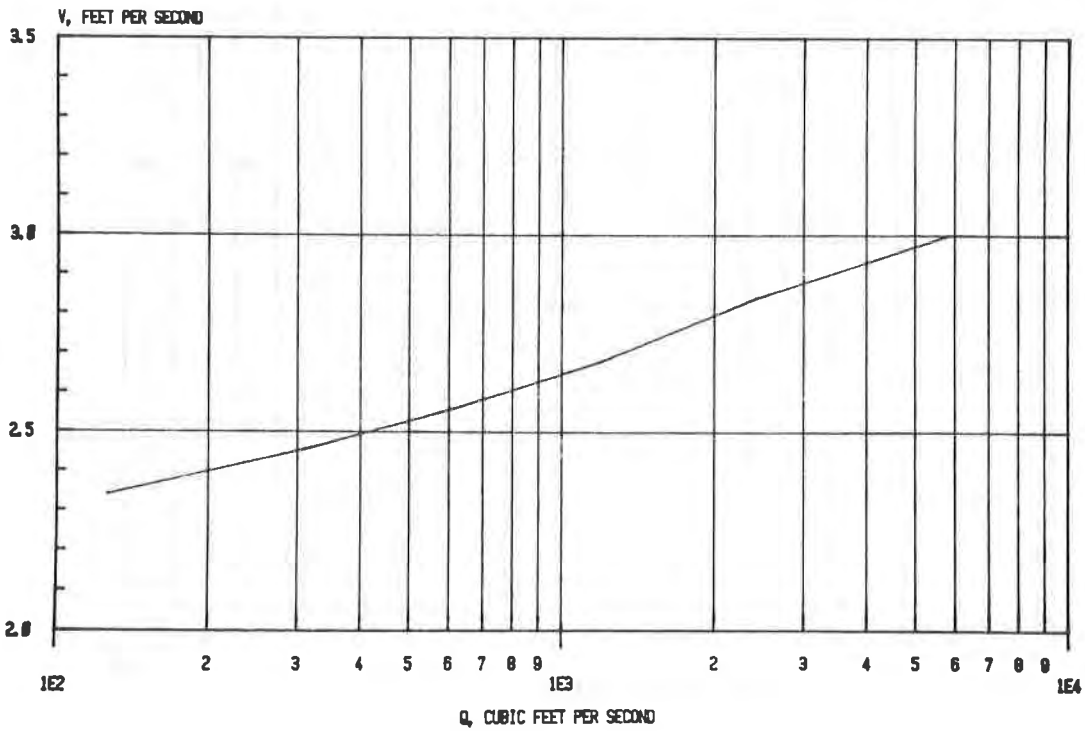
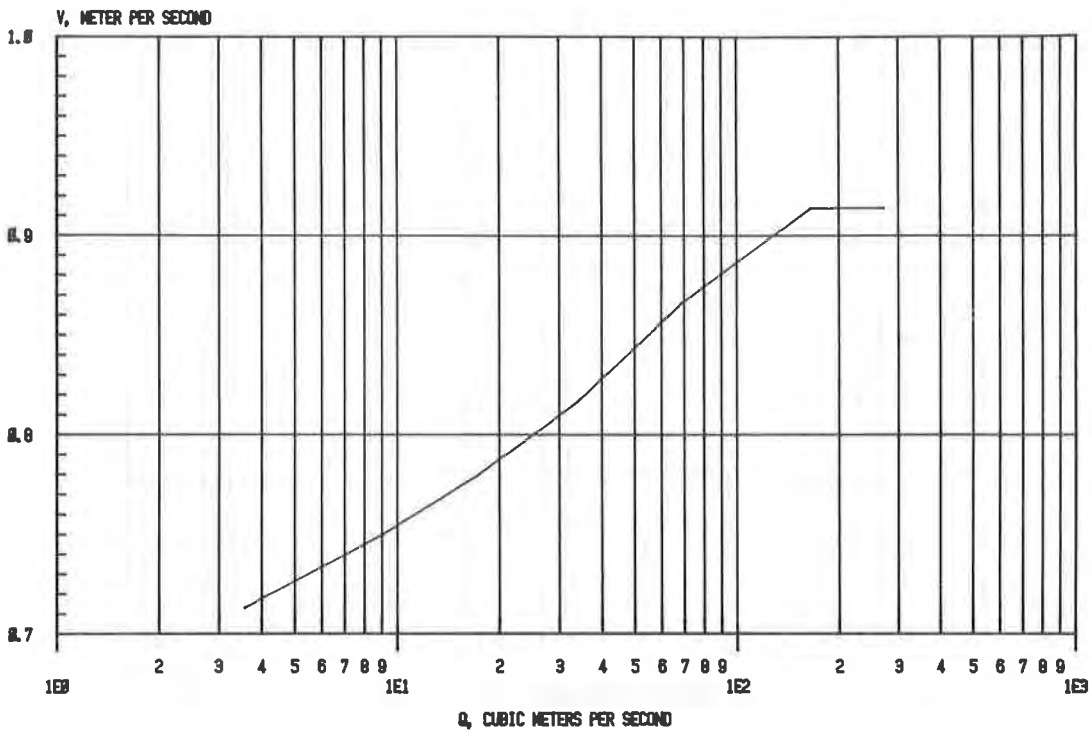


Figure 1. - Buried geomembrane canal lining system
Preferred design - maximum velocity

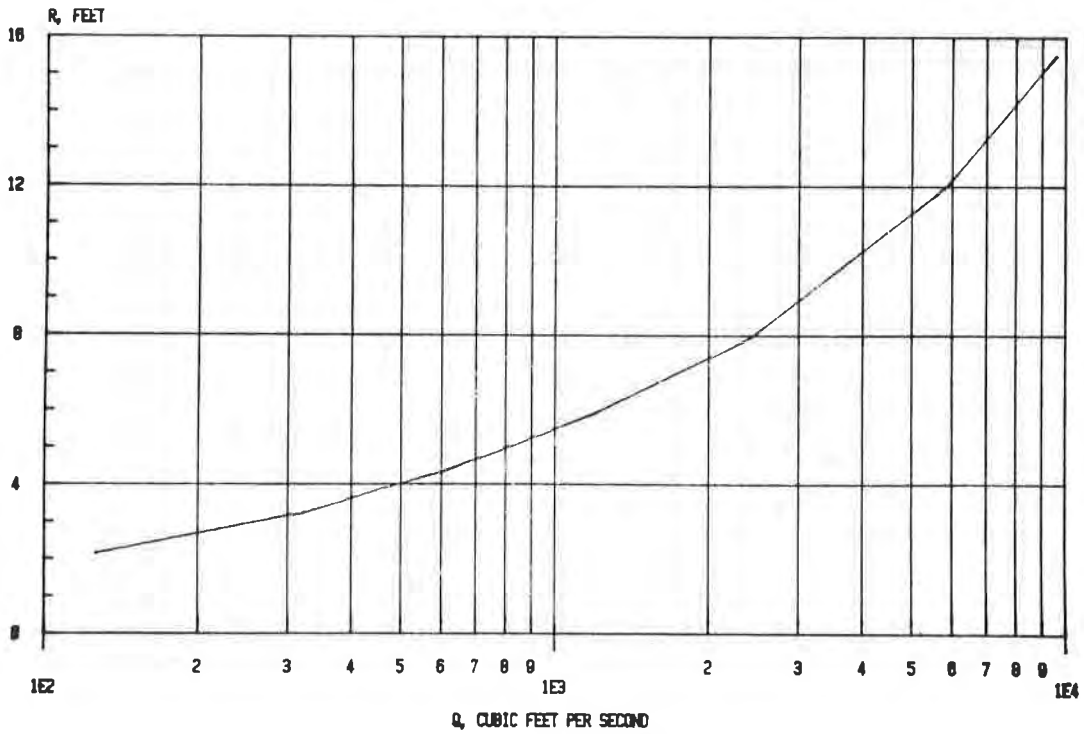
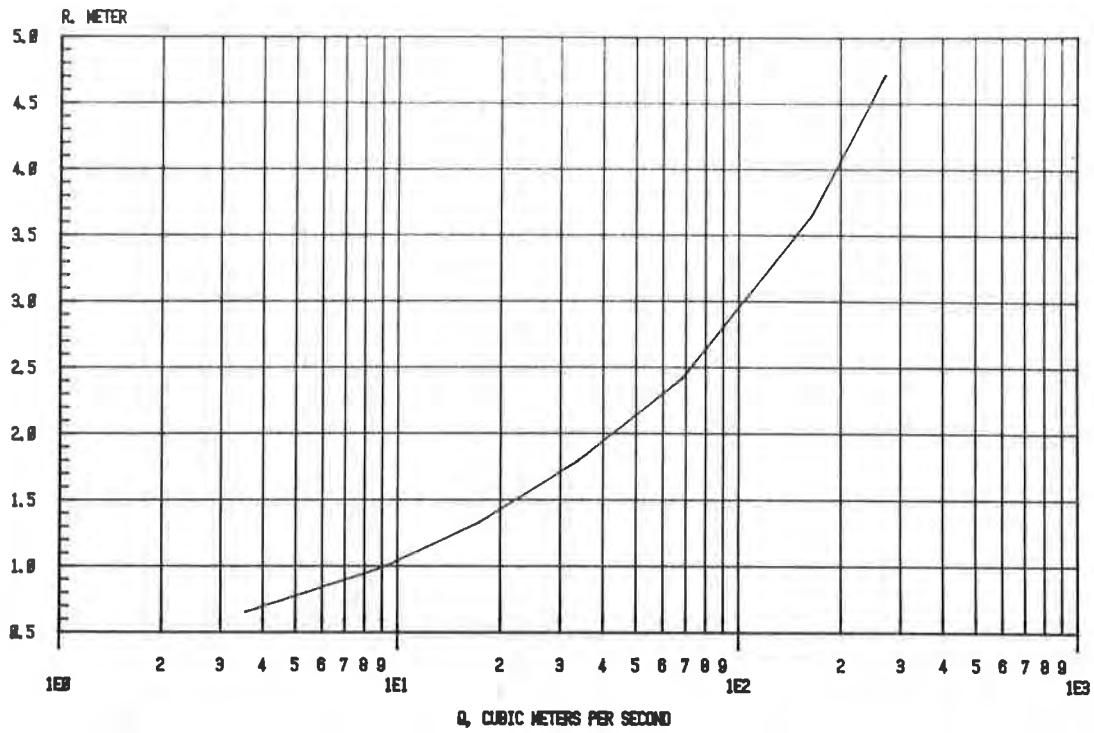


Figure 2. - Buried geomembrane canal lining system
Preferred design - hydraulic radius

Similarly, projects which involve construction in abnormally high temperatures will require attention both to the specifications for the geomembrane materials and the cover material. The cover material should not be open gravel which provides for free air movement to the geomembrane when the canal is dewatered. Such a situation promotes accelerated deterioration from heat aging (3).

The availability of earth materials suitable for a watertight earth lining will determine if this type of lining is economically feasible. A buried geomembrane lining system can be considered when cover materials of the appropriate gradation are available. An earth cover must be provided to protect the geomembrane lining from exposure to the elements and from injury by turbulent water, stock, plant growth, and maintenance equipment. The depth of cover depends on cover material, size of canal, water velocity, and canal side slopes. The minimum recommended total cover depth is 250 mm (10 in) plus 25 mm (1 in) for each 0.3 m (1 ft) of water depth.

To minimize costs, approved excavated material should be used for one-half the cover requirement. The upper layer should be a sand and gravel cover material conforming to the gradation limits shown on figure 3. If possible, the sand and gravel material should be obtained from an approved borrow area. The requirement of a sand and gravel layer for erosion protection is a major cost item in buried membrane lining construction. Using material that requires no blending lowers this cost. Larger gravel is generally required at the beach belt in larger canals for protection against wave action.

In some special situations, soil conditions are such that seepage is primarily vertical. Under such conditions, a bottom-only lining may be attractive. Since a completely watertight canal is not necessary, the small amount of seepage from the side slopes can be tolerated if the cost advantages are sufficient. Soil conditions which exhibit this seepage pattern are found in the loessal soils in some areas of Kansas and Nebraska. Field studies of such a lining were performed with the following results (4):

	Canal size		Seepage loss ft^3/ft^2 day		Percent reduction
	Q (ft^3)	b (ft)	Before lining	After lining	
Farwell Main Canal	290	18	.56	.27	52
Franklin Canal	230	14	1.01	.45	55
Upper Meeker Canal	284	16	1.13	.56	50

Cost considerations can impact in several ways the selection of geomembranes for canal lining systems and whether or not a geomembrane system is to be used. Obviously, the cost of the geomembrane material is an important consideration. Because of the rather modest engineering requirements and benign service conditions, higher priced materials such as reinforced geomembranes, heavy gauge HDPE, or specialty materials are usually not cost effective when compared to such materials as PVC and LDPE. Often the canal passes through high cost land. Since concrete-lined canals can be constructed with steeper side slopes and a smaller cross section than buried geomembrane-lined canals, the cost of rights-of-way makes concrete the more cost effective choice. The smaller cross section of a concrete-lined canal also makes it more cost effective if the canal passes through material difficult to excavate. Should suitable material for cover have to be hauled long distances or require extensive processing, the cost may be too high for a buried geomembrane lining to compete with concrete.

A buried geomembrane lining system is frequently selected for rehabilitation and betterment of existing canals when an existing earth-lined canal is found to have excessive seepage. Low cost lining with a geomembrane is a good method achieving water conservation and reducing high ground-water conditions in the surrounding land (5, 6). The engineering, design, construction, and cost considerations of a new canal should be reviewed for such a project. An important consideration is that often a canal is dewatered after the irrigation season. This involves construction during cold weather--a situation not often suitable for concrete lining. For small sections, a buried geomembrane lining can be constructed more economically than a concrete lining. This is because the competitive costs of a concrete-lined canal are related to the large mechanized paving equipment.

SERVICE CONSIDERATIONS

The purpose of the canal and expected operating and maintenance conditions can have an influence on materials which are selected. If the canal is to deliver potable water for municipal use, the lining system cannot introduce toxic substances. This may rule out the use of some geomembrane materials which could perform very well in industrial or toxic waste control situations. This is because the materials may leach small quantities of substances unacceptable in potable waters.

The water may be intended for agricultural crops especially sensitive to herbicides. In such situations, the introduction of aquatic weed problems and their control may have an impact on the lining system selected for the canal. In some areas, especially warmer climates where year-round irrigation is practiced, aquatic weed growths develop with such vigor that if left uncontrolled, the canal will cease to function. Aquatic weed control practices fall into four categories: mechanical, chemical, biological, and integrated. Mechanical includes underwater mowing, chaining, and removal by mechanical bucket. Chemical control involves the use of various herbicide. Herbivorous fish have recently shown to be a very effective biological control method but is not yet widely used. Further studies and approvals are needed before the method becomes commonplace. Integrated weed control includes all of these together with some environment manipulation like dewatering the canal.

With herbicide-sensitive crops and/or a water user organization aversion to use of chemicals, mechanical control is commonplace. If this situation exists, the lining system must be able to have frequent mechanical weed control operations performed without noticeable damage. Exposed geomembrane linings may inhibit the growth of weeds. However, windblown soil can result in sufficient sediment to begin a growth of an aquatic plant. Once this begins, the growth will expand as silt normally kept in suspension will deposit and encourage further growth. The end result is that the plants and soil must be removed mechanically or the weeds controlled. Mechanical cleaning poses serious hazards to exposed geomembranes.

The soil cover in a buried geomembrane lining, if properly constructed, can satisfactorily sustain carefully performed mechanical cleaning. However, the operation and maintenance staff must be aware that a proper thickness of cover must be maintained.

With the development of the use of herbivorous fish for aquatic weed control, the use of geomembranes for canal lining will be extended (7).

MATERIALS CONSIDERATIONS

After a selection of a buried geomembrane lining system has been made, the choice of alternative materials and their specifications and testing becomes an important engineering task.

The materials selected should have several important attributes:

- Durability. - The material should have the chemical and physical attributes to be able to sustain after installation the installed conditions and be able to function as a watertight membrane.
- Mechanical strength. - The geomembrane must have sufficient strength to be able to be installed without damage and to sustain the service conditions.
- Installability. - This includes availability of fabricated sizes large enough to be installed economically.
- Repairability. - Occasional installation and operation and maintenance accidents will occur causing holes and tears. Some successful measures of repair must be available. These factors are all involved in preparing materials specifications.

One of the most frequently raised issues by engineers and water users not familiar with geomembranes is durability. This involves several aspects of deterioration. Storage on the jobsite could produce ultraviolet damage even for geomembranes to be buried, if not adequately formulated. Some materials, if not properly compounded, could lose mechanical properties by water or soil leaching soluble constituents or heat aging during storage or in service. Bacterial accelerated deterioration is a potential for some materials in contact with the soil.

Mechanical strength of a geomembrane needs to be sufficient to permit installation without damage. The specific properties and values of these properties have not been determined by engineering analysis. Studies are being performed to compare materials. This is especially useful in comparing new materials with those known to be successful as a canal lining. However, years of experience have contributed to selection of important properties and defining their values. This includes properties such as tensile strength, elongation, and tear strength.

Installation requirements are based upon good construction practice which avoids unnecessary operations which could obviously damage the geomembrane. The service requirements have more limited demands on the mechanical properties of the geomembrane than installation. A canal should be carefully designed and constructed so that the subgrade is well consolidated. The prospects of major soil displacement, cavities, and sharp protrusions are engineered against. Thus, the requirement for material of special elastic properties is not necessary, and materials of a range of elasticity modulus and strength can perform satisfactorily (8).

The specifications matter is complicated by the fact that minimum mechanical properties adequate for installation and service as a canal lining may or may not assure obtaining a specific type material of satisfactory quality.

Factory seams represent a critical part of a geomembrane lining. They must have good mechanical, watertight, and durability qualities as does the geomembrane. Otherwise, the integrity of the lining will not be adequate (9).

Installability of the geomembrane goes beyond a material strong enough to permit reasonable installation. The material should be available in a single sheet or a fabricated blanket large enough to avoid excessive field seams. As a guideline,

the blankets should be wide enough to cover the complete perimeter of the canal and several hundred feet in length to minimize field seams. For most rehabilitation work, sheets of the PVC lining can be joined simply by lapping the downstream end of one sheet 1 m (3 ft) over the upstream end of the adjacent sheet. The PVC has a tendency of adhering to itself and, with the weight of the protective soil cover, a sufficiently bonded joint is obtained where 100 percent seepage control is not required. Where a more positive seal is required, the PVC should be overlapped a minimum of 0.3 m (1 ft) and a solvent cement (recommended by the manufacturer) applied to a minimum width of 50 mm (2 in). The seam is then hand rolled to complete the seal.

MATERIALS SPECIFICATIONS

Once a decision has been made to use a buried membrane lining, a materials specification is required for purchase of suitable material. A QC/QA (quality control and quality assurance) program is needed to ensure that the specified material is delivered to the jobsite.

Selection of which materials to specify involves knowledge of both the required properties and the properties and probable costs of available materials. Here, experience is an important factor. It has been found in several countries that PVC and LDPE have been acceptable and cost competitive for canal lining (3, 10, 11, 12). Other materials have been proposed and found to perform satisfactorily, but the costs are usually not competitive with compacted earth lining or PVC and LDPE (3).

Specifications for a satisfactory geomembrane is a combination of the properties experience shown to be required in order to perform satisfactory, and characterized properties which have been found necessary to adequately define and describe a quality material of required durability and adequate strength. In a consensus standard effort, the specifications for a number of materials was prepared and is available as NSF (National Sanitation Foundation) Standard No. 54 (13). Other materials standards have been proposed: ICID (International Commission on Irrigation and Drainage) Guidelines 108 (14); ASAE (American Society of Agricultural Engineers) Engineering Practice 340.2 (15); and SCS (Soil Conservation Service) Practice 428-B (16). Presently the Bureau of Reclamation is using the specifications conforming to table 1 of NSF Standard No. 54.

For extreme high or low temperatures, these specifications can be adjusted. The specification used by the Alberta Environment in Canada, is an example of a low-temperated PVC material.

QUALITY CONTROL/QUALITY ASSURANCE

It is essential that a QC/QA program be followed to assure that the specified material is used in the fabricated blankets and that the factory seams are proper. A QA/QC program is used by the Bureau of Reclamation. The Contractor has the option of furnishing PVC lining under one of two quality assurance programs. The PVC lining shall not be fabricated until the roll goods have been tested and approved by the Government.

Under quality assurance program No. 1, the Contractor submits certified test reports for approval for each day's production of roll goods to be used in fabricating the PVC lining. The certified test reports shall include results of key physical properties tests. A test sample [roll width by 0.3 m (1 ft) in length] from each roll

is also submitted for approval. The samples and certified test reports are submitted on a daily basis. The Contractor must provide qualified third party verification that the PVC formulation meets the resistance to soil burial requirements. Only roll goods meeting the physical property requirements are approved for use in fabricating the lining. Factory fabrication is subject to inspection by the Government at any time for compliance to these specifications. The Contractor submits certified test reports for approval for each day's fabrication process for the lining panels. The Government reserves the right to obtain samples of the factory seams for testing and approval in accordance with these specifications. Only fabricated PVC lining panels meeting the factory seam specification requirements are approved for installation.

Under quality assurance program No. 2., the Contractor provides a certification stating that the PVC lining roll goods proposed to be used in fabricating the lining are listed by NSF and meet the minimum physical property requirements of table 1 of NSF Standard No. 54. The Government reserves the right to obtain samples of the roll goods for testing and approval in accordance with these specifications. Roll goods meeting the physical property requirements of table 1 of NSF Standard No. 54 are approved for use in fabricating the PVC lining. The Contractor shall provide a certified test report for approval for each fabricated PVC lining panel showing that the factory seams meet the minimum requirements of table 1 of NSF Standard No. 54. The Government reserves the right to obtain samples of the factory seams for testing and approval in accordance with these specifications. Fabricated PVC lining panels meeting the factory seam requirements of table 1 of NSF Standard No. 54 are approved for installation.

FUTURE DEVELOPMENTS

Future developments are being made in both the engineering and materials field. Construction procedures with mechanized equipment are being developed and used for final trimming of the canal prism, laying the geomembrane, and placing the soil cover (17).

Combination of concrete and geomembranes have many attractive advantages. The concrete provides excellent protection for the geomembrane placed underneath. The geomembrane gives good overall seepage control, taking care of any random cracking of the concrete. Successful economic placement of the concrete over a geomembrane involves good placement of these two elements plus a material between them to prevent slippage of the concrete on the geomembrane and adequate moisture drainage between the two. Some work is now being done in the Middle East using this technique (3). Consideration is now being given by the Bureau of Reclamation of placing a concrete/geomembrane lining in an existing canal without dewatering. This could have important application for relining existing canals in warm climates, especially where municipal and industrial water is involved.

The geomembrane industry is now working on polymer alloys which could produce materials of good properties at competitive costs; alloys of HDPE, CPE, and very low density PE are some of the more promising materials. Texturizing the surface, geomembrane/geotextile composites, and geomembrane/geogrid composites which will minimize cover slippage are important developments now in progress.

The use of geomembranes as canal linings has been growing since their first use 18 years ago for limited rehabilitation purposes. They now are fully established as a good alternative for lining water conveyance canals.

REFERENCES

- (1) Design Standard 3, Canals and Related Structures, U.S. Bureau of Reclamation, Denver, Colorado, December 8, 1967.
- (2) Weimer, P., The Development of Large Scale Irrigation Canal Seepage Control Within Alberta Environment, Alberta Environment, Water Resources Management Services, Edmonton, Alberta, Canada, April 1984.
- (3) Hawkins, Gordon, "Development and Use of Membrane Linings for Canal Construction World Wide," Proceedings International Conference of Geomembranes, Denver, Colorado, Industrial Fabrics Association International, St. Paul, Minnesota, 1984.
- (4) "Special Membrane Canal Lining, Farwell Main and Lower Main Canals," prepared by the Bureau of Reclamation's Nebraska-Kansas Projects Office in cooperation with Loup Basin Reclamation District, November 1982.
- (5) Morrison, W. R. and J. G. Starbuck, "Performance of Plastic Canal Linings," REC-ERC-84-1, U.S. Bureau of Reclamation, January 1984.
- (6) Wilkerson, R. W., "Plastic Lining on the Riverton Project," ASCE Irrigation and Drainage Specialty Conference, Flagstaff, Arizona, July 1984.
- (7) Thullen, J. S. and F. L. Nibling, "Aquatic Weed Control with Grass Carp: Effectiveness in a Cool Water Irrigation Canal" Proceedings Environmental Quality and Ecosystem Stability, Bar Ilan University Press, Ramat-Gan, Israel, 1986.
- (8) Steffen, Heinz, "Report on Two Dimensional Strain Stress Behavior of Geomembranes With and Without Friction"; Proceedings International Conference on Geomembranes, Denver, Colorado, Industrial Fabrics Association International, St. Paul, Minnesota, 1984.
- (9) Frobel, Ronald K., "Methods of Constructing and Evaluating Geomembrane Seams," Proceedings International Conference on Geomembranes, Denver, Colorado, Industrial Fabrics Association International, St. Paul, Minnesota, 1984.
- (10) Staff, Charles E., "The Foundation and Growth of the Geomembrane Industry in the United States," Proceedings International Conference of Geomembranes, Denver, Colorado, Industrial Fabrics Association International, St. Paul, Minnesota, 1984.
- (11) Use of Plastics for Lining of Water Conveyance Systems - State-of-the-Art Report, Ministry of Irrigation, Central Water Commission, Government of India, March 1984.
- (12) "Laboratory and Field Studies in Plastic Films," Interim Report, Volume III, US/USSR Joint Studies on Plastic Films and Soil Stabilizers, U.S. Bureau of Reclamation, Denver, Colorado, December 18, 1982.
- (13) Standard No. 54, Flexible Membrane Liners, National Sanitation Foundation, Ann Arbor, Michigan, November 1985.

- (14) ICID Guideline 108, Use of Flexible Membranes for Irrigation Canal and Reservoir, Draft, July 1983.
- (15) ASAE Engineering Practice: ASAE Engineering Practice 340.2, Installation of Flexible Membrane Linings, Revised March 1986.
- (16) SCS Practice 428-B, Flexible Membrane Ditch and Canal Lining, October 1980.
- (17) Morrison, William R., "Progress Report on the Plastic Lining Construction for the Closed Basin Channel, San Luis Project, Colorado," Proceedings, Geotechnical Fabrics Conference '85, Industrial Fabrics Association International, St. Paul, Minnesota, 1984.

PFALSER, I.L.

Phillips Petroleum Co., U.S.A.

High Density Polyethylene Liners: A Users Experience

INTRODUCTION

The best guide to good engineering design and construction is experience. When new materials come on the market, the customer must rely on the manufacturers claims and test results. It is unfortunate that many times these claims are misleading due to the manufacturers eagerness to sell his products and services based on insufficient testing or experience.

In the case of high density polyethylene (HDPE), those involved in design and installation need not cope with inexperience with the material or its usage. HDPE has been around for a long time, and its use and applications are well known throughout the world. Even its use as a liner material is far from new.

The basic problem associated with HDPE liner systems is not the material, but improper installation and inspection. The blame can be directed to the installation contractor's poor workmanship practices, and the customer's inability to recognize an unacceptable job. This can only be controlled by use of a comprehensive set of construction specifications and rigid inspection by the customer. This paper presents our experiences with HDPE liner installations and is intended to increase awareness of potential installation problems.

EARLY LINER EXPERIENCE

Our experience with pond liners dates back to the very early 1960's. Since that time we have run the gamut of butyl rubber, polyvinyl chloride, asphalt plank, polyethylene, Hypalon, etc. All of these had various limitations. These materials vary in their vulnerability to ultraviolet light and petrochemical attack, as well as to long term climatic and operational conditions. Consequently, when the first state and federal environmental regulatory agencies' guidelines begin to take effect we were reluctant to specify liner materials for liquid waste ponds. We opted to specify 3 foot clay or bentonite amended soil liners, which appeared at the time to offer a service life appropriate to the intended pond usage.

Our first exposure with HDPE liner material was in 1978. We were invited to witness the installation of 100 mil liners in a waste containment facility in Tulsa, Oklahoma, and a few weeks later in a waste water pond in Bartlesville, Oklahoma. We were very impressed with the material as well as the installation workmanship.

As a manufacturer of HDPE resins, we were also interested in the liner material manufacturer as a prospective customer. An agreement was negotiated whereby we would supply the liner manufacturer a sufficient amount of our resin to enable the manufacturer to fabricate 100 mil sheet material for laboratory and a long term field testing. In 1979, the manufacturer lined a production field brine pond located in the Oklahoma City area with the test liner material. Field reports indicate that this liner is in good condition and has required no repairs to date.

By 1981, regulatory agency design guidelines had developed to the point that leak detection systems were required for certain types of liquid containment ponds. Our field operations required the construction of a 100,000 barrel brine containment pond in Gaines County, Texas. Based on our excellent experience with HDPE, we specified a HDPE primary liner, and a bentonite amended clay secondary liner system with a granular leak detection interbed system (see Figure 1).

Upon completion of the Gaines County brine pond the liner contractor started installation of a liner for a 175,000 barrel runoff storm water containment pond which was a part of a major expansion of our refinery located near Borger, Texas. This pond had been designed a nationally known design/construction management contractor had designed the storm water pond based on our Gaines County pond design. This design contractor also assisted in construction management and field inspection.

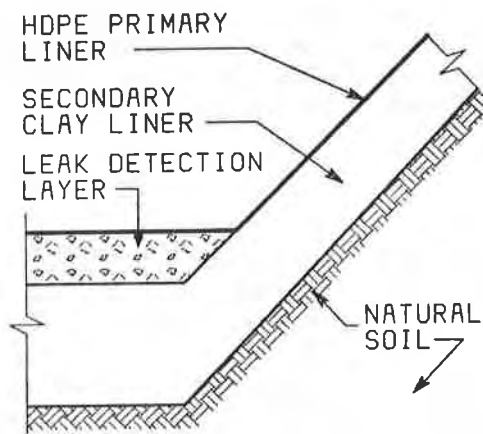


Figure 1. Single Synthetic Liner System

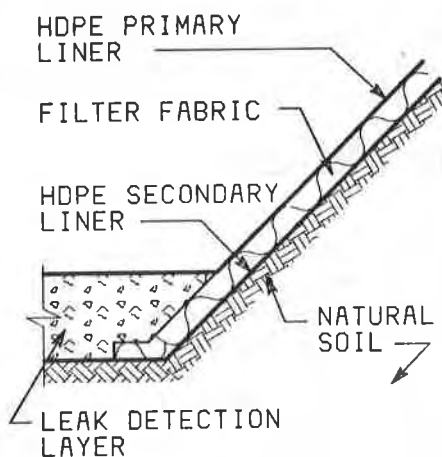


Figure 2. Double Synthetic Liner System

We subsequently designed a 3 million barrel brine containment pond installation for another Borger area facility. The design incorporated the use of a 100 mil HDPE primary liner, an 80 mil HDPE secondary liner, and a leak detection system (See Figure 2). We selected the same liner installation contractor for this project.

LINER PROBLEMS

In the fall of 1982, when the installation of the secondary liner of the 3 mm bbl. brine pond was started we received word from the Gaines County pond operators reported that there were severe problems with liner leakage, and Borger Refinery personnel reported excessive leakage flows from their storm water runoff containment pond. Installation of the secondary liner of the 3 million barrel brine pond was in progress at the time.

The liner installation contractor was immediately notified. A contingent of the contractor's quality control personnel and our engineers made a thorough inspection of all of the pond liners. The following describes the various problems that were discovered during these inspections:

- A. The lap seam fabrication method used by the liner contractor resulted in the weld bead being hidden from view, (see Figure 3) making inspection difficult.

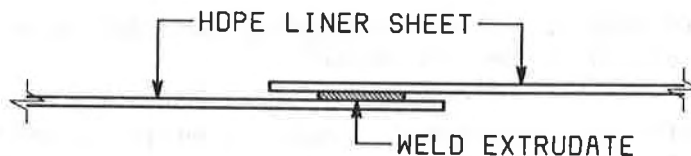


Figure 3. Lap Joint

Probing the weld bead by inserting a narrow bladed screw driver between the laps was somewhat effective. The inspection team determined that final judgment on welded seam integrity be based on peel tests of samples cut from the welded seams. It was agreed that a welded seam would be judged acceptable, provided the weld bead did not begin to peel before there was evidence of elongation or other deformation of the sheet material (See Figure 4).

The contractor had used fillet welds to reinforce and or repair the lap seams found to be inadequate during installation of the liner. The contractor's quality control people pointed out that surface sheen of the weld bead when compared to the surface sheen of the sheet material was a good indication of the degree of weld integrity.

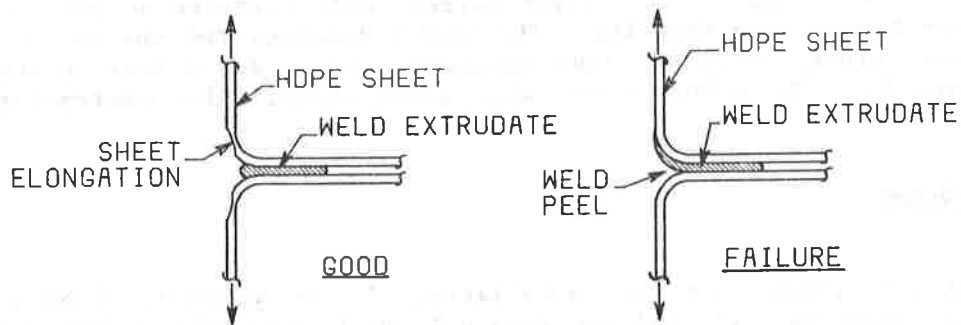


Figure 4. Weld Peel Testing

If the sheen of the weld bead was duller than the sheet material the extrudate was not hot enough when it was applied to form a good bond. If the sheen of the weld bead and the sheet material were about the same then the weld temperature was about correct, and a good weld could be expected. If the sheen of the weld bead was brighter than the sheet material then the extrudate was too hot when applied, resulting in a sheet material degradation. Peel tests were needed to verify the visual evaluations. In several cases, where the welding had overheated the sheet material. There was evidence of zipper type cracking of the sheet material adjacent to the weld. Similar sheet material failures were evident where excessive amounts of extrudate were used to form the fillet weld.

All agreed that weld seam integrity was the major problem and was directly related to the following:

1. Insufficient extrudate to produce a proper sized weld bead.
2. Insufficient extrudate temperature to assure a good bond.
3. Excessive extrudate temperature causing crystallization or weakening of the sheet material adjacent to the weld seam.
4. Excessive amounts of extrudate used to make fillet welds.

Two thirds or more of the peel tests conducted on weld samples removed from the Gaines County and 3 million barrel storm water ponds failed. An intensive study of the temperature of extrudate, sheet material and ambient air relationship would be required to develop reliable welding procedures.

- B. Prior to welding, the surfaces of the sheet material must be cleaned to remove any oxidation. This had been done by use of a hand held electric grinder. In several instances over grinding had occurred reducing the 100 mil liner sheet material thickness by over 50%. Scratch sizes indicated that the grinding wheel used was too

coarse. Removal of oxidation could have been achieved using a much finer grained grinding wheel.

- C. In the design of these ponds there was a concern with liner float-out since the specific gravity of HDPE is less than that of the contained liquid. Consequently, a layer of sand ballast was installed. Removal and clean up of the ballast prior to inspection and repair of the liners was time consuming and costly. To eliminate the need for ballast pumps were provided in the leak detection wells to maintain a lower hydrostatic liquid pressure in the leak detection system than in the pond, thereby preventing liner float-out.
- D. In addition to weld seam, leak sources included connections concrete inlet and outlet boxes, and other liner penetrations. It was evident that improved connection methods had to be designed and reinforcing pads installed around these openings to absorb stress buildup due to liner movement.
- E. During early operation of the Gaines County pond there were reports of fresh water seepage into the leak detection system. The inspection team found that the source was the liner anchor trench located at the top of the pond dikes. The liner seam welds did not extend past the turndown in the anchor trench, and the trench backfill had not been compacted (See Figure 5). Storm water had saturated the loose backfill and the excess water flowed in under the liner and down to the leak detection layer. In some areas, this water flow had severely eroded the soil dike surface. The uncompacted fill also created a problem for vehicle traffic on the top of the dike.

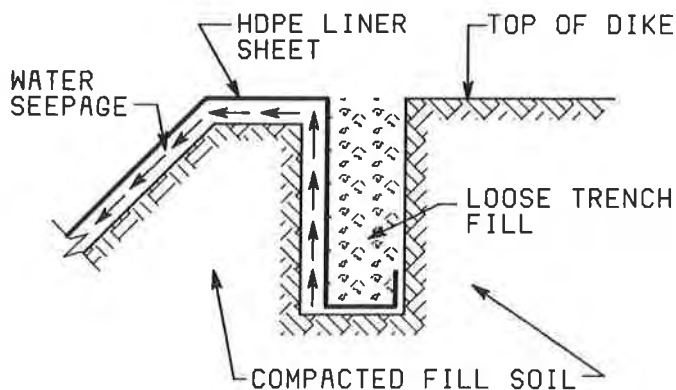


Figure 5. Liner Anchor Trench

- F. It was also found that some sheet material used in the Gaines County pond had thin spots and other manufacturing defects which were directly related to poor sheet manufacturing quality control.

The liner contractor volunteered to reweld all joints, overlay cracks, and replace all defective material at their expense. They also expressed a desire to collaborate with us in development of improved field installation quality control and testing procedures.

It is easy to point the finger of guilt at the material manufacture and installation contractor. However, to be fair, one must also look at his own short comings. We found the following:

1. We did not recognize the fact that over the ensuing time period since our first exposure to HDPE liner material, the manufacture and installation contractor had made major changes and additions to their personnel, and company operations procedures. Their previous strict adherence to field installation quality control had become lax.
2. We relied almost entirely on the contractor for material and field installation quality control.
3. Our field project engineers had no previous construction experience with any type of lined liquid containment pond facilities and therefore had little or no idea of the rights and wrongs of HDPE liner construction. In addition, our field project engineers spent the major portion of their time managing the construction of aspects of the overall project.

PROBLEM SOLVING

Using the 3mm bbl brine pond, which at the time had about 1/3 of its secondary liner in place, as a proving ground a joint effort to improve quality control and develop new installation methods was initiated.

- A. The contractor was using an ultra sonic conductivity type instrument to determine weld continuity and integrity in lap seams. The instrument was showing almost 100% integrity for every seam, even though there was visual evidence that this was not true. The screw driver probing test quickly revealed that the instrument was unreliable. Falling back on steel tank construction experiences we tried vacuum testing and found it to be very effective. The liner contractor began testing 100% of all the completed seam using standard, off the self, steel tank vacuum testing equipment (See Figure 6) we found over 150 failures in the previously tested seams.

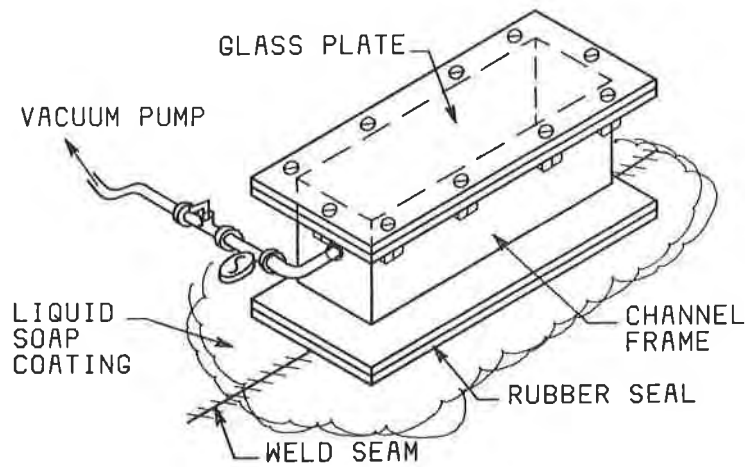


Figure 6. Vacuum Tester

To facilitate visual inspection for weld continuity the contractor was requested to begin placing the weld bead such that it was visible at the edge of the lap seam (See Figure 7).

In addition to 100% vacuum testing, the liner contractor cut one peel test sample from 150 foot of completed weld.

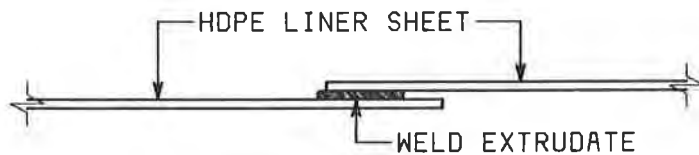


Figure 7. Lap Seam

- B. Plastics engineers from our Research Center contributed considerable welding and material expertise from their many years of research on the manufacturing and welding of HDPE pipe. They tested samples of the liner material to assure that it met our standards for material physical and chemical characteristics, and compounding make up. Due to national standards natural polyethylene resins are pretty much identical regardless of manufacturer. Resin compounders add various other materials to the natural polyethylene resins and coloring agents to give HDPE its reliable physical characteristics and color. We were concerned about the integrity of private resin compounding companies based on our experience in the industry, and consequently we required that the remainder of the liner material be produced using our own

compounded HDPE resin. Familiar material afforded us better control for weld test evaluation.

- C. We initiated welder and welding machine certification program was started. Certification tests were required at the start of each day after every 150 feet of seam welding, and when welding was interrupted for more than 30 minutes. The contractor began to monitor more closely the temperature controls on the welders, and the temperatures of the extrudite, the sheet material, and the ambient temperatures. A conservative allowable welding sheet temperature range of 55°F to 110°F was set and the rate of welding was also closely observed. This program produced reliable welds and there are indications that the allowable welding temperature range can be widened.
- D. Exposure to cold weather temperatures is the final and most severe test for weld seam integrity. HDPE has a high coefficient of thermal expansion, and this characteristic has always presented significant problems in its use. Unless sufficient slack is left in the liner material when it is installed severe stressing of the material can occur during cold weather. Inspections have been made of the pond liners each spring for seam or material failure. The first inspections revealed numerous failures weld seam that were repaired. The 1986 Spring inspection revealed only minor weld seam failures in one pond. There was some evidence elongation in the sheet material adjacent to the weld that displayed no distress. This would indicate that we are approaching maximum seam weld integrity through closer construction control and testing.

Small ponds are less vulnerable to cold weather seam failure problems than large ponds. This is to be expected because it is more difficult to uniformly distribute slack material over the long sides of the larger ponds to compensate for cold temperature contraction. In our first pond, we found tenting of the liner material at the toe of the dikes (See Figure 8) and at the corners when the ponds were empty. We now require the installer to leave sufficient slack to eliminate all tenting and additional slack based on the length of the pond side, thermal expansion of the liner material and anticipated temperature ranges.

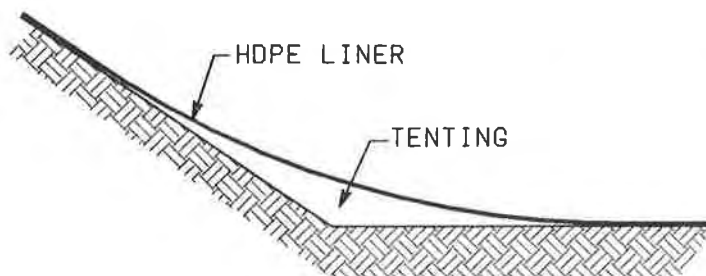


Figure 8. Tenting

To minimize the number of weld seams at the top of dikes exposed to temperature changes, we are considering placement of the top course of material circumferentially around the pond (See Figure 9).

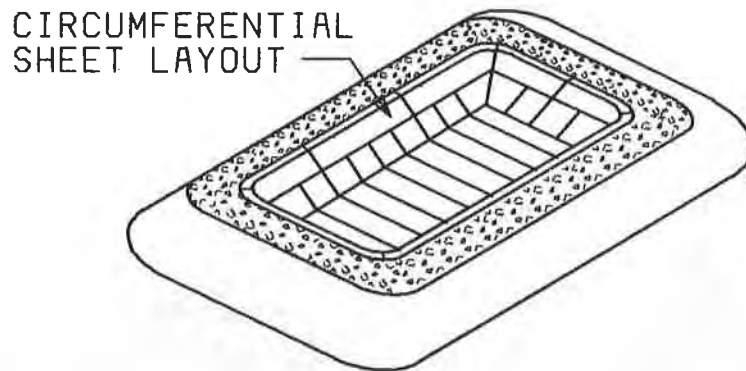


Figure 9. Pond Liner Sheet Layout

- E. As stated earlier there was also a problem with the anchor trench at the top of the dikes. Trench installations vary from those in which the liner material has doubled over with the end sticking out to those that were barely long enough to be embedded. The installation contractors prefer loose backfill in the trench so that as the liner begins to contract, it will relieve itself by slipping. However, if the top of the dike is to be used for inspection and maintenance of the leak detection monitoring well system, the backfill must be thoroughly compacted for trafficability. The compromise liner embedment is shown in Figure 10.

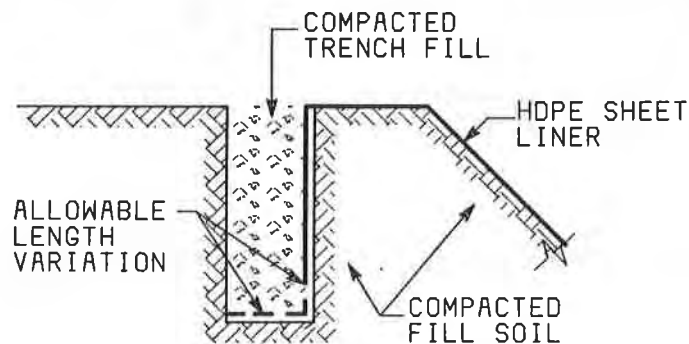


Figure 10. Liner Anchor Trench

F. We are still not satisfied with the present methods for sealing and attaching HDPE liner material to protrusions through the liner. Protrusions may range from concrete inlet/outlet structures to single pipes. We have used a number of methods as shown in Figure 11. In every case, one must carefully consider selection of metals, sealing materials or sealing compounds which are compatible with the liquids to be contained. To date we have not attributed any leakage problems to these connection. However, service time is still insufficient to make a positive evaluation of any of these systems.

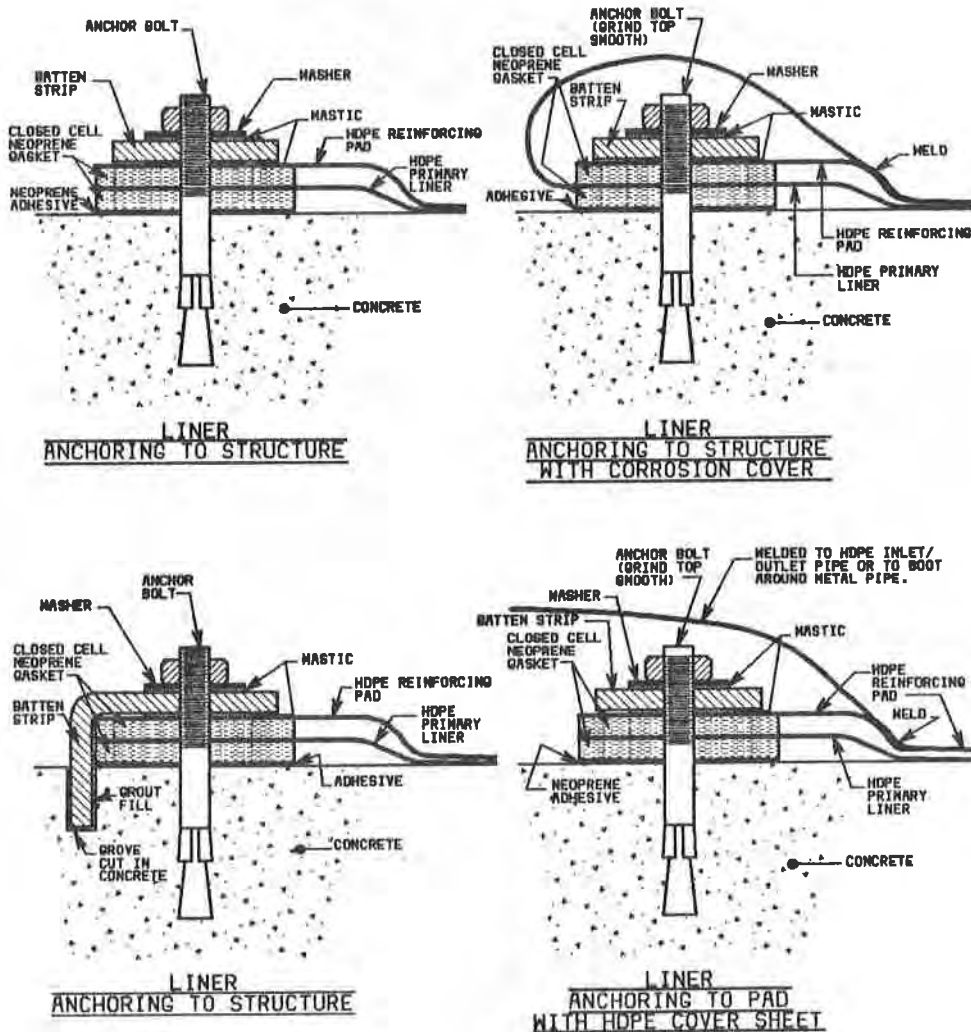


Figure 11. Liner Anchoring

CONCLUSION

At this time, we have nine operating waste containment sites lined with HDPE sheet material, and eleven in the design or construction stage. We are still have much more to the learn about the installation and inspection of HDPE as a liquid containment liner material.

The knowledge we have gained to date in the design, testing, and installation of HDPE liners makes us feel confident that we can produce a leak free containment system. However, we are equally aware of many remaining potential problem areas which can only be solved by further research, improved installation methods, and shared development knowledge and experiences.

To the potential owner of a lined containment facilities regardless of the type of liner material used I would like to emphasize the following:

1. Have a detailed liner material/installation specification for use as part of the construction contract or use as a guide in evaluation of the installation contractors proposed specifications.
2. Have your own quality control inspector on the site at all times to assure the contractors work and material are in compliance with the contract specifications.

IP/dh:1580-04

FROBEL, R.

Polyfelt Inc., U.S.A.

YOUNGBLOOD, W. and VANDERVOORT, J.

PolyAmerica, Inc., U.S.A.

**The Composite Advantage in the Mechanical Protection of Polyethylene Geomembranes
A Laboratory Study**

The use of geotextiles and geomembranes together in civil engineering applications continues to grow as both specifying authorities and material suppliers come to realize the benefits offered. The association of geotextiles and geomembranes is considered a natural one. In containment installations, the geomembrane acts as an impermeable barrier. A geotextile used in conjunction with the geomembrane insures increased mechanical protection for the geomembrane while providing an effective means to vent gas and drain liquids from beneath or between the liner system.

Environmental concerns have compelled engineers to include synthetic geomembrane lining systems in their containment design for waste disposal, mining leach pads and retention ponds as well as municipal landfills.

One class of materials, polyethylene, has become the design choice as a geomembrane because of a variety of factors. These factors include such things as chemical resistance, inertness to surrounding soils, ease and variety of seaming or weldability, and the fact that they provide the greatest overall mechanical tensile strength of any unsupported flexible

membrane liner. However, polyethylene materials, because of the semi-crystalline thermoplastic nature of the polymer, are subject to puncture and impact damage during installation and during the design life of the liner system. Specifiers of polyethylene geomembranes for use in waste containment, mining, and other applications, have been misled into believing that the thicker sheets of polyethylene with thickness ranges of 1.5, 2.0, and 2.5 mm (60, 80 and 100 mils) are the answer to mechanical protection for the geomembrane system. This is not the case and in fact, thicker is not always better. The fact that thin polyethylene geomembranes can and do function as an impermeable barrier as well as the thicker polyethylene geomembranes is a point of fact. However, polyethylene geomembranes need mechanical protection and the composite protection of a geotextile and a relatively thin geomembrane offers a viable alternative to the more expensive thick geomembrane systems.

This paper discuss geocomposites - the use of geotextiles in conjunction with geomembranes. In particular, data from four laboratory testing procedures which will be examined shows that a "technical" geotextile such as continuous filament, needle-punched

nonwoven will provide the necessary mechanical protection for the thinner polyethylene liners and will provide better mechanical protection than the unprotected thick high density polyethylene monolayers.

INTRODUCTION

Geomembranes have been used in a variety of containment applications since the early 1940s. Within the past 25 years, the use of flexible membrane liners in the form of prefabricated plastic or elastomeric sheet materials has increased rapidly in the construction industry. Such materials as butyl rubber, chlorinated polyethylene (CPE), chlorosulfonated polyethylene (CSPE or Hypalon), polyvinyl chloride (PVC), polyethylene (PE), ethylene propylene diene terpolymer (EPDM), and elasticized polyolefins, have been in use in a variety of applications to control the migration of fluids within the soil or from man-made structures. Examples of applications include: potable water pond liners, canals, tunnel linings, prefabricated tank linings, dams, curtain walls, slurry trenches, mining leach pads, hazardous waste disposal facilities and municipal landfills.

Because of our greater awareness of the dangers of pollution and water contamination, new regulations have been drafted and passed by the U.S. Environmental Protection Agency and state and local authorities to improve geomembrane specifications, design, and installations. In this light, one class of materials, polyethylene, has grown in popularity as a geomembrane system for several very important reasons. Among these are the following:

1. Polyethylenes have the best physical properties characteristics of any unsupported membrane liner.
2. Polyethylenes have the greatest overall chemical resistance over the widest temperature ranges.
3. Polyethylenes are inert, containing no migratory additives or plasticizers. They are not subject to microbiological attack.
4. Polyethylenes can be easily bonded in either factory or field environments by a variety of processes which provides bonds that are stronger than the parent material. (The parent material yields before the seam fails in either shear or peel test modes.)

Sheet polyethylene material presently available is generally classified into one of the following three categories:

1. Low density polyethylene (LDPE). Produced with high pressure polymerization giving a non-linear molecular chain. LDPE is not commonly used as a geomembrane because other higher density polyethylene materials have improved chemical resistance and physical properties.
2. High density polyethylene (HDPE). Produced with low pressure polymerization giving a linear molecular chain. Materials produced by this process are generally used as liners only when the natural resin density is below .942. Higher densities result in a less flexible material and would be sus-

ceptible to failing the environmental stress crack test (ASTM D1693) at 100°C. These materials can also be difficult to seam.

3. Linear medium density polyethylene (LMDPE). Produced with low pressure polymerization (Unipole or Dow process) creating a resin with linear molecular chains but lower in density. LMDPE is a recent addition to the polyethylene family. Due to its lower crystalline nature, LMDPE has greater flexibility and environmental stress crack resistance. The LMDPE now available demonstrates superior ultimate tensile, tear, and puncture properties over the more common HDPE liner systems.

Until recently, many polyethylene liner applications did not incorporate geotextiles, but were designed for strength in thickness of the material. In point of fact, polyethylenes, because of the semi-crystalline molecular structure are subject to mechanical damage due to puncture, impact damage caused by falling objects and abrasion. Polyethylene, regardless of thickness, is subject to this mechanical damage and must be protected. Until recently, of course, geotextiles were not used in conjunction with polyethylene. However, the use of geotextiles as discussed earlier, is a natural one and complements the properties of the geomembrane system. It is common knowledge that the increase in mechanical values such as tear and puncture, are relatively linear in relation to the thickness of unreinforced polyethylene. In recent years a number of studies have demonstrated that the use of geotextiles in conjunction with geomembranes can increase mechanical values such as puncture

resistance and impact resistance by substantial margins. The primary functions of a "technical" continuous filament, needle-punched nonwoven geotextile are protection, reinforcement and planar gas or liquid drainage. The separation and mechanical protection functions are the most underrated of all geotextile functions associated with geomembranes. Mechanical puncture and impact protection, not only offer long term survivability, but also contribute to ease in constructing of the geomembrane system in general. Thus, longer life and less maintenance should be expected with the use of a geotextile in conjunction with a geomembrane system.

There are many other side benefits to the use of a "technical" continuous filament nonwoven geotextile with a geomembrane. Among these are the following:

1. Installers are provided with a clean surface on which to place and seam the geomembrane. In the case of polyethylenes, this reduces the chance of poor welds due to weld surface irregularity.
2. The geotextile adds stability to underlying subsoil or to cover soil that is used on the slopes by providing a much greater increase in frictional resistance at the soil/geomembrane interface.
3. The geotextile can act as a basis for a leak detection system between two lining systems or under a primary liner.
4. The geotextile reduces the problem of abrasion of the liner as the liner is placed on the subgrade or as material is placed on top of the liner.

5. The geotextile provides gas venting underneath the geomembrane system.
6. Continuous filament needle-punched nonwoven geotextiles provide the necessary planar liquid transmissivity to direct water away from a primary lining system, especially in waste disposal containments.
7. The geotextile provides requisite mechanical protection for the geomembrane both during installation and for the life of the project.

In this particular study, the mechanical puncture and impact behavior of 0.5, 0.75 and 1.0 mm (20, 30 and 40 mil) LMDPE when associated with 200 and 400 gm/m² (6 and 12 oz/yd²), when associated with continuous filament, nonwoven needle-punched polypropylene geotextiles is addressed. The puncture and impact resistance of 1.5, 2.0 and 2.5 mm (60, 80 and 100 mil) high density polyethylene (HDPE) monolayers is also studied under the same test methods and the two types of systems are compared.

TEST METHODS

Two types of commonly used laboratory dynamic puncture methods were used to evaluate the various materials and material composites. The first puncture test is a modified form of ASTM D751, where the modification involves the use of a 5/16" (7.9mm) diameter blunt steel piston. The steel piston is pushed through the geomembrane or composite system using a CRT tensile/compressive testing machine at a rate of 300 mm/min. (12 in./min.) until failure of the system (see Figure 1).

The maximum load is recorded in pounds force (lbf).

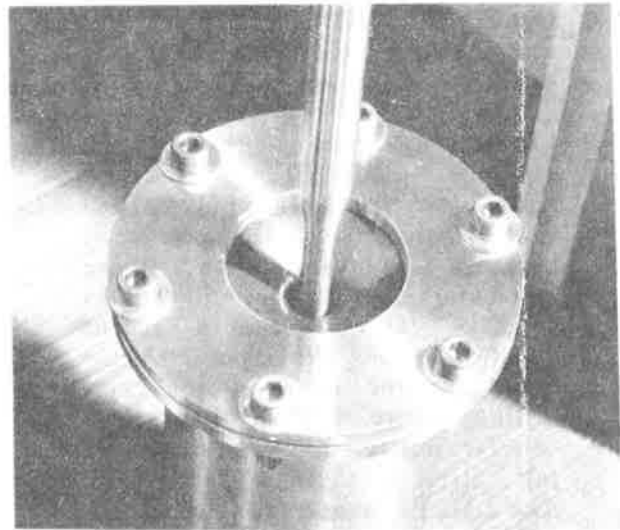


Figure 1: Photo Showing Rod Puncture Using Modified ASTM D751.

The second puncture method utilizes FTMS 101C Method 2065. This method incorporates a hemispherical point that is forced through the sample at the faster rate of 500 mm/min. (20 in./min.). The device is shown in Figure 2. The maximum load is recorded in pounds force (lbf).

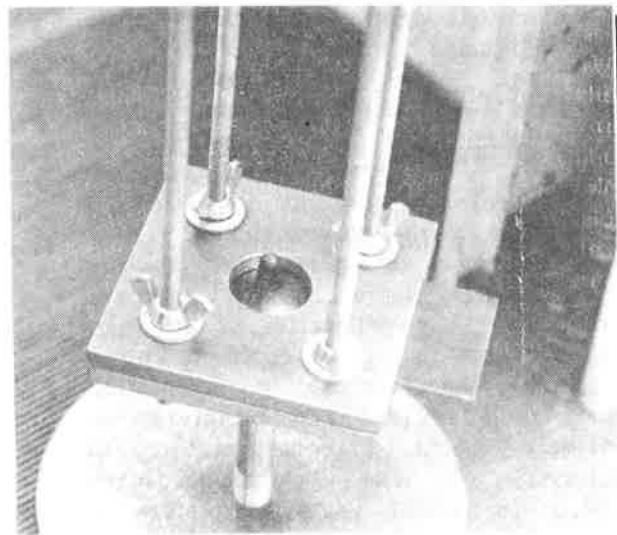


Figure 2: Photo Showing Rod Puncture Using FTMS 101C Method 2065.

In an effort to simulate actual field conditions of a geotextile/geomembrane composite system, a hydrostatic puncture resistance test method was also used. This method incorporates a hydrostatic test vessel as shown schematically in Figure 3. The hydrostatic test vessel was designed to investigate relatively large geomembrane area stress over irregular shapes on a compacted subgrade. The main advantage in testing sheet materials under stress over irregular shapes is in the simulation of field applied biaxial stress encountered in actual construction, as opposed to a point stress or unidirectional loading using standard laboratory tensile or puncture tests. The use of the hydrostatic vessel is an attempt at characterizing the given sheet material (in this case LMDPE and HDPE) when subjected to hydrostatic or overburden pressures. In this study, the mode of failure (puncture) due to an angular protrusion was studied under relatively static loading conditions. Stress was introduced by incrementally raising the hydrostatic pressure until rupture occurred. Early test equipment of this type was designed and built by J.M. Rigo of the University of Liege in Belgium and also designed and built at the U.S. Bureau of Reclamation Laboratories. The present equipment shown in Figures 4 and 5 consists of a 550 mm (22 in.) diameter pipe cap with bolted flanges and an insert pan containing three sided test pyramids (simulating sharp subgrade protrusions). The top of the hydrostatic vessel is placed over the membrane system and tested to a maximum burst pressure. The geomembrane is positioned over the subgrade which consists of the pyramids and sculptured sand. The top vessel lid is placed over the lining material and bolted in place. Water is then introduced to the top of the vessel and air

pressure is increased incrementally until the membrane fails.

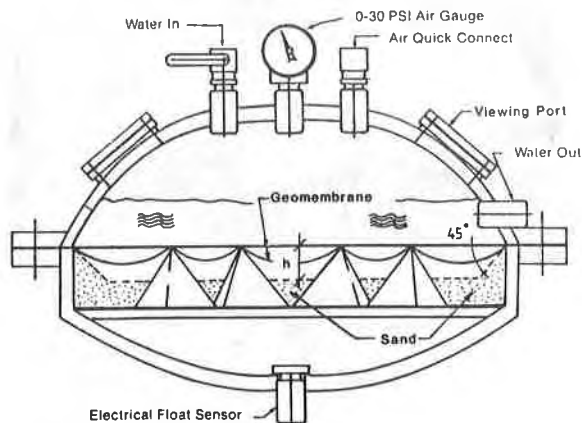


Figure 3: Hydrostatic Vessel Schematic.

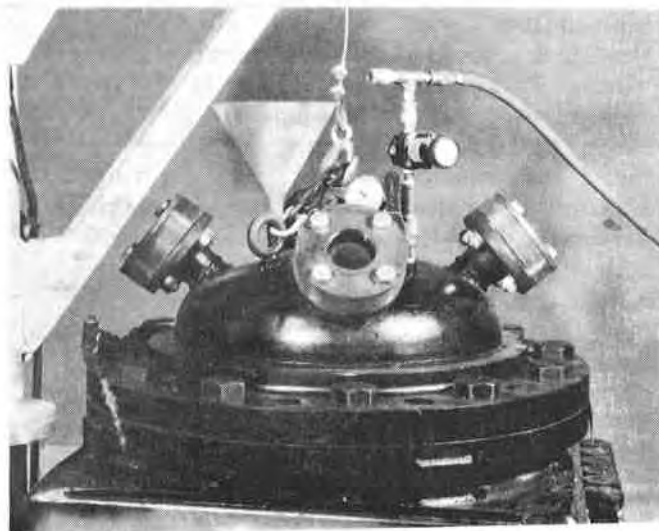


Figure 4: Photo Showing Hydrostatic Vessel.

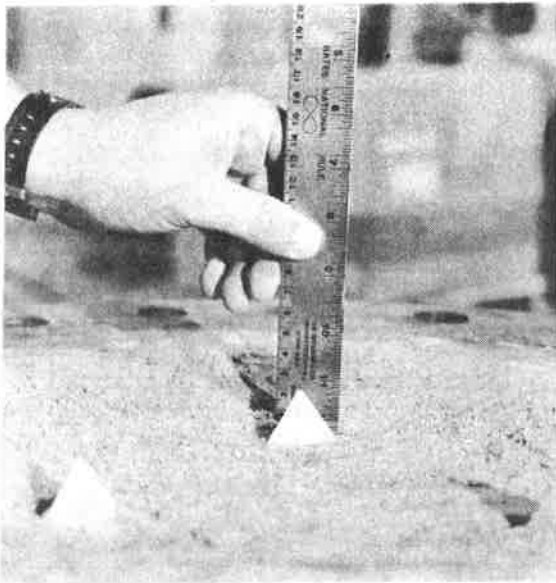


Figure 5: Photo Showing Insert Pan with Pyramids

In an effort to simulate the hydrostatic head, a compressed air on water system was selected similar to the U.S. Bureau of Reclamation device. This was used primarily to increase the range of operating pressures and in particular to maximize the hydrostatic head for testing. Maximum available pressure for this particular device is 4140 kPa (600 psi) or 432 meters (1280 feet) of water depth. The mating surfaces of the flanges were designed such that they would accept O-rings and minimize any potential water leakage during testing. A double O-ring seal has minimized any leakage. In fact, even welded seams in the polyethylene material can be tested hydrostatically in the vessel system.

During testing, the first test pressure increment is 6.9 kPa (1 psi), raised incrementally 6.9 kPa (1 psi) every 30 minutes until failure occurs. After all of the membrane

systems have been tested, the sand around the pyramids is lowered to give an increased height to the pyramid points. (Refer back to Figure 3.)

The pyramid design in the hydrostatic vessels was taken from J.M. Rigo's design and consists of three-sided pyramids with truncated tops. These pyramids simulate a sharp object protruding from an uneven subgrade. The equilateral pyramids are each 100 mm (4.0 in.) on a side with a height of 70 mm (2.8 in.). The faces have an apex angle of 70° and the pyramids are truncated 1 mm (0.04 in.) below the apex. Heights of the pyramids were chosen at 13 mm (0.5 in.), 25 mm (1 in.) and 38 mm (1.5 in.) so as to simulate an increase in size of sharp aggregate that would be situated on top of a compacted subgrade. The sheet materials tested without geotextiles included 0.5, 0.75 and 1.0 mm (20, 30 and 40 mil) thick LMDPE and 1.5, 2.0 and 2.5 mm (60, 80 and 100 mil) HDPE geomembranes. After initial testing, the LMDPE materials were protected by 200 and 400 gm/m^2 (6 and 12 oz/yd^2) non-woven, continuous filament needle-punched geotextiles. Puncture propagation was again observed and recorded as failure pressure and time to failure.

The incremental pressure increases of 6.9 kPa (1 psi) every 30 minutes allowed the materials to creep over the relatively sharp protrusions in the subgrade. These small pressure increases allow the material to elongate slowly, thus allowing a much less rapid rate of failure. Thus, this type of testing compliments the rapid machine test methods that were used in the rod puncture.

The fourth method to determine mechanical protection of the geomembrane

system is the dart impact method. This method provides a demonstration of the impact resistance of a geomembrane or geocomposite due to a falling object such as would be found with falling sharp rocks during construction of a geomembrane lined facility. The test method was derived from existing ASTM D3029 and ASTM D4495 test methods and incorporates the impact tester as shown in Figure 6 and a 2 kg (4.4 lb) dart with dimensions shown in Figure 7.

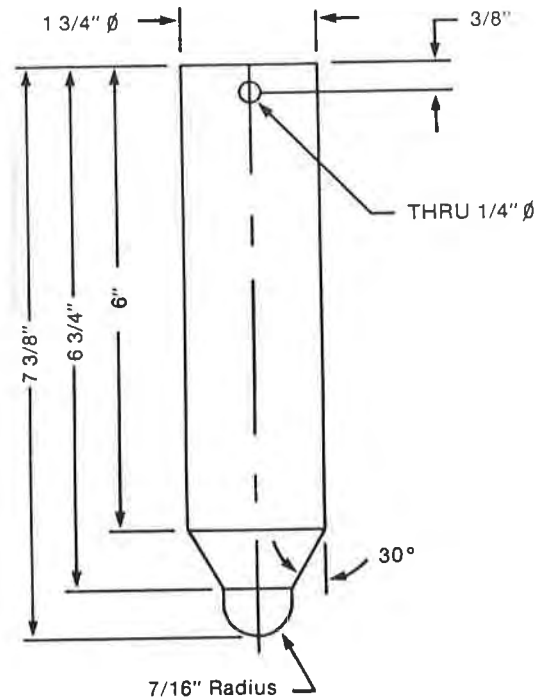


Figure 7: Dart Dimensions for the Impact Test.

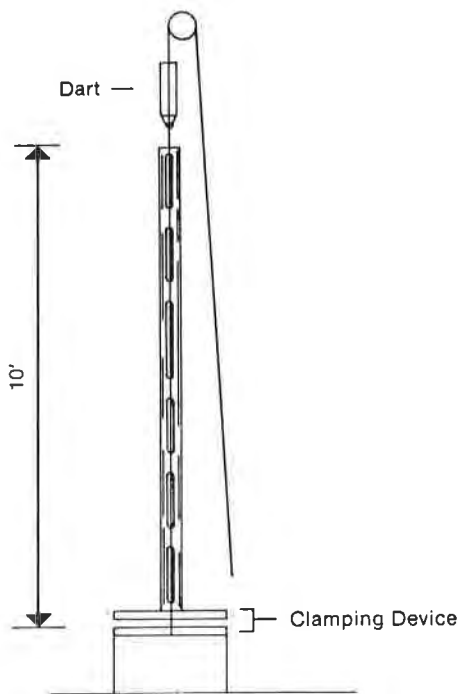


Figure 6: Impact Test Device (Modified ASTM D4495)

TEST RESULTS

Dynamic Puncture

The two types of dynamic puncture, modified ASTM D751 and FTMS 101C method 2065, both utilize a rod-type puncture device but differ in the rod end shape (flat vs. hemispherical) and speed of testing, 300 mm/min. vs. 500 mm min. (12 in./min. vs. 20 in./min.). Figure 8 represents puncture test results using the modified ASTM D751 procedure on LMDPE and composites and HDPE monolayers. It should be noted that with just a 200 gm/m² (6 oz/yd²) continuous filament needle-punched geotextile, the puncture resistance for the LMDPE is increased by a factor of 2 to 3. With the

heavier weight 400 gm/m² (12 oz/yd²) geotextile, puncture resistance is increased by another order of magnitude. As a direct comparison taken from Figure 8, note that a 1 mm/20 gm/m² (40 mil/6 oz/yd²) LMDPE/geotextile composite provides the same puncture resistance as a 2.0 mm (80 mil) HDPE monolayer and that a 1 mm/400 gm/m² (40 mil/12 oz/yd²) LMDPE/12 oz geotextile composite provides the same resistance as a 2.5 mm (100 mil) HDPE. Geotextiles on both sides of the geomembrane provide even greater protection for installations where both subgrades and cover protection is needed.

Figure 9 represents the same type of puncture test results as above but using FTMS 101C method 2065 test method and a 500 mm/min. (20 in./min.) rate. Generally, the same comparative results were realized; however, due to the faster rate of loading and shape of rod, higher puncture resistance results were obtained from the LMDPE and composite systems. The HDPE materials, however showed no increase in puncture resistance probably due to the lower yield point elongation at failure. It should be noted in Figure 9 that, as an example, a 0.75 mm/200 gm/m² (30 mil/6 oz/yd²) LMDPE/geotextile is now equivalent to an 2.0 mm (80 mil) HDPE monolayer in puncture resistance.

Hydrostatic Puncture Resistance

The hydrostatic puncture test was used to simulate a slower creep-related failure rate under sustained and increasing loading over a relatively large membrane surface area. Table 1 gives the actual test failure pressures and time to failure for the

LMDPE and composites and the HDPE monolayers over pyramid heights of 13 mm (0.5 in.), 25 mm (1 in.) and 38 mm (1.5 in.).

It is interesting to note that in this large area biaxial-type testing, the HDPE monolayer rapidly ruptures over sharp protrusions, whereas the LMDPE (with a flatter initial stress/strain curve, lower modulus and higher elasticity) conforms more readily over angular protrusions. The thicker HDPE materials failed as they approached their yield point where the material thinned out rapidly over the stress concentration of the pyramid point, again showing failure related to the lower yield point elongation of 10-12% (as compared to LMDPE yield elongation of 20%). With the added protection of a continuous filament nonwoven needle-punched geotextile, the LMDPE materials provide superior mechanical resistance to puncture and conform more readily over subgrade irregularities and sharp angular protrusions.

Impact Resistance

Figure 10 illustrates the increase in impact resistance for a composite system over the geomembrane alone. As an example, the impact resistance for 0.5 mm (20 mil) LMDPE is increased by a factor of 3 when protected by a 200 gm/m² (6 oz/yd²) geotextile and by a factor of 5 when protected by a 400 gm/m² (12 oz/yd²) geotextile. The geotextile, when placed over the geomembrane effectively protects it from falling objects such as would be found with falling or rolling rocks down a lined slope during construction. These concentrated stresses can and will damage a geomembrane system if not protected.

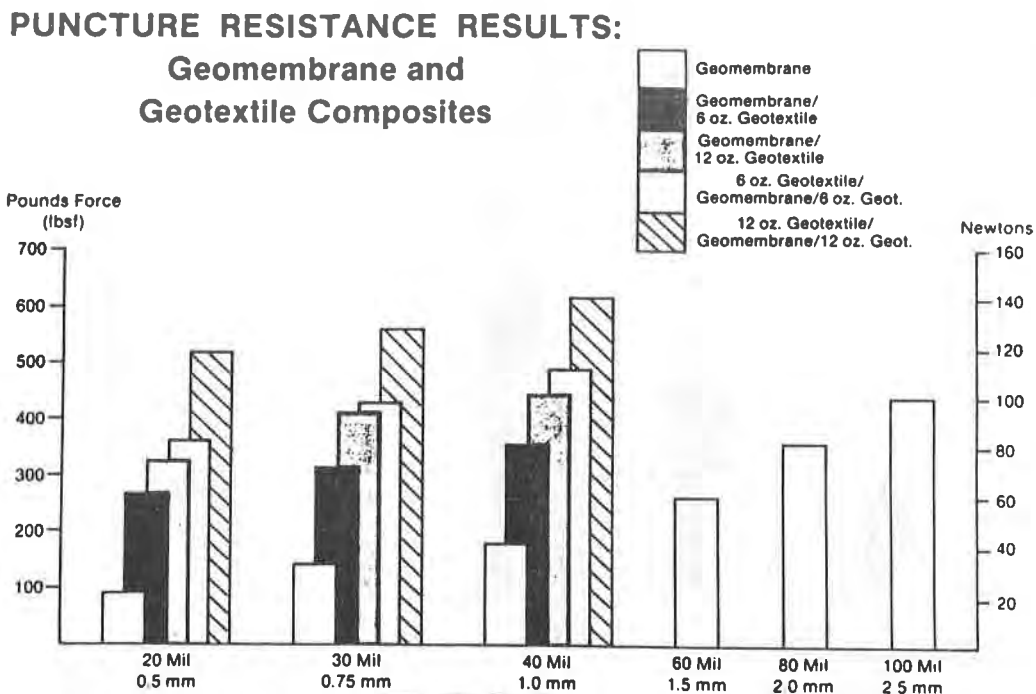


Figure 8: Puncture Resistance Results Using Modified ASTM D751 Test Methods.

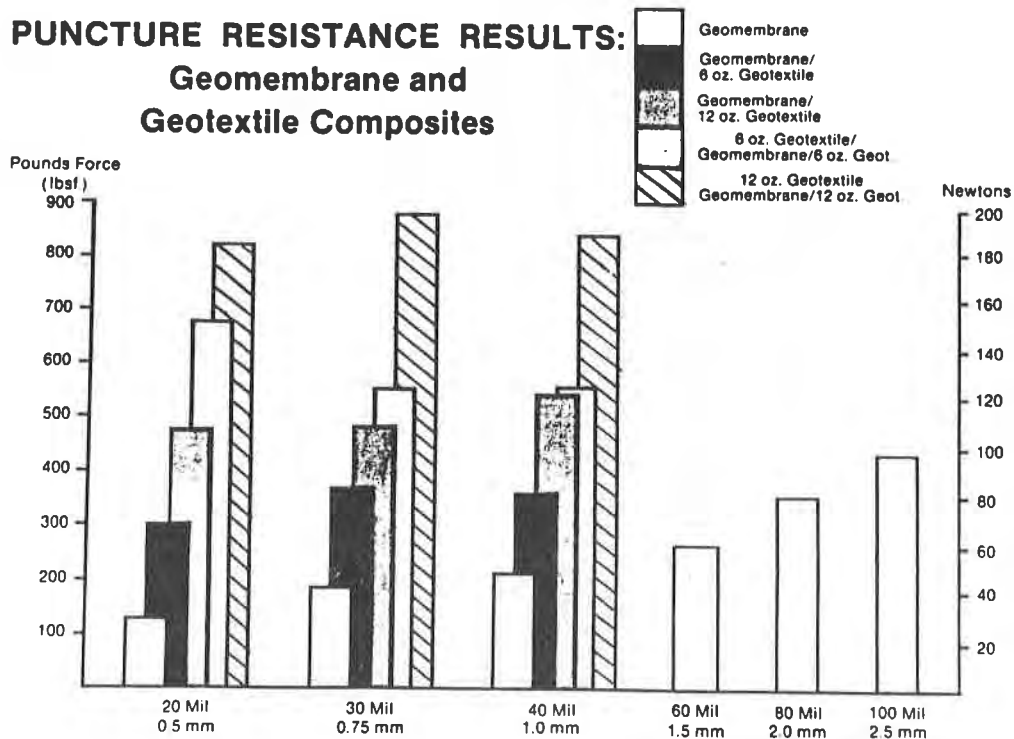


Figure 9: Puncture Resistance Results Using FTMS 101C Method 2065.

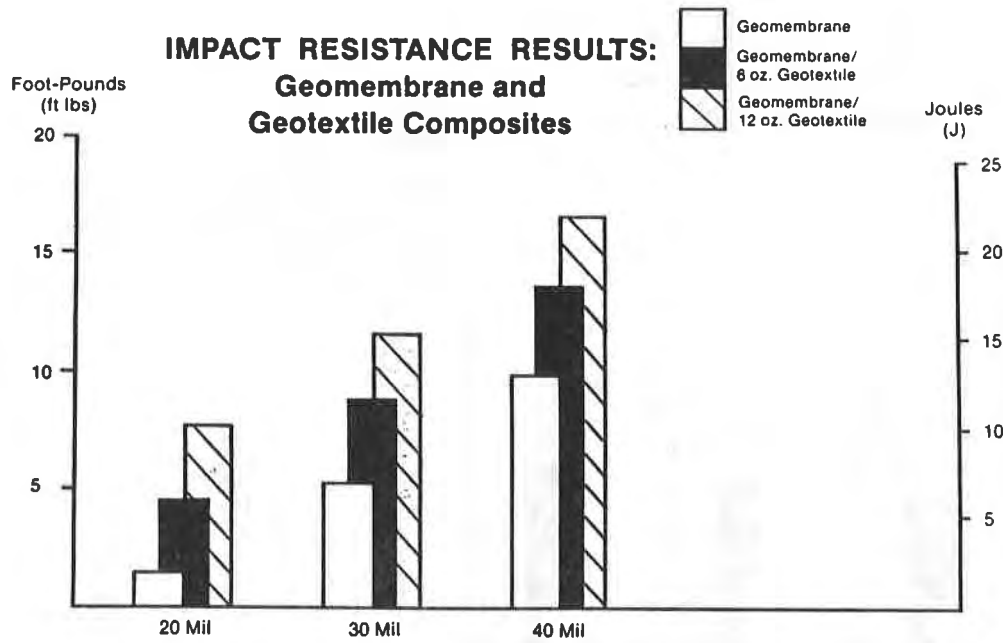


Figure 10: Impact Resistance Results Using Modified ASTM D4495 Test Method and LMDPE/Geotextile Composites.

Table 1. Hydrostatic Puncture Resistance Results for Geomembrane Systems Over Varying Pyramid Protrusions

Geomembrane System	Pyramid Height					
	13mm		25mm		38mm	
	Fail Pressure (kPa)	Fail Time (min)	Fail Pressure (kPa)	Fail Time (min)	Fail Pressure (kPa)	Fail Time (min)
0.5 mm Geomembrane	4.1	<2	2.4	<2	1.6	<2
0.5 mm Geomembrane with 200 gm/m ² Geotextile	21.4	95	6.9	28	6.9	12
0.5 mm Geomembrane with 400 gm/m ² Geotextile	213.9	930	20.7	94	13.8	34
0.75 mm Geomembrane	6.9	15	6.9	12	4.8	<2
0.75 mm Geomembrane with 200 gm/m ² Geotextile	69.0	308	27.6	142	27.6	130
0.75 mm Geomembrane with 400 gm/m ² Geotextile	345.0	1515	55.6	240	41.4	190
1.0 mm Geomembrane	19.9	63	6.9	15	13.8	63
1.0 mm Geomembrane with 200 gm/m ² Geotextile	158.7	763	27.6	145	22.1	92
1.0 mm Geomembrane with 400 gm/m ² Geotextile	441.4	1930	62.1	270	62.1	280
1.5 mm Geomembrane	17.3	75	6.9	20	6.9	<2
2.0 mm Geomembrane	26.6	116	13.8	38	6.9	12
2.5 mm Geomembrane	40.6	176	13.8	52	6.9	28

1 psi = 6.9 kPa
 1 oz/yd² = 34 gm/m²
 1 mil = .025 mm

SUMMARY AND CONCLUSIONS

The geotextile/geomembrane association is considered a natural combination. Geomembranes provide the imperviousness and geotextiles insure the increased mechanical protection while providing the effective means to vent gas and liquids from beneath or between the liner system as well as provide many other desirable benefits. Geotextile/geomembrane composite construction continues to grow in civil engineering applications as both specifying authorities and material suppliers see the obvious benefits of the composite system.

The laboratory tests that were conducted in this study illustrate the importance of geomembrane mechanical protection with a "technical" continuous filament, nonwoven, needle-punched geotextile. These tests were developed to simulate field stress situations such as would occur with objects on a compacted subgrade, landfill debris being pressed into a lining or any other puncture producing object, mechanism or situation.

It is obvious that the thinner LMDPE geomembranes provide the same function as the thick HDPE geomembranes. With the added benefits of the geotextile, especially when considering mechanical protection, the LMDPE/geotextile composite offers a superior system over HDPE monolayers while providing proven cost savings in materials, subgrade preparation and installation time.

With the advent of increased emphasis by regulatory agencies on performance criteria and functional design as opposed to material specification alone, the composite advantage will undoubtedly play a major role, especially when consideration of product

performance is a major criteria in the design of a geosynthetic containment system.

REFERENCES

- Giroud, J.P., "Design of Geotextiles Associated with Geomembranes", Proceedings - Second International Conference on Geotextiles, Vol. 1, Las Vegas, 1982, pp. 37-42.
- Koerner, R.M. and J.E. Sankey, "Transmissivity of Geotextiles and Geotextile/Soil Systems", Proceedings - Second International Conference on Geotextiles, Las Vegas, 1982, pp. 173-176.
- Koerner, R.M., et al., "Puncture and Impact Resistance of Geosynthetics", Proceedings - Third International Conference on Geotextiles", Vienna, 1986.
- Collins, T.G., and D.D. Newkirk, "The use of Geotextile Fabrics in Pond Construction beneath an Impermeable Membrane (Geomembrane)", Proceedings - Second International Conference on Geotextiles, Vol. 1, Las Vegas, 1982, pp. 13-18.
- Akber, S.Z., O. Dascal, A.L. Rollin and J. Lafluer, "Design of Dams using Geomembrane-Geotextile Sandwich, Robertson Lake Project, Lower Northshore, Quebec", Proceedings - International Conference on Geomembranes, Denver, Vol. 1, 1984, pp. 115-121.
- Hovater, L., "Geotextiles used with Geomembranes - Case Histories", Proceedings - International Conference on Geomembranes, Denver, Vol. 2, 1984, pp. 395-397.
- Koerner, R.M., Designing with Geosynthetics, Prentice Hall, Inc., Englewood Cliffs, New Jersey, 1986.

Frobel, R.K., "A Microcomputer-Based Test Facility for Hydrostatic Stress Testing of Flexible Membrane Linings", Proceedings - Colloque Sur L'Etancheite Superficielle Des Bassins, Barroges et Canaux, Vol. 2, Paris, 1983.

Frobel, R.K., "Design and Development of an Automated Hydrostatic Flexible Membrane Test Facility", REC-ERC-80-9, Bureau of Reclamation, Denver, 1981.

Rigo, J.M., "Correlation of Puncture Resistance over Ballast and the Mechanical Properties of Impermeable Membranes", University of Liege, Belgium, 1977.



SESSION 6A
TESTING

HAXO, H.E., Jr. and WALLER, M.J.
Matrecon, Inc., U.S.A.

Laboratory Testing of Geosynthetics and Plastic Pipe for Double-Liner Systems

INTRODUCTION

The use of polymeric products in civil-engineering applications has increased dramatically over the past decade, particularly in the design and construction of waste management facilities. These products include various rubber and plastic membranes that have very low permeability, woven and nonwoven textiles that have various degrees of permeability, special open constructions designed for high permeability and liquid flow, and plastic pipes (1). Except for plastic pipe, these products are called geosynthetics.

Of particular importance is the wide range of functions that polymeric products perform in double-liner systems for hazardous waste disposal facilities. These products are based on a wide range of polymers including rubbers (elastomers), plastics, fibers, and resins. With this great diversity in materials and products, an array of laboratory tests are being performed on the materials and the products to assess their quality and ability to perform in a specific application. Even for hazardous waste containment applications when a single type of material is the material of choice, thorough testing and evaluation of candidate materials are necessary due to the differences in polymers and additives used in both geosynthetics and plastic pipe.

This paper reviews some of the basic characteristics of the polymeric materials and products that are used in the construction of double-liner systems and indicates the effects of these characteristics on field performance and laboratory testing of these products. Emphasis is placed on the testing of polymeric geomembranes and compatibility testing.

POLYMERIC PRODUCTS IN A DOUBLE-LINER SYSTEM

Each construction material in a double-liner system requires testing and evaluation in terms of the specific facility and condition in which it is designed to perform. Thus, if a material will probably be exposed to a waste liquid or its vapors, it must be compatible with that particular waste stream and be able to maintain its properties over extended periods of time. Similarly, if the material is to be subjected to loads and to elevated temperatures, it must be able to function as required without failure.

The following polymeric materials of construction are being used or being suggested for use in double-liner systems (2):

Geomembranes--To provide a barrier between hazardous substances and mobile polluting substances and the groundwater; in the closing of landfills to provide a low-permeability cover barrier to prevent intrusion of rain water.

Geotextiles--To provide separation between solid wastes and drainage material and the leachate collection system or between the membrane and cover or embankment soils; to reinforce the membrane against puncture from the subgrade; to provide drainage, such as in leachate collection and leak-detection systems; to provide filtration around drainage pipes.

Drainage Nets--To provide drainage above and between liners; to provide reinforcement for side slopes and embankments.

Plastic Pipe--To provide drainage in leachate collection and leak-detection systems. Pipe is also used in the construction of monitoring ports, manholes, and system cleanouts.

Figure 1 presents a schematic of a double-liner system with indications of potential failure modes for the polymeric components used in the subsystems.

BASIC CHARACTERISTICS OF POLYMERIC MATERIALS

All of the geosynthetic materials, as well as plastic pipe, discussed in this paper are based on polymers, which are products of the chemical, plastics, rubber, and fiber industries. From the viewpoint of composition, an almost infinite range of polymeric materials can be produced. The polymeric materials used in the manufacture of geosynthetics and pipe are given in Table 1. Polymers within a type can vary according to grade and manufacturing process. In addition, considerable variation among compositions based on the same polymer is introduced by the product manufacturer through compounding with ingredients designed to enhance or develop specific characteristics. Knowledge of the composition of each geosynthetic and pipe can be important when dealing with waste liquids containing organics.

Four general types of polymeric materials are used in geosynthetics:

- Thermoplastics and resins, such as PVC and EVA.
- Crosslinked elastomers, such as neoprene and EPDM.
- Semicrystalline plastics, such as polyethylenes.
- Highly crystalline, oriented polymers, such as polypropylene and polyester fibers.

As all of these materials are polymeric, they have characteristics in common and require a broad array of tests to characterize them (3). In designing containment facilities and designing the tests needed to assess important design properties, recognition must be given to basic characteristics of polymers. Some of the important characteristics of the polymers used in products for the construction of double-liner systems are briefly discussed.

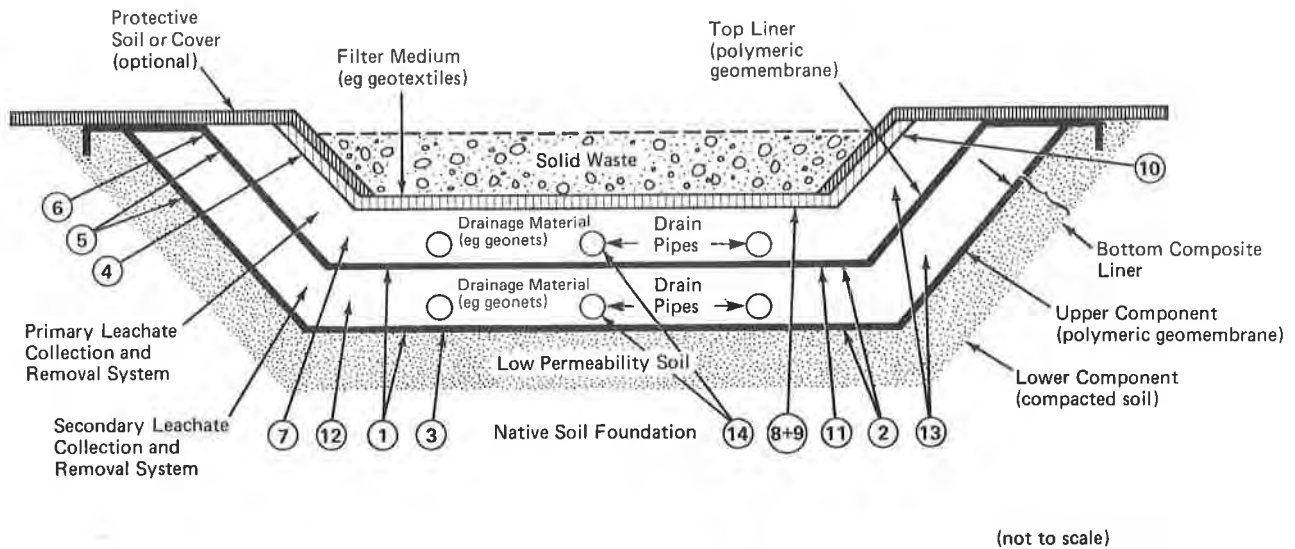


Figure 1. Schematic of a polymeric geomembrane/composite double-liner system for a landfill (2) and potential failure modes of the different components.

Potential failure modes of geomembranes:

1. Puncture due to settlement of components in leachate collection system or from irregularities in the subgrade.
2. Environmental stress-cracking of liner at bends and creases.
3. Bridging caused by localized subsidence in the subgrade.
4. Sloughing of protective soil cover due to low coefficient of friction between membrane and soils.
5. Tensile stress under load.
6. Thermal cycling.
7. Loss of properties due to waste incompatibility.

Potential failure modes of geotextiles:

8. Loss of properties due to waste incompatibility leading to reduced fluid flow.
9. Clogging or blinding of filter material by particles in the waste.
10. Tensile stress under load.

Potential failure modes of drainage nets:

11. Intrusion of membrane into the net, leading to clogging.
12. Loss of properties, leading to reduced fluid flow.
13. Collapse of the materials under waste load.

Potential failure modes of plastic pipe:

14. Collapse of pipe under load, particularly if incompatible with wastes.

TABLE 1. POLYMERS USED IN THE MANUFACTURE OF MAJOR PRODUCTS FOR THE CONSTRUCTION OF WASTE MANAGEMENT FACILITIES

Polymer	Type	Product			
		Geomem- branes	Geo- textiles	Geogrids and drain- age nets	Pipes
Acrylonitrile butadiene styrene	Resin	X
Chlorinated polyethylene	Rubber	X
Chlorosulfonated polyethylene	Rubber	X
Ethylene propylene rubber	Rubber	X
Ethylene vinyl acetate	Resin	X
Neoprene (chloroprene rubber)	Rubber	X
Polyamide (nylon)	Fiber/resin	X ^a	X
Polybutylene	Resin	X	X
Polyester	Fiber/resin	X ^a	X	X	...
Polyester elastomer	Resin/rubber	X
Polyethylene:					
Linear low-density	Resin	X
High-density	Resin	X	...	X	X
Polypropylene	Resin	...	X	X	...
Polyurethane	Resin/rubber	X
Polyvinyl chloride					
Plasticized	Resin	X
Unplasticized	Resin	X

^aUsed as reinforcing fabric in geomembranes.

Polymers Vary in Modulus and in Elongation at Break

Polymeric materials range from soft foam-like materials to high modulus structural materials. Polymeric materials that are used in waste management facilities are intermediate in modulus or stiffness. However, their elongation at break ranges from 15% to as much as 1000%. Both properties are important considerations in designing geosynthetics and plastic pipe.

Polymers are Sensitive to Organic Liquids and Vapors

As the polymeric compositions used in double-liner systems are organic in nature, they are sensitive to organic liquids; they can absorb organics from waste liquids and vapors and swell or can be leached and shrink. In either case, several properties of the composition can simultaneously change and their performance characteristics can be altered. This sensitivity to organics shows the need for compatibility testing.

Polymers are Viscoelastic and Sensitive to Temperature and Rate of Deformation

All polymeric materials are viscoelastic, that is, when undergoing a deformation they show, in varying degrees, both viscous and elastic behavior. The elastic component behaves like a spring and is independent of rate of deformation. The viscous component behaves like a dashpot and is highly dependent upon the rate of deformation and upon temperature. Rubbers, such as natural rubber and some

polyurethanes, tend to have highly elastic components, whereas many of the plastics have highly viscous components. In performing tests in extension or compression, the temperature and rate of deformation become important.

Most of the polymers used in geosynthetics and pipe vary greatly in properties with temperature, even within the temperature range in which waste containment facilities operate. At low temperatures some become glassy and brittle, and at high temperatures the thermoplastic polymers become soft and plastic. These characteristics will greatly affect the applications in which a polymeric material can be used.

Due to the viscous component of polymeric compositions, the speed at which they are deformed greatly affects the magnitude of the values that are obtained, e.g., tensile or tear values. At high test speeds, modulus values generally are considerably higher; the effect on tensile strength and elongation at break values varies with the polymer. In the case of semicrystalline materials, such as HDPE, high-speed testing will not allow time for crystals to align themselves during the test, thus resulting in lower tensile at break values than those obtained at lower speeds. In service environments deformation rates can range from rapid impacts to slow creep.

Polymers Tend to Creep and Relax in Stress

Polymeric materials have a relatively high tendency to creep, that is, to increase in length or change dimensions under load or to relax in stress when placed in constant strain. This characteristic is important to long-term exposure such as would be encountered in a double-liner system. For example, in-place drainage nets and pipes are under constant load and a geomembrane placed over a protrusion is under constant stress. The absorption of organics can aggravate this tendency.

High Coefficient of Thermal Expansion

All polymeric materials have thermal coefficients approximately 10 times greater than those of metals and concrete. For soft geomembranes, this is not a major problem; however, for stiff membranes, such as the polyethylenes, changes in temperature can cause considerable deformation and flexing of a liner when exposed to normal weather and high stress in the liner when exposed to cold weather.

Importance of Thermal and Strain History

Polymeric materials tend to have "memory," that is, the deformation during processing and forming into sheets leaves residual strain in many polymers, which is why tensile and tear testing should be performed in both machine and transverse directions. Residual strain can cause shrinkage in the machine direction and expansion in the transverse direction when the sheeting is warmed.

Elongation Under Biaxial Straining

Most of the tensile and tear testing for specification purposes is performed uniaxially, which can yield high elongations. Performing the tests biaxially, that is, deforming the materials simultaneously in machine and transverse directions, yields considerably lower elongation values. This can show up in the testing of puncture and hydrostatic resistances and in actual service.

Broad Range of Permeability

The permeability of the polymeric compositions to various gases and vapors can vary over several orders of magnitude. Generally, the presence of plasticizers increases permeability and the presence of crystalline structure reduces permeability. Also of importance is the relationship between the solubility characteristics of the permeant and the polymer; the more soluble the permeant is in the geomembrane, the higher the probability of permeation.

Stress-Cracking and Static Fatigue

Polymeric materials, as with other types of materials, are subject to fracture after being under stress and strain for extended periods of time. A material under constant stress loses tensile strength and elongation at break. Semicrystalline polymeric compositions, when placed under stress in environments that affect the surface of the material, can crack or craze. This phenomenon occurs with some grades of polyethylene and polyester elastomers. The stress-cracking resistance of semicrystalline polymers that might be used in contact with waste liquids over long periods of time should be assessed.

Amorphous and Crystalline Phases in Semicrystalline Polymers

Semicrystalline polymers, such as polyethylene, contain two basic phases: 1) an amorphous phase in which the molecular structure is random, such as in a rubber; and 2) a crystalline phase in which the molecular structure is highly ordered. The crystalline phase imparts stiffness to the polymer and resists the absorption of organic species, and the amorphous phase can absorb and transmit organics. Deformation of a semicrystalline polymer results over time in molecular rearrangement in the crystalline phase. Excessive deformation results in yielding and orientation of the crystalline phase and subsequent loss in strength in the direction perpendicular to the deformation.

Highly Resistant to Degradation

With proper protection through the use of stabilizers and antidegradants, polymers used in the manufacture of geosynthetics and pipe can be highly resistant to degradation, that is, with no adverse changes in molecular structure. Polymeric compositions are still subject to loss in properties due to swelling, but polymer molecular structure remains essentially undamaged.

Polymers in polymeric compositions are also highly resistant to biodegradation; however, some compounding ingredients, such as plasticizers, may be biodegradable. Biodegradation in such cases may result in adverse changes in the properties.

Combinations of Properties in Polymeric Compositions

A given polymer will tend to have a distinct pattern of properties which can be modified somewhat by compounding. Assessing materials based upon a single property, such as tensile strength, can lead to an incorrect selection of materials because of inadequate values for other important properties, such as chemical compatibility. For this reason, a group of tests are usually performed on a material and the resulting test values are assessed as a group before a selection should be made.

PURPOSE AND TYPES OF LABORATORY TESTS

A double-lined waste management facility is a complex system, each component of which must meet performance criteria for the service life of the facility. Failure of a single component could lead to failure of the system. Due to the inaccessibility of components of double-liner systems, rational selection and evaluation of each component is of critical importance to the long-term functioning of the facility. Rigorous testing programs designed to assess the properties of these materials are an indispensable part of the design process.

Laboratory tests are performed for the following reasons:

- To assess the ability of certain materials to perform in specific field environments.
- To aid in the selection of materials for the construction of a specific facility.
- To assess durability under some extreme conditions.
- To develop data useful in the designing of containment facilities.
- To ascertain for quality assurance purposes that the materials of construction placed in the field meet design specifications.
- To identify the materials and follow changes in composition during service.
- To monitor the properties of the liner during service.

Laboratory tests designed to assess the ability of these polymeric construction materials to perform as required in the design and to meet the challenges of the field environment are needed.

The types of tests used to assess the attributes of polymeric construction materials fall into several categories. Tests of mechanical properties are most commonly used to assess the characteristics of these materials. The test values are then used in the material specifications that are incorporated into the design documents. At the present state of liner technology, the relationships between mechanical properties of particular geosynthetics as measured in the laboratory and their field performance have not been well defined. Thus, when only laboratory test data on mechanical properties are available, the designer will often rely upon his experience in the field as the basis for design judgment.

Performance tests are designed to assess the ability of one or more materials to perform under a specific set of conditions that simulate those that exist in the field. Performance tests are generally complex, usually involve many steps, and need considerable control. Such tests are beginning to evolve for geosynthetics and plastic pipe in double-liner systems. EPA Test Method 9090 for liner compatibility with a waste liquid is a performance type of test because an actual waste liquid is used as the immersion medium (4).

A major difficulty in designing performance tests of the various materials under conditions encountered in double-liner systems is the necessity of reproducing in

the tests the field conditions in which the liner system will perform. For example, they might need to include identical soils, at the correct moisture contents, wastes, and construction materials that will be used. Tests that have been used and which relate to some aspects of field performance include:

- Permeability of geomembranes, e.g., pouch test (5).
- Frictional properties at the soil, membrane, and geotextile interface.
- Strength and elongation of geomembranes tested biaxially, e.g., hydrostatic resistance.
- Transmissivity, permittivity, and filter properties of geotextile, soil, and geogrid systems.

Most performance tests of geosynthetics and plastic pipe in waste containment applications as they exist today are in the early stages of development and require additional research in order to understand and control the test variables and to interpret the test results. At present, field verification data and long histories of use of these construction materials in waste liquid environments are meager.

Analytical tests are used to determine the composition of materials and to evaluate changes in composition over time under waste and environmental exposures (6). They include analyses for volatiles, ash content, analysis of the ash for trace metals, extractables (amount and composition), gas chromatography of extractables and by pyroprobe, differential scanning calorimetry of semicrystalline compositions, thermogravimetric analysis, and specific gravity. These tests can be used to "fingerprint" a polymeric material for quality control purposes.

The testing of the various polymeric components used or potentially used in double-liner systems are discussed in the following sections.

TESTING OF GEOMEMBRANES

The basic requirements of a geomembrane liner are low permeability to waste constituents, compatibility with the waste liquid to be contained, durability for the lifetime of the facility, and ease of construction and installation. Laboratory tests of these materials need to be selected or designed to assess these attributes. It is also desirable to be able to identify each geomembrane in order to be certain that an approved membrane is used in the final construction and to follow the effect of an exposure on a geomembrane through testing samples of the exposed liner. Table 2 presents a list of test methods that are being used in assessing the various types of polymeric geomembranes. The testing of geomembranes for use in the lining of waste disposal facilities has been discussed by Haxo (7) and in the an EPA Technical Resource Document (8). Specific test methods, including the modification of some ASTM methods, have been adopted by the National Sanitation Foundation (9).

Permeability

As the primary function of a liner is to prevent the flow of mobile liquids and other chemical species, permeability of the geomembrane to these species must

TABLE 2. APPROPRIATE OR APPLICABLE TEST METHODS FOR UNEXPOSED POLYMERIC GEOMEMBRANES

Property	Membrane Liner Without Fabric Reinforcement			
	Thermoplastic	Crosslinked	Semicrystalline	Fabric reinforced
<u>Analytical properties</u>				
Volatiles	MTM-1 ^a	MTM-1 ^a	MTM-1 ^a	MTM-1 ^a (on selvage and reinforced sheeting)
Extractables	MTM-2 ^a	MTM-2 ^a	MTM-2 ^a	MTM-2 ^a (on selvage and reinforced sheeting)
Ash	ASTM D297, Section 34	ASTM D297, Section 34	ASTM D297, Section 34	ASTM D297, Section 34 (on selvage)
Specific gravity	ASTM D792, Mtd A	ASTM D297, Section 15	ASTM D792, Mtd A	ASTM D792, Mtd A (on selvage)
Thermal analysis:				
Differential scanning calorimetry (DSC)	na	na	yes	na
Thermogravimetry (TGA)	yes	yes	yes	yes
<u>Physical properties</u>				
Thickness - total	ASTM D638	ASTM D412	ASTM D638	ASTM D751, Section 6
Coating over fabric	na	na	na	Optical Method
Tensile properties	ASTM D882, ASTM D638	ASTM D412	ASTM D638 (mod)	ASTM D751, Mtd A and B (ASTM D638 on selvage)
Tear resistance	ASTM D1004 (mod)	ASTM D624, Die C	ASTM D1004	ASTM D751, Tongue Mtd (modified)
Modulus of elasticity	na	na	ASTM D882, Mtd A	na
Hardness	ASTM D2240 Duro A or D	ASTM D2240 Duro A or D	ASTM D2240 Duro A or D	ASTM D2240 Duro A or D (selvage only)
Puncture resistance	FTMS 101B, Mtd 2065	FTMS 101B, Mtd 2065	FTMS 101B, Mtd 2065	FTMS 101B, Mtd 2031 and 2065
Hydrostatic resistance	na	na	ASTM D751, Mtd A	ASTM D751, Mtd A
Seam strength:				
In shear	ASTM D882, Mtd A (mod)	ASTM D882, Mtd A (mod)	ASTM D882, Mtd A (mod)	ASTM D751, Mtd A (mod)
In peel	ASTM D413, Mach Mtd Type 1 (mod)	ASTM D413, Mach Mtd Type 1 (mod)	ASTM D413, Mach Mtd Type 1 (mod)	ASTM D413, Mach Mtd Type 1 (mod)
Ply adhesion	na	na	na	ASTM D413, Mach Mtd Type 1 ASTM D751, Sections 39-42
<u>Environmental and aging effects</u>				
Ozone cracking	ASTM D1149	ASTM D1149	na	ASTM D1149
Environmental stress-cracking	na	na	ASTM D1693	na
Low temperature testing	ASTM D1790	ASTM D746	ASTM D1790 ASTM D746	ASTM D2136
Tensile properties at elevated temperature	ASTM D638 (mod)	ASTM D412 (mod)	ASTM D638 (mod)	ASTM D751 Mtd B (mod)
Dimensional stability	ASTM D1204	ASTM D1204	ASTM D1204	ASTM D1204
Air-oven aging	ASTM D573 (mod)	ASTM D573 (mod)	ASTM D573 (mod)	ASTM D573 (mod)
Water vapor transmission	ASTM E96, Mtd BW	ASTM E96, Mtd BW	ASTM E96, Mtd BW	ASTM E96, Mtd BW
Water absorption	ASTM D570	ASTM D471	ASTM D570	ASTM D570
Immersion in standard liquids	ASTM D471, D543	ASTM D471	ASTM D543	ASTM D471, D543
Immersion in waste liquids	EPA 9090	EPA 9090	EPA 9090	EPA 9090
Soil burial	ASTM D3083	ASTM D3083	ASTM D3083	ASTM D3083
Outdoor exposure	ASTM D4364	ASTM D4364	ASTM D4364	ASTM D4364
Tub test	b	b	b	b

^aSee reference (8).^bSee reference (12).

na = Not applicable.

be assessed. Transport through a geomembrane occurs on a molecular level and depends on the solubility of the permeating species and its diffusibility in the membrane. A concentration or partial pressure gradient across the membrane is the driving force for the direction and rate of transport. The species migrates through the membrane from higher to lower concentration; at a small difference in concentration, the transmission can approach zero for specific species. In contrast, soils and clays are porous and the driving force for permeation is the hydraulic head. Test methods that are available and have been used to assess the permeability of polymeric geomembranes include:

- ASTM D814, for determining organic vapor transmission.
- ASTM D1434, for determining gas transmission (10).
- ASTM E96, for determining moisture, vapor, and modified for organic vapor transmission (10).
- Pouch test, for determining transmission of organics in dilute solutions (5).

The permeability of geomembranes to different species can vary by orders of magnitude, depending on the composition and solubility of the migrating species in the geomembrane (10, 11). The permeation of a given species is also affected by such factors as crystallinity, filler content, density, crosslink density of the polymer, thickness of the geomembrane, temperature, and the driving force across the membrane. Also, swelling of a geomembrane during service can significantly increase its permeability to some species.

Compatibility with Wastes

The selection of a geomembrane depends on whether it is compatible with the liquid to be contained (12). A liner is compatible with a liquid if, on long exposure, its properties, e.g., permeability and mechanical properties, do not change more than reasonable amounts depending on the type of membrane. In the absence of criteria for determining the success or failure of materials under exposure to specific wastes, experience is required in interpreting changes or trends that develop over time.

EPA Test Method 9090 was designed to assess the compatibility of geomembranes and waste liquids by simulating some of the conditions a geomembrane would encounter as an unstretched coupon in representative samples of the waste liquids or leachates to be contained (4). In this test, liner samples in slab form are immersed for up to four months at 23 and 50°C in the waste liquid. Testing is performed on the unexposed membranes for baseline data and on samples exposed to the waste liquids for 30, 60, 90, and 120 days to assess the effects of immersion. Testing required by the method includes determination of tensile properties, tear resistance, puncture resistance, and hardness. In addition, the weight and dimensions of the individual test slabs before and after exposure are measured.

A major challenge in conducting the 9090 test is maintaining, as closely as possible, the composition of the waste liquid in the test cells for the duration of the tests as it would be encountered in the "real world." Changes in the concentration of dissolved constituents in a waste liquid can occur because of loss

of volatiles from the immersion cell or absorption by the geomembrane under test. Consequently, if the leachate contains volatile organics, it is necessary to seal the cells in which samples are immersed and to test the samples promptly after removal. Also, though not required by the 9090 test method, it may be necessary to change the liquid monthly at the time the sample is removed in order to maintain a constant concentration of the organics. Table 3 illustrates partitioning of organics between water and HDPE and the degree that organics are absorbed by the HDPE sample immersed in an aqueous solution of 10 organics in a 9090-type test. The acetone and methyl ethyl ketone preferentially partitioned to water, whereas the other 8 organics partitioned to the HDPE.

TABLE 3. PARTITIONING OF ORGANIC SOLVENTS BETWEEN WATER AND AN HDPE MEMBRANE AFTER 30 DAYS OF EXPOSURE IN A 23°C AQUEOUS SOLUTION SPIKED WITH TEN ORGANICS

Organic in spike	Initial spike ^a (mg/g)	Concentration in water at 30 days ^b (mg/g)	Concentration in HDPE membrane at 30 days ^c (mg/g)	Ratio ^d C_{PE}/C_W
Acetone	0.198	e	0.000	...
Methyl ethyl ketone	0.201	0.201	0.000	<0.002
Trichloroethane	0.335	0.000	1.42	>1400
Benzene	0.220	0.018	0.46	26
Trichloroethylene	0.366	0.032	1.58	49
Toluene	0.217	0.031	2.63	85
m-Xylene	0.072	0.0089	1.46	164
o-Xylene	0.073	0.0034	1.17	344
Tributyl phosphate	0.243	0.016	0.32	20
Di(ethyl hexyl) phthalate	0.247	0.0057	0.11	19

^aBased upon the solubility of individual organic in water.

^bConcentration determined by gas chromatography.

^cConcentration determined by headspace gas chromatography.

^dRatio of concentration of the organic in the HDPE membrane divided by the concentration in water.

^eNot detectable by the gas chromatograph.

Partial results of a 9090 test of an 80-mil HDPE geomembrane in a waste liquid containing organics are presented in Table 4. The test was conducted in a manner to prevent loss of volatiles and to maintain concentration of the organic constituents in the waste liquid. Determination of the volatiles and extractables of the exposed sample improves the interpretation of the results. The current EPA Test Method 9090 does not include testing of seams and the effect of strain on a geomembrane (4). Inclusion of such testing would enhance the method and make conclusions regarding compatibility more reliable.

Durability

A polymeric geomembrane used to line a hazardous waste storage and disposal facility must maintain its integrity and performance characteristics over the designed life of the facility. Liners must resist physical damage during installation and service; the integrity of the seams must be maintained so that cracks, breaks, tears, and other holes do not develop in the liner system. Fabric

reinforcement is used with CSPE, CPE, and other polymers to increase durability, particularly during installation. Ultimately, the service life of a given liner will depend on the intrinsic durability of the material and on the conditions under which it is exposed during service (13).

TABLE 4. PARTIAL RESULTS OF COMPATIBILITY TESTING OF AN 80-MIL HDPE GEOMEMBRANE ON IMMERSION IN A LEACHATE^a AT 23°C

Original Values of Properties and Percent Retention of Values after One, Two, Three, and Four Months of Immersion at 23°C

Property	Direction of test	Initial values	Exposure time, months			
			1	2	3	4
<u>Analytical properties</u>			<u>Test values</u>			
Volatiles, %		0.1	2.64	2.89	3.26	3.13
Extractables, %		≤0.6	0.90	1.43	1.40	^b
<u>Dimensional properties</u>			<u>Percent change</u>			
Weight ^c		...	+5.5	+6.0	+6.0	+5.9
<u>Physical properties</u>			<u>Percent retention</u>			
Tensile at yield	Machine	18.5 MPa	90	88	89	89
	Transverse	18.8 MPa	90	92	90	91
Tensile at break	Machine	29.9 MPa	89	91	102	93
	Transverse	30.7 MPa	91	82	97	83
Elongation at break	Machine	835%	98	99	105	98
	Transverse	830%	100	93	96	93
Stress at 100% elongation	Machine	13.0 MPa	90	89	90	90
	Transverse	12.7 MPa	91	93	92	91
Modulus of elasticity ^d	Machine	855 MPa	73	^e	60	62
	Transverse	811 MPa	75	69	63	61
Tear strength	Machine	148 kN/m	89	93	89	88
	Transverse	148 kN/m	86	91	89	88
Puncture resistance			<u>Test values</u>			
Maximum stress, normalized for 100-mil sheeting, N		717	725	669	657	672
Retention of stress for 100-mil sheeting, %		100	101	93	92	94
Elongation at puncture, mm		15.5	19.3	18.0	17.0	18.3
Hardness, Duro D points			<u>Change in points</u>			
5-second reading		63	-8	-8	-9	-7

^aLeachate was changed monthly.

^bNot measured.

^cWeight gain may be due to swell and/or encrustation of sample.

^dMeasured using 12.7 mm x 203-mm strip specimens with an initial jaw separation of 10 mm and an initial strain rate of 0.1 mm/mm min. Using a specimen with a 250-mm gage length, recommended as standard in ASTM D882-83, would result in somewhat higher values.

^eUnreliable result.

Laboratory tests for assessing the durability of geomembranes under different environmental conditions range from chemical analyses to tests of mechanical properties (e.g., tensile properties, tear resistance, puncture resistance, and impact resistance) under various exposures in aggressive environments, such as exposure to high and low temperatures, to ozone while under strain, to ultraviolet light, to stress and strain for extended periods of time, and to the combined effects of chemicals and stress. Specific tests to assess these properties are listed in Table 2 for different types of geomembranes.

Important in long-term service of a polymeric geomembrane liner is its ability to resist the effects of creep and biaxial strain that will occur when it is under load and rests on a nonplanar or irregular surface, such as exists at the bottom of a containment facility. Cracks and breaks can occur in a polymeric geomembrane at significantly lower stress values than are encountered in the simple uniaxial tensile test.

As with compatibility testing, maximum changes in properties that can take place without affecting overall performance have not been established. Nevertheless, laboratory testing of several properties can yield data indicative of durability.

Seamability and Quality of Seams

In constructing a large continuous leakproof liner from prefabricated sheeting, pieces of sheeting must be seamed. Sheetings of a roll width less than 1.8 m are seamed together in a factory to form panels which are brought to the field and seamed. Sheetings of a roll width greater than 6 m is brought to the field in rolls which are then seamed. In either case, the geomembrane must be seamable and yield reliable seams that are mechanically sound and can withstand exposure to waste liquids for extended periods of time. Thermoplastic materials which can melt or which can be dissolved in a solvent yield seams that can be monolithic and/or homogeneous, i.e., the interface between the layers has been eliminated. This contrasts to sheetings which are seamed with adhesives of a composition different from the parent material. Seams are tested in both peel and shear modes in accordance with methods given in Table 2. In addition, static tests can be run in peel and shear by dead-weight loading. All of these tests can be performed at elevated temperatures, after various aging periods, and after immersion in solvents or in waste liquids as part of EPA Test Method 9090.

Various measurements and observations can be made to assess the quality of the seams. In making an assessment, it is important not only to know the force required to break seams, but also to know the durability of the seam and the manner in which a test specimen of the seam breaks. The quality of a seam can be assessed by the following observations:

- Locus of break--a break in the parent material is desirable, such as a "film tearing bond." Failure at the interface between bonded surfaces is undesirable as it may be indicative of inadequate retention of adhesion on long exposure.
- Time to break when tested under tensile load in the static mode.
- Effects of temperature and other exposures on the magnitude or locus of break.

These observations can be used in setting specifications for seam quality. Laboratory tests should be performed on samples of seams cut from liners installed in the field as part of quality assurance.

Fingerprinting of Geomembranes

Because of the wide range of polymeric geomembranes that may be encountered, analysis and fingerprinting can be useful. For example, the analysis and fingerprinting of a polymeric geomembrane liner that has been tested for compatibility with a given waste liquid in accordance with EPA Test Method 9090 can be used at the time of liner installation for the following purposes:

- As a means of characterizing and identifying the specific sheeting.
- As a baseline for monitoring the effects of exposure on the liner.
- To determine which constituents of the waste liquid were absorbed during the 9090 test and thus could affect the chemical compatibility of the waste and liner in service.

Specific analyses that may be used for fingerprinting are suggested by Haxo (6). Table 2 lists specific test methods for many of these analyses.

TESTING OF GEOTEXTILES

The tests for characterizing geotextiles that have not been exposed to wastes are fully described by Koerner (14). Also, ASTM Committee D35 is developing specific test methods which can characterize the properties associated with the respective functions. Currently used test methods are:

<u>Property</u>	<u>Test method number</u>
Thickness	ASTM D1777 ^a
Mass/unit area	ASTM D3776-84
Percent open area	CWO 22125-86
Permittivity	ASTM D4491
Equivalent opening size	CWO 02215
Puncture	ASTM D3787 (modified)
Burst strength	ASTM D3786
Grab tensile/elongation (wide-width strip)	ASTM D1682 ^b
Ultraviolet resistance	ASTM D4355 ^c
Transmissivity	ASTM D35 Committee Draft, Designation 03.84.02

^a2 kPa loading.

^bSection 16 (Grab test G) using 100 mm x 200-mm sample, 75-mm gauge length, 25-mm wide x 50-mm long grip, strain rate 305 mm/minute, using a constant rate of extension tester.

^c500 hours.

For assessing geotextiles for use in waste containment applications, exposure to waste liquid for four months under EPA Test Method 9090 conditions is suggested. The laboratory performance testing of geotextiles in waste liquids under load poses a problem due to the size of the test specimens and the handling of large amounts

of waste liquids. In our laboratory we have performed compatibility testing of 75 mm x 150-mm geotextile specimens in accordance with ASTM D751 by the grab method. Wet specimens were tested throughout. The unexposed specimens were first immersed in water and then tested. The exposed specimens were dewatered with a roller and then wrapped in a thin polyethylene film and tested. As the elongation properties of the film exceeded that of the fabric, it did not break; thus, the waste liquid was contained.

Performance testing of geotextile/soil systems to determine filter characteristics are reported (15, 16). Martin et al, also performed tests on drainage material/soil systems to study the effects of overburden pressures on transmissivity of geotextiles (17). Raumann conducted similar tests on geogrids (18). Performance tests have also been conducted on geomembrane/geotextile/soil systems to evaluate the frictional coefficient at the material interfaces (14).

TESTING OF DRAINAGE NETS

This group of geosynthetics, which includes geogrids, geonets, and a variety of open constructions, are based primarily on polyethylenes and polypropylenes. As such, some of their attributes are similar to those of polyethylene geomembranes. Geonets that are used for drainage in double-liner systems must maintain their drainage capability over extended periods of time. As these materials are polymeric, they are subject to creep and compression under loads, which will tend to reduce their transmissivity. The polymeric geogrid probably will absorb organic constituents from the waste liquid, which will cause it to soften and lose compressive strength and result in greater creep and further loss of transmissivity. If the lateral mechanical stability decreases, the three-dimensional structure of the net could collapse and lose drainage capacity.

A test that would be indicative of the performance of the geogrid as a drainage medium is to place the geogrid between two stiff liners or plates while in contact with the waste liquid and under load, during which time the transmissivity is measured. It would be expected that the geonet would compress and creep with time. Reduction in transmissivity would be expected, but the magnitude would vary with the material, temperature, load, and chemical absorption; however, no test of this type has yet been developed.

A modified test procedure would involve testing samples of geonet for transmissivity after they have been exposed to a waste liquid. A load that corresponds in magnitude to service conditions would be applied and the transmissivity determined. This procedure would require that the load be applied for a sufficient length of time to allow for creep and compression of the tested sample. If water instead of waste liquid is used to determine transmissivity, some of the organics in the geogrid may leach out and cause changes in the properties of the geonet.

An alternate test procedure which we have followed to measure compatibility of geonets with waste liquids is to immerse samples of geonets for up to four months in a manner similar to that used for geomembranes, and measure such properties as tensile and compression modulus as a function of exposure time. Weight changes, volatiles, and extractables are also measured. Test results are treated similarly to those obtained on geomembranes.

TESTING OF PLASTIC PIPE

A wide variety of test methods for characterizing plastic pipe has been published by ASTM, the Plastic Pipe Institute, the Gas Research Institute, and the National Sanitation Foundation. Due to their good chemical resistance, plastic pipes have found considerable use in the handling of chemicals. However, the resistance can vary considerably from polymer to polymer. In waste containment facilities, PVC and HDPE pipes are used predominately. Nevertheless, pipes have collapsed due to organic solvent absorption and softening of the pipe.

Inasmuch as the leachate collection and leak-detection systems of double liner systems must function for extended periods of time, it is desirable to assess the compatibility of the pipe with the waste liquid. This can be done by exposing sections of pipe in waste liquid under conditions similar to those used in the EPA 9090 test and testing the sections after exposure in accordance with a method selected from ASTM D2412. The size of the pipe, e.g., 150 mm in diameter, and the need for replication may require large tanks and a considerable amount of waste liquid. The relatively large mass of the pipe could absorb considerable portions of the organic constituents in the liquid, resulting in a reduction of their concentrations and the need to replace the waste liquid.

In an alternate procedure which we have conducted, the pipe is tested for tensile properties parallel to the length of the pipe and for compressive modulus of a ring cut through the cross section. In this procedure, two types of specimens cut from the pipe are exposed and tested: cross-sectional rings 25 mm in length and longitudinal strips cut radially and machined to the proper thickness. The strips are tested for weight change, extractables and volatiles, tensile strength, elongation, and modulus of elasticity before and after immersion as in EPA Test Method 9090. The rings are tested in compression before and after exposure to the waste liquid to measure changes in modulus. Also measured are weight and hardness to determine changes in these properties.

DISCUSSION

As yet, maximum changes in properties which correlate with serviceability limits have not been established. Inasmuch as the effects of environmental exposures vary with the polymer, each material would have a separate set of maxima. Expert systems are being evolved by the U.S. Environmental Protection Agency to aid in assessing compatibility of liners and waste liquids (19). However, feedback from the field performance of liners and from testing liners that have been in service is needed to establish correlation between field performance and laboratory testing.

ACKNOWLEDGMENTS

The major portion of the work reported in this paper was performed under Contract 68-03-2173, "Evaluation of Liner Materials Exposed to Hazardous and Toxic Wastes," Contract 68-03-2969, "Long-term Testing of Liner Materials," and Contract 68-03-3213, "Use of Cohesive Energy Determinations for Predicting Membrane/Waste Chemical Compatibility and Service Life Estimates," with the Hazardous Waste Engineering Research Laboratory of the U.S. Environmental Protection Agency, Cincinnati, Ohio.

REFERENCES

1. Giroud, J. P. 1984. Geotextiles and Geomembranes. Geotextiles and Geomembranes, Vol. 1, pp. 5-40.
2. EPA/OSW. 1985. Minimum Technology Guidance on Double Liner Systems for Landfills and Surface Impoundments. EPA 530-SW-85-014, May 24, 1985. U.S. Environmental Protection Agency. Washington, D.C.
3. Mark, H. F., N. G. Gaylord, and N. M. Bikales. 1965-76. Encyclopedia of Polymer Science and Technology--Plastics, Resins, Rubbers, Fibers. Interscience, New York, NY.
4. EPA/OSW. 1984. Method 9090, Compatibility Test for Wastes and Membrane Liners. Noticed in the Federal Register, October 1, 1984, Vol. 49, No. 191, pp. 38792-93.
5. Haxo, H. E., and N. A. Nelson. 1984. Permeability Characteristics of Flexible Membrane Liners Measured in Pouch Tests. In: Proceedings of the Tenth Annual Research Symposium: Land Disposal of Hazardous Waste. EPA-600/9-84-007. U.S. EPA, Cincinnati, Ohio. pp. 230-251.
6. Haxo, H. E. 1983. Analysis and Fingerprinting of Unexposed and Exposed Polymeric Membrane Liners. In: Proceedings of the Ninth Annual Research Symposium: Land Disposal, Incineration, and Treatment of Hazardous Waste. EPA-600/9-83-018. U.S. EPA, Cincinnati, Ohio. pp. 157-171.
7. Haxo, H. E. 1981. Testing of Materials for Use in Lining Waste Disposal Facilities. In: Hazardous Solid Waste Testing, First Conference. eds., R. A. Conway and B. C. Malloy. ASTM Special Technical Publication 760. ASTM, Philadelphia, Pennsylvania. pp. 269-292.
8. Matrecon, Inc. 1983. Lining of Waste Impoundment and Disposal Facilities. SW-870 Revised. U.S. EPA, Washington, D.C. 448 pp. GPO #055-00000231-2.
9. National Sanitation Foundation. 1983. Standard Number 54, Flexible Membrane Liners. National Sanitation Foundation, Ann Arbor, MI.
10. Haxo, H. E., J. A. Miedema, and N. A. Nelson. 1984. Permeability of Polymeric Lining Materials for Waste Management Facilities. In: Migration of Gases, Liquids, and Solids in Elastomers. Education Symposium. Fall Meeting - Denver, Colorado. Rubber Division, American Chemical Society. The John H. Gifford Memorial Library & Information Center, The University of Akron, Akron, Ohio.
11. August, H., and R. Tatzky. 1984. Permeabilities of Commercially Available Polymeric Liners for Hazardous Landfill Leachate Organic Constituents. In: Proceeding of the International Conference on Geomembranes, June 20-24, 1984, Denver, Colorado. Industrial Fabrics Association International, St. Paul, MN. pp. 163-168.

12. Haxo, H. E., R. S. Haxo, N. A. Nelson, P. D. Haxo, R. M. White, and S. Dakessian. 1985. Final Report: Liner Materials Exposed to Hazardous and Toxic Wastes. EPA-600/2-84-169. U.S. EPA, Cincinnati, Ohio. 256 pp.
13. Haxo, H. E., and N. A. Nelson. 1984. Factors in the Durability of Polymeric Membrane Liners. In: Proceedings of the International Conference on Geomembranes, Denver, Colorado. Volume II. Industrial Fabrics Association International, St. Paul, Minnesota. pp. 287-292.
14. Koerner, R. M. 1986. Designing with Geosynthetics. Prentice-Hall, Englewood Cliffs, NJ. 424 pp.
15. Koerner, R. M., and F. K. Ko. 1982. Laboratory Studies on Long-Term Drainage Capability of Geotextiles. In: Proceedings of the Second International Conference on Geotextiles, Las Vegas, NV. Volume I. Industrial Fabrics Association International, St. Paul, Minnesota. pp. 91-96.
16. Koerner, R. M., and J. E. Sankey. 1982. Transmissivity of Geotextiles and Geotextile/Soil Systems. In: Proceedings of the Second International Conference on Geotextiles, Las Vegas, NV. Volume I. Industrial Fabrics Association International, St. Paul, Minnesota. pp. 173-76.
17. Martin, J. P., Koerner, R. M., and J. E. Whitty. 1984. Experimental Friction Evaluation of Slippage Between Geomembranes, Geotextiles, and Soils. In: Proceedings of the International Conference on Geomembranes, Denver, CO. Volume I. Industrial Fabrics Association International, St. Paul, Minnesota. pp. 191-196.
18. Raumann, G. 1982. In-plane Permeability of Compressed Geotextiles. In: Proceedings of the Second International Conference on Geotextiles, Las Vegas, NV. Volume I. Industrial Fabrics Association International, St. Paul, Minnesota. pp. 55-60.
19. Rossman, Lewis A., and H. E. Haxo. 1985. A Rule-Based Inference system for Liner/Waste Compatibility. In: Proceedings of the 1985 Speciality Conference of the American Society of Civil Engineers. ASCE, New York. pp. 583-590.

COIA, M.F.

Roy F. Weston, Inc., U.S.A.

SHERMAN, L.

Fondessy Enterprises, Inc., U.S.A.

HAXO, H.E., Jr.

Matrecon, Inc., U.S.A.

Performance of a Comprehensive Liner System Compatibility Testing ProgramABSTRACT

Fondessy Enterprises, Incorporated (FEI) recently completed a comprehensive program to evaluate the liner system performance of its interim status hazardous waste storage, treatment and disposal facility. FEI engaged Roy F. Weston, Inc. (WESTON) and Matrecon, Inc. to perform a laboratory testing program for chemical compatibility of its designed liner system and leachate conveyance system as well as to conduct a review of existing liner system regulations and a literature review of previous chemical compatibility experiments. This paper describes the results of 120-day immersion testing of the liner system materials (i.e., the 60-mil high density polyethylene (HDPE) flexible membrane liner (FML), the geotextile fabric layers, the geogrid layer and the leachate collection pipe within a synthetic laboratory leachate. The synthetic immersion leachate was comprised of FEI's existing facility leachate spiked with organic chemicals suspected as "aggressive" chemicals to the degradation of FML systems.

U.S. EPA Method 9090 procedures were utilized during the seven-month FEI Compatibility Testing Program. Extreme care was taken during this program to model within the laboratory the response of the FML to chemical exposure. Worse case compatibility conditions were tested by spiking the existing FEI facility leachate with 500 ppm of chlorinated organics (i.e., trichloroethylene and trichloroethane) and 500 ppm of aromatic organics (i.e., benzene, toluene, and xylene or BTX). Modifications were made to the Method 9090 testing cells in order to minimize the loss of volatile organics during exposure. Physical properties and chemical uptake of the FML and other leachate control devices were measured after exposure, and these values were compared with initial material properties.

The compatibility testing results generally indicated that the HDPE liner system was acceptable for use at the FEI hazardous waste facility. The HDPE liners, the HDPE geogrid matrix and leachate collection pipe, and the geotextile fabrics behaved within acceptable ranges of physical properties after chemical exposure.

BACKGROUND

FEI conducted a lining system performance evaluation program to develop information in response to RCRA Part B Permit Application comments by the U.S. EPA, Region V, dated 30 January 1985. A comprehensive information review and compatibility testing process was conducted as illustrated in Figure 1. The major components of this process focused on chemical compatibility of lining systems,

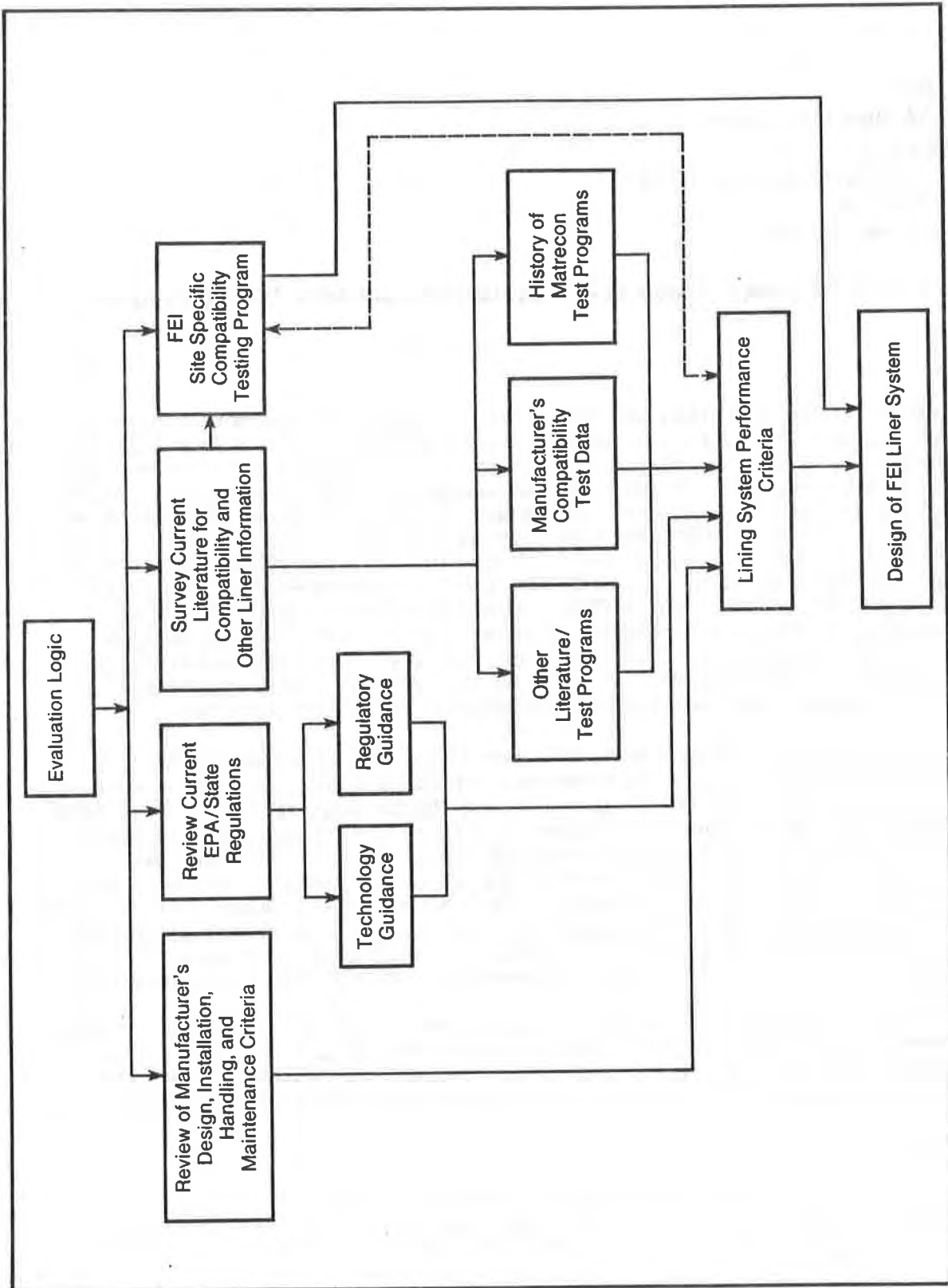


FIGURE 1 LINER SYSTEM EVALUATION MATRIX

including reviews of current regulations and literature as well as performance of the FEI site-specific compatibility testing program.

3

The EPA and Ohio state regulations were reviewed for the latest liner technology and regulatory guidance. Concurrent with a review of liner regulations, an extensive survey of current literature for liner information was conducted. This survey emphasized liner compatibility and included a compilation of existing manufacturer's compatibility test data, and a history of compatibility test programs, including those conducted by Matrecon, Inc. The objective of this survey was to obtain baseline information to aid in the design and development of a site-specific liner chemical compatibility testing program for FEI and to provide supplemental information for developing the liner system performance criteria.

A liner compatibility testing program, designed specifically for the FEI Oregon, Ohio, facility was conducted by Matrecon, Inc., in concurrence with Roy F. Weston, Inc. The objective of this experimental program was to test the chemical compatibility of the FEI liner system materials with a synthetic leachate designed to represent an "aggressive" leachate that could contact the landfill liner and leachate collection/removal system.

OVERALL COMPATIBILITY TESTING PROGRAM

Table 1 outlines the basic components of the FEI waste disposal cell lining system at the Oregon, Ohio facility. The primary leachate control device for the FEI lining system is the flexible membrane liner (FML), composed of 60-mil high density polyethylene (HDPE). The remaining leachate conveyance materials include geotextile fabric layers, geogrid layers, leachate collection pipes, and the sand and gravel packing. The FEI Compatibility Testing Program was performed to demonstrate the effectiveness of these leachate control systems in the presence of an aggressive and potentially degradative waste leachate of more severe quality than the anticipated active facility leachate.

WESTON and Matrecon performed a detailed assessment of the current FEI waste streams and the resulting facility leachate and developed a synthetic laboratory leachate comprised of suspected aggressive organic chemicals to HDPE liners. Leachate from the FEI facility's active Cell H was transported to Matrecon where its chemical composition and solubility characteristics were established. A leachate spiking procedure was developed, and liner compatibility experiments were performed. Development of the spiking procedure, spiking chemicals and concentrations was coordinated by FEI through EPA headquarters for concurrence.

U.S. EPA Method 9090 procedures ("Compatibility Test for Wastes and Membrane Liners") were utilized during the FEI Compatibility Testing Program, where each component of the leachate conveyance system was put into exposure with the synthetic leachate for 120 days during controlled laboratory experiments. The established Method 9090 procedures were developed for the U.S. EPA and are outlined in SW-846, "Proposed Sampling and Analytical Methodologies for Addition to Test Methods for Evaluating Solid Waste: Physical/Chemical Methods", and SW-870, "Lining of Waste Impoundment and Disposal Facilities". The Method 9090 procedures were published in Federal Register, October 1, 1984, Volume 49, No. 191.

TABLE 1
FEI WASTE DISPOSAL CELL LINING SYSTEM

<u>LINER SYSTEM COMPONENT</u>	<u>MATERIAL</u>	<u>DESIGN</u>
1. <u>Natural Subgrade</u>	In-situ native clay	90% Proctor Compaction 10 ⁻⁷ cm/sec permeability
2. <u>Secondary Composite Liner</u>		
o Recompacted Clay	Excavated grey-blue clay from site	Minimum of 36 in. thick 10 ⁻⁷ cm/sec permeability; 95% Proctor Compaction
o Secondary Liner	HDPE Liner	60-mil thickness
3. <u>Secondary Leachate Collection</u>		
o Leachate Collection Zone	Sand & Gravel; HDPE Leachate Pipes	12 inches thick
o Geotextile	Drainage/Filter Fabric	Promotes in-plane leachate transmissivity
4. <u>Primary Composite Liner</u>		
o Recompacted Clay	Excavated grey-blue clay from site	24 inches thick; 10 ⁻⁷ cm/sec permeability; 95% Proctor Compaction
o Primary Liner	HDPE Liner	60-mil thickness
5. <u>Primary Leachate Collection</u>		
o Leachate Collection Zone	Sand & Gravel; HDPE Leachate Pipes	12-18 inches thick
o Geotextile	Drainage/Filter Fabric	Promotes in-plane leachate transmissivity
o Protective Layer	Soil/Clean Waste	6 inches thick
6. <u>Side Slope Flow Zone</u>	HDPE Geogrid Mesh	Promotes in-plane leachate transmissivity

FEI believes that this Compatibility Testing Program is the most comprehensive study of HDPE liners to date. Extreme care was taken during this program to model within the laboratory the response of the FML to chemical exposure. Existing facility conditions were tested using FEI's Cell H leachate, and worse case conditions were tested by spiking this leachate to produce an aggressive chemical leachate for 9090 testing. Spiking was performed using chlorinated and aromatic organic chemicals, including Trichloroethylene (TCE), and 1,1,1-Trichloroethane (TCA), as well as Benzene, Toluene, and Xylene (BTX). The U.S. EPA was involved with the early development of this Compatibility Testing Program by establishing leachate spiking requirements for chlorinated and aromatic chemicals, as well as spiking concentrations. Standard EPA Method 9090 procedures were followed in the laboratory, and special care was taken to develop and incorporate experimental steps to minimize the loss of volatile organics during the program. Physical properties and chemical uptake of the FML and other leachate control devices were measured after exposure, and these values were compared with initial material properties.

Table 2 highlights the Method 9090 physical tests and analytical measurements performed as part of the FEI Lining System Compatibility Testing Program. Physical properties were measured before and after exposure to the aggressive chemical leachate, and leachate quality was analyzed throughout the program to ensure that the worst case synthetic leachate was maintained during experimental conditions.

Two synthetic test solutions were prepared by spiking the active FEI facility Cell H leachate. These included:

- o Baseline Test Leachate: Cell H leachate was spiked with 250 mg/l or ppm each of TCE and TCA to achieve a final 500 ppm level of chlorinated organic spike as well as with 167 ppm each of benzene, toluene and xylene (BTX) to achieve a final 500 ppm level of aromatic organic spike. This test leachate was used during the Baseline Compatibility Program where each of the liner system components was tested with 120-day Method 9090 experiments.
- o Supplemental Test Leachate: Cell H leachate spiked with TCE, TCA and BTX at the solubility limit for each chemical. This test leachate was selected as a worse case condition for the disposal cell, where chemical leaching from hazardous wastes will be limited by the solubility characteristics of the chemicals. Laboratory experiments were conducted to assess the solubility of each chemical in the Cell H leachate, and this test leachate was used during a short-term 30-day Supplemental Compatibility Program where the Gundle 60-mil HDPE liner was evaluated.

In conducting FEI's Liner System Compatibility Program, Matrecon and WESTON worked in close cooperation to insure development and performance of comprehensive testing procedures. While testing of the HDPE membranes was performed in accordance with the U.S. EPA's Method 9090 procedures, the following general additions to specified procedures were required to conduct FEI's overall Program:

- o Exposure testing procedures were conducted for the geotextile fabrics, geogrid, leachate collection pipe, and sand and gravel aggregates. No standardized testing protocols had been previously established for these materials.

TABLE 2
FEI LINER SYSTEM COMPATIBILITY PROGRAM
METHOD 9090 EXPERIMENTS

6

<u>Test/Measurement</u>	<u>2 Liners</u>	<u>Geotextile Fabrics</u>	<u>Geogrid</u>	<u>Pipe</u>
1) Pre-Test GC/MS Leachate Analysis	X	X	X	X
2) Gauge Thickness	X	X	X	X
3) Mass	X	X	X	X
4) Length and Width	X	X	X	X
5) Tear Resistance (Machine and Transverse Directions)	X			
6) Puncture Resistance	X			
7) Tensile Properties (Machine and Transverse Directions)	X	X	X	X
8) Hardness	X			X
9) Elongation at Break	X	X	X	X
10) Compressibility			X	
11) Post-Test Leachate Analysis	X	X	X	X
12) Materials Uptake of Organics (GC Analysis)	X	X	X	X

NOTE: All tests were performed after 30, 60, 90, and 120 days exposure; pre-test GC/MS analyses were performed each period; cell leachate was replaced each period with freshly spiked leachate.

- o Immersion leachate was changed monthly to ensure exposure of materials to the maximum concentrations of synthetic leachate constituents.
- o Fresh leachate was spiked with a mixture of organic solvents (chlorinated and aromatic hydrocarbons) at the beginning of each monthly exposure period. The spiking mixture was added to the individual immersion test cells.
- o Synthetic leachate from selected immersion cells was analyzed by gas chromatography before spiking, after spiking, and at the end of each exposure period in order to characterize the synthetic leachate and to track the presence of the organic solvent spiking chemicals.
- o The volatile and extractable organics content of the HDPE membrane samples was measured before and after exposure in order to evaluate chemical uptake characteristics of the liner material.
- o The immersion test cells, as well as stirrers, were made of 316 stainless steel and sealed with Teflon gaskets to reduce the loss of volatiles. Volatile losses were reduced further by maintaining a zero headspace in each cell.

METHOD 9090 COMPATIBILITY TESTING PROCEDURES

Apparatus

The Method 9090 procedure for FEI's Compatibility Program involved the use of standard stainless steel exposure cells (immersion tanks) with a liquid capacity of approximately 5.2 gallons and with provisions for supporting liner specimens so that they could not touch the bottom or sides of the tank or each other. The immersion tanks were sealed to minimize volatile organic losses during the testing periods, and the synthetic leachate levels were maintained completely filled to eliminate the presence of a head space within the apparatus. The tanks were equipped with the means for slowly stirring the leachate to provide continuous agitation within the tank and to minimize the potential for layered phase separation of the synthetic leachate. Tank temperatures were thermostatically controlled to maintain testing conditions of either 23°C or 50°C. Some evaporation took place during the study, especially within the elevated temperature exposure tanks, but this was controlled through use of leachate-filled standpipes which supplied additional synthetic leachate as necessary. Figure 2 illustrates the exposure testing cells used during the FEI Compatibility Testing Program.

Liner Compatibility Testing

Physical properties testing was performed on samples of the unexposed liner materials prior to compatibility experiments as well as the samples after chemical immersion. Matrecon tested representative samples of each of the liner system materials as received, to determine their baseline physical properties. Physical properties testing for this FEI study included all of the Method 9090 procedures as well as modifications developed by Matrecon to expand the standard U.S. EPA methodology. Table 3 describes a comparison

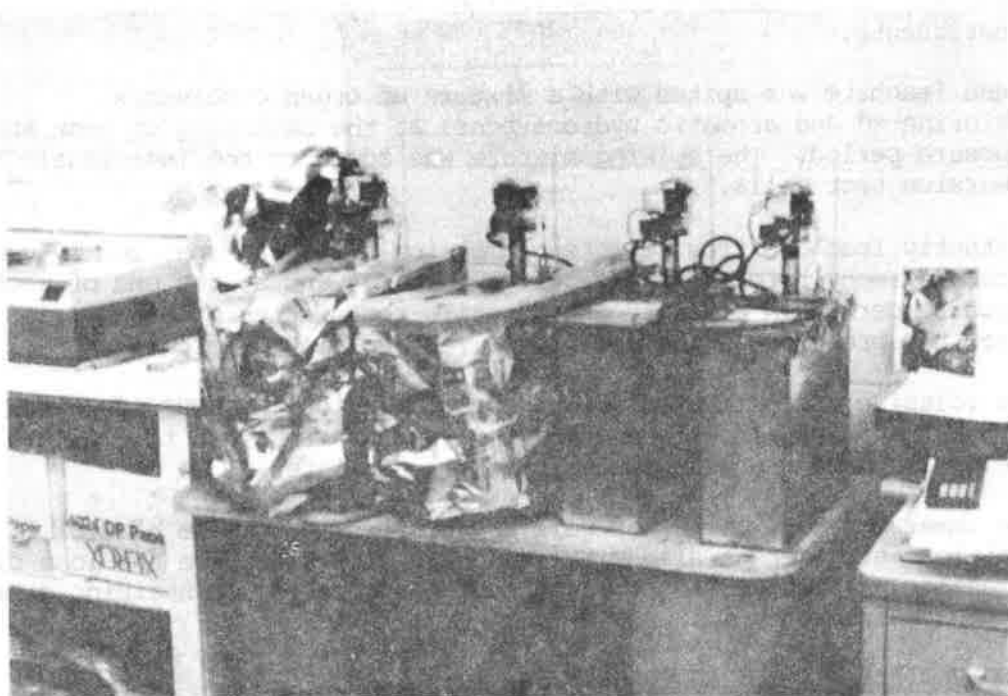


FIGURE 2 IMMERSION TESTING APPARATUS FOR FEI STUDY

between the standard Method 9090 procedures and the comprehensive Compatibility Testing Program conducted for FEI. It should be noted that the additional experimental procedures were performed along with the required Method 9090 testing to augment the Compatibility Program by describing the chemical characteristics and chemical uptake properties of the liner materials as well as the modulus of elasticity and specific gravity properties.

At the end of the liner/leachate exposure (i.e. after 30, 60, 90, and 120-day exposure periods), the specimen sheets were removed from the test cells for analysis of their physical and chemical properties. Waste leachate and/or precipitates were removed from the specimens, allowing them to be rinsed well with deionized water. This procedure was a necessary experimental preparation and decontamination step to comply with testing procedures and OSHA standards to protect the health and safety of analytical personnel. Die cutting and sample punching operations were then performed according to prescribed patterns, and the cut specimens were immediately placed in labeled polyethylene bags to prevent them from drying out and to minimize volatile organic losses. Exposed sample testing was performed shortly after the cutting operations as follows:

- o Analysis of volatiles and extractables content of the liner samples to determine the concentration of chemicals taken up by the specimens during exposure. Matrecon performed MTM1 and MTM2 procedures to assess percentages of total volatiles and extractables, respectively. WESTON performed GC/MS analysis of the liner samples to determine chemical-specific concentrations absorbed in the liner sheets.
- o Physical testing of the specimens after exposure were conducted in the same manner as described in Table 3.

Formulate the Synthetic Leachate

Formulation of the FEI synthetic leachate represented the culmination of nearly a year's research and experimentation. FEI utilized the recommended approach cited in a memorandum from Chris Rhyne of U.S. EPA, Washington, D.C. to James Brossman of U.S. EPA, Region V (30 January 1985 EPA Memorandum) as well as existing laboratory testing results of HDPE compatibility studies (Gundle, National Seal, and Matrecon testing) to develop the proposed synthetic leachate for its Compatibility Program (1 March 1985 FEI proposal to U.S. EPA, Region V). The U.S. EPA recommendation was to combine the present Cell H leachate with aggressive compounds listed in RCRA Appendix VIII, where "aggressive" was taken to mean that the chemicals may have an adverse effect upon the HDPE liner material.

The U.S. EPA memorandum (30 January 1985) ruled out the need to test all inorganic compounds in the FEI synthetic leachate, including strong acids and bases, due to the known inertness of HDPE to these chemicals. Existing liner manufacturers and Matrecon testing results confirm this conclusion. Therefore, only organic chemicals were considered by FEI for use in its spiking solution to formulate a representative synthetic leachate. Based upon the FEI review of existing compatibility testing data, two classes of organic chemicals were identified which could potentially cause absorption and swelling of the HDPE material, thereby weakening an HDPE liner system.

TABLE 3

LINER SYSTEM COMPATIBILITY STUDY FOR FEI WASTE STREAM
COMPARISON OF METHOD 9090 AND MATRECON PROCEDURES

<u>TEST PROPERTIES</u>	<u>TEST METHOD 9090 (Basis of Program)</u>	<u>MATRECON PROCEDURE (Used During FEI Program)</u>
<u>TESTING OF LEACHATE</u>		
1. Chlorinated Organics	<u>Not Required</u>	WESTON GC and GC/MS
2. Aromatic Organics	<u>Not Required</u>	WESTON GC and GC/MS
<u>TESTING OF UNEXPOSED MEMBRANE LINERS</u>		
1. Volatiles	<u>Not Required</u>	NTM* 1 & WESTON GC/MS
2. Extractables	<u>Not Required</u>	MTM 2 & WESTON GC/MS
3. Tear Resistance	ASTM D1004	ASTM D1004
4. Puncture Resistance	FTMS 101B, Method 2065	FTMS 101B, Method 2065
5. Tensile Properties	ASTM D638	ASTM D638
6. Hardness	ASTM D2240	ASTM D2240
7. Modulus of Elasticity	<u>Not Required</u>	ASTM D992, Modified
8. Specific Gravity	<u>Not Required</u>	ASTM D792
9. Thermogravimetric Analysis	<u>Not Required</u>	MTM TGA
<u>TESTING APPARATUS</u>		
1. Exposure Tanks	<u>Not specified, but with stirring plus reflux condensor</u>	316 Stainless steel, sealed with Teflon seal gasket, with stirring, with leachate level controls
<u>EXPOSURE CONDITIONS</u>		
1. Temperature	23°C and 50°C	23°C and 50°C
2. Duration Tests	120 days (30, 60, 90, and 120-day periods)	120 days (30, 60, 90 and 120-day periods)
3. Spike Leachate with Aggressive Chlorinated Organic Chemicals	<u>Not Required</u>	500 ppm concentration of aggressive chlorinated organics (TCE and TCA)
4. Spike Leachate with Aggressive Aromatic Organic Chemicals	<u>Not Required</u>	500 ppm concentration of aggressive aromatic organics (BTX chemicals)

*MTM refers to Matriecon Test Method

TABLE 3 (continued)

LINER SYSTEM COMPATIBILITY STUDY FOR FEI WASTE STREAM
COMPARISON OF METHOD 9090 AND MATRECON PROCEDURES

<u>TEST PROPERTIES</u>	<u>TEST METHOD 9090 (Basis of Program)</u>	<u>MATRECON PROCEDURE (Used During FEI Program)</u>
<u>HANDLING OF SPECIMEN AFTER EXPOSURE</u>		
1. Liner Samples	Cool slab for 1 hour in fresh waste at room temperature; then rinse and place in bag until test	Allow cell to cool to room temperature before opening; then rinse well with water and place in bag; minimize time to testing
<u>TESTING OF EXPOSED MEMBRANE LINERS</u>		
1. Volatiles	<u>Not Required</u>	MTM 1 & WESTON GC/MS
2. Extractables	<u>Not Required</u>	MTM 2 & WESTON GC/MS
3. Tear Resistance	ASTM D1004	ASTM D1004
4. Puncture Resistance	FTMS 101B, Method 2065	FTMS, 101B, Method 2065
5. Tensile Properties	ASTM D638	ASTM D638
6. Hardness	ASTM D2240	ASTM D3340
7. Modulus of Elasticity	<u>Not Required</u>	ASTM D882, Modified
<u>TESTING OF LEACHATE COLLECTION SYSTEM</u>		
1. Physical Testing of Geotextile Fabrics after Exposure	<u>Not Required</u>	Tensile properties and elongation at break.
2. Physical Testing Geogrid after Exposure	<u>Not Required</u>	Tensile properties and elongation at break
3. Physical Testing of Leachate Collection Pipe after Exposure	<u>Not Required</u>	Tensile properties, hardness, elongation at break, and compressibility
4. Physical Testing of Aggregate (Fine and Coarse Aggregate) After Exposure.	<u>Not Required</u>	Grain size analysis and material dissolution into leachate.

These included halogenated or chlorinated hydrocarbons and aromatic hydrocarbons. Table 4 provides an overall comparison of the existing Cell H leachate composition with the two synthetic test solutions used for the FEI compatibility testing program. As the table indicates, the testing solutions contained chlorinated and aromatic organic constituents in the range of 3-5 orders of magnitude greater concentrations than those presently within FEI's facility leachate. 12

FEI COMPATIBILITY STUDY CONCLUSIONS

The FEI Liner System Compatibility Program results generally indicated that the HDPE liners, the HDPE geogrid matrix and leachate collection pipe, and the geotextile fabrics behaved within acceptable ranges of physical properties after chemical exposure. Considering the conservative test conditions for the FEI Compatibility Program, the liner system and leachate control components are considered appropriate for the proposed hazardous waste management application as described within the FEI Part B permit application.

FEI performed a state-of-the-art compatibility study for their liner system and leachate control components. The Program required considerable method development to describe the compatibility of the geotextile fabrics, geogrid matrix and the leachate collection pipe. Conservative procedures were applied when developing a synthetic leachate and performing the exposure testing. Some of the key activities which describe the conservative nature of this research-oriented compatibility study are outlined below:

METHOD 9090 REQUIREMENTS	MEETS REQUIREMENTS	EXCEEDS REQUIREMENTS
Use representative leachate	Yes	Performed tests with Cell H leachate spiked with 500 ppm of chlorinated organics and 500 ppm aromatic organics.
Perform 30, 60, 90 and 120-day exposure	Yes	Performed exposure testing with all liner system components (i.e. geotextiles, geogrid, pipe, and aggregate materials) Performed volatile and extractable organic analyses on the exposed liner samples. Performed rigorous additional test of the Gundle liner with highly concentrated synthetic leachate.

TABLE 4

COMPARISON BETWEEN CELL H AND CONSERVATIVE SYNTHETIC LEACHATES
FEI LINER SYSTEM COMPATIBILITY STUDY

<u>CHEMICAL CONSTITUENT</u>	<u>CELL H LEACHATE CONCENTRATION mg/l</u>	<u>BASELINE TEST SYNTHETIC LEACHATE(1) mg/l (% Increase)</u>	<u>SUPPLEMENTAL TEST SYNTHETIC LEACHATE(2) mg/l (% Increase)</u>
Trichloroethylene	0.6 - 1.9	250 (13 x 10 ³)	500(3) (26 x 10 ³)
Trichloroethane	2.7 - 8.0	250 (3 x 10 ³)	520 (6 x 10 ³)
Benzene	0.2 - 0.3	167 (56 x 10 ³)	1400 (467 x 10 ³)
Toluene	0.01 - 6.0	167 (3 x 10 ³)	910 (15 x 10 ³)
Total Xylenes	0.005 - 3.0	167 (5 x 10 ³)	6000 (200 x 10 ³)

- (1) Baseline tests performed on all FEI Liner System components during 120-day compatibility Method 9090 program.
- (2) Supplemental tests performed with Gundline HDPE Liner.
- (3) TCE solubility concentration found to be 120 mg/l or ppm in FEI leachate.

Previous Method 9090 testing work has generally utilized existing leachate, surface impoundment liquids or other dilute solutions. For this program, additional research was conducted with HDPE liners using highly concentrated chemicals in order to identify any "aggressive" chemicals which may adversely affect HDPE. These aggressive materials were further tested in aqueous solutions up to their solubility limits in an attempt to identify critical concentration ranges. Existing research to date has not been successful in developing design correlations to predict liner failures, and liner evaluations have focused on the expertise of the materials testing laboratory. To this end, FEI chose Matrecon, a recognized leader in the field of liner testing, to complete its Liner System Compatibility Program.

FEI's Test Program not only met the Method 9090 requirements for compatibility testing in the normal range of expected leachate values, but also performed the testing using aggressive synthetic leachates with chemical concentrations greatly exceeding the actual facility leachate values. This is one of the first times that Method 9090 testing with spiked leachates has been attempted and should be considered as a model for future revisions to existing compatibility testing procedures. The use of a range of aggressive leachate concentrations makes evaluation and approval of a liner for use in containment possible with a high degree of certainty.

From the information described herein and the Matrecon evaluations of the test results, it should be concluded that the FEI Compatibility Program was very conservative. The testing values were determined to be within or near guidelines for acceptable liner performance, indicating that the FEI liner system materials are compatible with the leachate currently generated at the facility and with the aggressive synthetic leachate which could reflect any future changes in leachate quality. As demonstrated within the results, the Gundline 60-mil HDPE liner, after 120 days of exposure, performed in excess of any known criteria or proposed guidelines. The National Seal liner also performed well under exposure, with the possible exception of the elongation at yield physical parameter. The elongation at yield parameter is most important during liner installation and the initial placement of waste materials. Since these sitework activities will precede actual waste/liner exposures, this physical property is not believed to be a major concern at the FEI facility. The geogrid matrix, geotextile fabric, and leachate collection pipe components have been evaluated under this Compatibility Program, and no important degradation of physical properties which could impair their function has been identified.

LANDRETH, R.E.

United States Environmental Protection Agency, U.S.A.

The EPA Testing Program for Components of Treatment, Storage, and Disposal Facilities

INTRODUCTION

Land disposal continues to be a popular and economical method for disposing of hazardous wastes. Though poor practices in the past have led to significant environmental problems, today's properly designed, constructed, and operated, land disposal facility can ensure that wastes will not be a source of health and environmental concern for many decades. In November 1984, the Hazardous and Solid Waste Amendments (HSWA) of 1984 were signed into law. Liners and leachate collection components are required for surface impoundments and waste piles under Section 3004(0) and 3015 of the Resource Conservation and Recovery Act (RCRA) as amended by the HSWA minimum technological requirements for hazardous waste landfills. Among these provisions are:(1)

- o New units and lateral expansions and replacements including all types of treatment, storage and disposal facilities, must be double-lined and must have leachate collection systems, and
- o New units and lateral expansions and replacements at interim-status waste piles must meet the requirements for single liners and leachate collection.

The U.S. Environmental Protection Agency (EPA) has published two documents establishing minimum technology guidance on single and double liner systems.(2),(3) These documents provide guidance for owners/operators and regulatory personnel on design, construction, and operation of systems believed by the Agency to meet the requirements of Sections 264.221(a), 264.251(a), and 264.301(a) of RCRA. This guidance also identifies specifications that can be used by owners/operators to meet the above requirements for HSWA.

This paper discusses some of the tests required by the Agency to evaluate the adequacy of liner and leachate collection materials. These laboratory tests subject the candidate materials to the physical, biological, and chemical stresses that are intended to duplicate conditions found in a treatment, storage, or disposal facility (TSDF). Some unresolved testing concerns are also discussed.

CURRENT TESTING PROTOCOLS

The more common testing programs for liners and leachate collection components evaluate their physical properties before and after exposure to the liquids being contained.

Method 9090

Method 9090 incorporates an elevated temperature to accelerate the potential chemical attack.⁽⁴⁾ Physical properties are measured before exposure and 1, 2, 3, and 4 months after exposure. Data from exposures at room temperature and at elevated temperature are compared to detect any change or rate of change in the physical property values caused by exposure. Rejection criteria values based on the amount of change cannot be given since the change affects the performance of different materials in different ways and to different degrees.

The use of Method 9090 by testing and development companies has generated questions regarding materials testing. Among these questions are the following:

- (1) Should environmental stress cracking (ESC) be added to Method 9090?
- (2) Should the leachate be changed during the immersion period?
- (3) What other liner and leachate collection system components are required by current regulations to be compatible with wastes?

The Agency has offered supplementary guidance on these question in Directive No. 9480.00-13.⁽⁵⁾

-Including Environmental Stress Crack

Testing for ESC is not currently included in Method 9090. However, recently reviewed data and discussions with technical experts, including polymer manufacturers, have re-emphasied the need to require an ESC test for crystalline and semicrystalline polymeric membrane liners. Stress cracking tests such as ASTM A 1693-70⁽⁶⁾ accelerate physical failure by starting with a standard incision and measuring its propagation. The Standard warns against using the results of ESC tests in direct engineering applications, since they do not quantitatively determine the effect of exposure on material strength. Though other tests have been suggested to evaluate ESC, the use of ASTM D-1693-70 by the manufacturers and testing companies remains the test of choice due to the large data base developed over the years. The Agency is reviewing Method 9090 and is considering ESC test methods. Until specific ESC tests are developed to simulate conditions at a TSDF, the Agency encourages the owner/operator to conduct the D-1693 test.

-Changing the Leachates

Changing of the leachates during the exposure of candidate materials is another issue addressed by Directive No. 9480.00-13. The question centers around the concern that some of the constituents in the leachate may be volatile or have an affinity for the candidate materials being tested. Since most TSDF's release leachate that is generally consistent in chemical composition, the owner/operator must assure that the chemical composition of the leachate used for testing remains relatively constant during the test to provide a representative environment for specimens being immersed. The owner/operator must also attempt to seal the immersion vessel as tightly as possible to prevent a loss of volatiles. In addition, the concentrations of leachate chemicals that are suspected to affect the sample (e.g., aliphatic and halogenated hydrocarbons) must be checked during the exposure time to ensure that the leachate composition does not change significantly. If the constituents change

significantly, the owner/operator should replenish the leachate frequently enough to assure that the liner samples are experiencing exposure conditions similar to those in the field.

-Chemical Compatibility of Other System Components

Directive No. 9480.00-13 also addresses other system components that need to be evaluated for chemical compatibility. Section 264.301(a)(2) of RCRA requires that the leachate collection and removal system be constructed of materials that are chemically resistant to the waste managed at the TSDF. Suggested general procedures for meeting this requirement include testing of plastic piping, geotextiles, and earthen materials, as follows:

1. Plastic piping - Plastic piping should be prepared for strength testing per ASTM D 2412 or its equivalent. At least one prepared sample should be subjected to the same immersion test as performed on the liner material (e.g., the immersion test outlined in Method 9090). After the immersion test, the pipe sample should be dried (per Method 9090) and subjected to a strength test (see especially ASTM D 2412, paragraphs 6-9). Testing of a control specimen (a sample not subjected to the immersion test) should be performed. A report should be prepared similar to that outlined in ASTM D 2412 paragraph 11 (including 11.1.7 and 11.1.9) comparing the test results of the immersed and control samples.
2. Geotextiles - Geotextiles can be used to perform any of three major functions in the land disposal unit: (1) protection of the flexible membrane liner, (2) filtration, or (3) transmission of liquid (water or leachate). Testing procedures for a given geotextile depend on its function. When the geotextile is used either as a filter or as a protective medium for the flexible membrane liner, it should receive immersion testing like that for flexible membrane liners. After any immersed specimens are dried, they and the identical control specimen(s) should be subjected to the ASTM D 1682 grab strength test and the ASTM D 751 puncture strength test to determine whether a significant loss of strength has occurred.

Synthetic materials used for leachate drainage (e.g., nets) should also be immersed in the expected waste/leachate. Following immersion, both a control specimen and the immersed specimen should be tested for in-plane transmissivity. No ASTM method presently exists to evaluate in-plane transmissivity, but the Federal Highway Administration's Geotextile Engineering Manual references a technique by Koerner and Bove.⁽⁷⁾ This or another method can be used to compare the in-plane transmissivity of the immersed specimen with that of a control specimen.

The transmissivity test should include the following conditions:

- (1) The pressure exerted on the geotextile should be at least 1.5 times the maximum expected pressure to be experienced during the active life and post-closure period of the unit.
- (2) The geotextile should be placed in the apparatus under expected field conditions--that is, both sides of the geotextile should be placed against the materials experienced in the field (e.g., soil, sand, gravel, flexible membrane liner, or other geotextile).

3. Earthen materials - When rock or gravel is used as drainage material in the leachate collection system, the owner/operator should verify that the mineral content of the rock is compatible with the waste/leachate mixture. The owner/operator will need to demonstrate that the rock will not be dissolved or form a precipitate that would clog the leachate collection system.

Soil used as a liner or a component of a composite should be subjected to EPA Method 9100 using the expected leachate to determine its effect on the hydraulic conductivity of the compacted, low-permeability soil. The owner/operator may use the fixed-wall or triaxial test.

A wide range of compositions and constructions has been reported for the same generic liner.(8) This range may be the result of changes made in the basic formulations to meet a specific exposure requirement, changes made in the base polymer as a result of manufacturing processes, or other factors. Regardless of the reason for the change, generic names are insufficient to identify a liner material. This fact becomes extremely important when materials used in TSD's have had extensive compatibility testing and the design is based on the properties of a specific material. The potential for change in composition between the time of testing and construction forms the basis for a "fingerprint" test procedure. A procedure outlined by Haxo(9) can provide valuable information to characterize and identify a specific material. The information then serves as a baseline for monitoring the effects of exposure on the liner and helps assess the aggressive nature of leachate constituents. The recommended procedure includes the following analyses for liners before and after exposure: volatiles, ash, extractables, gas chromatography, thermogravimetric analysis, differential scanning calorimetry (crystalline materials), and specific gravity. The results of these analyses can be used to demonstrate that the liner material tested for chemical compatibility in Method 9090 is the same as that being installed at a TSD--even if the testing and installation are separated by a significant time period. The results could also be compared with the results of period similar tests of exposure coupons to determine whether changes in the liner properties are occurring during laboratory exposure to leachate. Thus the liner performance could be monitored for early warning of potential liner failure. The results of the fingerprint analysis could also be used to identify aggressive leachate constituents that are attacking the liner. Such constituents could then be removed from the waste stream.

FUTURE TESTING

Recognizing that no laboratory test fully duplicates field exposure, the Agency is constantly reviewing and developing procedures to produce laboratory results that will correlate with field performance. The ideal procedure would be to have a short-term test that predicts the performance for several hundred years. The performance would be predicted for both chemical resistance and physical stresses to which the liner components would be subjected during the active life of the facility and post-closure period.

Some consideration has been given to stressing components during the Method 9090 test procedure. Harwell Laboratory(10) used elevated temperature and weighted sample specimens to produce a stress condition during chemical compatibility testing. Steffen(11) has suggested that field conditions are better simulated when the component is stressed during exposure. Since the material actually experiences stress e.g., during settlement or placement of the wastes, during the site life, it

is logical to add this condition to current procedures. Details of stressing the liner materials during exposure must still be developed, and additional research is required to interpret the results.

After the initial disposal unit at a given site has been tested by Method 9090 coupon testing(12) may be used as an alternative to Test Method 9090 for subsequent disposal units built at the site, providing the waste characteristics do not change. Exposure coupons in the leachate sump area of landfills or directly in surface impoundments are probably more representative of actual field conditions than most laboratory tests. However, the large number of sample specimens for the liner and drainage collection materials will almost certainly require a large area for testing. Also, the agitation of the leachate in the sump must be taken into account. Since the temperature in the sump area will most likely be near ground temperature (i.e., approximately 55°F), the time of sample exposure should be extended longer than the exposure time of Method 9090. Method 9090 currently does not require exposure temperatures of 55°F because longer exposure times would be required. Though some work has been completed on acceleration of aging with increased temperatures, few data are available on the effects of lowering the temperature and reducing the time required to produce a given change at these temperatures.

Concern exists over the quality of the data that are being submitted to EPA for review of Part B permits. Decisions need to be made about developing and running a laboratory testing certification program. Standards are not generally available to perform round-robin tests or to evaluate variances in test procedures or between laboratories. Though the Agency has limited resources for this research, EPA remains very interested in the subject area.

Probably the single most important issue raised in the overall testing program--and one about which the Agency is very concerned--is that of data interpretation. Because only a few individuals can interpret the data accurately and predict chemical compatibility based on short-term exposures, the Agency has assembled some of this expertise in a computer system. This system can be used by both owners/operators and the regulatory community. The system is part of an artificial intelligence program made up of discrete computer-based, user-friendly programs that incorporate the knowledge, experience, and expertise of those individuals who analyze TSDf components. The liner chemical compatibility system(13) is now being readied for verification testing. The success of this project will provide consistent permit reviews, save time and money, and synthesize large amounts of expert, heuristic knowledge into a form that can help determine the adequacy of various technical interpretations and best engineering judgments.

SUMMARY AND CONCLUSIONS

Testing of liners and leachate collection components should be performed to duplicate the conditions of actual containment systems. EPA has presented test protocols that represent the conditions to which construction materials will be subjected. The Agency continuously reviews these protocols and develops new procedures to improve the ability to predict what will actually happen in the environment.

Current test protocols include Method 9090, which uses elevated temperature to accelerate the potential chemical attack. Tests for chemical compatibility should be performed on liners as well as other system components, including plastic piping, geotextiles, and earthen materials. A "fingerprinting" procedure can provide valuable information for characterizing and identifying a specific material.

Future testing may include an environmental stress crack test for crystalline and semicrystalline polymeric membrane liners stressing of components during the Method 9090 test, coupon testing at certain sites, and a computer system that incorporates the knowledge, experience, and expertise of individuals who analyse TSDf components.

REFERENCES

1. USEPA (1985). Guidance on Implementation of the Minimum Technological Requirements of HSWA of 1984, Respecting Liners and Leachate Collection Systems. Reauthorization Statutory Interpretation #5. Washington, D.C.: U.S. Environmental Protection Agency. USEPA 530/SW-85-012.
2. USEPA (1985). Minimum Technology Guidance on Single Liner Systems for Landfills, Surface Impoundments and Waste Piles - Design, Construction and Operation. Washington, D.C.: U.S. Environmental Protection Agency. USEPA 530/SW-85-013.
3. USEPA (1985). Minimum Technology Guidance on Double Liner Systems for Landfills - Design, Construction and Operation. Washington, D.C.: U.S. Environmental Protection Agency. USEPA 530/SW-85-014.
4. USEPA (n.d.). Method 9090. Washington, D.C.: USEPA Office of Solid Waste.
5. USEPA (1986). Supplementary Guidance on Determining Liner/Leachate Collection Compatibility. Washington, D.C.: USEPA Office of Solid Waste and Emergency Response, Directive No. 9480.00-13, August 7, 1986.
6. ASTM (1985). ASTM Standard Testing Method for Environmental Stress-Cracking of Ethylene Plastics. ASTM D1693-70 in Annual Book of ASTM Standards. Philadelphia, PA: American Society for Testing and Materials.
7. Koerner, R. M. and Bov, J. A. (1983). In-Plane Hydraulic Properties of Geotextiles. *Geotextile Testing Journal*. GTJODJ 6(4):190-195.
8. USEPA (1983). Lining of Waste Impoundments and Disposal Facilities, Cincinnati, OH: U.S. Environmental Protection Agency, USEPA SW-870, NTIS PB81-166-365.
9. Haxo, H. E., Jr. (1983). "Analysis and Fingerprinting of Unexposed and Exposed Polymeric Membrane Liners," Proceedings of the Ninth Annual Research Symposium: Land Disposal of Hazardous Waste. Cincinnati, OH: U. S. Environmental Protection Agency, EPA 600/9-83-018, pp. 157-171.
10. Smith, A. S. and Parker, A. (1979). Comparison of the Durability of Potential Landfilling Lining Materials - Results of Accelerated Tests. Harwell Laboratory, Harwell, England.
11. Steffen, J. (1984). "Report on Two Dimensional Strain Stress Behavior of Geomembranes With and Without Friction." Proceedings of the International Conference on Geomembranes, Denver, CO, June 20-24, 1984. St. Paul, MN: Industrial Fabrics Association International.
12. Tratnyek, J., et al. (1985). Proposed Methodology for Removable Coupons Testing. Washington, D.C. Contract No. 68-02-3968, Task 36.
13. USEPA (in preparation). Feasibility of Using Expert System for Determining Liner/Waste Chemical Compatibility. Cincinnati, OH



SESSION 6B

OTHER GEOSYNTHETIC APPLICATION

WILLIAMS, N.D.

Georgia Institute of Technology, U.S.A.

HOULIHAN, M.F.

Law Environmental Services, U.S.A.

Evaluation of Interface Friction Properties Between Geosynthetics and Soils

Interface friction parameters were evaluated for 35 surfaces, 7 soils and 5 geosynthetics. The friction parameters were measured using a modified direct shear friction device under boundary conditions which approximate typical field conditions. Descriptions of the equipment and methodology used to perform the analyses are presented. The results of the analyses indicate 3 primary modes of failure: sliding between the soil and geosynthetic, sliding on a failure surface in the soil or sliding between multiple layers of geosynthetics. The location of the sliding surface and magnitudes of the interface friction parameters are primarily a function of the surface roughness, type and elastic modulus of the geotextile; the type, composition, grain size, density and water content of the soil; and the confining stress and stress history.

1.0 INTRODUCTION

The interface friction parameters between soils and geosynthetics are used in the design of many engineering works. In solid or hazardous waste landfills (Figure 1A), the consolidation of the waste induces movement of the waste relative to the geomembrane. Or, if the geomembrane is restrained, deformation between the geomembrane and the soil. As the deformation progresses, increased shear stress is mobilized at the interface between the soil and the geomembrane. The stability of the slope is largely a function of the interface shear strength. The stability of composite landfill covers (Figure 1B) on slopes is a function of the interface friction properties between the vegetative cover layer and the relatively thin nonwoven geotextiles separating the vegetative cover layer from the synthetic drainage layer or sand drainage layer. As the soil moves down the slope, shear stresses are mobilized on each of the interfaces in the drainage layer. The mobilized interface shear stress must be large enough to support the soil layer if the slope is stable.

In many areas new embankments or embankment extensions are constructed over soft subgrades (Figure 1C). In many cases this construction would not be possible without the tension reinforcement provided by a geosynthetic placed at the interface between the embankment and the soft soil or waste subgrade. Nonwoven and woven geotextiles and geogrids have all been successfully installed in embankments over soft subgrades. As the embankment is placed over the geosynthetic, settlements occur in the subgrade. If the subgrade is very soft, the settlements may be very large. As settlement occurs, the geosynthetic elongates, mobilizing shear stress between the geosynthetic and the subgrade. Continued loading results in an increase in shear stress at the interface and an increase in the tension force mobilized in the geosynthetic. These forces resist additional displacements making it possible to construct relatively high embankments over very weak subgrade materials.

Reinforced walls (Figure 1D) utilize multiple layers of geosynthetics to provide tension reinforcement. Woven and nonwoven geotextiles and geogrids have all been successfully installed in reinforced walls. As the wall deflects away from the soil mass shear stress is mobilized at the interface between each sheet and the adjacent soil. This shear stress allows tension forces to be mobilized in the geosynthetic.

In railroad embankments (Figure 1E) two types of geosynthetics have been used to maintain rail alignment. In new track installation, thick nonwoven geotextiles may be used at the interface between the new ballast and the existing subgrade. As the ballast is placed and compacted displacements occur in the soil subgrade, resulting in shear stress mobilization between the ballast and the geotextile. These shear stresses mobilize tension forces in the geotextile which resist lateral deformation of the ballast under live loads.

When track maintenance is performed, the top 30 to 45 cm (12 to 16 inches) of fouled ballast is typically removed. A geosynthetic may be placed above the fouled ballast prior to placement of the new ballast. A thick nonwoven is typically used in areas where the ballast is relatively shallow and where the ballast is fouled by the penetration of the subgrade clay or silt soils. In areas where the ballast is relatively thick, geogrids or thick nonwoven geotextiles may be used. In these areas, the use of higher modulus materials may be beneficial because less strain is induced in the geosynthetic during placement. Since the strains are smaller, a higher modulus material should be utilized to mobilize equivalent tension forces in the geosynthetic.

Geosynthetics may also be used to improve the performance of unpaved roads (Figure 1F). Nonwoven and woven geotextiles and geogrids have all been successfully installed in unpaved roads. The geosynthetic is typically placed above the subgrade soil and covered with a thin layer of granular soil. The soil is then tracked and compacted by the construction equipment. This tracking causes ruts to form in the soil subgrade, inducing large strains in the geosynthetic. As the geosynthetic elongates, shear stresses are mobilized at the interface between the soil or embankment and the geosynthetic. These shear stresses cause tension forces to be developed in the geosynthetic which in turn resist additional deformation in the subgrade soils.

While these engineering works are quite dissimilar in application, they all use interface friction properties for design. These interface friction properties may be measured in either a direct shear test or a pullout test, depending on the desired boundary conditions. This paper described the direct shear testing device, discusses the methodology employed for analysis of the interface friction parameters and presents the results of direct shear friction analyses between several geosynthetics and several types of soils.

2.0 BACKGROUND

The direct shear device applies a normal stress across a soil/geosynthetic interface. A horizontal load is then applied to a soil layer inducing movement of the soil relative to the geosynthetic. The horizontal load may be applied using either stress control or strain control methods. Stress control friction analyses are typically used to model construction or transient loading conditions. Strain control friction analyses are used to measure interface friction parameters for static and long term stability analyses.

The direct shear device has been used in soil mechanics for many years to evaluate the internal friction angle and cohesion of soils on a prescribed sliding surface or failure plane. A conventional direct shear device typically uses a soil mold which is 5 to 6.5 cm in diameter by 5 to 10 cm in height. The displacement rates vary considerably between devices but are typically in the range of 0.1 mm/min to 100 mm/min.

In a fine grained soil, the deformation required to mobilize the peak and residual shear stresses is a function of the average particle diameter and the confining stress. This deformation is typically in the range of 0.3 to 1.0 cm. When soils are displaced relative to a very rough geosynthetics the deformation required to mobilize the residual shear stress is in the range of 2 to 7 cm. Therefore, when evaluating the interface friction parameters between soils and geosynthetics the contact area in the shear box needs to be much larger than the contact area of the shear box in a conventional direct shear device for soils. Most direct shear devices used to measure the interface friction parameters between soils and geosynthetics have a contact area of at least 0.3 by 0.3 m.

Direct shear devices have been used by several investigators to evaluate interface friction parameters between soils and geosynthetics. A summary of the available soil/geosynthetic interface friction data is presented in Table 1. The table provides a brief description of the direct shear devices used in the analyses, the compaction data and grain size data for the soils, and the soil/geotextile interface parameters. It is apparent from the data in Table 1 that two sets of boundary conditions have been employed in the analyses. Myles (1982), Degouette (1986) Martin et.al. (1984) and Miyamori (1986) placed the soil on only one side of the geotextile. The other side of the geotextile was then glued to a plate. Saxena et al. (1986) placed soil on both sides of the geosynthetic. The boundary conditions used in the analyses by Formazin et al (1986) were not described.

3.0 EQUIPMENT

The direct shear apparatus (Figure 2) at the Georgia Institute of Technology is designed to evaluate the interface shear strength for a soil/geosynthetic composite. The device reproduces the field conditions in order to model the factors contributing to the interface shear strength. Since the friction analysis models field conditions, it is considered a design test. The friction analyses should be performed using the site soil, placed and compacted in a manner which simulates field conditions.

The direct shear device has a relatively large shear box, 30.5 cm by 30.5 cm (12 inches by 12 inches) in order that the large strains required to cause sliding at the soil/geosynthetic interface do not induce inordinately large and unaccountable boundary effects. A force is applied perpendicular to the sliding surface by a pneumatic piston and yoke, which is mounted on linear ball bushings to reduce the inherent friction in the device. The bottom soil layer is attached to the table and does not move during the test. The horizontal force is applied to the top box by another pneumatic piston device. The horizontal and vertical forces acting on the specimen during the test are measured by electronic load cells and signal conditioning equipment. The maximum normal stress which can be applied by the device is in the range of 0 to about 100 kPa (2000 psf).

Deflection of the top soil box results from the lateral force applied by lateral piston device. Figure 3 shows the pressure application system. The analyses may be performed at a constant stress by applying the pressure directly into the piston device, or at a constant rate-of-strain by introducing a constant flow of oil into the piston. This constant rate of inflow is controlled by a needle valve and, since oil is relatively incompressible, provides a constant rate of flow through the needle valve orifice and thus a constant rate of deformation. Deformation rates may be varied from approximately 0.003 to 3.0 mm/min (0.0001 to 0.01 in/min) on this device (in the strain control mode). Displacement of the top soil box relative to the lower box is measured with a dial gage or LVDT. All tests conducted for this project were performed at a constant rate-of-strain.

Due to the low total stress capacity of the system, the apparatus is best described as compliant. That is, the stress builds up slowly until the peak stress is reached, at which point there is a sliding along the weakest plane in the system at a constant rate-of-strain. The slow buildup of stress in the system induced under the strain - control option makes it possible to determine the peak stress, which corresponds to the static coefficient of friction, and the residual stress, which corresponds to the dynamic coefficient of friction.

4.0 APPROACH

Friction characteristics were determined for 35 interfaces, using seven different soils and five different geosynthetics. The geosynthetics were chosen to give a representative sampling of surface textures of products commonly used in current engineering practice. The soils were chosen to give a wide range of soil characteristics in order to evaluate the influence of soil properties relative to the interface frictional characteristics.

4.1 Soils

4.1.1 Ottawa 20/30 Sand. This soil is a quartzite, rounded to well rounded, highly

uniform sand, with a uniformity coefficient of 1.3 and a USCS classification of SP. All of the sand passes the No. 20 sieve and is retained on the No. 30 sieve (0.6 to 0.85mm diameter). The sand was compacted to a density of 1.57g/cm^3 (98 pcf), with a relative density of about 95%. The soil was placed, compacted and tested in a dry state.

4.1.2 Concrete Sand. This soil is a limestone sand, with subrounded to subangular particles. It has a USCS classification to of SW, and was compacted to a dry density of 1.51g/cm^3 (94 pcf) which corresponds to a relative density of 95%. The sand has a uniformity coefficient of 4. The concrete sand was placed, compacted, and tested in a dry condition.

4.1.3 Glacial Till. The glacial till was obtained from the region of southern Illinois. It is a composite of gravel to silt-size particles and a large percentage of non-plastic clay particles created during glacial advance and recession. The soil has approximately 60% fines but is basically nonplastic (Plastic Limit (PL) = Liquid Limit (LL) = 17). The soil has a Modified Proctor maximum dry density of 2.22g/cm^3 (138 pcf), an optimum moisture content of 7.5% and has a USCS classification of ML. The glacial till was compacted 2% wet of optimum at a dry density of 2.18g/cm^3 (133 pcf).

4.1.4 Saprolite. This soil is a residual soil typical of the piedmont region of the Southeastern United States. This soil, as do most residual soils, has a true cohesion in-situ, but no cohesion upon remolding. The soil is a subangular to angular medium to fine sand with a small (0.5% - 1%) percentage of mica. The uniformity coefficient of the saprolite is 2 and the USCS classification is SP. The soil is nonplastic and has a Modified Proctor maximum dry density of 1.62g/cm^3 (101 pcf) at an optimum moisture content of 12%. The saprolite was compacted at 2% wet of optimum moisture content at a dry density of 1.55g/cm^3 (97 pcf).

4.1.5 Gulf Coast Clay. This soil is a medium-plasticity, marine deposited clay from the South Louisiana area. It has a Plasticity Index (PI) of 14, a Modified Proctor maximum dry density of 1.84g/cm^3 (115 pcf) at an optimum moisture content of 15.5%, and a USCS classification of CL. The clay was compacted at 2% wet of optimum moisture content and a dry density of 1.78g/cm^3 (111 pcf). At the time of testing, the void ratio was 0.74 and the degree of saturation was 63%.

4.1.6 Ottawa 20/30 Sand - 5% Bentonite. This soil is a laboratory mixture of sand and Bentonite clay. The PI is 20 and the Modified Proctor maximum dry density is 1.76g/cm^3 (110 pcf) at an optimum moisture content of 9%. The clay adds some plasticity to the soil but does not completely fill the voids. The void ratio at the time of testing was 0.70 and saturation was 43%. The soil was compacted at 2% wet of optimum at a dry density of 1.70g/cm^3 (106 pcf).

4.1.7 Ottawa 20/30 Sand - 10% Bentonite. This soil is also a laboratory mixture of sand and Bentonite clay. The PI is 27 and the Modified Proctor maximum dry density is 1.91g/cm^3 (119 pcf) at 12.6% moisture content. The void ratio at time of testing is 0.64 and the degree of saturation is 62%. This soil was also compacted at optimum plus 2% moisture content to a dry density of 1.84g/cm^3 (115 pcf).

4.2 Synthetics

4.2.1 Trevira 1155. A Nonwoven, continuous filament polyester geotextile from Hoechst Fibers Industries. The tensile strength is 92 kN/m (525 lbs/in) in the machine direction.

4.2.2 Typar 3401. A nonwoven, heat bonded, continuous filament polypropylene geotextile from DuPont. The grab tensile strength is 26 kN/m (150 lbs/in) in the machine direction.

4.2.3 Nicolon 900-M. A woven, polyester geotextile from Nicolon with a wide width tensile strength of 165 kN/m (950 lb/in) and a tensile modulus of 550 kN/m (3167 lb/in).

4.2.4 Polyvinyl Chloride (PVC). A smooth, 30-mil thick PVC membrane from Staff Indus-

tries. The grab tensile strength is 32 kN/m (183 lb/in).

4.2.5 High Density Polyethylene (HDPE). A smooth, 60-mil HDPE from Gundle Lining Systems. The grab tensile strength is 63 kN/m (360 lb/in) and the elastic modulus is 800,000 kPa (110,000 psi).

5.0 SOIL TESTING

All soils used in this testing program were individually tested for Atterberg limits, compaction characteristics, grain size distribution, and shear strength in direct shear. The soils were tested in direct shear at the same moisture content, density, and normal load used during the analysis for frictional characteristics at soil/synthetic interfaces. The test results are tabulated in Table 2. The shear strengths of the soils were measured using a conventional direct shear device (6.25 cm diam.). At the deformation rates employed in the analyses, excess pore pressures may have developed in the Gulf Coast Clay Specimen resulting in a low friction angle and high cohesion measurements.

6.0 METHODOLOGY

The direct shear friction test is used to evaluate the design interface friction parameters between layers of soil and geosynthetics. The soil and geosynthetic are placed in the device under the boundary conditions which approximate field conditions. To perform the analysis, the soil is compacted in the bottom box at the desired moisture content and density. Then, the geosynthetic(s) is trimmed to about 30.5 X 46 cm (12 by 18 inches) and placed above the soil as shown in Figure 4. The soil is then compacted in the upper soil box, also at the desired moisture content and density.

Two mounting procedures may be used to perform the direct shear friction analysis between soils and geosynthetics. First, the geosynthetics may be placed unanchored between the two soil boxes (Figure 4A). This configuration is used when sliding is expected to occur along the interface of interest. The second mounting procedure involves anchoring the geosynthetic(s) as shown in Figure 4B. This configuration may be necessary to induce sliding along a surface with a higher shear strength.

After the specimen has been placed in the device the top portion of the shear box is attached to the yoke, as shown in Figure 2. The normal loads, which were 890, 1110 and 2225 Newtons (100, 250 and 500 lbs. respectively) for this testing program, are then applied using a pressure regulator and piston device. Once the normal load has been applied, the oil reservoir is pressurized to 1670 kPa (80 psi) using the high-pressure regulator (see Figure 3).

The needle valve is then adjusted to provide the desired rate-of-strain, and the three-way-valve is set to strain control. The horizontal displacement (HDG) and horizontal load are then monitored for the duration of the test. When the desired load, either peak or residual, is reached the pressures in the system are released, the soil is removed and recompacted, and the system is reconfigured for the next desired normal stress.

7.0 DATA REDUCTION

The interface coefficient of friction, which is tabulated in Table 3, is the dynamic coefficient of friction at a strain rate of approximately 0.3 mm/min (0.01 in/min). The residual stress during sliding is obtained from the graph of shear stress versus strain. The coefficient of friction at the interface is evaluated from a graph of the residual shear stress as a function of the applied normal stress (see Figure 5). The residual shear stress is calculated as follows:

$$\gamma = \frac{T - f}{A} \quad (1)$$

Where, T = The horizontal load (F),

- f = The device friction (F),
- A = The contact area between the sliding layers at the interface (L^2),
- τ = The shear stress (FL^{-2}).

The contact area between the sliding layers at the interface varies as a function of time because the top portion of the shear box slides relative to the bottom portion of the shear box. The contact area at any instant in time is evaluated using the horizontal displacement:

$$A = A_i - (W)HDG \quad (2)$$

- Where,
- A_i = The initial contact area at the beginning of the analysis (L^2),
 - W = The width of the specimen (L), and
 - HDG = The horizontal displacement (L).

The normal stress, σ , is equal to the vertical load, N, divided by the contact area, A. The coefficient of friction, u, is the slope of the best fit straight line when the residual shear stress is plotted versus the corresponding normal stress. The interface friction angle, δ , is computed as follows:

$$\delta = \tan(u) \quad (3)$$

The intercept of the best fit straight line is the adhesion at the interface. The adhesion, a, is the shear stress at the interface when the normal stress is zero. Even though the adhesion contributes to the shear stress and friction mobilized at the interface, the adhesion may be neglected or reduced in stability evaluations.

8.0 RESULTS OF FRICTION ANALYSES

The results of the 35 friction analyses are shown on Table 3. These results are analyzed to give a quantitative assessment of sliding on the different interfaces and a qualitative assessment of general trends in soil-geosynthetic interface shear strength.

Three types of sliding surfaces may develop during the direct shear friction analysis:

- 1) Sliding along the interface between the soil and the geosynthetic. This sliding surface develops under low confining stresses and when very smooth, relatively stiff geosynthetics are evaluated against granular soils.
- 2) Sliding along a failure surface which develops in the soil parallel to the geosynthetic layer. This sliding surface develops during most of the direct shear analyses.
- 3) Sliding along a failure surface which develops in the the geosynthetic. This failure surface commonly develops when multiple layers of geosynthetics are evaluated as discussed in Williams and Houlihan (1986).

8.1 Interface Shear Failure Results

Sliding occurred on the interface between the soil and the geosynthetic for the HDPE versus all soils, the PVC versus the fine grained soils and Typar 3401 versus the granular soils. For this type of sliding surface the primary modes of frictional resistance are sliding of the soil grains against the surface of the geosynthetic and rolling of granular soil grains on the surface of the geosynthetic. The shear strength at the interface for this type of sliding surface is primarily a function of the smoothness, tensile strength and modulus of the geosynthetic, the soil type and water content and the confining stress.

An 80 mil HDPE sheet with a high tensile strength and modulus was used in the analyses. At the normal stresses used in this testing program, the soils did not penetrate into the polyethylene sheet. Therefore, sliding along the surface was the primary mode of failure.

The interface shear strength was lower than the shear strength of the adjacent soil for all soils tested. The Sand-Bentonite mixtures gave a lower interface shear strength than the HDPE vs Ottawa Sand alone, primarily because the clay particles obscured the sand particle contacts with the HDPE sheet. We anticipate that, for a completely saturated clayey soil, a horizontal failure envelope would develop with an unconsolidated-undrained type of failure mode.

The PVC material exhibited a higher shear strength than the HDPE versus similar soils except for tests against the Gulf Coast Clay. Also, adhesion values were typically higher for tests of soil against the PVC. The PVC has a lower elastic modulus than the HDPE resulting in embedment of the soil particles in the surface of the synthetic. This causes higher shear stresses to be mobilized at the interface.

Sliding at the soil/geotextile interface also occurred between Typar 3401 and the sandy soils. Typar 3401 is a heat-bonded polypropylene geotextile with a relatively smooth surface and a comparatively high elastic modulus. The mechanism of failure for sands versus this material was primarily sliding and rolling.

8.2 Soil Sliding Surface Friction Results

Sliding on a failure surface which develops in the soil parallel to the geosynthetic was the primary sliding surface for the Trevira 1155 and Nicolon versus all soils and Typar 3401 versus the cohesive soils. For sliding in the soil the primary modes of frictional resistance are dilation, interlock, rolling and sliding of the soil grains on the sliding surface, and adhesion. The shear strength on the soil sliding or failure surface is primarily a function of the roughness and modulus of the geosynthetic; the type, grain size, grain size distribution, structure, fabric, void ratio, density and water content of the soil; and the state of stress and stress history.

The Trevira 1155 is a thick, continuous filament nonwoven polyester geotextile with a pliable texture, which has a rough texture on a soil-particle size scale. The voids in the textile surface are large enough for silt to clay-sized and fine to medium sand-sized particles to become lodged in the geotextile matrix. This causes the shear stress applied to the system to be transferred from the surface of the geotextile into the adjacent soil layer. This is evidenced by the high interface friction parameters for Trevira 1155 relative to all of the soils tested. The soil sliding surface developed at a distance of approximately 0.04 to 0.32 cm from the surface of the geotextile.

The Nicolon 900-M geotextile is a woven fabric with a distinctly rugged surface caused by the weave pattern. The depth of the undulation of the weave is large enough to constrict the sliding of clay and sand-sized particles over the surface of the geotextile. This induces a failure in the soil similar to that induced by the Trevira 1155. However, since the surface texture is significantly rougher, there is less contribution of sliding and rolling to failure and more contribution due to dilation of soil particles. This effect is most pronounced in sands. Therefore, the interface shear strength for Nicolon 900-M versus sands was significantly higher than for the sands versus any other fabric. For all soils, the shear strength of the system approached the shear strength of the adjacent soil. The soil sliding surface developed at a distance of about 0.04 to 0.32 cm from the surface of the geotextile.

Typar 3401 induced a partial soil failure in the Glacial Till, Gulf Coast Clay, and Saprolite soils. In these soils, the particle sizes are significantly smaller than for the other soils, allowing some interlock of the fabric with the smaller soil particles. This resulted in some component of dilation and rolling, which increased the strength of these systems. However, since sliding along the surface predominated as a mode of failure, the strength values of Typar 3401 were lower than those for Trevira 1155 and Nicolon 900-M.

9.0 CONCLUSIONS

The following conclusions and observations are developed as a result of the friction

analyses for the materials evaluated.

- 9.1 For the sandy soils, geosynthetics with very rough surfaces shift the sliding surface into the adjacent soil, resulting in a higher interface friction angle.
- 9.2 For the cohesive soils, geosynthetics with moderately rough surfaces were sufficient to shift the sliding surface into the adjacent soil layer.
- 9.3 Adhesion is primarily a function of the soil type, soil water content and density, and the surface roughness of the geosynthetic.
- 9.4 The interface friction angle is primarily a function of soil type and void ratio, surface roughness of the geosynthetic, confining stress, type of geosynthetic, and tensile strength and modulus of the geosynthetic.
- 9.5 Total displacements required to mobilize residual interface friction values may be on the order of 2 to 7 cm or more for thick geosynthetics with rough surfaces.
- 9.6 At very low confining stresses, the failure surface is typically between the soil and geosynthetic since little interlock occurs.
- 9.7 At intermediate confining stresses, the sliding surface is typically in the soil adjacent to the geosynthetic, parallel to the outermost location of the geosynthetic. The distance of this failure surface varies but is typically 0.04 to 0.32 cm from the surface of the geosynthetic. The higher the offset distance, the more sensitive the results to the size of the specimen.
- 9.8 The conventional direct shear device (6.25 cm diameter) should not be used to evaluate interface friction parameters between soils and most geosynthetics due to the large deformations required to mobilize the residual shear stress.
- 9.9 The difference between peak and residual interface friction angles likely results from changes in the soil void ratio during shear.
- 9.10 For clay soils and nonwoven geotextiles, the interface friction angle may increase and the adhesion decrease during the analyses at intermediate and high confining stresses due to consolidation of the soil adjacent to the geotextile.
- 9.11 Multiple anchorage methods may be required to evaluate the interface friction parameters on the high shear strength interfaces of multiple layer systems.
- 9.12 The interface friction angle and the adhesion are strain rate dependent. In general, the higher the strain rate, the higher the interface friction angle and the adhesion.
- 9.13 In the range of 0.03 to 3.0 mm/min, the interface friction parameters are relatively insensitive to the strain rate.
- 9.14 For highly cohesive soils which are near complete saturation, the rate of deformation during testing should be slow enough to allow complete dissipation of excess pore pressures.

TABLE 1. INTERFACE FRICTION VALUE FROM EXISTING LITERATURE

REFERENCE	DEVICE DESCRIPTION	GEOSYNTHETIC	S (σ)	a (kPa)	SOIL DESCRIPTION	φ (°)	c (kPa)	$\frac{c}{\sigma}$ (kn/m ²)	w (%)	
Mylon, B. (1982)	Conventional Shear Box	Heat Bonded Polypropylene Polyethylene	40	0	Fine Sand (0.1 to 0.2 mm)	48	0	—	DRY	
		Heat Bonded Polypropylene	42	0						
		Light Weight Woven Polypropylene	42	0						
		Heat Bonded Polypropylene, Polyethylene	38	0	Fuel Ash	44	0	—	DRY	
			Needle Punched Polypropylene	38						0
			Light Weight Woven Polypropylene	40						0
		Heat Bonded Polypropylene, Polyethylene	38	0	Coarse Sand (0.2-1.0 mm)	46	0	—	DRY	
			Needle Punched Polypropylene	44						0
			Light Weight Woven Polypropylene	40						0
	DIRECT SHEAR DEVICE Area = 0.3 by 0.3 m Soil Depth = 10 to 12 cm Soil One Side Displacement Rate = 10 to 75 mm/min Normal Stress = 30, 50, 300 kPa	Needle Punched Polypropylene	35.5	0	Leighton Burnard Sand (0.8 to .85 mm)	38	0	—	DRY	
Heat Bonded Polypropylene Polyethylene		34	0							
Heavy Polyester Woven		38	0							
Light Polyester Woven		32	0							
Polished Steel		28	0							
Miyamoto, T., Iwai, S. and Makiuchi, K. (1986)	DIRECT SHEAR Area = 0.3 by 0.3 m Soil Depth = 12.0 cm Soil One Side Displacement Rate = 0.5 mm/min Normal Stress = 0-200 kPa	Needle Punched & Resin Bonded Polyester	37	12	River Sand G = 2,867 Cu = 1.83 e = 1.00 s = 0.85	44	0	18	DRY	
		Needle Punched Polypropylene	41	0						
		Needle Punched & Resin Bonded Polyester	35	2		35	0	14.5	DRY	
		Needle Punched Polypropylene	32	4						
		Needle Punched & Resin Bonded Polyester	33	2		32	0	18	8	
		Needle Punched Polypropylene	34	0						

REFERENCE	DEVICE DESCRIPTION	GEOSYNTHETIC	δ [deg]	α [kPa]	SOIL DESCRIPTION	θ [deg]	c [kPa]	γ_s [kN/m ³]	w [%]
Martin, J.P., Koerner, R.M., & Whitty, J.E. [1984]	DIRECT SHEAR Area = 0.1 by 0.1 m Soil Depth = 2.54 cm SOIL ONE SIDE Displacement Rate = .127 mm/min Normal Stress = 14 to 100 kPa	EPDM FML	24	0	Concrete Sand $d_{10} = 0.20$ mm, $C_u = 2.6$	24	0	90 % Standard Proctor (ASTM D898)	Saturated
		PVC (Rough) FML	27	0					
		PVC (Smooth) FML	25	0					
		CSPE FML	25	0					
		HDPE FML	18	0					
		Crown Zellerbach 800	30	0					
		Type 3401	28	0					
		Polyfilter X	28	0					
		Miraf 500 X	24	0					
		EPDM FML	20	0					
		CSPE FML	21	0	Ottawa Sand $d_{10} = 0.42$ mm $C_u = 1.8$	28	0	90 % Standard Proctor (ASTM D898)	Saturated
		HDPE FML	18	0					
		Crown Zellerbach 800	28	0					
		Miraf 500 X	24	0					
		EPDM FML	24	0	Mica Silted Silty Sand (SM) $d_{10} = 0.057$ $C_u = 5.1$	28	0	90 % Standard Proctor (ASTM D898)	Saturated
PVC (Rough) FML	25	0							
PVC (Smooth) FML	21	0							
CSPE FML	23	0							
HDPE FML	17	0							
Crown Zellerbach 800	25	0							
Miraf 500 X	23	0							
Saxena and Budiman [1988]	DIRECT SHEAR Area = .25 x .25 m Soil Depth = .27 to 7.6 cm Soil Two Sides Displacement Rate = 0.78 mm/min Normal Stress = 72-288 kPa	Celanese 800 X	14	14	45% OS, 5% Bent. 50 % Kaolinite	12.8	7.8	17.8	Saturated
		Monanto C-34	15	22					
		Celanese 800 X	24	50	Limestone	40	0	20	Saturated
		Monanto C-34	8	100					
Formazin and Batareu [1988]	Shear Box	Nonwoven	35	0	$d_{50} = 0.2-2$ mm = 2-5 mm = 5-10 mm	---	---	---	Saturated
			31	0					
			27	0					
		Woven	31	0	$d_{50} = 0.2-2$ mm = 2-5 mm = 5-10 mm	---	---	---	Saturated
			27	0					
			22	0					
Degoutte and Mathieu [1988]	Direct Shear Area = 3m x 0.3m Soil Depth = 15cm Normal Stress = 200-1200 kPa Soil One Side	Geotextile	38	---	Sand $d_w/d_{10} = 2$, $d_{50} = 0.3$	38	0	---	Dry
		PVC	38.5	---		38	0	---	Saturated
		PVC	38.5	---		38	0	---	Dry
		Geotextile	38	---	Sandy Clay $PL = 13\%$	33.5	50	---	12.5
		PVC	35	---		33.5	50	---	12.5
		Direct Shear Area = 5cm x 5cm Normal Stress 200-800 kPa	Geotextile	34	---	Sand $d_w/d_{10} = 2$ $d_{50} = 0.3$ mm	38	0	---
	34			---	38		0	---	Dry
	22.5			---	38		0	---	Dry

TABLE 2. SUMMARY OF SOIL TEST RESULTS

SOIL	USCS CLASSIFICATION	ATTERBURG LIMITS			COMPACTION CHARACTERISTICS			SHEAR TEST RESULTS		
		LL	PL	PI	γ_{max} [KN/m ³]	w _{opt} [%]	D100	u [-]	ϕ [deg]	c [kPa]
Ottawa Sand	SP	—	—	NP	—	—	104	0.78	38	0
Concrete Sand	SM	—	—	NP	—	—	100	0.72	38	—
Ottawa Sand/2% Bentonite	BP	38	18	20	17.1	10.0	—	0.73	38	—
Ottawa Sand/10% Bentonite	SP	47	20	27	18.7	13.3	—	0.73	38	—
Saprolite	SP	—	—	NP	15.8	12.0	—	0.71	38	—
Gulf Coast Clay	CL	42	28	14	18.1	15.5	—	0.38	20	57
Glacial Till	ML	17	17	NP	21.7	7.5	—	0.73	38	31

TABLE 3. RESULTS OF FRICTION ANALYSES

TEST NUMBER	SLIDING SURFACE	μ [-]	δ [deg]	σ [kPa]
1	Ottawa Sand/HDPE	0.35	19	0.8
2	Ottawa Sand/PVC	0.48	28	0.3
3	Ottawa Sand/Typar 3401	0.47	26	0.8
4	Ottawa Sand/Trevira 1155	0.53	28	1.4
5	Ottawa Sand/Nicolon 800-M	0.68	35	0.0
6	Concrete Sand/HDPE	0.51	27	0.7
7	Concrete Sand/PVC	0.85	33	0.8
8	Concrete Sand/Typar 3401	0.50	27	0.8
9	Concrete Sand/Trevira 1155	0.68	34	1.2
10	Concrete Sand/Nicolon 800-M	0.70	35	1.2
11	Sand-5% Clay/HDPE	0.28	14	0.8
12	Sand-5% Clay/PVC	0.35	19	0.8
13	Sand-5% Clay/Typar 3401	0.41	22	0.8
14	Sand-5% Clay/Trevira 1155	0.51	27	1.4
15	Sand-5% Clay/Nicolon 800-M	0.80	31	1.1
16	Sand-10% Clay/HDPE	0.30	17	0.8
17	Sand-10% Clay/PVC	0.35	19	0.7
18	Sand-10% Clay/Typar 3401	0.41	22	0.8
19	Sand-10% Clay/Trevira 1155	0.52	27	1.4
20	Sand-10% Clay/Nicolon 800-M	0.68	34	0.1
21	Saprolite/HDPE	0.38	21	0.4
22	Saprolite/PVC	0.53	28	0.5
23	Saprolite/Typar 3401	0.54	28	0.8
24	Saprolite/Trevira 1155	0.58	30	1.5
25	Saprolite/Nicolon 800-M	0.59	31	1.5
26	Gulf Coast Clay/HDPE	0.47	25	1.0
27	Gulf Coast Clay/PVC	0.42	23	1.8
28	Gulf Coast Clay/Typar 3401	0.62	38	1.3
29	Gulf Coast Clay/Trevira 1155	0.88	45	1.8
30	Gulf Coast Clay/Nicolon 800-M	0.88	43	2.0
31	Glacial Till/HDPE	0.41	22	0.7
32	Glacial Till/PVC	0.48	25	1.0
33	Glacial Till/Typar 3401	0.85	33	0.4
34	Glacial Till/Trevira 1155	0.75	37	0.5
35	Glacial Till/Nicolon 800-M	0.70	35	2.5

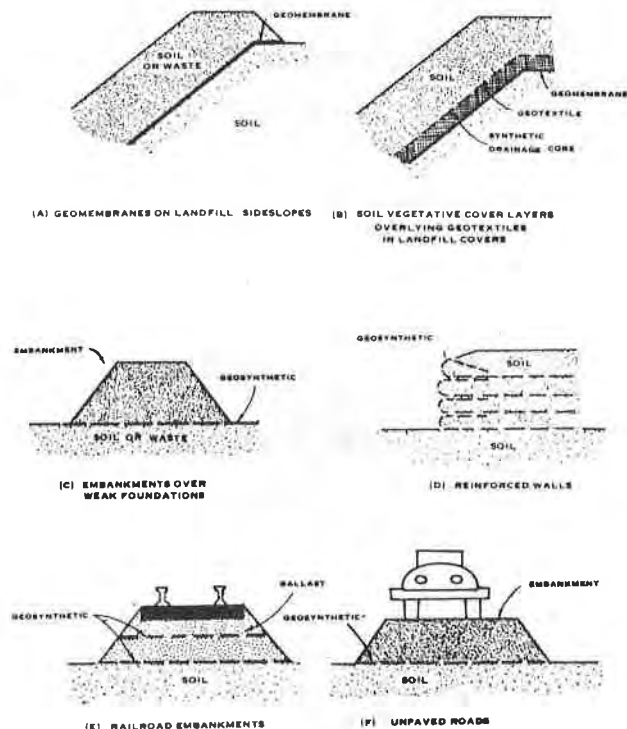


FIGURE 1. COMMON EXAMPLES OF THE APPLICATION OF INTERFACE FRICTION PROPERTIES FOR THE DESIGN OF GEOSYNTHETICS IN ENGINEERING WORKS

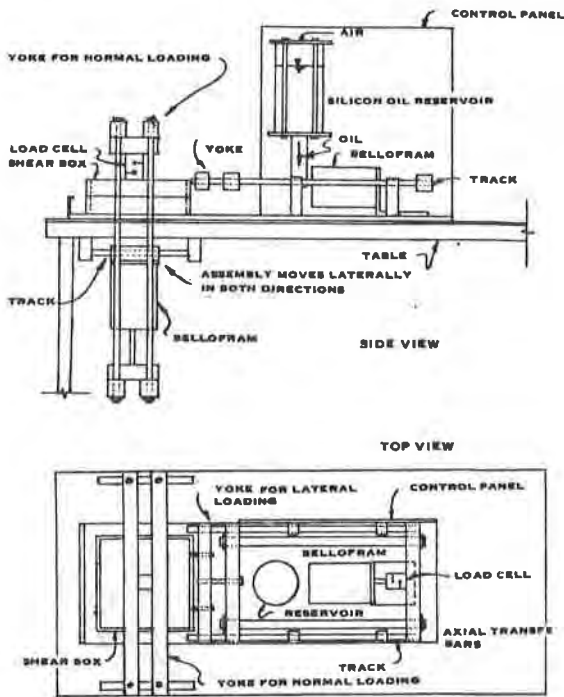


FIGURE 2. MODIFIED DIRECT SHEAR DEVICE

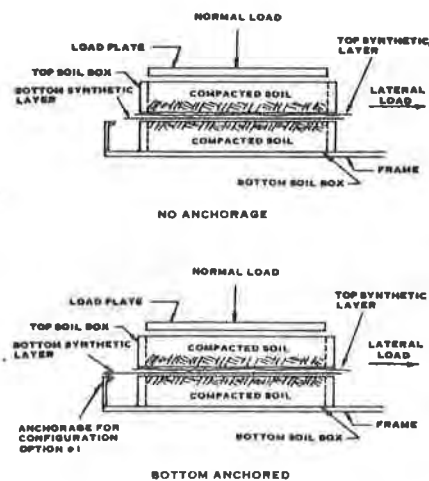


FIGURE 3. SPECIMEN CONFIGURATION OPTIONS

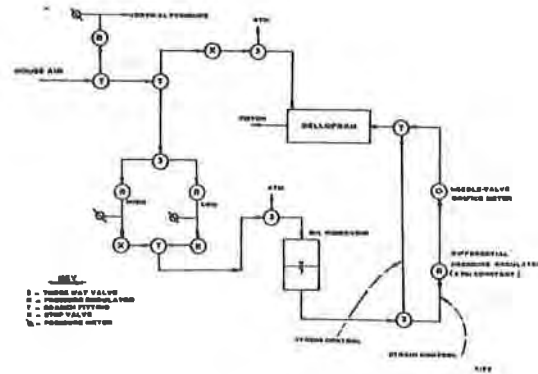


FIGURE 4. DIRECT SHEAR FRICTION DEVICE
HYDRAULIC LOADING SYSTEM

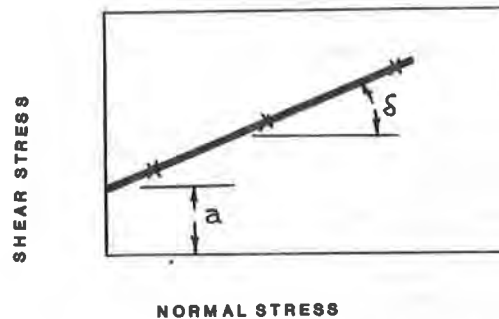


FIGURE 5. Interface Friction Parameters

10. REFERENCES

Degoutte, G., and Mathieu, G., "Experimental Research of Friction Between Soil and Geomembranes or Geotextiles Using a 30x30 cm² shearbox," *Proceedings of the Third International Conference on Geotextiles*, Vienna, Austria, 1986, p.p. 791-796.

Cul-Vermaoui, A., and Novatski, E., "Effect of Confining Pressure on Geotextiles in Soils," *Proceedings of the Second International Conference on Geotextiles*, Las Vegas, U.S.A., 1982, p.p. 799-804.

Formain, J., and Batareou, C., "The Shear Strength Behavior of Certain Materials on the Surface of Geotextiles," *Proceedings of the Eleventh International Conference on Soil Mechanics*, San Francisco, U.S.A., 1985, p.p. 1773-1775.

Jacobson, M. M., "Stability of Earth Structures Reinforced by Geotextiles," *Proceedings of the Eleventh International Conference on Soil Mechanics*, San Francisco, U.S.A., 1985, p.p. 1781-1785.

Hertin, J.P., Koerber, R.M., and Whitly, J.Z., "Experimental Friction Evaluation of Slippage Between Geomembranes, Geotextiles and Soils," *Proceedings of the International Conference on Geomembranes*, Denver, U.S.A., 1984, p.p. 191-196.

Mitchell, James K. *Fundamentals of Soil Behavior*, John Wiley and Sons, Inc., 1976.

Miyawaki, T., Iwai, S., and Makiuchi, E., "Frictional Characteristics of Non-Woven Fabrics," *Proceedings of the Third International Conference on Geotextiles*, Vienna, Austria, 1986, p.p. 701-705.

Myles, R., "Assessment of Soil Fabric Friction by Means of Shear," *Proceedings of the Second International Conference on Geotextiles*, Las Vegas, U.S.A., 1984, p.p. 787-791.

Baxena, S.K., and Budiman, J.S., "Interface Response of Geotextiles," *Proceedings of the Eleventh International Conference on Soil Mechanics*, San Francisco, U.S.A., 1985, p.p. 1801-1804.

Williams, R.D., and Houliban, M., "Evaluation of Friction Coefficients Between Geomembranes, Geotextiles, and Related Products," *Proceedings of the Third International Conference on Geotextiles*, Vienna, Austria, 1986, p.p. 891-896.

PARTOS, A.M. and KAZANIWSKY, P.M.
SITE Engineers, U.S.A.

Geoboard Reduces Lateral Earth Pressures

ABSTRACT

A two level below grade parking garage under a forty story office building adjacent to a low rise retail plaza is nearing completion in Philadelphia, Pennsylvania. A subway is located adjacent to the south property line. The exterior grades at the north are approximately 2.2 m (7 ft) higher than those at the south. The difference in elevations and the potential for a future excavation along the subway would result in unbalanced lateral earth pressures at the location of the plaza. It was not feasible to brace the north wall of the garage below the plaza or employ permanent tiebacks. A design was completed to reduce lateral at-rest earth pressures against the north basement wall by mobilizing active lateral earth pressures. Prefabricated, expanded polystyrene bead drainage geoboards were installed against the exterior face of the north basement wall. Compacted backfill was constructed against the 25 cm (10 in.) thick drainage geoboards. Load cells and extensometers were installed to monitor the magnitudes of lateral earth pressures and deflections of the drainage boards. This paper presents the design and monitoring system data together with conclusions regarding the performance of the system.

INTRODUCTION

Figure 1 shows the project site which occupies a full city block in the business center of Philadelphia, Pennsylvania. The completed project will consist of a forty story west office tower, a future forty story east office tower, and a centrally located plaza with one and two story retail areas. Two basement levels will provide parking below the entire site. The nearly completed west office tower is supported on drilled piers socketed in mica schist rock. The garage below the west tower and plaza is completed and supported on drilled piers and spread footings, respectively.

Figure 2 presents a cross-section through the plaza area. The lowest garage floor and the Market Street subway platform are approximately at the same elevation. Market Street grade is 2.2 m (7 ft) below JFK Boulevard grade. A temporary retention system consisting of soldier beams, wooden lagging, and soil tiebacks protected the north, west, and south sides of the approximately 10 m (33 ft) deep excavation. A 1.9 m (6 ft) diameter storm sewer was installed along the north wall of the excavation.

SITE engineers, inc. was retained by the owner to provide geotechnical engineering services in connection with design and construction. Figure 3 presents a summary of subsurface conditions based on borings drilled along the north retaining wall.

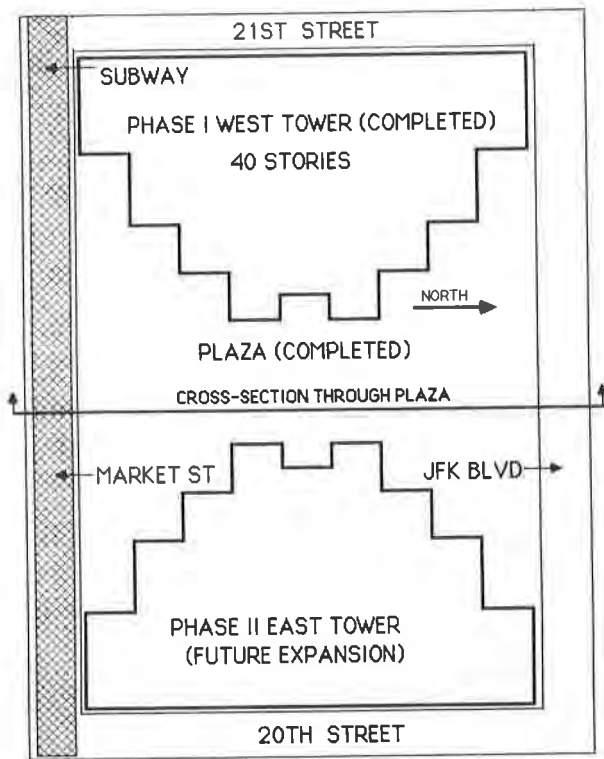


FIG. 1 LOCATION OF COMMERCE SQUARE TWIN TOWERS

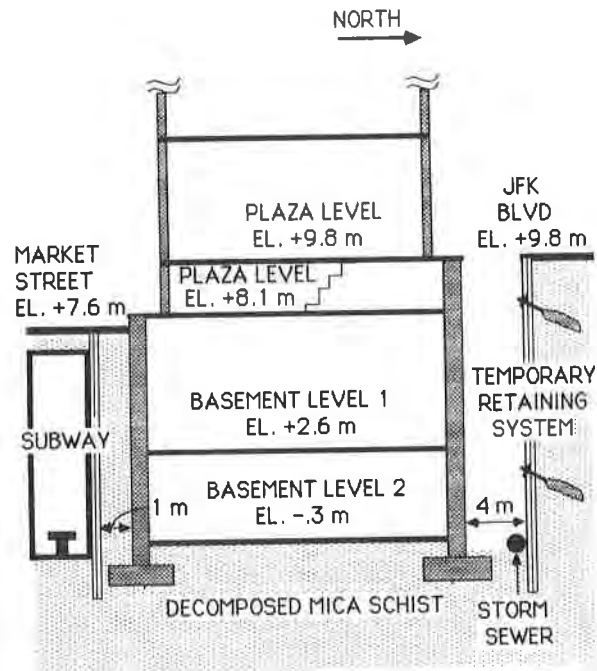


FIG. 2 CROSS SECTION THROUGH PLAZA DURING CONSTRUCTION

PRESENTATION OF PROBLEM

All below grade walls were designed to be non-yielding, braced by floors, and designed for the at-rest earth pressures computed on the basis of the existing soil conditions behind the temporary retention system. The design at-rest earth pressures are shown in Figure 3.

Due to the differences in elevations between Market Street and JFK Boulevard, unbalanced lateral earth pressures exist for the length of the plaza as shown in Figure 4. The unbalanced design load computed by the Structural Engineer was on the order of 233 kN/lin m (16 kips/lin ft) of wall.

Future excavation along the Market Street subway for repair or reconstruction could further increase the unbalanced loading conditions, but such additional loading was not considered in the design since maintaining stability would be the responsibility of others.

The Structural Engineer's review disclosed that modification to the light plaza steel frame by providing bracing to resist the lateral loads was not feasible. Permanent tiebacks anchored under JFK Boulevard could not be considered due to easement problems beyond the JFK Boulevard property line. Therefore, it was necessary to search for methods of reducing the lateral earth pressures against the north wall of the plaza.

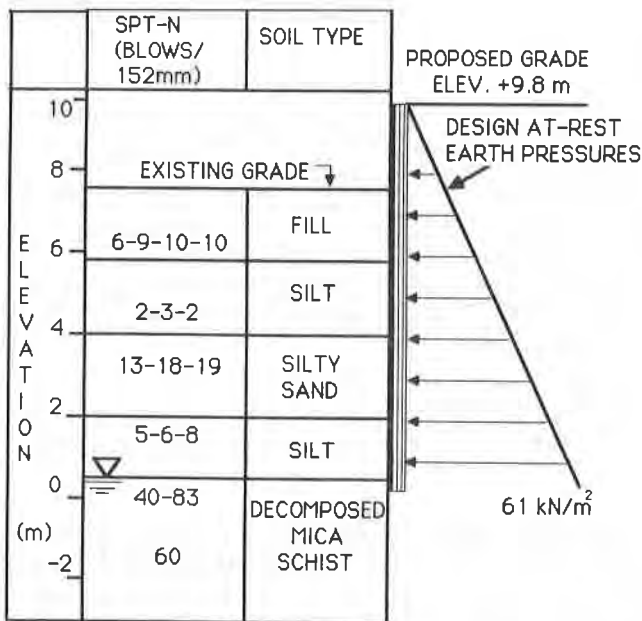


FIG. 3 TEST BORING RESULTS AND DESIGN AT-REST EARTH PRESSURES AT JFK BLVD WALL

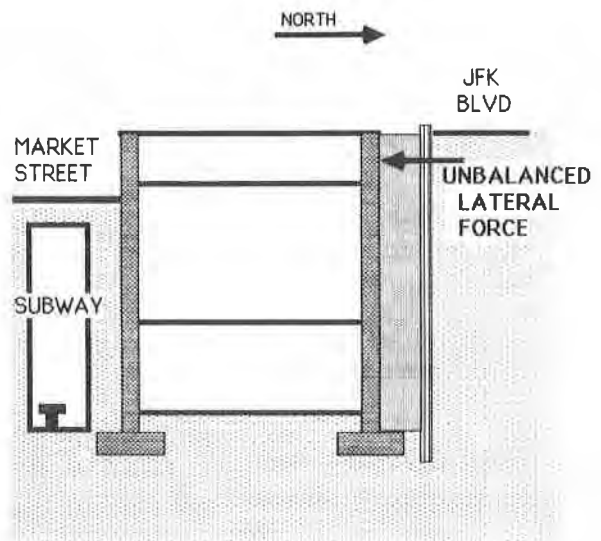


FIG. 4 UNBALANCED LATERAL FORCE AGAINST PLAZA NORTH WALL

METHODS OF REDUCING LATERAL EARTH PRESSURES

Several schemes were considered as listed in Table 1. The relevant functions of each method are also listed.

Table 1: Descriptions of Methods of Reducing Lateral Earth Pressures

<u>Description of Method</u>	<u>Function</u>
1. Light Weight Cellular Concrete Backfill	- Reduction in density - Mobilization of high value of cohesion
2. Stabilized Backfill	- Increase of angle of internal friction - Increase of cohesion
3. Elastic Drainage Board on Face of Wall	- Inducing quasi-active stress conditions by providing yielding media

After taking into consideration costs, scheduling, etc., the Construction Manager selected the drainage board scheme.

DRAINAGE BOARD DESCRIPTION AND PROPERTIES

The basic use for drainage boards is to provide rapid drainage capability for below grade structures, thus eliminating build-up of hydrostatic pressures against retaining walls, foundations, etc. Most drainage boards consist of rigid, thin "egg crate" like sheets molded from polystyrene. One product, the "Geotech Drainage Board," consists of molded blocks of expanded polystyrene beads bonded together with adhesive compound. It deforms during load application. Available thicknesses vary from 2.5 cm (1 in.) to 60 cm (24 in.). This product was selected on the basis of the predictability of stress-strain relationships and the availability of varying thicknesses.

A 3.8 cm (1.5 in.) thick by approximately 15 cm (6 in.) square manufacturer's sample was tested by uniaxial loading in an unconfined condition. The stress-strain relationships are presented in Figure 5.

Testing of two and three samples stacked-up provided results similar to those of the single sample board. The observed modulus of elasticity for the drainage board was approximately 220 kN/m^2 (2.34 tsf) in the load range up to 12 kN/m^2 (0.13 tsf) and on the order of 414 kN/m^2 (4.4 tsf) above that load interval. These values are in general agreement with the stress-strain data provided by the manufacturer.

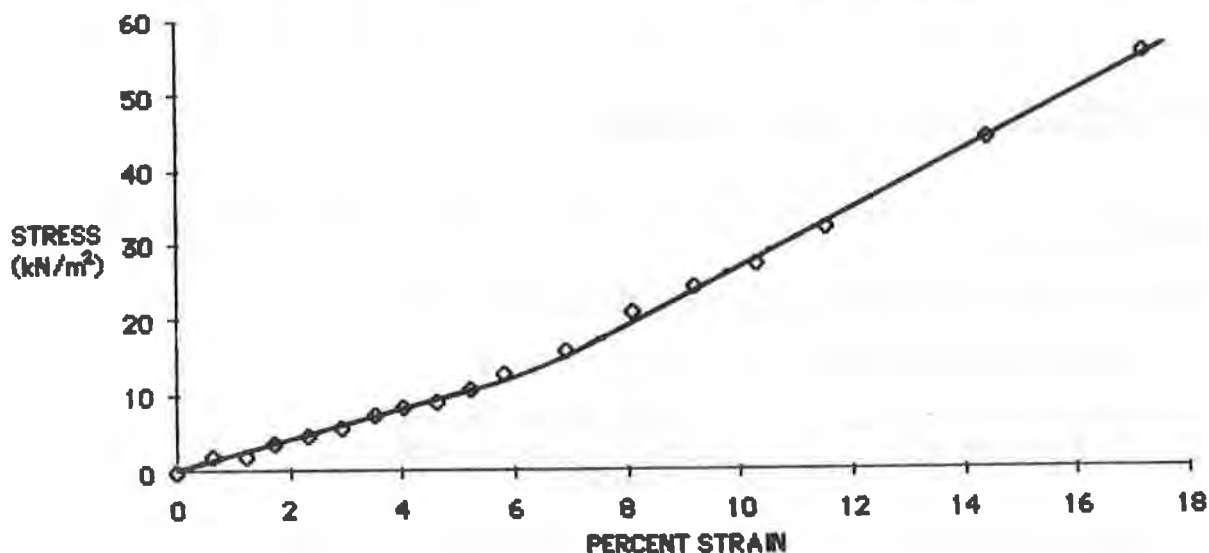


FIG. 5 LABORATORY STRESS-STRAIN
RELATIONSHIP FOR "GEOTECH" DRAINAGE BOARD

BACKFILL SOIL PROPERTIES AND DESIGN OF DRAINAGE BOARD

The excavated on-site granular materials were proposed as backfill for the full height of the retaining walls. The physical and engineering properties of the on-site granular soils based on laboratory testing and the anticipated field properties are presented in Table 2.

Table 2: Design Backfill Soil Properties

Soil Description: Well graded sand, some gravel, some silt
USC Classification: SW-GW
Maximum Laboratory Dry Density*: 20 kN/m^3 (128 pcf)
Laboratory Void Ratio (e) at Field Density: 0.36
Angle of Internal Friction: 36°
Cohesion (c) : 0
Anticipated Average Field In-Place Dry Density: 19 kN/m^3 (121 pcf)
Anticipated Average Field In-Place Moisture Content: 10%
Field Percentage of Maximum Dry Density: 93% to 95%

* (ASTM D698)

A well graded, coarse, very angular crushed aggregate (stone) was specified around the storm sewer line to approximately Elev. 0.9 m (Elev 3 ft). The estimated angle of internal friction is on the order of 60° , and the in-place density is approximately 22.8 kN/m^3 (140 pcf).

The drainage board thickness was then selected on the basis of the anticipated maximum earth pressure (at-rest condition) as shown in Figure 3, and compression of the board during translational displacement. A translational movement equal to approximately 0.3% of the wall height was estimated to mobilize a quasi-active state condition. (1)

The key design parameters are presented in Table 3.

Table 3: Design of Drainage Board:

Maximum Design Wall Pressure: 61 kN/m^2 (1300 psf)
Maximum Compression of Board : 2.5 cm (1 in.)
Minimum Thickness of Board: 15.2 cm (6 in.)
Selected Thickness of Board: 25.4 cm (10 in.)

The 25.4 cm board thickness was selected to provide a greater margin of safety because of the possibility that over-compression and some damage to the board could occur during backfill operations.

The vertical extent of the board was from approximately Elev. 1.5 m to Elev. 8 m (Elev. 5 ft and Elev. 25 ft).

The recommended method of installation required gluing the 1.2 m by 1.2 m by 0.25 m (48 in. by 48 in. by 10 in.) thick panels to the wall in advance of the backfill operations. Since protection of the board was crucial, temporary protection (plywood on exterior face) was also specified, if conditions required.

Backfill specifications required placing fill in 20 cm to 30 cm (8 to 12 in.) thick lifts and compacting with a light duty self propelled vibratory roller, to achieve 93% to 95% of maximum dry density (ASTM D698).

INSTRUMENTATION

As part of the quality control during construction, it was critical to evaluate the behavior of the proposed system in order to assess the validity of the design. To provide data on actual lateral earth pressures against the retaining wall and the magnitude of drainage board compression, instruments were installed in the wall along a near vertical line as shown in Figure 6. The instrumentation consisted of the following:

Stress Monitoring Instruments

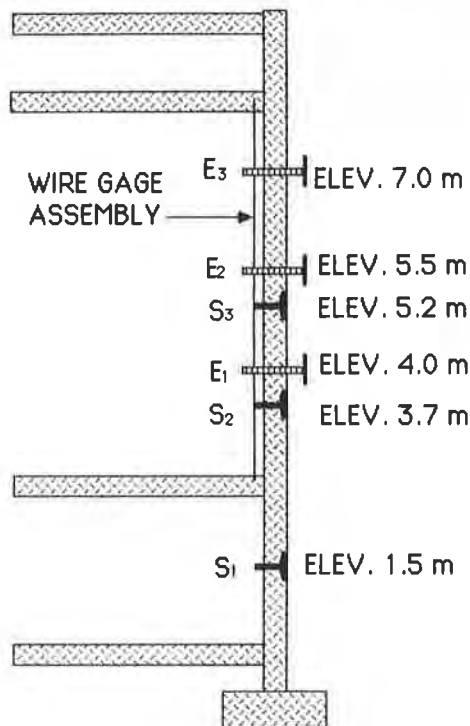
Type: Carlson S-25 Soil Stress Meter

Description: Resistance type "interface" stress meter approximately 28 cm (11 in.) in diameter, installed in the retaining wall behind the drainage board.

Number of instruments: 3

Pressure Range: 0 to 170 kN/m² (0 to 25 psi)

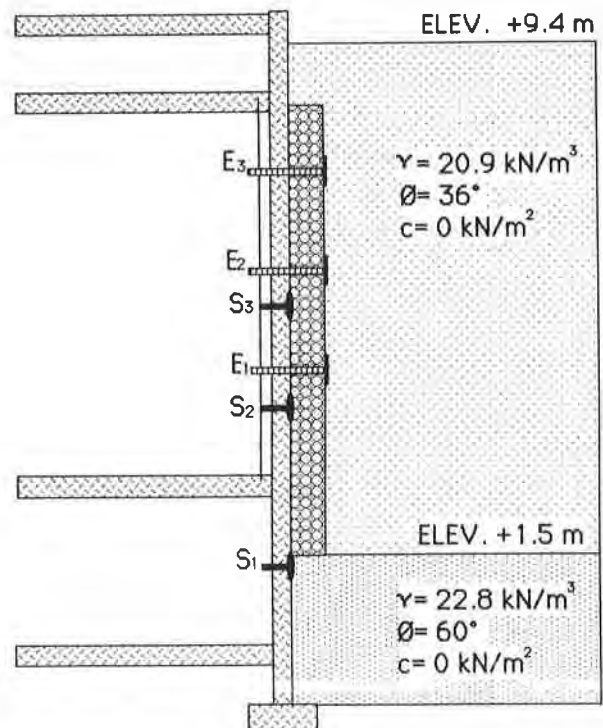
Accuracy: ±2% of full scale



LEGEND

- EXTENSOMETER (E)
- STRESS METER (S)

FIG. 6 STRESS METER AND EXTENSOMETER ELEVATIONS ON JFK RETAINING WALL



LEGEND

- EXTENSOMETER (E)
- STRESS METER (S)
- CRUSHED STONE BACKFILL
- SAND AND GRAVEL BACKFILL
- "GEOTECH" DRAINAGE BOARD

FIG. 7 BACKFILL MATERIALS (AS-BUILT)

Compression (Deflection) Monitoring Instruments

Type: Extensometer

Description: Field fabricated steel plate (.6 m x .6m) (2 ft by 2 ft) in size, installed on the exterior face of the drainage board. Plate is provided with a steel rod and a scale which projects through a sleeve to the inside of the wall. Movements were read against a wire gauge suspended between floor and ceiling.

Number of Instruments: 3

Accuracy: $\pm .25$ cm (0.1 in.)

BACKFILL CONSTRUCTION AND DATA ACQUISITION

An addendum to the specifications was issued covering installation of instrumentation, the drainage board, and the placement and compaction of backfill. The instrumentation became a part of the quality control procedures. Backfill construction was completed in two phases. The initial backfill phase consisted of placement of the crushed stone layer. The contractor elected to backfill the entire width of excavation up to approximately Elev. 1.5 m (5 ft) with crushed stone after the stress meters were installed as shown in Figure 7. The crushed stone fill extended above the lowest stress meter S-1, which had not been anticipated. Installation of the drainage board and backfilling (Phase 2) commenced approximately one month later. Installation of drainage boards and extensometers was done during backfilling with increasing fill heights. Backfill was placed in accordance with the recommended procedures with the exception that protection of the drainage boards with plywood panels was not required. Total densities from 20.3 to 20.9 kN/m³ (129 to 133 pcf) were measured in the field.

Stress and extensometer readings were obtained daily. Fill placement was completed in approximately two weeks time. Readings were also obtained for a period of four months after completion of the backfill.

Figure 8 presents the relationship between stresses and increasing fill heights at each of the three stress meter locations.

The data from Figure 8 are replotted and presented in Figure 9 to show the relationships between effective net fill heights above meter S-2 and S-3 and the corresponding lateral pressures.

Figure 10 shows the relationship between fill elevation and the corresponding compression of the "Geoboard" for each of the extensometers. The computed field strain-stress relationship and the laboratory stress-strain data are shown in Figure 11.

Figure 12 shows the actual measured and theoretical at-rest and active lateral earth pressures for the completed backfill condition.

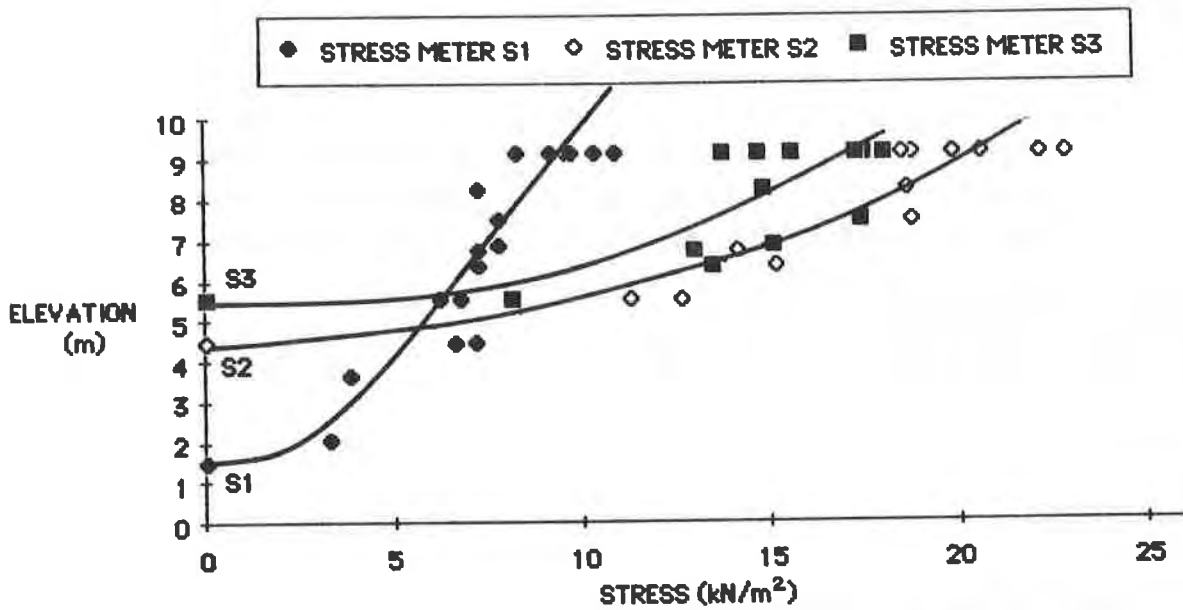


FIG. 8 FILL AND STRESS METER ELEVATIONS AND CORRESPONDING STRESS AT INDIVIDUAL METERS

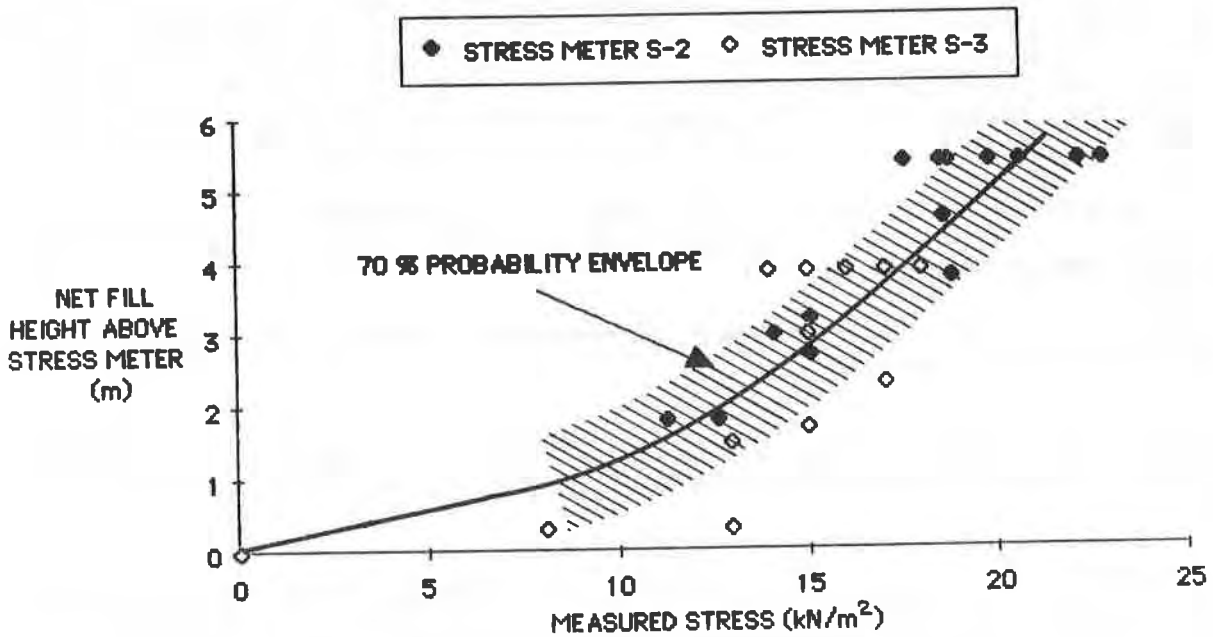


FIG. 9 RELATIONSHIP BETWEEN NET FILL HEIGHT AND STRESS

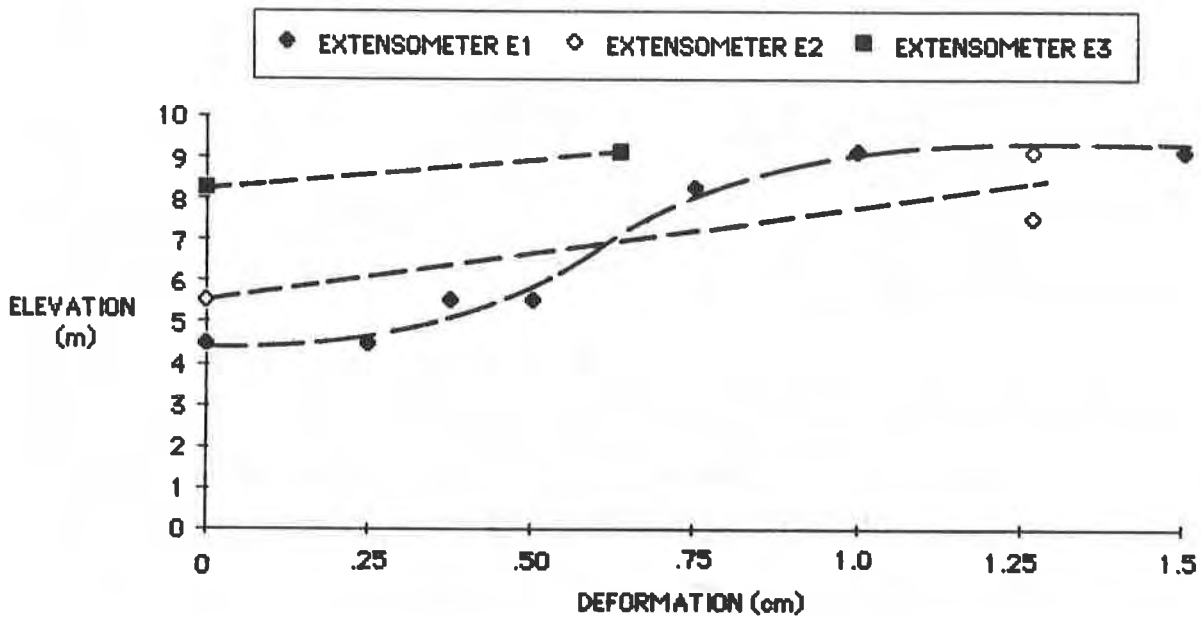


FIG. 10 FILL ELEVATION AND CORRESPONDING DEFORMATION OF "GEOTECH" DRAINAGE BOARD

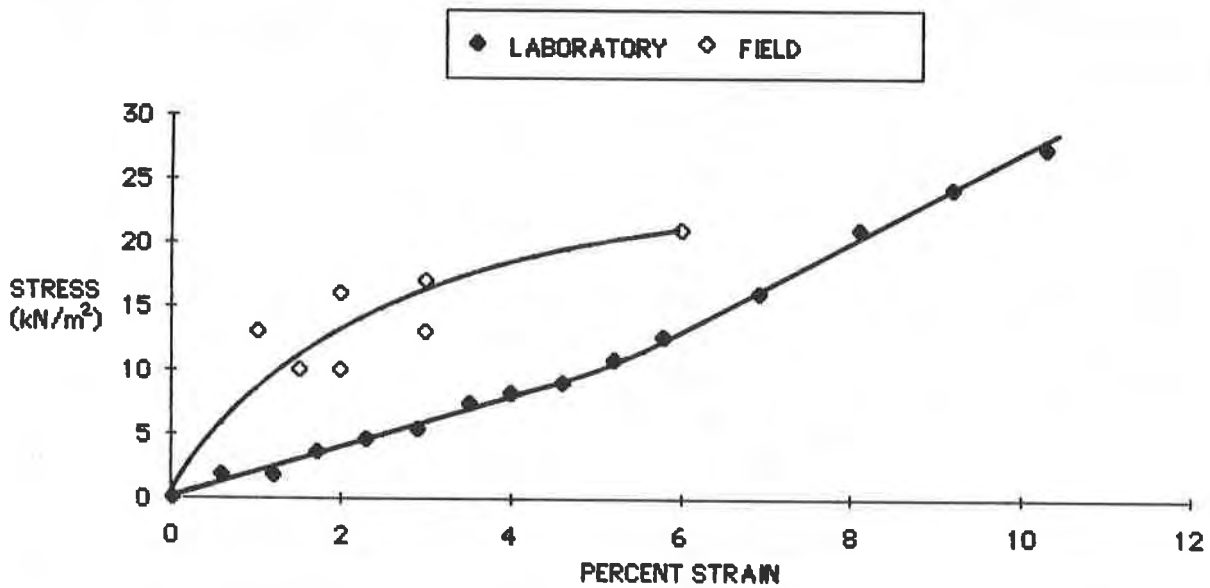


FIG. 11 LABORATORY AND FIELD STRESS-STRAIN RELATIONSHIPS FOR "GEOTECH" DRAINAGE BOARD

CONCLUSIONS

1. Application of the "Geotech Drainage Board" against a non-yielding retaining wall mobilized a quasi-active lateral pressure by allowing translational displacement of the wall backfill.
2. The instrumentation and monitoring programs discussed in this paper were done as part of the quality control procedures for this project and were not done for research purposes. Thus, the accuracy of the instrumentation, particularly deformation measuring, could be improved.
3. We are not aware of work by others to reduce lateral earth pressures against non-yielding retaining structures. We propose that "Geotech Drainage Board" or similar products could be used for this purpose, but further field and laboratory testing by manufacturers, researchers, etc., is warranted.
4. We offer to share our experience (good and bad) with those interested in similar applications.

REFERENCES:

1. Fang, Y.S. and Ishibashi, I., "Static Earth Pressures with Various Wall Movements," Journal of Geotechnical Engineering, ASCE, Vol. 112, No. 3, March 1986, pp. 317 - 333.
2. Gould, J.P., "Lateral Pressures on Rigid Retaining Walls", (1970) Specialty Conference: Lateral Stresses in the Ground and Design of Earth Retaining Structures, ASCE, NY, NY, pp. 219-270.
3. Morgenstern, N.R. and Eisenstein, N. "Methods of Estimating Lateral Loads and Deformation," 1970 Specialty Conference: Lateral Stresses in the Ground and Design of Earth Retaining Structures, ASCE, NY, NY, pp 51-102.
4. Tshebotarioff, G.P., Foundation, Retaining and Earth Structures, 2nd Edition (1973), McGraw-Hill Book Co., NY, NY, pp 382-388.
5. Winterkorn, M.F. and Fang, H.Y., Foundation Engineering Handbook, Van Nostrand Reinhold Co., NY, NY, 1975, pp 197-220.

Acknowledgements:

The authors thank John DiGenova, geotechnical engineer, SITE engineers, inc. for his assistance during field work and preparation of this paper; and Kelly A. Romayko for her dedicated assistance in the preparation of this manuscript.